MACROTIDAL SEDIMENTS, BEDFORMS AND HYDRAULICS, COBEQUID BAY

DOCTOR OF PHILOSOPHY (1977) McMASTER UNIVERSITY
(Geology) Hamilton, Ontario.

TITLE: Sediments, bedforms and hydraulics in a macrotidal environment, Cobequid Bay (Bay of Fundy), Nova Scotia

AUTHOR: R. John Knight, B.A., B.Sc. (Queen's University)

SUPERVISOR: Professor G. V. Middleton

NUMBER OF PAGES: xxvii, 693

ABSTRACT

Macrotidal environments, such as Cobequid Bay which has a mean tidal range of 11.7 m (maximum measured range of 16.3 m) near its mouth, are not uncommon in the world's coastal ocean. Such areas are, however, the least studied compared to other areas with smaller tidal ranges.

Cobequid Bay is a large, funnel-shaped estuary located at the head of the Bay of Fundy. The bay's waters are well-mixed due to the large tidal range and because river input is small compared to the tidal exchange. The morphology and distribution of sediments and bedforms is mainly the result of the tides. The bay is flanked by an intertidal bedrock platform that is either exposed or covered with a veneer of sediments. Suspended sediment concentrations are high (up to 2700 mg/l), but mudflats occur only in the small estuaries and bay. Sand deposition is localized in the centre of the bay as an intertidal to subtidal channel-bar complex. The sand bars are elongate features, 1 to 5 km long, asymmetrical in transverse section, oriented parallel to the currents, and covered with megaripples (length = 1-12 m) and sand waves (length = 10-30 m). The bars are composed of well-sorted, medium-grained sands that range from 5 to 15 m thick (decreasing in thickness and relief towards the head of the bay), and that are underlain by local accumulations (up to 10 m) of premodern (possibly Pleistocene) sediments and bedrock.

The tidal currents are semidiurnal, reversing and time-velocity asymmetrical. Maximum near bottom (0.5 m) speeds ranged from 0.3 to 1.0 m/s over the bars, and up to 2.0 m/s in the channels. Flow durations averaged 4.5 and 3.5 h for the ebb and flood over the bars, and 7.0 and 5.5 h for the ebb and flood in the channels. Current strengths and durations decreased towards: the shore, the bar crests and the head of the bay. The ebb and flood are dominated by a high-water 'sheet-flow' and a low-water 'channel-flow' relative to the low water emergence of the bar crests. The currents flow across the bars at an oblique angle to the crestlines during the 'sheet-flow' phase. The strength, duration and asymmetry of the currents are controlled by topographic shielding on and by the bars, the different hydraulic geometries and hypsometries

of the channels and the variation of tidal range during the lunar month. The gently sloping sides of the bars are flood-dominated and the steep sides are ebb-dominated.

The measured vertical velocity profiles indicate that velocities are proportional to the logarithm of the depth despite the presence of large bedforms and large depths of flow. Three types of velocity profile shape are related to the location of the measured vertical over the bedforms and to time during the tidal cycle.

Bedform scale, internal and external geometry, and net migration rates differ with sediment size, and flow strength, duration and asymmetry. Megaripples move faster (0.2 to 0.8 m/tidal cycle) than sand waves (0.1 to 0.3 m/tidal cycle), and become larger and more three-dimensional with increasing flow strength and duration. The sequence of bedform development (plane bed→ripples→sand waves→megaripples) with increasing flow strength on the bars is similar to that observed in flumes and other sedimentary environments. Seven different bedform facies are defined from the external morphology and scale of the intertidal bedforms on the bars and their areal distribution is described relative to a typical macrotidal sand bar. Megaripples reverse their asymmetry during each ebb and flood, but sand waves do not. Most of the preserved sedimentary structures in the intertidal bedforms are flood-oriented and are from ripples and megaripples. Sets of cross-bedding are separated by 'reactivation surfaces' and surfaces of discontinuity, and "herringbone cross-bedding" is uncommon.

The flow friction factor changes during the tidal cycle with different stages of bedform development and reversal, and suspended sediment concentrations. The friction factor at the time of maximum ebb speeds varies from about 0.032 for small megaripples to 0.050 for larger megaripples.

In winter, the presence of the frozen crust and the grounding of drift ice on the bars effectively stops the development of large bedforms, and obliterates or reduces the size of the bedforms from the summer.

The asymmetry of the currents results in the residual circulation of currents and sediment around the bars, or parts of the bars, within closed, or nearly closed, "elliptical loops." Coriolis effects are

unimportant with respect to the pattern of general circulation within the bay which resembles a large "ebb tidal delta." The general properties of the sediments, bedforms and current hydraulics of the sand-body complex in Cobequid Bay are similar to those of other tidal environments, despite dissimilarities of tidal range and the scale, relief and topographic complexity of the elongate sand bars in a macrotidal environment.

"The tide was out, and miles of basin bottom lay red and shining in the sunlight."

"It was dreamlike to see the tide creeping in over the shining red sand and ooze, and changing their vivid tints by blending with them its own colours to make tones strange both to sea and sand."

(Frank Bolles, from his essay From Blomidon to Smoky, in Goldthwaite, 1924, p. 132 & 134)

SEDIMENTS, BEDFORMS AND HYDRAULICS IN A MACROTIDAL ENVIRONMENT, COBEQUID BAY, (BAY OF FUNDY) NOVA SCOTIA

By

R. JOHN KNIGHT, B.A., B.SC.

A Thesis

Submitted to the School of Graduate Studies

in Partial Fulfilment of the Requirements

for the Degree

Doctor of Philosophy

McMaster University

January 1977

ACKNOWLEDGMENTS

I am greatly indebted to Dr. G. V. Middleton, my thesis supervisor, for numerous discussions and his patient guidance throughout the study. I would not have learned as much from the thesis research without his suggestions and criticisms.

Drs. S. B. McCann, R. G. Walker and M. Woo, the writer's supervisory committee, have reviewed the progress of the study from time to time. Drs. McCann and Walker critically read an early draft of the thesis and offered many useful suggestions.

I wish to thank the Atlantic Geoscience Centre (A. G. C.) of the Geological Survey of Canada for their financial and logistical support of the project. Special appreciation is expressed to Dr. B. R. Pelletier (presently with the G.S.C., Ottawa) who encouraged the project from its initiation and throughout in a variety of important ways. Many people from A. G.C. provided substantial administrative and logistical support; Lyle Brown, Caroline Clarke, Verne Coady, Georges Drapeau (presently with the Applied Oceanography Centre, Rimouski, Quebec) and Al Grant were most prominent. Al Grant's assistance with the interpretation of the 'Sparker records' was greatly appreciated. Others, from the Atlantic Oceanographic Laboratory (Environment Canada) who provided assistance on several occasions included: Fred Barteaux, Charlie Butler, Winston Goodwin, Bob Lively, Bud Martin, Roy Peck, Ed Verge, and others.

Further financial support was given by grants from the Geological Society of America (Penrose Bequest Grant No. 795-73) for the winter studies, and also from the Department of Energy, Mines and Resources and the National Research Council of Canada.

An 'instantaneous water sampler' was loaned for the project by the Inland Waters Directorate (Environment Canada, Ottawa) through Mr. E. R. Peterson and Mr. P. I. Campbell.

I am indebted to Jack Whorwood for his help with the photography and to John Cekr for his advice in technical matters. Maureen Dickson helped with some of the sediment analyses, and Mrs. Joyce Allen assisted in the typing of the final manuscript. Appreciation is also expressed to other university faculty members and to the departmental secretaries

who contributed to the project on various occasions.

Many useful discussions were had with my fellow graduate students. I would like to thank Doug Cant, Bob Dalrymple and Joe Lambiase in particular.

Special thanks go to the field people who made some of the largest contributions to the project. The principal field assistants were Kathy Warner (1971), Mike Beattie (1972) and Chris Lawson (1973). The boat cockswains, who often did more than they were required to do, were Aubrey Scott from Noel, and Doug Jamieson and John Pellerin from the Atlantic Oceanographic Laboratory (Environment Canada, Dartmouth). The writer is indebted to the many kind people from the field area, specifically Noel and Noel Shore, who made life so enjoyable in the field through their warm friendship and generous hospitality. Without the assistance of all of the field people, the project could not have been completed.

Many thanks to all of my family for their encouragement and support throughout the thesis work. Particular thanks go to my mother, Mrs. D. E. Knight, for typing most of the final thesis manuscript in her usual expert way.

Finally, I offer my deepest appreciation to my wife, Sherrill, who was my photographic scale, field assistant, draftswoman, darkroom assistant, and 'girl-Friday' on many occasions, for her patience and understanding throughout the thesis project. In many respects, my wife perhaps deserves to be a coauthor.

TABLE OF CONTENTS

LEAF xii OMITTED IN PAGE NUMBERING.

Appendices

LIST OF FIGURES

LIST OF TABLES

UNITS, NOTATIONS AND ABBREVIATIONS

Units

Metric units (S. I.) are employed throughout except where specifically noted.

Notations

A	value of Fr at nominal motion (Ackers and White, 1973)
A_o, A_1, A_2	constants in the linear regression equations
Az	orientation of bedform crest lee-face
c	celerity of tidal wave
C	coefficient in Ackers and White (1973) sediment transport function; Chezy coefficient
C_D	drag coefficient
C_1, C_2	constants of integration
d	sediment grain size
d_{35}, d_{50}, d_{65}, d_{84}, d_{90}, etc.	proportional size limits in a grain size distribution
D	water depth
D_{gr}	Ackers and White (1973) dimensionless particle size
f, f', f"	function of ...; Darcy-Weisbach friction factor; grain roughness; form roughness
F_{gr}	Ackers and White (1973) dimensionless sediment mobility numbers
Fr	Froude number
g	acceleration of gravity
G_{gr}	Ackers and White (1973) dimensionless sediment transport
h	flow duration
H, H_R, H_D	bedform height; ripple height; dune height

k_s	equivalent sand roughness
L, L_D	bedform length; dune length
L/H	ripple index
m	constant; exponent in Ackers and White (1973) sediment transport function
Mz	mean grain size
N, n	number of observations
n	transitional exponent of Ackers and White (1973) transport function depending on sediment size.
q	discharge per unit width
q_{st}	total-sediment load per unit width; rates in volume per unit time per unit width
Re	Reynolds number
Re_b	boundary Reynolds number
s	sediment specific gravity or relative density
S	hydraulic gradient (or theoretical slope of water surface)
S_e	salinity of ebb
S_f	salinity of flood
S_o	standard deviation of grain size distribution (sorting)
t_e, t_f	duration of ebb; duration of flood
T_1, T_2	times of high and low water slacks
u	velocity
u'	horizontal turbulent velocity component
u_1, u_2, etc.	velocity at y_1 and y_2 from the boundary; velocity at one metre from bottom, etc.

$\bar{u}$	mean flow velocity
u_{max}	maximum, mean surface flow velocity
u_*	shear velocity
V_e	volume of ebb tidal prism
V_{ev}	volume lost by evaporation from surface of the bay
V_f	volume of flood tidal prism
V_i	water volume discharged into the bay
V_o	water volume discharged out of the bay
V_p	volume of precipitation on to surface of the bay
V_r	volume of river runoff into the bay
V_E, V_F	average velocity of ebb and flood (Biswas and Chakrabarti, 1974)
w'	vertical turbulent velocity component
X	sediment transport, mass flux per unit mass flow rate (Ackers and White, 1973)
y	normal distance from the boundary
y_o	height of boundary roughness
z_o	roughness height
δ'	thickness of laminar sublayer
κ	von Karman's constant (0.4)
μ	dynamic viscosity of water
ν	kinematic viscosity of water
ρ	fluid density

ρ_s	sediment density
Σ	summation
τ	shear stress
τ_o	shear stress at bed
ϕ	phi grain size; $-\log_2 d$
ω	stream power

Abbreviations

A.S.C.E.	American Society of Civil Engineers
ATPEMC	Atlantic Tidal Power Engineering and Management Committee
B. P.	before present
C.H.S.	Canadian Hydrographic Service
^oC	degrees Celsius
D.M.T.S.	Department of Mines and Technical Surveys
E, e	ebb
ENB	East Noel Bar
F, f	flood
GV	Great Village Bar
h	hours
HW	high water
Kg	kilograms
m, km	metres; kilometres
MC	Middle Channel (see Fig. 4.1)
min, h	minutes; hours

ml, l	milli-litres; litres
mg/l	milligrams/litre
m/s, km/h	metres per second; kilometres per hour
m^3/s	cubic metres per second
NBB	Noel Bay Bar
NSB	Noel Shore Bar
N.A.P.L.	National Air Photo Library
pers. comm.	personal communication
r	correlation coefficient
SB	Selma Bar
T, t	time
t	metric tons; = 1000 kg
TR	tidal range
y	year
μ	microns

CHAPTER 1

INTRODUCTION

1.1 THE PROBLEM

Tidal currents are the "horizontal water movements associated with the rise and fall of the sea surface" (Gross, 1972, p. 283) and caused by the tide-producing forces of the moon and sun. According to Johnson and Belderson (1969, p. 393): "Tidal currents are at present the dominant sediment-moving force over a significant portion of the world's continental shelves and a secondary source over the remaining part." Thus, it is of no surprise that tidal currents and their deposits are of scientific interest to sedimentologists. Other reasons for the present interest in tidal sedimentation can be attributed to several influcences, including: man's determination to seek an understanding of poorly known or unstudied sedimentary systems; the possible significance of tidal deposits in the geologic past (Ginsburg, 1975; Off, 1963); the potential importance of tidal deposits as oil and gas reservoirs, and of tidal currents for power development (ATPEMC, 1969; Charlier, 1969 a and 1969 b; Clarke, 1972; Gray and Gashus, 1972; Richards, 1976) during the current "energy crisis"; and the need to acquire information about tidal systems for environmental management and development (e.g., maintenance of navigable waterways, development of tidal power schemes, problems associated with offshore oil exploration and pipeline construction, and environmental consequences of man-made developments in the coastal ocean).

Intensive and systematic study of tidal deposits began with the founding of Senckenberg am Meer at Wilhelmshaven, West Germany by Richter (Ginsburg, 1975; Spencer, 1957) in 1929. Since that time, a relatively large literature (see bibliography by Reineck, 1972) has accumulated about modern intertidal and shallow subtidal sediments. Until recently, the most common studies in the literature were concerned primarily with sedimentary facies descriptions and their application to the interpretation of sedimentary sequences in the geologic record, e.g., Evans (1965) in the Wash; Hantzschel (1939), Reineck (1963, 1967), Reineck and

Singh (1967; 1973, p. 280-372), van Straaten (1954, 1961) and Terwindt (1971 a, 1973) from the Dutch and German coasts of the North Sea; Bajard (1966), Mathieu (1966), and Phlipponeau (1956) in the Baie du Mont-Saint-Michel; Klein (1964, 1970 a) in the Minas Basin; Thompson (1968) in the Colorado River delta. Studies on the movement and accumulation of fine-grained tidal sediments are also relatively common, e.g., McCave (1969, 1970), Postma (1954, 1961), Reineck and Wunderlich (1968), van Straaten (1957), van Straaten and Kuenen (1958), Terwindt (1967), Terwindt et al. (1968), and Terwindt and Breusers (1972).

Although the literature on tidal sedimentation is seemingly large, tidal studies are "currently very active, with many old problems to be solved or unsolved, and new riddles to be discovered" (Garrett, 1974 a, p. 14). Indeed, there are many gaps in our knowledge of tidal sedimentation with respect to both imperfectly known systems and unexplained problems (e.g., Fig. 1.1).

Any natural tidal sedimentary system consists of a set of material and geometry factors that are more or less adjusted to a set of energy factors. The individual characteristics or interaction of these factors within a sedimentary system is best considered as a process-response problem (Fig. 1.2), wherein the material, geometry and energy elements of the system interact through various processes (e.g., sediment transport, current mechanics) to produce specific time-space sedimentologic responses (e.g., properties of the sediments, bedform development and distribution, geometry of the deposits). Many studies have directed their attention towards the morphological and material characteristics of tidal systems, but little consideration has generally been given to the energy factors (particularly from a sedimentologic viewpoint) or to their interaction with other system elements (e.g., specifically the material and geometry elements). As well, relatively few studies have attempted to test the applicability of experimental and theoretical steady-uniform flow results in natural flows, or to derive empirical explanations of tidally produced bedforms and internal sedimentary structures in terms of hydraulic and hydrodynamic factors. Some examples of this type of study include: Boothroyd and Hubbard (1975); Dyer (1970 and 1971); Klein and Whaley (1972); Ludwick (1970 a and b, 1972, 1974 and 1975); Nece and Smith (1970); Smith (1968 and 1969);

A comic strip from the Hamilton Spectator, July 31, 1974.
(Broom Hilda)

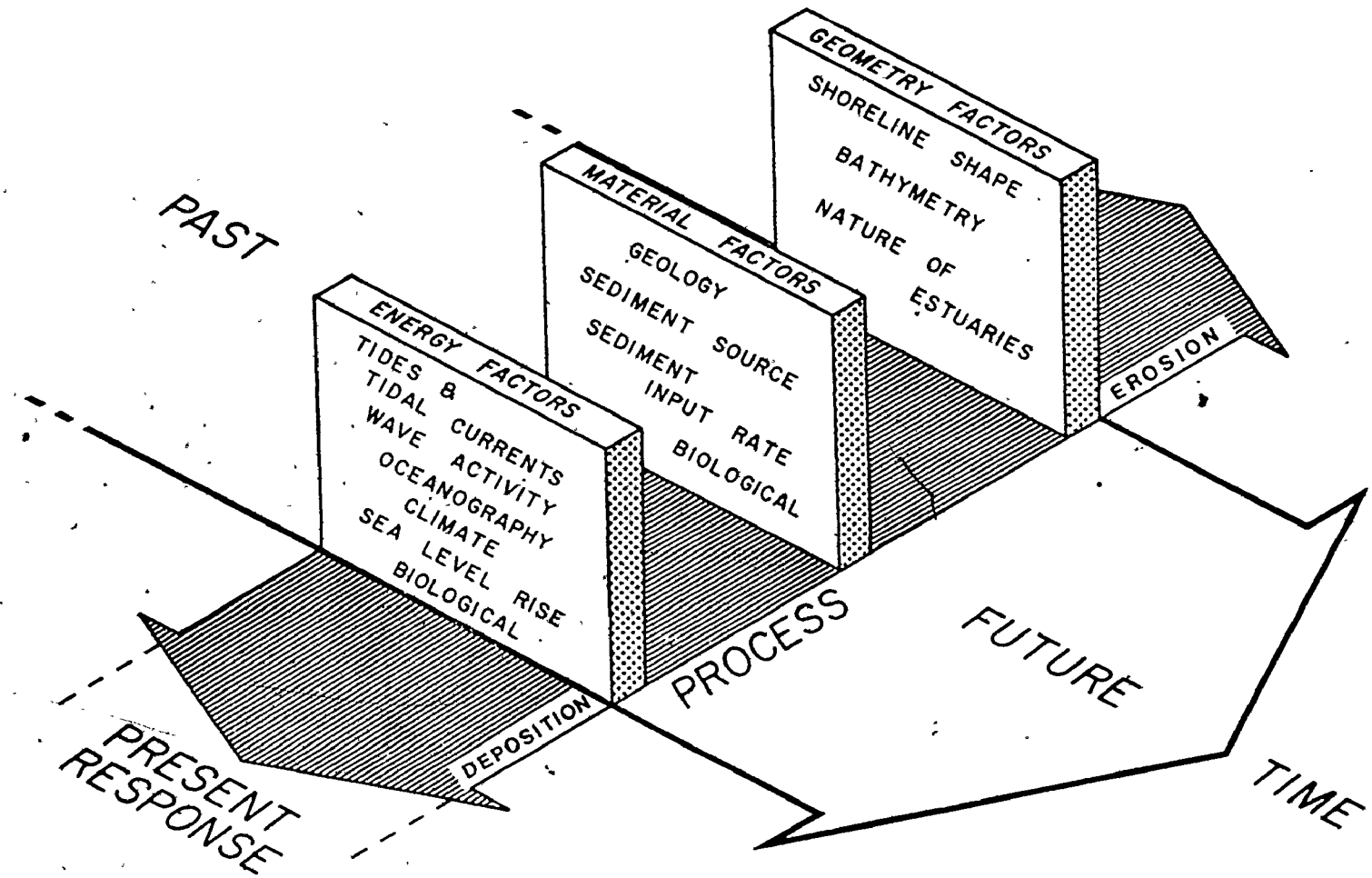

FIGURE 1.2: Summary of some of the energy, material and geometry factors operative in a tidal sedimentary system.

and Sternberg (1966, 1967, 1968, 1970, 1971, and 1972).

Most tidal studies, in terms of Davies' (1964) tidal range classification, have dealt primarily with areas that have micro- (less than 2 m) to mesotidal (2 to 4 m) ranges. Only a few studies have been conducted in areas where the tidal range is greater than 4 m. This is surprising because about one-third of the world's coastline has macrotidal ranges (Fig. 1.3).

Furthermore, little is known about the formation and maintenance of linear tidal sand ridges (or bars) that characterize many macrotidal, and some mesotidal, areas of the coastal ocean (Hayes, 1975; Swift, 1975). Swift (1975) distinguished between 'tide-formed' and 'tide-maintained' sand ridges by the absence of any reference to the former type (a convenient way of not getting into that problem). He groups the 'tide-maintained' ridges into three categories: (i) ridges in embayments, or the mouths of embayments, e.g., Gironde River estuary (Allen, et al., 1972). Tay River estuary (Green, 1975), Ord River estuary (Wright, Coleman and Thom, 1975), German Bight of the North Sea (Reineck, 1963), Rhine River estuary (Oomkens and Terwindt, 1960; Terwindt et al., 1963), Chesapeake Bay entrance (Ludwick, 1972, 1974, and 1975), Vineyard Sound (Smith, 1968 and 1969), Thames River estuary (Robinson, 1960), and Minas Basin (Klein, 1970 a; Swift and McMullen, 1968); (ii) ridges off capes and promontories, e.g., Cape Cod and Georges Bank (Off, 1963; Swift, 1975), Norfolk coast (Robinson, 1966); and (iii) ridges on open shelves and shelf-edges, e.g., Georges Bank (Jordan, 1962; Steward and Jordan, 1965), Sable Island (James and Stanley, 1968), offshore North Sea (Caston, 1972; Caston and Stride, 1970; Houbolt, 1968; Stride et al., 1972). Whether correct or not, some workers consider that all sand ridges are similar to each other and thus, should be considered together regardless of their location. To substantiate or refute either approach, more studies of tidal ridges are required, particularly from areas which are generally less accessible (e.g., such as the outer continental shelves) and those areas with macrotidal ranges. Also, the relationship between the internal sedimentary structures and the three-dimensional geometry of tidal sand ridges is not well known.

In comparison to most other depositional environments, tidal deposits and their depositional mechanics are poorly known. For example,

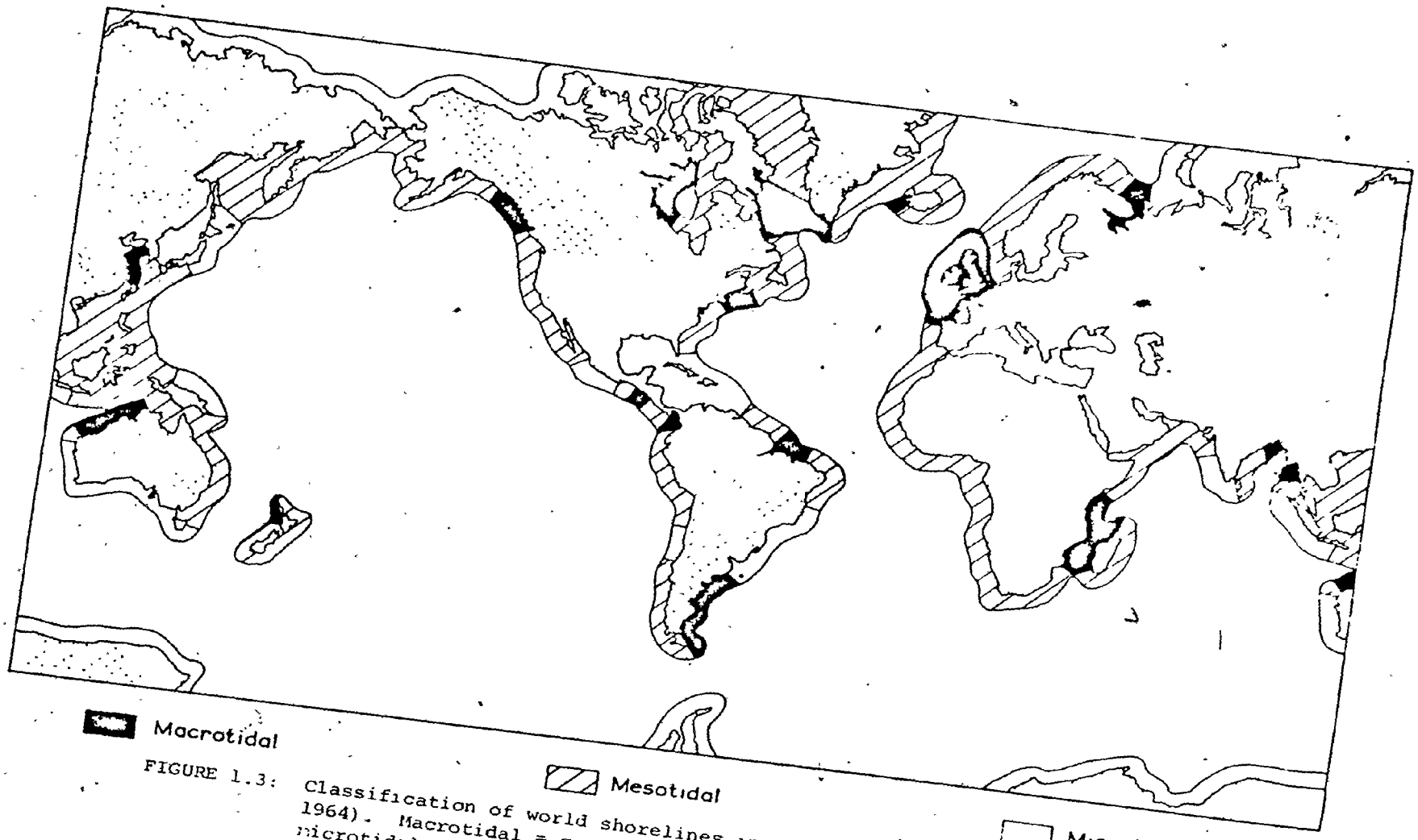

FIGURE 1.3: Classification of world shorelines in terms of tidal range (after Davies, 1964). Macrotidal = greater than 4 m; mesotidal = 2 to 4 m; and microtidal = less than 2 m.

fluvial deposits are well-enough studied and understood that models have been constructed to synthesize most of the important characteristics of meandering and braided reaches (Walker, p. 63-79, in Harms et al., 1975; Walker, 1976). Klein (1971 and 1972) formulated a model for "prograding clastic tidal shorelines in embayed areas, lagoons, and open coasts ..." (1971, p. 2585), but the model does not satisfactorily characterize all aspects of tidal sedimentation, particularly subtidal deposits. Because there are still many gaps in our knowledge of tidal sedimentation, no overall model exists that combines all of the basic characteristics of tidal systems in the coastal ocean.

In view of the many deficiencies concerning our understanding of tidal deposits, the major emphasis of this study will be to contribute the knowledge of: (i) the geometry, structure and development of linear sand bars; (ii) the hydraulics of tidal currents in a macrotidal system; and (iii) the mechanics of tidal sedimentation (e.g., tidal bedform development).

1.2 FIELD PROGRAMME

Study Area

The Bay of Fundy lies between New Brunswick and Nova Scotia (Fig. 1.4) on the east coast of Canada. At the head of the bay, it divides into Chignecto Bay (including Shepody Bay and Cumberland Basin) which extends towards the northeast and Minas Basin-Cobequid Bay which extends to the east (Fig. 1.5). Field studies were carried out in Cobequid Bay (Fig. 1.5) which is situated to the east of Minas Basin at an approximate latitude and longitude of 45°20'N and 63°20"W to 63°50'W respectively (see also C.H.S. chart 4010 and D.M.T.S. map sheets 11E/5E, 11E/5W and 11E/6W at 1:50,000).

The field work was carried out during the summers (usually May through August) of 1971 to 1973. Winter observations were made during the last week of February, 1973 and during the first three weeks of February, 1974.

According to Yuen (1969): "The Bay of Fundy has attracted the attention of the mariner, the scientist, and the curious onlooker for many years because of its remarkable tides." McWhirter and McWhirter

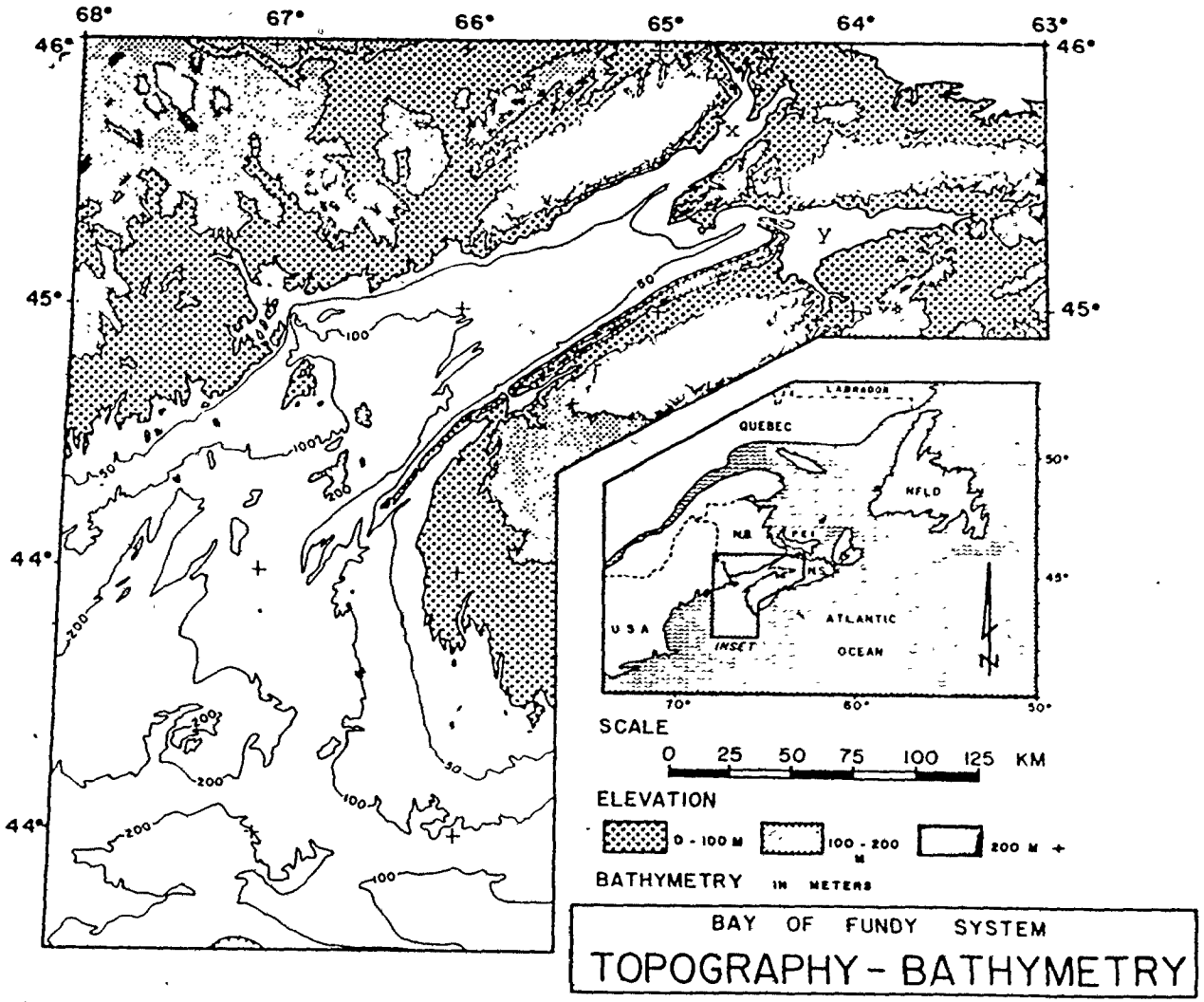

FIGURE 1.4: Map of the Bay of Fundy system showing location, bathymetry and local topography. Chignecto Bay (x) and Minas Basin-Cobequid Bay (y) are located at the head of the Bay.

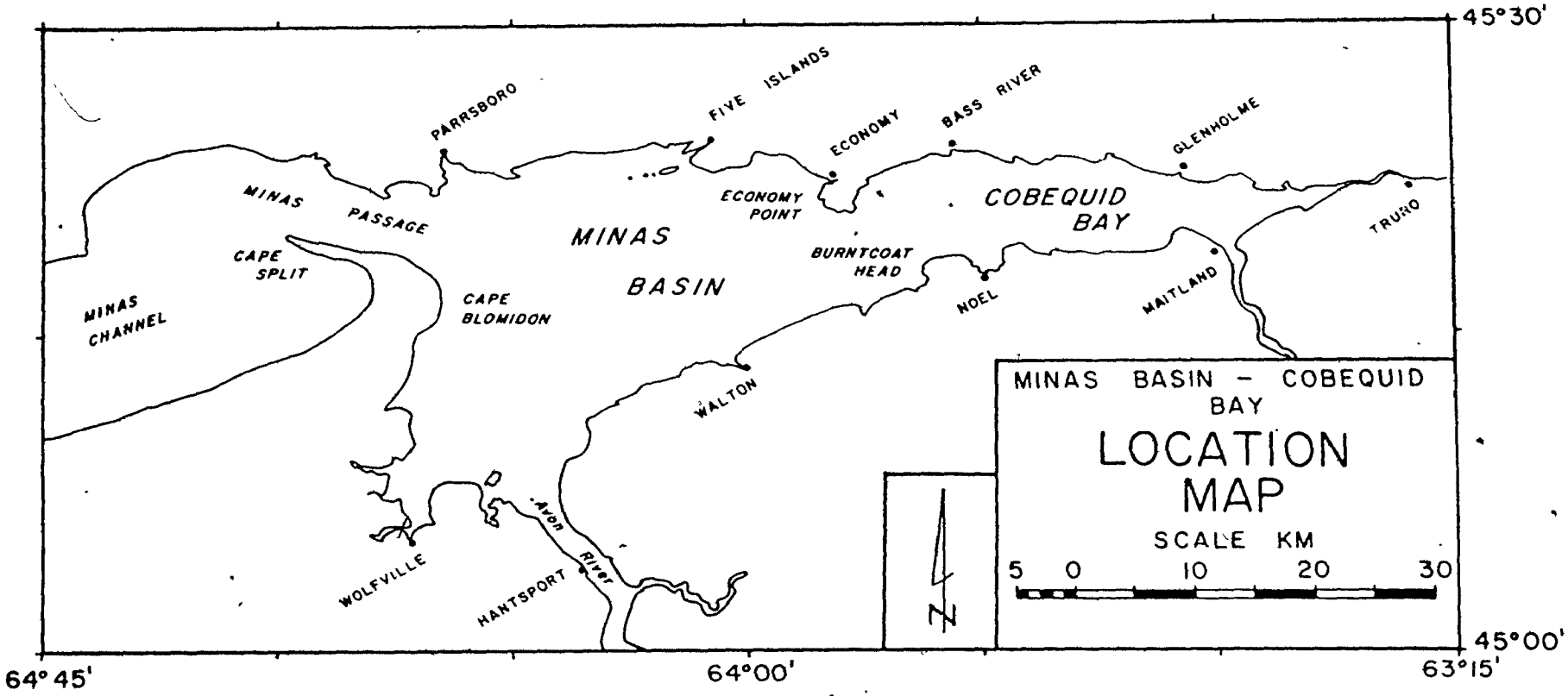

FIGURE 1.5: Location map of Minas Basin-Cobequid Bay region showing place names.

(1972, p. 56) reported that the largest tides in the world occurred at Burntcoat Head near the head of the Bay of Fundy system (Fig. 1.5). The maximum measured range is 16.3 m (Dawson, 1917) from the west side of Burntcoat Head.

Despite the extremely large tidal range and the supposed interest of many people, sedimentological studies in the bay are much less complete than those in areas elsewhere (e.g., the North Sea and the Massachusetts coast). This is surprising because the tidal currents move large quantities of sediments, and these sediments accumulate locally as elongate sand bars and extensive mudflats that are exposed at low tide (Fig. 1.6). Other reasons that justify the study of macrotidal sedimentation in Minas Basin-Cobequid Bay include: (i) the area has been considered as a potential site for the development of tidal power (ATPEMC, 1969; Clarke, 1972); (ii) the emergence of many of the linear sand bars in Cobequid Bay at low tide makes it possible to study many aspects of tidal ridge formation and maintenance directly that can only be studied indirectly in tidal areas elsewhere; and (iii) if tidal deposits represent an important part of the geologic record and the moon was at one time considerably closer to the earth (Klein, 1971 and 1972; Merifield and Lamar, 1970; Olson, 1970 and 1972), then a better understanding of modern areas of macrotidal sedimentation is important for the interpretation of ancient deposits.

Previous work on the linear sand-bodies in Minas Basin-Cobequid Bay include: Balaz and Klein (1972); Brisbin (1974); Dalrymple (1973 a and b, 1974 a and b, 1975 and 1976); Dalrymple et al., 1975); Klein (1968 a and b and 1970 a); Klein and Whaley (1972); Knight (1971, 1972, 1973 a and b); Knight and Dalrymple (1976); Lambiase (1974); Middleton (1972); Middleton et al., (1975 and 1976); Swift and McMullen (1968) and Wehrfritz (1973). Pelletier and McMullen (1972) described the general distribution of bottom sediments in the bay. ATPEMC (1969) reported the results of studies and surveys carried out in the bay to determine the physical and economic feasibility of tidal power. Their report provides extensive background data to the Minas Basin-Cobequid Bay area. Dr. C. Amos (Atlantic Geoscience Centre, pers. comm., 1975) is currently investigating the sediment budget of Minas Basin-Cobequid Bay. Figure 1.7 shows the main areas of previous sedimentologic work in Minas Basin-

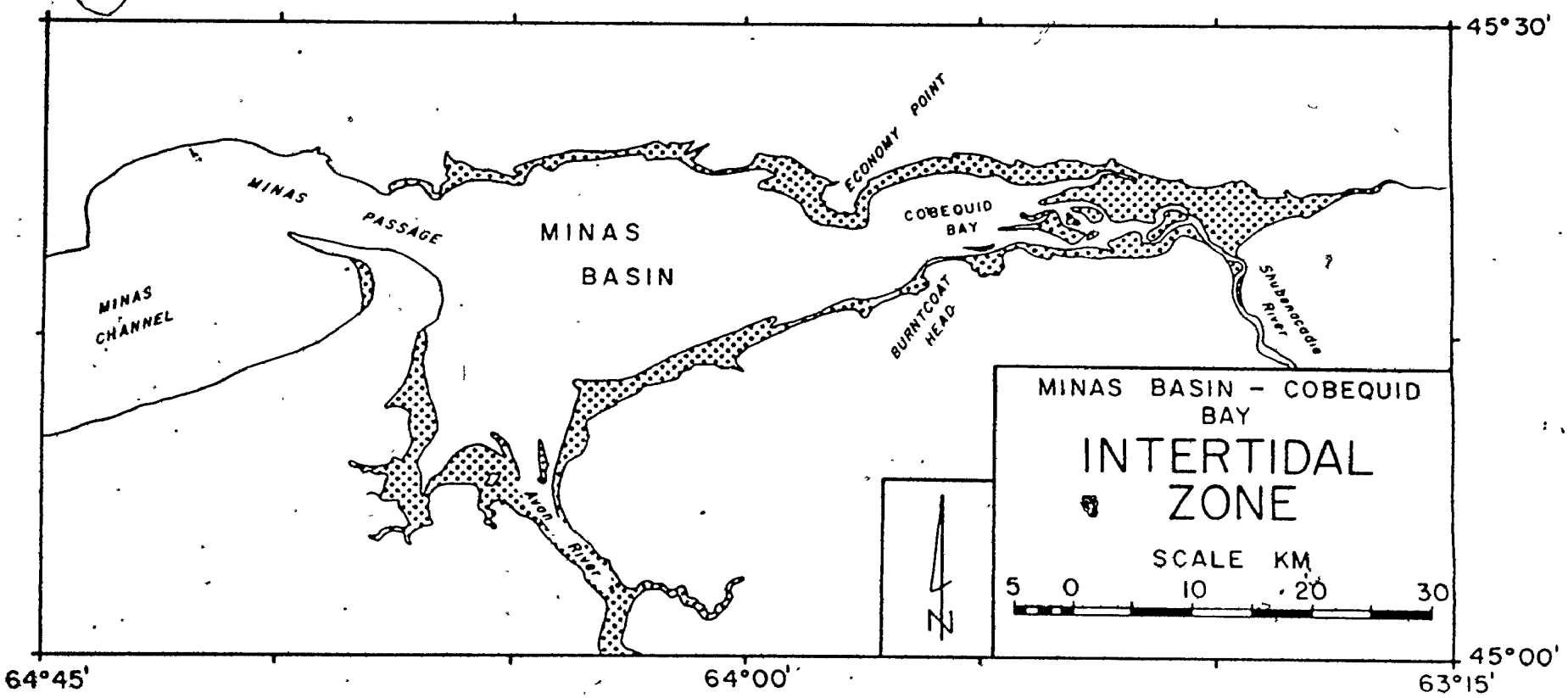

FIGURE 1 Map of the intertidal areas in Minas Basin and Cobequid Bay.

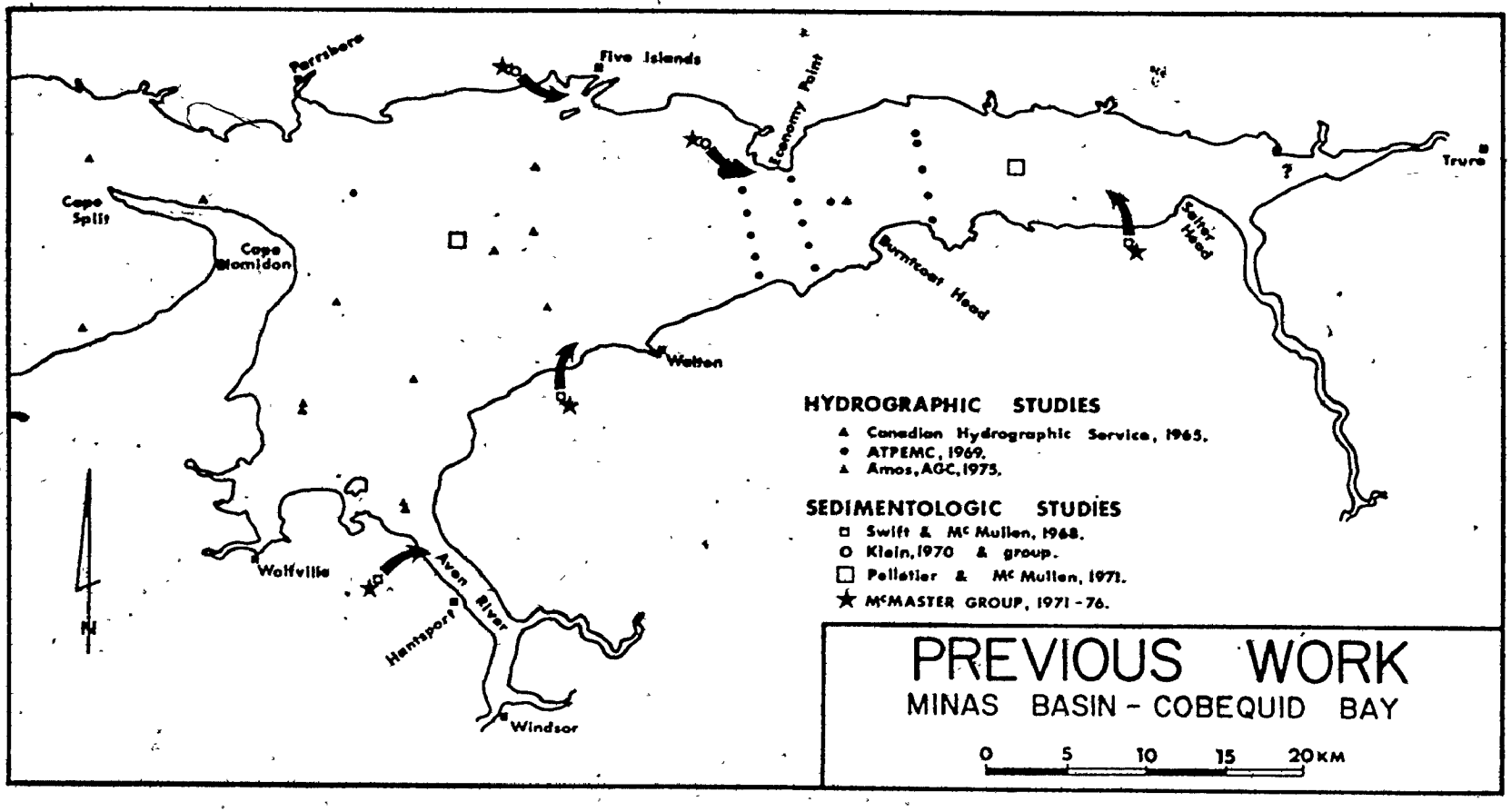

FIGURE 1.7: Generalized locations of previous work in Minas Basin Cobequid Bay.

Cobequid Bay, including the areas that are being studied by the McMaster University group.

Plan of the Study

The main objective of the field investigation was to study the sedimentary dynamics associated with the formation and maintenance of large scale bedforms (e.g., megaripples and sand waves) and linear sand bars in a macrotidal area. Because any sedimentary system comprises a set of dynamically and complexly interrelated components, it is best studied in terms of the material, geometry and energy elements (Fig. 1.2) of the system, using as much information as possible from experimental studies, the geologic record and natural tidal systems elsewhere. The project had three specific goals: (i) to define the process elements within the system (e.g., energy, material and morphological factors); (ii) to determine the energy and mass transfer events that lead to sediment erosion and deposition (e.g., tidal current hydraulics and sedimentation mechanics); and (iii) to analyse the system's response elements relative to the environmental conditions under which the process and transfer factors interact (e.g., characteristics of the tidal deposits, the areal variation of process and transfer elements, sediment transport, etc.).

The field work concentrated on three main aspects of data collection. Firstly, considerable emphasis was placed on the measurement of tidal current velocities (speed and direction) as a function of time, depth and location in the sand-body complex. These measurements were used to derive several hydraulic parameters (Appendix IV) in order to evaluate the nature and degree of interaction between individual process elements (e.g., energy, material and geometrical factors) in the system. The second area of data collection comprised a study of the large scale bedforms that covered the surface of the intertidal sand bars (e.g., types, scale, and areal variations; relationships to hydraulics, sediments and bar morphology; time-variant properties; internal sedimentary structures). And thirdly, data was collected to investigate the rates and patterns of sediment transport relative to the formation, maintenance of morphology of the large scale bedforms (e.g., megaripples and sand waves) and the linear sand bars.

An attempt was made to adapt as many observations as possible to instrumented measurement so that the nature of such observations would be easier to assess and be more reliable. The field work resulted in the acquisition of a large volume and variety of data. Because of the potential value of much of the data for other workers, it is reported in full at the end of the thesis (i.e., Appendices I to V).

The results of the investigation will hopefully contribute toward the understanding of macrotidal sediment mechanics and deposits, not only with respect to the study area but also to macrotidal areas elsewhere.

1.3 Preview of Results

In stratigraphic section, the sand-body complex in Cobequid Bay resembles a clastic wedge that has prograded from the head of the bay. The general morphology and pattern of circulation within the sand-body complex is mainly the result of the tides and is similar to that of a large "ebb tidal delta", following the model proposed for tidal inlets with mesotidal ranges. As a result of the asymmetry and the interdigitation of the ebb and flood tidal currents, the gently sloping sides of the bars and the channels located along the north and south margins of the sand-body complex are dominated by the flood, and the steeply sloping sides of the bars and the major channels located along the axis of the sand-body complex are dominated by the ebb. Sand is circulated around the bars or parts of the bars within closed or nearly closed loops at faster rates than the lateral rates of migration of the bars. There is no indication from the last 100 years of historic record of a major change in the volume of sand in the sand-body complex, suggesting that the sand-body is in some sort of dynamic equilibrium with the modern tidal regime. The general properties of the sediments, bedforms and current hydraulics are similar to those of other tidal environments, despite differences of tidal range, and the scale, relief and topographic complexity of the macrotidal sand bars in Cobequid Bay.

The general characteristics of the setting of the sand-body complex in Cobequid Bay are discussed in Chapters 2 and 3. Chapter 4 presents the results of the current measurements and some of the derived hydraulic

parameters. Description and discussion of the large scale bedforms and their internal sedimentary structures, and some of the hydraulic controls on bedform development, is found in Chapter 5. In Chapter 6, the general circulation of currents and sediments on the sand bars and within the sand-body complex are discussed with reference to the formation and maintenance of the elongate sand bars in Cobequid Bay. Chapter 7 briefly summarizes the main findings and conclusions of the study.

CHAPTER 2

SETTING

2.1 PHYSIOGRAPHY

The almost completely enclosed, triangular-shaped body of water at the eastern end of the Bay of Fundy includes Minas Basin and Cobequid Bay (Figs. 1.3 and 1.4). The physiographic region bounding Minas Basin-Cobequid Bay can be divided into two parts for convenience of discussion: (i) the subaerial topography; and (ii) the submarine bathymetry.

Topography

The area surrounding Minas Basin and Cobequid Bay, comprising the subaerial topography, consists of three physiographic subdivisions (Bostock, 1970, Goldthwaite, 1924; Figs. 2.1 and 2.2): (i) the Nova Scotia Highlands; (ii) the Atlantic Uplands; and (iii) the Minas-Annapolis Lowlands. Each of these subdivisions comprises a distinct unit of the landscape that is closely related to the underlying bedrock geology of the region.

The Nova Scotia Highlands, locally referred to as the Cobequid Hills, form the northern boundary to the Minas Basin-Cobequid Bay physiographic region. The hills extend in an east-west direction, parallel to the north shore of Minas Basin and Cobequid Bay. The surface of the highland forms a rolling upland between 290 and 300 m.

The Atlantic Uplands occur along the entire Atlantic coast of Nova Scotia (Fig. 1.3), forming the southern border and part of the western edge of the Minas Basin-Cobequid Bay region. Along the southern margin of the region, the highlands are gently rolling hills that reach 180 to 240 m elevation. On the western edge of the region, North Mountain, also part of the Atlantic Uplands, is a flat-topped, steep-sided ridge that extends from the curved hook of Cape Blomidon and Cape Split to the southwest along the south shore of the Bay of Fundy (Fig. 1.3). The average surface elevation of the ridge is a little over 200 m.

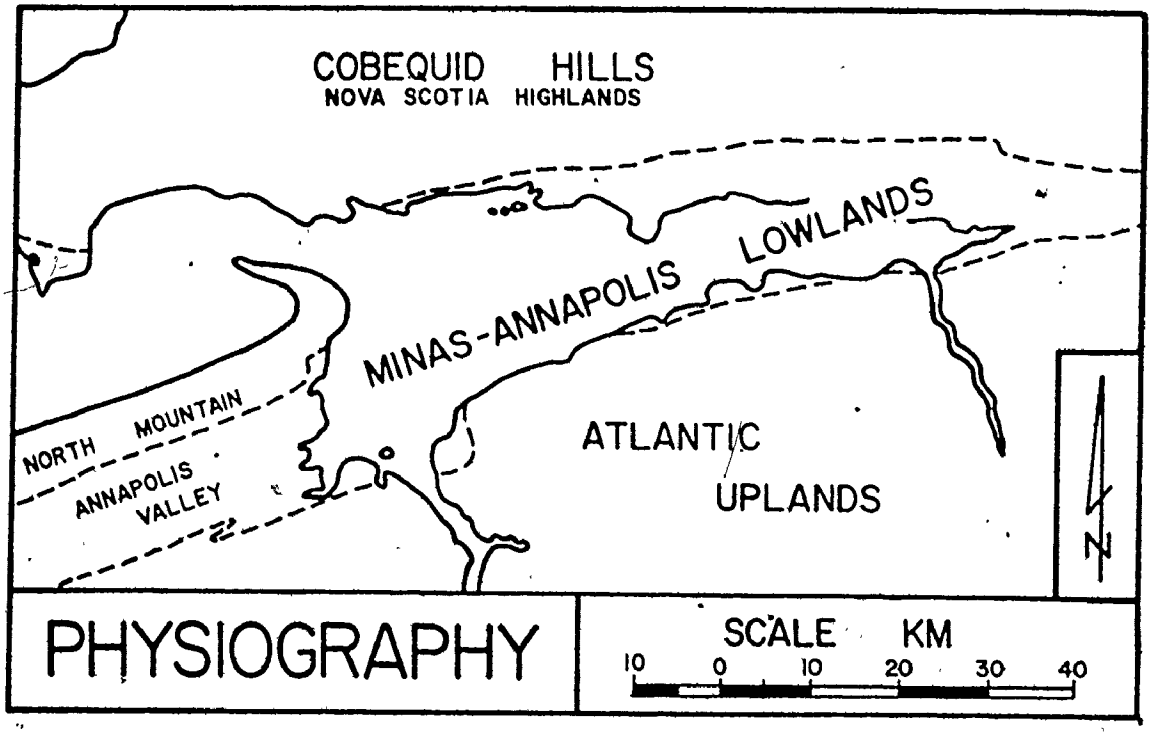

FIGURE 2.1: Physiographic subdivisions of the Minas Basin-Cobequid Bay region (after Bostock, 1970).

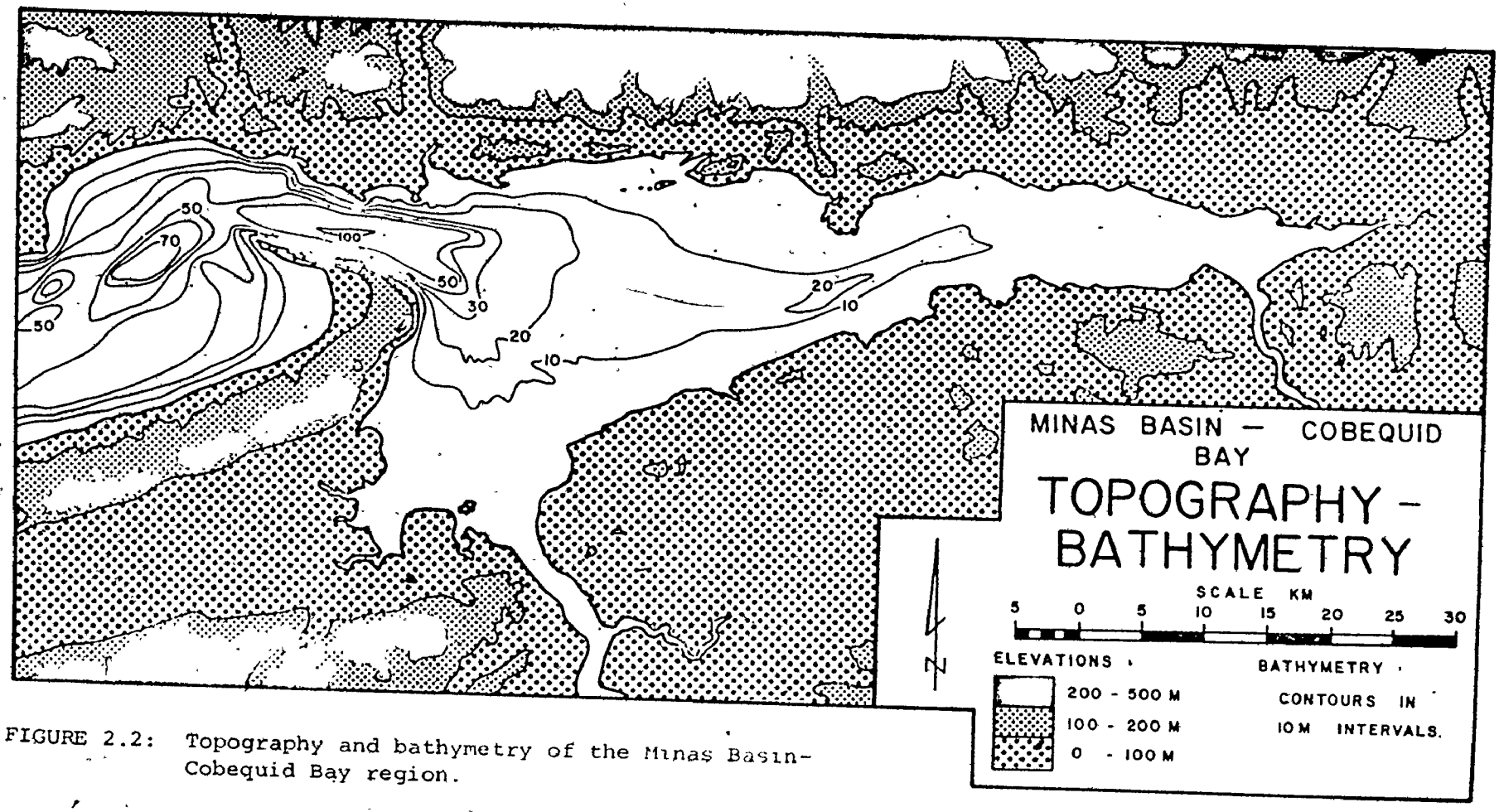

FIGURE 2.2: Topography and bathymetry of the Minas Basin-Cobequid Bay region.

The Minas-Annapolis Lowlands occur on both sides of Minas Basin and Cobequid Bay (Figs. 2.1 and 2.2). The lowland surface consists of broad gently rolling hills with an average elevation of 20 m. The lowlands terminate abruptly in bedrock seacliffs that are about 10 m in height along the shoreline of Minas Basin-Cobequid Bay. On some promontories, the seacliffs reach a height of 30 m. Rivers crossing the lowlands are incised with broad, flat-bottomed valley floors covered in alluvium. Many of the river estuaries and streams are tidal and bordered by saltmarshes for some distance upstream from their entrances (e.g., the Salmon and Shubenacadie Rivers; see Fig. 3.1).

Bathymetry

Minas Basin and Cobequid Bay together (Fig. 2.2) measure over 70 km in length and almost 31 km wide at the widest point, and constitute almost 1050 km^2 of water surface. Minas Basin refers to the area west of a line joining Economy Point on the north shore to Cape Tenny on the south shore. Cobequid Bay is the funnel-shaped extension of the system to the east of the line.

The system is connected to the main Bay of Fundy through the Minas Passage-Minas Channel (Figs. 1.3 and 1.4). The channel is relatively deep (up to 120 m) and narrow (about 5 km) at the widest point of separation. Water depths (Fig. 2.2) in the central part of the Minas Basin and near the entrance to Cobequid Bay (in the vicinity of Economy Point and Burntcoat Head) are generally in the order of 10 to 20 m below lowest normal tide levels. A fairly pronounced trough extends up the axis of the system from Minas Passage towards the entrance to Cobequid Bay. Water depths do not change appreciably along the length of this bathymetric low, but east of Burntcoat Head in Cobequid Bay (Fig. 1.5) the seafloor shallows rapidly into a relatively complex channel-bar system.

At low tide, an extensive intertidal zone (area about 200-300 km^2) is exposed around the perimeter of Minas Basin-Cobequid Bay (Fig. 1.5). As the seabed gradient is somewhat shallower from the north shore than from the south toward the centre of the bay (Fig. 2.2), the width of the intertidal zone is slightly wider along the north side than along the south.

2.2 GEOLOGY

The regional physiographic subdivisions of the previous section generally conform to the regional geological subdivisions (compare Figs. 2.1 and 2.3). A more complete account of the Minas Basin-Cobequid Bay regional geology can be obtained from Bell (1929, 1960); Belt (1964, 1965); Crosby (1962); Goldthwaite (1924); Harris (1975); Harris and Schenk (1975); King and Maclean (1974); Klein (1962); Powers (1916); Schenk (1975); Smitheringale (1960); Stevenson (1958); and Weeks (1948).

Regional Geology

The Nova Scotia Highlands are geologically referred to as the Cobequid Complex. The hills comprise a parallel-sided block of resistant granites, volcanics and partly metamorphosed sediments of Silurian and Devonian ages which have been denuded less rapidly than sandstones and other sedimentary rocks around its margins. Both the north and south margins of the hills are marked by fault scarps. Along the south, the Cobequid Fault separates the Cobequid Complex from Carboniferous rocks found to the south. The Complex developed by block faulting of the basement rocks during the late Pennsylvanian and Triassic periods. The faulted basement was eventually buried by sandstones deposited during the Triassic, later to be exhumed and modified by denudation.

The Atlantic Uplands are developed about equally on metamorphic rocks of the Cambro-Ordovician Meguma Group and Lower Devonian granites. The upland is a tilted block which dips to the southeast beneath the ocean. The Meguma rocks are the oldest in the area, and consist primarily of slates and quartzites. The rocks of the Meguma Group were folded and intruded by massive granites during the Acadian Orogeny in the Devonian period. Later, these rocks were covered by Triassic sandstones that have since been eroded, exposing the present Atlantic Upland surface.

The Minas-Annapolis Lowlands include friable red sandstones and conglomerates, shales, and basaltic lavas. These rocks represent sedimentation in local basins during Triassic times. Minas Basin-Cobequid

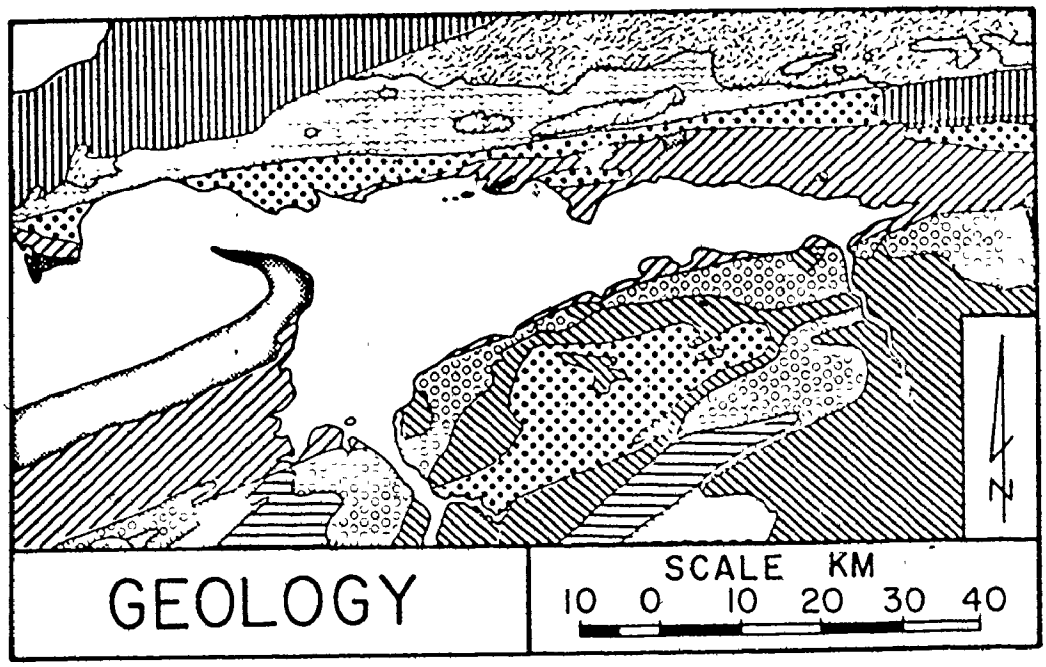

FIGURE 2.3: Regional geology of the Minas Basin - Cobequid Bay area.

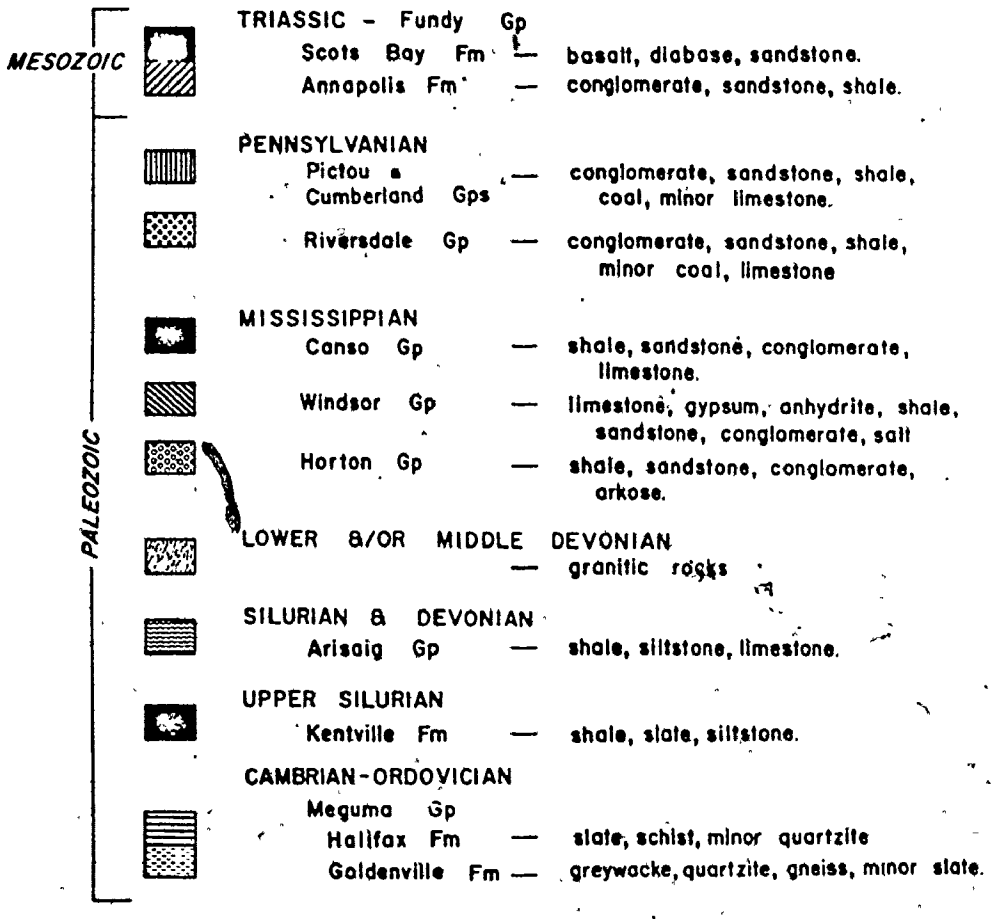

Bay is a submerged lowland from which the rocks have been removed. The rocks in this eastern extension of the Bay of Fundy are preserved in a syncline between the Atlantic Uplands and the Cobequid Hills (Nova Scotia Highlands). The axis of the syncline extends from Truro at the head of Cobequid Bay westwards through Scots Bay into the Bay of Fundy (Fig. 2.3; King and McLean, 1974). The Triassic Lowlands extend farther from the north shore of the system than from the south shore. Along the south shore, the Triassic rocks form only a fringing border with intermittent exposure in the coastal headlands.

Although North Mountain is part of the Atlantic Uplands physiographic region, it is considered here because it is of Triassic age. North Mountain consists of a 300 m thick sequence of basaltic lava flows. The flows dip to the northwest where they are exposed along the shoreline in cliffs over 20 m high. The lavas are underlain by older Triassic sedimentary rocks of the Fundy Group (Annapolis Formation) and disconformably overlain by the Scots Bay Formation.

Glacial Geology

Discussions about the glacial geology of the region can be found in Borns and Swift (1966); Glass (1972); Goldthwaite (1924); Grant (1970); Greenwood and Davidson-Arnott (1972); Prest et al. (1968); Prest and Grant (1969); Prest (1970) and Swift and Borns (1967 a and b).

During the Wisconsin glaciation, the region was glaciated by a continental ice sheet which flowed from the north across the Cobequid Hills towards the south and southwest. Evidence along the south shore of Minas Basin-Cobequid Bay indicates that early flow varied from southwest to southeast, and that later flow was diverted along the pre-existing axis of the present marine system. Bedrock in the region is commonly mantled with till, morainic materials, kames, outwash sands and gravels, local lacustrine deposits and in some areas, e.g., the Annapolis Valley, with wind-blown loess deposits. Most of the stream valleys draining from the north shore of Minas Basin-Cobequid Bay are filled with outwash sediments (e.g., Groundwater Probability Map 1160A, G.S.C., 1966).

The Wisconsin ice sheets began their retreat from the area about 12,000 BP. As the ice disappeared, lobes of ice continued to extend

down many of the valleys entering the Minas Basin-Cobequid Bay system. Meltwaters from the glacier margins carried outwash sediments through the valleys to the edge of the marine system where prograding marine deltas developed and continued to build upwards as sea level rose. Prior to this time, sea level was lower than it is today. Maximum sea level invasion occurred about 14,000 y BP.

The region began to emerge when the rate of isostatic rebound became greater than the eustatic rise of sea level. As the uplift proceeded, the upper surfaces of the deltas became emergent and dissected. Meanwhile, the retreating ice front continued to supply outwash sediments. These sediments were deposited as subaerial fans on top of the marine deltas. The sea eventually returned to the area about 5000 to 6000 y BP when the rates of rebound slowed.

Since then, the region has undergone submergence at a rate three to five times faster than the 6 cm per century rate of eustatic sea level rise. Grant (1970) believed that about half of the anomalous rate of submergence was related to an increase in the tidal range as the Bay of Fundy system (including the Gulf of Maine) widened and deepened during the past 6000 years. The remainder of the abnormal submergence rate is attributed to "geosynclinal downwarping and relaxation of a former ice-marginal bulge."

The influence of the complex changes of sea level are visible at several locations in the region. At Advocate Harbour, Borns and Swift (1966) and Swift and Borns (1967 a and b) described a raised glacio-fluviomarine outwash terrace. Wightman (1975) described a raised beach at Cape Chignecto with evidence of a postglacial tidal range of only 3 to 4 m. On the southwest side of the Minas Basin, drowned forests are discernible in the shoreline at low tide. Radiocarbon dates show that these trees were living about 3000 to 4000 y BP (Wolfville, N.S.).

Origin of the Bay of Fundy System

The origin of the Bay of Fundy System has received the attention of several investigators (e.g., Johnson, 1925; Koons, 1941 and 1942; Klein, 1962; Shepard, 1930 and 1942; and Swift and Lyall, 1968). Johnson and Koons believed that the Fundy System represented a submerged Triassic fault trough lowland, later modified by fluvial erosion.

Shepard, however, suggested that glacial erosion was responsible for the excavation of the bay. This interpretation was rejected by Klein. He proposed that the bay's origin resulted from a persistance of the structural control and fluvial erosion which had produced the early Triassic basin. Klein's supposition was supported by Swift and Lyall (1968), but they argued that the present form of the bay was, nevertheless, largely a product of the Wisconsin glaciation.

2.3 SEDIMENTS

Sediment Sources

The sediments found in Minas Basin and Cobequid Bay have three main sources (Fig. 2.4): (i) coastal erosion; (ii) bottom erosion; and (iii) fluvial discharge. Pelletier and McMullen (1972) suggested that some sediment may be brought into the system from outside through the Minas Passage, but concluded that this source was of little importance.

Most of the shoreline materials bounding the system are Triassic sedimentary rocks, and Pleistocene glacio-fluvial and till sediments, both of which are relatively easy to erode. The importance of coastal erosion is inferred by: (i) the broad tidal current and wave-cut bench around the margins of Minas Basin-Cobequid Bay (Fig. 2.8 A and B); (ii) the similarity in colour and lithology between the shoreline source materials and the adjacent intertidal sediments (Balaz and Klein, 1972; Klein, 1964 and 1970 a); (iii) the observed rapid rates of lateral shoreline erosion -- rates up to 2 meters per year (ATPEMC, 1969; Churchill, 1924; Klein, 1968 a and b); and (iv) the similarity in mineralogy between coastal materials and suspended sediments and other fine-grained sediments found in the intertidal zone (Miller, 1966; Pelletier and McMullen, 1972).

Regional geology maps (e.g., King and Maclean, 1974) show that Minas Basin-Cobequid Bay is entirely underlain by Triassic sedimentary rocks similar to those exposed in the shoreline cliffs. Swift and McMullen (1968) indicated that the seabed was composed of almost equal proportions of Triassic sedimentary rocks and Pleistocene glacial sediments. Thus, it is possible that a significant proportion of the

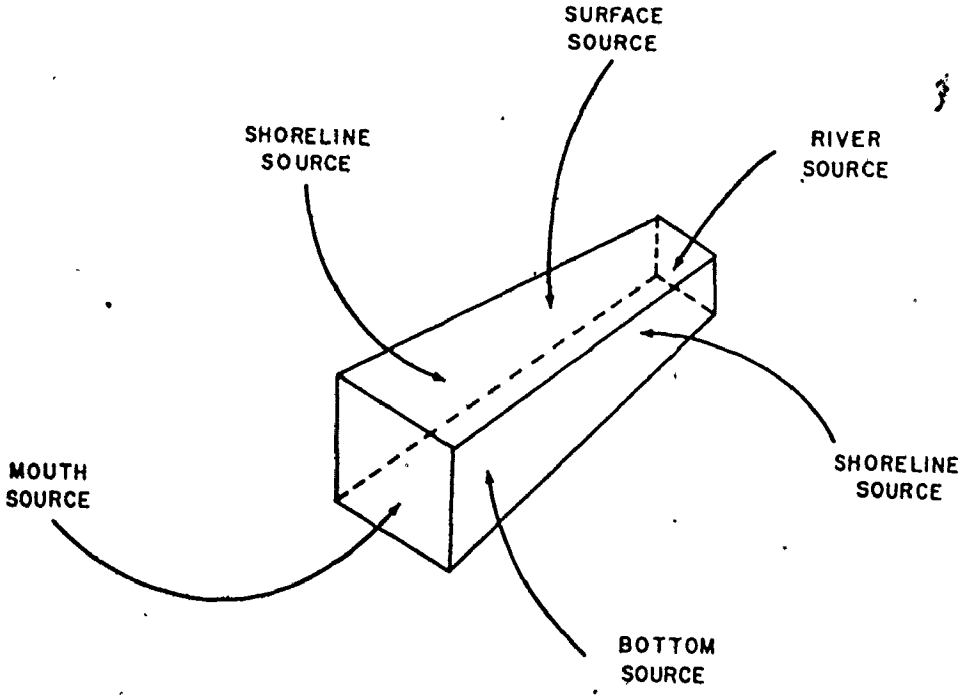

FIGURE 2.4: Generalized sources of modern sediments in Minas Basin-Cobequid Bay.

Holocene sediments presently in the system were derived from the erosion and reworking of submarine materials by tidal currents and storm-wave action.

It is impossible to determine the relative importance of coastal erosion versus bottom erosion. Both shoreline and submarine sources have similar lithologies, erosion potential and relative proportions of material types. Thus, both should be considered as important Holocene sediment sources. Studies in the main Bay of Fundy (Miller, 1966) indicate that the seabed is presently either depositional or in a state of sedimentary equilibrium. This observation, although not necessarily applicable to Minas Basin-Cobequid Bay, supports the relative importance of coastal erosion as the main source of modern sediments. A further factor to consider is that the relative importance of coastal and submarine sediment sources has most likely changed with time. Much of the present intertidal sediments may have been derived from Pleistocene sediments reworked from the whole area of the bay as sea level rose (i.e., about 4000 B.P.). If this is the case, then the source of intertidal sediments in Minas Basin-Cobequid Bay would be analogous to those in the North Sea.

Rivers entering Minas Basin and Cobequid Bay have small drainage basins. The average watershed size along the north and south shores is 84 and 362 km^2 respectively. As most of the region is drained by relatively small rivers and streams, they do not presently contribute large volumes of water or sediment to the marine system. The three principal rivers are the Avon, Salmon and Shubenacadie (Figs. 1.4 and 3.1).

There is little information about the hydrology and sediment loads of rivers in the region. R. S. Smith (1969) has studied the sedimentology of the Moose and Diligent rivers along the north shore of the Minas Basin. Stichling (1973) reported that Maritime rivers in general have suspended sediment concentrations (a measure of watershed erosion activities) less than 60 milligrams per liter (which is at the low end of concentrations compared to other Canadian rivers). Rivers entering Minas Basin-Cobequid Bay along the north shore have annual suspended sediment yields (amount of sediment produced by a river

system from a unit drainage area in one year) from 18 to 88 metric tons per square kilometer, while rivers along the south shore have annual yields ranging from 2 to 9 metric tons per square kilometer. The dissimilarity between north and south shore rivers reflect the differences in lithology and river gradient on either side of the bay.

The Salmon River flowing into the head of Cobequid Bay past Truro (Fig. 3.1) is the only river in the region for which there is independent hydrologic and sediment discharge data (Fig. 2.5). Data for this river has been collected since mid-1964 at Murray which is located above any tidal influence on the river (Hennigar, 1972; J. E. Peters, pers. comm., 1974). The Salmon River drains a watershed area of approximately 363 km^2 and has a mean daily discharge of about 11 m^3/s (with mean maximum and minimum daily discharges of 113 and 0.6 m^3/s respectively). The mean annual discharge of the river is about 4.38×10^8 m^3. Annual discharges are strongly bimodal (Fig. 2.5) with maxima occurring during the February to May period (spring snowmelt runoff) and from October to December (cyclonic storm activity). August commonly has the lowest discharge.

The mean annual suspended sediment concentration for the Salmon River is 9.6 mg/l (which is greater than the value reported by the ATPEMC, Table A3-5, 1969) and the mean daily suspended sediment discharge is approximately 20.3 t. Fluvial suspended sediments are generally fine-grained, except perhaps during periods of maximum runoff, and do not show any mineralogical similarities to the marine suspended and intertidal zone sediments (Miller, 1966).

Areal Distribution

There is a wide variety of sedimentary environments in Minas Basin-Cobequid Bay (Klein, 1964 and 1968 a). The distribution of intertidal sediments is closely related to the shoreline lithology and relative exposure to wave and current activity. Figure 2.6 summarizes the relation of sediment types found in the intertidal and subtidal zones in terms of 'relative exposure energy' and 'relative tidal position'.

There are two types of shoreline: (i) the cliffed shoreline with or without an intertidal zone; and (ii) the saltmarsh or low bank

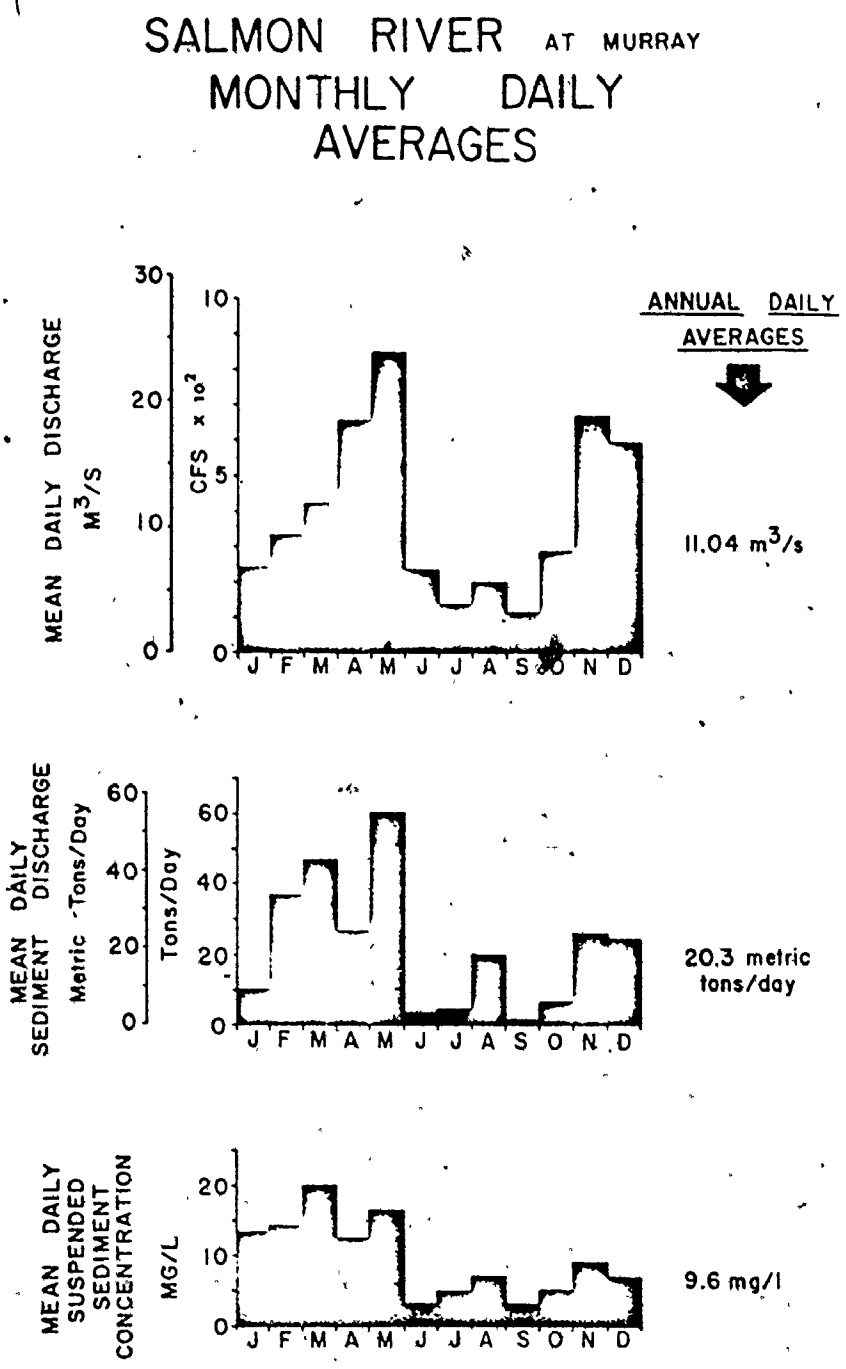

FIGURE 2.5: Mean daily discharge, suspended sediment discharge and suspended sediment concentration (for an average year) for the Salmon River at Murray, N.S. Graphs based on data from Water Resources Branch, Environment Canada (J.E. Peters, pers. comm., 1974).

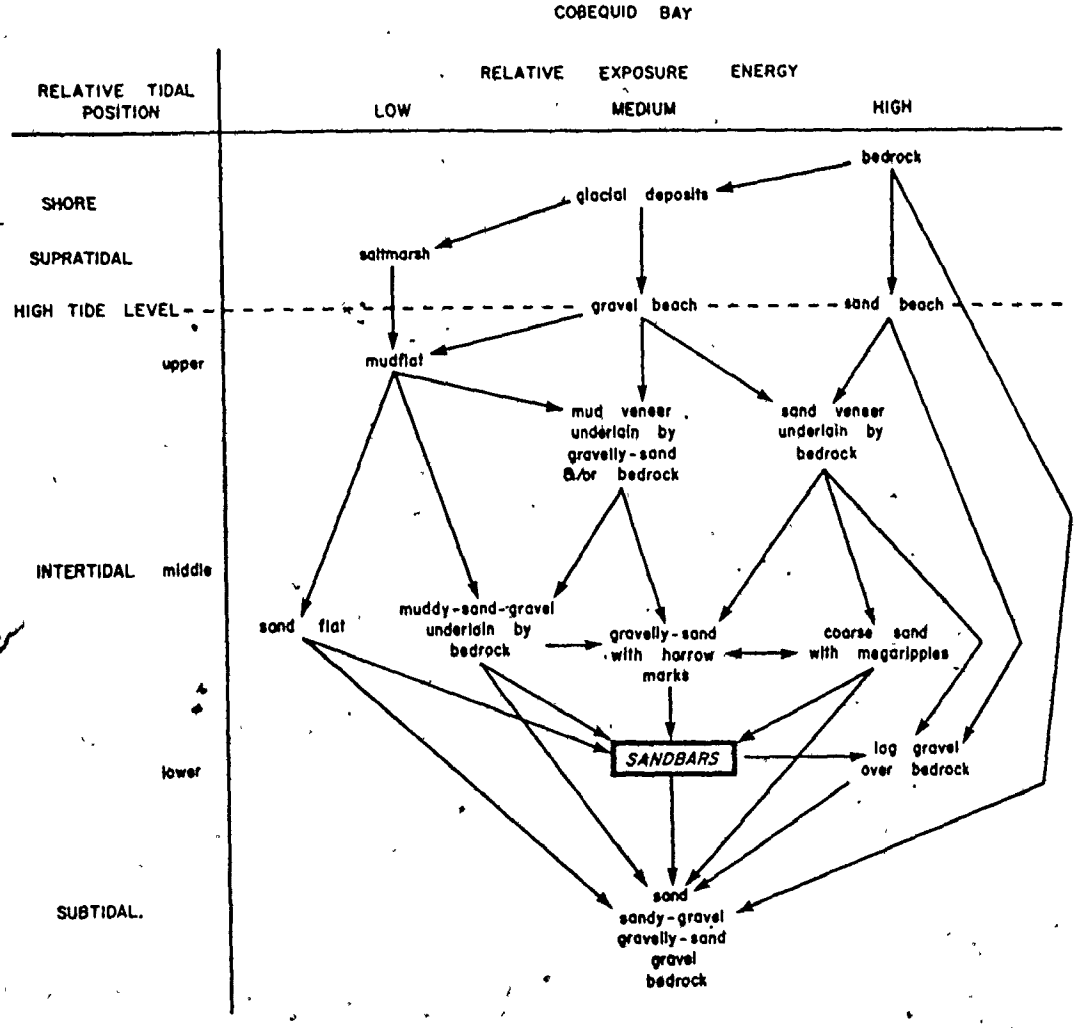

FIGURE 2.6: Generalized relationships of sediment facies to relative tidal position and exposure energy.

shoreline with an extensive intertidal zone.

Most of the shoreline consists of bedrock seacliffs with an erosional platform that may (Fig. 2.7A) or may not be intertidal. Cliffed shorelines without an intertidal platform are uncommon and generally restricted to coasts that have resistant lithologies, e.g., basaltic cliffs in Scots Bay. Where there is no intertidal zone, the submerged area at the base of these cliffs is commonly covered with a thin layer of sand-sized sediments similar in lithology to the adjacent cliffs.

Cliffed shorelines, composed of Triassic sandstones and Pleistocene deposits, generally have an extensive intertidal platform whose width (up to one kilometre) is controlled by the adjacent and underlying bedrock lithology. On bedrock shorelines, where the high tide line reaches the cliff face, the water level is marked by erosion hollows and holes (Fig. 2.7B and C). Where the high tide level occurs in front of or at the base of the cliff, there is a lag gravel beach composed of pebble-sized materials eroded from the cliff (Fig. 2.7D). Away from the shoreline, the platform may be covered with a veneer of sand (up to 0.2 m thick; Fig. 2.7D) and (or) patches of lag gravel (Fig. 2.7E), or it may be a scoured and striated bedrock surface (Fig. 2.7B). The long axes of the scours and striation are generally parallel to the direction of tidal current flow. Early studies in the area mistakenly attributed their formation to glaciation.

During 'normal' tidal conditions, the intertidal platform in front of the bedrock cliffs undergo small amounts of erosion and reworking with each tidal cycle, while the cliffs suffer little erosion. However, during storms and periods of unusually high tides, both the intertidal platforms and the cliff-face are extensively eroded (e.g., Fig. 2.7C), scoured and reworked by wave and current action. ATPEMC (1969), Churchill (1924) and Klein (1968 a) report annual rates of shoreline retreat up to 2 m in friable Triassic sandstones and unconsolidated glacial deposits.

Topographic lows in the bedrock shoreline are generally occupied by glacial sediments that form small coastal cliffs of unconsolidated materials up to 5 m in height (Fig. 2.7F and 2.8A). A residual gravel

FIGURE 2.7: Views of cliffed shoreline in Cobequid Bay.

A. Oblique air photo of erosional platform at Burntcoat Head. Seacliffs are composed of red Triassic sandstones and are approximately 10 to 15 m in height.

B. View of scoured and striated erosional platform at Noel Head. Note hollows and holes in cliff face marking the high tide level. Seacliffs are approximately 10 to 15 m in height.

C. Evidence of coastal erosion in sandstone seacliffs at Noel Head. Cliff height is approximately 7 m.

D. View (to the west at Noel Head) of sand veneer covering the erosional platform and lag gravel at high tide level. Note person for scale.

E. View of erosional platform near Noel Head (looking northwest) showing chaotic patches of sand, gravel and boulder cover. Scale is 1 m.

F. View of Pleistocene seacliff near Selma and sandy-gravel and boulder-strewn intertidal foreshore. Seacliffs are approximately 5 m (maximum) in height.

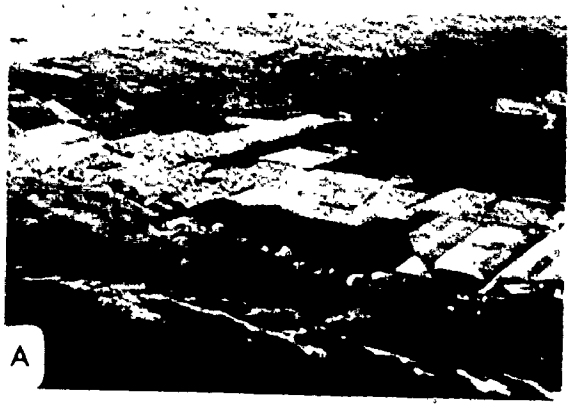
A


B

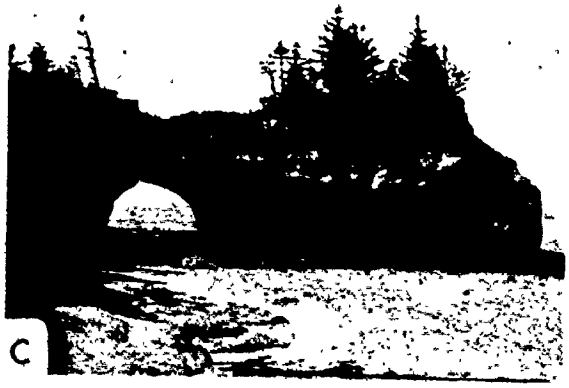
C

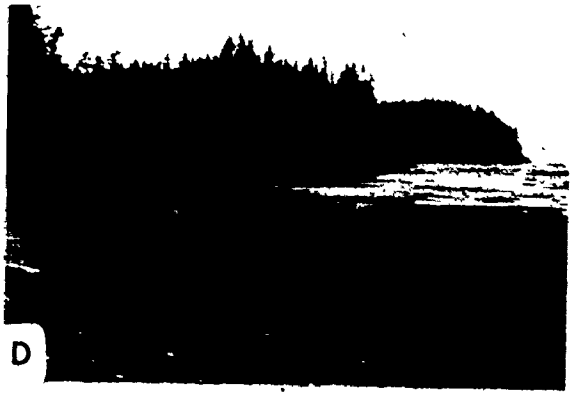
D


E


F

FIGURE 2.8: Views of intertidal foreshore adjacent to a Pleistocene cliffed shoreline near Selma.

A. View of intertidal zone sediment facies distribution. Note megaripples and sand waves on sandbar in middle background.

B. View of mud veneer overlying sandy-gravel sediments (foreground) and lag gravel beach at high water level. The shoreline is composed of Pleistocene tills. Note shallow drainage rills across the mud veneer that are dotted with small gastropods. Truck in background is scale.

C. Closeup view of mud veneer surface showing current ripples and extensive burrowing. Scale is in centimetres and inches.

D. View of lower intertidal foreshore with small megaripples (length = 1 m; height = .2 m) and sandy-gravel lag.

E. Current produced harrow-marks along the lower intertidal foreshore. Scale in foreground is 1 m. View is to the west.

F. Gravel spit in middle to upper part of intertidal foreshore. Tidal currents flood from left to right. Note drainage pattern on the lower foreshore and emergent sandbar in background.

A

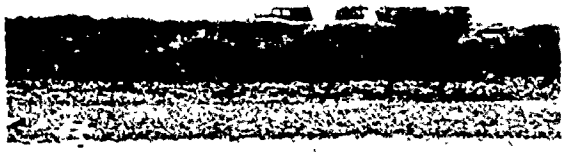

B

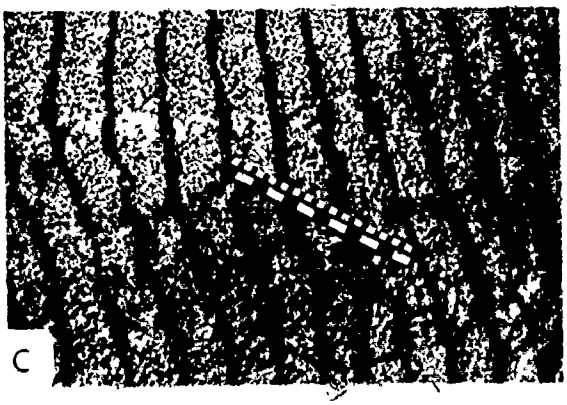

C

D

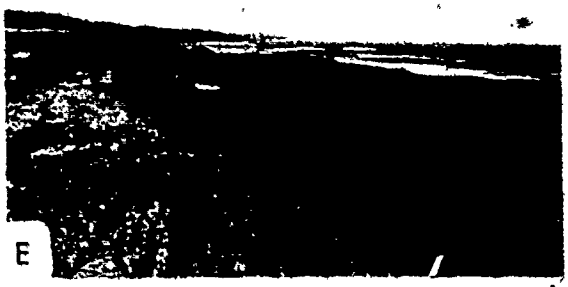

E

F

beach composed of pebble-sized materials from the shoreline occurs at the base of these cliffs, marking the high tide level. Away from the shore, the gravel beach may grade into an intertidal foreshore composed of sandy-gravel and boulders (Fig. 2.7 F) or it may change abruptly into mud (Fig. 2.8 A and B). The mud forms a veneer, 0.05 to 0.15 m thick, overlying a sandy-gravel lag which appears to be laterally continuous with the high tide gravel beach. The muddy sediments are commonly rippled (Fig. 2.8 C) and burrowed (Craig, 1973). Further away from shore, the muddy area thins and grades into a sandy-gravel zone with megaripples (Fig. 2.8 D and (or) harrow marks (Fig. 2.8 E) at the seaward edge of the intertidal foreshore (lower intertidal zone). Rock fragments up to boulder size are present in many places on the foreshore (Fig. 2.8 A, D and E), and both bedrock and glacial till outcrop throughout the zone.

Wave and current action has built small swash bars and gravel spits (Fig. 2.8 F) from some headlands and across the mouths of many small streams that discharge across the foreshore. Small streams with dendritic and (or) braided patterns drain much of the intertidal foreshore at low tide (Fig. 2.8 F). Some of these streams have cut through the intertidal zone sediments (up to 0.15 m depth), exposing bedrock and (or) gravel bottoms.

In small estuaries and bays (Fig. 2.9 A and 2.10 A) that are protected from strong wave and current activity, extensive mudflats occur in front of saltmarsh shorelines, e.g., Noel Bay, west side of Salter Head, estuaries of the Salmon and Shubenacadie Rivers. The mudflats display many of the topographic, structural, textural and faunal features and zonations that are described from simlar environments elsewhere, e.g., Dutch Wadden Sea (Klein and Sanders, 1964; van Straaten, 1954; Reineck, 1967). The mudflats are composed of silt- and clay-sized sediments with some occurrences of sand near the upper and lower limits of the flats adjacent to exposures of bedrock, glacial sediments and (or) marsh deposits. Other features include: meandering and dendritic drainage patterns (Fig. 2.9 B, C and D); soft sediment deformation in channels (Fig. 2.9 C); lateral channel migration (Fig. 2.9 D); discontinuities in bedding and topography from ice action (Fig. 2.9 E; see later section); burrowing (Fig. 2.9 F and G; Craig, 1973); parallel, wavy, flaser and lenticular bedding (Fig. 2.9 H) Reineck and

FIGURE 2.9: Intertidal mudflats in Cobequid Bay.

A. Oblique air photo of Noel Bay (right centre) and Noel Bay Bar (lenticular sandbar to left of Noel Bay). Burntcoat Head is located in the left foreground.

B. Oblique air photo of mudflats near Selma showing dendritic tidal channels.

C. Broad, flat-bottomed tidal channel cutting mudflat in the middle to lower intertidal zone. Channel width is about 60 m.

D. V-shaped, meandering tidal channel cutting mudflat in the upper intertidal zone. Channel width is about 10 m.

E. Surface of mudflat near Selma showing shallow depressions (left centre) and small drainage channels. Note cliffed seaward edge of the salt marsh in the middle background. View is to the south; the scale is 1 m.

F. View of burrowed mudflat surface. Lens cap is about 5.5 cm across.

G. Burrows of Corophium (U-shaped) and Macoma (Craig, 1973) in mudflat sediments near Selma. Lens cap is about 5.5 cm across.

H. Parallel and wavy laminated muds and silts exposed in mudflats. Scale is 1 m.

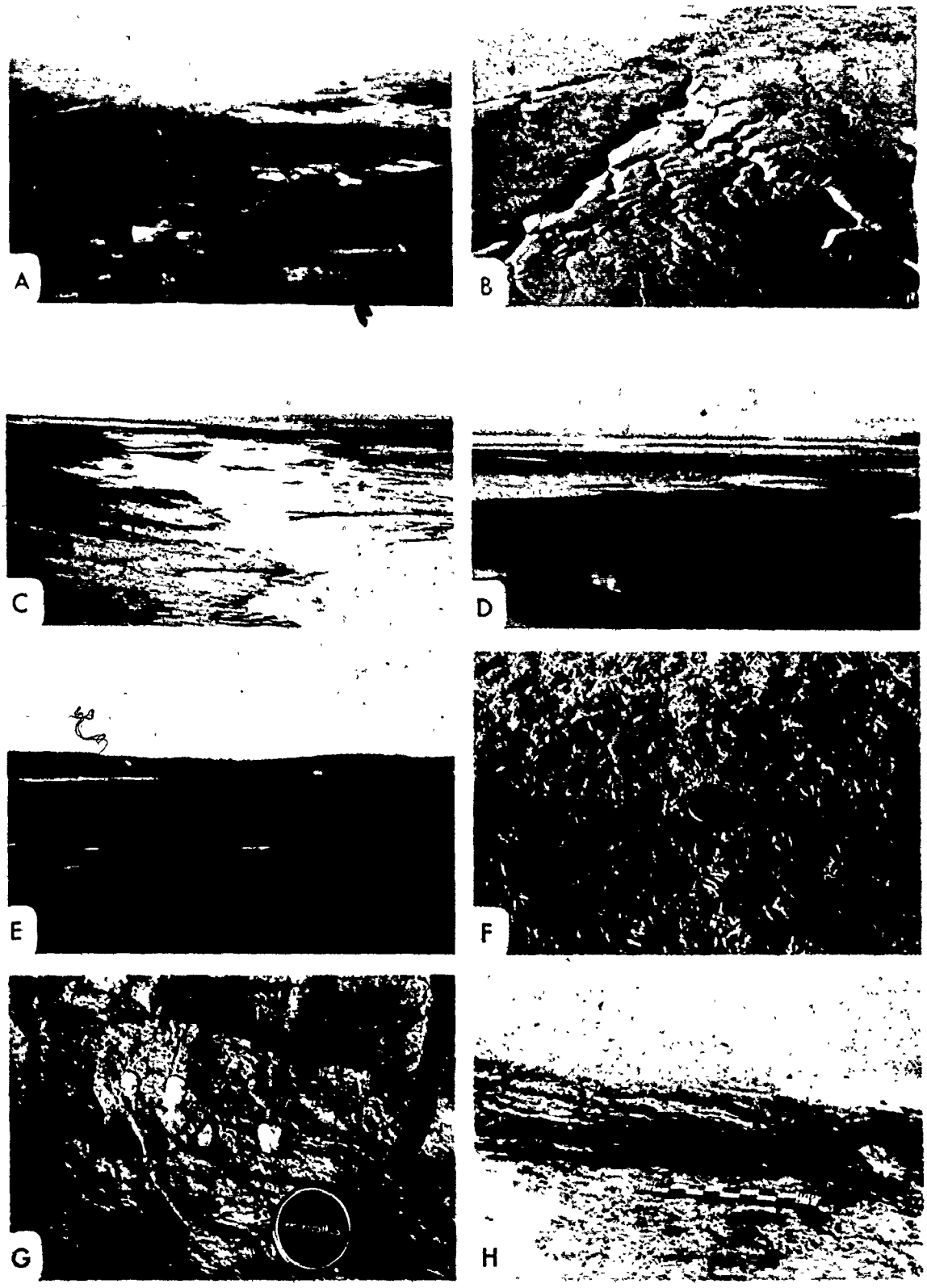
A
B
C
D
E
F
G
H

Wunderlich, 1968); and vertical oxidation-reduction zonation (Berner, 1970 and 1971, p.202-208). The bottoms of the channels are usually sandy with some terrigenous and mud pebbles.

Towards the seaward edge of the mudflats, grain size increases as a result of the increased exposure to wave and current action which prevents or limits mud deposition. The coarsening seaward sequence is best developed in the estuaries of the Salmon and Shubenacadie rivers. Here, the estuarine mudflats grade into broad sand flats (Fig. 2.12 E and F) with ripples and a few large-scale bedforms. These flats are cut by channels to give a braided pattern (Swift and McMullen, 1968). These sand flats grade towards the shore into interbedded sand and mud (the "mixed flats" of German writers), then into mudflats in the upper part of the intertidal zone. The seaward zonation of sediment types is somewhat analogous to that described by Evans (1965) and Reineck (1972).

Above the mean high water level, mudflat areas are backed by supratidal saltmarshes (Fig. 2.10A and B) which are extensively flooded by high spring tides. The seaward margin of the marsh is commonly truncated by a small erosional scarp up to 2 m in height (Fig. 2.10B and C), possibly indicative of the postglacial rise of sea level in the last 4000 years. The marsh surface is cut by meandering channels (Fig. 2.10A and D) up to 4 m in depth.

The surface of the marshes are covered primarily by Spartina juncea and Juncus gerardii (Goldthwaite, 1924, p. 136) which traps suspended sediment that settles during high spring tides or is brought there by drift-ice. Internally, the marshes consist of a brown coloured surface horizon, 0.05 to 0.3 m thick, with marsh grass roots, plant debris and trapped mud. This horizon is underlain by a zone of silty-clays and plant debris that is blue-gray to black in colour (Fig. 2.10E). The lower part of the marsh is dark because the organic materials have been reduced from the interaction of bacteria, iron oxides in the sediments and sulphates in the seawater to produce hydrogen sulphide and pyrite (Berner, 1970 and 1971, p. 202-208).

The sediments of the subtidal and lower intertidal zones, seaward of the intertidal foreshores in Minas Basin-Cobequid Bay, are areally

FIGURE 2.10: Views of saltmarsh in Cobequid Bay.

A. Oblique air photo of mudflat and saltmarsh near Selma (Salter Head is to the lower left). Note the patterns of tidal channels crossing the intertidal zone.

B. View of transition from mudflat to saltmarsh. Note truncated seaward margin of saltmarsh. Width of meandering tidal channel is about 10 m.

C. Truncated seaward margin of saltmarsh showing internal structure. Scale is 1 m.

D. View (to the north) across saltmarsh near Noel at low tide showing development of marsh grasses and meandering tidal channel. Channel width is about 15 m (maximum).

E. Oxidation-reduction zonation in saltmarsh materials. Note the thin (2.5 cm), light coloured layer overlying a darker (reduced) layer. Scale is in centimetres.

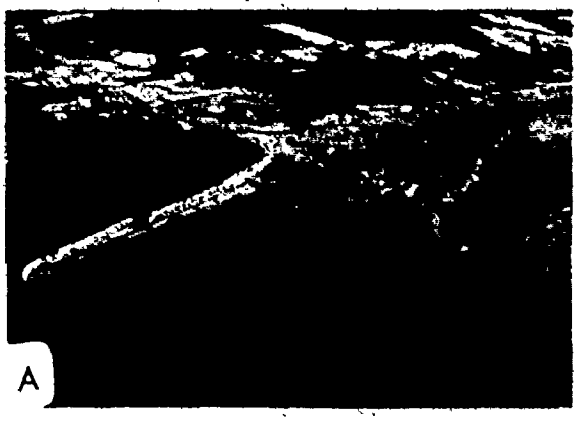
A


B


C


D


E

and volumetrically the most extensive. Pelletier and McMullen (1972) have described and mapped the distribution of subtidal sediment types in the basin and bay. Most of the bottom sediments are sand, or sand and gravel (Fig. 2.11). Continuous seismic profiles (ATPEMC, 1969; Huntec, 1966; Swift and McMullen, 1968) indicate that the recent sediments occur as local accumulations (up to 25 m thick) underlain by glacial deposits and (or) bedrock. Some of these sediments have been moulded into broad, lenticular sand bars which are roughly parallel to the shore (Fig. 2.12 A and B) and to the direction of the tidal currents. The channels between the bars are commonly scoured down to bedrock, glacial sediments or a 'basal' gravel. The upper parts of most of these bars are emergent at low tide (up to 6 m above low water), e.g., Avon River estuary, Economy Point, Five Islands, Walton-Cambridge (Fig. 1.5) and Cobequid Bay (see Chapter 3). Previous studies of these intertidal-subtidal deposits were cited in Chapter 1 and the sand bars investigated in this study are discussed fully in Chapter 3.

The grain size of the sands on all the bars is primarily medium sand. The coarsest sizes on the bars are found closest to the shoreline, and in the adjacent channels. The finest sizes are generally found along the crestline of the bars. Grain size, on the bars studied, is examined in Chapter 3.

Bed material movement occurs primarily by traction and intermittent suspension close to the bed on the intertidal sand bars. The surface of the bars are covered with a variety of current produced bedforms, including: (i) ripples, with wavelengths less than 0.15 m and heights less than 0.05 m; (ii) megaripples (or dunes), with wavelengths from 1 to 12 m and heights from 0.10 to 0.70 m (Fig. 2.12D); and (iii) sand waves, with wavelengths from 10 to 30 m and heights from 0.40 to 1.50 m (Fig. 2.12C). These bedforms can be directly observed on the bars at low tide. As a consequence, they are either ebb-oriented or ebb-modified flood oriented features, and commonly show some modification due to low tide emergence and wave action (particularly in stormy weather). Further discussion of bedforms is given in Chapter 5.

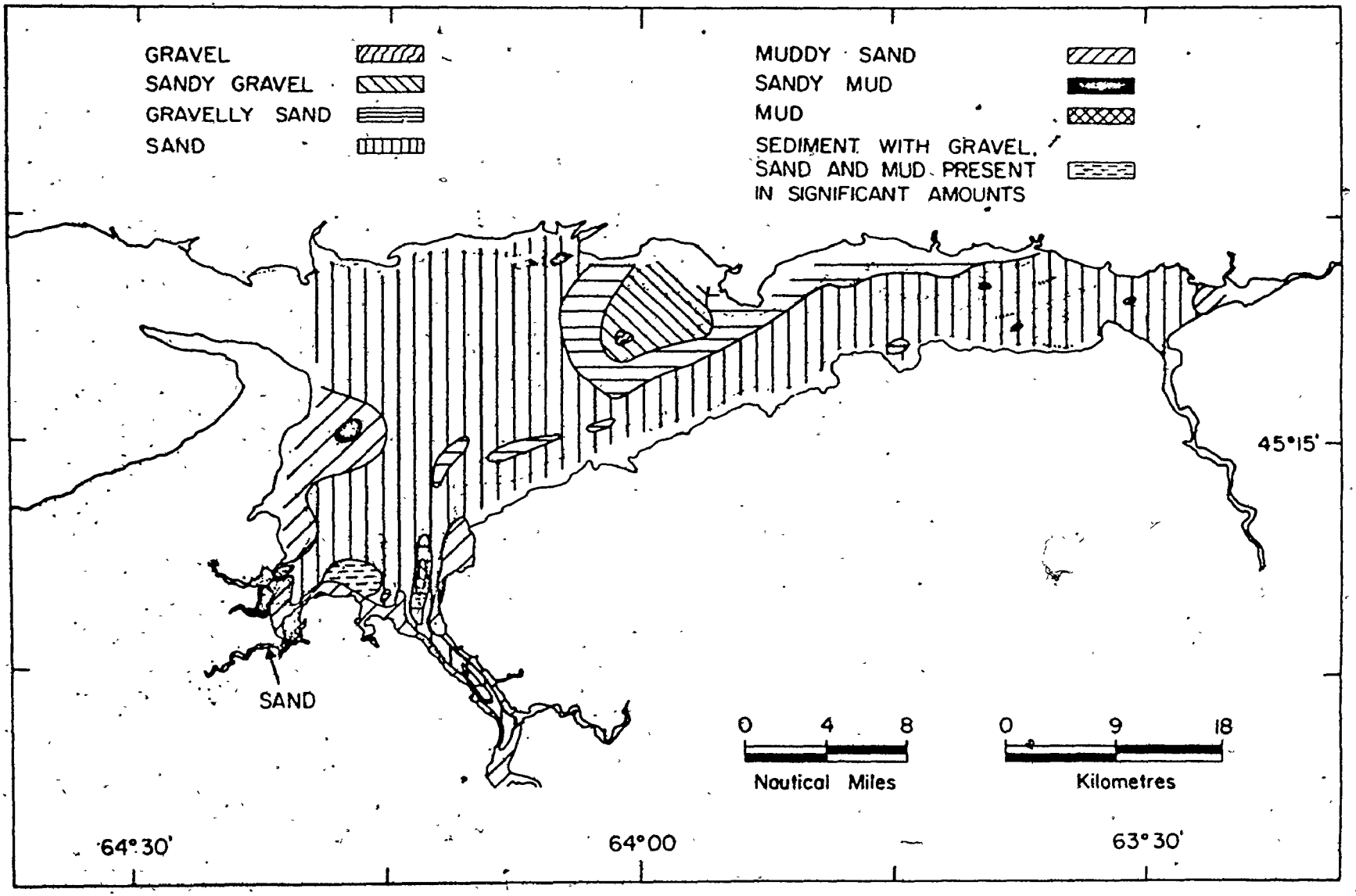

FIGURE 2.11: The distribution of bottom sediment types in Minas Basin-Cobequid Bay (after Pelletier and McMullen, 1972).

FIGURE 2.12: Sand bars and Sand flats.

A. Oblique air photo of sand bars in Cobequid Bay (looking to the southwest). Great Village Bar (foreground); Noel Shore Bar (middle); and Noel Bay (X). The tide level is about 1 h before low water.

B. Oblique air photo from south side of Cobequid Bay showing the position of Selma Bar relative to the shoreline. Note Salter Head (SH); and Great Village Bar (upper left). View is to the NE.

C. Oblique air photo over central part of Selma Bar showing the occurrence of flood asymmetric sand waves (in the foreground) with wavelengths greater than 12 m and ebb oriented megaripples (in the background) with wavelengths from 5 to 6 m.

D. Oblique air photo of megaripples (wavelengths of 8 to 12 m) on the north side of Selma Bar. View is to the SSW.

E. Oblique air photo of Salmon River estuary. Note sediment zonation from saltmarsh to mudflat to sandflat (left to right) and meandering channel of the estuary. View is to the east.

F. Oblique air photo of sandflats northeast of Salter Head. Note the few large bedforms (wavelengths = 5 to 8 m) and the braided channel pattern. View is to the NE.

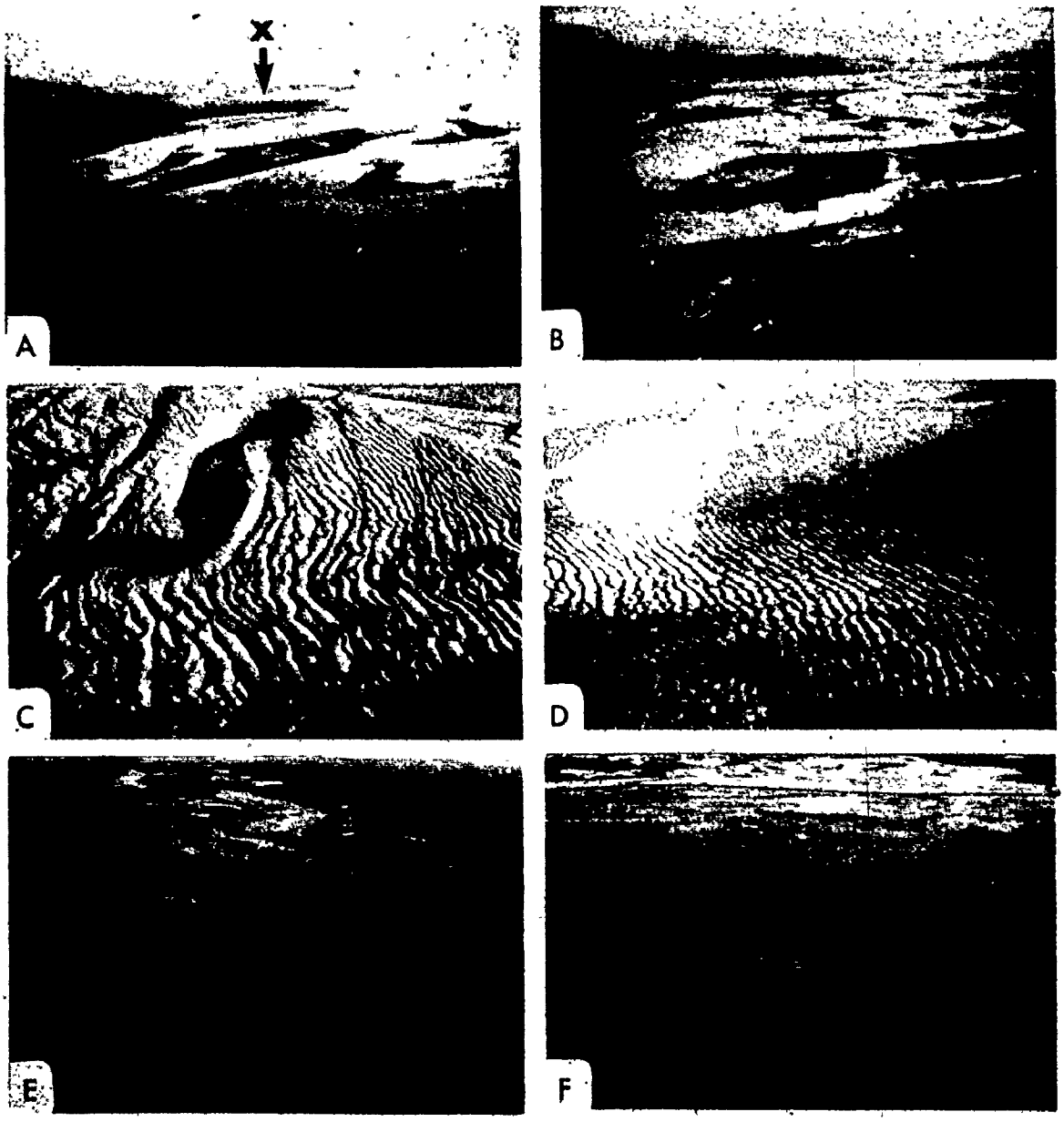
X
A
B
C
D
E
F

2.4 DYNAMIC SETTING

Climate

The Minas Basin-Cobequid Bay region experiences a humid, temperate climate with a strong continental influence due to the easterly movement of air masses from the midcontinent over the area. Temperatures are modified to a certain extent by the proximity of the ocean. The mean monthly temperatures of an average year based on meteorology records for the five year period between 1968 and 1972 (from Monthly Summaries, Meteorological Observations in Canada, Dept. of Transport, 1968 to 1972) are given in Figure 2.13. The average summer temperature (includes all months with a mean temperature above freezing) is 12°C, while the average winter temperature is -5.2°. July is the warmest month with a mean daily temperature of 20°, and January, with a mean daily temperature of -6°, is the coldest month.

The mean annual precipitation over the same five-year record period is 1.18 m. Precipitation is fairly evenly distributed throughout the year (Fig. 2.13). The slight maximum that occurs in November and December can be attributed primarily to early snowfall. The mean annual snowfall for the region is about 2.6 m.

Further information on temperatures and precipitation can be found in Environment Canada (1970).

Wind and Waves

The prevailing winds are from the west throughout the year (Fig. 2.14 B), but with a slight bias to the southwest during the summer and to the west-north-west during the winter (Fig. 2.14 A). Average wind speeds in winter (17.4 km/h) are slightly higher than in summer (14.8 km/h) (from Monthly Summaries, Meteorological Observations in Canada, Dept. of Transport, 1968 to 1972).

Over the five year period analyzed, wind conditions were calm about 8% of the time, less than 20 km/h for about 61% of the time, and between 20 and 60 km/h for about 31% of the time. Wind speeds exceeding 60 km/h were rare events and always associated with severe storms. Most storms occur during the winter months, but the occasional hurricane passes close to the area during August-September. Storm winds gener-

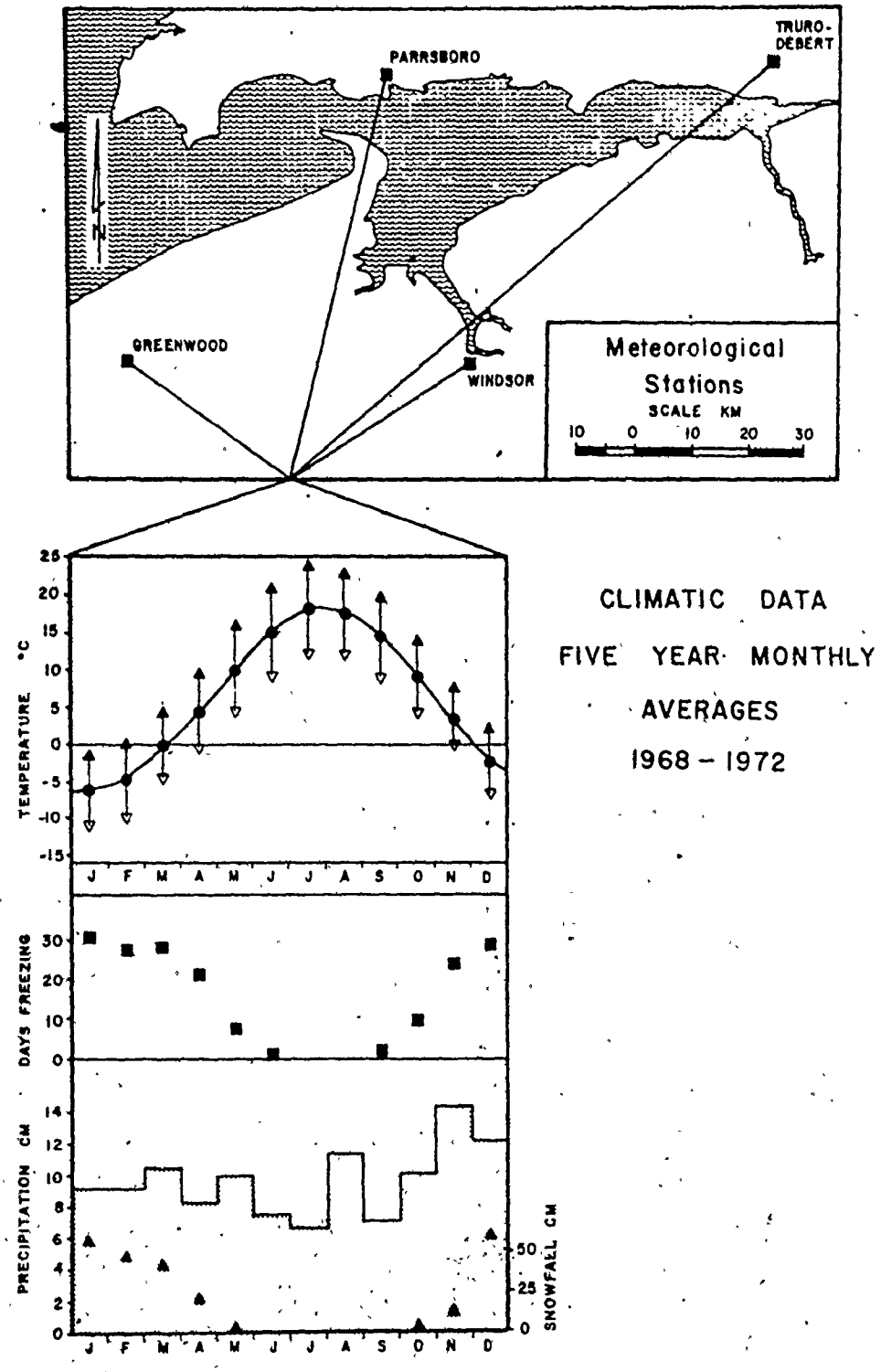

FIGURE 2.13: Monthly averages of temperature, precipitation and days freezing. The bars on the temperature curve show the maximum and minimum monthly averages.

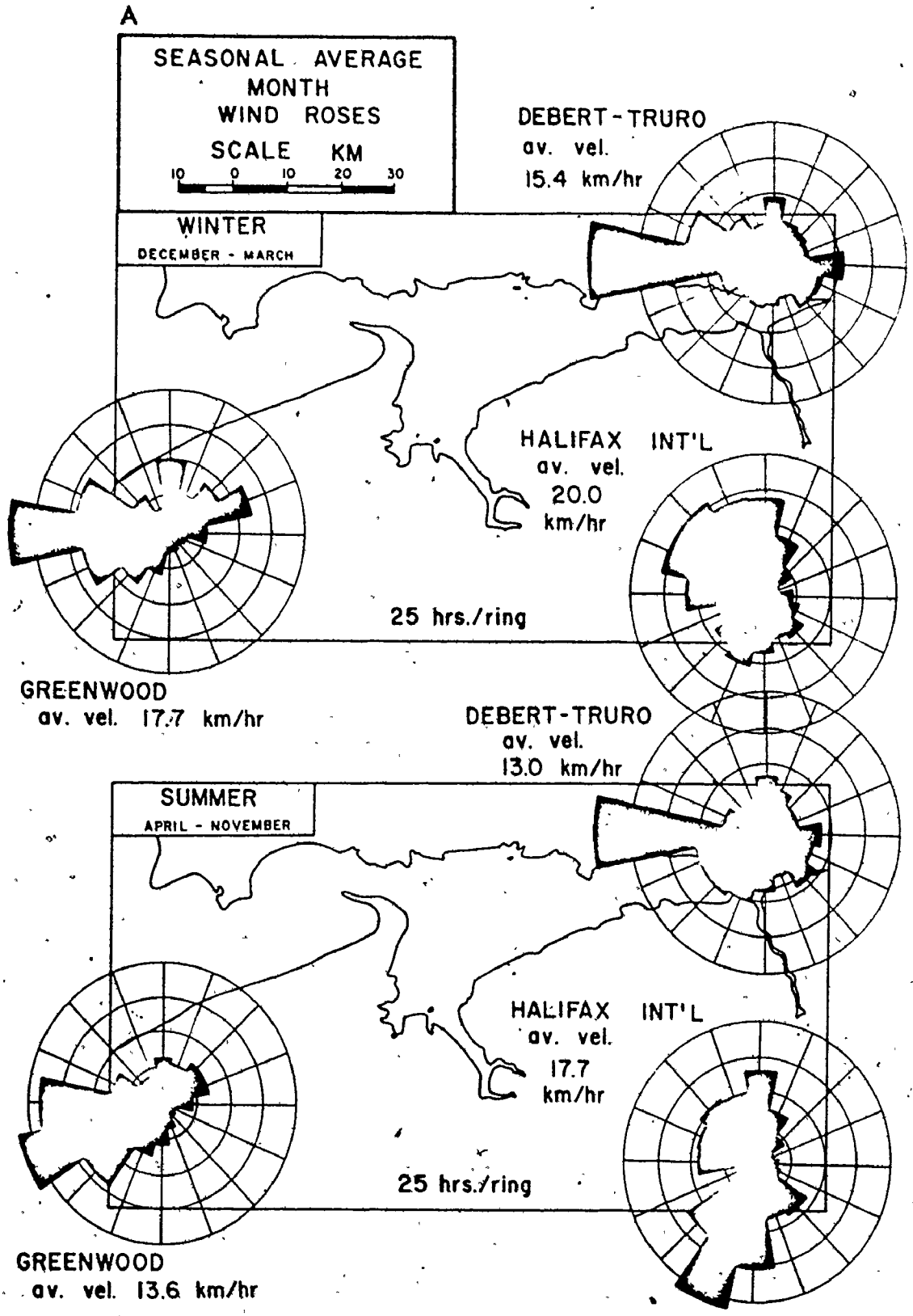

FIGURE 2.14; A. Seasonal average month wind roses.

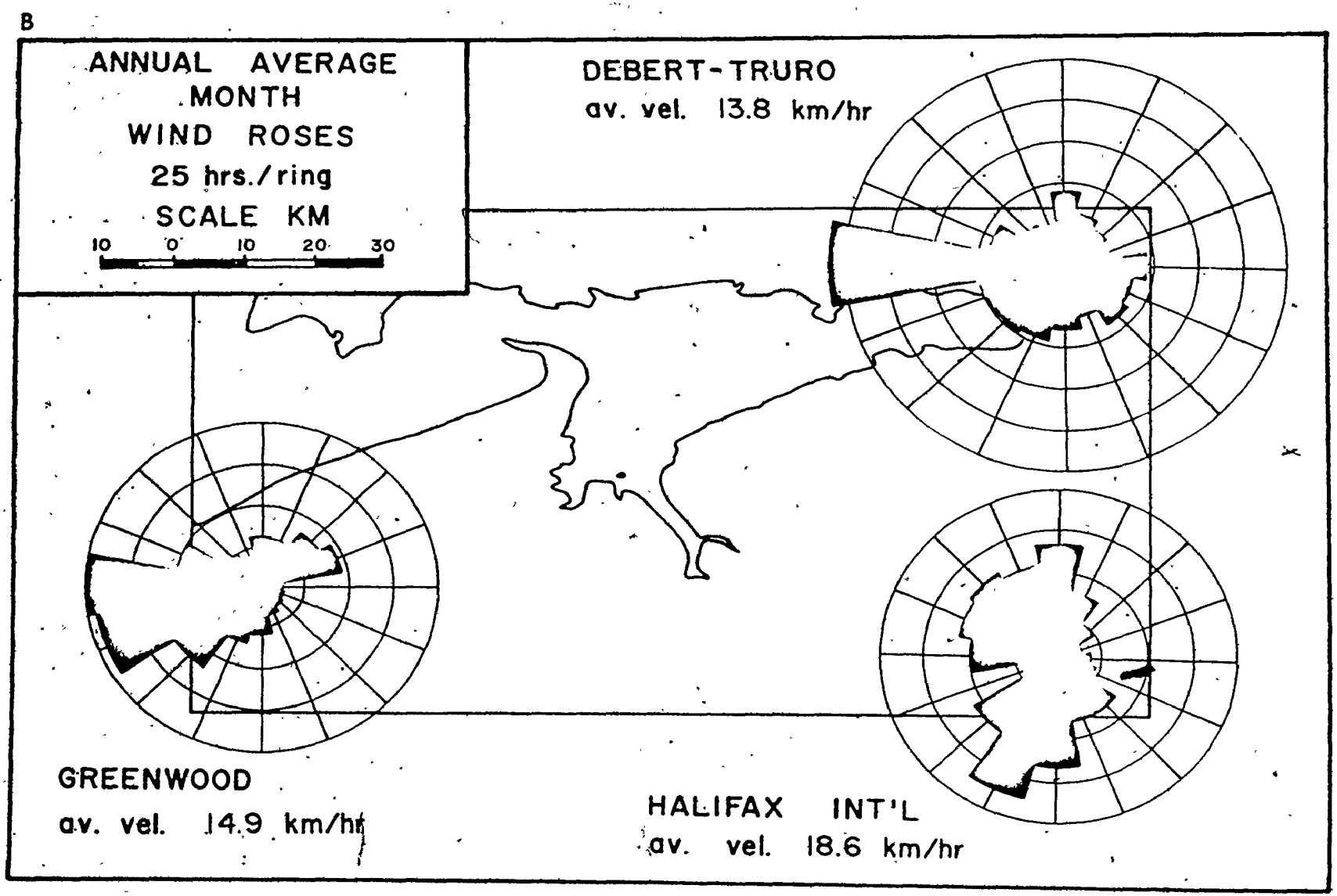

FIGURE 2.14: B. Annual average month wind roses.

ally blow from the west and southwest. The computed annual maximum winds (average of Truro, Debert and Greenwood) for 30, 50 and 100 y periods are 99, 115, and 132 km/h (Environment Canada, 1975, p. 140 - 144).

Little information is available about wave conditions in Minas Basin-Cobequid Bay because very few measurements of actual conditions have been made. Wave conditions are best developed for waves generated from the west as this is the direction that corresponds to the prevailing winds and to the direction of maximum over-water fetch (compare Figs. 2.14 and 2.15). Fetch distances from other directions in the system are much less. Wave development is restricted because of the relatively small size of the bay, and by its isolation from the main Bay of Fundy (ATPEMC, 1969). Thus, most waves in the bay are developed within the system. Refraction on Headlands (e.g., Economy Point and Burntcoat Head: ATPEMC, 1969, Plate A4-3) and shoaling of the sea bed (e.g., on the crests of exposed sand bars; Fig.2.16 E) further diminish the effectiveness of wave action. In Cobequid Bay, most of the wave energy is dissipated at the seaward margin of the sand bar complex, obliterating most bedforms on the sand bars (Fig. 2.16 F). Towards the head of the bay, wave action is negligible (Fig. 2.16 G).

Assuming a maximum wind fetch of 50 km from the west to a location near the entrance to Cobequid Bay, opposite Noel Bay (Fig. 2.15; still in relatively deep water -- 20 m), and an average overland wind speed of 15 km/h (add 20% for overwater speed, ATPEMC, 1969), it is possible to generate a wave with a 2 to 2.5s period with a height of approximately 0.5 m (U.S. Army Coastal Engineers, 1973, Fig. 3-30).

Qualitative observations during the summer indicate an average wave height of about 0.25 to 0.5 m, although rare waves up to 2 m have been observed during storms. Wavelengths are generally small (less than 4 m). Wave heights become steeper relative to their lengths when the wind direction opposes tidal current flow. Klein (1970 a) reported wind-generated currents during slack water periods of 0.1m/s.

The large tidal range in the area, and its rapid rate of rise and fall, effectively disperse wave action over the entire intertidal zone. The relatively small fetch distances are the limiting factor on

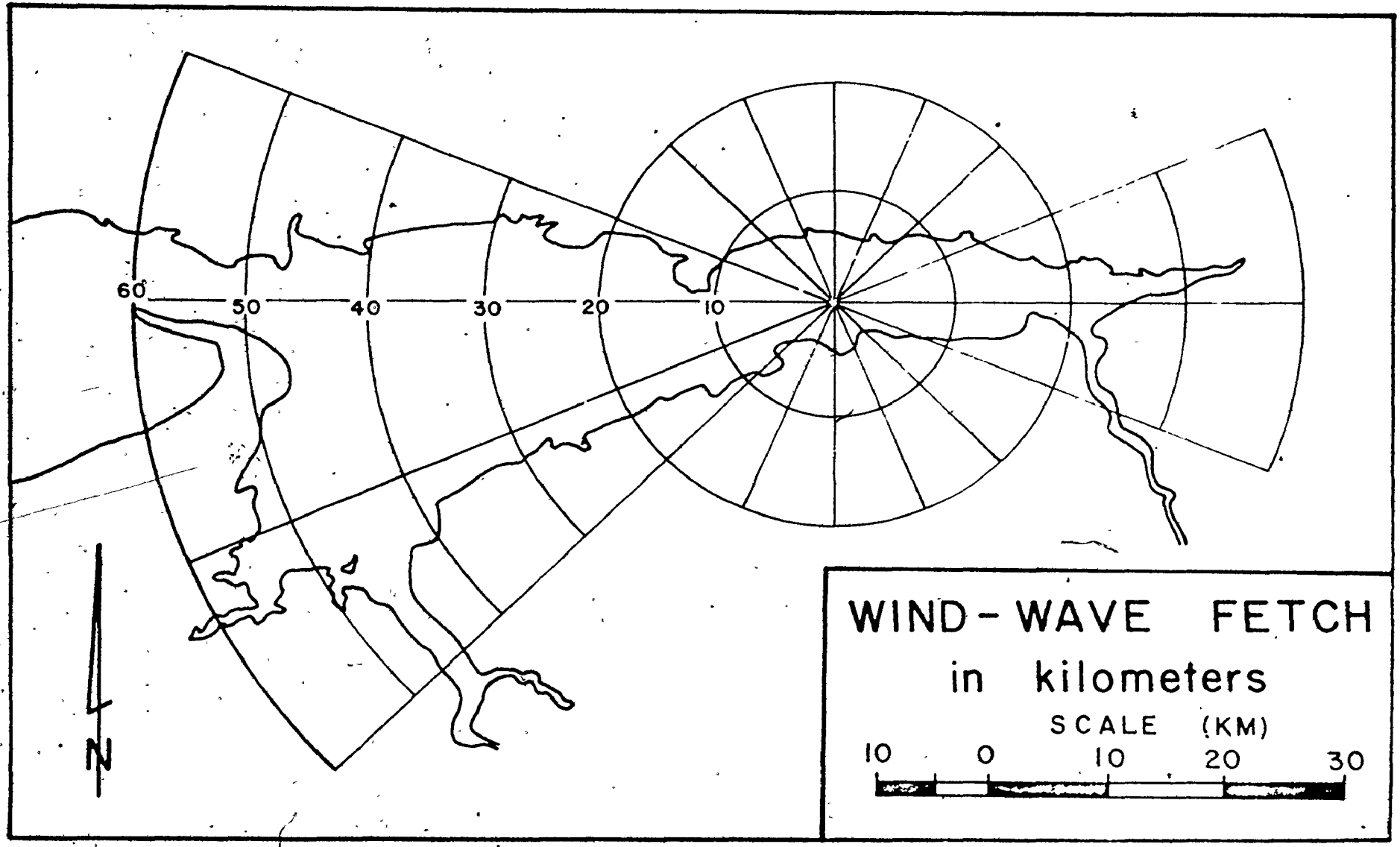

FIGURE 2.15: Wind-wave fetch to a point near the entrance to Cobequid Bay.

wave size and period. During the winter months, the formation of an ice-foot along the shoreline, combined with the damping of wave activity by drift ice, greatly reduces the effectiveness and importance of waves.

Tides

The Bay of Fundy is famous for its large tides (Fig. 2.16 A, B, C and D), but details of the tides are poorly known and imperfectly understood, partly because tidal records are not extensive. There is only one permanent tide gauge in the entire Fundy system. It is located at St. John, New Brunswick and records are available back to 1896. The large tides, however, occur near the head of the system in Cobequid Bay and not near the entrance to the Bay of Fundy. Only temporary tide gauges have been used in Minas Basin-Cobequid Bay for short periods of time and at only a few locations (ATPEMC, 1969, Plate A1-2), e.g., from August 6 to September 6, 1960 on the west side of Burntcoat Head.

The most comprehensive information about the tides near the head of the Bay of Fundy system is presented by Dawson (1917). Further information about predicted times and heights of high and low water are available in the Canadian Tide and Current Tables (Canadian Hydrographic Service).

Tidal Characteristics - The type of tide in any coastal location is in part a reflection of the type of adjacent oceanic tide, as well as a function of the dimensions (specifically length and depth) of the coastal system. The Bay of Fundy tides have a semidiurnal periodicity (Fig. 2.17) as does the North Atlantic Ocean. The lunar semidiurnal component of the tide (with a period of 12.42 h) accounts 86% of the mean spring tidal range (Yuen, 1969). Despite the dominance of the lunar semidiurnal component, the solar component (which represents about 10% of the spring range) and the diurnal components produce significant tidal forces that affect the characteristics of the tide.

Changes in the distance of the moon from the earth have a greater effect on the tidal range than changes of the moon's phase, thus the tides are anomalistic. For example, a variation of ±20% in the tidal range results from differences in the moon's distance from earth.

FIGURE 2.16: Tides and Waves.

A. View from south side of Cobequid Bay (looking to the northwest) showing the high level near the west end of Selma Bar.

B. Same view as A., but showing low tide level. Note extensive intertidal foreshore and sand bars in the background.

C. High tide level in tidal creek at Noel on the south shore of Cobequid Bay. View is to the north. Boat is 6.4 m long.

D. Same view as C., but showing low tide level. Note position of saltmarsh, the mud banks of the tidal channel and gravel channel bottom.

E. Wave activity along the crest of Selma Bar just prior to emergence. View is to the NW.

F. Oblique air photo of the exposed west end of Noel Shore Bar showing the almost complete obliteration of megaripples as a result of wave action.

G. Wave-washed megaripple crests on the crest of Selma Bar. View is to the south; scale is 1 m. Note the negligible effects of wave action on the bedforms compared with F.

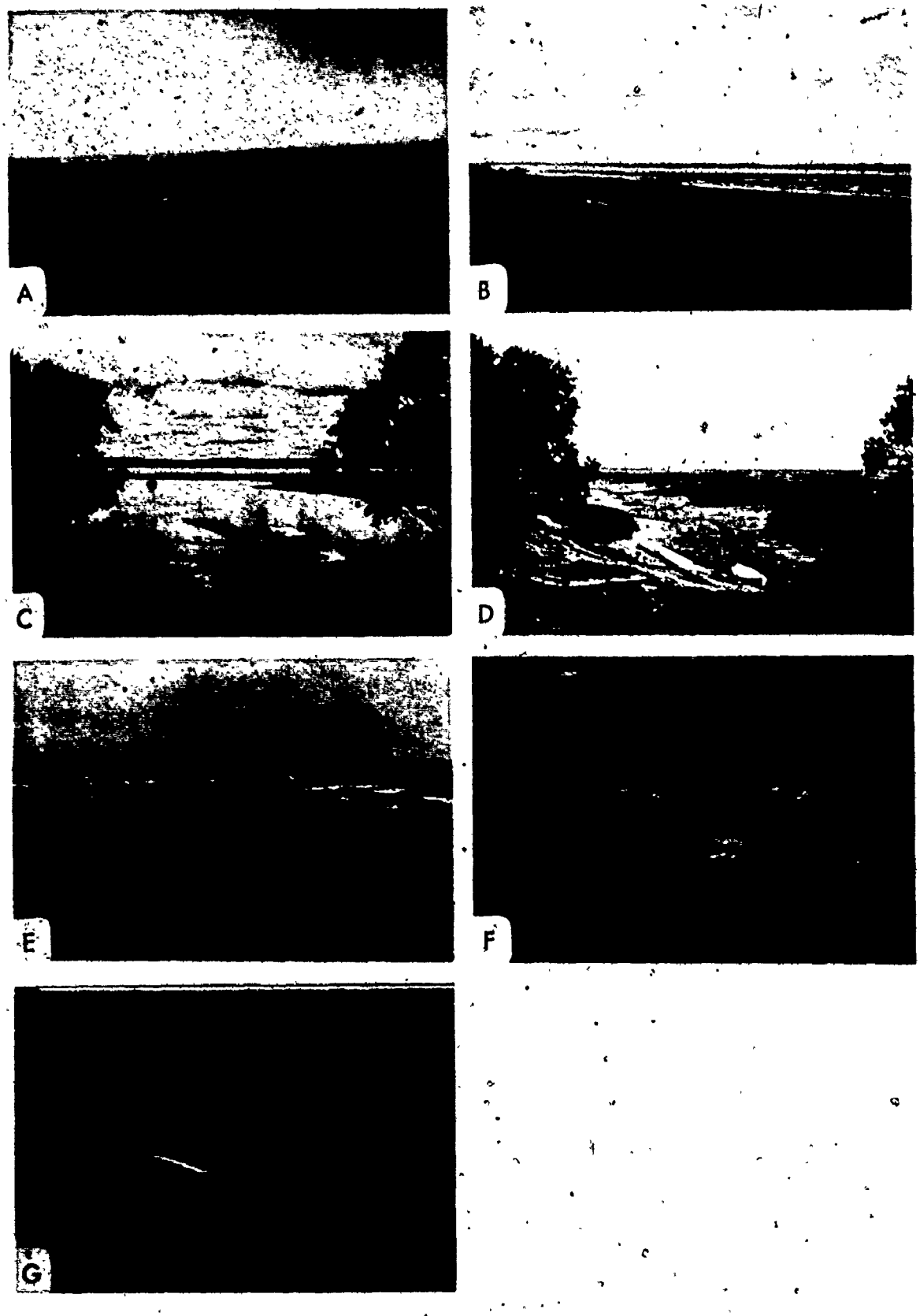
A
B
C
D
E
F
G

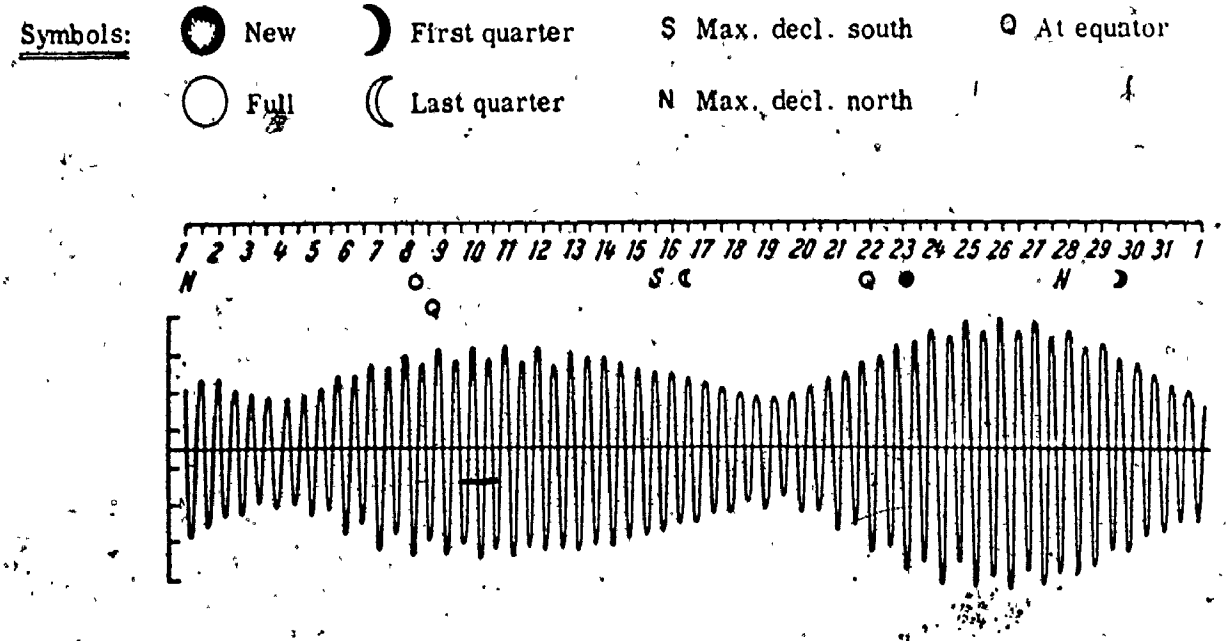

FIGURE 2.17: Diagram of semidiurnal tidal variations during a lunar month (from Dohler, 1966). Note the variations in the timing of the spring and neap tides relative to the new and full moon.

The tides have a diurnal inequality (a difference in the level of successive high and low waters when the moon is at maximum declination north or south of the equator) that is generally less than 0.8 m (Dawson, 1917).

The tidal range is affected by the moon's nodal cycle (the gradual change of the moon's declination with respect to the plane of the earth's orbit about the sun) of approximately 18.6 years. The moon's declination changes ±5° to either side of the earth's ecliptic. Larger tides are experienced during the ascending node. According to Bleakney (1972) and Kaye and Stuckey (1973), maximum nodes occur near the years 1904, 1922, 1940, 1958 and 1976. Thus, the period of observation in this study were made during an ascending node.

Tidal Range - The mean tidal range at Burntcoat Head is 11.7 m (Dawson, 1917). The mean spring range (at lunar perigee) is 15.4 m and the mean neap range (at lunar apogee) is 12.3 m. The largest tide actually measured, with a range of 16.3 m, was observed by Dawson (1917) on the west side of Burntcoat Head.

By comparison, the ATPEMC (1969, Table A1-1) report a maximum spring range of 15.2 m and a mean tide of 11.3 m at Burntcoat Head. The Admiralty Tide Table (1976) give a mean spring and neap range of 12.9 and 9.6 m respectively for Burntcoat Head.

Severe storms have some affect on tidal range. The "Saxby tide" of October 5th, 1869 (ATPEMC, 1969, A4-3; Dawson, 1917) reached an estimated range of 17.3 m as a result of a major storm. Otherwise, the tide would not have been particularly large.

The confusion about the actual tidal ranges at Burntcoat Head makes comparisons with other coastal locations difficult. The large tides of the Bay of Fundy system are amongst the largest in the world (Admiralty Tide Table, 1976; Bauer, 1933; Davies, 1964; Gierloff-Emden, 1961; Skinner and Turekian, 1973), if not the largest (McWhirter and McWhirter, 1972, p. 56). The Fundy tides are certainly not unique, as shown by the occurrence of large tidal ranges (greater than 5 m) throughout the world (Table 2-1 and Figs. 1.2 and 2.18).

TABLE 2 - 1

REPRESENTATIVE WORLD TIDAL RANGES GREATER THAN 5 METRES

(after Admiralty Tide Tables, 1975)

		MEAN SPRING TIDAL RANGE (m)	MAX. RANGE RECORDED
EUROPEAN WATERS			
East Coast of England			
	Thames River	6.6	7.9
	Humber River	6.5	8.4
West Coast of England			
	Mersey River	8.4	10.5
	Morecombe Bay	8.4	
Bristol Channel			
	Swansea	8.6	10.5
	Cardiff	11.1	13.4
	Newport	12.1	
	Severn River	8.4 - 12.4	
	Avon River	11.0 - 12.3	14.5
NW Coast of France			
	Dieppe	8.5	9.8
	Boulogne	8.0	9.3
	Le Havre	6.8	8.0
	St. Helier	9.8	12.3
	St. Malo	10.7	
	Granville	11.5	
	Brest	6.1	7.8
White Sea		10.0	

TABLE 2 - 1 (cont'd)

	MEAN SPRING TIDAL RANGE (m)	MAX. RANGE RECORDED
NORTH AMERICA		
East Coast of Canada		
Frobisher Bay	8.8	
Hudson Strait	9.9	
Ungava Bay	10.4 - 11.5	
Quebec	5.0	6.2
Bay of Fundy		
St. John	7.4	9.2
Chignecto Bay	9.8 - 12.4	
Minas Basin	9.6 - 12.9	(Burntcoat Head)
Annapolis Valley	7.8 - 9.2	
West Coast of Canada		
Prince Rupert	5.3	7.5
West Coast of U.S.A.		
Cook Inlet	8.6 - 9.0	
Colorado River Estuary	9.0	
SOUTH AMERICA		
Argentina		
Puerto Gallegos	10.4	13.2
Puerto Santa Cruz	9.5	
Golfo San Matias	7.7	
Chile		
Puerto Montt	5.8	7.4
Chonos Archipelago	~5.0	
AFRICA		
Mozambique		
Beira	5.6	6.9

TABLE 2 - 1 (cont'd)

	MEAN SPRING TIDAL RANGE (m)	MAX. RANGE RECORDED
ASIA		
India		
Gulf of Cambay (Bhaunagar)	8.8	11.9
Hooghly River	5.0	5.7
Burma		
Rangoon River	5.8	7.4
China		
Hangchow Bay	5.9	
Korea		
Inch On	6.1	10.2
AUSTRALIA		
Northwest Australian Coast		
Port Hedland	5.8	7.8
Broome	8.2	
King Sound	9.8	
Buccaneer Archipelago	8.2 - 9.2	
Collier Bay	8.9 - 10.5	
Darwin	5.5	7.8
East Australian Coast		
Broad Sound	~5.0	

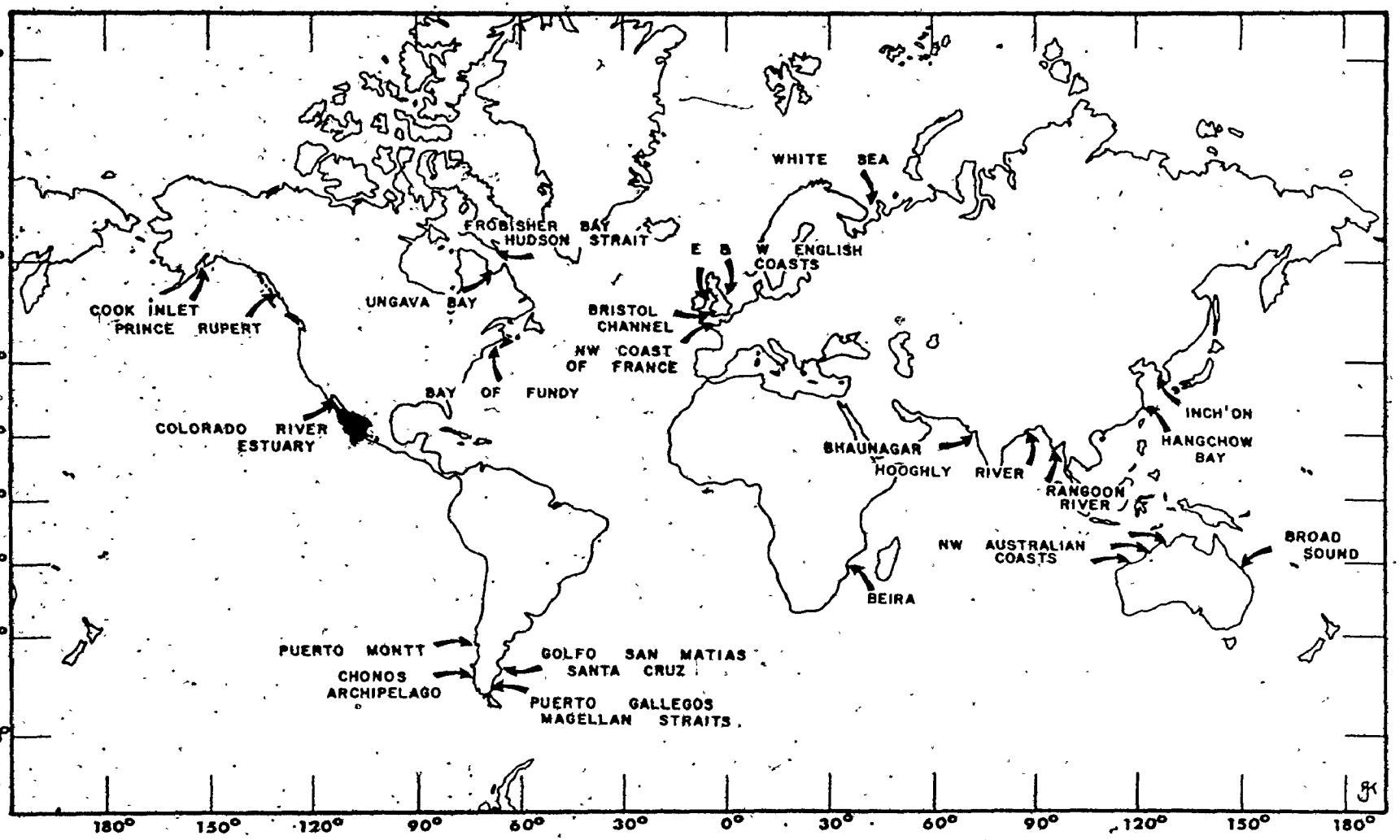

FIGURE 2.18: WORLD SITES WITH LARGE TIDAL RANGES greater than 5 m

Origin of the Large Tides - An extensive literature exists on the mechanics of tides and tide generating forces (e.g., Clancy, 1969; Defant, 1958 and 1961; Ippen and Harleman, 1966; McClellan, 1965; Proudman, 1953, Sverdrup, Johnson and Fleming, 1942), but there are still many unanswered questions. The cause and age of the large tides near the head of the Fundy system is a much debated topic. The deficiency of tidal records and of study of postglacial stratigraphy throughout the Bay of Fundy is partly responsible for the confusion and conflict concerning the origin of the large tides.

Honda et al. (1908, cited in Garrett, 1972 and Goldthwaite, 1924, p. 125), Proudman (1953) and Defant (1961) believed that the large tidal range is the result of resonant amplification of the lunar semidiurnal constituent of the tide within the Bay of Fundy. Ippen and Harleman (1966), Rao (1968), Redfield (1950) and Yuen (1969) questioned this explanation and suggested that the resonant period of the bay is significantly different from the semidiurnal period. Rao (1968) determined that the natural period of the lowest longitudinal mode of the bay is 9.047 hours as compared to the lunar semidiurnal period of 12.42 hours. The results indicated that the Bay of Fundy was too short for resonance, and that bottom shoaling and coastline convergence also could not explain the large tides.

Duff (1970) suggested that if the Bay of Fundy was extended to include the Gulf of Maine, the enlarged system would approximate the conditions necessary for resonance of the lunar semidiurnal constituent to occur. Garrett (1972, 1974 a) found that the natural period of the enlarged system is 13.3 hours, i.e., that it is a little larger than the period of the lunar semidiurnal component. He concluded that the resonant period of the Fundy system is "forced by the lunar semidiurnal component of the North Atlantic" to produce the large tides near the head of the Bay of Fundy.

Wightman (1975) has determined a maximum tidal range of 3 to 4 m for a Pleistocene (13,000 BP) beach at Advocate Harbour, where the present maximum tidal range is 12.6 m. Grant (1970) suggested that the main growth of tidal range took place as eustatic sea-level rise widened and deepened the entrance to the Bay of Fundy, and, on the

average, the bathymetry shallowed. If the large tides are caused by resonance, they must have been susceptible to changes in the dimensions of the system. The present configuration of the system has resulted from a combination of rising sea-level and isostatic rebound only during the last 6000 y. Most of the increased tidal range has taken place during the last 4000 y (Grant, 1970).

Field Observations - In view of the confusion about the range of the tides at Burntcoat Head and the deficiency of tidal information further towards the head of the bay, an attempt was made to set up a temporary tide gauge at Anthony Park (near Noel Shore). Unfortunately, difficulties with the Ottboro 'pressure type water level recorder' (Dohler, 1970) prevented successful operation of the tide gauge. The recommended maximum separation between the recorder and the pressure diaphragm (using 1.02 mm capillary tubing) is 100 m. The shortest distance across the intertidal foreshore was about 350 m (requiring 12 - 30.5 m sections of tubing and thus increasing the probability of leaks with so many sections).

In order to compare the predicted times and ranges of the tide at Burntcoat Head with locations further towards the head of the bay, the times and levels during a single rise and fall of the tide were recorded and surveyed across the intertidal foreshore near Mungo Brook (east of Noel Shore) on July 24, 1973 (weather conditions were calm).

The results (Fig. 2.19 and Table 2-2) show that high water occurred at about the same time as the predicted time of high water at Burntcoat Head (Canadian Tide and Current Tables, Canadian Hydrographic Service, 1973), but that the time of low water was approximately 44 minutes later at Mungo Brook (relative to Burntcoat Head).

The survey results indicate that the tidal range at Mungo Brook was 12.3 m while the predicted range at Burntcoat Head was 12.5 m. It is beyond the limits of this study to ascertain whether the difference is significant and to suggest possible causes for the difference.

The duration of the ebb and flood phases of the tide from the predicted times at Burntcoat Head (and as measured by Dawson, 1917) are approximately equal. However, at Mungo Brook the ebb tide lasts 1.32 h longer than the [illegible] of the [illegible]. The rates of

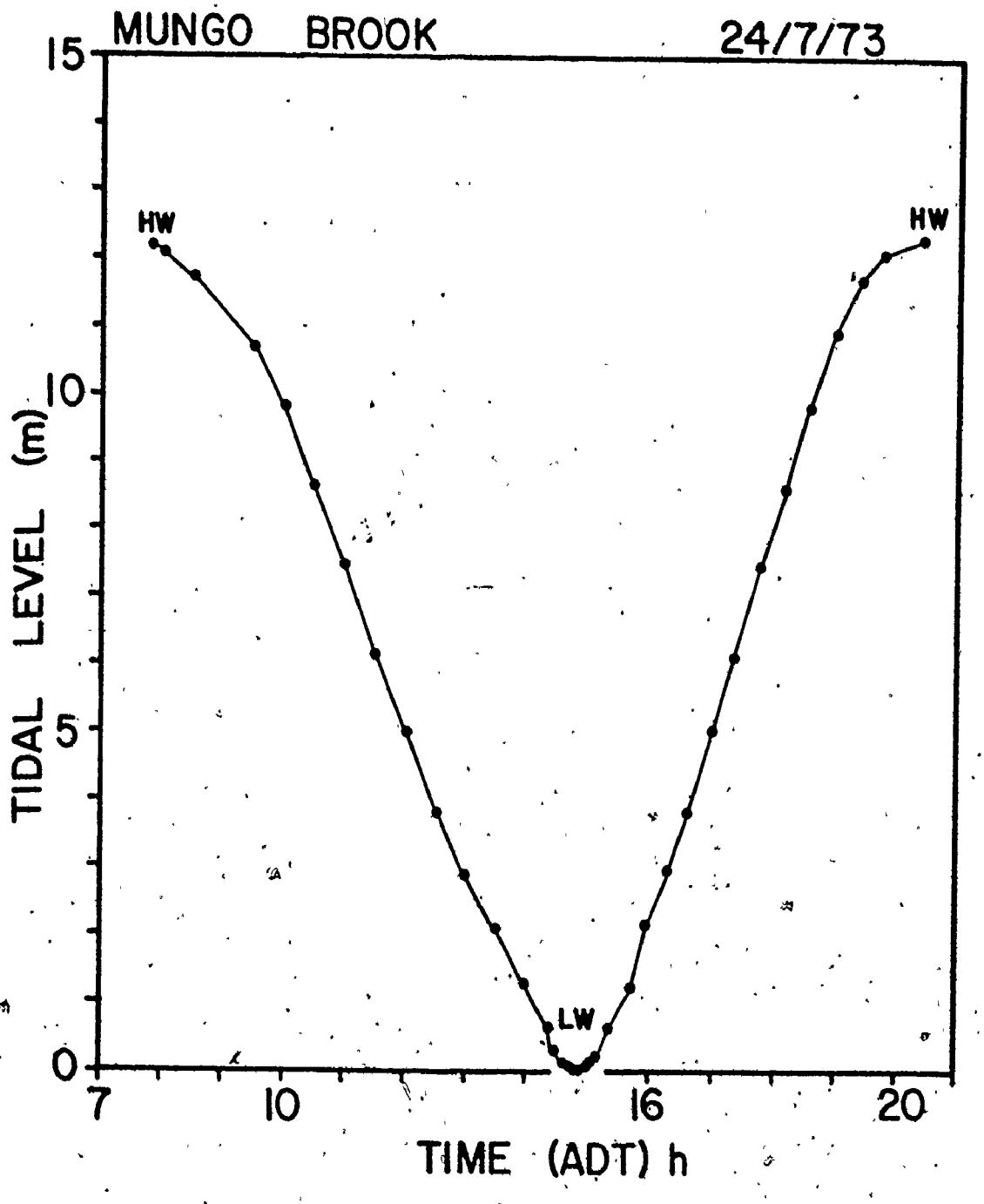

FIGURE 2.19: The time-variation of the tidal level during a single tidal cycle at Mungo Brook on July 24, 1973.

T A B L E 2 - 2

COMPARISON OF TIMES AND RANGES OF THE TIDE BETWEEN MUNGO BROOK AND BURNTCOAT HEAD, JULY 24, 1973.

	Mungo Brook	Burntcoat Head*	Differences
Times			
High Water	0755	0753	+2 min
Low Water	1450	1406	+44
High Water	2025	2023	+2
Duration (hours)			
Ebb	6.91	6.22	+41 min
Flood	5.59	6.28	-41
Range (meters)			
Ebb	12.21	12.19	+.02 m
Flood	12.35	12.70	-.35
Mean	12.28	12.45	-.17
Rates of Rise and Fall			
Ebb	1.77	1.96	-.19 m/h
Flood	2.21	2.02	+.19

Note: * predicted times and ranges from the Canadian Tide and Current Tables (Canadian Hydrographic Service, 1973)

tidal rise and fall at Mungo Brook and Burntcoat Head (based on ebb and flood durations, and tidal ranges) are 1.77 and 2.21 m/h, and 2.0 m/h (for both rise and fall) respectively. The rates of rise and fall slow for a short time on either side of high and low water (Fig. 2.19).

Figure 2.20 shows the predicted tidal height variations for Burntcoat Head during the three summer field seasons.

Tidal Currents

In coastal areas, such as the Bay of Fundy, the tidal currents generally reverse their direction by almost 180°. By contrast, tidal currents in the open ocean are not restricted by coastlines, and they follow rotary patterns (with clockwise rotation in the northern hemisphere). Oceanic currents are continuous and constantly change direction whereas the reversing currents, typical of confined bays and straits, commonly have a slack period between the ebb and flood. The oceanic ebb and flood are separated only by a current speed minimum. Even in the central part of Minas Basin (Fig. 2.23 B), the currents reverse their direction by almost 180° (Anonymous, 1966) and are uniform in direction from top to bottom (C. Amos, pers. comm., 1975). However, current directions may be modified by storm winds, peak runoff from rivers (e.g., snowmelt, storms), and by local irregularities in bathymetry and shoreline morphology.

The strength and periodicity of the currents depends on the tidal range and characteristics of the tide. Tidal currents have a semi-diurnal period in Minas Basin-Cobequid Bay. In spite of the large tidal range, tidal currents generally range from 0.5 to 2 m/s (C. Amos, pers. comm. 1975; Anonymous, 1966; ATPEMC, 1969; Forrester, 1958; Godin, 1968; Klein, 1968 a and 1970 a; Klein and Whaley, 1972; Swift, 1966; Swift and McMullen, 1968). In the central part of Minas Basin and near the entrance to Cobequid Bay (Fig. 2.23 A), current speeds are generally less than 1.5 m/s. Over intertidal areas where water depths are shallower and the bathymetry is relatively more complex, speeds are generally less than 1 m/s and vary considerably between locations. The strongest currents occur in the channels adjacent to sand bars and in Minas Passage (where speeds up to 5.6 m/s have been recorded, Cameron, 1961).

FIGURE 2.20: Predicted tidal height variations for Burntcoat Head during the three field seasons (June, July, and August).

A. 1971

B. 1972

C. 1973

Data compiled by Marine Environmental Data Service, Environment Canada, (D.G. Mitchell, pers. comm., 1974).

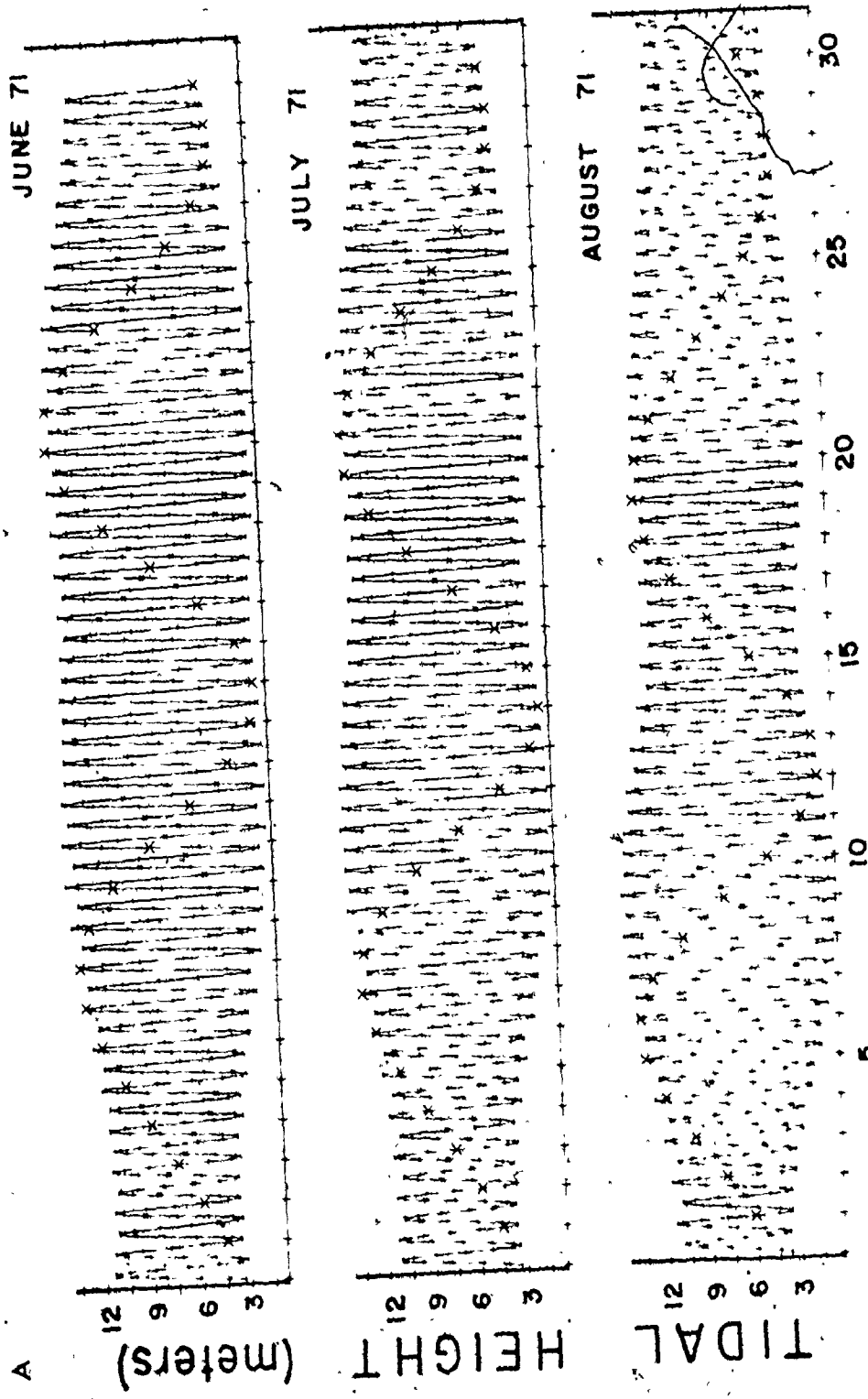
A
TIDAL HEIGHT (meters)
JUNE 71
JULY 71
AUGUST 71
12 9 6 3
5 10 15 20 25 30
TIME (days)

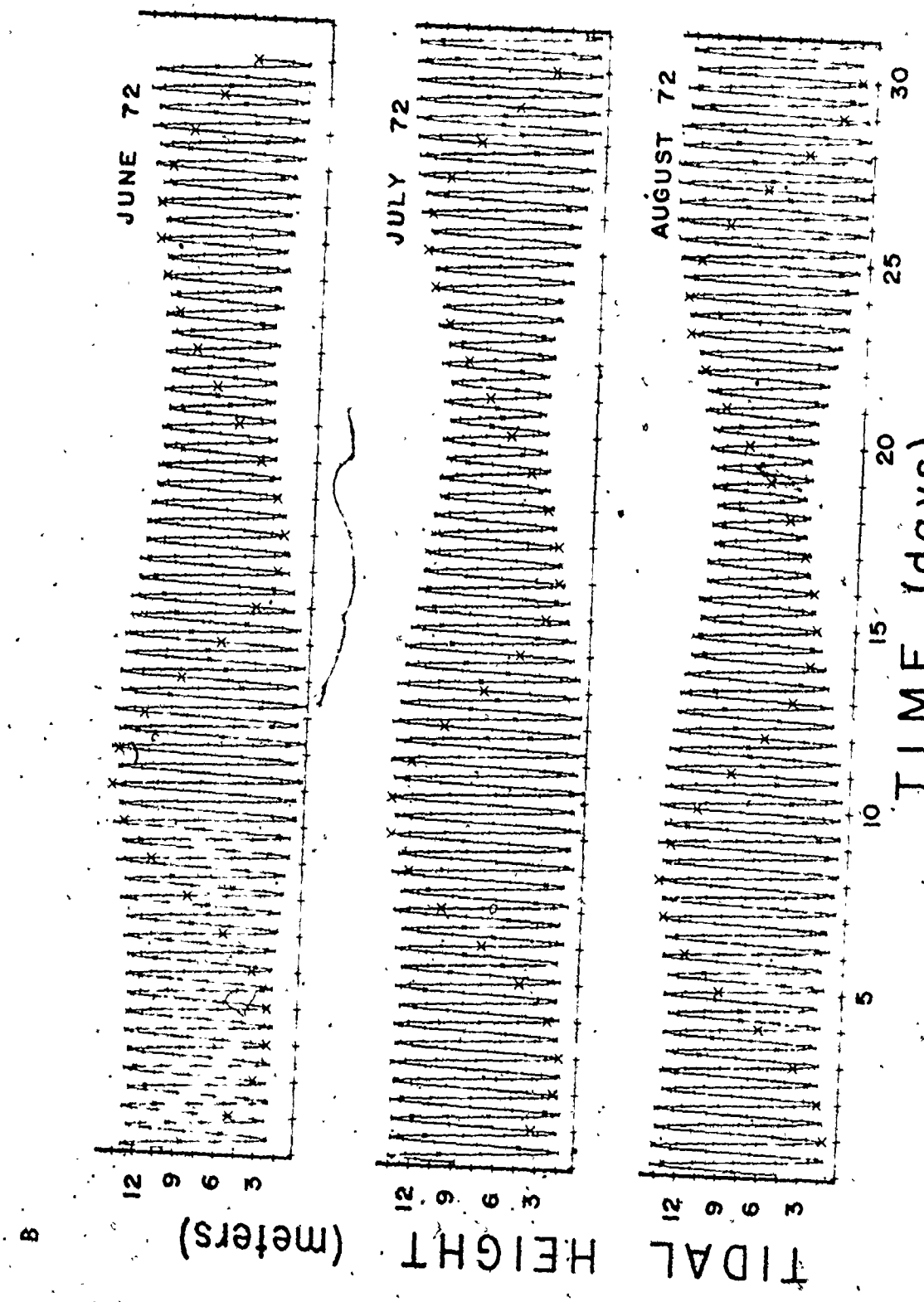

FIGURE 2.20 - con't'd.

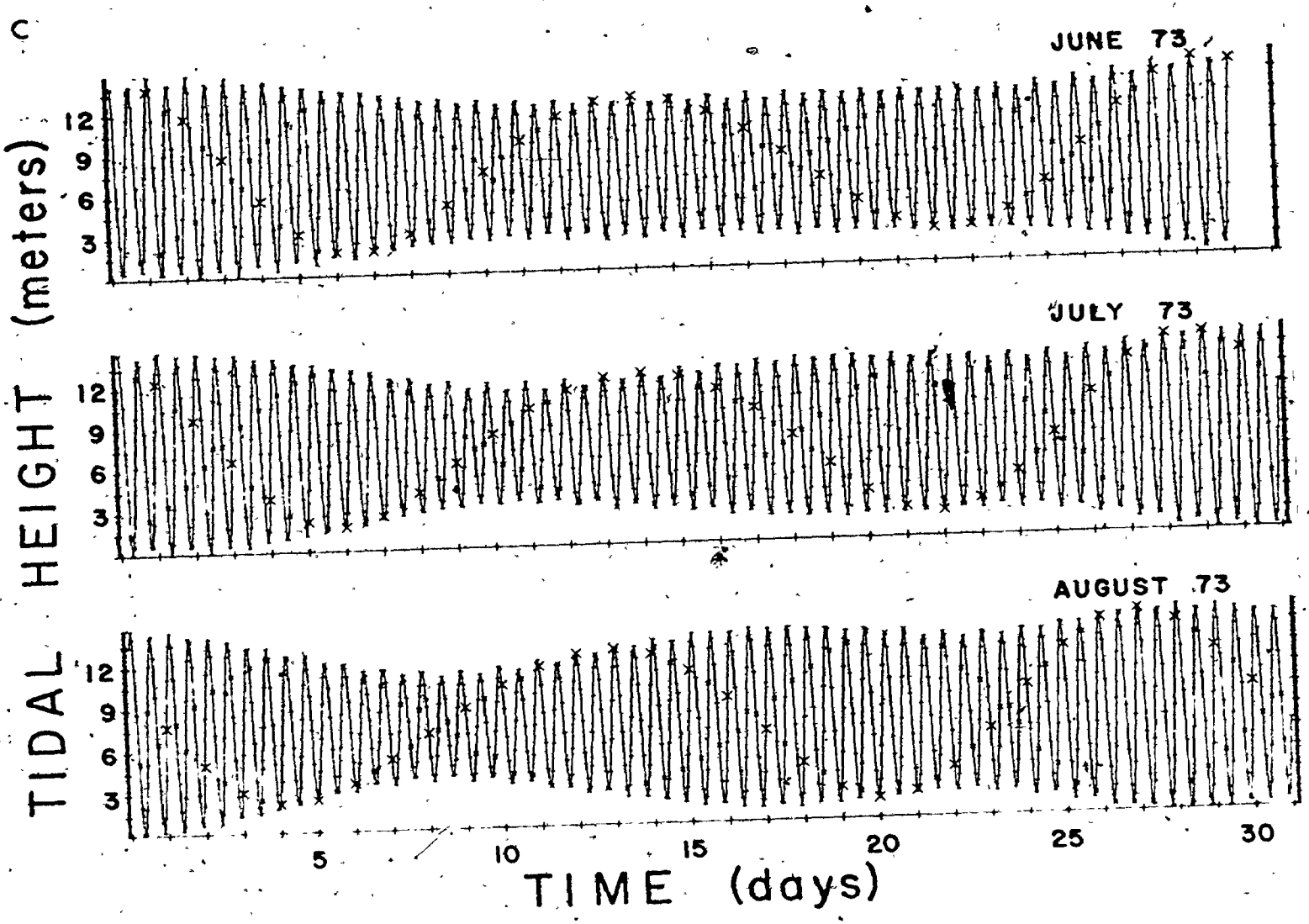

FIGURE 2.20 - cont'd

Seawater Properties

There are only a few measurements of seawater properties in Minas Basin-Cobequid Bay (e.g., ATPEMC, 1969; Pelletier and McMullen, 1972). More work has been done of the properties of seawater and circulation patterns in the main Bay of Fundy (e.g., Bailey et al., 1953; Bumpus, 1959; Bumpus and Lauzier, 1965; Miller, 1966; Pelletier and McMullen, 1972; Swift et al., 1973).

The seawater properties of any marine system depend to a large extent on the tidal range, the amount of vertical mixing and patterns of water circulation. The large tides in Minas Basin-Cobequid Bay result in the flushing of large volumes of water into and out of the system and in good vertical mixing. These characteristics should be reflected in seawater properties (e.g., water temperature, salinity, suspended sediment concentrations).

Some measurements of water temperature and suspended sediment concentrations were made during the study to supplement existing data. The field methods used for the collection of these data are discussed in Appendix I.1.

Temperature and Salinity - Vertical profiles of temperature and salinity both show negligible gradients as a result of good vertical mixing (ATPEMC, 1969; Swift et al., 1973) at most locations, particularly towards the head of the Fundy system. Amos (pers. comm., 1976) reports that salinity profiles in Minas Basin show bottom to surface differences of the order of $0.4^{o}/_{oo}$.

Water temperatures become significantly warmer and salinities lower at all depths towards the head of the Bay of Fundy system (Bousfield and Leim, 1959). Mean surface temperatures range from 1.2^{o}C in March to 11.5^{o}C in September (Bailey et al., 1953) in Passamaquoddy Bay near the entrance to the Bay of Fundy. Amos (pers. comm., 1976) reported water temperatures of 15.2^{o}C and 11.2^{o}C for low and high tide respectively during July in the centre of Minas Basin. In Cobequid Bay, mean bottom (0.5 m) temperatures range from 12^{o} to 20^{o}C during the summer months (Figs. 2.21 and 2.22). The extensive intertidal zone in Cobequid Bay plays an important role in controlling water temperatures. As the water surface area of the bay at low

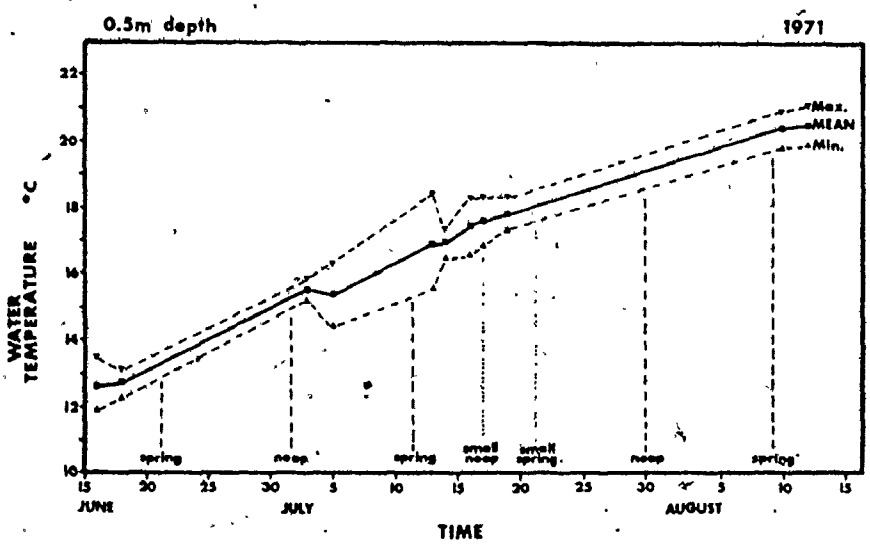

FIGURE 2.21: The time-variation of water temperature during the summer of 1971 over Noel Bay Bar.

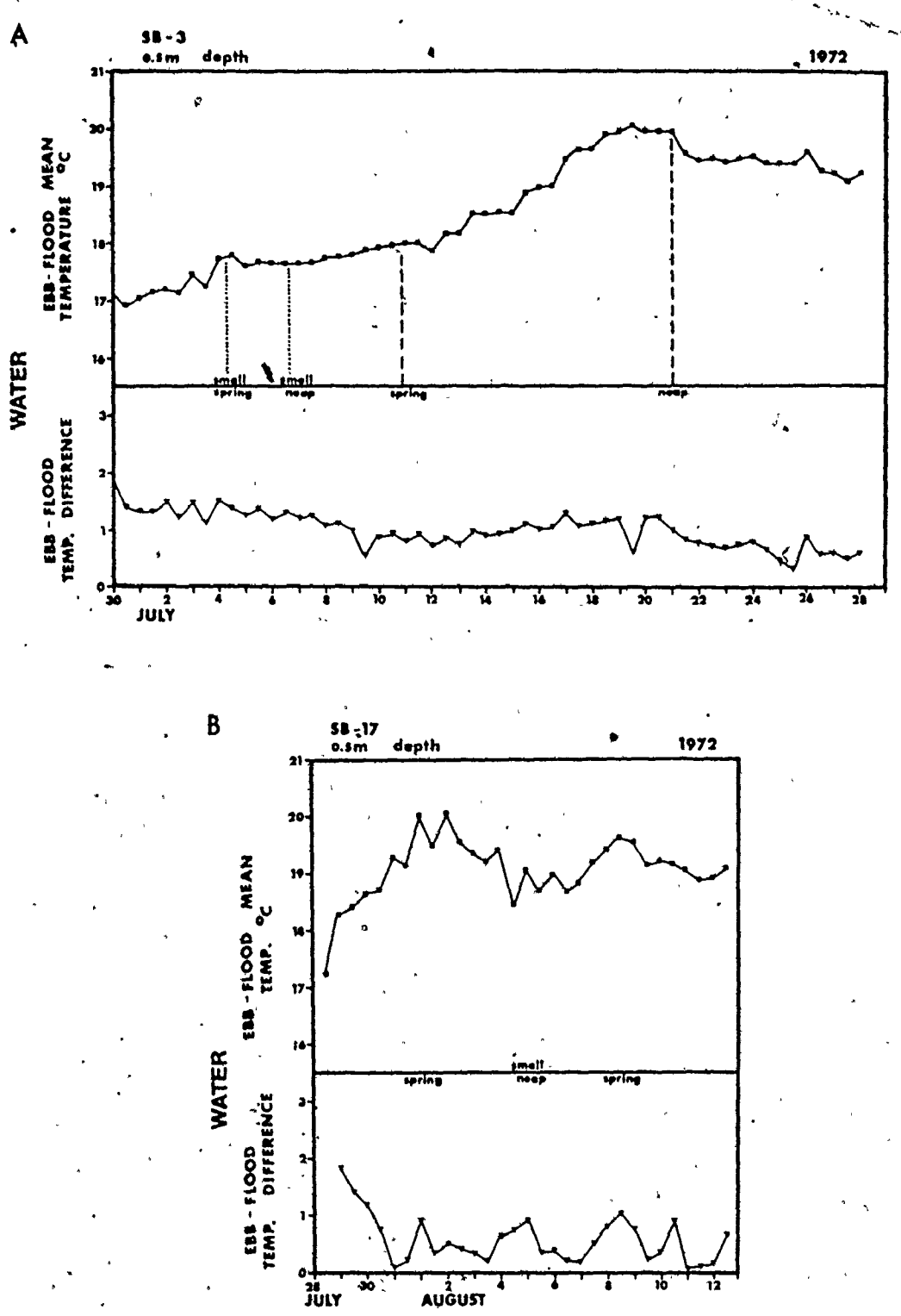

FIGURE 2.22: The time-variation of water temperature during the summer of 1972 at two locations over Selma Bar: A. SB-3; and B. SB-17. Locations are shown in Fig. 4.1.

tide is small relative to the area of the exposed intertidal zone, summer temperatures tend to be warmer and winter temperatures colder than the waters of the main Bay of Fundy. In winter, water temperatures drop to freezing in Cobequid Bay, but no detailed measurements have been made during this season.

Figures 2.23 C and 2.24 summarize the variation of water temperatures in Cobequid Bay during a single tidal cycle. The difference between the ebb and flood water temperatures is particularly apparent in Fig. 2.22 C (ATPEMC, 1969). During the ebb, temperatures become progressively warmer until low tide (Fig. 2.23), while the reverse is true during the flood. There is some suggestion in Figs. 2.22 and 2.24 that water temperatures may also be governed by the phase of the tide (i.e., water temperatures are warmer during neap tide periods than during spring periods).

Salinities in Passamaquoddy Bay (Bailey et al., 1953) range from 31.1$^{o}/_{oo}$ in May to 32.9$^{o}/_{oo}$ in October. The spring minimum is related to dilution from snowmelt runoff. Swift et al. (1973) measured salinities that ranged from 32.0 to 33.8$^{o}/_{oo}$ in Chignecto Bay. Amos (pers. comm., 1976) found that salinities in Minas Basin and Minas Passage averaged about 32.3$^{o}/_{oo}$. Salinities are noticeably diluted towards the head of the Minas Basin-Cobequid Bay system (Fig. 2.23 D), where they range from 25 to 30$^{o}/_{oo}$.

Figure 2.23 D also indicates the variation of mid-depth water salinities during a tidal cycle at the entrance to Cobequid Bay. The mid-ebb and mid-flood salinities average 28.3 and 28.4$^{o}/_{oo}$ respectively. Salinities are lowest before and highest after low water.

The colder temperatures and higher salinities during the flood are related to the incursion of fresh seawater into Cobequid Bay from the main Bay of Fundy. The lower salinities and warmer temperatures during the ebb reflect a small, but measurable dilution of seawater from freshwater input at the head of the bay (e.g., from the Salmon and Shubenacadie Rivers). According to Gross (1972, p. 296): "An estuary is a semienclosed part of the coastal ocean where fresh water from the land mixes with seawater." The temperature and salinity measurements considered above thus indicate that Minas Basin-

FIGURE 2.23: Current characteristics and seawater properties at the entrance to Cobequid Bay during a tidal cycle.

A. Bottom current speed.

B. Bottom current direction.

C. Mid-depth water temperature.

D. Mid-depth water salinity.

E. Mid-depth suspended sediment concentration.

A BOTTOM VELOCITY m/s

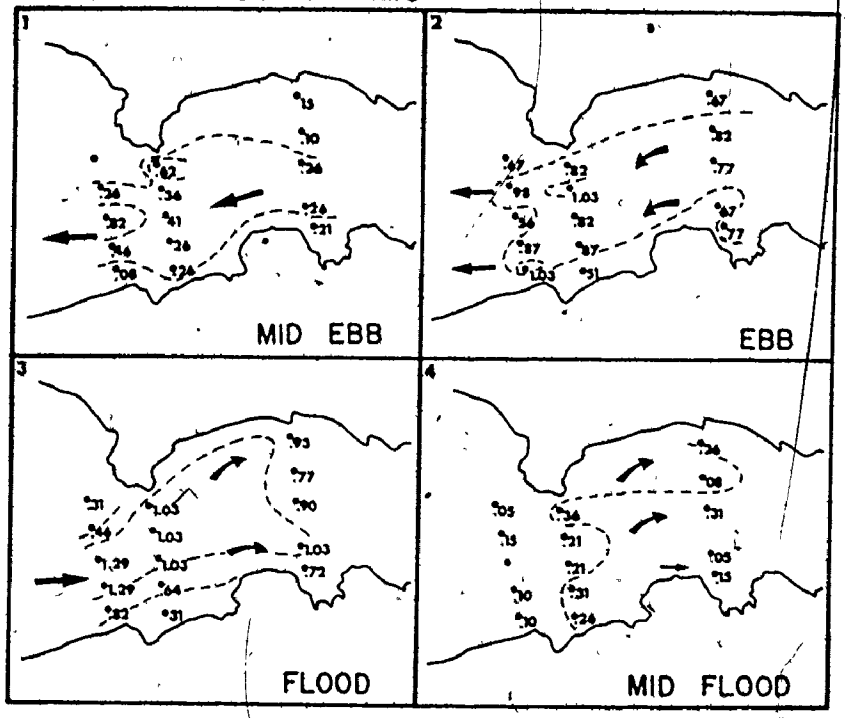

(after ATPEMC, 1969)

B CURRENT DIRECTION bottom .5m

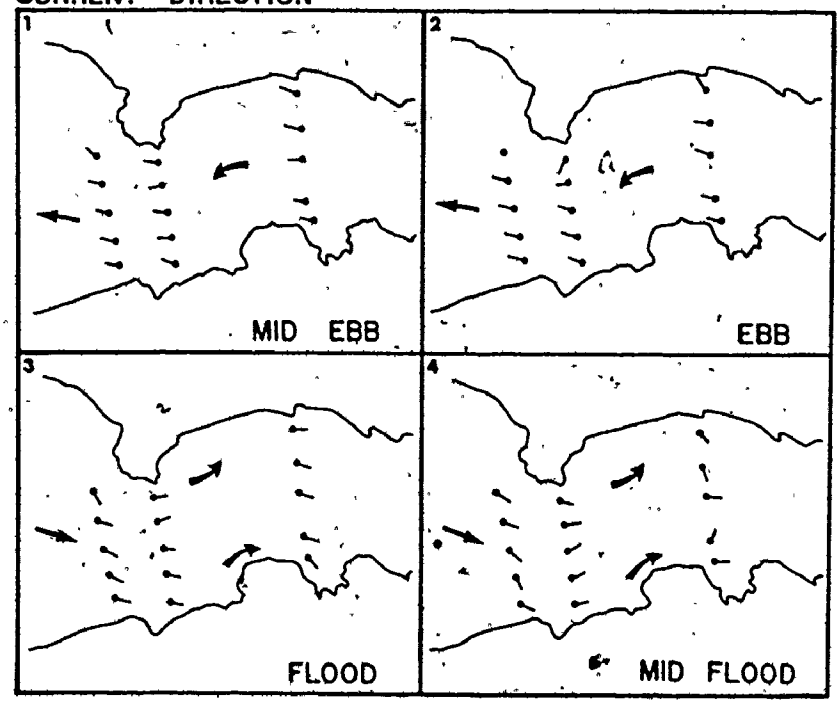

(after ATPEMC, 1969)

C WATER TEMPERATURE °c mid depth

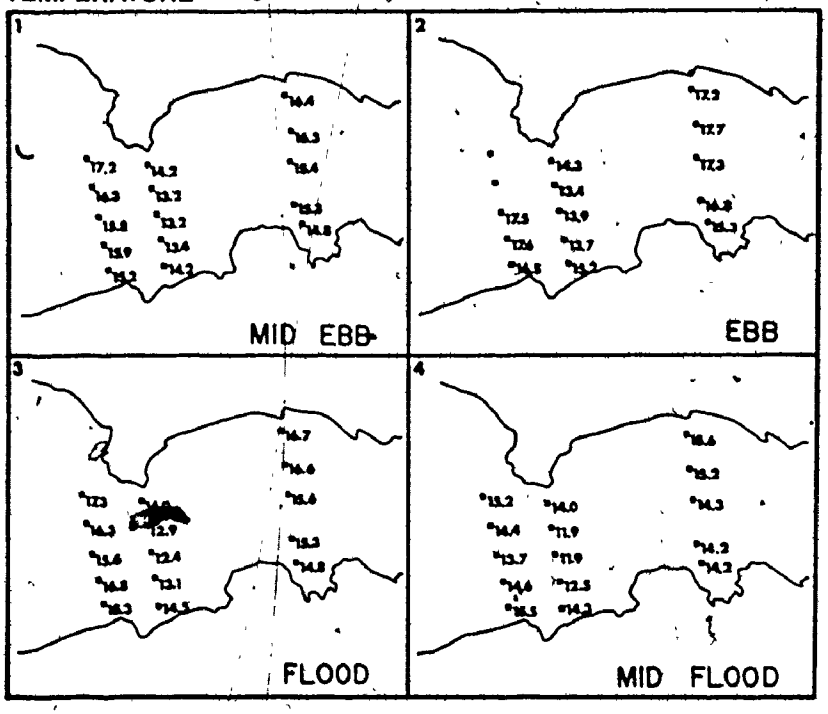

(after ATPEMC, 1969)

D SALINITY ‰ mid depth

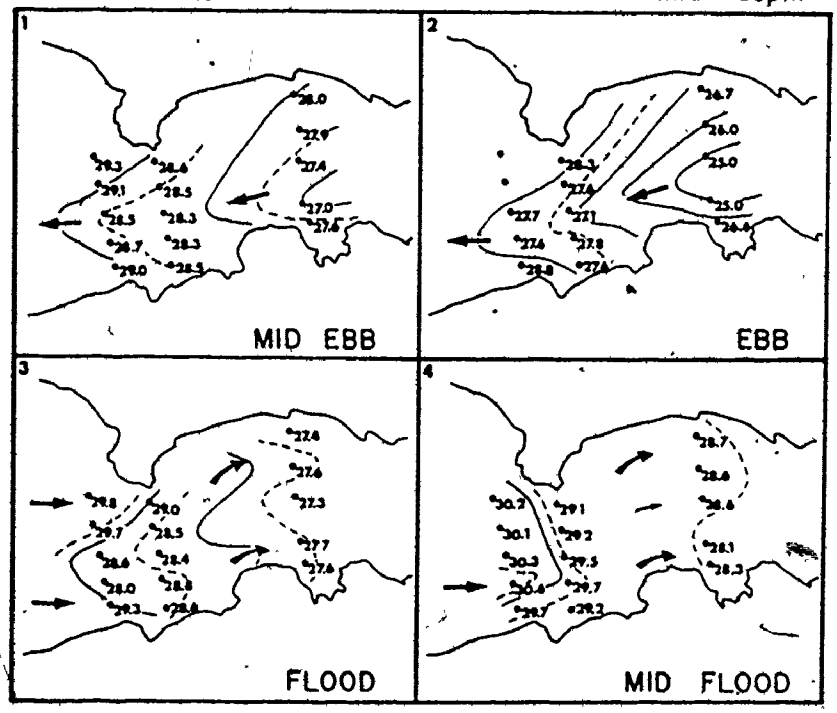

(after ATPEMC, 1969)

FIGURE 2.23 - cont'd.

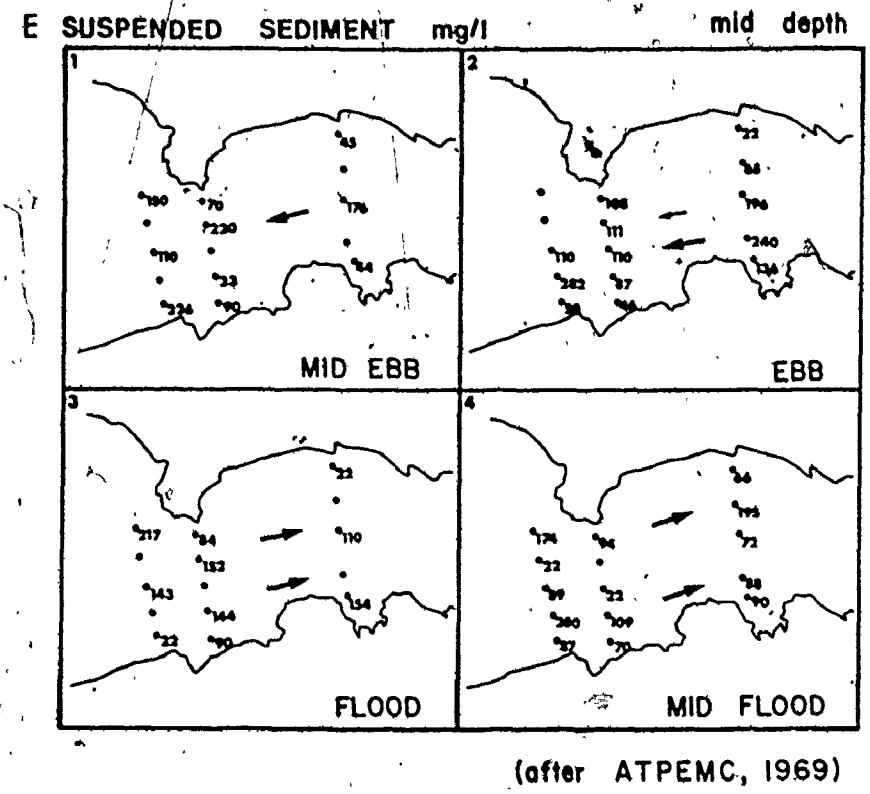

FIGURE 2.23 - cont'd.

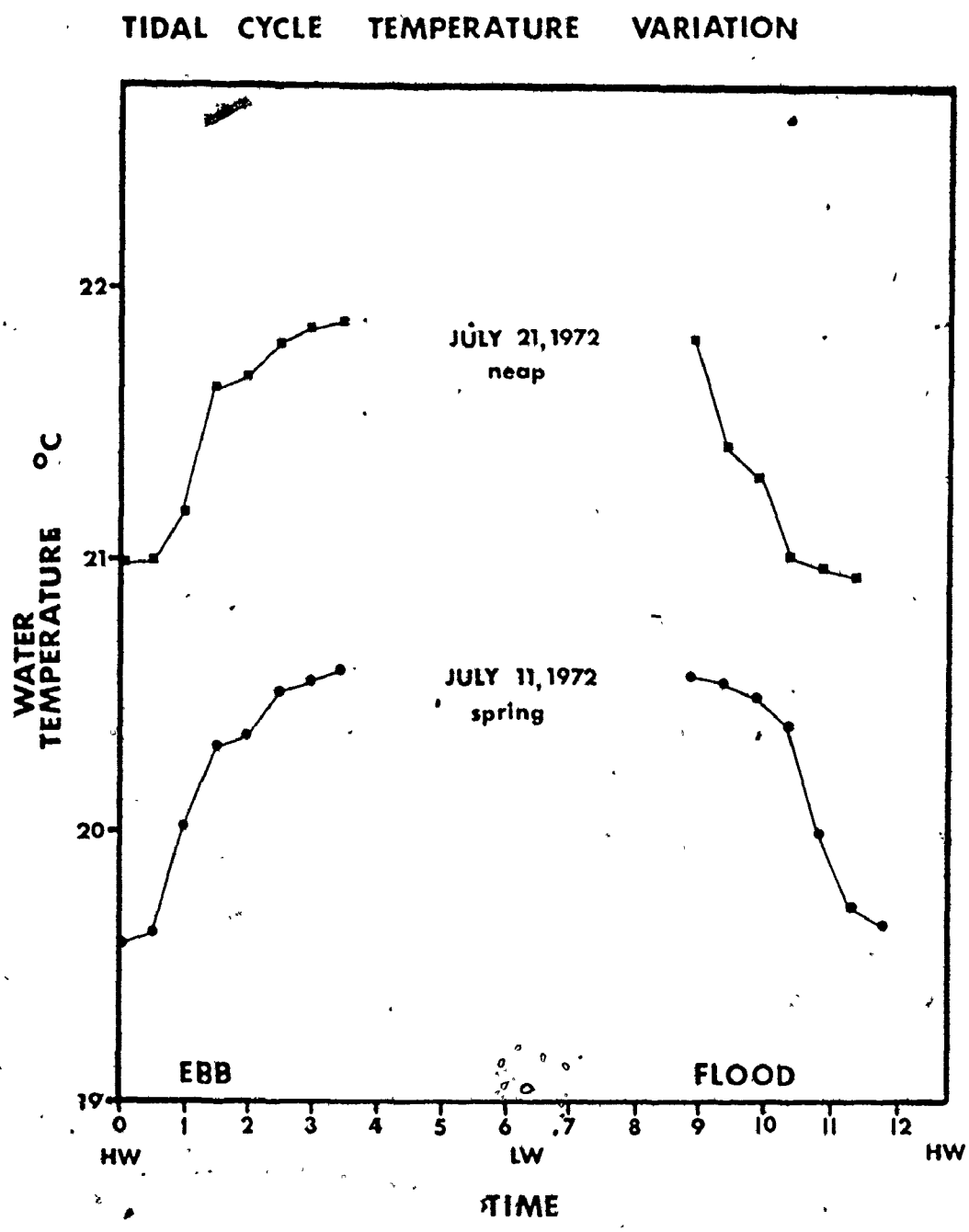

FIGURE 2.24: Time-variation of water temperature during a spring and neap tidal cycle in Cobequid Bay.

Cobequid Bay is a well-mixed tidal estuary.

Water temperatures are larger during spring tides than during neaps because the spring tidal prism is larger and relatively more cold, oceanic water is exchanged with the main Bay of Fundy. During neap periods, the tidal prism is relatively smaller (i.e., less cold water enters Minas Basin-Cobequid Bay).

The data presented in Fig. 2.23 (ATPEMC, 1969, Tables A1-22 and A3-10) shows some characteristics of the circulation pattern at the entrance to Cobequid Bay during a tidal cycle. During the ebb, salinities are lower and temperatures are generally found along the axis of the bay during the ebb, implying that the main ebb flow is concentrated there. During the flood, the highest salinities and lower temperatures (to a lesser extent) occur to either side of the bay's central axis. This suggests that the flood currents are deflected towards the sides of the bay by the seaward flowing ebb currents during the early flood (e.g., Fig. 2.23 D-3). After the tide has completely turned (Fig. 2.23 D-4) flood currents are concentrated along the axis of the bay. Bottom velocities and current directions (Figs. 2.23 A and B) show a somewhat similar circulation pattern. This pattern of circulation will be discussed more extensively in Chapter 6.

None of the data considered above suggests the existence of a counter-clockwise system of residual currents (Pelletier and McMullen, 1972; Swift and McMullen, 1968) in Minas Basin-Cobequid Bay. The Coriolis Effect on circulation patterns in the system is small. For a tidal current speed of 1 m/s, (at a latitude of 45^{o}N), the residual current speed would be approximately 1.03×10^{-6} m/s (McLellan, 1965, p.65).

Suspended Sediment - The large exchange of water with each tide keeps a large amount of fine-grained sediments in suspension. Suspended sediment concentrations in the main Bay of Fundy range from 0.2 to 30.4 mg/l with an average of 6.6 (Miller, 1966). Concentrations in the lower bay show negligible vertical gradients. Near the head of the system, concentrations range from 72 to 2680 mg/l according to Pelletier and McMullen (1972). These values are considerably higher than concentrations found in the main bay and in the open ocean

(average of 2 mg/l). The vertical distribution of suspended sediments shows an increase in the vertical gradient as one moves towards the head of the system. Here, bottom concentrations are considerably higher than those in near-surface samples (ATPEMC, 1969, Table A3-10), particularly near mid-ebb, mid-flood and low tide.

The total amount of sediment in suspension varies during the tidal cycle (Fig. 2.25). Highest values occur near low tide. The flood tide tends to have larger sediment concentrations (Fig. 2.25; ATPPB, 1969, Table A3-10) than the ebb. Fig. 2.26 shows the relation between suspended sediment concentration and mean current velocities. The concentration lags velocity in a manner similar to that described by Allen (1974), Postma (1954, 1957) and van Straaten and Kuenen (1957, 1958). Lag times are generally of the order of 1 h.

The accumulation of fine-grained sediments in the middle to upper intertidal zone (e.g., towards the head of Cobequid Bay) can be explained in terms of settling and scour lag effects (Postma, 1954 and 1957; van Straaten and Kuenen, 1957 and 1958). This mechanism is best summarized by Postma (1957): "Towards high tide, when the flood current velocity has decreased sufficiently far, nearly all material sinks to the bottom. The sediment is not again brought in suspension by the returning ebb current before the latter has reached a velocity considerably higher than that of the flood current at the moment of deposition. In this manner the material is resuspended in a water mass the relative position of which is farther inward than that of the water mass which carried the material during the flood."

"At low tide a considerable part of the material remains in suspension and is thus not subjected to a process similar to that at high tide, which would otherwise approximately compensate the latter. Consequently, over a whole tidal cycle, this material undergoes a net inward displacement."

"The reason for the different behaviour between high tide and low tide is the fact that the time span during which current velocities are sufficiently low to permit settling of fine material is much longer at high tide than at low tide. The causes of this difference between the two tidal phases are, first, the decrease of mean velocities from

FIGURE 2.25: Diagrams showing the time-variability of suspended sediment concentrations during a tidal cycle at five locations in Cobequid Bay:

A. SB-2b

B. SB-3a

C. SB-6c

D. SB-18

E. SB-20a

Locations are shown in Fig. 4.1.

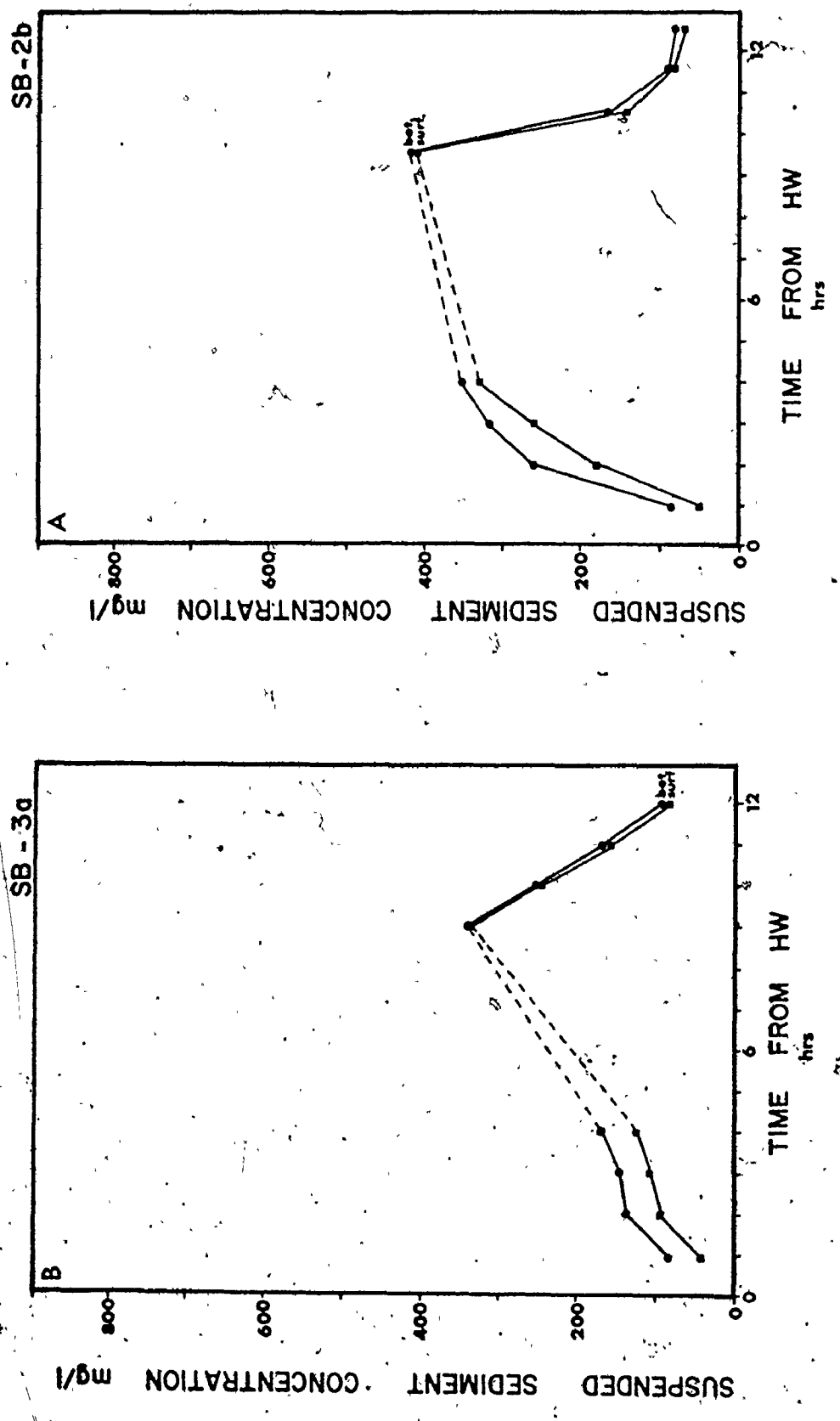
SB-2b
A
SUSPENDED SEDIMENT CONCENTRATION mg/l
800
600
400
200
0
0
6
12
TIME FROM HW hrs
SB-3a
B
SUSPENDED SEDIMENT CONCENTRATION mg/l
800
600
400
200
0
0
6
12
TIME FROM HW hrs

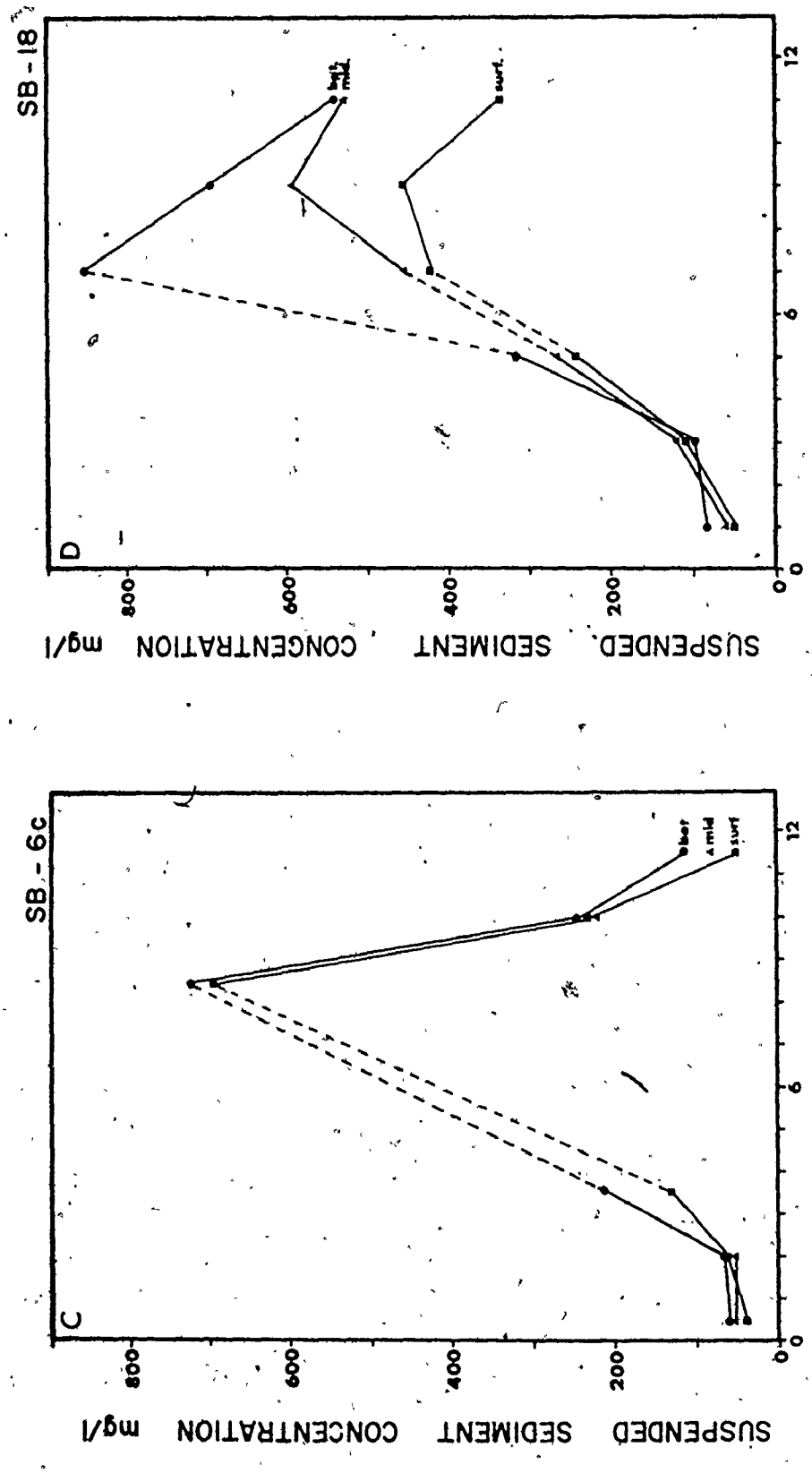

FIGURE 2.25 - cont'd.

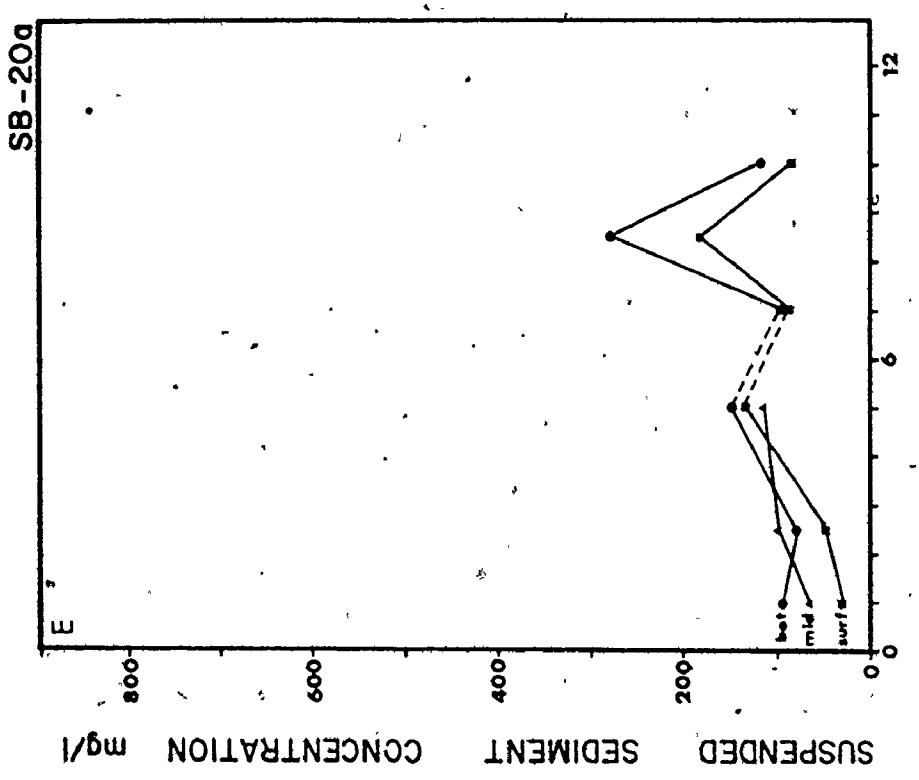

FIGURE 2.25 - cont'd.

FIGURE 2.26: Diagrams showing the relation between suspended sediment concentration and mean current velocity near the surface and bottom during a tidal cycle at five locations in Cobequid Bay:

A. SB-2b

B. SB-3a

C. SC-6c

D. SB-18

E. SB-20a

Locations are shown in Fig. 4.1. Numbers indicate sequence of variation from high water to low water to high water.

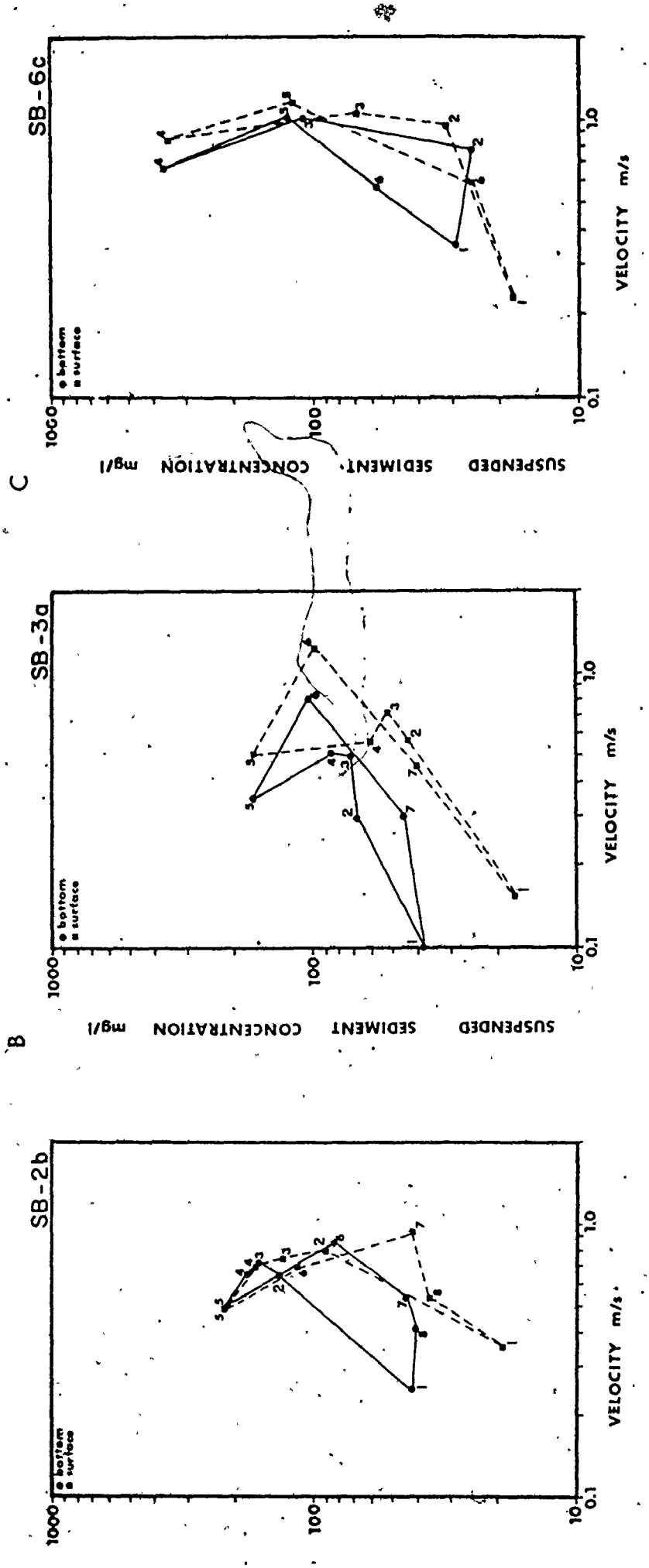
SB-6c
SB-3a
SB-2b
SUSPENDED SEDIMENT CONCENTRATION mg/l
1000
100
10
0.1
1.0
VELOCITY m/s
bottom
surface
C
B

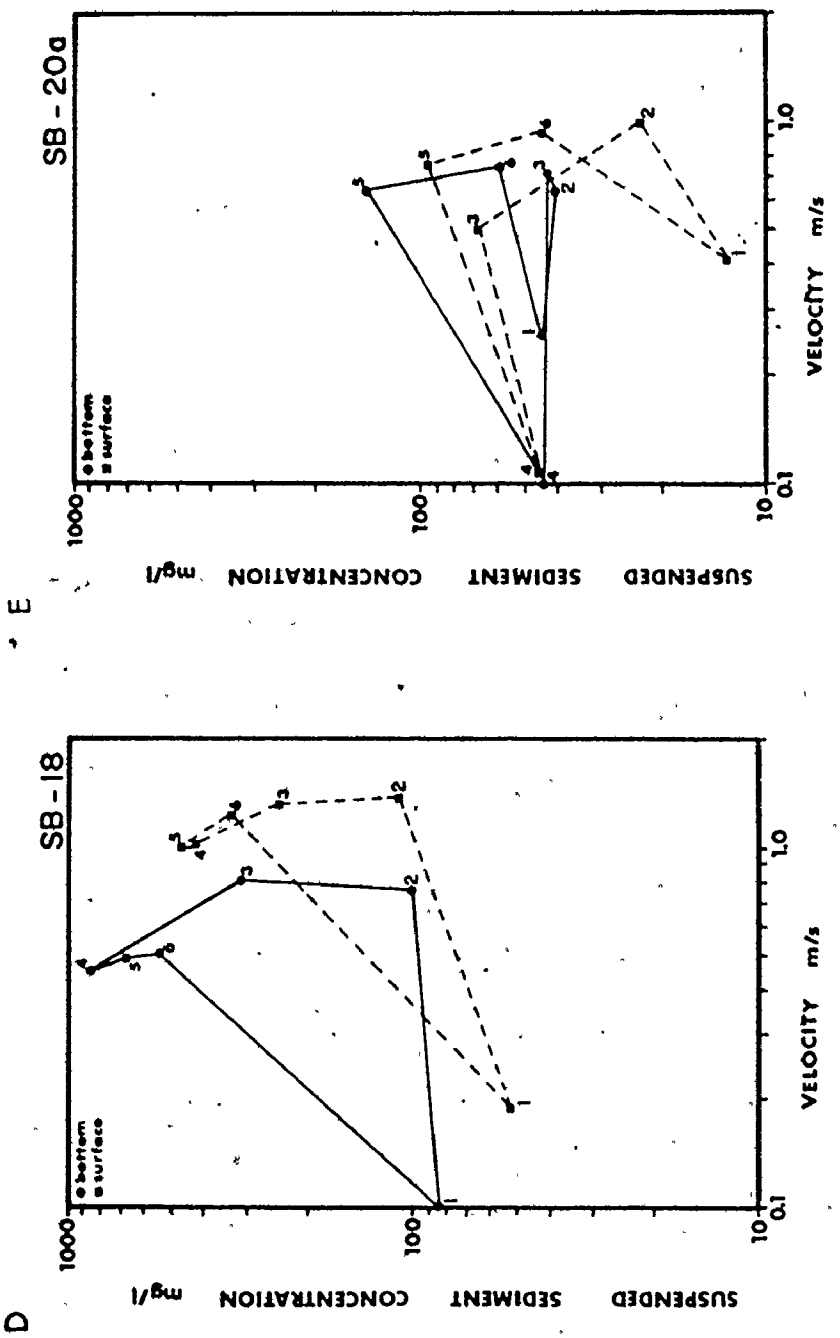

FIGURE 2.26 - cont'd.

tidal inlets towards the coast, and, secondly, the asymmetrical shape of the ebb and flood curves in the small tidal channels, the velocity maxima of which, compared with the maximum of the sinus curve, are shifted towards low tide."

Most of the sediment in suspension in Cobequid Bay and Minas Basin is silt and clay sized (less than 0.0625 mm size). Some fine to medium grained sand is found in some of the near-bottom samples. These grain sizes are well within the size limits suggested by Postma (1957) for the operation of settling and scour lag effects.

WATER BUDGET

To show the dominance of the tidal prism (the volume of water displaced between high and low tide levels) on the hydrological cycle in the Minas Basin-Cobequid Bay region, a water budget was estimated for a single 12-hour tidal cycle.

For a constant water volume, the volume of water that comes into the system (V_i) must equal the volume of water leaving the system (V_o). Therefore,

$$V_i = V_o$$

The amount of water entering the system is a sum of the volumes due to the influx of river runoff (V_r), precipitation directly onto the surface of the bay (V_p) and the flood tidal prism (V_f). Therefore,

$$V_i = V_r + V_p + V_f$$

The water leaving the system is a sum of the volume lost by evaporation from the surface of the bay (V_{ev}) and the volume of the ebb tidal prism (V_e). Therefore,

$$V_o = V_{ev} + V_e$$

Thus, for a perfectly balanced water budget,

$$V_r + V_p + V_f = V_{ev} + V_e$$

ATPEMC (1969) estimated that the average tide moved approximately 2.94×10^9 m^3 of water through the Minas Passage roughly every 6^+ hours. The volume of river runoff entering the bay can be determined from the

size of the watershed area draining into Minas Basin-Cobequid Bay (by planimeter) and from the unit watershed discharge computed for the Salmon River drainage basin (Hennigar, 1972--7412 m^3/km^2 per tidal cycle). The amount of precipitation and evaporation are based on values of 1.18 m/y and .66 m/y respectively (McClellan, 1965, p. 136). The results of these calculations are summarized in Table 2-3.

For a constant content of salt in the bay, the salinities of the ebb and flood tidal prisms must be different. Ebb salinities (S_e) are less than flood salinities (S_f) in the bay (ATPEMC, 1969), therefore

$$V_f S_f = V_e S_e$$

and

$$V_f = \frac{S_e}{S_f} V_e$$

If the average ebb tide moves $2.94 \times 10^9 m^3$ of water with a salinity slightly less than that for the flood tide,

e.g., $S_e = 30.2$ and $S_f = 30.5^o/_{oo}$ then

$$V_f = 0.99 V_e$$

and the average flood tide must move $2.91 \times 10^9 m^3$.

Compiling all of these values and relationships into a budget equation, we find that with only a $0.3^o/_{oo}$ difference in salinity between the ebb and flood tidal prisms, the bay has a balanced water budget. The amount of water gained by precipitation and river runoff equals the amount lost by evaporation and ebb outflow from the bay. From this budget, the combined effect of the ebb and flood tidal exchange accounts for 98.94% of the total flux into and out of the bay. Together, river runoff, precipitation and evaporation represent about 1.06% of the bay's water flux.

TABLE 2 - 3

WATER BUDGET FOR MINAS BASIN-COBEQUID BAY

Total surface area of system (Minas Basin + Cobequid Bay)	1220 km^2
Total watershed area surrounding the system	8130 km^2
Average 6h tidal flux through Minas Passage	2.94×10^9 m^3

Volume In (m^3)	Volume out (m^3)
$V_r = 6.02 \times 10^7$	
$V_p = 1.97 \times 10^6$	$V_{ev} = 1.10 \times 10^6$
$V_f = 2.91 \times 10^9$	$V_e = 2.94 \times 10^9$
$V_i = 2.97 \times 10^9$	$V_o = 2.97 \times 10^9$

Combined ebb and flood flux	= 5.94×10^9 m^3	(98.94%)
River input	= 6.02×10^7 m^3	(1.01%)
Precipitation	= 1.97×10^6 m^3	(0.03%)
Evaporation	= 1.10×10^6 m^3	(0.02%)
Total water flux	= 6.00×10^9 m^3	

Winter Conditions

Very little previous work has been undertaken concerning the effects of ice within the Bay of Fundy. Hind (1875) presents some early observations of the possible consequences of ice formation and movement in this macrotidal environment. It was not until the late sixties that further studies were undertaken by ATPEMC (1969) to ascertain the possible effects of winter ice phenomena in the Bay of Fundy System. In both studies, although brief mention is made of the estimated volumes of sediment trapped in ice, the emphasis was placed on potential engineering difficulties as a result of ice. The sedimentological significance was essentially overlooked. The results discussed here are published in Knight and Dalrymple (1976).

Ice Types - Ice begins to form in December when extended periods of freezing temperatures occur. Ice formation is most rapid during continued intervals of extremely cold weather, heavy snowfalls, and rising tides (towards spring tide conditions). From January to early April, much of Cobequid Bay is covered with drift ice and the shoreline bordered with an ice-foot. From observations made by local inhabitants and ATPEMC (1969), ice persists in Minas Basin-Cobequid Bay until early April each year.

There are basically three modes of ice occurrence: the ice-foot, the drift ice, and the frozen ice crust which covers most of the intertidal zone sediments.

(i) Ice-foot - The ice-foot (Fig. 2.27 A, B and C) begins to form along the high tide level in late December and it remains throughout the winter. It grows during periods of sub-freezing air temperatures through the combined accreting actions of wave spray and wave wash, snowfall and overtopping by high spring tides. Also drift ice floats onto the ice-foot and becomes stranded during high spring tides and(or) onshore storms, producing an irregular, hummocky surface. The ice is relatively dense due to repeated cycles of freezing and thawing experienced at the high tide level as a result of recurrent submergence and emergence by tides and waves. The ice-foot remains attached to the bottom throughout the winter and can therefore be considered as shorefast.

FIGURE 2.27: Ice-foot and drift ice.

A. Ice-foot on a bedrock headland along the south shore of Cobequid Bay (Noel Head). Note sediment concentration in the ice. Arrow points to a shovel 1 m in length.

B. The intertidal foreshore with development of an ice-foot approximately 1.5 m thick and 10 m across at the high tide level. Note that the foreshore sediment facies distribution in winter is similar to that in summer (Fig. 2.8A).

C. The same intertidal foreshore as in B, but packed solidly with grounded drift ice after a period of northeasterly winds. Hinge-line (arrows) occurs at edge of dirty ice, the seaward edge of the shorefast ice. Grounded ice can be seen on the topographic highs of Selma Bar in the middle background.

D. Variable sizes and types of drift ice grounded in the inter-tidal zone of Cobequid Bay, e.g., slush ice, sheet ice, and composite ice. The large ice block in the left foreground is approximately 2 m in length.

E. Elliptical keel shapes of some ice blocks resulting from collisions and from dragging along the bottom in shallow water. Hammer is .3 m in length.

F. A large composite ice block grounded in the intertidal zone; note rimmed upper edges and sediment content. Shovel (arrow) is 1 m.


A


B


C


D


E


F

The overall morphology, mode of formation and nature of the ice-foot is similar to that described from other areas (Davis, R. A., 1973; Dionne, 1970, 1973 a and McCann and Carlisle, 1972). The height and width of the ice-foot is variable and can be related to the steepness of the foreshore slope and the general shoreline morphology. On intertidal foreshores with relatively shallow gradients, an ice-foot of 1.5 to 2 m in height and 10 to 30 m across (perpendicular to the shore) forms (Fig. 2.27 B and C). However, along the truncated seaward edges (up to 2 m in height) of salt marsh deposits, the ice-foot reaches 4 m in height. The greatest thickness of shorefast ice forms on bedrock headlands where rock ledges are exposed at low tide and the intertidal foreshore is relatively steep. In these areas, the ice-foot can reach heights up to 9 m (Fig. 2.27 A), with widths generally less than 5 m.

Sediment is incorporated into the ice-foot by several mechanisms: (1) by freezing of muddy seawater; (2) by mass wastage processes onto the surface of the ice-foot from the adjacent shore; (3) from stranded drift ice; (4) or from freeze-thaw action at the ice-sediment interface beneath the ice-foot. Sediment within the ice reduces the albedo which enhances surface melting during warm days. Subsequent refreezing of the melt-water when temperatures dip below freezing tends to smooth out and glaze the upper surfaces of the ice-foot. Progressive melting concentrates sediment near the upper surface of the ice-foot.

(ii) Drift Ice - According to ATPEMC (1969), drift ice cover increases through early January and mid-February, reaching a maximum in late February. At this time, Minas Basin-Cobequid Bay is 70 to 90% covered with medium to thick drift ice. At no time does the field area become frozen over with a continuous unbroken ice cover. The tidal currents break up large floes and keep the blocks in continual motion. Winds add a variable, cross-bay component to the drift ice motion which can produce striking differences in the foreshore zone appearance from day to day as shown by the photos in Fig. 2.27 B and C. Southerly winds drive the ice to the north side of Cobequid Bay, leaving the southern foreshore almost entirely cleared of ice (Fig. 2.27 B). On the other hand, winds from the north pack the drift ice onto the southern foreshore producing ten-tenths cover (Fig. 2.27 C). When onshore winds prevail

over an extended period of time, the individual blocks become temporarily welded together, and this newly formed ice pack rises and falls with the tide seaward of a hinge line (Fig. 2.27 C) which is located along the outer edge of the ice-foot.

Four distinct types of drift ice can be distinguished in Cobequid Bay on the basis of external and internal form:

1) Slush ice (Fig. 2.27 D) is composed of an unconsolidated mass of ice crystals and water with no definite shape or structure. The individual ice crystals are derived from: the initial freezing stages of seawater; snowfall; and the erosion of ice blocks by collisions during transport.

2) Pan ice (Fig. 2.27 D) is approximately 0.1 to 0.15 m in thickness, and may reach up to 10 m across. It has a smooth upper surface and forms from the freezing of surface waters in sheltered embayments and estuaries. Individual pieces of pan ice are broken off by the rise and fall of the tide and are redistributed by currents and wind.

3) Cake ice (Fig. 2.27 D) forms as independent, near-equidimensional ice blocks, commonly less than 1 m across, from the direct accretion of seawater onto smaller pieces of drift ice. This ice typically but not always has an elliptical base (Fig. 2.27 E) and rimmed top edges which result from collisions with other blocks of drift ice and from grounding out at low tide.

4) Composite ice (Fig. 2.27 F) is an amalgamation of all ice types present and forms from the freezing together of small pieces of ice. Subsequent enlargement occurs by the rafting of other blocks into its surface, and by the direct accretion of seawater and snowfall. Size and shape of composite ice is variable, but it generally occurs as semi-equant blocks which range up to more than 5 m in thickness. The keel of composite ice blocks may be somewhat elliptical as a result of collisions or grounding.

Any type of drift ice can become stranded in the intertidal zone as the tide drops. Most of the blocks float off as the tide rises again, but some become frozen to the bottom during the low tide period and cannot be lifted by the rising water. Ice that has been anchored to the bottom in this manner is called "rooted" ice. Blocks of rooted ice

grow by the accretion of seawater and may achieve sufficient buoyancy to break free eventually, often taking some of the substrate with them. The formation of rooted ice is most common in the higher parts of the intertidal zone (e.g., sand bar crests, and upper surfaces of the ice-foot) where blocks are stranded for a longer time, and on the supratidal marshes near the tidal channels (Fig. 2.28 E, F and G) where they are left behind during spring tides.

The drift ice in Cobequid Bay contains a wide variety of sediment sizes, ranging from clay up to cobbles and larger. ATPEMC (1969) found 8 to 63% sand, and 5 to 30% clay in three samples from the Salmon River estuary. Samples collected along the south shore of Cobequid Bay (Table 2-4) contained 0 to 20% gravel, 35 to 87% sand, and 12 to 47% clay. The total amount of incorporated sediment also varies widely. Hind (1875) reported sediment concentrations of 2.4 to 5.5 gm/m^3 from the Avon River estuary near Windsor. ATPEMC (1969) reported concentrations of 1.3 to 18.1% by weight. Ice collected in Cobequid Bay contained up to 22% sediment by weight (Table 2-4), but with concentrations generally less than 5% by weight. High sediment contents were usually the result of the pick-up of coarse material while grounded or rooted. Low sediment contents can be attributed to the direct incorporation of suspended fines from seawater.

(iii) Frozen Crust - The third mode of ice occurrence in Cobequid Bay is in the form of an ice and sediment crust which covers and immobilizes most of the intertidal sediments (Fig. 2.28A). This crust is usually continuous over many hundreds of meters and gives the sediment surface a smooth, rounded and glazed appearance. The crust varies from about 10 mm in thickness when newly formed, to a maximum of 0.45 to 0.50 mm. Internally, the crust is composed of alternating ice and sediment laminae, up to 10 mm in thickness, which appear to be laterally continuous, and to parallel the surface of the crust over distances of several meters (Fig. 2.28 B). Ice crystals within the crust are commonly elongated in a vertical direction. Sediment concentrations usually range from 30 to 40% by weight, with values as high as 68% in one sample. Although no values of specific gravity are available for the frozen crust, some fragments of the crust floated in seawater, indicating a

T A B L E 2 - 4

ICE-SEDIMENT CONCENTRATION AND TEXTURAL ANALYSIS

Sample No.**	Weight % Total Solids	% Gravel	% Sand	% Mud
1	4.98	--	83.61	16.39
2	13.84	0.75	71.95	27.31
3	21.98	3.93	70.20	25.87
4	0.07	--	80.08	19.92
5	0.08	--	--	--
6	0.17	--	--	--
7	1.26	--	62.38	37.62
8	0.78	--	67.76	32.24
9*	48.97	0.84	52.32	46.83
10*	68.44	1.79	44.05	54.16
11	0.59	--	--	--
12	0.60	--	--	--
13	0.81	--	67.11	32.87
14	1.73	--	69.67	30.33
15*	40.99	0.88	80.62	18.50
16	0.73	--	70.44	29.56
17	5.97	8.43	42.23	47.35
18	3.64	10.80	57.81	31.39
19*	28.96	23.61	64.49	11.50
20	0.07	--	66.92	33.08
21	15.71	--	87.84	12.16
22	22.23	--	83.06	16.94
23	1.11	--	78.14	21.86

Continued.....

Table 2 - 4 -- Continued

24	0.85	--	--	--
25	0.65	--	33.23	66.77
26	0.78	--	55.98	44.02
27*	43.84	--	81.32	18.68

* Denotes sample from frozen ice-crust.

** Sample numbers 1 to 18 collected from drift ice and shorefast ice along intertidal foreshore from the south shore of Cobequid Bay. Sample numbers 19 to 27 collected from drift ice and frozen crust on Selma Bar.

FIGURE 2.28: Frozen crust and saltmarsh in winter.

A. General view of frozen crust covering Selma Bar sediments.

B. Close-up of frozen crust showing interlaminated ice and sediment. Lens cap is 0.05 m.

C. Frozen crust on the mudflat surface near Selma. Crust thickness is 0.08 m.

D. Frozen ice and sediment crust on Selma Bar, approximately 0.45 m thick.

E. Same view as Fig. 2.10D showing the flooding of the saltmarsh surface during a high spring tide in winter. Note close-packing of drift ice along axis of the tidal channel.

F. Same view as in E., but showing the tidal channel at low tide during the winter. Note the chaotic nature of ice grounded in the channel and on the surface of the saltmarsh, and the sediment content of the ice.

G. Erosion of the tidal channel walls by the rise and fall of ice with the tide in the channels. Hammer (right centre) is 0.3 m in length.


A

B


C


D

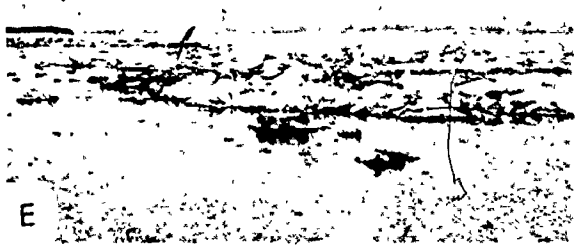
E


F


G

density slightly less than that of the water.

The crust was observed to form when the sediment surface is exposed to freezing air temperatures. In general, the crust was thickest over areas which were topographically high, and which therefore, had relatively long periods of low tide emergence (2.5 to 5 hours). At lower elevations, the crust became thinner and then non-existent near the low water level, where exposure time was too short to allow the development of a crust which was sufficiently rigid to withstand erosion by the flood tide. In areas continuously covered by standing or running water, such as bedform troughs and presumably in the subtidal as well, a crust did not form, and the sediments remained unfrozen and mobile.

The formation of the ice and sediment crust is believed to involve both downward freezing of pore water in the sediment and upward accretion. The vertical build-up of the crust takes place by one or more of the following processes: 1) freezing of sluch ice on the sediment surface; 2) freezing of snowfall; 3) freezing of late stage ebb runoff which occurred as thin sheet flow; and 4) once the crust is initiated, by freezing of water out of the laminar sub-layer of the overlying water. The sediment laminae within the crust is believed to be derived from the small amount of remaining available sediment transported by the tidal currents. The relative importance of downward freezing and upward accretion in crust formation is difficult to determine. The low sediment content, the laterally continuous, laminae parallel to the surface, and the lack of preserved sedimentary structures within the crust indicate that upward accretion is a major factor. On the other hand, in unfrozen sands, a thin surface layer of pore water can freeze within a single low tide period; and on the overturned bases of crust fragments sediment is found frozen into the ice. As well, the thickness of the crust varied with the sediment grain size and porosity. In areas of muddy impermeable sediments, the frozen crust does not exceed 0.08 m in thickness (Fig. 2.28 C), whereas on sandy areas the crust is more than 0.1 m in thickness (Fig. 2.28 D). These features indicate that downward freezing of water in the interstitial pore spaces could also be of importance.

2.5 SUMMARY

The study area in Cobequid Bay is located at the eastern end of the Bay of Fundy system. The bay is funnel-shaped, about 40 km long and about 10 km wide at the mouth where it adjoins the broader and deeper Minas Basin. Most of Minas Basin and Cobequid Bay is bordered and underlain by Triassic sandstones and some Pleistocene glacial sediments (i.e., till and outwash).

The area is reknowned for its large tides which have average spring ranges up to 15 m. The tides are semidiurnal with a small diurnal inequality. The large tides are believed to be due to resonant amplification of the lunar tide as it moves across the continental shelf southwest of Nova Scotia into the Bay of Fundy. The large tides developed largely within the last 4000 years as the bay reached resonance dimensions through the combined effects of the eustatic rise of sea level, the sinking of the land and the erosion of the shoreline and seabed.

The tidal currents, measured 0.5 m from the bottom, attain speeds up to 1.5 m/s in the channels and in the range of 0.3 to 1.25 m/s over the intertidal sand bars which is comparable to current strengths in many areas with smaller tidal ranges. The tidal currents are reversing in character because of the close proximity of the shoreline. The directional modes of the ebb and flood are separated by about 180°.

During both summer and winter, winds blow mainly from the west and average about 16 km/h (Fig. 2.14). This direction is also the direction of maximum fetch in the bay, but because the fetch is limited to about 50 km (Fig. 2.15), waves are generally less than 1 m in height and because of the large tidal range, wave action is dissipated over the broad intertidal zone. Most of the wave energy generated is expended on the bedrock headlands and at the western end of the linear sand bar complex in Cobequid Bay. The sediment regime and pattern of facies is related almost entirely to the tidal currents, and is little affected by wave action.

The climate of the area is continental-marine, with relatively cold winters (Fig. 2.13). The mean annual temperature is about 6°C and the mean annual precipitation about 1.18 m. There is ice in the bay for

three to four months each year (i.e., December to March). The effects of ice on the sediments have been described by Knight and Dalrymple (1976). The formation of an ice foot (Fig. 2.27) and the presence of drift ice greatly reduces shore erosion by wave action.

The formation of an ice-sediment crust (Fig. 2.28) over much of the intertidal zone generally reduces the amount of sediment movement. Some sediment is moved by drift ice (Table 2-4) that has been temporarily stranded in the intertidal zones (i.e., ice rafting). Sediment concentrations range up to 68% in the ice-sediment crust and up to 23% in drift ice (weight %).

Most of the modern sediments in the bay were derived from the erosion of the shoreline and seabed. The rivers entering the bay are presently contributing little sediment (Fig. 2.5), but were no doubt more important as sources of sediment during the post-Pleistocene retreat of the continental ice-sheets (e.g., glacial outwash sediments).

Figure 2.6 summarizes the general sediment facies in the bay relative to tidal position and exposure to wave and current activity. The perimeter of Cobequid Bay is marked by cliffs cut in Triassic bedrock (Fig. 2.7) or Pleistocene deposits (Fig. 2.8). At the base of these cliffs, a broad, steeply inclined wave and current cut rock platform (Figs. 2.7) extends across the intertidal zone. The bedrock platform is either exposed (Figs. 2.7 and 2.8) or covered with a veneer of sand, gravel and/or sand. The existence of the platform reflects the presence of easily eroded bedrock in the shoreline, the exposure of the shoreline to strong wave action and the progression increase of sea level as the tidal range increased, the land sank and eustatic sea level rose. Textural and mineralogical studies (Balaz and Klein, 1972; R. W. Dalrymple, pers. comm., 1976) and estimated rates of shoreline erosion (up to 2 m/y) suggest that coastal erosion is an important source of modern sands in the bay.

Although suspended sediment concentrations are large in the bay, thick deposits of mud are relatively uncommon. Mud accumulates only in areas that are sheltered from strong wave and current action around the margins of the bay (e.g., in small bays and estuaries). The mudflats (Fig. 2.9) exhibit characteristics (e.g., sediment texture and organism zonation) that are generally similar to those reported from mudflats elsewhere (e.g., the Dutch and German North Sea). The mudflats are

backed by a supratidal saltmarsh (Fig. 2.10).

The central part of the bay is almost entirely filled with sand (Figs. 2.11 and 2.12) that has been moulded into a number of intertidal and subtidal bars separated by a system of tidal channels. The bars are generally elongate parallel to the tidal currents and are covered with large current-produced bedforms (megaripples and sand waves).

The amount of suspended sediment in the waters of the bay is much higher than that in the rivers above any tidal influence. Suspended sediments form a "turbidity maximum" in the major estuaries as described from estuaries elsewhere. In Cobequid Bay, suspended sediment concentrations (based on 77 water samples) vary during the tidal cycle (Fig. 2.25), ranging from 70 to over 2700 mg/l. The largest concentrations occur during the late ebb and early flood when water depths are relatively shallow and shortly after the time of the maximum ebb and flood current velocities (Fig. 2.26). Concentrations during the early flood are often more than 50% higher than those during the ebb. The higher concentration of suspended sediment during the flood, compared with the ebb, is due to the affects of "settling and scour lag" mechanics discussed by Postma (1967). The large amount of suspended sediment in the waters of the bay is likely related to the resuspension of mud from the intertidal mudflats by wave and current activity. Most of the suspended sediments are clay and silt, not sand-sized.

Because of the large tidal prism and the relatively small volume of freshwater input into the bay (Table 2-3), the waters of the bay are well-mixed and vertical stratification of temperature and salinity are almost totally absent. During the flood, water temperatures and salinities are about 2 to 3°C lower and 1 to 2 °/oo higher respectively compared to those during the ebb (Figs. 2.23 C and D, and 2.24), reflecting the influx of the colder, more saline ocean waters from the main Bay of Fundy. Summer temperatures generally average about 16°C. In winter, water temperatures drop just below freezing. Water salinities in Minas Basin-Cobequid Bay range from 25 to 30 o/oo. During spring tides, the differences of temperature and salinity between the ebb and flood are slightly larger (Fig. 2.24) than during neap tides (e.g., ebb and flood temperature differences during spring tides are about 0.5°C while during neap tides are about 0.2°C). The lunar tidal month variation of water temperatures

and salinities reflects the variations in the net volumetric exchange of the tidal prism (i.e., net loss during springs and net gain during neaps). Temperatures and salinities of the waters also varied by 1 to 2°C and 2 to 3 o/oo during the semidiurnal tidal cycles (Fig. 2.24).

The areal variation of tidal current directions, water temperatures and salinities during a tidal cycle (Fig. 2.23) do not support the existence of an anti-clockwise Coriolis force circulation pattern in Cobequid Bay as proposed by Pelletier and McMullen (1972) and Swift and McMullen (1968).

CHAPTER 3

COBEQUID BAY SAND-BODY COMPLEX

3.1 INTRODUCTION

Cobequid Bay is a funnel-shaped estuary that extends approximately 45 km from the west side of Burntcoat Head to the Salmon River estuary at the head of the bay (Fig. 3.1). From the entrance to Salter Head, the width of the bay averages about 9 km. East of Salter Head, the shorelines converge.

Because of the large tidal range, an extensive intertidal zone is exposed at low tide (Fig. 3.2). Fig. 3.3 shows the distribution of intertidal sediment facies in Cobequid Bay. Note that the central part of the bay is almost entirely filled with sand. Around the margins of the bay, bedrock platforms are exposed (e.g., adjacent to headlands), or veneered with sand and gravel, or mud.

The sand-body complex in Cobequid Bay is similar in many respects to Hayes' (1975, p. 17 and Fig. 17) morphological model for a macrotidal estuary: "The most prominent feature of this type of estuary is the overwhelming dominance of tidal currents. Such estuaries are usually broadmouthed and funnel-shaped. Sand deposition is normally concentrated in the centre of the estuary, away from shore, which is usually dominated by broad, muddy tidal flats. The sand bodies are long linear features oriented parallel with the tidal currents." The sand-body in Cobequid Bay comprises two subfacies, the first of which is the chief concern of this study: (i) the asymmetrical-shaped, elongate sand bars covered with megaripples and sand waves situated in the outer bay (Fig. 2.12 A and B); and (ii) the broad sand flats with ripples and few large bedforms situated in the inner bay (Fig. 2.12, E and F). The sand-body subfacies also differ with respect to two other aspects; the sediments of the outer bay are primarily medium-sized sands, while those of the inner bay are chiefly fine-grained sands; and, the outer bay is characterized by

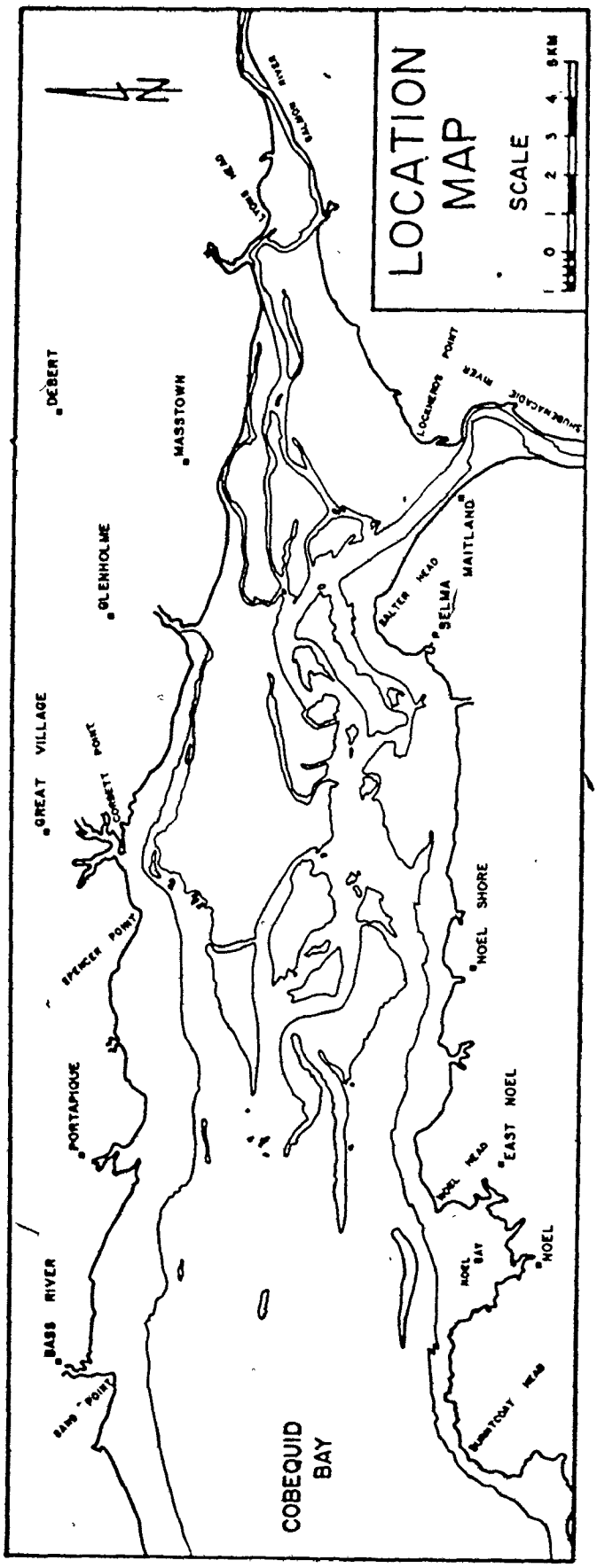

FIGURE 3.1: Location map of Cobequid Bay showing local place names.

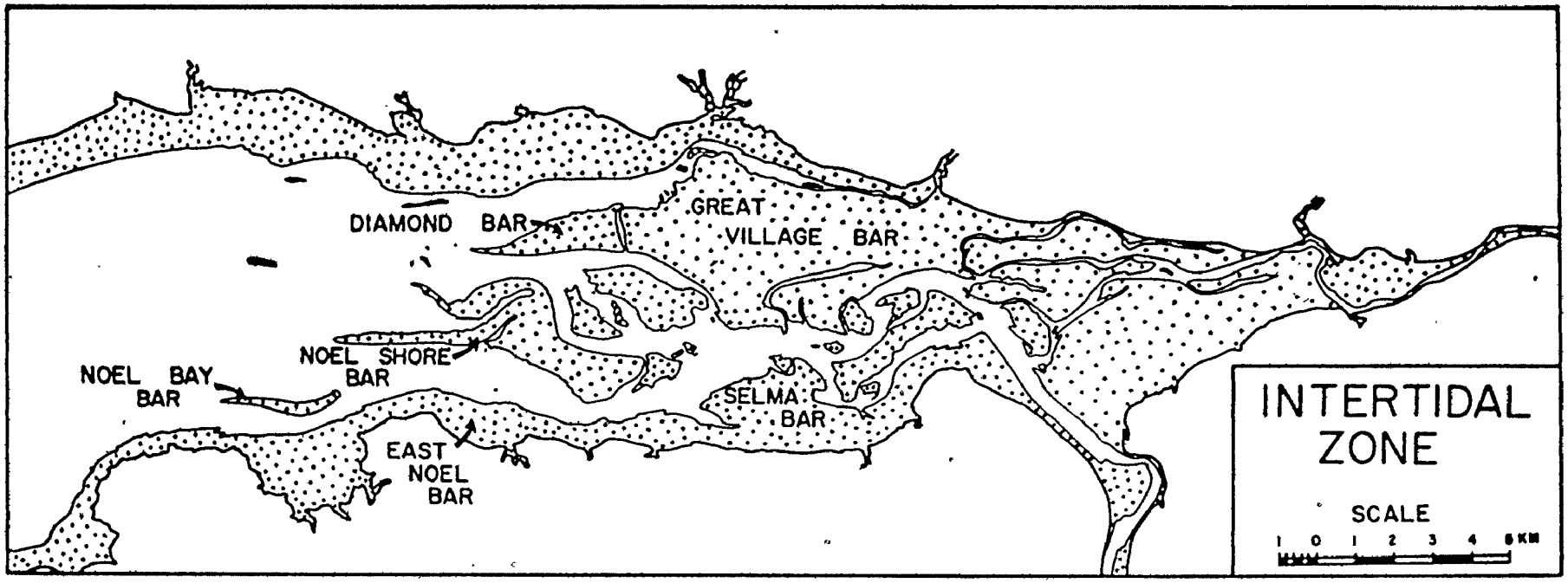

FIGURE 3.2: Map showing the extent of the intertidal zone in Cobequid Bay and the names of the main sand bars. Outline of shoreline and intertidal zone is based on air photographs taken in 1973.

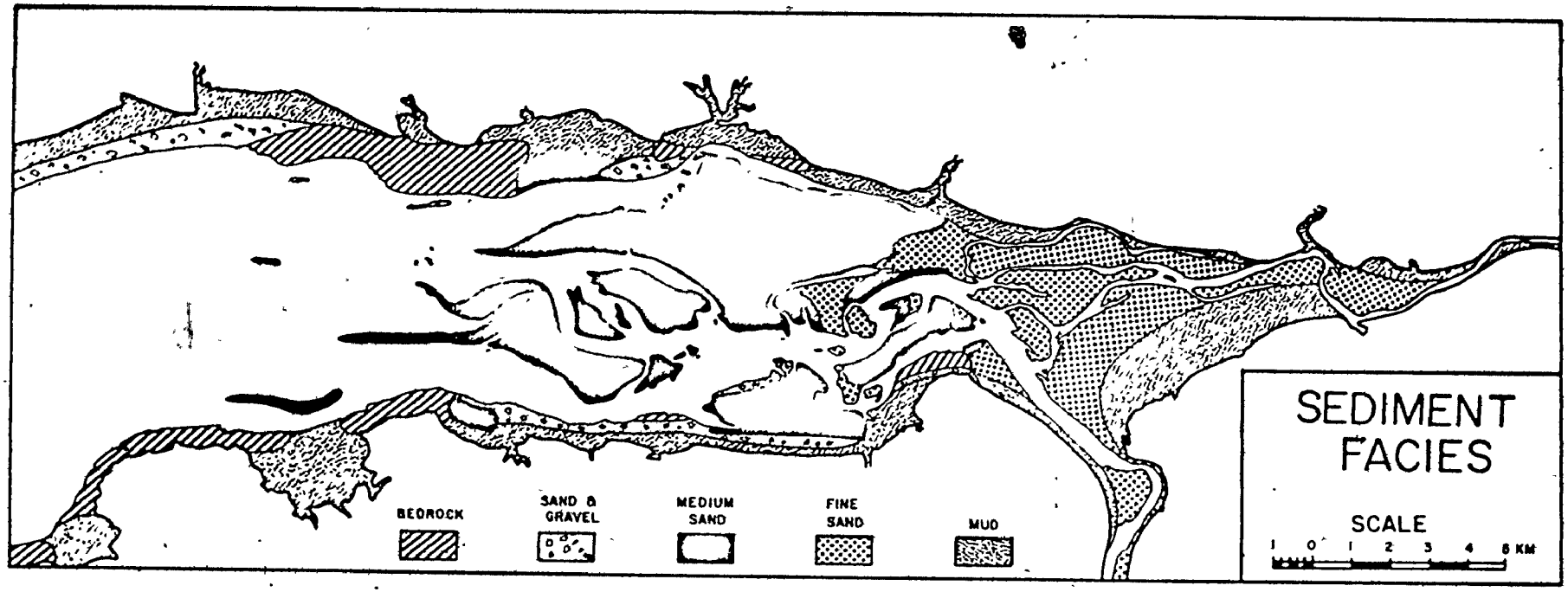

FIGURE 3.3: Map showing the distribution of the intertidal sediment facies in Cobequid Bay (based on fieldwork and air photos taken in 1973).

several major channels, while the channel pattern of the inner bay is braided (with many small anastomosing channels).

3.2 BATHYMETRY

The submarine morphology of Cobequid Bay was initially determined from Canadian Hydrographic Chart 4010, the only bathymetric chart available for the region which is, unfortunately, out-of-date. The high water line was charted from the D.M.T.S. maps (11E) which were compiled from air photographs taken in 1933 and 1938, and from field surveys done between 1938 and 1942. The low water line (chart datum), including the soundings, were mapped from British Admiralty Chart Number 353 which is based on surveys carried out in 1860 (E. M. Walsh, Canadian Hydrographic Service, pers. comm., 1973). Although the relative position and configuration of the shoreline has not changed noticeably since Chart 4010 was printed, the bathymetry of Cobequid Bay has undergone considerable modification. Nevertheless, Chart 4010 is useful as a historical document.

A bathymetric survey of the bay, between Burntcoat Head and Salter Head (Fig. 3.4), was undertaken in early August, 1973, to provide an up-to-date map of the area where the field work was to be concentrated. The survey and reduction methods are discussed in Appendix I, Sections 2, 3, and 4.

Figure 3.5 shows the bathymetry of the sand-body complex in Cobequid Bay. Near the entrance of the bay, the bathymetry is relatively simple and water depths, in the centre, are greater than 30 m. Towards the head of the bay, the bathymetry becomes more complex and water depths shallower.

The actual sand-body complex begins to the east of a line connecting Sand Point and Noel. The western part of the complex has three main channels (compare Figs. 3.2 and 3.5): (i) a northern channel that is situated between the bay's north shore, and Diamond and Great Village Bars; (ii) a central channel that separates Diamond and Great Village bars from Noel Shore Bar; and (iii) a southern channel that is located between the south shore of the bay and Noel Shore Bar. The northern

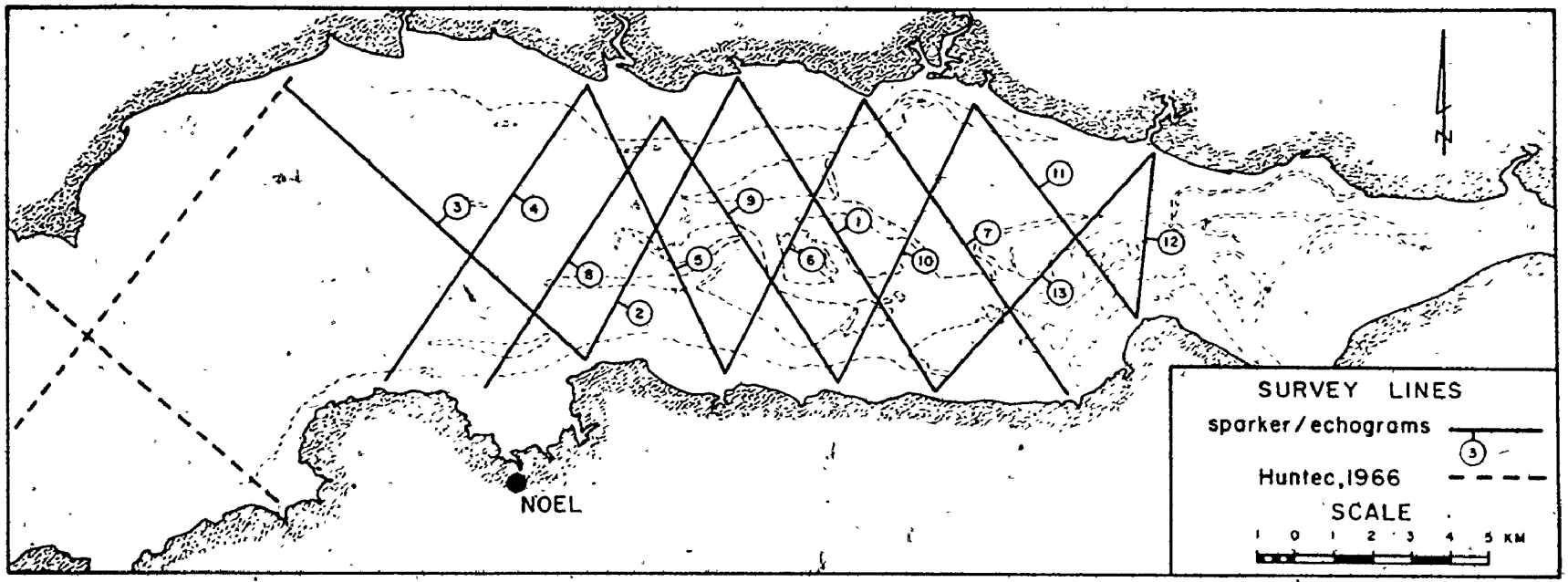

FIGURE 3.4: Location of echogram and sparker survey lines relative to the sand-body complex in Cobequid Bay.

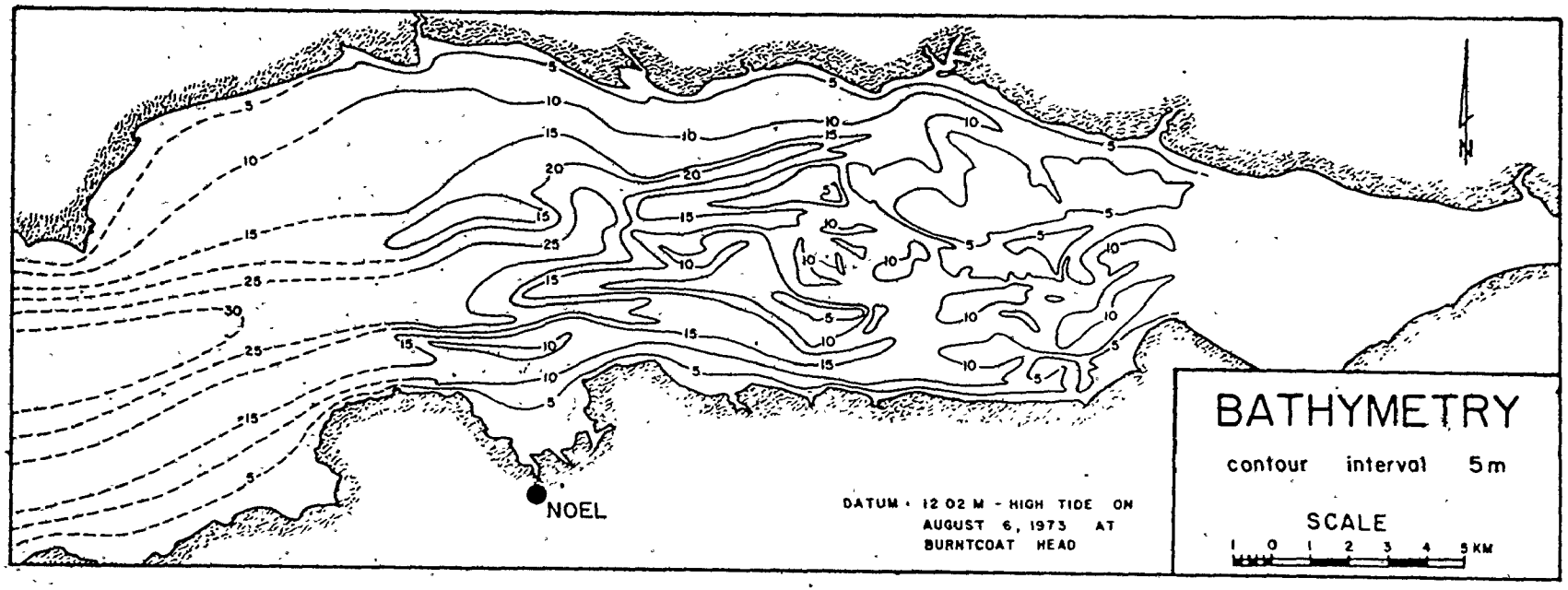

FIGURE 3.5: Bathymetry of Cobequid Bay. Sounding datum is 12.4 m above 'chart datum' (Dohler, 1970).

channel terminates at the shoreline south of Glenholme, while the central and southern channels merge into a single channel (northeast of Noel Shore) that extends past Salter Head.

Although not evident in Figure 3.5, the channels and bars are asymmetrical in cross-section (Figs. 3.7 and 3.8). The southern margins of Diamond Bar, Great Village Bar, Noel Bay Bar and the west end of Noel Shore Bar are steeper than the northern sides. The reverse is true for many of those bars, or parts of bars, not listed (e.g., Selma Bar, the north and southeastern sides of Noel Shore Bar).

Figure 3.6 summarizes some of the general features of the Cobequid Bay bathymetry. Towards the head of the bay, water depths become shallower. The maximum bathymetric relief near Burntcoat Head exceeds 25 m, while near Salter Head, the average relief is less than 5 m. The elevation of the sand bar crests increases from west to east (from about 10 m to less than 5 m depth relative to sounding datum).

3.3 STRUCTURE AND GEOMETRY

Because the relief of the sand bars ranges from 5 to 10 m (i.e., beyond the approximately 1.5 m maximum depth of trenching), seismic methods must be used to study the internal structure and geometry of the sand-body complex.

Previous seismic studies in the bay (ATPEMC, 1969; Huntec, 1966; Swift and McMullen, 1968) were not done with the specific intention of determining the size, shape, and the internal geometry and stratigraphy of the intertidal-subtidal sand-body. The earlier surveys were primarily concerned with the engineering properties of the sediments as they related to sites of possible barrages for a tidal power project in the bay.

In order to investigate the sedimentologic aspects of the sand-body structure and geometry in Cobequid Bay, a shallow-penetration, continuous seismic survey was carried out in conjunction with the bathymetric survey (Fig. 3.4) in the early part of August, 1974. The field and reduction methods used in the survey are discussed in Appendix I.5.

The continuous seismic profiling records (Figs. 3.7 and 3.8) show

FIGURE 3.6: Variation of cross-sectional and longitudinal bathymetric profiles in Cobequid Bay (drawn from Fig. 3.5).

A. Location of cross-sectional and longitudinal profiles.

B. Cross-sectional profiles.

C. Longitudinal profiles.

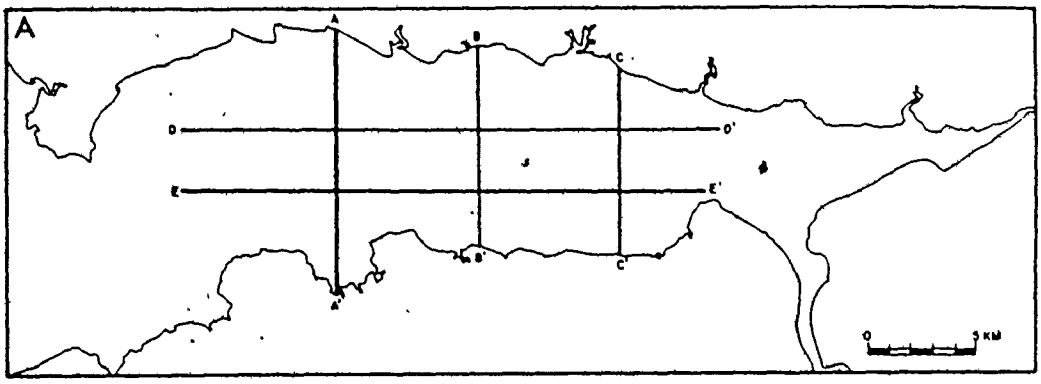

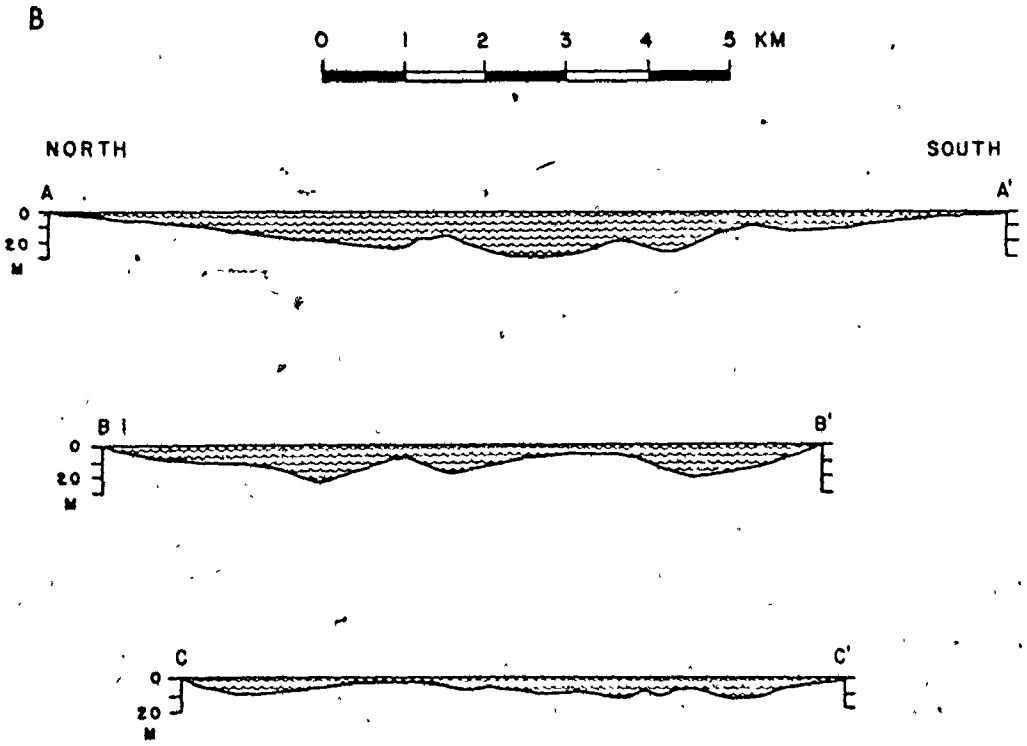

COBEQUID BAY CROSS-SECTIONAL PROFILES

HIGH WATER DATUM = 12.02 M

C

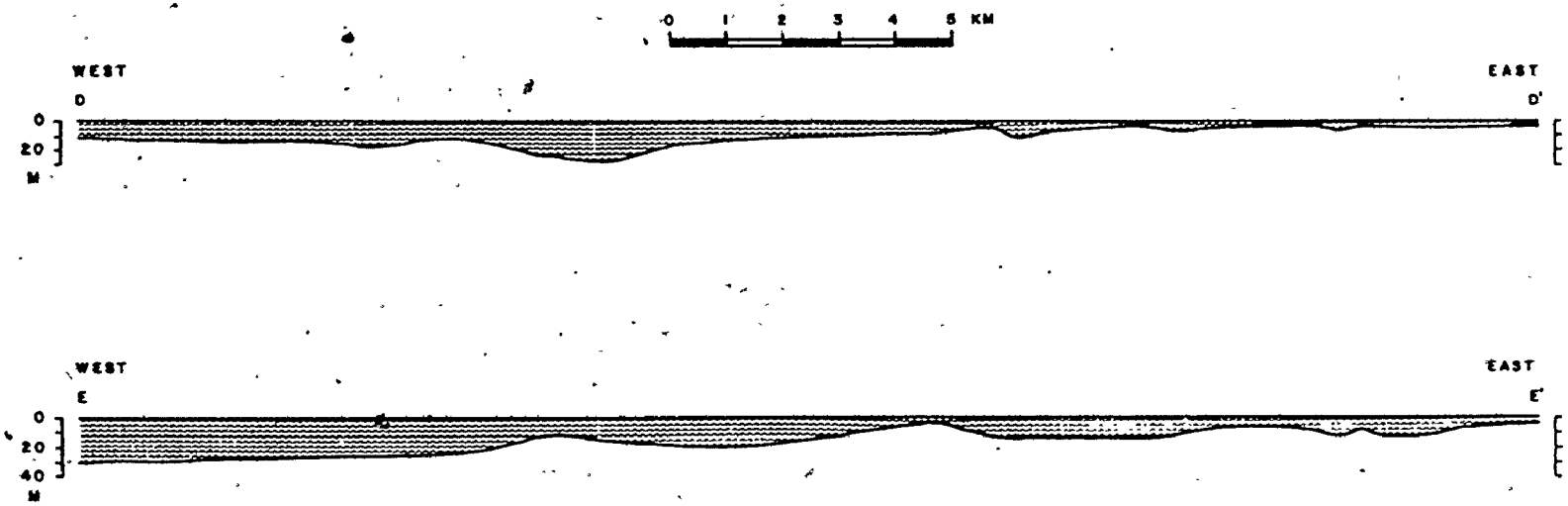

COBEQUID BAY LONGITUDINAL PROFILES

HIGH WATER DATUM = 12.02 M

FIGURE 3.6 - cont'd.

FIGURE 3.7: Continuous seismic profiles in Cobequid Bay from representative sections of the bay showing the original record and structural interpretations.

Line 2: Across Noel Shore Bar from NE to SW.

Line 4: Across the subtidal part of the small sand bar located to the west of Diamond Bar from SW to NE.

Line 6: Across Diamond Bar from SW to NE.

Line 9: Across Diamond Bar and Noel Shore Bar from NW to SE.

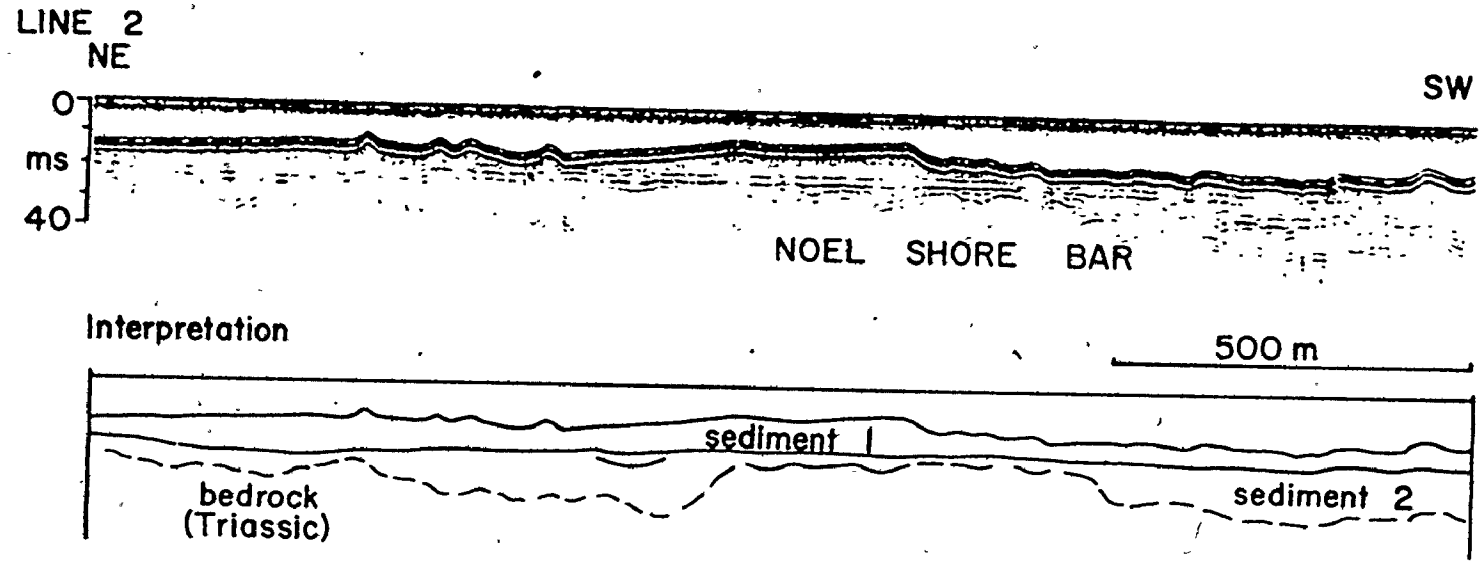
LINE 2
NE
SW
0
ms
40
NOEL SHORE BAR
Interpretation
500 m
sediment 1
bedrock
(Triassic)
sediment 2

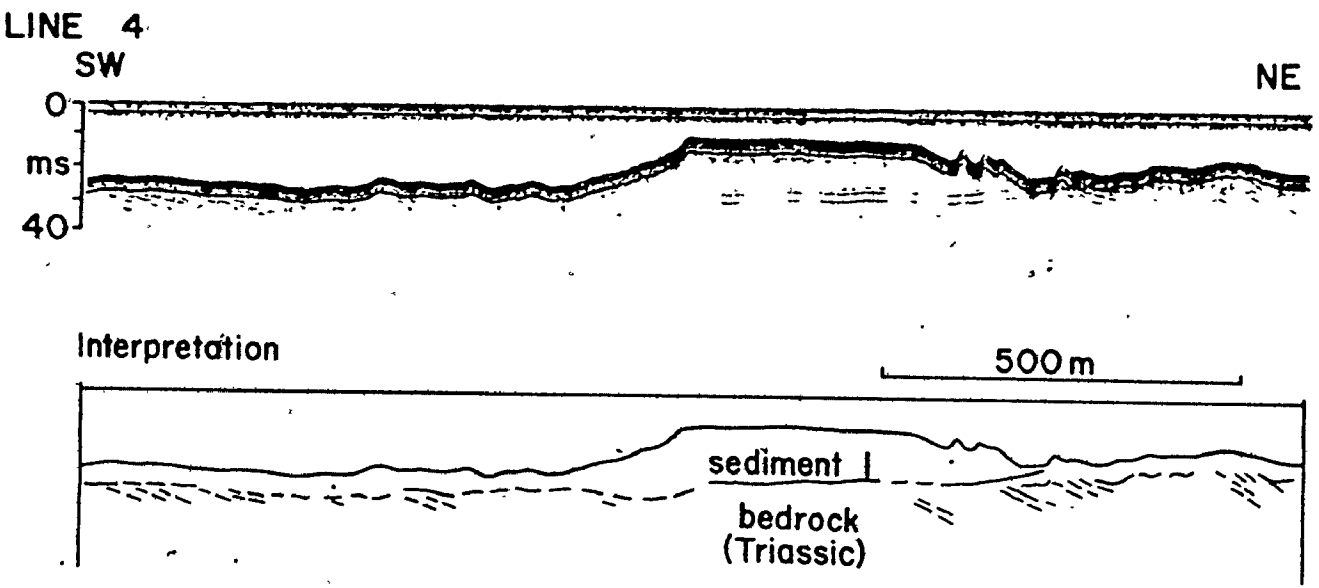
LINE 4
SW
NE
0
ms
40
Interpretation
500 m
sediment 1
bedrock
(Triassic)

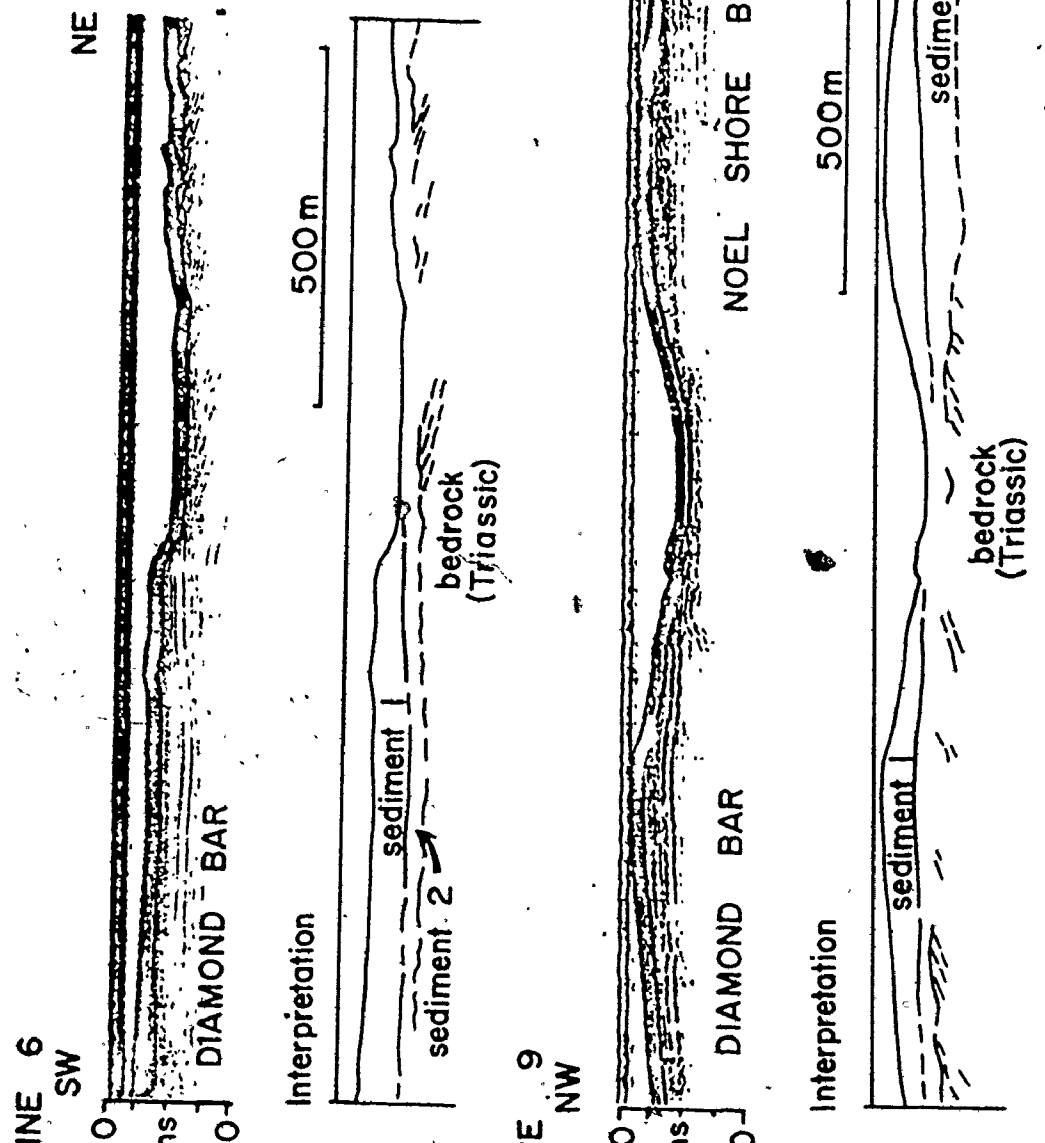

FIGURE 3.7 - cont'd.

FIGURE 3.8: Interpreted structural cross-sections (Fig. 3.4) of the intertidal-subtidal sediments from the continuous seismic profile records in Cobequid Bay.

Lines 1 - 13.

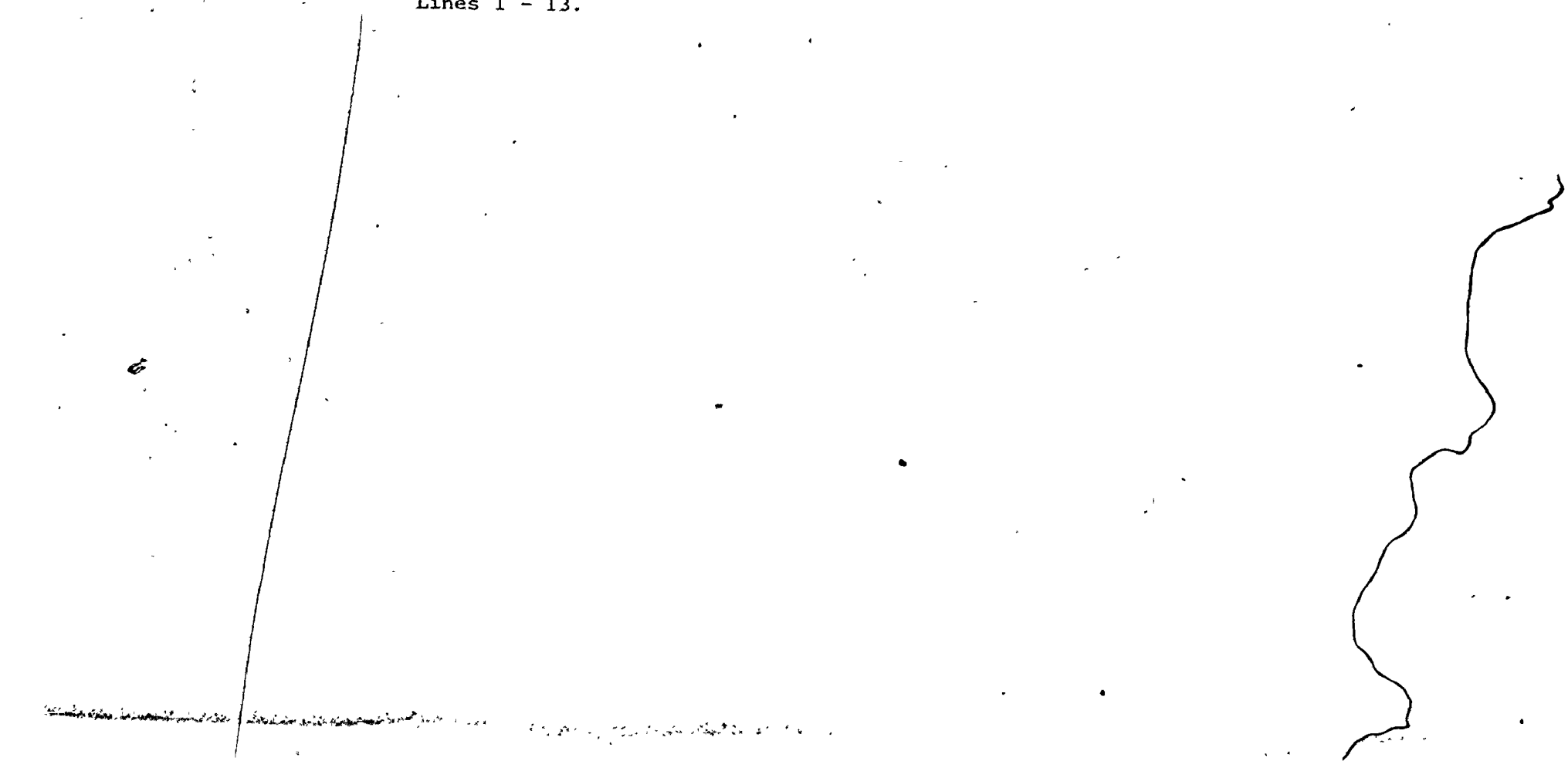

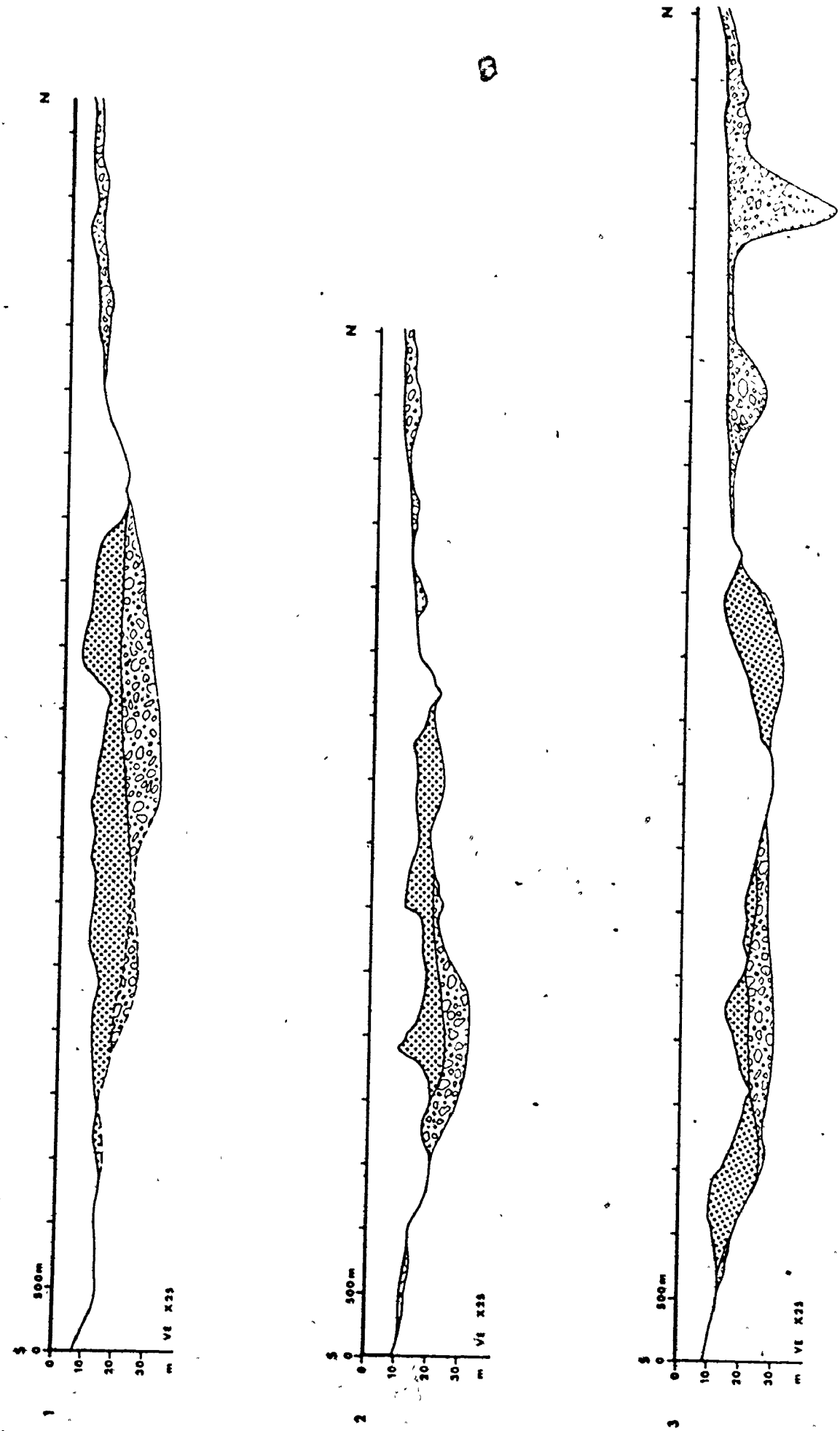
N
S
500m
0
10
20
30
m
Ve X2
1
2
3

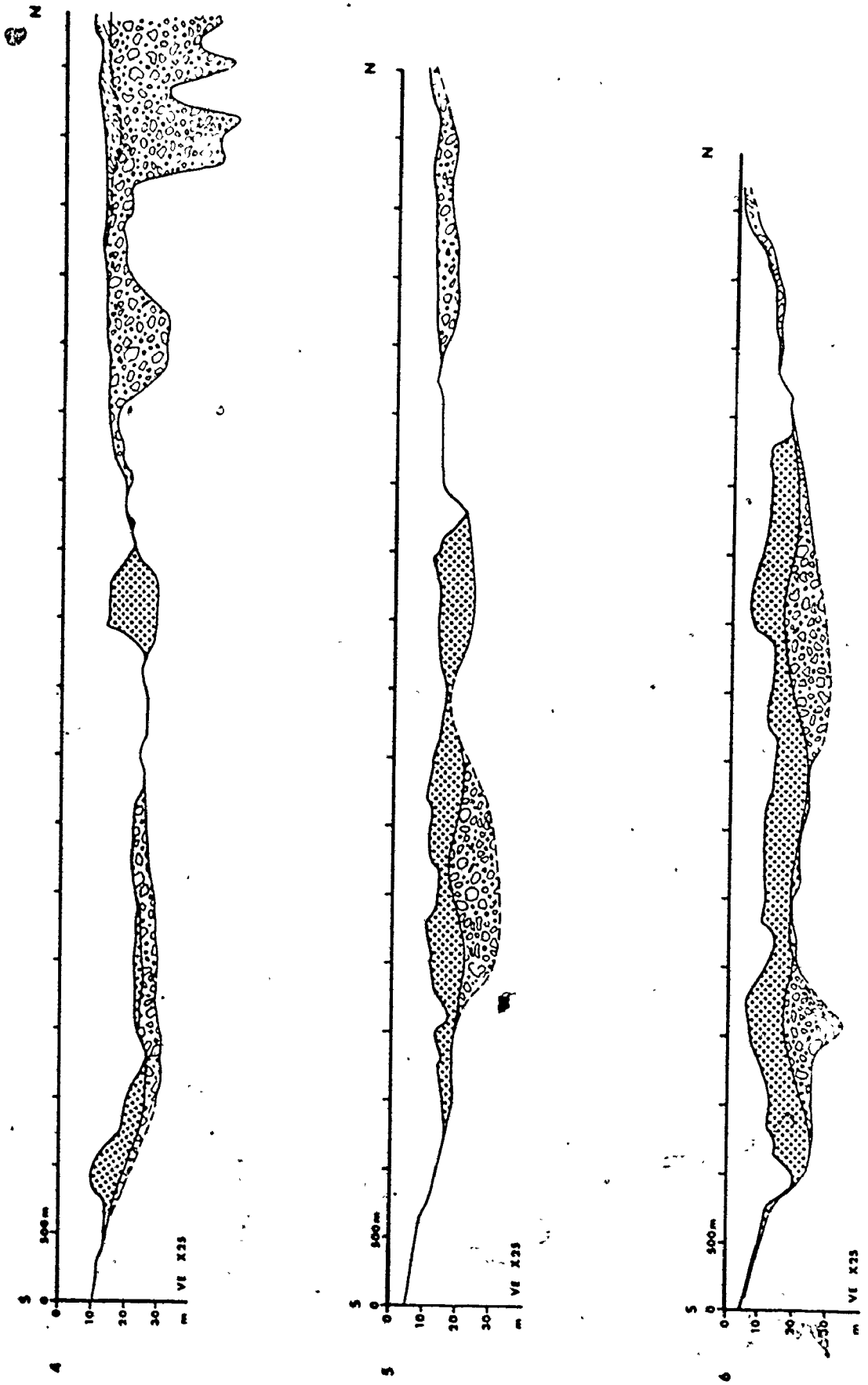

FIGURE 3.8 - cont'd.

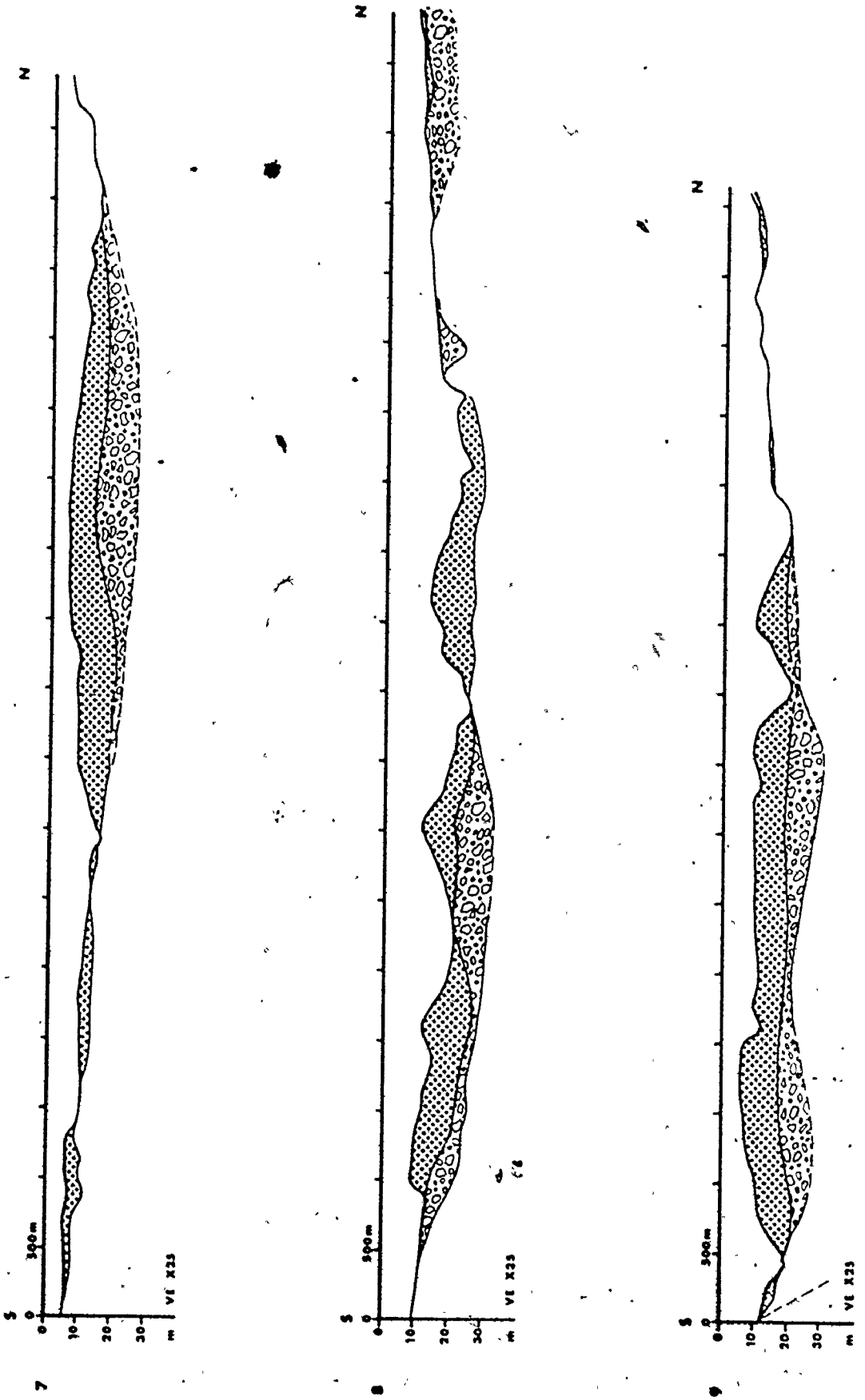

FIGURE 3.8 cont d.

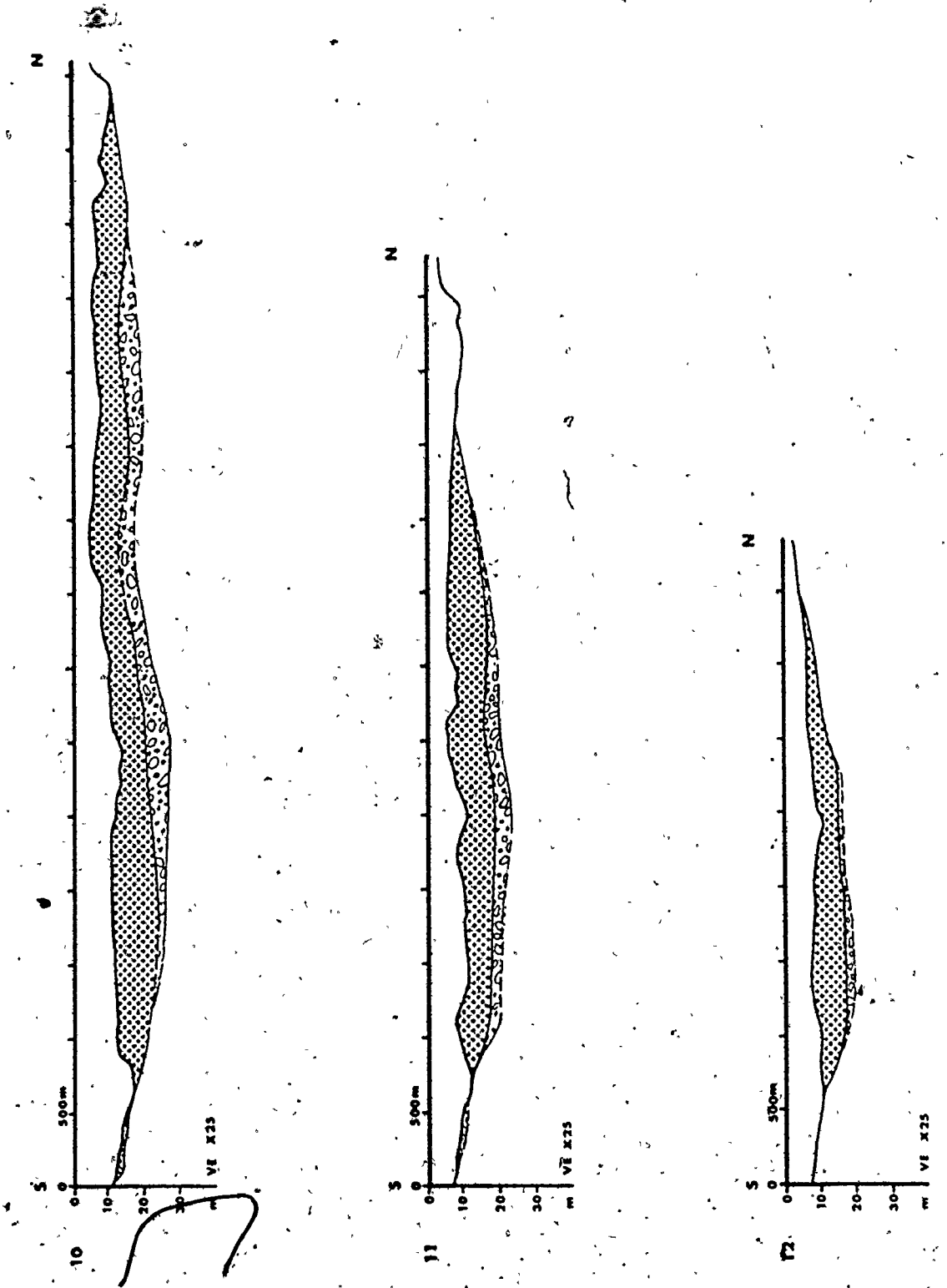

FIGURE 3.8 - cont'd.

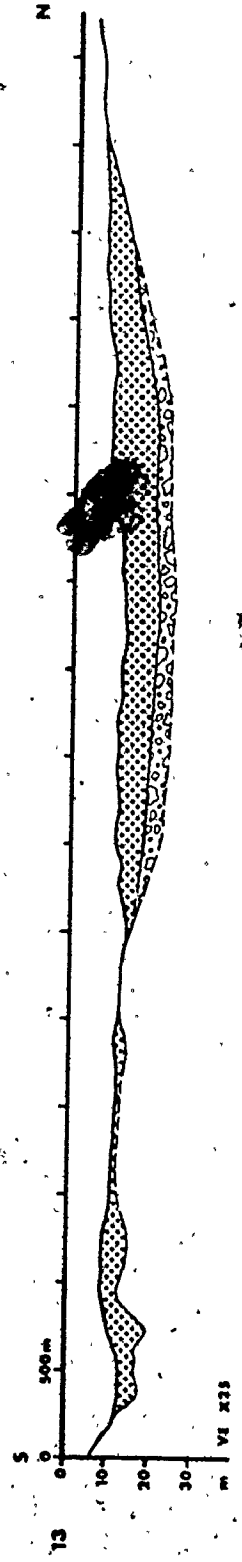

FIGURE 3.8 - cont'd.

that the 'recent' sand-body in Cobequid Bay occurs as local or pseudo-tabular accumulations (up to 15 m thick) that are concentrated in the central part of the bay, overlying a fairly uniform and flat surface of either bedrock (Triassic) or a second sedimentary deposit (up to 10 m thick). Individual accumulations range from 0.5 to 6 km in width.

Figure 3.9 shows the contours on the Triassic bedrock surface that underlies the Holocene sediments in the bay. The bedrock surface forms a generally flat-floored, longitudinal depression along the central axis of the bay that gradually shallows (by about 25 m from Economy Point to Salter Head) towards the head of the bay. The depression divides into two relatively shallow lows south of Spencer Point for a short distance, then merges north of Selma Bar (Fig. 3.2). Two narrow, but deep channels (up to 30 m deep) occur to the east of Economy Point, extending north-eastwards towards the shoreline between Bass River and Portapique.

The morphology of the bedrock surface (Fig. 3.9) is an important control on the accumulation of Holocene sediments. Figure 3.10 shows the isopachs of the second sedimentary deposit lying directly on the bedrock surface. These sediments are concentrated along the depression in the bedrock surface as elongate accumulations roughly parallel to the longitudinal axis of the bay. These local accumulations of sediment are about 5 to 10 km long, 1 to 6 km wide and range up to 25 m thick. The maximum thickness of accumulation (greater than 25 m) occurs beneath Noel Shore Bar. The deep bedrock channel near Economy Point is filled with more than 30 m of sediment. In this latter area, the record is very clear in the interval above the bedrock surface. This may indicate the presence of a fairly uniform lithology, possibly silt or mud, in contrast to the coarser sands and gravels that overly it.

Figure 3.11 shows the contours on the surfaces of the second sedimentary unit and bedrock together. The contours indicate that the second sedimentary unit has effectively infilled many of the irregularities in the bedrock surface (i.e. the relief of this surface is less than that of the bedrock surface), but a central longitudinal depression remains. The surface shoals about 15 m from Burntcoat Head to Salter Head (compared with about 25 m for the bedrock surface).

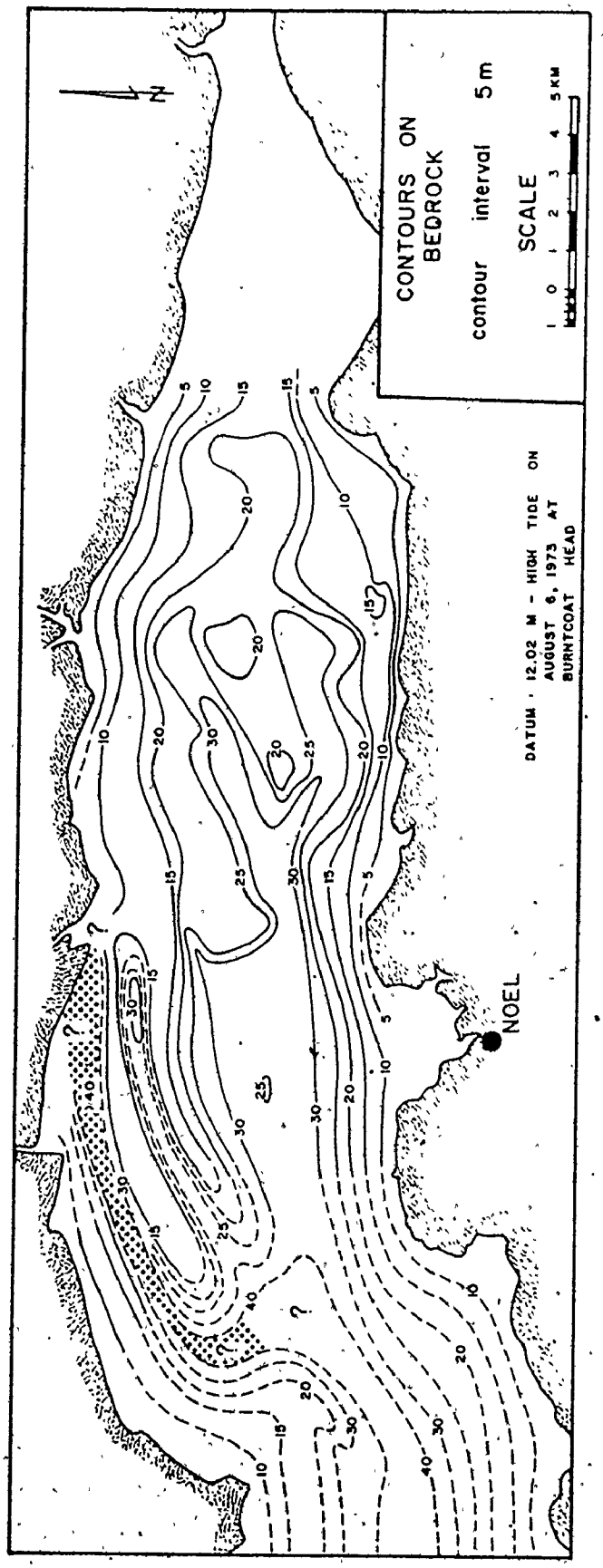

FIGURE 3.9: Contours on the bedrock surface underlying the 'modern' sediments in Cobequid Bay.

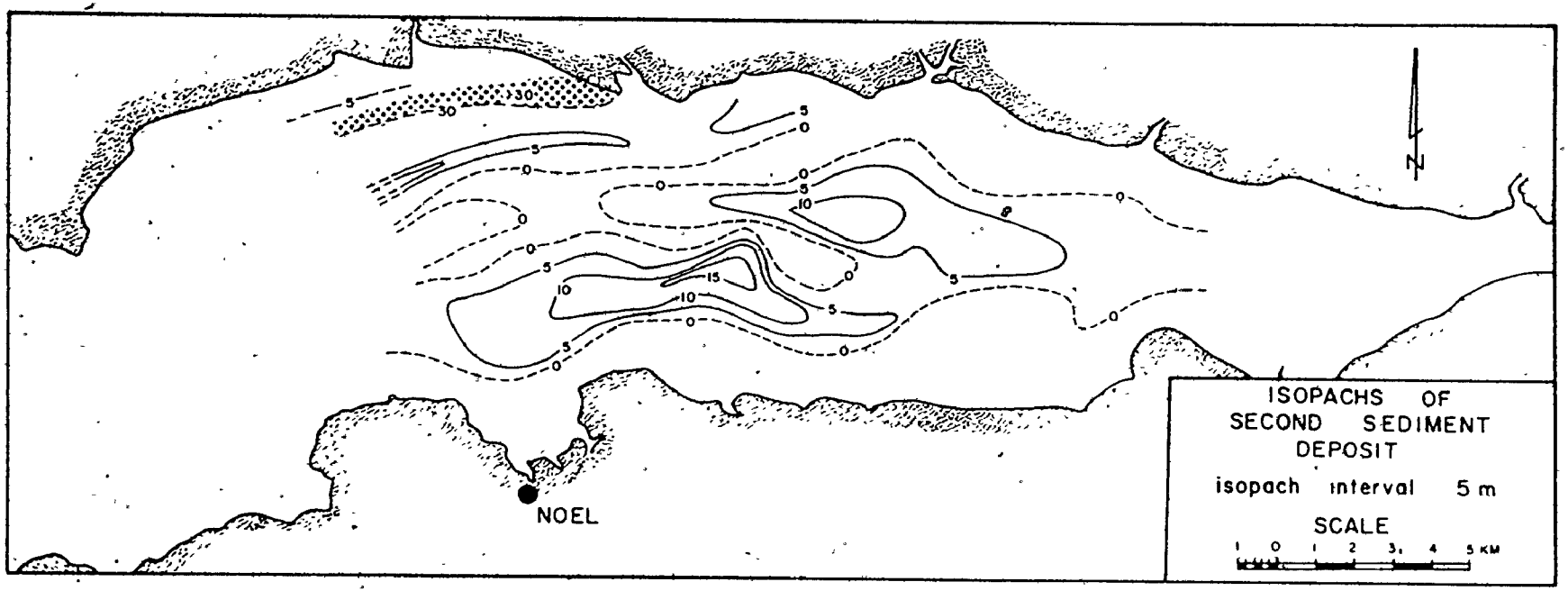

FIGURE 3.10: Isopachs of the second sedimentary deposit.

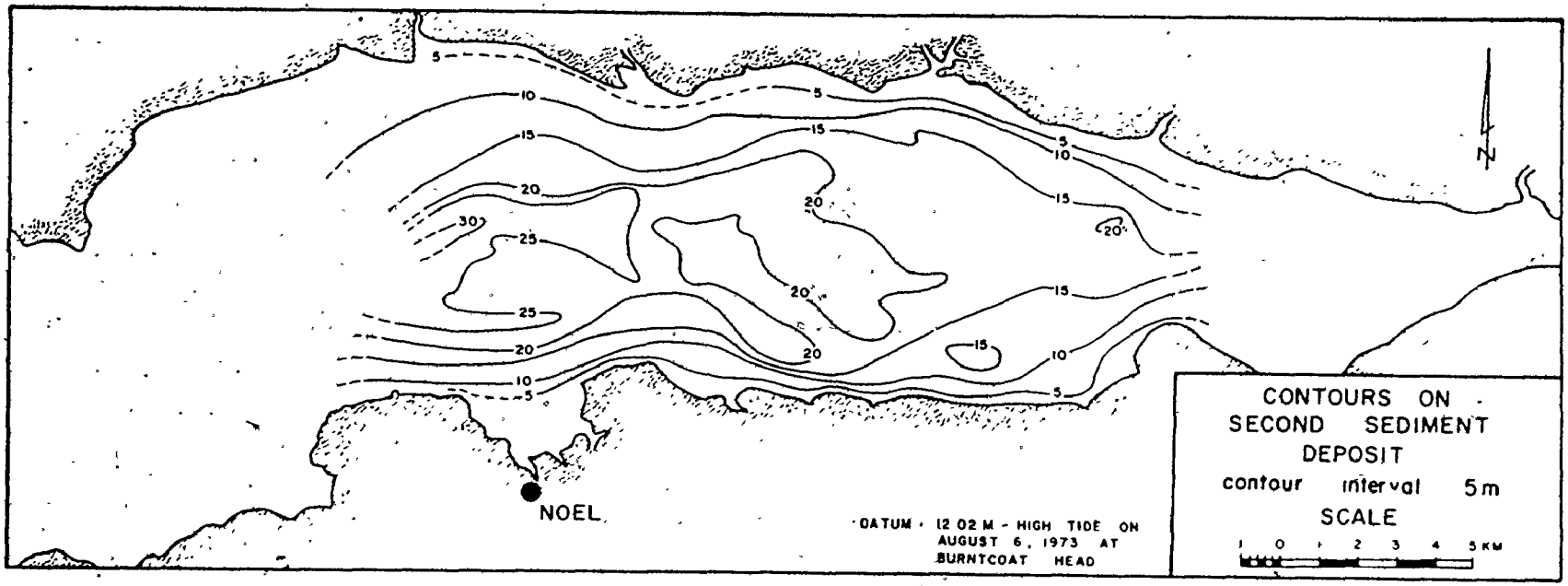

FIGURE 3.11: Contours on the surface of the second sedimentary deposit and bedrock together.

The uppermost sedimentary deposit (Fig. 3.12) comprises an irregular shaped sand-body that is concentrated along the centre of the bay. The upper unit is referred to as the 'recent' or 'modern' sediments. The 'recent' sediments are areally more extensive and morphologically more complex than the underlying sedimentary unit. Maximum sediment thickness is about 15 m beneath the crests of some of the sand bars (compare Figs. 3.5 and 3.12), particularly near the west end of the sand-body complex. The average thickness is about 10 m. The present bathymetric relief of the sand bars closely approximates the thickness of the 'recent' sediments and the intertidal outline of some of the bars. The north and south margins of the 'recent' sediments is generally defined by the absence of sand-sized sediments (compare Figs. 3.3 and 3.12). Where sand occurs on the intertidal foreshore, it is less than 0.5 m thick.

Figure 3.13 shows the isopachs of the total unconsolidated sediments overlying the Triassic bedrock (King and McLean, 1974) surface in Cobequid Bay. The contour patterns are similar to those for the 'recent' sediments. The maximum thickness of sediment is found beneath Noel Shore Bar (greater than 30 m). Note the thick accumulations of sediment in the bedrock channel east of Economy Point. This channel extends to the Bass and Portapique river valleys which are filled with glacio-fluvial sediments (D. Wightman, Dalhousie Univeristy, pers. comm., 1975).

The sediments and bedrock were identified from exposures in either the intertidal zone or from the shoreline. Unfortunately, exposures of the second sedimentary unit were poor. Without borehole data, there are two possibilities for the identity of this unit: (i) the unit may represent Pleistocene glacial materials deposited as either till or glacio-fluvial sediments, and possibly reworked during the postglacial marine transgression; or (ii) the unit may represent the lower part of a 'multistory' stacking of Holocene tidal sand-bodies developed in response to the postglacial rise of sea level and an increase of tidal amplitude causing frequent lateral shifting and vertical accretion of the channel-bar complex.

Some previous workers (Huntec, 1966; Swift and McMullen, 1968) did

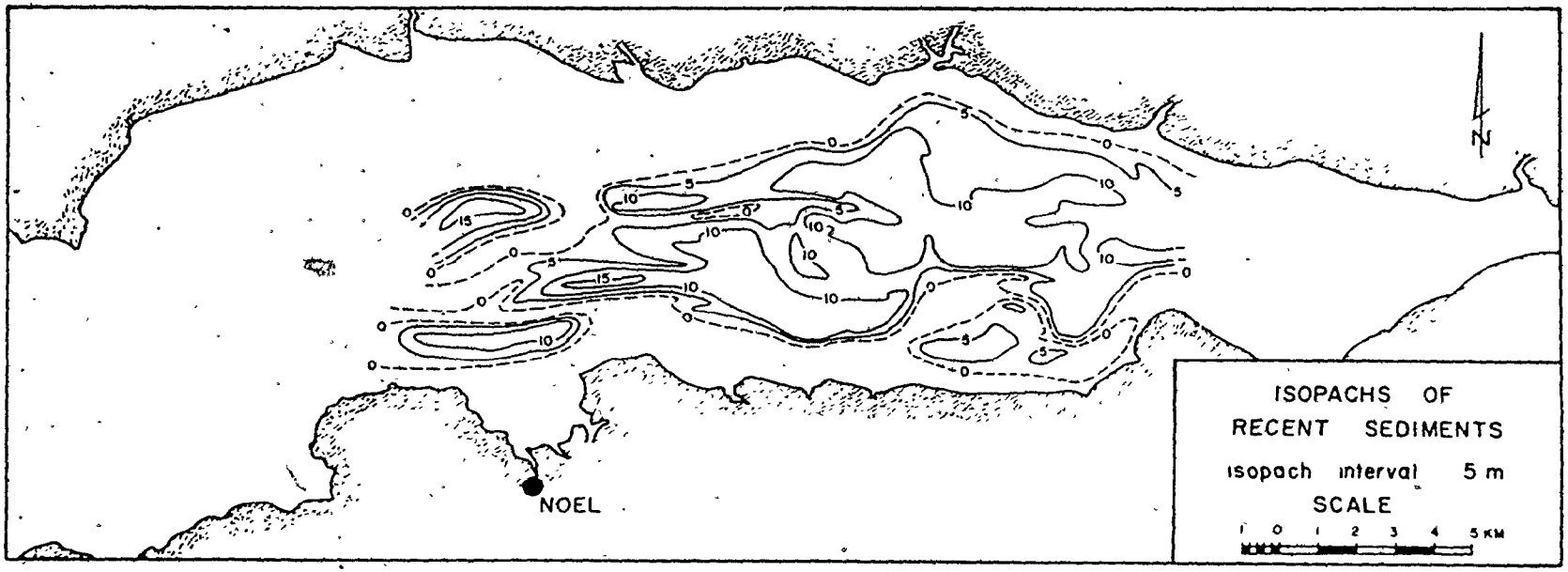

FIGURE 3.12: Isopachs of the 'recent' sedimentary deposit in Cobequid Bay.

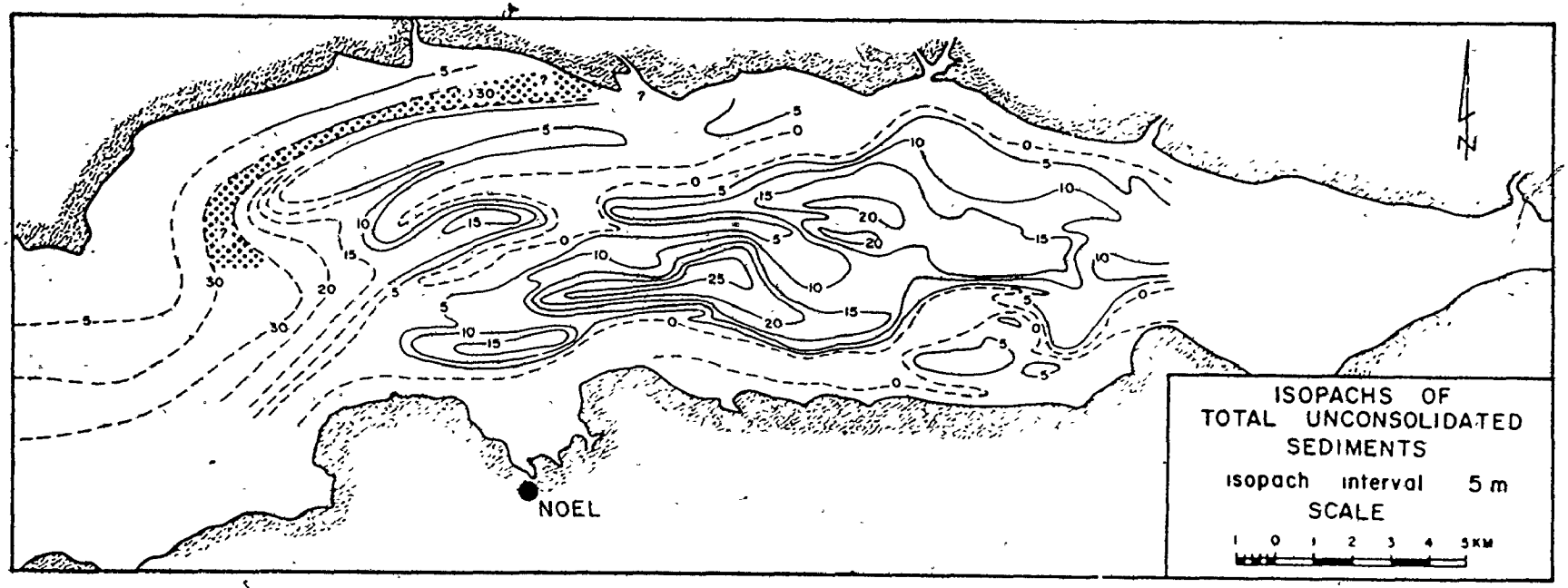

FIGURE 3.13: Isopachs of the total unconsolidated sediments overlying the Triassic bedrock surface in Cobequid Bay.

not recognize the presence of the second sedimentary deposit in Cobequid Bay which is evident in Figure 3.7 A, C, and D. They believed that there was a single sand-body overlying the bedrock surface. ATPEMC (1969) made a brief reference to a second sedimentary deposit found beneath three sand bars in Cobequid Bay (p. A3-34 and Plate A3-24), but they were unable to identify the deposit, so included it with the other Holocene sediments overlying the bedrock surface. They concluded that the second deposit was related to some reddish-brown clayey-silts recovered from boreholes along a lone between Economy Point and Cape Tenny. This conclusion is unsubstantiated. Without further data from boreholes, it is still not possible to identify the second unit reliably. Where possible, the second unit appeared to merge with the sandy-gravel sediments overlying the bedrock surface, which tends to support the second possibility for the identity of the second sedimentary unit. These results, however, are inconclusive without further stratigraphic data.

3.4 INTERTIDAL ZONE

The configuration and lateral extent of the intertidal zone in Cobequid Bay (Fig. 3.2) has remained relatively stable through time, except for some small local changes. The historical changes in the intertidal zone were examined from maps (British Admiralty Chart 353; DMTS map sheets 11/5E, 5W and 6W; Canadian Hydrographic Survey Chart 4010) and vertical air photographs (National Air Photo Library photos from 1938, 1947, 1948, 1961 and 1963). Additional air photos of the bay at low tide were contracted from Atlantic Air Survey (Halifax, N.S.) in 1972 and 1973 to obtain recent information about the intertidal zone. Several flights were also made over the bay in a Cessna 172 (Keith Stephens, Tennycape) during low water periods on June 7, 1971, August 23, 1971, and August 25, 1975. An additional flight was made in June, 1975, by R. W. Dalrymple (a fellow graduate student). Oblique air photographs were taken during each flight with a 35-mm camera.

As mentioned in Section 3.2, the configuration of the intertidal zone on various maps of Cobequid Bay is based either on old surveys or

on air photos. Although each air photo set gave areally comprehensive information about the distribution of the intertidal zone sediments, absolute comparisons of the intertidal zone configuration between photo sets were impossible because: (i) flight times relative to low water times were different for each photo set; and (ii) the elevation of the low tide level was different for each photo set. Some relative comparisons were made between photo sets to determine the historical variability of the intertidal zone using the flight data in Table 3-1 (based on flight reports at the National Air Photo Library, Ottawa).

Figure 3.14 shows the extent of the intertidal zone in Minas Basin and Cobequid Bay from a section of British Admiralty Chart 353 (compiled from surveys carried out in 1860-E. M. Walsh, Canadian Hydrographic Service, pers. comm., 1973).

Figure 3.15 shows the historical variation of the intertidal zone extent and configuration in Cobequid Bay since 1860. Note that the configurations of the intertidal zone are almost identical in Figures 3.14 and 3.15 A. The latter was traced from C.H.S. Chart 4010, the most up-to-date hydrographic chart of the bay. Recall that some of the variation in the outline of the intertidal zone in Figure 3.15 results from differences in the time and level of low tide relative to the actual flight time.

Although the shoreline reportedly experiences high rates of erosion, no major changes in the configuration or position of the shoreline were readily apparent from the available maps and air photos.

The sequence of maps in Figure 3.15 generally shows that: (i) the intertidal sand bars are elongate in an east-west direction, with their blunt ends oriented towards the head of the bay; (ii) the channel pattern in the western part of the complex is characterized by two or three major channels; and (iii) the channel pattern towards the head of the bay looks similar to the alluvial portion of a coastal plain river with a meandering and braided channel pattern. The channel-bar complex appears to have remained in the same general position, and maintained roughly the same relative volume during the past 110 y.

Although the accuracy of the 1860 surveys is open to question, the 1860 intertidal zone shows several broad similarities to the geometry of the complex in 1973 (compare Figs. 3.15 A and E), e.g., channels

TABLE 3 - 1

AIR PHOTO SUMMARY FOR COBEQUID BAY (low tide only)

Date		Flight No.[1]	Time Relative to Low Tide[2] (hours)	Low Tide Elevation[3]	Tidal Range[3]
1938	April	A-5923,-5924 & -5925	-1.5, -1.1	1.89	11.1
1947	November 4	A-11765	-1.0	2.07	10.8
1948	May 16	A-11787	-0.4	1.86	10.6
	June 23	A-11790	-1.0	1.65	11.8
1961	August 1	A-174-4	0.0	1.74	13.4
1963	April 25	A-18060	-1.2	1.28	14.4
	May 26	A-18061	-1.0	1.71	13.5
1972	July 22		-0.1	2.65	9.6
1973	June 5		0.0	1.04	12.9

Note: 1. N.A.P.L. flight numbers where applicable. Flights in 1972 and 1973 were flown by Atlantic Air Survey.

2. Calculated from median of flight interval from flight reports (N.A.P.L., Ottawa) and times of low tide (C.H.S. Tide Tables). Negative sign denotes time before low water; positive sign denotes time after low water.

3. Tidal range and elevation at Burntcoat Head (C.H.S. Tide Tables).

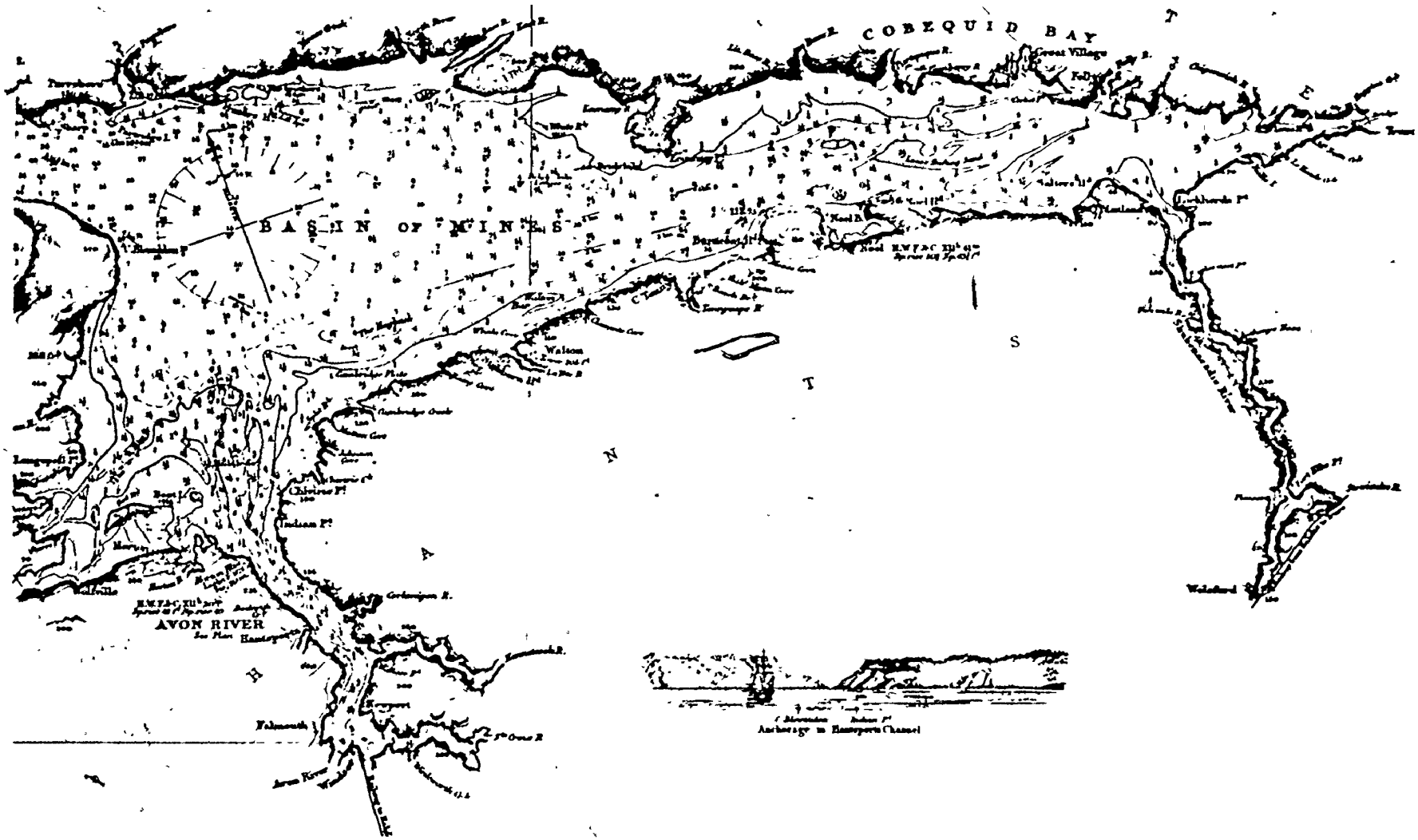

FIGURE 3.14: A section of British Admiralty Chart 353 showing the extent of the intertidal zone in Cobequid Bay from surveys carried out in 1860. The full chart is available from the Canadian Archives, Ottawa.

FIGURE 3.15: The historical variation of the intertidal zone extent and configuration in Cobequid Bay between 1860 and 1973.

A. 1860

B. 1938

C. 1947

D. 1961-63

E. 1973

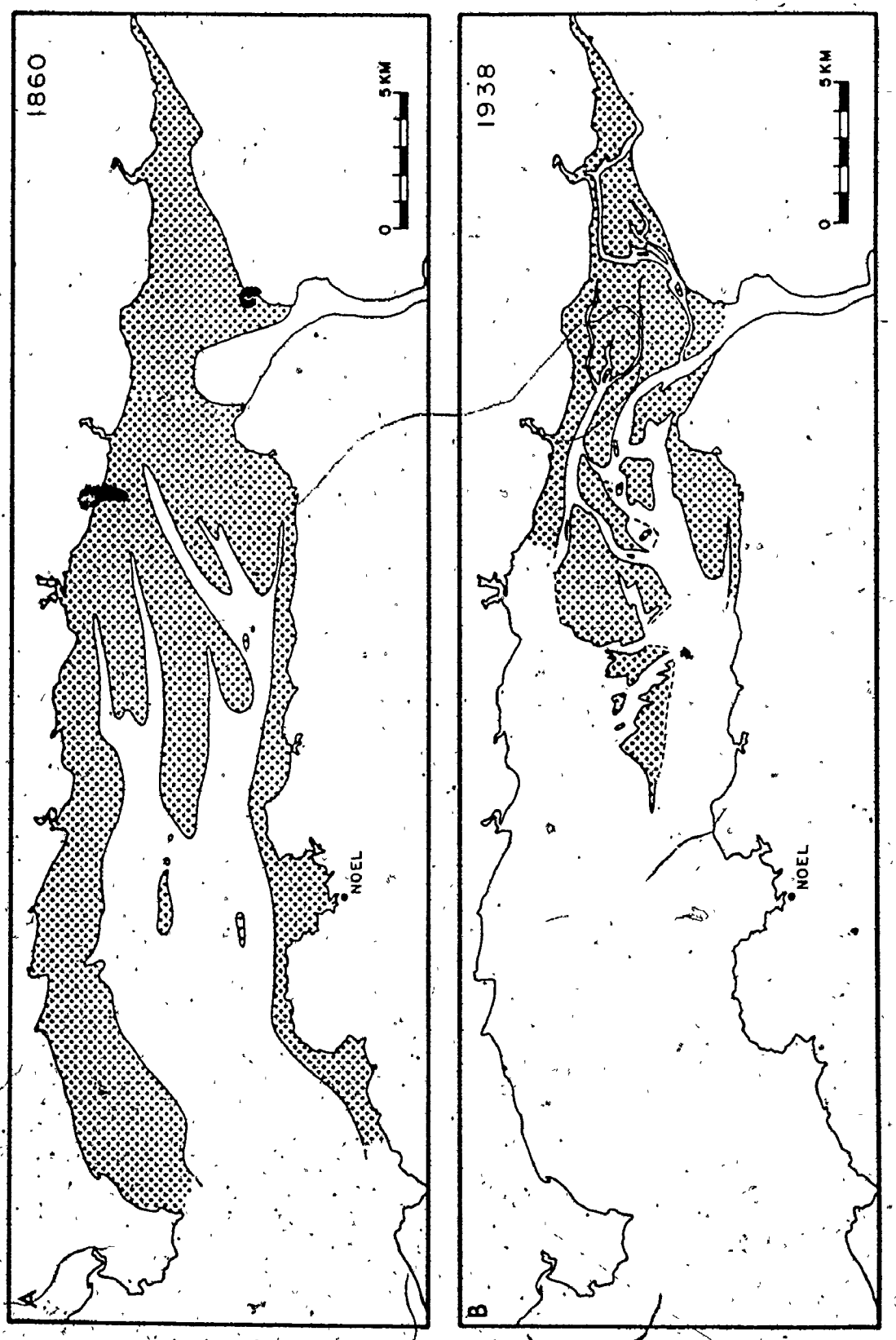
1860
5KM
0
NOEL
A
1938
5KM
0
NOEL
B

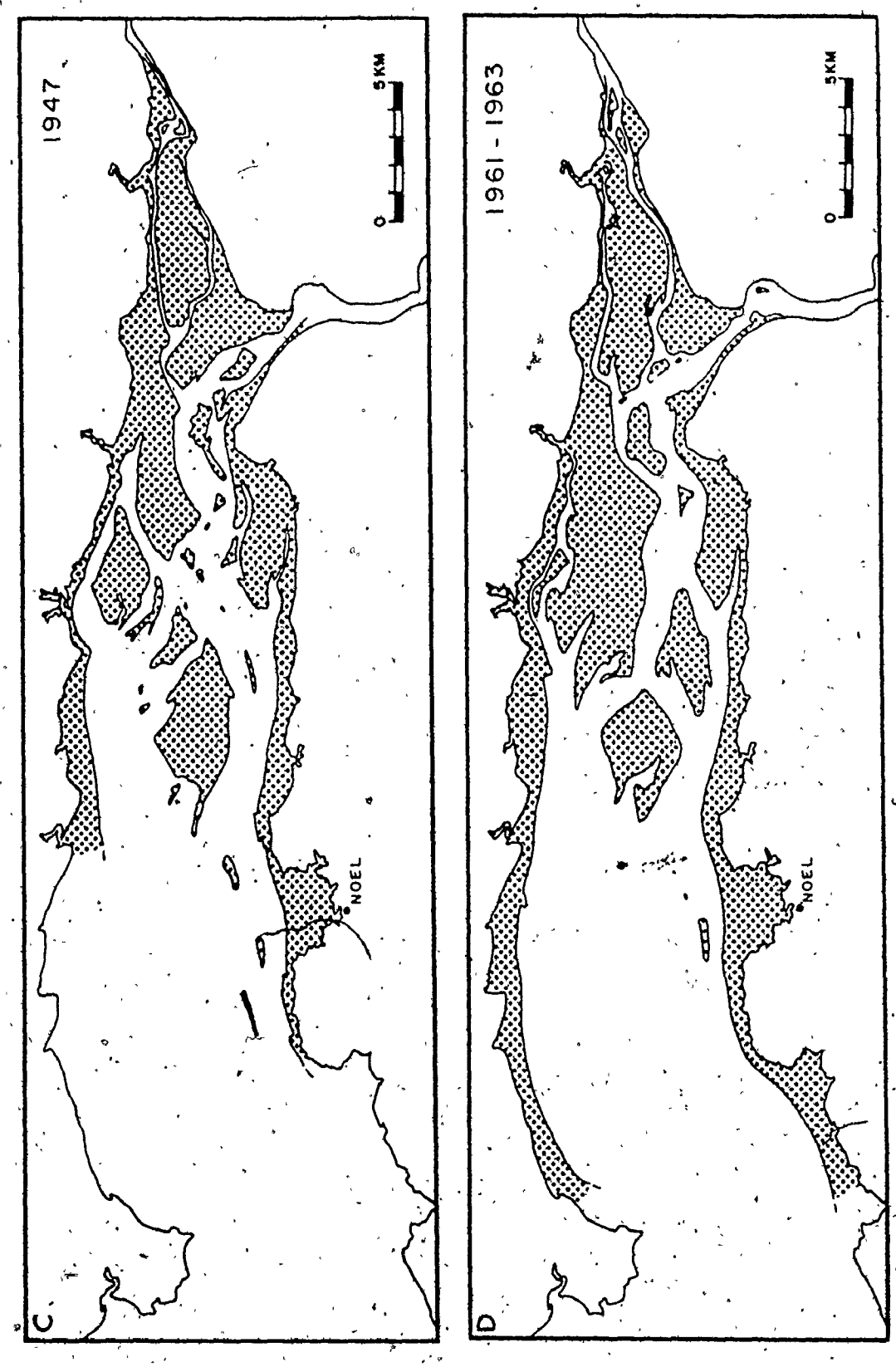

FIGURE 3.15 -- cont'd.

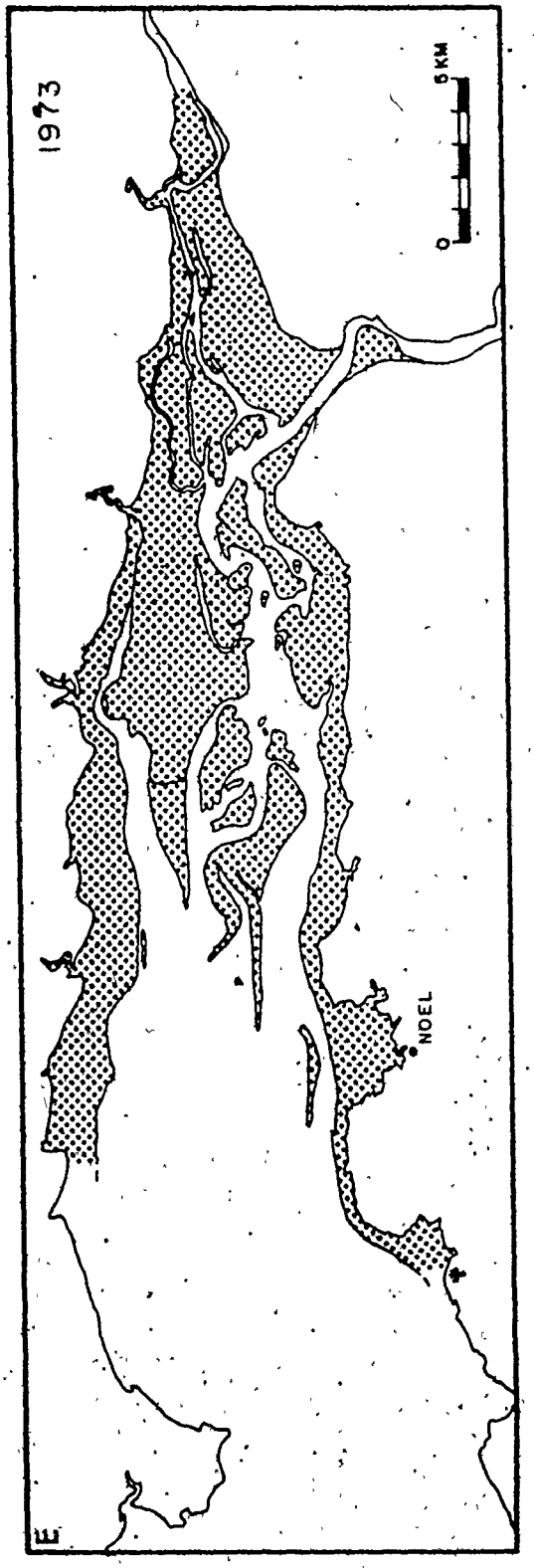

FIGURE 3.15 - cont'd.

extend along the north and south edges of the intertidal sand-body, and several of the sand bars seem to have maintained the same relative position (e.g., Noel Bay Bar, Noel Shore Bar, Great Village Bar and Selma Bar). The same similarities, as well as some differences, can be recognized in the other maps of Figure 3.15.

The sequence of maps in Figure 3.15 show that the channel draining the Salmon River estuary has changed its position several times since 1938. In 1938, the channel meandered across the full width of the estuary, while in 1947 it was positioned primarily along the north shore (but with a secondary channel extending part way towards the head of the estuary along the south shore). In the 1961-63 map (Fig. 3.15 D), the main channel has switched to the south side of the bay (with the north channel playing a secondary role). By 1973 (Fig. 3.15 E), the major intertidal channel from the Salmon River estuary is along the north side of the bay (similar to its position in 1947).

The different positions of the major intertidal channel in the Salmon River estuary suggests that it may have migrated laterally through time. If this were the case, the average rate of lateral migration would be approximately 180 m/y. Based on field observations from 1970 to 1974, this figure is too high, so there must be another explanation. Closer examination of the air photos shows that two channels generally drain the estuary at low tide: a major channel from the Salmon River; and a secondary channel that does not extend all of the way to the head of the estuary. Thus, the changing position of the major channel appears to occur by avulsion to the secondary channel rather than by lateral migration of a single, major channel.

3.5 SAND BARS

Four sand bars were selected from the intertidal sand-body in Cobequid Bay for detailed study (Fig. 3.2): Noel Bay Bar, East Noel Bar, Noel Shore Bar and Selma Bar. The reason why these particular bars were selected included: (i) accessibility, e.g., East Noel Bar and Selma Bar could be reached from shore on those days when a boat could not be used because of weather conditions; and (ii) diversity of bar-location and -type for comparative studies within the bay from west to

east (e.g., East Noel Bar and Selma Bar relative to Noel Shore Bar and Noel Bay Bar).

The purpose of this section is to describe the setting, geometry (topography and bathymetry) and sediment textures of the bars selected for detailed study. Field methods and laboratory techniques are discussed in Appendix III. Sediment sample locations, distributions and statistics are listed in Appendix III. Bedforms are discussed in Chapter 5.

Noel Bay Bar

Noel Bay Bar is located at the southwest margin of the sand-body complex in Cobequid Bay (Fig. 3.2), immediately to the north of Noel Bay. Figures 3.16 and 3.17 show the position of the bar relative to the south shore of Cobequid Bay, and the distribution of the local intertidal sediment facies.

At low tide, the bar is about 3.2 km long and has a maximum width of about 365 m. The bar is elongate in an east-west direction and slightly arcuate in plan (i.e., its outline is convex to the south). The east end of the bar is blunt relative to the west end. The intertidal margin of the bar is relatively smooth along the south side from an absence of bedforms, while the north side of the bar has a serrated outline from megaripples that extend into the subtidal zone. The intertidal, and parts of the subtidal, are covered with megaripples.

Including the subtidal parts of the bar (Fig. 3.18), its length and maximum width are about 5 km and 1 km respectively. The upper surface of the bar has little variation of relief compared with other bars in the complex. The surface has three small topographic highs (of about 1 m relief); two of which are apparent in Figure 3.18, and a third near the west end of the bar. At low tide, the bar has a maximum emerged relief of about 3.5 m.

Figure 3.19 shows the bar's bathymetric position relative to the shoreline and its asymmetric (north-south) cross-sectional shape. The bar has an intertidal crestal platform that slopes to the north from 1 to 2°. The bar's crestline occurs along the sourthern edge of the bar (note the relatively smooth intertidal margin of the bar along the south side in Figure 3.16). South of and perpendicular to the bar's crestline,

FIGURE 3.16: Vertical air photo mosaic showing Noel Bay and Noel Bay Bar (photos taken near low tide in 1973 by Atlantic Air Survey; see Table 3-1).

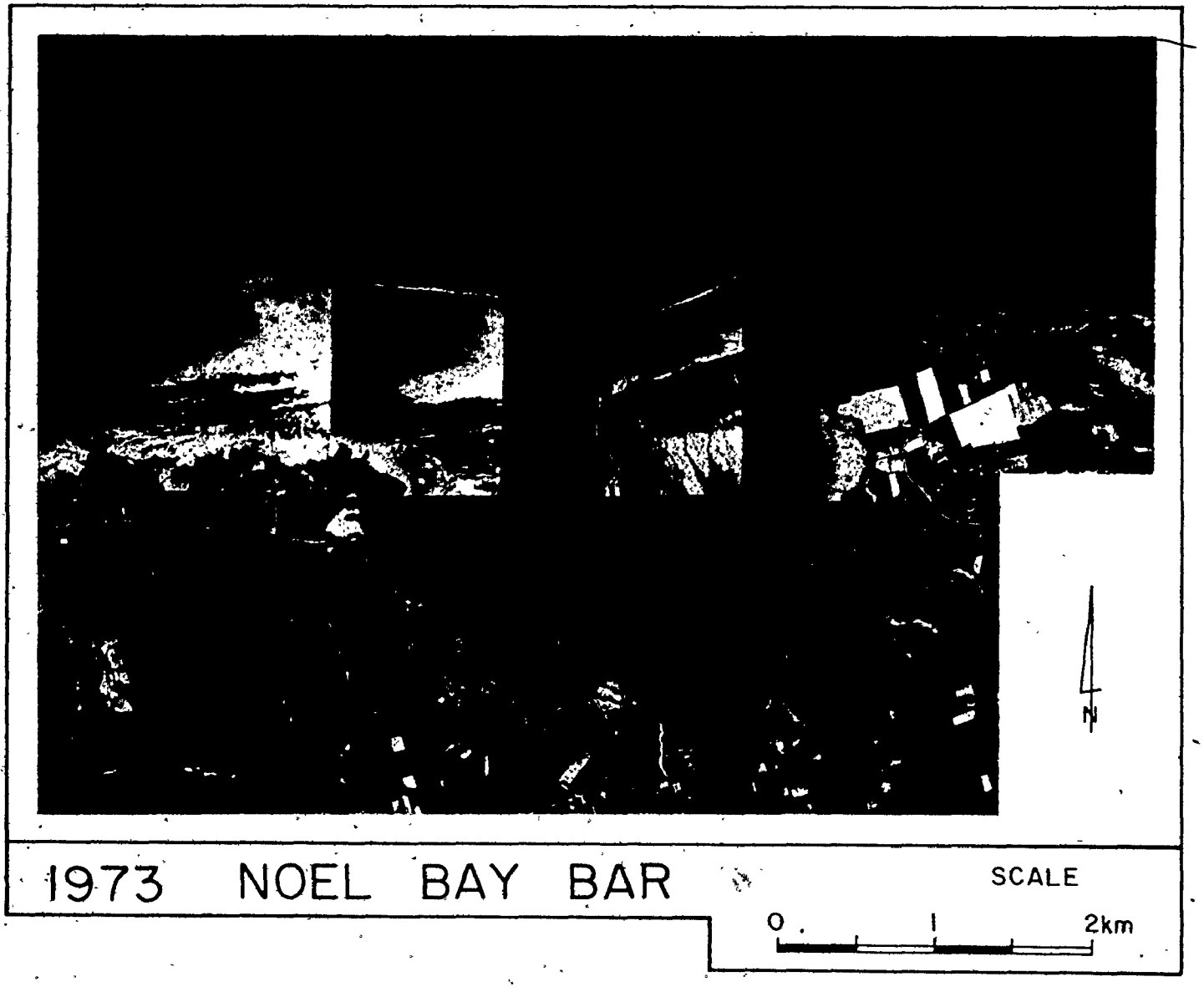
N
1973 NOEL BAY BAR
SCALE
0
1
2km

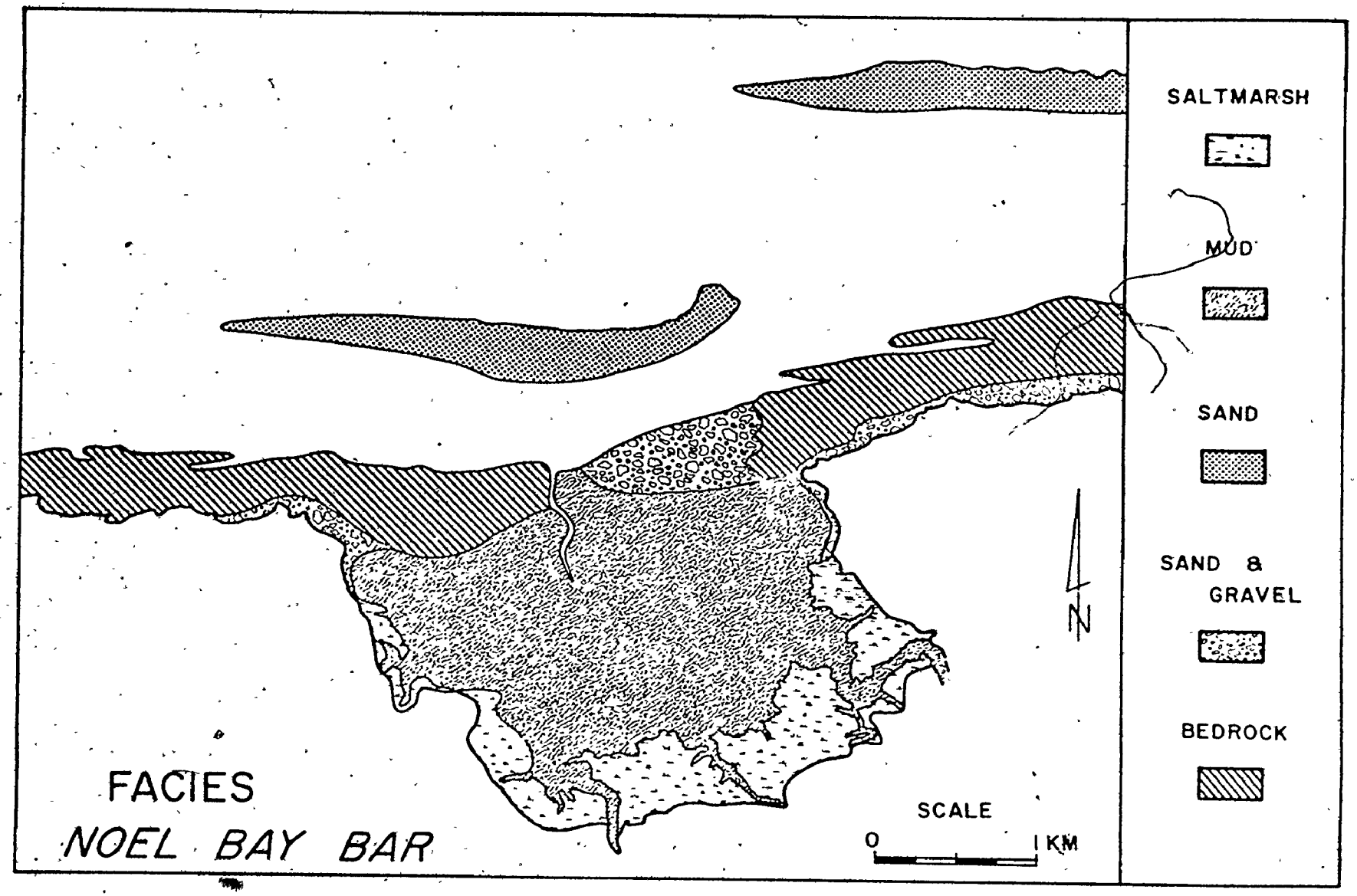

FIGURE 3.17: Distribution of the intertidal sediment facies in the vicinity of Noel Bay Bar.

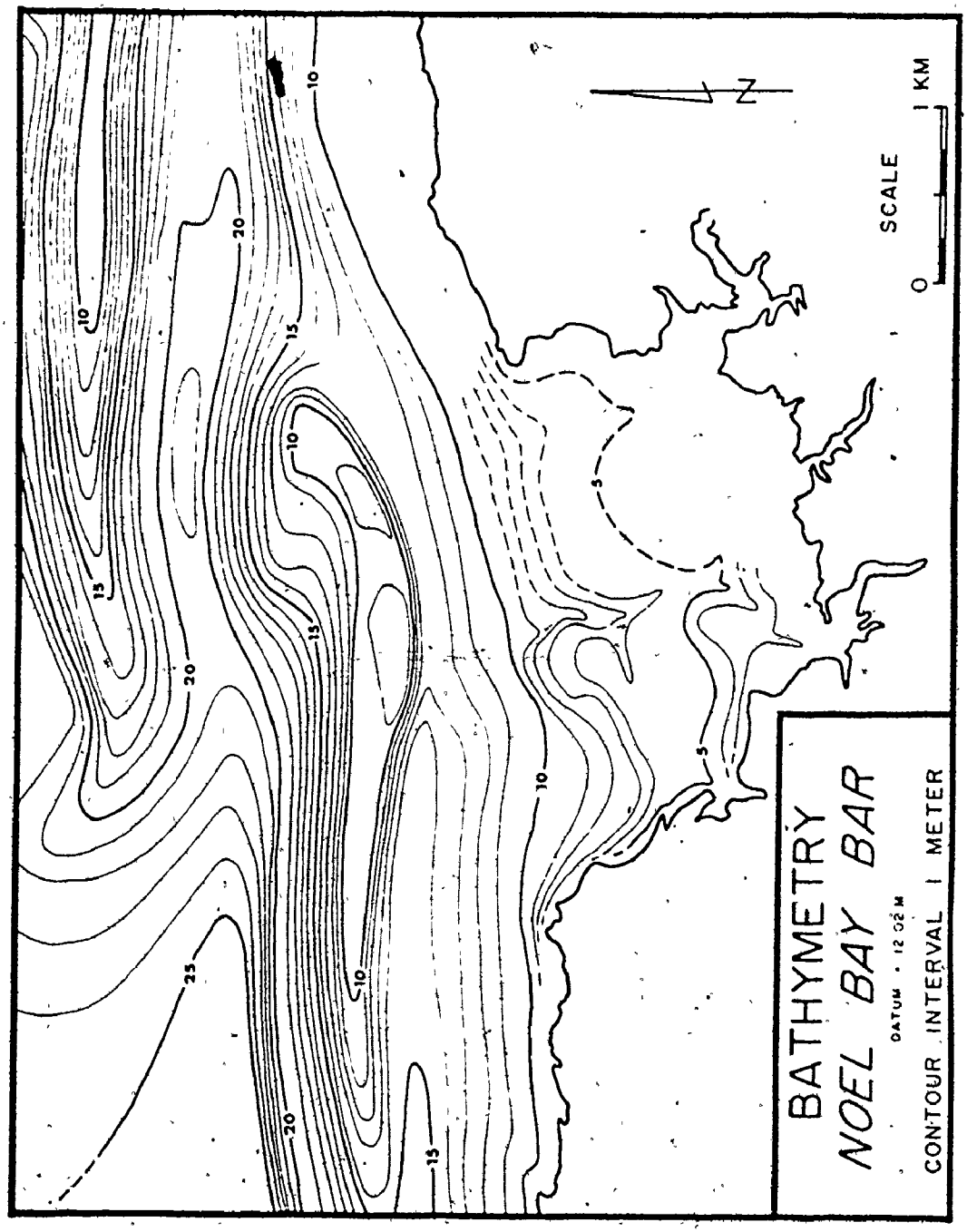

FIGURE 3.18: Bathymetry of the Noel Bay-Noel Bay Bar area.

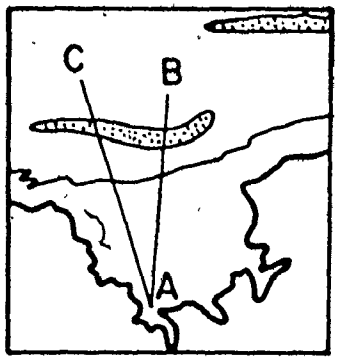

NOEL BAY & BAR

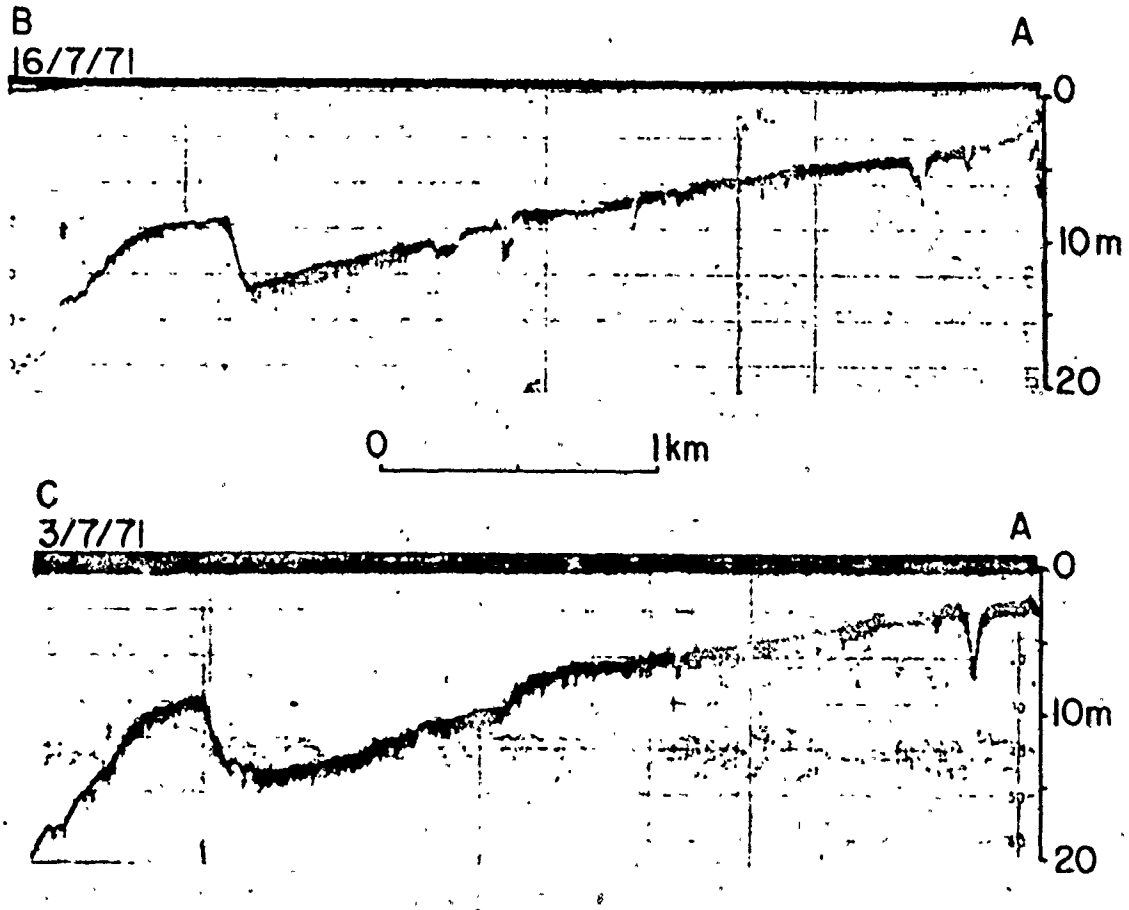

FIGURE 3.19: Representative sounding records showing the relative bathymetric position of Noel Bay Bar and its cross-sectional shape.

the bar surface slopes between 4 to 12° into the subtidal channel to the south. To the north of the crestline, the bar surface slopes (into the subtidal channel to the north) are generally less than 3°.

The bar is bounded by subtidal channels to the north and south (Fig. 3.18). The channel to the north is about 7 m deeper than the channel to the south of the bar (Figs. 3.18 and 3.19), and considerably wider (Figs. 3.2, 3.17 and 3.18). The southern channel ranges from about 500 to 800 m in width at low tide, while the northern channel extends to the centre of the bay. The thalweg gradient of the southern channel is steeper (about 1m/km than that along the northern channel (about 0.65m/km).

Sparker records over Noel Bay Bar show that the 'recent' sediment cover has a maximum thickness of about 15 m, while the second sedimentary body is about 5 m thick.

Figure 3.20 shows several representative sediment size distributions and Figure 3.21 shows the areal distribution of mean grain size, sorting and skewness of the sediments on Noel Bay Bar and in the adjacent channels. The bar sediments are mainly medium grained sands that are well-sorted. The representative distributions (Fig. 3.20) and maps (Fig. 3.21) indicate that: (i) sediment size is finer and sorting is generally better along the bar's crestline (i.e., the highest parts of the bar); (ii) sediment size decreases slightly from northeast to southwest (i.e., sediment phi size increases from east to west); and (iii) the sediments at the west end of the bar tend to be positively skewed while those at the east end are negatively skewed. Sediment samples and SCUBA observations indicate that the channels are floored by bedrock and (or) an admixture of medium to coarse sized sands, pebbles and cobbles.

Figures 3.22 and 3.23 show the relative position of Noel Bay Bar in 1947 and 1961-63. Although not totally emergent (see Table 3-1), it appears that the bar may have developed in a west to east direction (compare the position of bar in Figs. 3.16, 3.22 and 3.23).

FIGURE 3.20: Several representative sediment size distributions from Noel Bay Bar. Station locations are shown in Figure A11.1.

A. Variation of sediment size distributions from the west to east end of the bar.

B. Variation of sediment size distributions from north to south across the western part of the bar.

C. Variation of sediment size distributions from north to south across the eastern part of the bar.

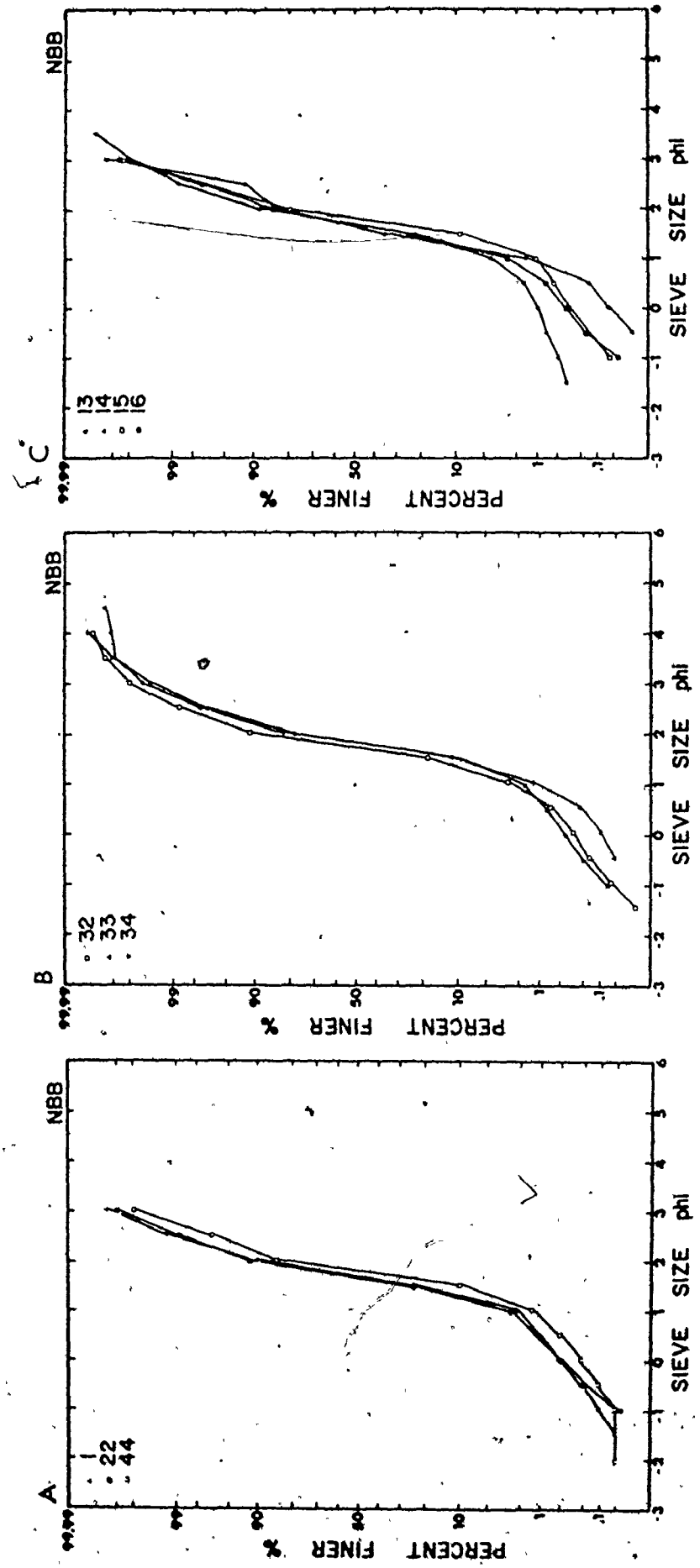
NBB
A
1
22
44
B
32
33
34
C
13
14
15
16
PERCENT FINER %
SIEVE SIZE phi

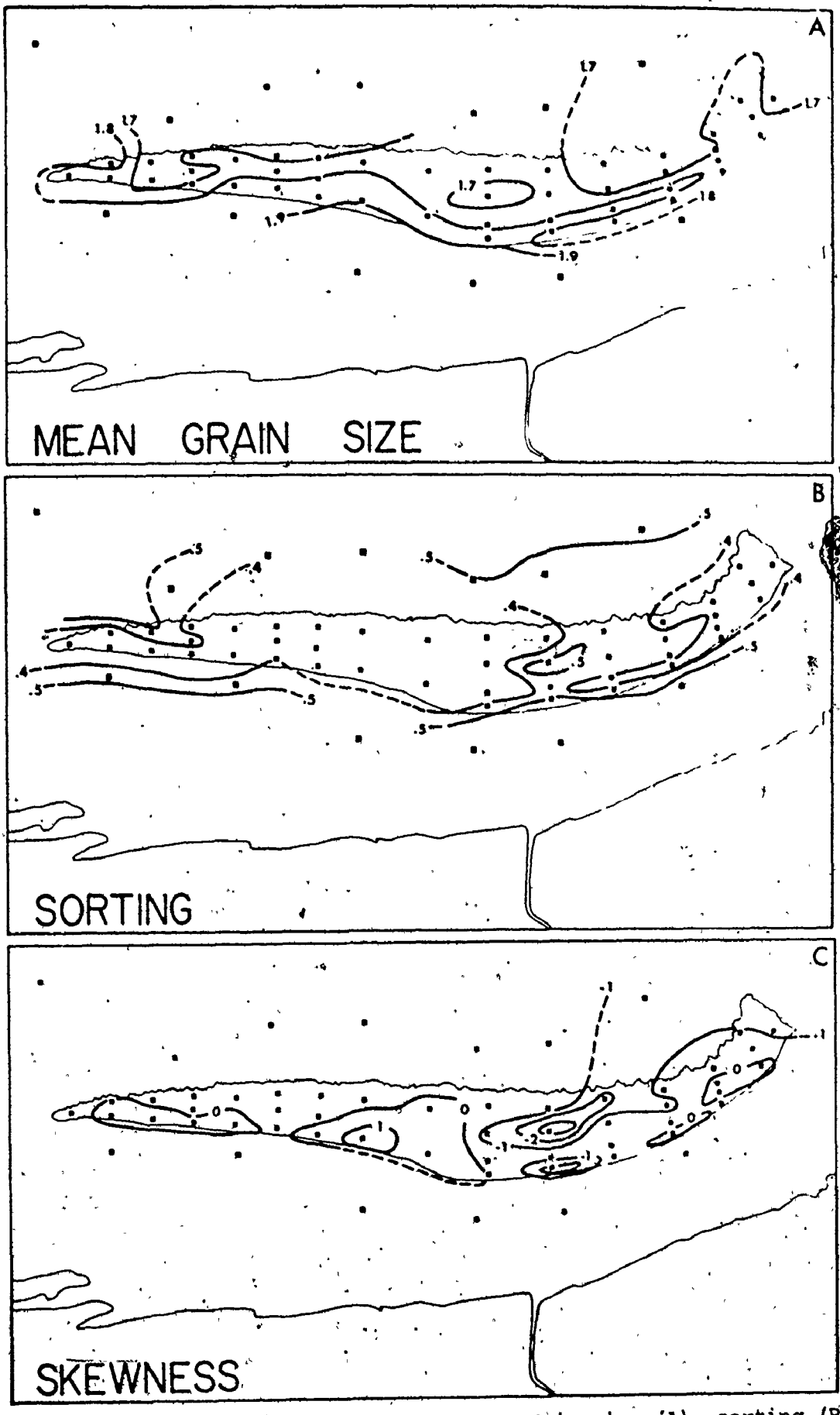

FIGURE 3.21: Areal distribution of mean grain size (A), sorting (B) and skewness (C) of the sediments on Noel Bay Bar and in the channels.

FIGURE 3.22: Vertical air photo mosaic of the south side of Cobequid Bay in 1947 (N.A.P.L. photos). See Table 3-1 for the time and level of the tide relative to the flight time.

1947 SOUTH SHORE COBEQUID B

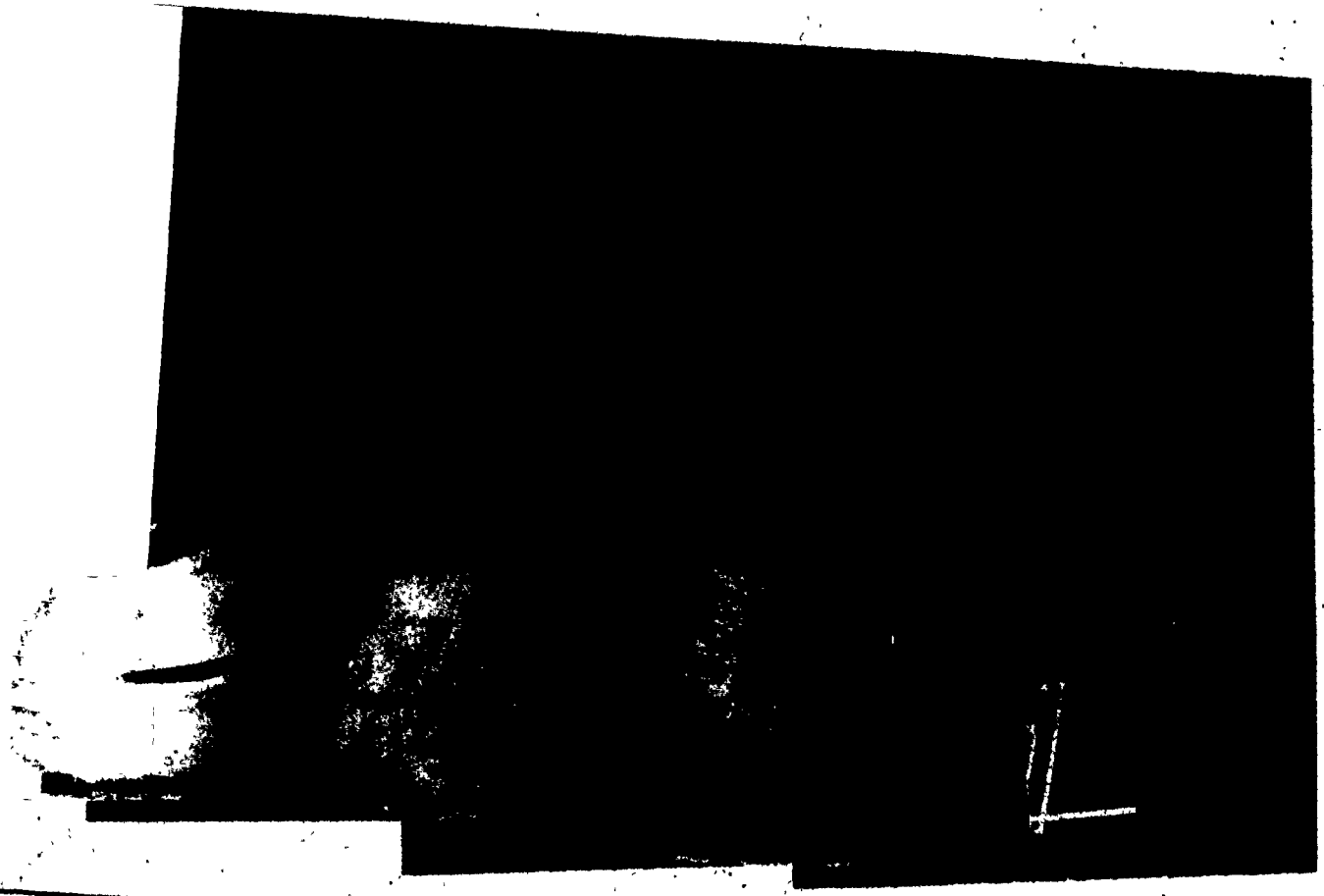

UID BAY

SCALE 0 1 2 3 4 5 km

FIGURE 3.23: Vertical air photo mosaic of the south side of Cobequid Bay in 1961-63 (N.A.P.L. photos). See Table 3-1 for the time and level of the tide relative to the flight time.

1961 - 63 SOUTH SHORE

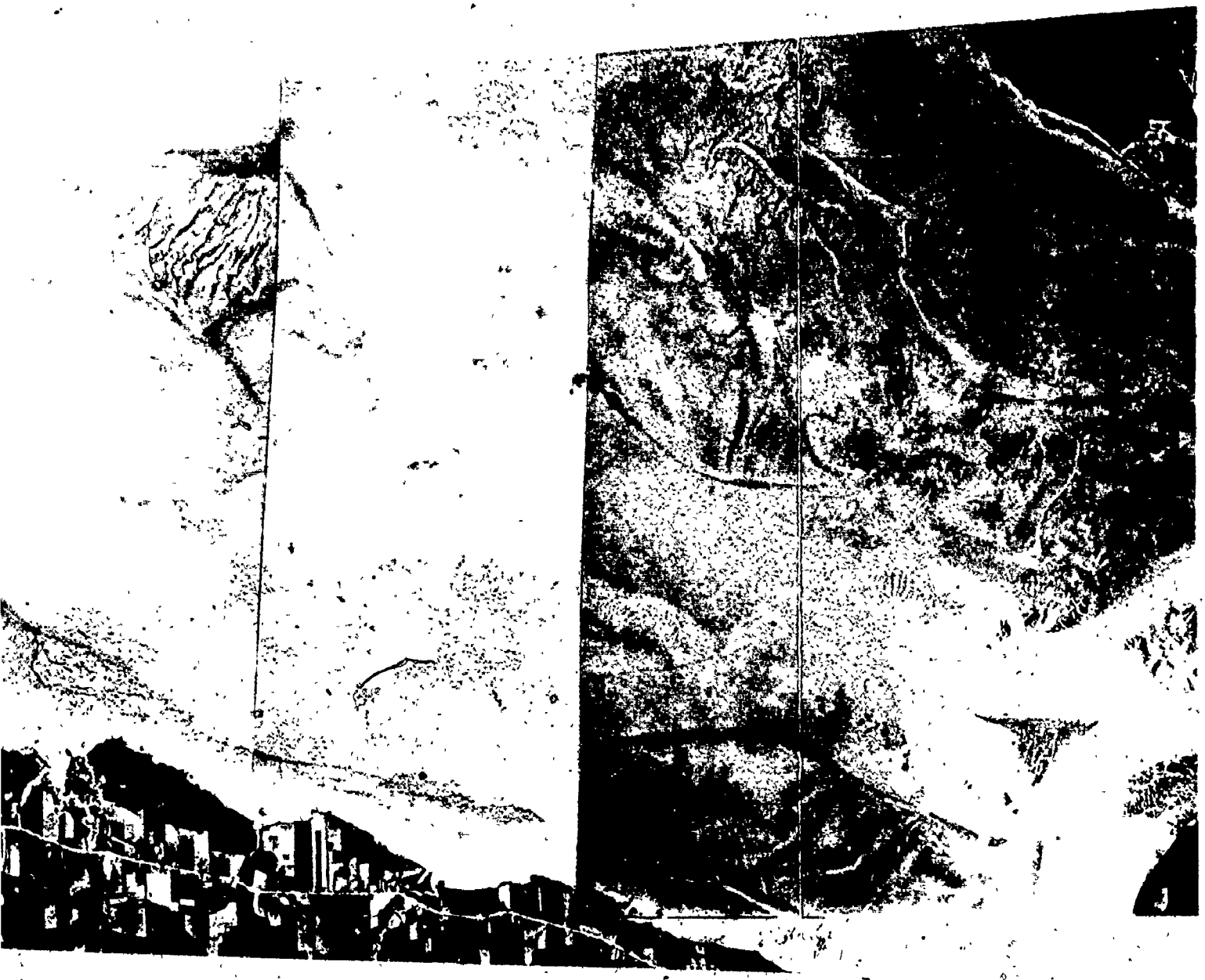

COBEQUID BAY

SCALE 0 1 2 km

East Noel Bar

East Noel Bar is a small sand-body, about 1.25 km long and 500 m wide, that is located along the south shore of Cobequid Bay (Fig. 3.2) in the lee of Noel Head (Fig. 3.24). Figures 3.24, 3.27 and 3.28 show the position of the bar relative to the shoreline and the distribution of intertidal sediment facies. The bar is roughly elliptical in outline with its long axis extending from the northwest to southeast.

The bar occurs in the middle part of the intertidal zone on a bedrock platform. It is flanked to the south by a small intertidal creek and mudflat foreshore. To the north, east and west, the bar is bounded by an exposed or veneered (mostly gravel) bedrock platform. The bar is shielded from strong flood currents and wave activity by Noel Head and intertidal bedrock ledges to the west. The east end of the bar is exposed to strong ebb currents but sheltered from strong wave action by the sand-body complex to the northeast and east.

The topography of the bar (Fig. 3.29) has less than 3 m relief and is morphologically simple compared to Noel Shore Bar and Selma Bar. The bar has no distinct crestline, although there is a small topographic high that extends along the northwest and northeast sides of the bar (apparent by the light colour along the edges of the bar in Figure. 3.24).

The thickness of sediment in the bar is thin (generally less than 1 m). Although the surface of the bar is covered with megaripples (Fig. 3.24), bedrock or gravel is exposed in many of the bedform troughs, particularly near the east end of the bar, and the surface of the bar is dotted with rock fragments (up to boulder size, i.e., more than 2 m in diameter). The boulders and the exposed bedrock and gravel on the bar have the same lithology (primarily Triassic sandstone) as the bedrock and gravel in the shoreline. The thickness of sediment generally increases from east to west across the bar because of the shielding and entrapment by the bedrock headlands and intertidal ledges at the west end of the bar.

Figure 3.25 shows several representative sediment size distributions from East Noel Bar. Mean grain sizes fall within the medium sand size, but there is a wider range of sizes and the sediments are coarser and more poorly sorted than those found on Noel Bay Bar or Noel

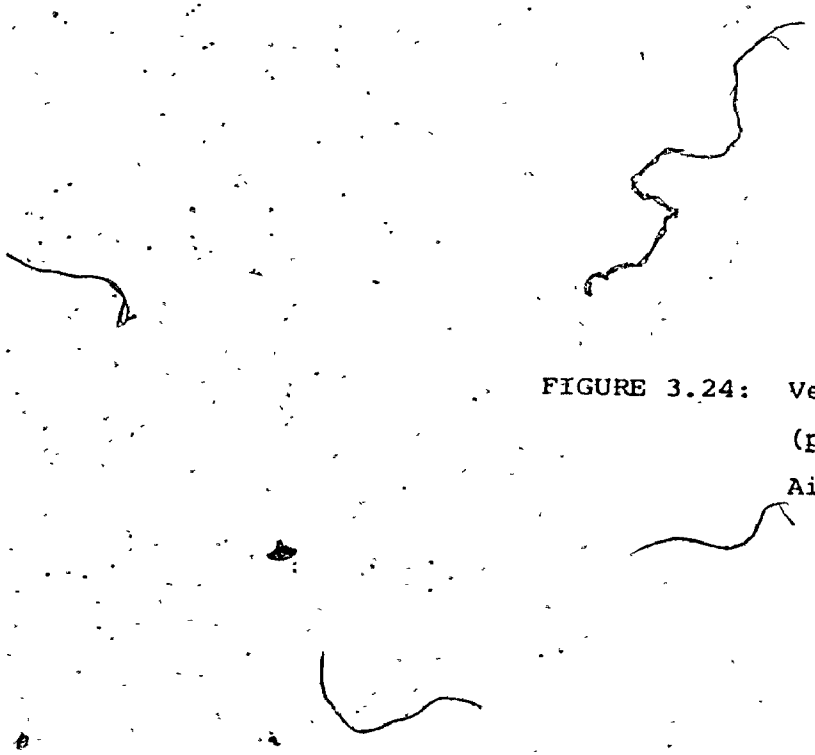

FIGURE 3.24: Vertical air photo mosaic showing East Noel Bar (photos taken near low tide in 1973 by Atlantic Air Survey; see Table 3-1).

1973 EAST NOEL BAR

SCALE 0 1 2 km

FIGURE 3.25: Several representative sediment size distributions from:

A: East Noel Bar

B. Selma Bar

Station locations are shown in Figure A II.1.

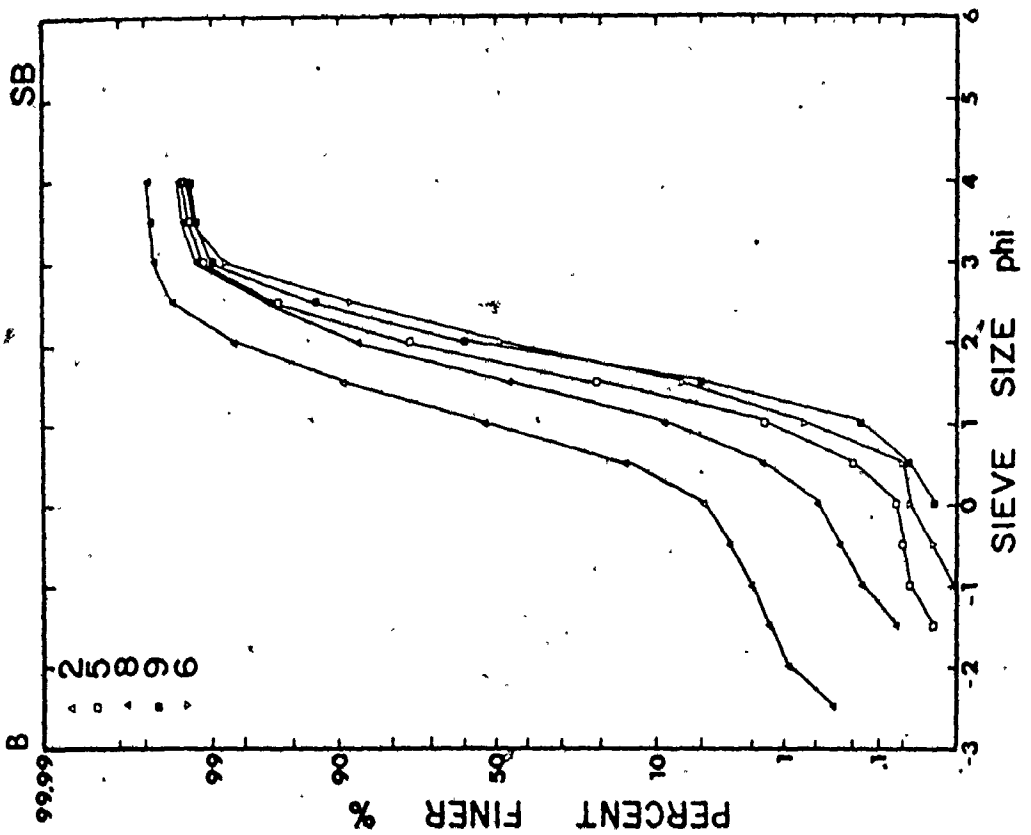
SB
B
25
8
9
6
99.99
99
90
50
10
1
.1
PERCENT FINER %
-3
-2
-1
0
1
2
3
4
5
6
SIEVE SIZE phi

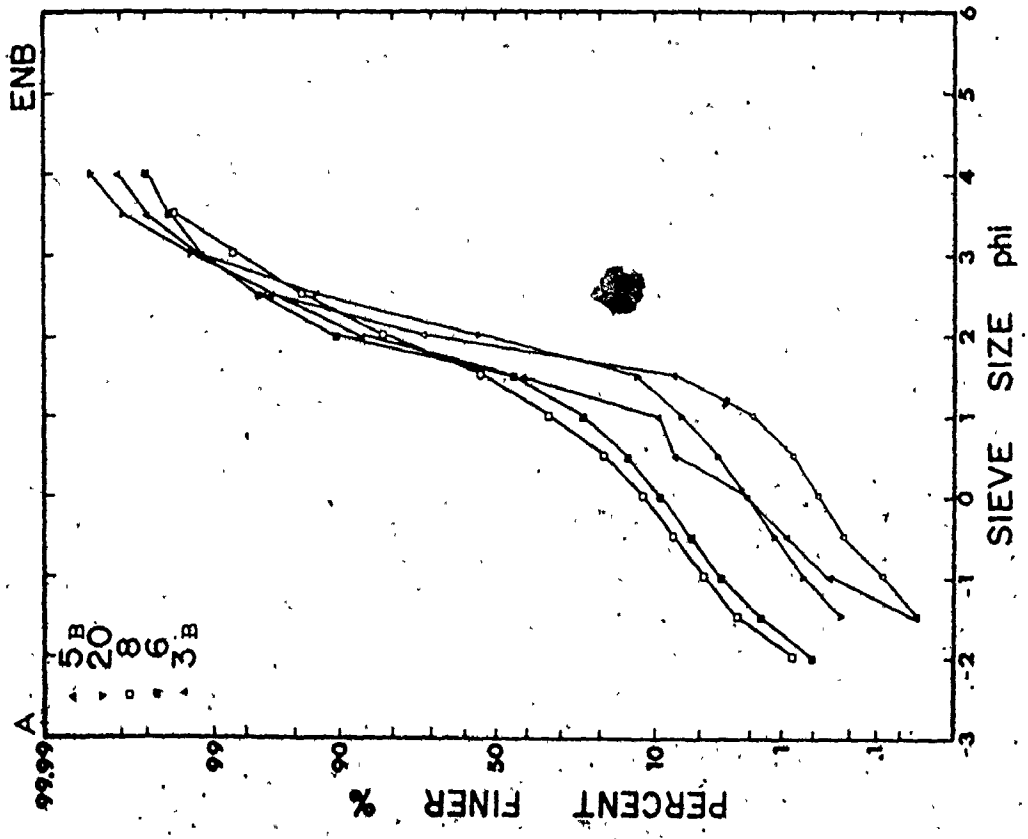
ENB
A
5B
20
8
6
3B
99.99
99
90
50
10
1
.1
PERCENT FINER %
-3
-2
-1
0
1
2
3
4
5
6
SIEVE SIZE phi

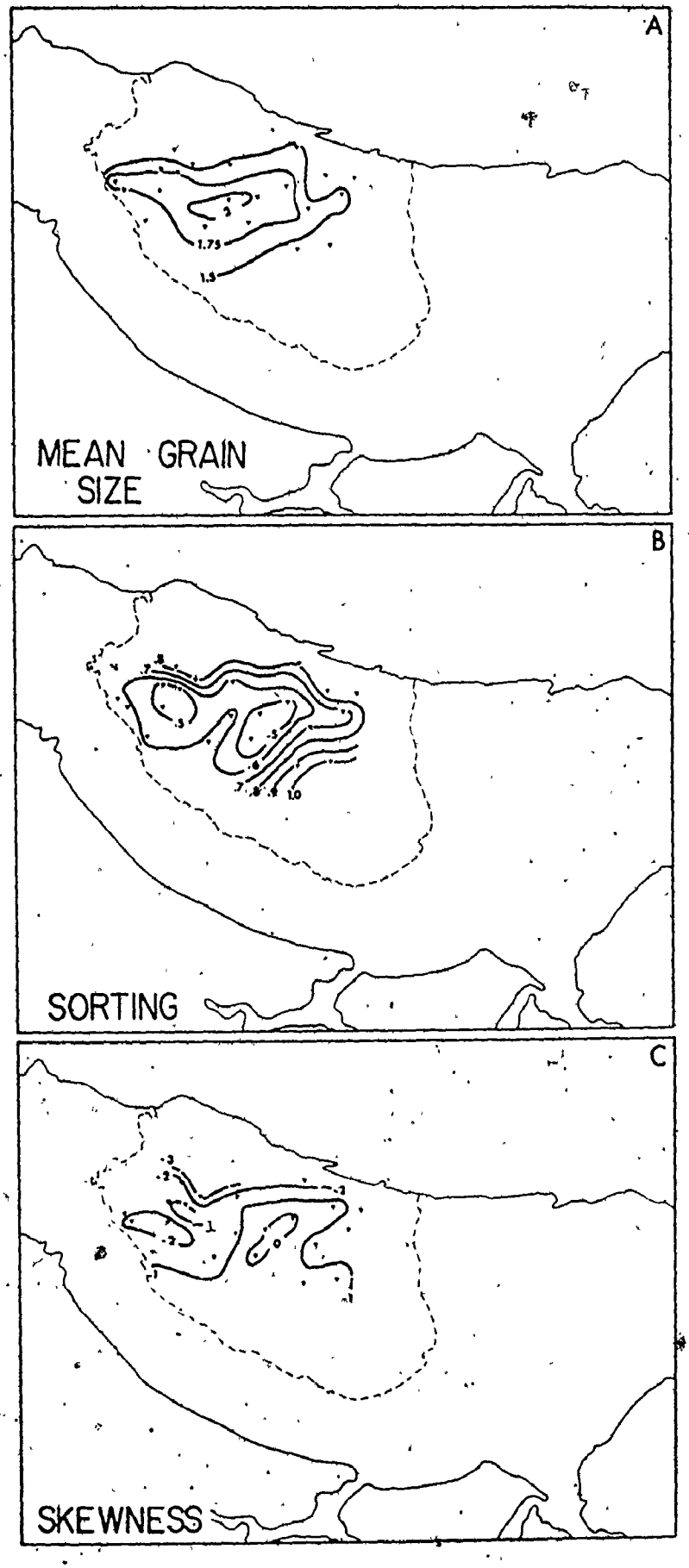
A
MEAN GRAIN SIZE
B
SORTING
C
SKEWNESS

FIGURE 3.27: Vertical air photo mosaic showing Noel Shore Bar (and East Noel Bar). Photos were taken near low tide in 1973 by Atlantic Air Survey; see Table 3-1.

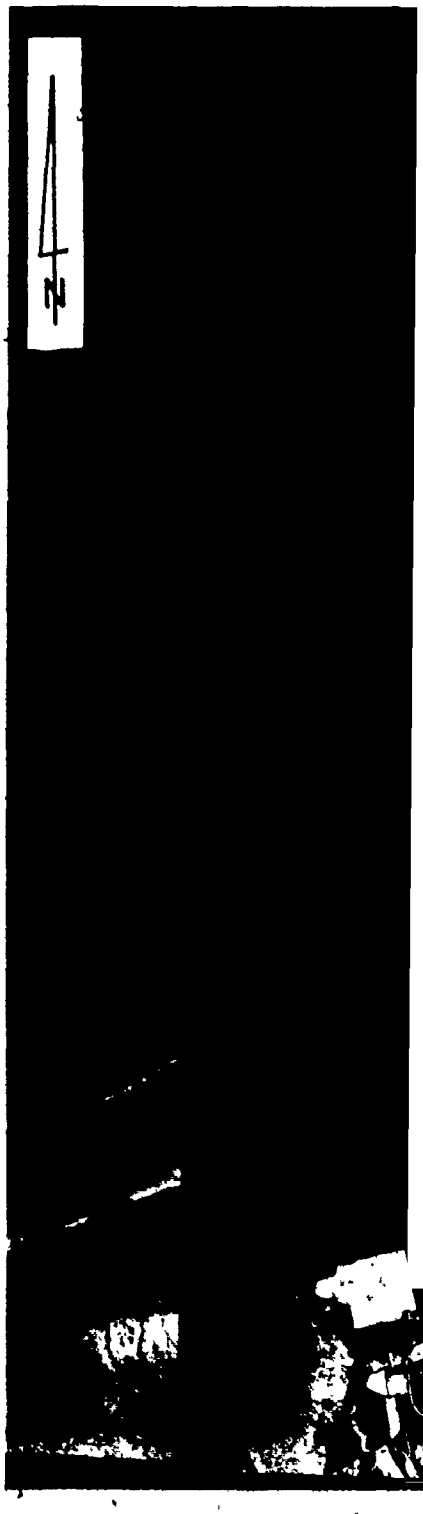

1973 EAST NOEL BAR & N

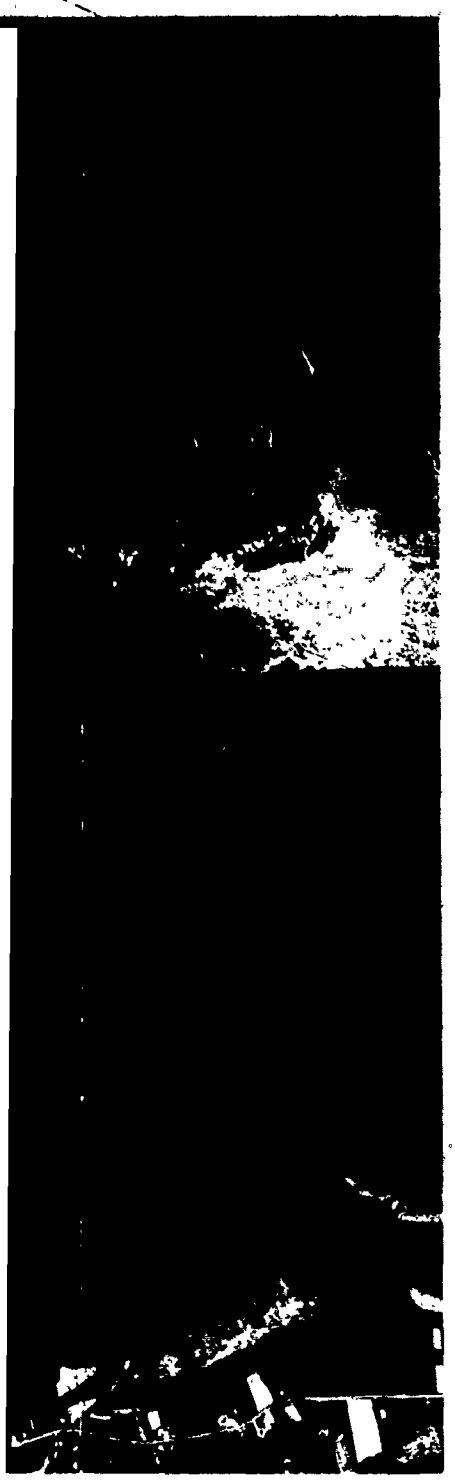

BAR & NOEL SHORE BAR

SCALE

0 1 2km

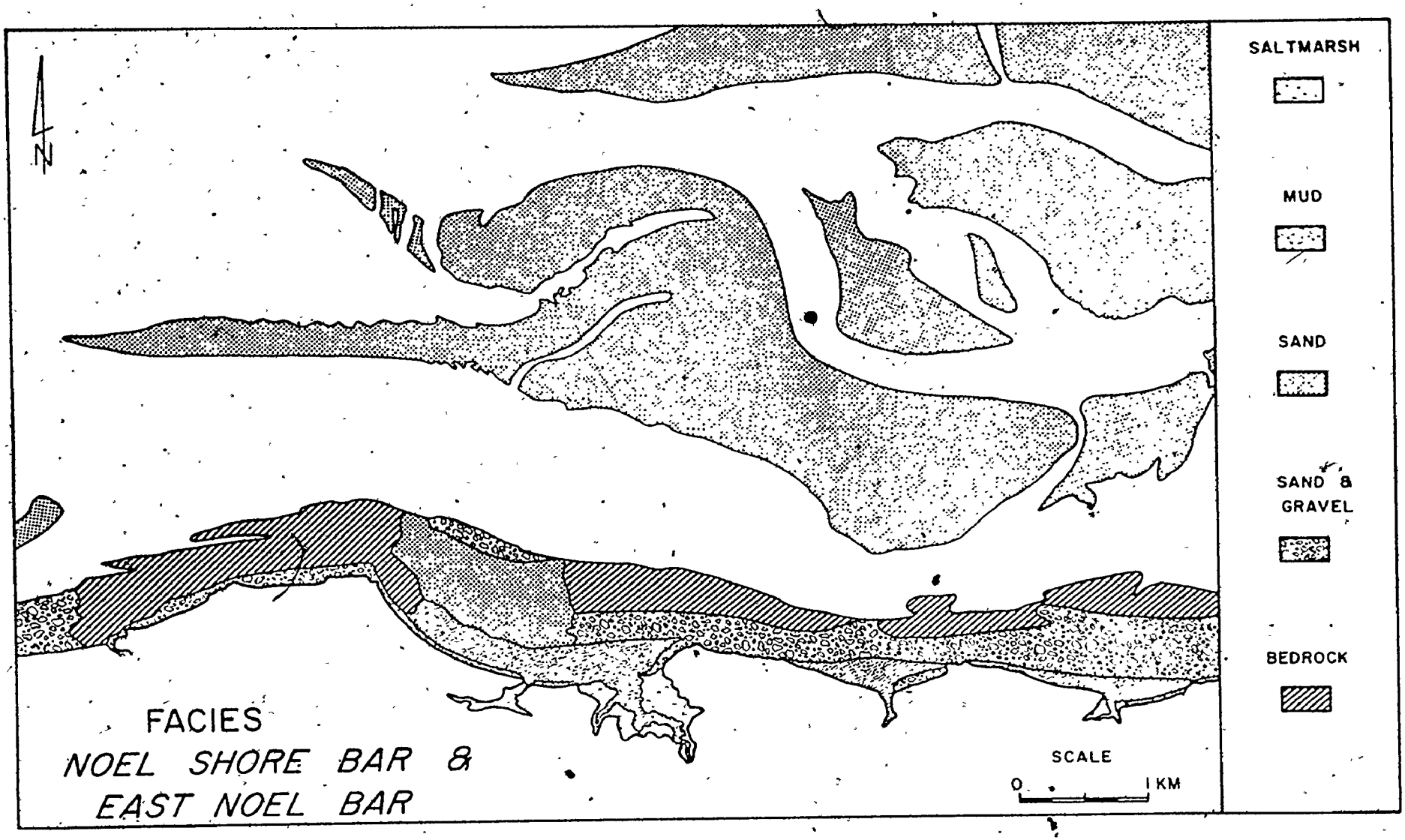

FIGURE 3.28: Distribution of the intertidal sediment facies in the vicinity of East Noel Bar and Noel Shore Bar.

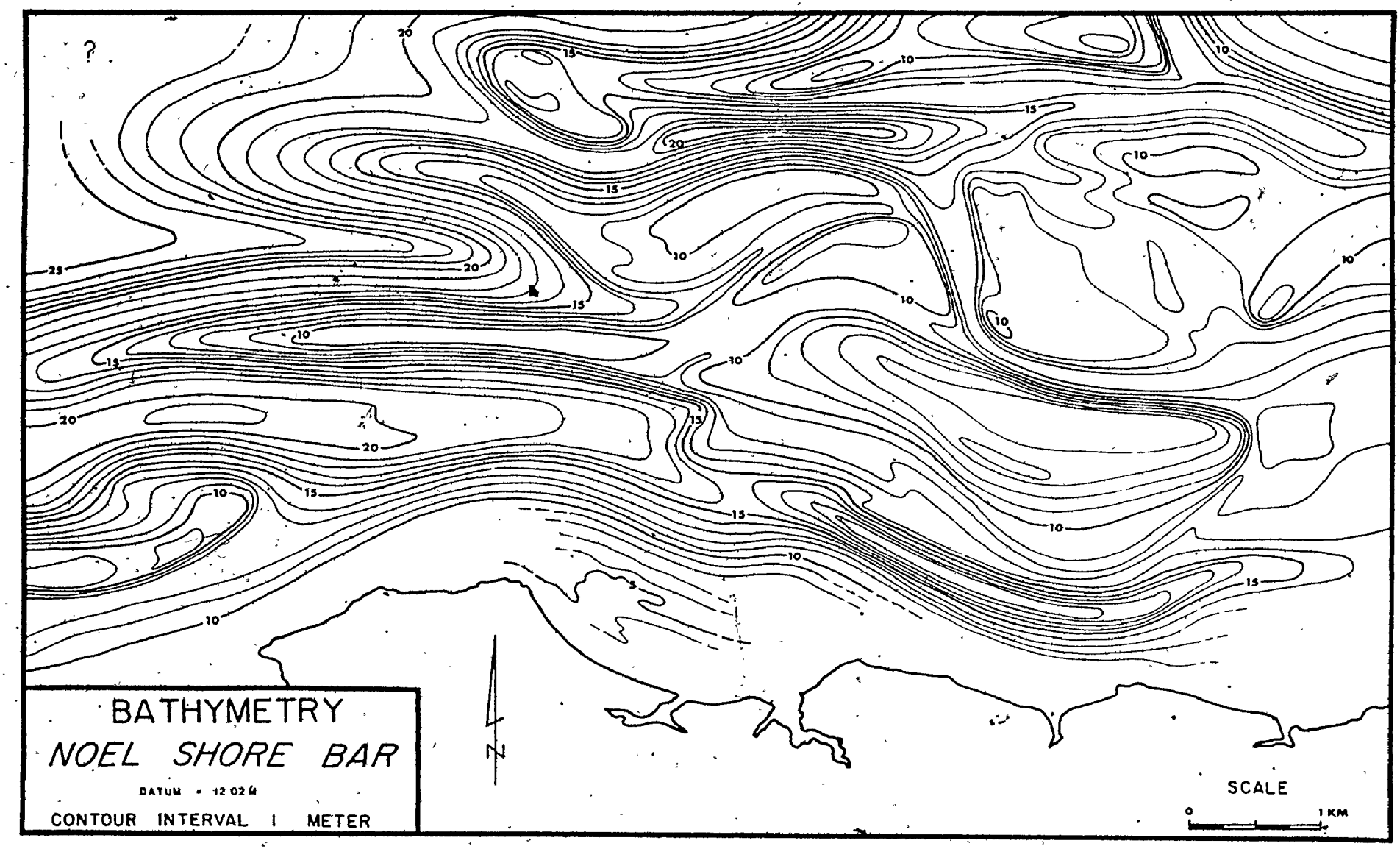

FIGURE 3.2?: Bathymetry of the Noel Shore Bar and East Noel Bar area

Shore Bar, sediment size (Fig. 3.26 A) decreases and sorting improves towards the centre of the bar. The areas of poorest sorting and coarsest grain size (to the east and southeast) presumably occur near the source of sediments for the bar (e.g., from erosion of the shoreline and intertidal foreshore east of the bar, and from the channel along the northeast side of the bar). The sediments are negatively skewed (increasing from southeast to northwest).

Figures 3.22, 3.23 and 3.24 show that the size of East Noel Bar has increased slightly from 1947 to 1973. In 1947, the areal extent of the bar was smaller and the main accumulation of sand was located closer to the intertidal creek along the southwest side of the bar. By 1961-63, the areal extent of the bar was almost the same size as the bar-configuration in 1973, but the sand surface appeared to be bisected by a sandy-gravel zone along the axis of the bar. Bedform size on the sand bar does not appear to have changed.

Noel Shore Bar

Noel Shore Bar is a large, topographically complex sand bar that is located opposite East Noel Bar (Fig. 3.2) on the north side of the southern channel extending into the sand-body complex. It lies about 2 km from the south shore of Cobequid Bay and extends in an east-west direction about 8.2 km. The bar ranges from about 300 m to 2.1 km in width. Figures 3.27 and 3.28 show the relative position of the bar to the shoreline and to the distribution of intertidal sediment facies.

The low tide outline of the bar is relatively compl[illegible] compared with Noel Bay and East Noel Bars. The bar comprises: an eastern part that is about 1 to 2 km wide and 5 km long; a western part that is about 350 m wide and 4.5 km long; and a northern part that is about 3.5 km long and ranges about 0.5 m to 1 km in width. The three parts of the bar are separated by two swatchways (Robinson, 1960, p. 186) that extend from the southwest to the northeast (Fig. 3.27). The northern swatchway opens to the west into the deepest part of the bay at the edge of the sand-body complex. The southern swatchway intersects with the deep channel along the south side of the bar, opposite East Noel Bar.

Because the north part of the bar was exposed for such short periods of time at low tide, no detailed field observations were

carried out on this part of the bar. Most of the field work was concentrated on the western and eastern parts of the bar. Figure 3.29 shows the bathymetry of the bar and adjoining areas of the subtidal zone.

The crestline of the eastern part of the bar occurs along the north side (Figs. 3.27 and 3.29). North of the crestline, the bar surface slopes to the north at about 6 to 10° and the surface is devoid of largescale bedforms. To the south of the crestline, the bar surface slopes gently southwards at about 1 to 2° across the crestal platform, then dips at about 5 to 8° into the channel south of the bar. A small topographic high extends from the main crestline to the south near the eastern end of the bar (into the area of relatively large bedforms on the southeast side of the bar in Figure 3.27). A relatively large swash platform is evident in Figure 3.27 near the western end of the eastern part of the bar. This part of the bar is covered with a wide range of largescale bedforms (see Chapter 5).

The western part of the bar is well-exposed to wave action from the west (e.g., Fig. 216 F). The crestline occurs near the south side (Fig. 3.27 and 3.29). The surface of the bar slopes at about 3 to 5° to either side of the crestline (north and south). The absence of large-scale bedforms in some areas along the south side of the bar (which is slightly steeper than the north side) gives a relatively smooth low tide outline. Several largescale bed features occur to the north of the crestline (Fig. 3.34 A), extending laterally into the channel north of this part of the bar. These features are asymmetrical towards the head of the bay and have wavelengths ranging from 100 to 200 m. Their presence along the north side of the bar gives a jagged appearance to the low tide outline. Megaripples are superposed over the whole western part of the bar.

The western end of the northern part of the bar is also relatively well-exposed to wave action from the west. The crestline in this part of the bar occurs along the northern edge near the central channel (Fig. 3.29) that extends into the sand-body complex. This part of the bar is convex-concave in planimetric shape from east to west. The western end is dissected by several shallow channels (1 to 2 m depth). The surface of the bar is covered with megaripples that are similar to some of those

on the eastern part of the bar (Fig. 3.27).

The bar is bounded to the north and south by relatively deep (up to 25 m) channels that extend eastwards into the sand-body complex (Fig. 3.29). The channel along the south side of the bar continues relatively unobstructed from east to west into the deeper parts of Cobequid Bay. The channel along the north side of the bar, however, is obstructed by a shallow shoal near its western terminus where it divides into three small channels (about 15 m deep) to the northeast of the bar.

At low tide, the intertidal relief of the bar ranges from zero to almost 6 m. Seismic records indicate that the thickest accumulation of sediment in the sand-body complex occurs beneath Noel Shore Bar (totalling about 30 m maximum beneath the eastern part of the bar).

Figure 3.30 shows several representative sediment size distributions from Noel Shore Bar and Figure 3.31 shows the areal distributions the mean grain size, sorting and skewness of the sediments. The sediments fall into the medium sand size (about the same size and sorting as the sediments on Noel Bay Bar, but finer than those on East Noel Bar). Mean grain size generally decreases from west to east across the bar. The finest and best sorted sediments occur along or near the bar crestlines (particularly along the south side). The areal variation of sorting does not show a very regular change across the bar. Sorting values are generally lower near the east end of the bar. Sorting improves from north to south across the western part of the bar, and from northeast to southwest across the eastern part. Note the areal distribution of skewness values (negative in flood dominated areas and positive in ebb dominated areas).

The low tide outline and surface morphology of Noel Shore Bar has changed considerably since the late nineteenth centry (compare Figs. 3.15, 3.22, 3.23 and 3.27). The bar was originally called 'Betsy Bob' Bar by the local people and Swift and McMullen (1968), but it is no longer recognizable in recent air photographs. The bar has, however, maintained about the same location through time for the eastern part of the bar, but the western and northern parts have grown steadily westwards. The distribution of bedforms and the position of swatchways has also changed considerably. In 1947 (Fig. 3.22) and 1961-63 (Fig. 3.23),

FIGURE 3.30: Several representative sediment size distributions from Noel Shore Bar. Station locations are shown in Figure A II.1.

A. Variation of sediment size distributions from the west to the east end of the bar.

B. Variation of sediment size distributions from north to south across the western end of the bar.

C. Variation of sediment size distributions from north to south across the eastern part of the bar.

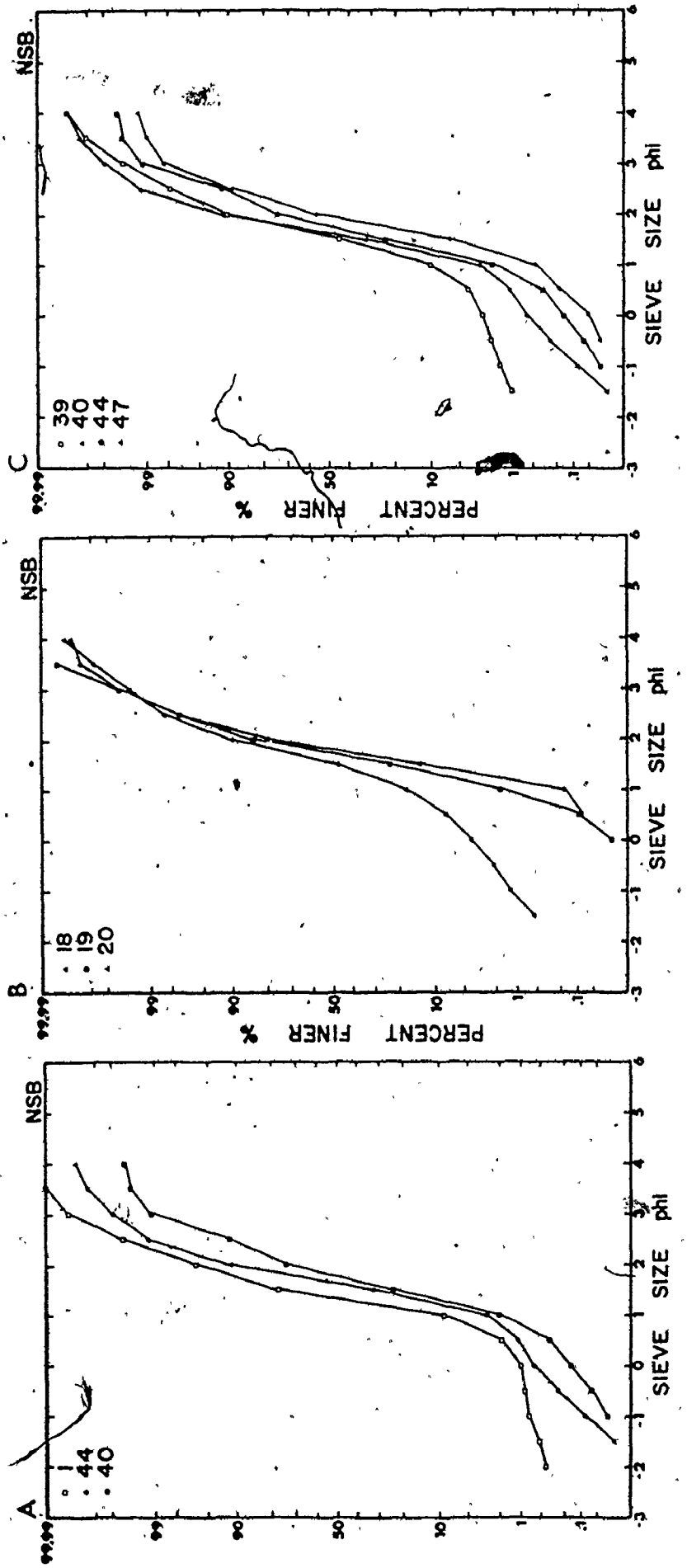
A
NSB
44
40
B
NSB
18
19
20
C
NSB
39
40
44
47
PERCENT FINER %
SIEVE SIZE phi

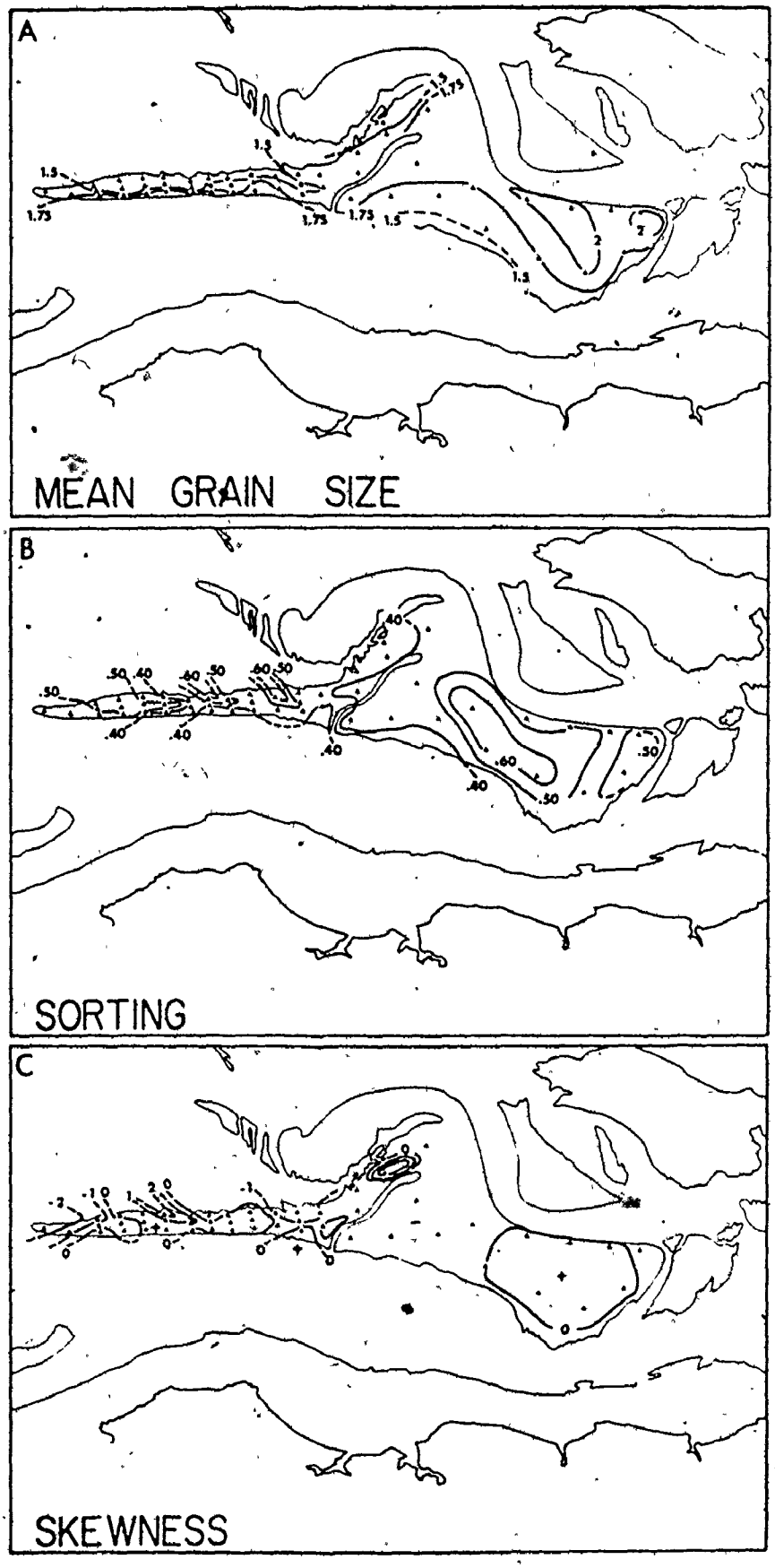

FIGURE 3.31: Areal distribution of mean grain size (A),

there seems to be more largescale megaripples on the north side of the bar than are apparent in 1973 (Fig. 3.27) when the reverse seems to be true.

Selma Bar

Selma Bar is a large sand bar, about 4.1 km long and ranging from 900 m to 2.1 km wide. It is located just off the south shore of Cobequid Bay (Fig. 3.2) to the east-southeast of Noel Shore Bar. The bar is elongate in an east-west direction, parallel to the shore. It is partly shielded from ebb currents by Salter Head to the east, but flood currents have a relatively unobstructed approach to the western end of the bar. Figures 3.32 and 3.33 show the relative position of the bar to the shoreline and to the distribution of intertidal sediment facies. Between the sand bar and Salter Head is an extensive area of mudflats. The transition from the sand bar to the mudflats occurs abruptly (Fig. 3.34 E). The bar is separated from the shore along the entire south side by a low area (Figs. 3.32 and 3.34), most of which emerges only at low water.

The sand bar is divided into two parts by a swatchway that extends from the southwest to the northeast across the middle of the bar (Figs. 3.32, 3.34 B, 3.35). The main crestline of the bar extends along the north side. Secondary crestlines occur on either side of the diagonal swatchway and to the northwest from the main crestline.

The eastern part of the bar slopes gently from north to south (Fig. 3.35) and is traversed by several northeast-southwest oriented, shallow swatchways (Fig. 3.32) with up to 1.5 m relief. The north side of the bar slopes steeply to the north (Fig. 3.34 F and G).

The western part of the bar is topographically simple compared with the eastern part (Figs. 3.32 and 3.35). The bar surface slopes gently to the southwest and steeply away from the main crestline to the north.

The surface of the whole bar is covered with a complex hierarchy of bedforms including sand waves (on the eastern part of the bar only) and megaripples (superposed on the sand waves and on the western part of the bar). A more extensive discussion of bedforms is found in Chapter 5.

FIGURE 3.32: Vertical air photo mosaic showing Selma Bar (photos were taken near low tide in 1973 by Atlantic Air Survey; see Table 3-1)

1973 SELMA BAR

N

SCALE 0 1 2km

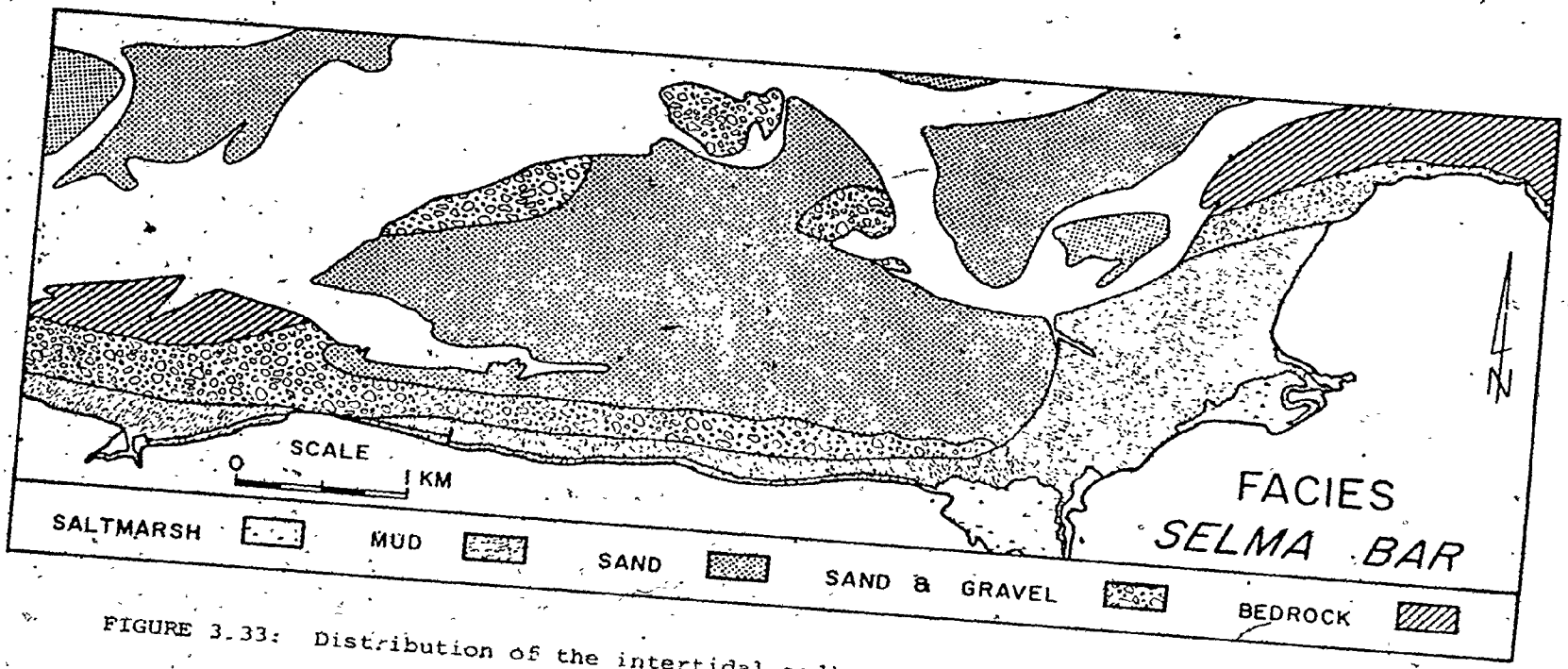

FIGURE 3.33: Distribution of the intertidal sediment facies in the vicinity of Selma Bar.

FIGURE 3.34: Photos of Noel Shore Bar and Selma Bar.

A. The western part of Noel Shore Bar showing the large asymmetrical bedforms on the surface of the bar. The large-scale features are flood oriented (asymmetrical towards the head of the bay). View is to the north.

B. Oblique air photo of the central part of Selma Bar showing the diagonal swatchway that divides the bar surface into eastern and western parts. Note the sand waves on the eastern part (right of swatchway) and the megaripples on the western part (to the left). The south shore and intertidal foreshore are located in the foreground. View is to the NNE.

C. Oblique air photo of the eastern end of Selma Bar showing the edge of the intertidal zone in 1973. View is to the northeast.

D. Oblique air photo of the eastern part of Selma Bar showing the edge of the intertidal zone in 1974 (photo courtesy of R. W. Dalrymple). View is to the northeast.

E. Oblique air photo of the eastern end of Selma Bar showing the abrupt transition between the sand bar and the mudflats. View is to the north.

F. View of the northeast side of Selma Bar showing the eroded, steep northern slope. View is to the east; scale is 1 m long.

G. View of the northern side of Selma Bar showing the steep slope (10 to 15°) and erosion from the low water dewatering of the bar. Scale is 1 m long.

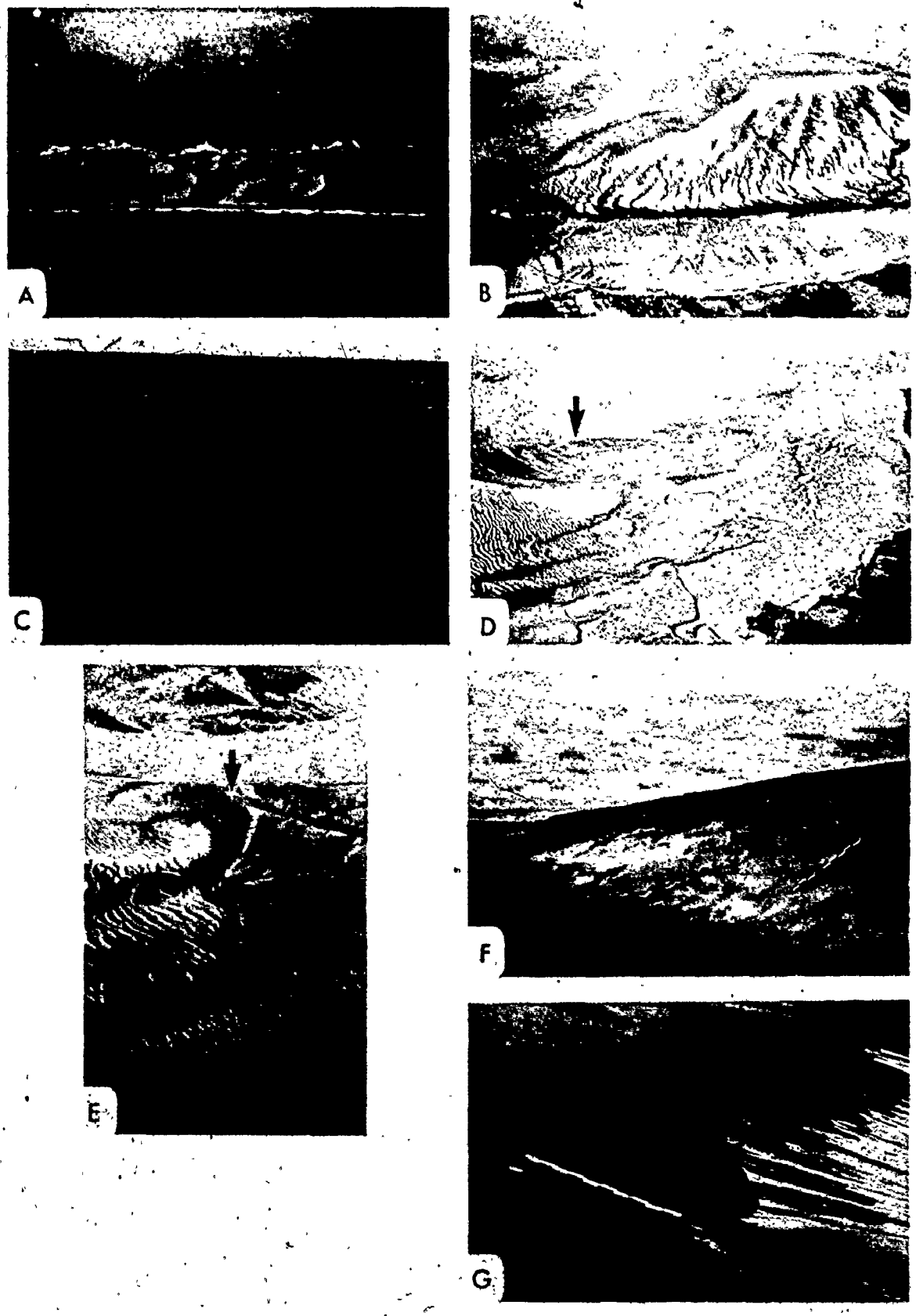
A
B
C
D
E
F
G

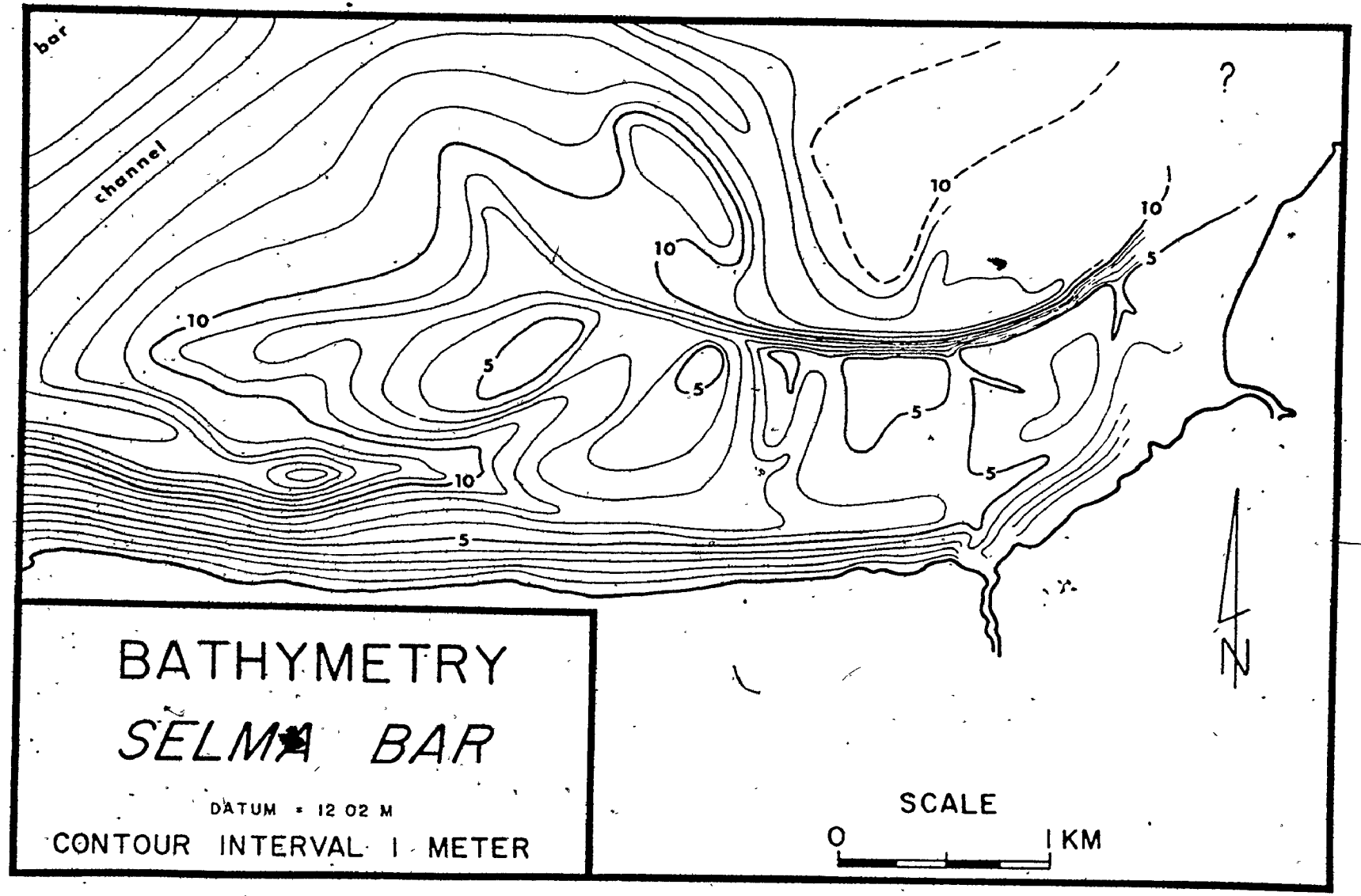

FIGURE 3.35: Bathymetry of the Selma Bar area.

Seismic records show that the thickness of sediment is generally less than 5 m. The sediments rest directly on bedrock and (or) a gravel lag which is exposed along the northern edges of the bar and which appears to be laterally continuous with the sands and gravels of the intertidal foreshore.

Figure 3.25 shows several representative sediment size distributions from Selma Bar and Figure 3.36 shows the area variation of mean grain size, sorting and skewness of the bar sediments. The coarsest and poorest sorted sediments are found along the south side of the bar presumably because this area is closest to the major sources of sediment (in the cliffs south and west of the bar). Almost all of the sand in the bar falls into medium sized sands. Mean grain size decreases and sorting improves towards the crestline of the bar. The best sorting occurs along the north side and western end of the bar away from likely sources of coarser sediment and where current action is strongest. The flood dominated parts of the bar (e.g., northwest end and south of main crestline) tend to have negatively skewed sediments.

Selma Bar has remained in the same relative position for over 100 y (compare Figs. 3.15, 3.22, 3.23 and 3.32).

In 1938 (Fig. 3.37, the bar extended much further to the north and east than it did in 1973 (Fig. 3.32). The mudflat now present to the east of the bar was of only limited extent at that time. The crestline was located along the north side of the bar, but was very simple in outline, i.e., there were no secondary crestlines and only small late stage ebb-runoff channels across the bar surface. The bedforms appear to be primarily large megaripples with few sand waves. The intertidal foreshore south of the bar has changed very little.

In 1947 (Fig. 3.22), the north side of the bar had begun to retreat towards the south, and the bar had extended somewhat further towards the west. The mudflat area was beginning to become more extensive as it prograded over the sand bar surface west of Salter Head. The crestline of the bar was still relatively simple near the eastern end of the bar, but it bent towards the southwest near the western part of the bar as the diagonal swatchway began to develop.

In 1961-63 (Fig. 3.38), the air photos indicate that the outline

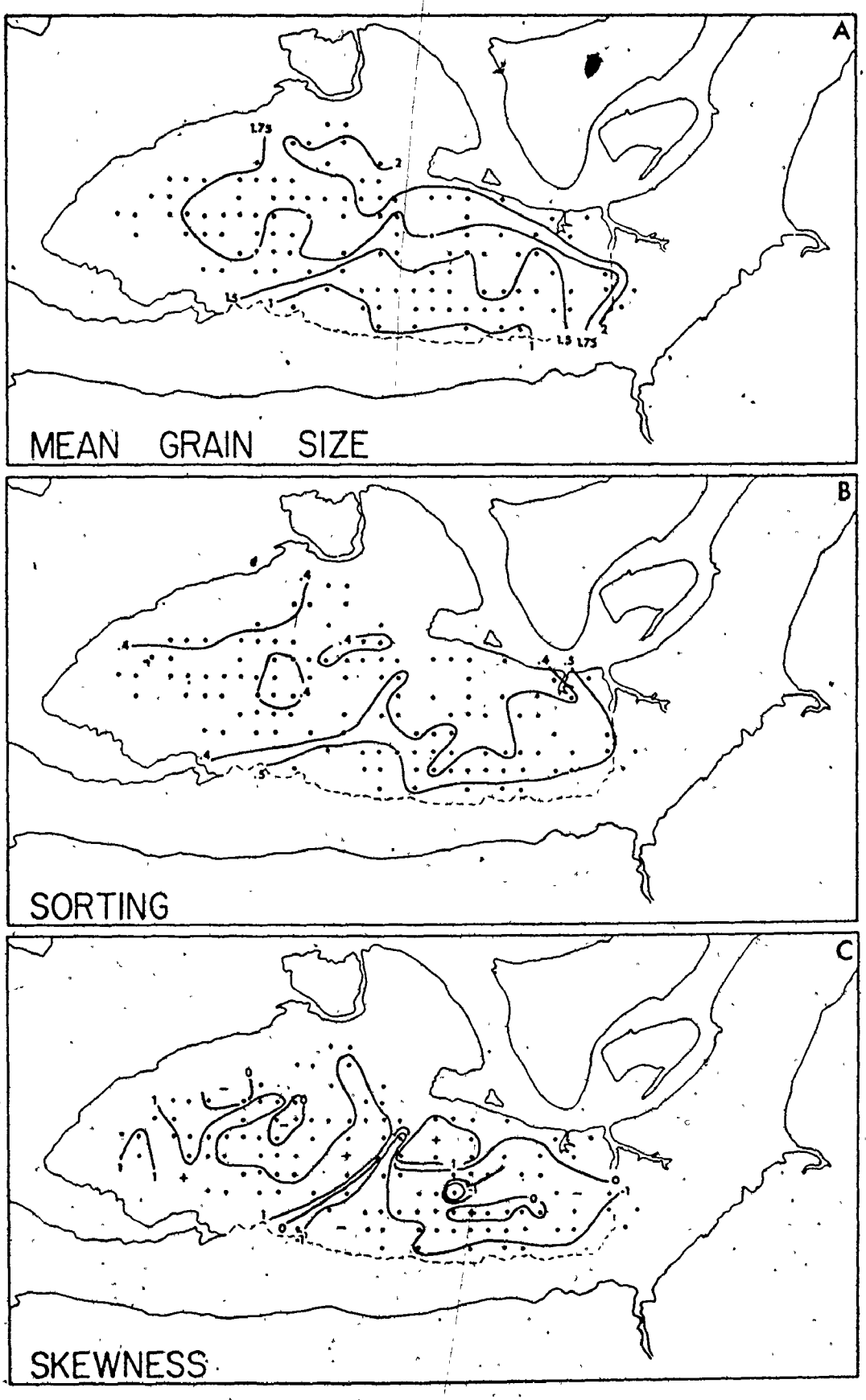

FIGURE 3.36: Areal distribution of mean grain size (A), Sorting (B)

FIGURE 3.37: Vertical air photo mosaic of Selma Bar in 1938 (N.A.P.L. photos). See Table 3-1 for the time and level of the tide relative to flight time.


1938 SELMA BAR
0 SCALE 1 2km

FIGURE 3.38: Vertical air photo mosaic of Selma Bar in 1961-63 (N.A.P.L. photos). See Table 3-1 for the time and level of the tide relative to flight time.

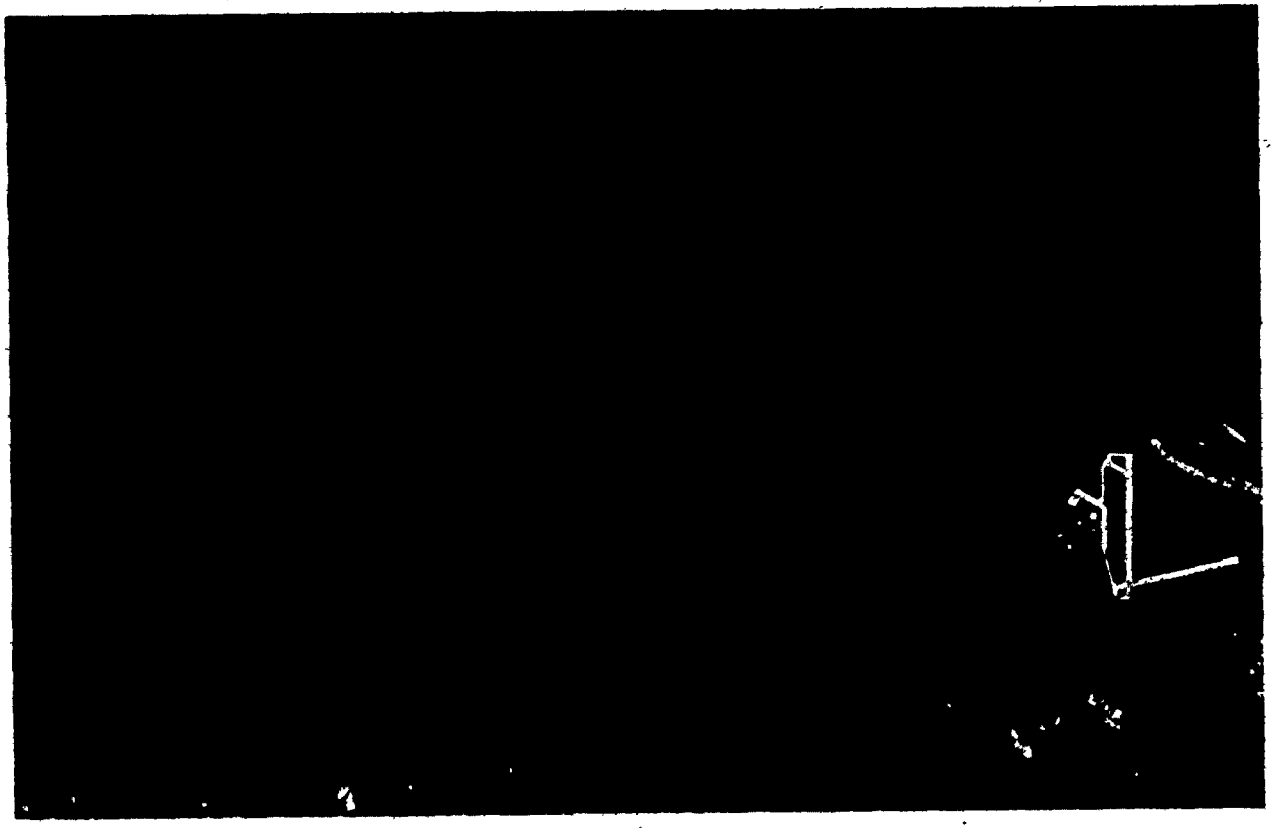

N

1961 - 1963

SELMA BAR

SCALE

0 1 2 km

of Selma Bar was very similar to the present outline (1973-Fig. 3.32), but that the surface morphology was still quite different. There were at least two swatchways extending across the bar surface, but they showed little similarity to the present surface pattern. The bar's crestline was becoming more complex as the secondary morphology of the surface developed.

During August, 1973, the northeastern edge of Selma Bar began to retreat at a rapid rate (Fig. 3.34 F) of about 0.3 m/tidal cycle. Figure 3.34 C shows the position of the northern edge of Selma Bar in 1973 which was close to the maximum position of retreat. Figure 3.34 D shows the position of the same part of Selma Bar, but now the channel north of the bar has changed its course and the northern edge of the bar has accreted northwards.

3.6 SUMMARY

The sand-body complex is concentrated in the centre of Cobequid Bay (Fig. 3.3), generally away from the shore. The intertidal shore is dominated by wave and current cut bedrock platform that is either exposed or covered with a veneer of sediments and by mudflat deposits. The area of sand deposition is characterized by two subfacies (Fig. 3.3): (i) the broad intertidal, fine-grained sand flats with ripples and few large bedforms, and a braided pattern of tidal channels situated near the head of the bay; and (ii) the intertidal to subtidal, lenticular sand bars with many large bedforms and relatively few, but deep major tidal channels situated in the central to western part of the bay. In this study, detailed examination of several of the major intertidal sand bars were made from the latter subfacies, and included Noel Bay Bar, East Noel Bar, Noel Shore Bar and Selma Bar (Fig. 3.2).

The bathymetry of the sand-body complex (Fig. 3.5) was determined from 13 echo-sounding transects of the bay (Fig. 3.4) totalling over 70 km of survey line, plus individual surveys of the four sand bars studied in detail (echo-sounding and level). The sand bars are separated from the shore and each other by relatively deep (5 to 15 m deep relative to the surface elevation of the bar tops; see Figs. 3.5 and 3.6) tidal chan[illegible] The bars vary [illegible] in siz[illegible] in geo-

metrical and topographical shape (Figs. 3.2, 3.5 and 3.6), but are generally almost parallel to the tidal currents, asymmetrical in transverse section, and about 3 km long, 1 km wide and 5 to 15 km thick. In plan, the eastern ends of the bars are relatively blunt (Fig. 3.2) while the western ends are relatively pointed. In transverse section, the gently sloping sides of the bars are generally inclined between 3 to 5 degrees, while the steeply sloping sides of the bars slope between 4 and 12 degrees into the adjacent channel. The steep slope of the bars, located to the south of the bay's longitudinal axis, generally face to the north, while the steep slope of those bars, located to the north of the bay's axis, generally face south. The relief of the bars decreases from about 25 m in the west to about 5 m in the east (Figs. 3.5 and 3.6) of the sand-body complex. The duration of intertidal exposure increases from about 2.5 hours to over 4 hours towards the head of the bay. The sand-body is dominantly subtidal at the seaward end of the bay, and increasingly intertidal towards the east. At high tide, the tops of the bars are covered by up to 10 m of water near the western edge and less than 5 m near the eastern end of the complex.

In tidal areas elsewhere, such as the North Sea, the relief and relative level of the tops of linear sand ridges are believed to be controlled by the base level of strong wave activity. In Cobequid Bay, the largest waves approach from the west and most wave energy is dissipated near the seaward edge of the sand-body complex. Wave action is progressively decreased by increased bottom friction (i.e., shallow water depths and relatively complex bathymetry) towards the head of the bay and therefore, the bars there can be built higher into the intertidal zone than those at the exposed seaward margin of the bay. There is a detectable west to east gradient along the surface of individual bars (Fig. 3.6) showing that the western ends of the bars are somewhat lower (by about 2 to 3 metres) than the eastern ends.

The structure and internal geometry of the sand bars were determined with a continuous 'sparker' survey done at the same time as the bathymetric survey (see Fig. 3.4 for the location of the survey lines). The thickness of the bars (Fig. 3.12) ranges from 5 to 15 m, and generally decreases towards the head of the bay and is roughly equal to the maximum bathymetric relief of the sand bars (compare Figs. 3.5 and 3.12).

The sand bars overlie a relatively flat surface of either older sediments (Figs. 3.7, 3.10 and 3.11) that is probably Pleistocene or Triassic bedrock (Figs. 3.7 and 3.9). The major tidal channels separating the sand bars from each other are generally cut down to bedrock through the modern and premodern sediments in many locations (Figs. 3.7 and 3.13). The premodern sediments occur as small, elongate deposits up to 10 m thick beneath the sand bars. The topography of the surface underlying the modern sediments in the bay forms a shallow depression (Figs. 3.9 and 3.11) along the longitudinal axis of the bay that shallows and decreases in relief from the mouth to the head of the bay. Thus, the sand-body complex appears in stratigraphic cross-section to be a clastic wedge that has prograded over the bedrock surface from the head of the bay.

The historical record (Figs. 3.14 and 3.15) of air photos since 1937 and charts since 1860 shows the relative stability of the position of the intertidal sand bars. The sand bars located near the shore (e.g., Selma Bar and East Noel Bar) have changed little in position while the sand bars situated offshore have moved primarily by lateral migration of the interbar channels or avulsion of the interbar channels into bar swatchways. The surface topography, and the distribution of large-scale bedforms (i.e., megaripples and sand waves) on the sand bars (based on air photos, e.g., Figs. 3.16, 3.22, 3.23, 3.24, 3.27, 3.32, 3.37 and 3.38) have changed appreciably during the last 40 years, but there is no evidence that there has been a major net progradation or reduction in the size of the intertidal part of the sand-body complex (i.e., the volume of sand in the bay has remained relatively unchanged).

The sands of the sand-body complex are generally medium-grained (about 0.34 mm) and well-sorted. Grain size decreases and sorting improves away from the shore towards the head of the bay. The poorest sorted and coarsest grained sands are commonly found near the shore or in the interbar channels, while the best-sorted and finest-grained sands are found along and near the crests of the bars. There is a tendency for the sands of the flood dominated areas of the bars to be negatively skewed while those of the ebb dominated areas are positively skewed. Postma (1957, p.337) suggested that there were three possible controls

on the areal variation of grain size distributions in an intertidal environment: (i) the intensity of water movement; (ii) the origin of the sediment (provenance); and (iii) the direction of transport. All three factors seem to be important in controlling the areal variation of the sediments in the sand bars of Cobequid Bay.

CHAPTER 4

TIDAL CURRENTS

4.1 INTRODUCTION

In 1929, the German paleontologist, Richter, founded the Senckenberg am Meer at Wilhelmshaven as an institute for the study of modern intertidal and shallow subtidal marine sediments to aid in the study of ancient rocks (Spencer, 1957). Since that time, there has been a very large increase in the number of published studies of intertidal areas, particularly in the North Sea (Boersma, 1967, 1968; Boersma et al., 1968; Evans, 1965; Hantzschel, 1939; Postma, 1957; de Raaf and Boersma, 1971; Reineck, 1967; Reineck and Singh, 1967; van Straaten, 1953; and Terwindt, 1971 a).

Over approximately the same period of time, also beginning in Germany, with the work of Prandtl (1926), his students Nikuradse (1933) and Shields (1936) and his associate Von Karman (1930), theoretical and experimental work by hydraulic engineers has led to great advances in the understanding of the fundamental physics of flow and sediment transport. This knowledge has recently been summarized in books by Raudkivi (1967 a), Graf (1971) and Yalin (1972). In attempting to apply these new concepts to natural sedimentary systems, the main effort has been directed towards rivers (Shen, 1971). There have been few studies of the tidal environment (Allen, 1976 b; Dyer, 1970; Gordon, 1975; Ludwick, 1972, 1974, 1975; Smith, J.D., 1969; Sternberg, 1966, 1967, 1968, 1970, 1971, 1972; Sternberg and Kachel, 1971; and a few others).

Current measurements (vertical velocity profiles and point velocities 0.5 m from the bottom) were made over a variety of bed configurations at several selected locations in Cobequid Bay (Fig. 4.1). The current meters and the field and analytical techniques are discussed in Appendix III (Sections 1 and 2). The velocity profile measurements are listed in full in Appendix III.3, and the point velocity data are summarized in

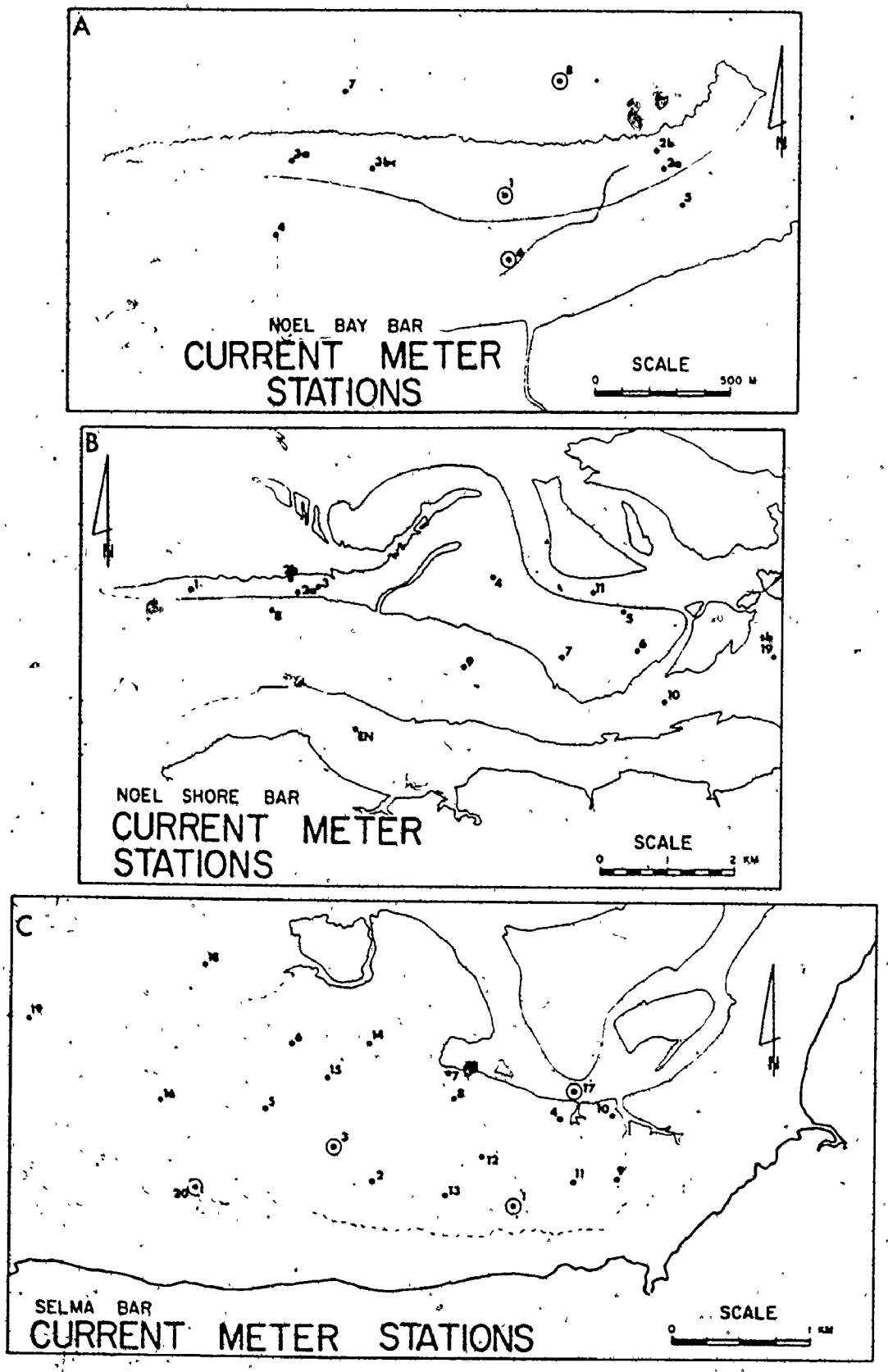

FIGURE 4.1: Location of current meter stations on Noel Bay Bar (A), Noel Shore and East Noel Bars (B), Selma Bar (C) and in Cobequid Bay (D). Circled stations indicate locations of automatic recording current meters. All stations indicate locations of vert

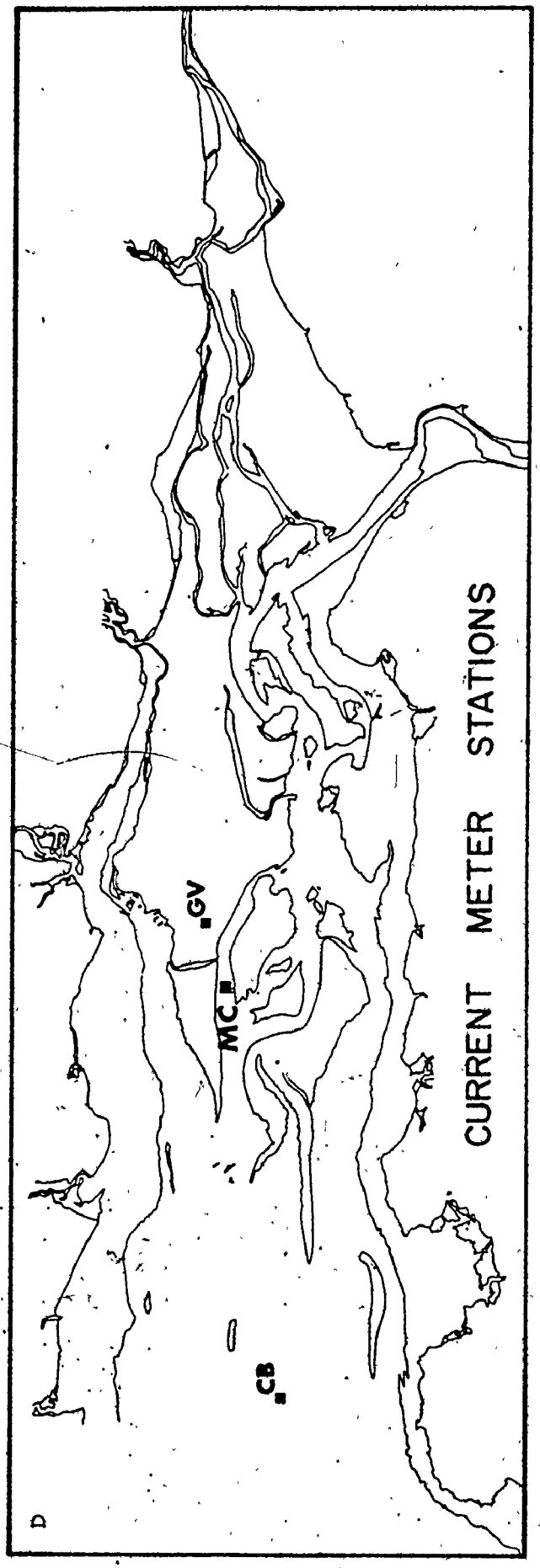

FIGURE 4.1 - cont'd.

Appendix III.4. The purpose of this chapter is to present and discuss the results of the current measurements and some of their hydraulic relationships in the sand-body complex. The derived hydraulic variables are listed in Appendix IV.

4.2 THEORETICAL CONSIDERATIONS

The basic problems in understanding the dynamics of sediment movement are similar for rivers and for tidal currents. Several textbooks summarize the knowledge of open channels (Chow, 1959; Henderson, 1966; Rouse, 1950;). The rate and mode of sediment movement, and the form of both small and large scale sediment accumulations (bedforms, bars, etc.) must be related to hydraulics, but the exact form of the relationship is not fully understood, either in the laboratory or the flume. One major problem for the investigator, therefore, is the choice of appropriate hydraulic variables.

Experience in laboratory flumes and in rivers suggests that two of the most important variables are depth (D) and mean speed ($\bar{u}$) (Brooks, 1958; Colby, 1964; Southard, 1971; Vanoni, 1974). Two fundamental properties of fluids are the density (ρ) and dynamic viscosity (μ). The two may be combined as the kinematic viscosity ($\nu = \frac{\mu}{\rho}$). For flows with a free surface, account must be taken of the gravitational acceleration (g).

These five fundamental variables may be combined to produce two dimensionless numbers, whose significance in hydraulics has long been established:

the Reynolds Number, $$Re = \frac{\bar{u} D}{\nu} \qquad (4.1)$$

and the Froude Number, $$Fr = \frac{\bar{u}}{\sqrt{gD}} \qquad (4.2)$$

where $\bar{u}$ = the mean flow velocity and D = the flow depth. The Reynolds Number expresses the ratio of viscous to inertial forces in the flow. For Re less than 500, viscous forces control the flow character, which is laminar. If Re is greater than 750, inertial forces dominate and flow is turbulent. Transitional regimes occur between

these limits. Turbulent flow occurs in almost all natural open channels. The Froude Number represents the ratio of inertial to gravitational forces. For Fr less than 1.0, gravitational forces dominate and the flow is 'subcritical' or 'tranquil'; this is the normal circumstance in most tidal flows. For Fr greater than 1.0, inertial forces dominate, and flow becomes 'supercritical' or 'rapid'.

Most engineers have also attempted to relate sediment movement to the shear-stress acting on the bed (τ_o) or to the shear-velocity (u_*), which is related to shear-stress by the equation:

$$u_* = \sqrt{\tau_o/\rho} \qquad (4.3)$$

This is because shear-stress measures the fluid force acting on the bed. It was also shown by Shields (1936) to be the principle variable that determines the beginning of sediment movement on a flat bed. Inman (1949) and Bagnold (1966) and many others have demonstrated that the intensity of turbulence close to the bed is directly proportional to the shear velocity. Bagnold (1956, 1966) has suggested that the stream power ($\bar{u}\ \tau_o$), the rate at which a flow performs work on its bed, is a fundamental variable for sediment transport and bedform development.

Thus, it seems important to include some estimation of shear-stress among the hydraulic variables measured in the field. Field measurements of shear-stress, however, is not as simple as the measurement of depth and average current speed. There are five techniques for determining or estimating the boundary shear-stress:

1. Direct measurement with a Preston-tube. This technique has been used quite successfully in laboratory experiments for open channel flows over rigid boundaries, but it has found only limited utility in the field. Smith, J.D. (1969) and Nece and Smith (1970) have discussed the numerous problems.

2. Reynolds Stress. This technique requires some means of measuring the apparent shear-stress ($\tau=-\rho\overline{u'w'}$) at two levels near the bed in a turbulent flow and assuming a linear variation of the stress to yield the boundary shear-stress. The apparent shear-stress depends on measurement of the fluctuating turbulent velocity components u' and w'. McQuivey (1973 a and b) has discussed the assumptions and calculations involved.

Such measurements, using hot-wire and hot-film devices, have become commonplace for studies in air and in some flumes, but the operation and results of such devices in natural channels have generally proven to be unreliable. Three exceptions are Church (pers. comm.) in some British Columbia rivers, and measurements in tidal currents by Bowden and Fairbairn (1956, with small electromagnetic flowmeters) and Grant et al. (1962, with a hot-film flowmeter).

3. Momentum Analysis. This is an indirect method used in boundary layer studies. It is based on velocity profiles measured normal to the bed at successive stations and then solution of the boundary shear-stress using momentum principles. Several complications exist when this method is attempted in tidal channels: current speeds vary both in magnitude and direction, and pressure gradients vary with time because the water surface slope changes. The momentum analysis approach has been used, with several simplifications, in some tidal channel studies (Bowden and Fairbairn, 1952; Bowden, Fairbairn, and Hughes, 1959). These studies were made in channels with few and small bed irregularities so that development of a nonuniform velocity field would not be a significant factor. Solution of a nonuniform velocity field by momentum analysis would be impractical.

4. Water Surface Slope. This method is commonly used in river studies. The boundary shear-stress is computed from the equation:

$$\tau_0 = \rho g D S \qquad (4.4)$$

where ρ is the water density, g is the acceleration of gravity, D is the water depth and S is the water surface slope (an approximation of the slope of the energy surface). Equations of this form are valid only for steady uniform flows of homogeneous fluids. The major requirement for use of this method is accurate measurement of the water surface slope. Such methods are common in straight reaches of rivers using survey techniques (e.g., Jordan, 1965; Scott and Stephens, 1966; and many others), but may involve errors of ±10%. Sea-surface slopes are

seldom known accurately in shallow-marine areas. Direct measurement of water-surface slopes were attempted in this study by sighting with a theodolite (a Wilde T2) to several buoys moored at various locations over one of the nearshore sand bars (Selma Bar) periodically through a tidal cycle. The results of the survey were rejected because: (a) the distance from the theodolite station to the individual buoy locations could not be determined precisely; (b) the distance from the theodolite to the buoys was large (1000 to 1500 m) for precise measurement of the vertical position changes of the buoys through the tidal cycle; and (c) the buoys were dragged beneath the surface during periods of maximum current flow, and therefore could not be accurately located.

5. Quadratic Stress Law. This technique is based on experimental evidence that the boundary shear-stress is proportional to the fluid density and the square of the mean velocity:

$$\tau_o \propto \rho \bar{u}^2 \qquad (4.5)$$

or,

$$\tau_o = C_D \rho \bar{u}^2 \qquad (4.6)$$

if the proportionality coefficient, C_D, is introducted. C_D is a dimensionless drag coefficient. The problem of choosing a value for C_D is similar to that of choosing a value of Manning's n or Chezy's C, except that tables of n are relatively common whereas the variations in C_D are less well established (Ludwick, 1975 ; Nikuradse, 1933; and Sternberg, 1968).

6. Velocity Profiles. In the present study, shear-stress or shear-velocity was estimated from the measured velocity profiles. The theoretical basis for this lies in the theory of turbulent boundary layers as originally developed by Prandtl and von Karman (see Schlichting, 1968). Numerous workers have used this method for river flows (e.g., Jordan, 1965; Scott and Stephens, 1966; and others) and for tidal flows (Charnock, 1959; Dyer, 1970; Lesser, 1951; Ludwick, 1974; Revelle and Fleming, p. 480, in Sverdrup et al., Smith, 1969; and Sternberg, 1966,

1968). The basis for this method is discussed in detail in the next section.

Velocity Distributions - The first theoretical derivations of the velocity distribution within a fully developed turbulent boundary layer was given by Prandtl and von Karman (see Schlichting, 1968; Yalin, 1972). Their derivations led to the "law of the wall".

$$du/dy = \frac{\kappa}{u_* Y} \qquad (4.7)$$

where du/dy is the slope of the depth-velocity relationship, and κ (kappa) is called the von Karman "universal constant." Integration of the law of the wall up to the limits, $u=u_{max}$ at $y=D$ gives

$$\frac{u_{max}-u}{u_*} = -\frac{2.3}{\kappa} \log_{10} \frac{D}{y} \qquad (4.8)$$

This is the "velocity defect law." The indefinite integral of the law of the wall yields

$$\frac{u}{u_*} = \frac{2.3}{\kappa} \log_{10} y + C_1 \qquad (4.9)$$

where C_1 is a constant of integration, having the dimension of length. The value of C_1 depends on the boundary roughness (Yalin, 1972, p. 27-28), i.e., whether the bed surface is hydraulically smooth or hydraulically rough.

Application of the theoretical velocity distribution depends on the nature of the boundary layer close to the wall, which in turn is related to the flow and boundary characteristics. If the boundary is relatively smooth, a laminar sublayer persists in the region close to the boundary even after the development of the turbulent boundary layer. If, however, large roughness elements project through the laminar sublayer into the turbulent region, the laminar sublayer may be partly or wholly destroyed.

The exact conditions for the existence of a laminar sublayer were first investigated by Nikuradse (1933) using pipes whose interior sur- had been rou by gluing on a of

grains. Nikuradse found (see Schlichting, 1968, p. 567 and 579-586) that the nature of the flow at the boundary was determined by a Boundary Reynolds Number, Re_b,

$$Re_b = \frac{u_* k_s}{\nu} \qquad (4.10)$$

where k_s was the diameter of the sand grains, and ν is the kinematic viscosity. For Re_b less than 5, the roughness elements were entirely contained within the laminar sublayer and the roughness has no direct effect on the flow. This boundary is considered to be hydraulically smooth. The velocity distribution and the boundary shear-stress or the frictional resistance of the boundary to the flow are entirely determined by the flow Reynolds Number $Re = \frac{\bar{u} D}{\nu}$). For Re_b greater than 70, the roughness elements completely destroy the laminar sublayer. This boundary is considered hydraulically rough. The velocity distribution and the shear-stress (or the frictional resistance of the boundary to the flow) are determined by the mean velocity, the depth, and the relative roughness (k_s/D). For values of Re_b between 5 and 70, the laminar boundary layer is only partly destroyed and the boundary roughness is considered hydraulically transitional. It can be shown that, for smooth and transitional boundaries,

$$Re_b \sim 11.6 \frac{\delta'}{k_s} \qquad (4.11)$$

where δ' is the thickness of the laminar sublayer. It should be noted that these critical values of the Boundary Reynolds Number apply only to flat boundaries roughened by uniform sand grains. For different types of roughness, the height of the roughness elements does not necessarily correspond to the sand grain diameters used by Nikuradse (e.g., Morris, 1955). However, as long as the total effect of the roughness on the flow can be expressed as a length, this length can be expressed as an "equivalent sand roughness" (k_s). In nature, boundary roughness results not only from sediment grains, but also from bedforms such as ripples and megaripples. A further discussion of k_s is deferred until a later section.

In equation 4.9, the constant C_1 can be assumed to be a logarithm:

$$C_1 = -\frac{2.3}{\kappa} \log_{10} y_o \qquad (4.12)$$

where the nature of y_o depends on whether the boundary surface is hydraulically smooth of hydraulically rough. The value of y_o has been found experimentally to be a function of Re_b, the Boundary Reynolds Number. Substitution of equation 4.12 into equation 4.9 gives

$$\frac{u}{u_*} = \frac{2.3}{\kappa} \log_{10} \frac{y+y_o}{y_o} \qquad (4.13)$$

If y_o, which is a constant, is assumed to be small compared with y, then equation 4.13 can be rewritten

$$\frac{u}{u_*} = \frac{2.3}{\kappa} \log_{10} \frac{y}{y_o} \qquad (4.14)$$

For a smooth boundary, y_o depends only on u_* and ν. Nikuradse found that

$$y_o = \frac{m\nu}{u_*} \qquad (4.15)$$

where m is a constant (a generalized Reynolds Number) equal to about 1/9 for smooth pipes. For rough boundaries, he found that m depends on the height, k_s, of the surface roughnesses. Thus,

$$y_o = mk_s \qquad (4.16)$$

where m is a constant equal to approximately 1/30.2.

Keulegan (1938) found from a study of Nikuradse's (1933) pipe data and Bazin's (1865) open-channel data that the uniform flow equation for open-channel velocity over smooth boundaries was:

$$\frac{u}{u_*} = \frac{2.3}{\kappa} \log_{10} \frac{yu_*}{\nu} + 5.5 \qquad (4.17)$$

For flow over rough boundaries, it was:

$$\frac{u}{u_*} = \frac{2.3}{\kappa} \log_{10} \frac{y}{k_s} + 8.5 \qquad (4.18)$$

This is the result most commonly used for rivers (e.g., Einstein, 1950).

Less frequently used in natural flows is the velocity defect law in either the logarithmic (eqn. 4.8) or parabolic form (Ludwick, 1974, p. 719; 1975, p.20)

$$\frac{u_{max} - u}{u_*} = C_2 \left(1 - \frac{y}{D}\right)^2 \qquad (4.19)$$

Equation 4.19 represents a parabola open in the -u direction with the vertex and the principal axis at the water surface, where $du/dy = 0$. Ludwick (1974, 1975) used Hama's (1954) empirical formula with $C_2 = 9.6$. Keulegan (1938), on the other hand, used $C_2 = 6.25$.

The equations discussed thus far assume two-dimensional steady-uniform flow over rigid boundaries and no sediment movement. Such conditions are nowhere realized under natural flow conditions. Several important differences must be discussed (Mahmood and Simons, 1975; and Simons and Richardson, p. 9-1 to 9-89, in Shen, 1971):

(i) in natural flows, the flow and the boundary interact in a much more intimate manner because they are to some extent interdependent. A non-cohesive sediment bed (e.g., sandy) deforms by developing ripples and dunes as the nature of the flow changes. The resultant boundary geometry and rate of change of the bedforms in turn affects the nature of the flow.

(ii) With bedform development, the "equivalent sand roughness" (k_s) depends on both the geometry and the scale of the ripples and dunes, rather than on a single, invariant, characteristic scale only (roughness height).

(iii) Sediment moving close to the bed by rolling, sliding and saltation alters the hydraulic roughness, even for a flat bed.

(iv) The movement and changing geometry of bedforms causes some unsteadiness in the flow.

(v) When bedforms develop to a height comparable in scale to the depth, the flow becomes nonuniform.

Unfortunately, the development of theory for real, three-dimensional unsteady-nonuniform flow over moveable beds with sediment transport is not comparable to the theories available for ideal flows (e.g., two-dimensional, steady-uniform flows over rigid boundaries with no sediment movement). Therefore, it is necessary to continue to make use of the classical rigid boundary results, while recognizing that the results are at best only approximately correct when applied in the field.

Having established the theoretical velocity profile for rigid boundaries, there are a number of possible modifications. In order of complexity, these are:

1. Different types of boundary roughness give different constants in the equation (Eqn. 4.17 and 4.18) from those established in Nikuradse's experiments. Refer back to equations 4.15 and 4.16. For example, Keulegan (1938) gave the following numerical coefficients in the equations for the average channel velocities (derived by integration of equations 4.17 and 4.18):

for smooth boundaries $$\frac{\bar{u}}{u_*} = \frac{2.3}{\kappa} \log_{10} \frac{yu_*}{\nu} + 5.5 \qquad (4.20)$$

for rough boundaries $$\frac{\bar{u}}{u_*} = \frac{2.3}{\kappa} \log_{10} \frac{y}{k_s} + 8.5 \qquad (4.21)$$

He also found that the coefficients may vary $\pm$10% (3.23 to 16.92) with different types of boundary roughness. The values of the coefficients in the above equations (4.20 and 4.21) represent average values taken from a study of Nikuradse's pipe flow data and Bazin's open-channel data.

2. The "equivalent sand roughness" (k_s) is dependent on the roughness of the bed surface, and thus, it varies with the size and spacing of the roughness elements. According to Einstein (1950) the value of k_s for flow over a flat sediment bed equals the grain diameter (d) when the bed consists of uniform material (e.g., Nikuradse used d_{50} in his experiments), and the grain size at which 65 percent of the mixture

(by weight) is finer (d_{65}) when the bed consists of non-uniform material. Other workers have suggested using d_{84} or d_{90} (Church and Gilbert, 1975, p. 33-34; Leopold, Wolman and Miller, 1964, p. 159-160; Wolman, 1955, p. 17 and 51-53) for non-uniform grain roughness. A boundary composed of moving sediment (even if still a plane boundary) has a different roughness from one composed of the same sediment that is not moving (Lovera and Kennedy, 1969).

3. The presence of large amounts of suspended coarse sediment alters the value of Von Karman's 'universal constant' (κ) and may make the velocity distribution close to the boundary non-logarithmic. For clear-water flows with no sediment movement, the Von Karman 'universal constant' (κ) has been found to have a value approximating 0.4 in flume experiments (A.S.C.E., Task Committee, 1963 b; Nikuradse, 1933). However, high concentrations of suspended coarse sediment in a flow have generally been found to lower the value of κ to as low as 0.2 (A.S.C.E., Task Committee, 1963 b; Einstein and Chien, 1955; Elata and Ippen, 1961, in Graf, 1971; Vanoni, 1941, 1946 and 1953, in Graf, 1971; Vanoni and Nomincos, 1959). Although it is generally agreed by workers that the presence of high concentrations of suspended sediment in a flow lowers the value of κ, there is little general agreement on the reason for the effect on the flow.

It has been suggested by several workers that the logarithmic velocity distribution for clear-water flow is inadequate when applied to large scale flows with high concentrations of suspended sediment. Vanoni (1941 and 1946, in Graf, 1971), from experimental data, showed that the logarithmic distribution of velocity may be inadequate only in some cases in flumes. Einstein and Chien (1955) suggested that the logarithmic law was valid for the whole flow over a plane sand bed except in the lowest part of the flow (see their Fig. 16, Eqns. 27 and 30). Mahmood and Simon's (1975) approach was essentially the same except that they added a third zone of surface effects close to the water surface. Toffaleti (1965) seems to be one of the few who completely rejects the logarithmic law. In the field, it is not possible to measure the velocity profile in the region close to the boundary because of: (i) the practical difficulty in accurately determining the position of the

current meter above the bed; (ii) the relatively large size of the current meter; and (iii) the boundary is composed of sand that would be scoured by flow moving around the current meter.

4. Moulding of the movable bed into bedforms creates form resistance rather than grain resistance (Alam and Kennedy, 1969; A.S.C.E. Task Committee, 1963; Chang, 1970; Einstein and Barbarossa, 1952; Garde and Raju, 1966; Simons and Richardson, 1962 a & b; Vanoni and Hwang, 1967; and summaries in Graf, 1971, p. 303-320; Raudkivi, 1967 a, p. 222-251; and Yalin, 1972, p. 37-40 and p. 262-286). The "equivalent sand roughness" (k_s) with the development of bedforms (ripples and dunes specifically) now becomes the sum of: (i) the grain roughness of the moving bed surface; (ii) the form roughness of the bedforms; and (iii) the roughness due to grain material diffused into the flow (mainly the suspended load). The relative contribution of these factors to the total k_s for bedforms is summarized by Yalin (1972, p. 266-267). Factor (i) is particularly important for flow over plane bed, before and just after the initiation of sediment movement (grain roughness; see 2, this section), and factor (iii) for flow over a moving plane bed in the upper flow regime (bed material in suspension). For ripples and dunes, the size and shape of the bedforms (form roughness) is by far the largest component of the total k_s (e.g., Garde and Raju, 1966, Table 3, p. 85; Vanoni and Hwang, 1967, Table 3, p. 128-129, Tables 4 and 5, p. 134-135).

5. If the bedforms are large compared to the flow depth, the flow becomes nonuniform, and cannot be logarithmic, except (a) very close to the boundary, (b) in that part of the flow that is sufficiently far from the boundary to be little affected by the nonuniformity of the boundary, or (c) over the crestline of bedforms.

The vertical velocity distribution in the region very close to the boundary is beyond the scope of this study for the reasons listed near the end of comment 3, and thus will not be discussed further.

Vanoni and Hwang (1968, Fig. 11; closure to discussions of their 1967 paper) and Mahmood and Blinco (1972, Fig. 11; discussion of Rifai and Smith, 1971) show that the flow is approximately logarithmic in the

region between y=2H (where H is the height of the bedforms) and the water surface. The thickness of the nonlogarithmic region relatively close to the boundary is directly influenced by the location of the velocity profile with respect to the bedform. Over ripples and dunes, the flow separates from the boundary at the bedform crest and reattaches on the upstream slope (or stoss-side) of the next bedform downflow. Profiles measured through the separation eddy commonly show reverse flow near the bed and nonuniform flow up to about y=2H due to expansion and wake generation in the lee of the bedform crest.

Profiles recorded over the upstream (or stoss-side surface, between the point of flow reattachment and the bedform crestline, show the effects of flow contraction within a thin zone that decreases towards the crestline of the bedform. Over the crestline of the bedforms, the contraction of the flow suppressed the effects of nonuniformity and produces a velocity distribution that is logarithmic throughout the main part of the flow (Khanna, 1970; Raudkivi, 1963, 1966; Rifai and Smith, 1971; Vanoni and Hwang, 1967, 1968). In the field, the relatively large flow depth and high water turbidity make it impossible to determine the location of the profile with respect to the bedform.

Vanoni and Hwang (1968) and Mahmood and Blinco (1972) show that some variation in the slope of the depth-velocity distribution occurs on either side of the slope predicted for the known average u_* if κ is determined by the conventional method (e.g., Scott and Stephens, 1966, p. J23; Vanoni and Hwang, 1968, Eqn. 22). The κ values determined vary from too small to too large depending on the position of the mean bed elevation. The average value, however, is still about 0.4 or a little less.

Flume and field studies have shown that the value of κ determined by comparing the slope of logarithmic velocity profiles with the value of u_* determined from Equation 4.4 may vary considerably to either side of 0.4, even for clear-water flows. Sayre and Albertson (1961) report values of κ ranging from 0.34 to 2.77 for clear-water flow over isolated roughness baffles. Many river studies report a wide range for κ. For example: Colby and Hembree, 1955, κ=0.42-2.80 from the Niobara River, Nebraska; Nordin and Dempster, 1963, κ=0.15-1.20 from the Rio Grande and the Rio Puerco, New Mexico; Jordan, 1965,

κ=0.21-0.62 (average=0.35) and Scott and Stephens, 1966, κ=0.31-0.40 (average=0.38) from the Mississippi River at St. Louis, Missouri.

Non-uniformity of flow also has the effect of leading to development of secondary currents. Secondary circulation may also result from sediment in suspension (Graf, 1971, p. 181-182). Secondary circulation may itself have an important effect on the velocity distribution of the flow and hence on the measured value of κ.

6. For relatively deep flows, the frequency (or time scale) for large scale turbulence, which is limited only by the size of the channel, is longer than the time available for making velocity measurements (generally less than 3 min). For example, Cannon (1971) reported that macroturbulence in a coastal plain estuary (4 m deep) had a natural period of approximately 7.5 min. From vertical velocity measurements in the Columbia River, Savini and Bodhaine (1971) found that the 66-min mean velocity varied ±5.1% (Fig. 4.2) and that the optimum measurement period was 1 to 4 min. Thus, even if a long term average showed close approximation to a logarithmic distribution, actual measurements would show large departures.

The net result of all the factors listed in the preceding section, but particularly 5 and 6, is that field measurements in rivers and in tidal currents frequently show large deviations from logarithmic distributions. If it is assumed that the 'true' ("stochastic mean") distributions are logarithmic and least squares are used to fit the best line, the determined values of u_* and k_s may deviate substantially from the 'true' average values in the channel. This deviation is shown, for example, by the large range of values for the von Karman constant (κ) computed from the velocity profiles where the average value of u_* is known (see discussion under 5 above).

4.3 VERTICAL VELOCITY PROFILES

The measured vertical velocity profiles were analyzed in terms of: (i) the applicability of the iterative procedure (described in Appendix III.2) outlined by Inman (1963) and Sverdrup et al. (1942, p. 480);

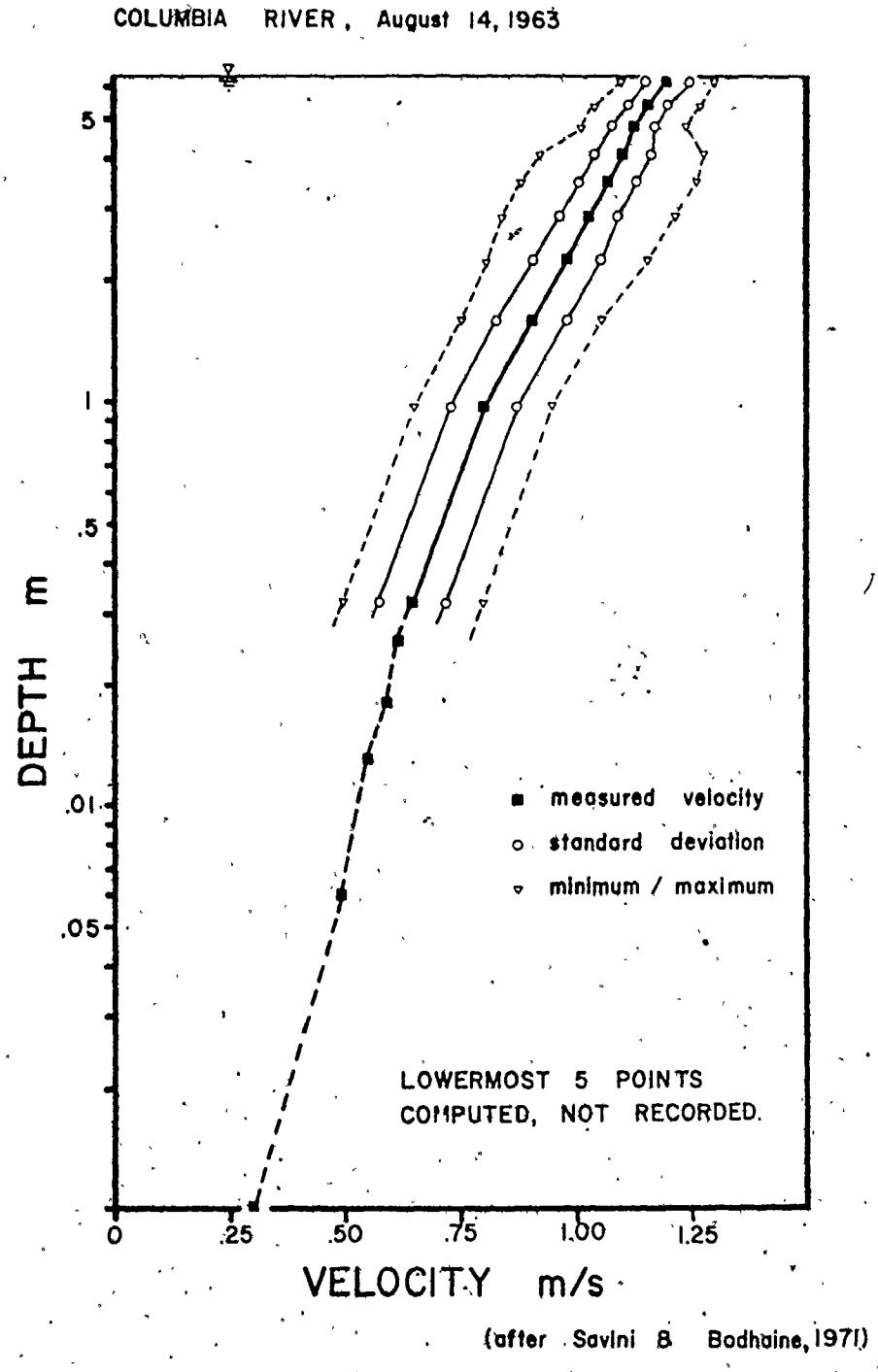

FIGURE 4.2: See caption above.

(ii) the statistical significance of the linear and quadratic regression models fitted to the vertical velocity distributions; (iii) the shape of the velocity profiles; and (iv) the magnitude and distribution of velocity deviations from the profile regression line.

Iteration Procedure

The iteration procedure is a means of improving the fit of the linear regression line to each velocity profile (Inman, 1963; Sverdrup et al., 1942, p. 480). For each iteration, a value of the regression line intercept (y_o = the distance above the profile datum at which u = 0) is determined. The profile datum is shifted in a positive direction (away from the boundary) in increments of the computed y_o-value with each iteration. The iteration continues until the value of the intercept and the correlation coefficient converge towards a unique value for the given flow and boundary conditions.

The results of the iteration analysis on several test profiles (Table 4-1) indicated that y_o and r generally converged within 5 or 6 iterations. Although the values of y_o and r increased with each iteration, the difference between the original and the converged values were generally small to negligible. The iteration technique does not seem to be justifiable in view of the small improvement in fit in most cases. The scatter about the regression line, due largely to turbulence and nonuniformity of the flow produced by the large bedforms, particularly at shallow depths (late ebb, early flood), makes it impossible to determine the exact bed location by this method (e.g., Clauser, 1956; Simons and Richardson, p. 9-1 to 9-89 in Shen, 1971; Vanoni and Hwang, 1967; Yalin, 1972, p. 37-40).

Statistical Significance of the Regression Models

The "goodness of fit" of the regression line fit to the vertical velocity profile was determined with a correlation coefficient (Davis, J. C., 1973, p. 73-80 and 197-198). These coefficients are listed with the hydraulic data in Appendix IV.

An 'F-test' (Davis, J.C., 1973, p. 99-105, 201-204 and 215-217) was used to test the statistical significance of the linear and quadratic regression models (Appendix III,2), and whether or not the improvement in fit due to the addition of quadratic terms was statistically significant.

T A B L E 4 - 1

SUMMARY OF ITERATION RESULTS ON SEVERAL
REPRESENTATIVE VERTICAL VELOCITY PROFILES (NBB-1a)

Time (A.D.T.)	Linear y_o (m)	Regression r(%)	Iterated no. of iterations[1]	Regression y_o (m)	r(%)
0525	0.05	92.3	6	0.07	92.8
0546	0.12	89.9	5	0.17	91.0
0603	0.21	91.7	7	0.44	94.3
0615	0.11	89.6	6	0.17	90.5
0631	0.27	91.8	7	0.67	93.9
0700	0.017	95.9	4	0.018	96.0
0720	0.02	95.9	3	0.03	96.0
0806	0.27	88.1	5	0.41	89.1
0840	0.04	98.0	3	0.05	97.9
0911	0.05	99.0	6	0.07	100.0

NOTE: 1 Number of iterations required to achieve convergance of y_o and the "best fit" (r).

TABLE 4-2

SUMMARY OF F-TEST RESULTS FROM REGRESSION ANALYSIS OF VELOCITY PROFILES (PERCENT)

	Linear			Quadratic			Addition by Quadratic		
	Ebb	Flood	Total	Ebb	Flood	Total	Ebb	Flood	Total
Signif. at 99% level	71.3	67.2	69.5	77.6	70.5	74.5	37.1	17.2	28.4
	80.9	80.3	80.6	89.0	87.9	88.5	51.5	34.4	44.0
Signif. Between 95 and 99%	9.6	13.1	11.1	11.4	17.4	14.0	14.4	17.2	15.6
Signif.	19.1	19.7	19.4	11.0	12.1	11.5	48.5	65.6	56.0
Total %	100.0	100.0	100.0	100.0	100.0	100.0	100.0	100.0	100.0
No. of Profiles[1]	628	482	1110	536	407	943	515	401	916

NOTE: 1. Profiles with negative regression slopes and those with insufficient data points (i.e. less than 3 for linear regression and less than 5 for quadratic) not included in total.

Table 4-2 summarizes the results of the 'F-test' on the velocity profiles. Those profiles with too few data points (i.e., less than 3 for the linear model and less than 5 for the quadratic model) or negative correlation coefficients were excluded from the analysis. The majority of the velocity profiles were significant at the 95% level of confidence. From 1110 profiles regressed by the linear model, 80.6% were significant at the 95% level (69.5% at the 99% level). The quadratic regression increased the number of profiles significant at the 95% level by 7.9% (5.0% at the 99% level) to 88.5% (74.5%) from 943 velocity profiles. A larger number of profiles were significant at the 95% level from the quadratic regression because the correlation always increases with the addition of regression terms (or degrees of freedom), but the number of significant correlations does not necessarily increase.

A comparison of the explained sum of squares for each model (linear and quadratic) and the additional variance explained by the quadratic regression indicates that only a small addition can be attributed to the quadratic fit and that the addition is significant in only 44.0% of the profiles at the 95% confidence level (28.4% at the 99% level). Fifty-six percent of the profiles (from 916 profiles) showed no significant improvement.

Table 4-2 also shows the results of 'F-tests' done ebb and flood profiles separately. The velocity profiles measured during the ebb and flood respectively have about the same proportion of statistically significant profiles.

Profile Shapes

Although the linear regression model generally gave more statistically significant results, a study of the distribution of velocity deviations from the fitted regression line

Deviation Velocity = Observed Velocity - Estimated Velocity

showed that a regular, non-random variation of deviations was common. The profiles could be classified into one of three types (Fig. 4.3): (i) profiles exhibiting deviations greater than the linear model (faster velocity) near the bottom and top of the profile, but deviations less than the fitted line (slower velocity) in the middle part of the

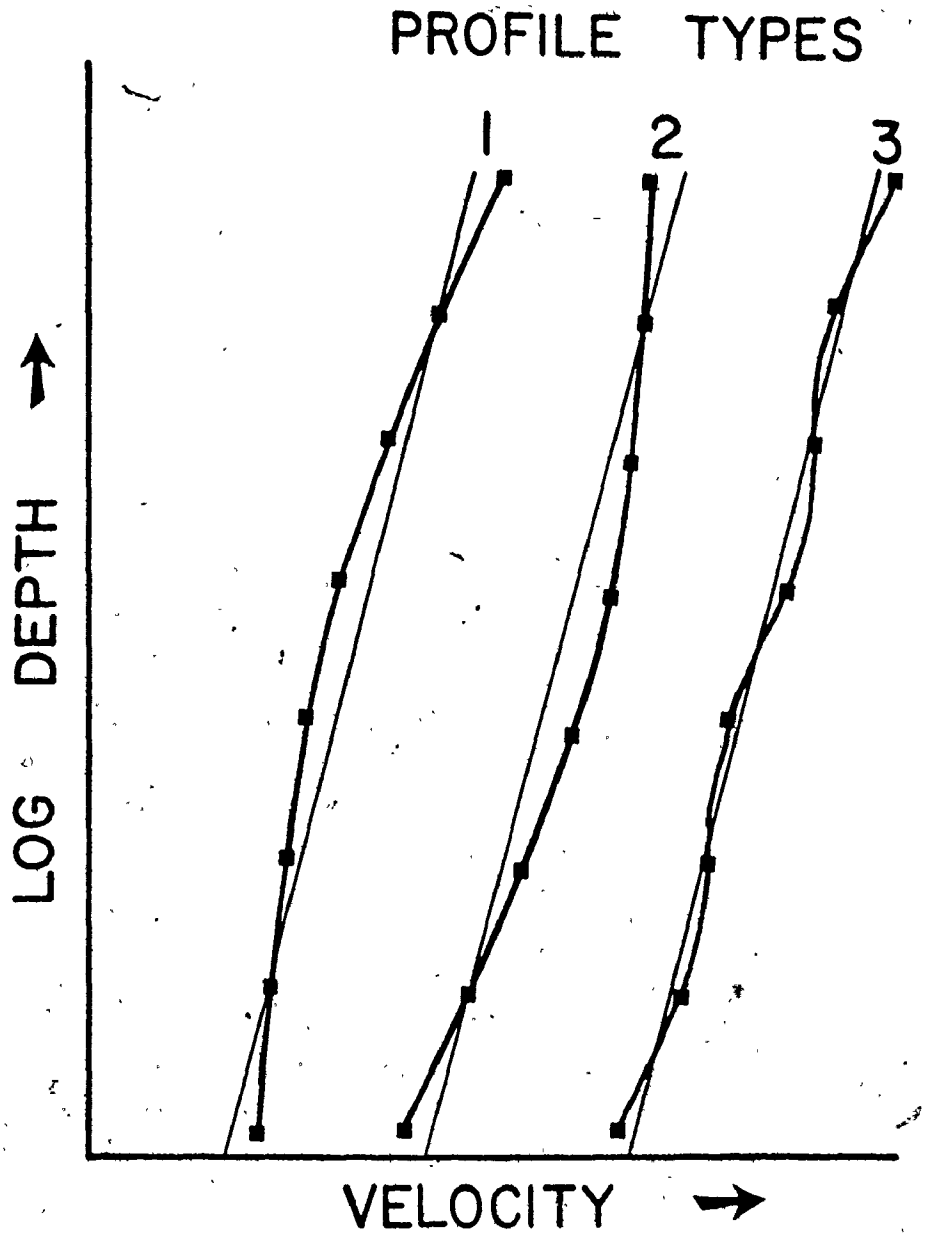

FIGURE 4.3: Diagram of the three types of vertical velocity profile shapes.

profile; (ii) profiles showing the reverse shape to those of 'Type 1', i.e., deviations near the bottom and top of the profile were less than the fitted line, while those in the middle of the profile were greater than the estimated velocity; and (iii) profiles with a more or less linear trend, or display a random distribution of observed velocity points to either side of the fitted line.

Each of the measured vertical velocity profiles was classified according to the shape type using plots of depth versus velocity and a tabulation of the deviation velocities. The results are summarized in Table 4-3. Almost 44% of the profiles could be classified as Type 1, with about 20% as Type 2 and 36% as Type 3 (from 1132 profiles). Further study showed that most profiles (about 53%) were Type 1 during the ebb and Type 3 (about 41%) during the flood (Table 4-3).

The ebb and flood were each divided into two equal parts (on the basis of the respective ebb and flood flow durations). Eighty percent of the profiles during the first half of the ebb were Type 1 distributions. Most of the profiles (55%) during the second half of the ebb were Type 3. During the flood, an equal percentage of profiles were Types 1(38%) and 3 (38%) for both parts of the flood. These results are summarized in Table 4-4.

Figures 4.4, 4.5 and 4.6 show the variation of vertical velocity profile shapes during a tidal cycle at three representative locations on Selma Bar (over megaripples and sand waves).

Profile Deviations

The deviations of the measured profile point velocities from the fitted linear regression are distributed both positively and negatively about the line. Ludwick (1974) used a standard deviation of the velocity departures as a measure the magnitude of the 'waviform departures' from the fitted regression.

$$\text{Waviform Departure} = \sum_{i=1}^{n} \left[\frac{\text{Estimated Velocity} - \text{Observed Velocity}}{n-2} \right]^{\frac{1}{2}}$$

where n = the number of velocity points in the profile. If the 'waviform departure' is divided by u_* (determined from the profile), the result is a dimensionless measure of the magnitude of the point velocity departures from the fitted regression line. This value is called a

T A B L E 4-3

SUMMARY OF EBB AND FLOOD PROFILE SHAPES (PERCENT)

Type	Ebb	Flood	Total
1	53.0	34.4	43.7
2	15.5	24.2	19.9
3	31.5	41.4	36.4
TOTAL	100.0	100.0	100.0
Number of Profiles*	641	491	1132

NOTE: * Profiles with only 2 data points or negative regression slopes deleted.

TABLE 4-4

SUMMARY OF PROFILE SHAPES FOR THE EARLY AND LATE PARTS OF THE EBB AND FLOOD PHASES OF THE TIDE

Type	Ebb		Flood	
	1st Half	2nd Half	1st Half	2nd Half
1	77.9	28.1	37.8	31.0
2	14.3	16.6	24.4	24.1
3	7.8	55.3	37.8	44.9
TOTAL	100.0	100.0	100.0	100.0
Number of Profiles*	321	320	246	245

NOTE: * Profiles with only 2 data points or negative regression slopes deleted.

FIGURE 4.4: Vertical velocity profiles measured during a tidal cycle on Selma Bar over sand waves. The time from high water (h) is indicated at the top of each profile. The velocity origin of each plotted profile is offset one velocity unit to the right with time from high water.

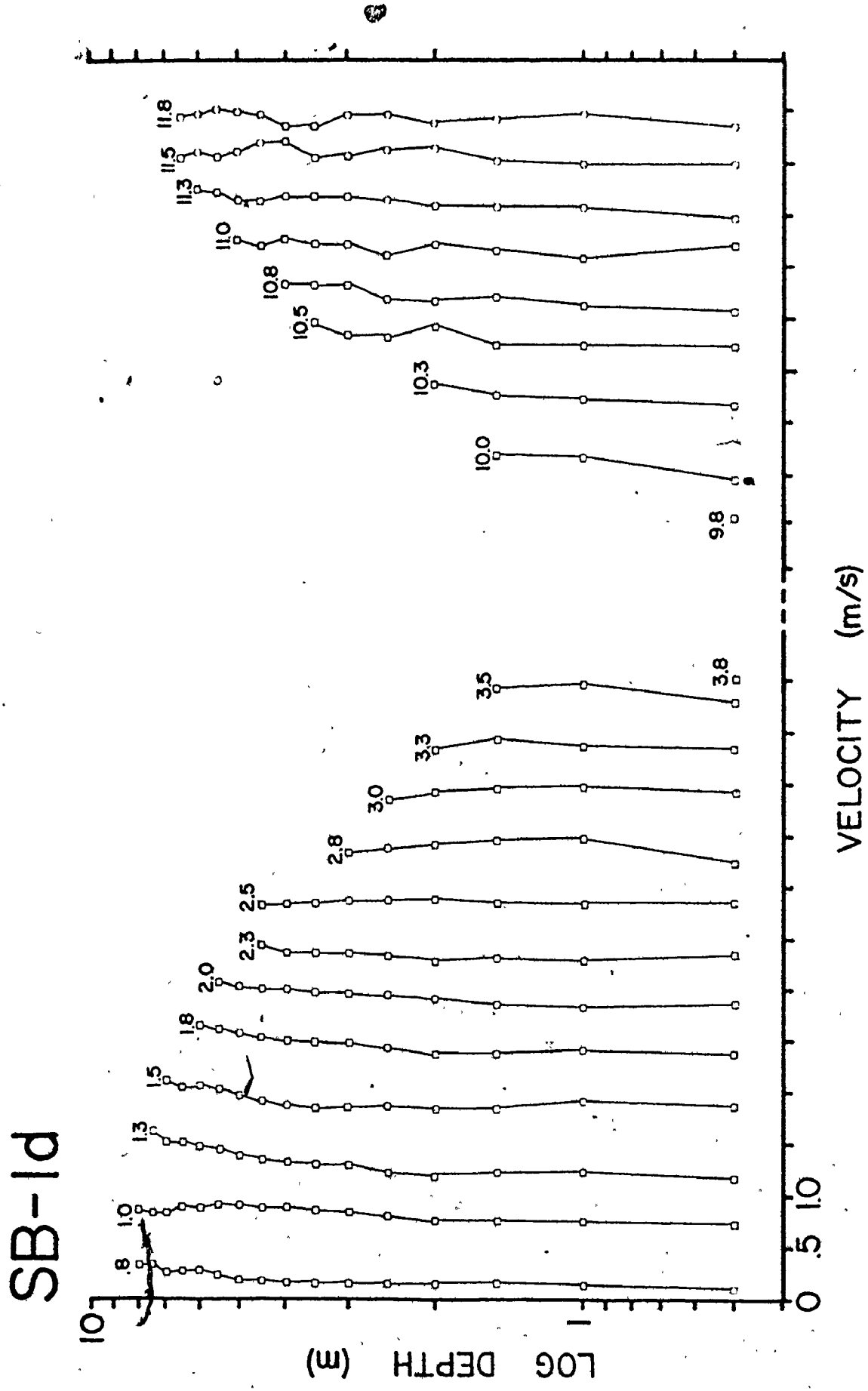
SB-Id
LOG DEPTH (m)
VELOCITY (m/s)
0
.5
1.0
1
10
.8
1.0
1.3
1.5
1.8
2.0
2.3
2.5
2.8
3.0
3.3
3.5
3.8
9.8
10.0
10.3
10.5
10.8
11.0
11.3
11.5
11.8

FIGURE 4.5: Vertical velocity profiles measured during a tidal cycle on Selma Bar over small megaripples (flood dominated area). The time from high water (h) is indicated at the top of each profile. The velocity origin of each plotted profile is offset one velocity unit to the right with time from high water.

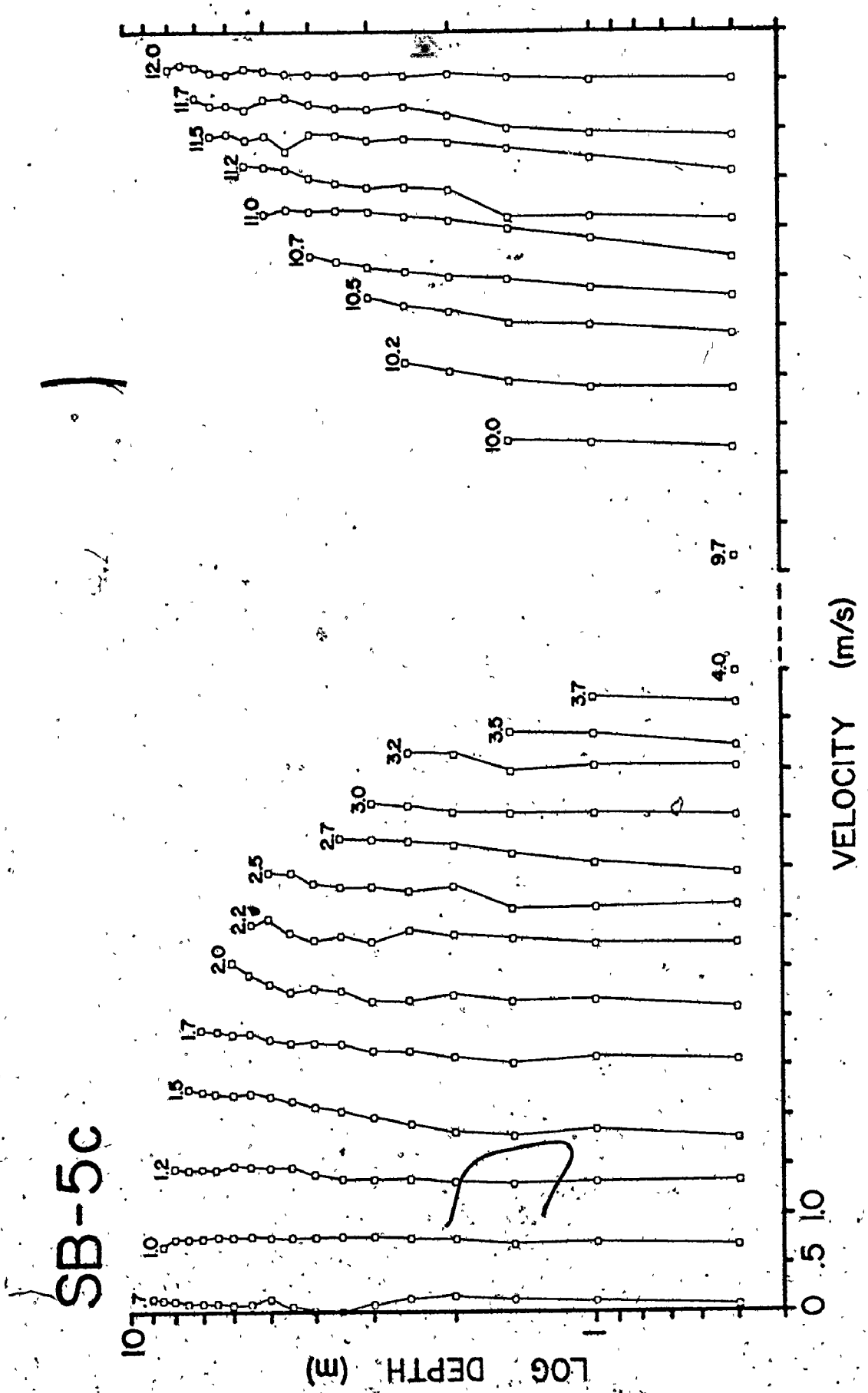
SB-5C
LOG DEPTH (m)
VELOCITY (m/s)
0 .5 1.0
10
1
12.0
11.7
11.5
11.2
11.0
10.7
10.5
10.2
10.0
9.7
4.0
3.7
3.5
3.2
3.0
2.7
2.5
2.2
2.0
1.7
1.5
1.2
1.0
.7

FIGURE 4.6: Vertical velocity profiles measured during a tidal cycle on Selma Bar over large megaripples. The time from high water (h) is indicated at the top of each profile. The velocity origin for each plotted profile is offset one velocity unit to the right with time from high water.

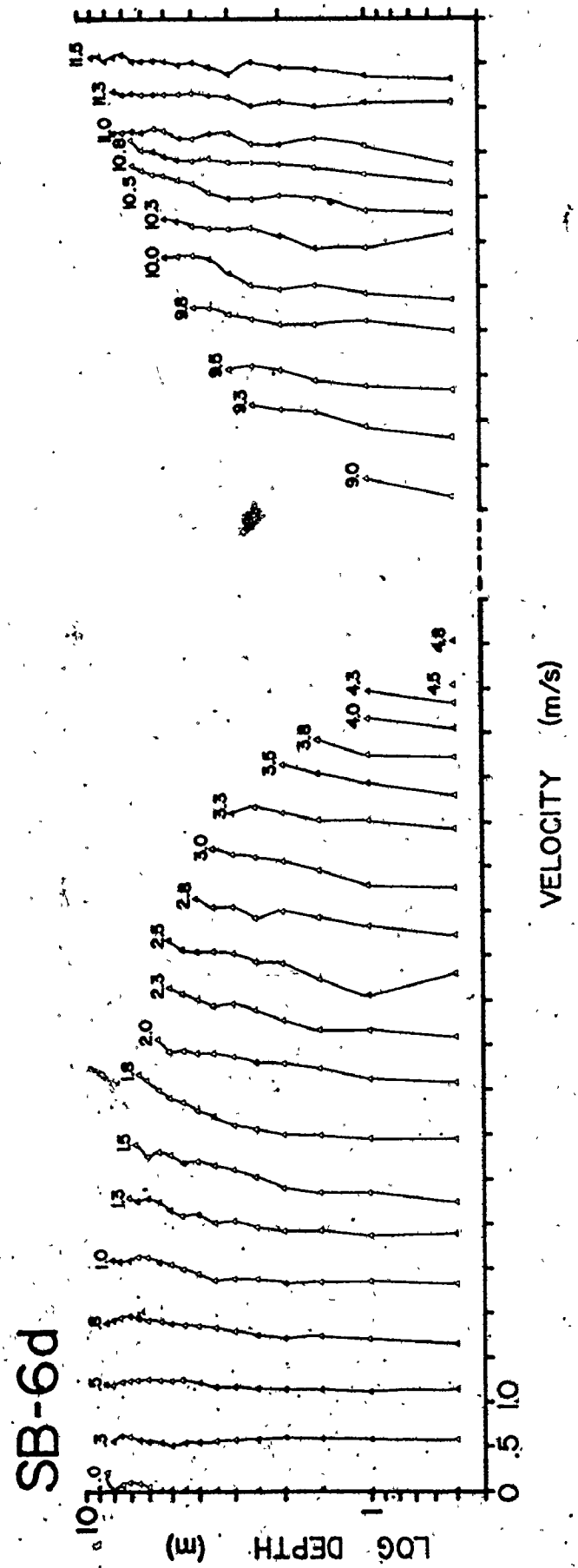
SB-6d
LOG DEPTH (m)
VELOCITY (m/s)
0
.5
1.0
1
10
0.0
.3
.5
.8
1.0
1.3
1.5
1.8
2.0
2.3
2.5
2.8
3.0
3.3
3.5
3.8
4.0
4.3
4.5
4.8
9.0
9.3
9.5
9.8
10.0
10.3
10.5
10.8
11.0
11.3
11.5

'turbulence coefficient' in Appendix IV.

Values of the turbulence coefficient are generally less than 2.0, except for those profiles with large, possibly spurious, velocity residuals. There is little difference in the magnitude of the coefficient between the ebb and flood, but the values seem to be somewhat larger during the early and late ebb, and during the early part of the flood. This temporal variation of the coefficient is, however, evident in only a few tidal cycles monitored. In many cases, the variation of the coefficient appears to be multimodal or random.

The absolute value of the velocity departures (i.e., Ludwick's 'waviform departure') ranged from 0.02 to 0.05 m/s which are comparable to values determined from profile measurements in rivers (e.g., data from Jordan, 1965; and Scott and Stephens, 1966).

Discussion

Because of the lack of established theories about turbulent flow over boundaries composed of sand, or for that matter over large roughness elements, recourse is made to theories of clear water, turbulent flows over rigid boundaries. This kind of approach is one way to improve the understanding of flow over sandy boundaries because many of the hydraulic aspects of the flow can be studied in isolation and under controlled limits.

For flow over boundaries composed of sand or over roughness elements (artificial or natural), there are several unanswered questions such as: What is the depth origin in velocity profiles? What is the correct representative velocity profile? What is the distribution of boundary shear velocity? These are all parameters that are important in describing the flow.

In flow over sand boundaries, the presence of bedforms of relatively large size compared to the depth of flow tends to generate nonuniformity in the flow. The flow accelerates over the upstream slope or the stoss-side of the bedforms, separates at the crests and reattaches on the upstream surface of the next bedform downstream. For relatively larger depths of flow (or relatively smaller bedforms), the nonuniform effects of the boundary decrease towards the surface of the flow. In nature, the three dimensional characteristics of bedforms, and their variation of

shape, size and movement in time present a more complex situation. Nevertheless, whether the flow is in a flume under controlled conditions or in nature, the questions are still the same: where should a representative velocity profile be measured with respect to the bed form, and is one representative profile sufficient to adequately describe the flow over a boundary with bedforms present?

The vertical velocity distribution at different locations over a bedform has been studied in several investigations, e.g., in flumes (Khanna, 1970; Raudkivi, 1966 and 1967 a, p. 206-207; Rifai and Smith, 1971; Vanoni and Hwang, 1967 and 1968), in rivers (Culbertson et al., 1972; Jackson, 1975; Smith, J.D., 1969) and in tidal channels (Dyer, 1970). The results from these studies show the nature of velocity profiles in fully developed flow over bedforms. For example, in the study of Vanoni and Hwang (1967, Fig. 3 and 1968, Fig. 11; Figure 4.7, this study), the semilogarithmic velocity profiles over a stabilized ripple bed show several features: (i) the maximum velocity at the bed occurs near the bedform crests; (ii) velocity profiles in the lee of bedforms show a region of retarded or reverse flow; and (iii) the measured velocity profiles generally show nonrandom departures from the fitted linear regression. The occurrence of the maximum near bottom velocity in the proximity of the bedform crests is caused by flow contraction and acceleration over the upstream surface of the bedforms. Immediately downstream of the bedform crests, the separation of the flow from the bed and the generation of turbulent wakes shed from the bedform crests causes a slackening and/or a reversal of the flow (related to flow expansion and energy dissipation) within the bedform leeside eddy.

Some of the measured profiles that deviate in shape from the fitted regression model can be related to the location of the profiles in the region of the leeside eddy. The apparently larger number of Type 1 profiles in the Vanoni and Hwang data is probably because more profiles are measured over the stoss-side of the bedforms than through the separation zone.

The characteristics of the length/height ratio of bedforms makes it more likely that profiles will be measured over the stoss-side (Type 1 profiles) than through the separation zone (Type 2 profiles) of bedforms.

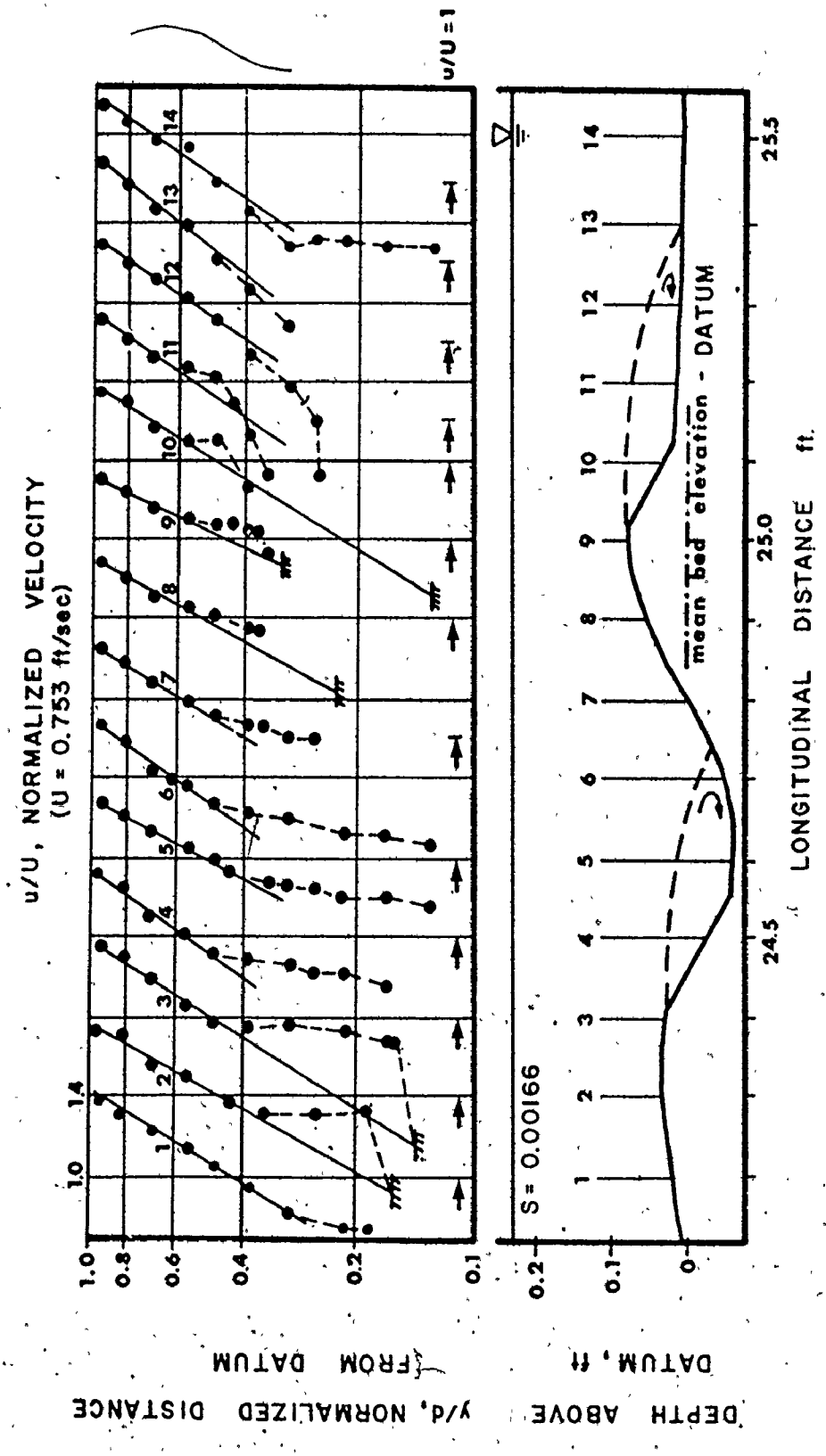

FIGURE 4.7: VERTICAL VELOCITY PROFILES OVER DUNES VANONI and HWANG 1967 and 1968

Blatt et al. (1972, p. 127) and Simons and Richardson (p. 9-57, in: Shen, 1971) state that the length of the separation zone is approximately 6 to 8 times and 10 to 12 times the height of bedforms (measured from trough to crest) respectively. For example, if the boundary were covered with megaripples with a length of 8 m and a height of 0.4 m, the separation zone would be approximately 3 m (assuming that the separation zone is related to approximately 8 times the bedform height). Thus, with a random or an equal-spacing system of locating velocity profiles over a bedform, the probability is that more profiles will be measured over the stoss-side.

That many of Vanoni and Hwang's profiles are similar to the Type 1 profile shapes can probably be explained by: (i) most of the profiles are measured over the bedform stoss-side; and (ii) because flow convergence over the stoss-side of bedforms produces relatively higher velocities relatively close to the bed.

The velocity profile characteristics from the flume in Vanoni and Hwang (1967 and 1968) are representative of the findings in other studies, e.g., see the results of Culbertson et al. (1972, Fig. 6), Dyer (1970, Figs. 4 and 5), Raudkivi (1966, Fig. 4), Rifai and Smith (1971, Fig. 2), and Smith, J.D., (1969, Figs. 16 and 17) from flows in flumes, rivers and tidal channels over bedforms. Savini and Bodhaine (1971) measured the vertical distributions of velocity in the Columbia River over boundaries composed of cobbles and boulders (90 to 396 mm). Plots of the vertical velocity profiles (e.g., for the section below Priest Rapids Dam) show that the profile shapes are generally Type 3 which suggests that flow convergence over well rounded cobbles and boulders is relatively unimportant with respect to possible alteration of the shape of the vertical velocity distribution.

Thus far, the various types of profiles described for fully developed turbulent flow were in situations where the location of the profile was known with respect to the bedform cross-section (e.g., as in flumes, and in relatively shallow and clear flows with relatively large bedforms compared with the flow depth) or where the knowledge of the profile location with respect to the boundary geometry was apparently unimportant (e.g., as in flows over cobble and boulder beds). The

question now arises: what type of velocity profile should be expected if only one profile were measured and if the exact position of the profile relative to the bedform was unknown? Such situations commonly occur where the depth of flow is relatively large and the water turbidity is high.

An example of velocity profile measurements in a relatively deep flow over bedforms and with high water turbidity is the work that has been done in the Mississippi River at St. Louis, Mississippi (Jordan, 1965; Scott and Stephens, 1966). In the reach studied, suspended sediment concentrations ranged from 314 to over 1690 mg/l and the boundary was covered with large dunes (average heights from 0.6 to 2.4 m and average lengths from 76 to 274 m; bedform index = roughly 120). There was no attempt to determine the position of the profiles relative to the bedforms. More than 46 percent of the profiles measured by Jordan, and more than 56 percent of those measured by Scott and Stephens were Type 1 (Table 4-5).

Table 4-5 also summarizes the different frequencies of profile types recorded by Dyer (1970) and Ludwick (1974). In Dyer's investigation of a tidal channel in the West Solent, about 64 percent of the profiles measured were Type 1. Analysis of Ludwick's measured profiles at the entrance to Chesapeake Bay show that only 50 percent are Type 1 and almost 43 percent are Type 2. Dyer attributed the variation in the profile shape to the location of the vertical measurement with respect to large bedforms on the boundary (heights from 0.3 to 1 m and lengths from 5 to 18 m). Ludwick, on the other hand, related the 'nonrandom, depth-zoned departures' of the measured velocity profiles from the regression model to the difference between the surface and the bottom current speed which he believed was a function of the local hydraulic geometry (i.e., zig-zag shoals) and the tidal range at a given location, not the bedforms (with heights of about 1.8 m and lengths of about 240 m).

In Cobequid Bay, the relatively large depths and high water turbidity make it impossible to determine the exact position of the measured velocity profile relative to the bedforms (i.e., it is not known whether an individual profile was measured above the crest or the trough of a megaripple). These conditions are similar to those encountered by Jordan (1965), Ludwick (1974) and Scott and Stephens (1966).

TABLE 4-5

SUMMARY OF PROFILE SHAPES FROM OTHER SOURCES

Type	Tidal Dyer[1]	Ludwick[2]	River Jordan[3]	Scott & Stephens[4]
1	64.3	50.0	46.3	56.3
2	7.1	42.8	24.0	20.7
3	28.6	7.2	29.7	23.0
TOTAL	100.0	100.0	100.0	100.0
Number of Profiles	14	14	121	87

NOTE:
1. Dyer (1970, p. 158) tidal channel, West Solent, England.
2. Ludwick (1974, p. 720-721, Fig. 2 & 3) tidal entrance to Chesapeake Bay, Virginia.
3. Jordan (1965, Table 4), Mississippi River at St. Louis, Missouri.
4. Scott & Stephens (1966, Table 3) Mississippi River at St. Louis, Missouri.

The shape of most of the velocity profiles measured over bedforms were Type 1, while those over sandy-gravel channel bottoms (without bedforms) were generally Type 3.

Many of the velocity profiles had a zone up to 3 m from the bottom with a different slope than the upper part of the profile (excluding the top one or two readings which commonly reflect a velocity 'cutback' because of wave activity, frictional resistance between the water and air, or interference caused by the presence of the boat). The thickness of the lower profile zone did not vary regularly during a tidal cycle (i.e., with respect to possible development during the ebb and flood); nor was there any relation of the zone's thickness to bedform type or scale. Specific trends and (or) relations might have been detected with more velocity points in a profile and more profiles during a tidal cycle.

The prevalence of Type 1 profiles possibly indicates that the velocity distributions should be analysed in two segments: (i) a lower zone characterized by the development of a turbulent wake generated from bedform crests and other nonuniformities of the flow related to the interaction of the flow and bedforms; and (ii) an upper zone of 'normal' statistically uniform turbulent flow (Morris, 1955; Morris and Wigert, 1972, p. 50-51) that is sufficiently removed from the effects of boundary roughness. The accuracy of the velocity measurements in this study, however, do not conclusively warrant this kind of analytical approach.

The substantial differences in the distribution of profile types through a tidal cycle cannot be simply due to the effects of random sampling. There are basically two aspects of the profile data that require explanation: Why are Type 1 profiles more common than either Types 2 or 3? and why are Type 1 profiles more abundant in the early part of the ebb?

A possible explanation for the first question is that more profile measurements were made over the bedform stoss-sides because of the characteristic length/height ratios of the bedforms, and that flow over the stoss-sides converge towards the bedform crest producing relatively high velocities comparatively close to the bed (e.g., Fig. 4.7).

An explanation of the larger number of Type 1 profiles during the early part of the ebb is more difficult. During the early ebb, flow depths are relatively large compared with the height of the bedforms

on the boundary and bedforms are flood oriented (produced by flood currents). Figure 4.8 is a diagram depicting the hypothetical flow conditions that might be expected during the early ebb. Note that: (i) there is no flow separation in the lee of the megaripple; (ii) there is a small flow separation in front of the flood megaripple lee-slopes; and (iii) there is a low velocity gradient in the main part of the flow and a sharp gradient close to the boundary. The implication of this diagram is that the separation zones are not yet well-developed during this part of the tidal cycle; consequently turbulent mixing is not fully developed across the whole flow and the velocity gradient tends to be steep close to the boundary.

Under 'normal' conditions, there is generally a velocity 'cutback' at the top of velocity profiles (from the generation of secondary flows caused by inertial and surface tension effects). In many of the measured velocity profiles, current speeds are larger near the surface during the early ebb (rather than less). This is possibly caused by the relatively sudden drop or draw-down of the water surface after the tide turns at high water. The negative wave produced by the drawdown retreats towards the head of the bay (see discussion on negative waves by Henderson, 1966, p. 294-313) and dissipates exponentially. Because water moves faster in the upper part of the wave than near the boundary (James, W., pers. comm., 1976), this might explain the larger velocities near the surface in the measured profiles particularly during the early ebb.

During the late ebb when flow depths are changing relatively rapidly and are shallow compared with bedform heights, the bedforms are adjusted to the ebb flow and the boundary layer is well-developed. The larger frequency of Type 3 profiles indicates the development of a logarithmic velocity distribution in the late ebb currents.

During the early flood, the occurrence of Type 1 profiles might be explained in the same way as for the ebb profiles, except that the re-reversal of bedforms and the establishment of a new equilibrium boundary layer is expected to occur more rapidly because flow depths are initially shallower. The depth of flow is again relatively large compared with bedform heights and the flow is slowly decelerating during the late flood, thus more Type 3 profiles occur.

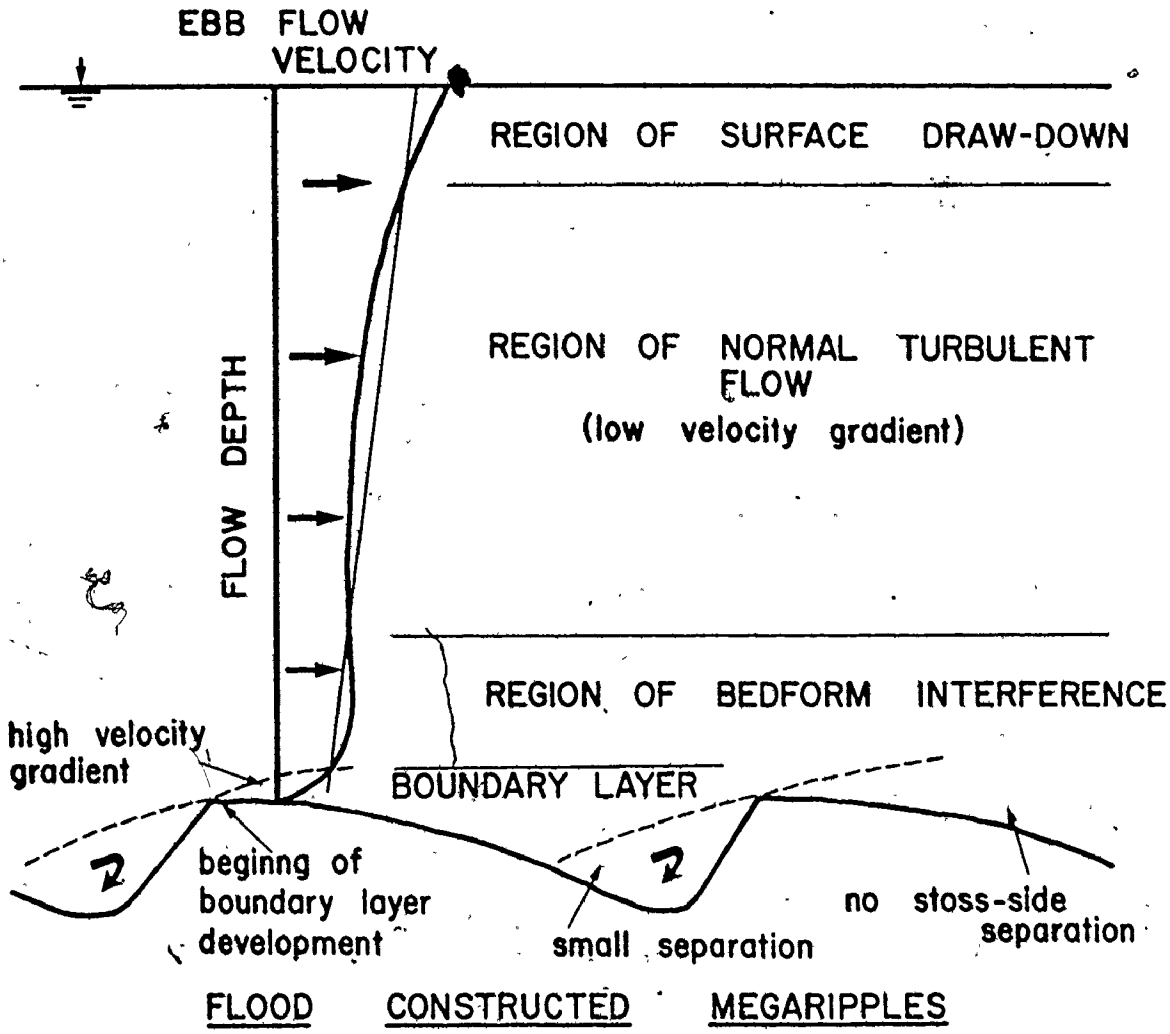

FIGURE 4.8: Hypothetical flow structure during early ebb. See text for explanation.

The foregoing explanation of the variation of profile shapes is hypothetical, but it indicates the possible form of some of the complex inter-relationships that exist between the flow and boundary. The discussion clearly indicates the need for more detailed measurements of velocity profiles in the field to provide a larger number of measurements per profile and per tidal cycle, and accurate location of the profile with respect to the bed morphology. With such data, it may be possible to analyze velocity distributions as more than one simple linear function (e.g., possibly similar to the approaches of Einstein and Chien, 1955; Morris, 1955; Morris and Wigert, 1972, p. 48-59; and Mahmood and Simons, 1975).

It is a relatively common practice for sedimentologists to describe the velocity distribution of and to determine the shear velocity from measured vertical velocity profiles by regression analysis (e.g., from flumes: Raudkivi (1967 a), Vanoni and Hwang, (1967 and 1968); from rivers: Jordan (1965), Scott and Stephens (1966); and from tidal channels: Dyer (1970), Ludwick (1974). No workers, to the writer's knowledge, have reported making comparisons to more than one regression method. For example, Sternberg (1965) used a linear model (Eqns. 4.13 and 4.22), but considered the velocity distribution logarithmic only if 4 out of the 6 near bottom measurements fell within ±10% of the fitted regression line. Dyer (1970) applied the same regression model to his data, but used only the two lowermost points in the profile (at 0.15 and 0.3 m from the bottom) to calculate the shear velocity. This method is unorthodox and questionable considering that: (i) there is little theoretical justification for the approach; and (ii) there are problems of measuring the velocity near the boundary in the presence of bedforms (bedforms in his area had heights from 0.25 to 2 m and lengths from 5 to 18 m) and with a relatively large current meter (0.13 m diameter). Ludwick (1974) achieved reasonable fits with the quadratic regression model (Eqns. 4.19 and 4.25), but does not discuss whether or not any other regression models were tried to obtain a 'best-fit' model. Jackson (1975) chose the best fitting regression line visually (linear versus quadratic) from depth-velocity plots.

In this study, regression analysis with both a linear and a quadratic

model showed that: (i) there was little difference between the results of the models in terms of the number of statistically significant profiles; (ii) the linear model permitted the analysis of a larger number of profiles (i.e., it required fewer data points per profile) and it generally gave a better fit; and (iii) the results from this and other studies generally agree with the theoretical argument that velocity is proportional to the logarithm of the depth. Because of these results, the linear model was used for the calculation of shear velocities and all other subsequent calculations requiring the vertical distribution of the velocity (Appendix IV).

The intensity of turbulence in a tidal flow is usually determined from the instantaneous velocity fluctuations in the direction of current flow with such devices as: an electromagnetic flowmeter (Bowden and Fairbairn, 1956; Bowden and Howe, 1963); a hot film flowmeter (Cannon, 1971; Gordon, 1975; Gordon and Dohne, 1973; Grant et al., 1962); and an acoustic current meter (Wiseman, 1969).

The strength of the local turbulence intensity (or velocity component) is generally expressed as the root-mean-square of the turbulence component of velocity, e.g., $(\bar{u'}^2)^{\frac{1}{2}}$ (the equivalent of the standard deviation of the turbulent component of a velocity). The root-mean-square is commonly expressed as a relative turbulence intensity, e.g., $(\bar{u'}^2)^{\frac{1}{2}}/u$ or $(\bar{u'}^2)^{\frac{1}{2}}/u_*$, where $\bar{u}$ is the mean velocity in the main flow direction and u_* is the shear velocity. For examples of this usage, see Blinco and Partheniades (1971), Mahmood and Blinco (1972), McQuivey and Richardson (1969), Richardson and McQuivey (1968), Rifai and Smith (1971) and A.S.C.E. Task Committee (1963 b).

Direct measurements of turbulence intensity could not be made in this study because the current meter was unsuitable. Dalrymple (pers. comm., 1976) used an Endeco current meter in Cobequid Bay to record flow fluctuations every 5 seconds for periods up to 20 minutes over megaripples. His measurements were made at 0.75 m from the boundary and at 0.5 m from the surface. The standard deviations of the current speed at these two measurement levels were 0.80 and 0.57 m/s respectively. The large value of the standard deviation from the near bottom velocity measurements was related to the high velocity gradient and the relatively

intense interaction between the flow and boundary in this region (e.g., the nonuniformity of the near boundary flow is caused by the presence of bedforms, the generation of turbulent wakes shed from bedform crests, and the separation and reattachment of the flow from the boundary downflow of the bedform). These boundary effects are dissipated upwards from the bottom towards the surface where smaller values of the standard deviation of velocity fluctuations are expected.

The values of the 'waviform departures' determined from the 'turbulence coefficients' in Appendix IV., although slightly smaller in magnitude, are comparable to Dalrymple's results cited above, and to the findings of other workers who have used 'normal' methods of measuring relative turbulence intensities (e.g., Blinco and Partheniades, 1971; Richardson and McQuivey, 1968).

No regular variation of the 'turbulence coefficients' could be observed during the tidal cycle because: (i) the velocity profiles were referred to a local bed elevation rather than a mean bed elevation which caused a distortion of the velocity profile from the logarithmic distribution in the region close to the boundary (Mahmood and Blinco, 1972); and (ii) the position of the measured velocity profiles relative to the bedforms on the boundary were not known. Several experimental studies have shown that the intensity of turbulence varies both with respect to the distance from the boundary and to location over bedforms (e.g., Raudkivi, 1963 and 1967 a, p. 206-207; Rifai and Smith, 1971).

4.4. TIME-VARIANT CHARACTERISTICS

In recent years, there has been increased interest in the time-variant properties of present-day tidal transport and sedimentation processes in tidal inlets, estuaries and shelves (e.g., Salsman et al., 1966; Swift and McMullen, 1968; Coastal Research Group, 1969; Postma, 1961, 1967; Daboll, 1969; Farrell, 1970; Hartwell, 1970 Swift et al., 1972; and several papers in Cronin, 1975). Time series analysis of tidal currents is a fundamental aspect of tidal flow description and analysis, and it is a prerequisite for the study and understanding of a particular tidal system's evolution, maintenance, geometry, structure, bedforms, sediments, etc.

In this study, the time-variant properties of the tidal currents in Cobequid Bay were measured within two time scales: (i) during individual semidiurnal tidal cycles (i.e., from high water to low water to high water); and (ii) during lunar-tidal month (i.e., spring to neap tide variations). The serial properties of the measured and derived variables (e.g., velocity, depth and direction; see Appendix IV.2) will be described and discussed. Specific reference to the development and distribution of bedforms and sediments, and the evolution and maintenance of the channel-bar complex with respect to these variables is deferred to the succeeding two chapters.

Semidiurnal Variations of the Tidal Currents

Current Speeds and Flow Duration - The velocity profile data, discussed in the last section, are quite cumbersome to use for the recognition of any specific serial characteristics of tidal currents, and further detailed analysis would be extremely laborious and time-consuming relative to the information gained. A more direct approach is to select a representative variable (e.g., mean velocity or unit discharge) from each measured vertical velocity distribution and then to characterize the temporal variation of this parameter during a tidal cycle. Unfortunately, there is no standard vertical profile variable that is used by all workers. Sternberg (1968, 1970) and Ludwick, (1974), for example, used a mean-bottom velocity, the current speed one metre from the boundary. Others have used mean surface velocities (e.g., Boothroyd and Hubbard, 1975), mean flow velocities or unit flow discharges. The flow strength parameter chosen makes little difference to the recognition of the specific time-variant characteristics of tidal currents. The inconsistencies in the parameter selected from one worker to the next, however, greatly complicates any attempts to make absolute comparisons between different studies.

The measures of flow strength used in this study are the mean flow velocity ($\bar{u}$) and the unit flow discharge (q). See Appendix IV.1 for details.

The mean flow velocity is commonly determined by one (or more) of several possible methods (Gray, 1970, p. 8.86-8.88; Savini and Bodhaine, 1971): (i) integration of the vertical velocity profile (i.e., average

velocity of the vertical is proportional to the arean enclosed by the velocity distribution divided by the depth of flow); (ii) average of all point velocities in the profile if they are equidistantly spaced from the boundary; (iii) average of the point velocities at 0.2D and 0.8D above the boundary; (iv) measurement of, or determination (from profile measurements) of the point velocity at 0.368D above the boundary; and (v) measurement of the velocity at the surface multiplied by 0.9. All of these methods have their advantages and disadvantages. Savini and Bodhaine (1971) compared the results of several methods (i, ii, iii, and iv) and found that the mean velocities determined from the various methods differed from each other by only ±0.3%. Thus, the different methods have about the same degree of variability, and any method will give results comparable to those of the others.

For this investigation, the two-point method (i.e., method (ii) above was used to determine mean velocities from the linear regressions fitted to the measured velocity distributions. This method was selected because: (i) it was simple to use; (ii) it used two representative point velocities from the vertical profile (thus, it is better than only a single value, e.g., methods iv & v); and (iii) it is commonly used by workers investigating river hydraulics (e.g., Jordan, 1965; Scott and Stephens, 1966).

The calculated mean flow velocities from each vertical profile during a tidal cycle were then graphed against time. According to Postma (1961), the time-velocity relationship at a given location has a unique form which is a function of the hydraulic and boundary conditions of that site, at that moment in time.

There are two aspects of time-velocity relationships that are commonly described: (i) the nature of velocity variation within individual ebb and flood phases of the tidal cycle; and (ii) the similarities and/or differences between the ebb and flood velocity variations for a complete tidal cycle. The first aspect concerns the duration of the particular flow and the time of the maximum current speed relative to the time of high or low water. Ebb and flood time-velocity relationships are frequently asymmetrical (i.e., the time of the maximum current speed occurs either early or late during the tidal phase -- the relationship would be symmetrical if the maximum current speed occurred in the

middle of the tidal phase); hence the expression 'time-velocity asymmetry' (Postma, 1961). The second aspect of time-velocity description is the symmetry or asymmetry of the ebb and flood relationships for a complete tidal cycle with respect to flow duration and maximum speed.

The time-velocity relationships over the four bars studied are discussed in the following section.

Noel Bay Bar - Figure 4.9 shows the time-velocity relationships for three locations on Noel Bay Bar (NBB-6, NBB-8 and NBB-1; see Fig. 4.1 for locations) that were collected with an automatic recording current meter (Appendix III.1). The three relationships show that: (i) the maximum near-bottom current velocities were larger in the channel south of the bar (NBB-6; ebb = 0.95 to 1.59 m/s and flood = 1.12 to 1.56 m/s) than in the channel north of the bar (NBB-8; ebb = 0.57 to 1.46 m/s and flood = 0.71 to 1.24 m/s) and on the bar itself (NBB-1; ebb = 0.75 to 1.12 m/s and flood = 0.68 to 1.18 m/s); (ii) the maximum ebb speeds were generally less than the maximum flood speeds in the channels, but the reverse was somewhat true at NBB-1; (iii) for all three locations, the maximum ebb and flood speed occurred between mid to low tide (late ebb) and low to mid tide (late flood) respectively, i.e., there was a relatively long period to either side of high water when current speeds were lower; (iv) the degree of time-velocity asymmetry during a tidal cycle was different for each location, decreasing from NBB-6 to -8 to -1 (particularly during the ebb); and (v) the ebb tended to last longer than the flood at NBB-6 and -8, while the reverse was slightly true at NBB-1.

Figure 4.10 shows several representative time-velocity relationships for different locations over Noel Bay Bar (NBB-1d, -2a, -3a, -6a and -7) that were based on measurements from the direct reading current meter (see Fig. 4.1 for locations). Raw data for other locations on Noel Bay Bar are listed in Appendix IV.1.

The relationships in Figure 4.10 show much the same time-velocity characteristics as those discussed from Figure 4.9. The time-velocity relationships are both ebb and flood asymmetrical, and tidal cycle asymmetrical. Maximum ebb speeds were greater than maximum flood

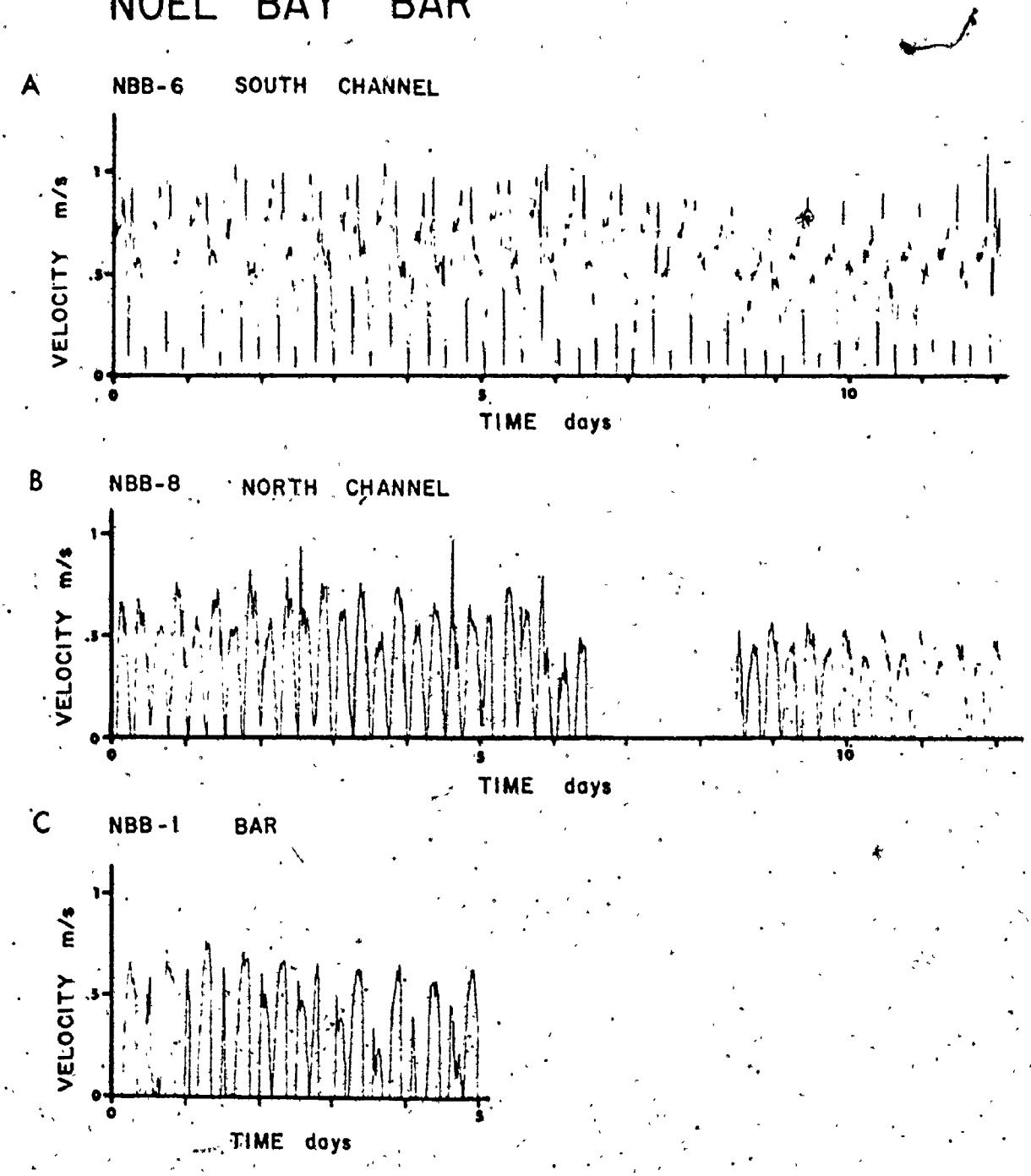

FIGURE 4.9: Time-velocity relationships (0.5 m from bottom) for three locations on Noel Bay Bar. Data recorded by a Plessey automatic recording current meter in 1971. The periods of operation were: July 7 to July 19 at NBB-6; July 19 to August 1 at NBB-8; and August 1 to August 19 at NBB-1. Some parts of the original record have been deleted at the beginning end because of spurious measurements.

FIGURE 4.10: Representative time-velocity relationships (standardized mean velocities) from Noel Bay Bar and East Noel Bar. Station locations are shown in Figure 4.1.

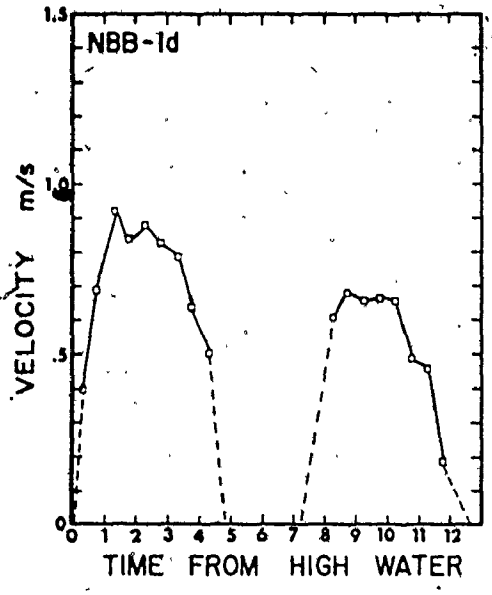
NBB-1d
VELOCITY m/s
TIME FROM HIGH WATER

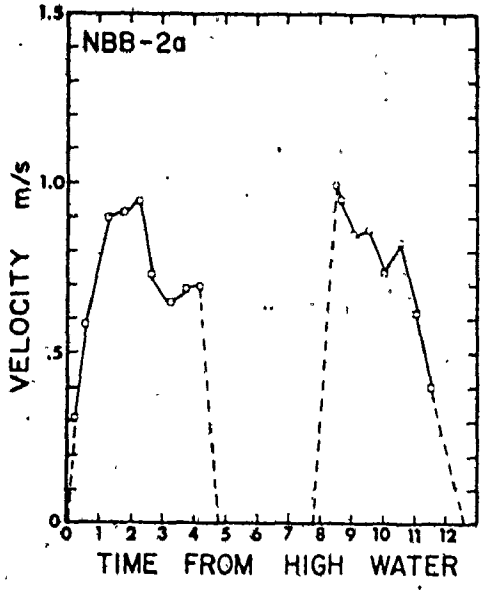
NBB-2a
VELOCITY m/s
TIME FROM HIGH WATER

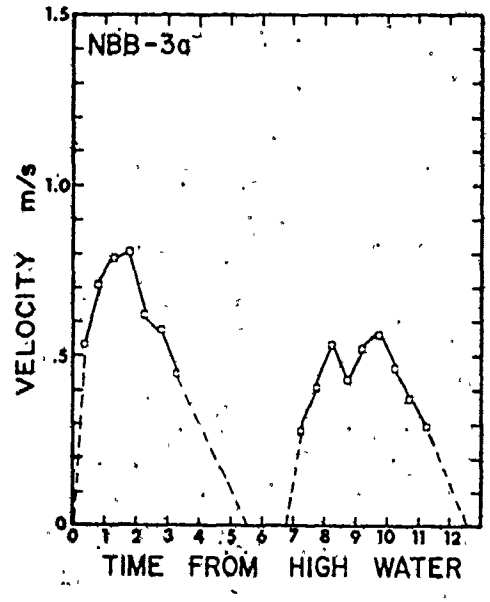
NBB-3a
VELOCITY m/s
TIME FROM HIGH WATER

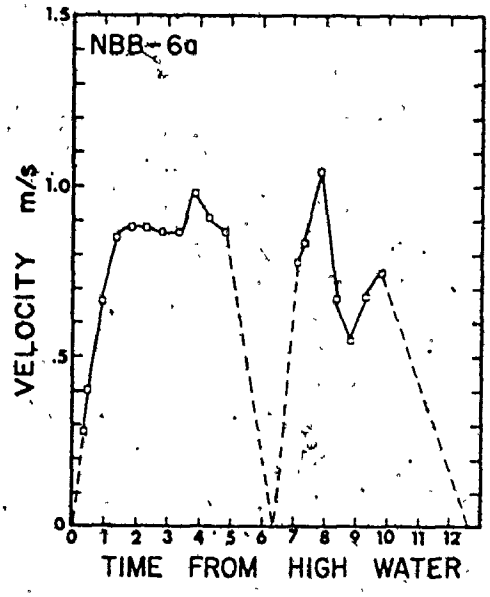
NBB-6a
VELOCITY m/s
TIME FROM HIGH WATER

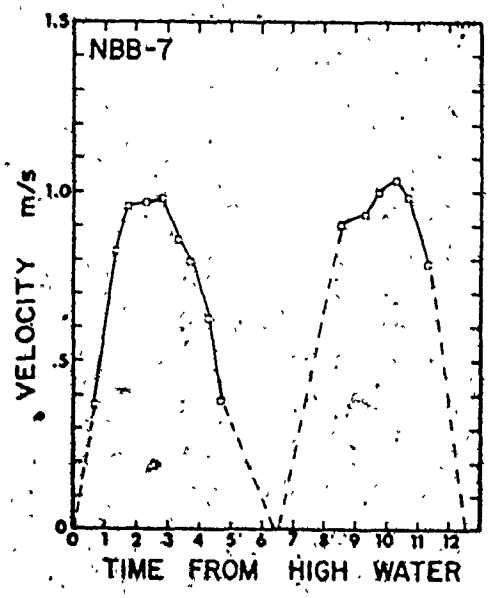
NBB-7
VELOCITY m/s
TIME FROM HIGH WATER

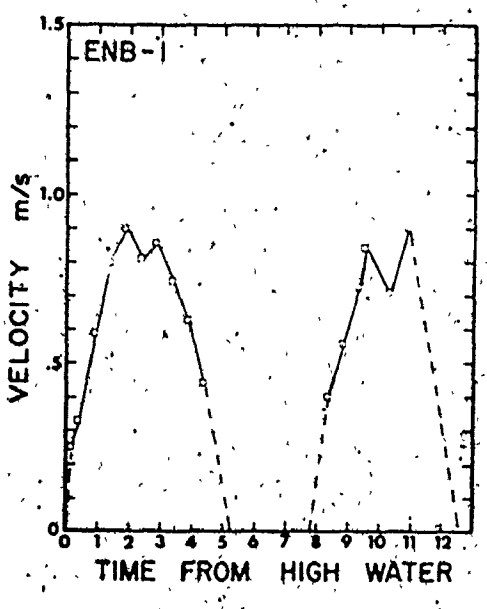
ENB-1
VELOCITY m/s
TIME FROM HIGH WATER

speeds in the channel south of the bar (average ebb speed = 0.96 m/s; average flood speed = 0.75 m/s) and over the bar (average ebb speed = 0.86 m/s; average flood speed = 0.76 m/s), while the opposite was true for the channel north of the bar (average ebb speed = 0.97 m/s; average flood speed = 1.04 m/s). The average duration of the ebb flow was longer than the flood in the channel locations (ebb average = 6.4 h; flood average = 6.0 h). On the bar, the average ebb duration (4.9 h) and average flood duration (4.9 h) were approximately equal. Maximum current speeds tended to occur during the late ebb and early flood at channel locations, and during the early ebb and early to mid flood at bar locations.

Table 4-6 summarizes the ebb and flood flow durations for several locations on Noel Bay Bar. Figure 4.11 shows the areal distribution of the ebb and flood maximum mean current speeds over the bar, and the areas of ebb and flood dominance (with respect to current speed). The bar was ebb dominant to the south of the crestline and flood dominant to the north. Maximum current speeds decreased towards the crest of the bar.

Average ebb and flood unit discharges averaged approximately 6.43 x 10^4 and 4.69 x 10^4 m^3 respectively (difference = 1.74 x 10^4 m^3 in the ebb direction). Table 4-7 summarizes the unit discharges at several locations over Noel Bay Bar. Unit discharges were approximately an order of magnitude greater in the channel locations than over the bar. The areal variation of unit discharges shows about the same pattern as the current speeds in Figure 4.11 (i.e., flood dominant north of the bar crestline; ebb dominant to the south).

East Noel Bar - Tidal currents were monitored on East Noel Bar at only one location (on two separate occasions, see Appendix III.1). A representative time-velocity relationship is shown in Figure 4.10. Both the ebb and flood were only slightly time and velocity asymmetrical (e.g. average ebb and flood flow durations = 4.9 and 4.7 h respectively; average ebb and flood maximum current speeds = 0.88 and 0.83 m/s respectively). The average unit discharge during the ebb (6.24 x 10^4 m^3) was approximately 1.15 x 10^4 m^3 greater than the flood (5.09 x 10^4 m^3); thus, the bar is ebb dominant.

TABLE 4-6

EBB AND FLOOD FLOW DURATIONS ON NOEL BAY BAR AND MIDDLE CHANNEL (hours)

Location	Ebb	Low Tide Emergence	Flood	Difference Flood-Ebb
NOEL BAY BAR				
1 A	4.70	3.25	4.64	-.07
B	4.57	2.50	4.95	.38
C	5.12	2.50	4.88	-.24
D	4.78	3.00	5.22	.44
	(4.73)[1]		(4.92)	
2 A	4.62	3.00	4.72	.10
B	5.03	3.00	4.38	-.65
	(4.83)		(4.55)	
3 A	5.50	1.62	5.38	-.12
B	4.83	2.00	5.47	.64
C	5.28	2.25	4.97	-.31
	(5.10)		(5.27)	
4	6.42	--	6.08	-.34
5	6.33	--	6.17	-.16
6 A	6.25	--	6.08	-.17
B	6.20	--	5.30	-.90
	(6.23)		(5.69)	
7	6.42	--	6.08	-.34
8	6.42	--	6.08	-.34
MIDDLE CHANNEL				
MC	7.13	--	4.30	-2.83

NOTE: 1. Station average.

FIGURE 4.11: The areal distribution of maximum mean current speeds (average of three maximum speeds) during the ebb and flood, and the areas of ebb and flood dominance on Noel Bay Bar. Current speeds used were standardized (see Appendix IV.1).

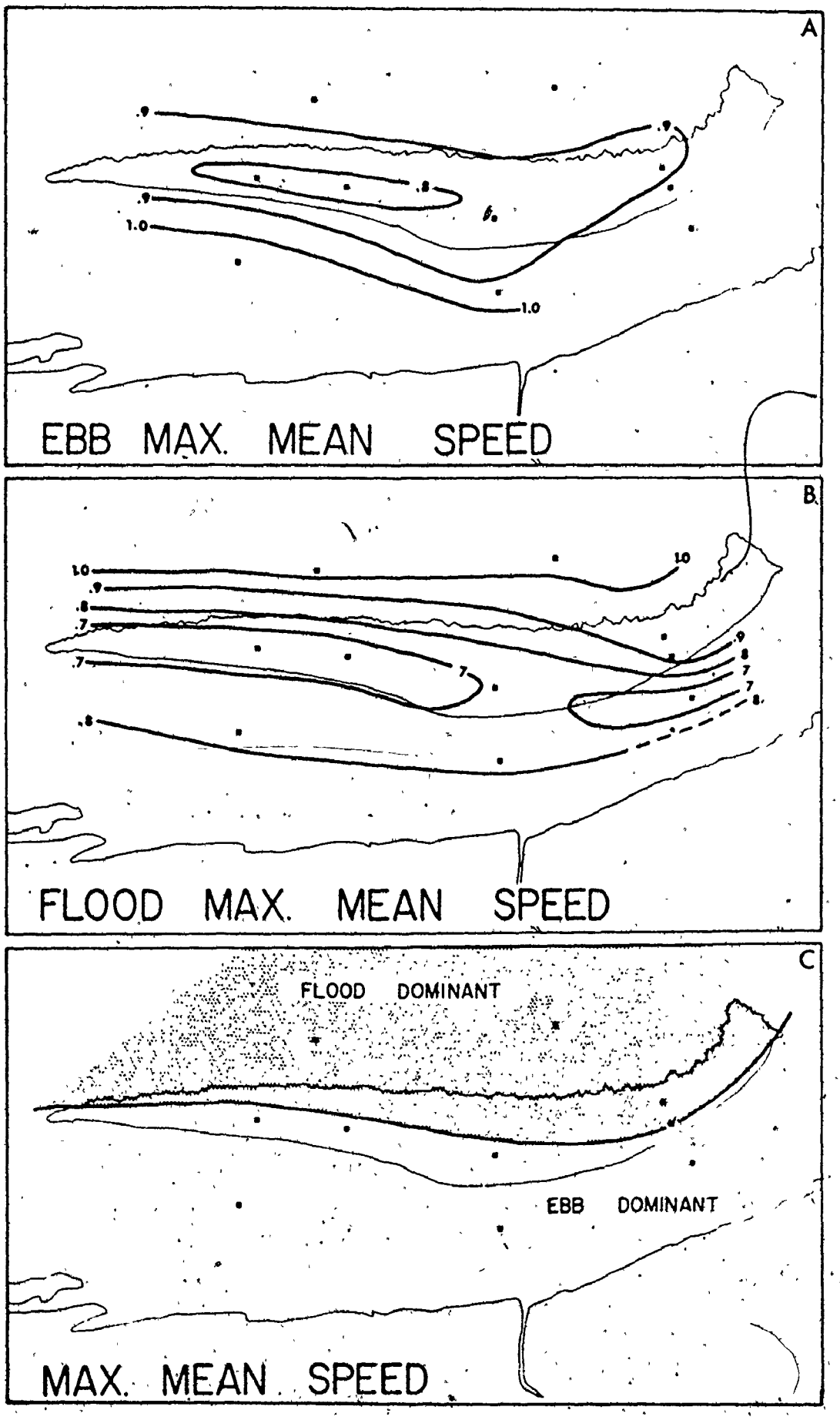
A
.9
.9
.8
.9
1.0
1.0
EBB MAX. MEAN SPEED
B
1.0
1.0
.9
.8
.7
.7
.9
.8
.7
.7
.8
FLOOD MAX. MEAN SPEED
C
FLOOD DOMINANT
EBB DOMINANT
MAX. MEAN SPEED

TABLE 4-7

EBB AND FLOOD DISCHARGE PER TIDAL CYCLE (m^3) [1]

Location	Ebb	Flood	Diff. [2]
NOEL BAY BAR			
1A	81547.243	44306.132	-37241.111
1B	59486.068	44910.858	-14575.210
1C	66362.381	45857.852	-20504.529
1D	62647.194	43020.675	-19626.519
2A	64713.143	59494.486	- 5218.657
2B	78536.181	48370.482	-30165.699
3A	48919.435	44090.196	- 4829.239
3B	50114.832	41383.804	- 8731.028
3C	66303.518	50763.693	-15539.826
4	151804.313	111932.021	-39872.292
5	163148.196	90620.213	-72527.983
6A	131038.212	89599.570	-41438.642
6B	72154.181	30586.100	-41568.081
7	144520.860	167169.880	22649.020
8	161771.426	158496.561	- 3274.065
MIDDLE CHANNEL			
MC1	250849.948	225103.561	-25746.387

NOTE: 1. Data not standardized.
2. Negative sign indicates ebb dominance; positive is flood dominant.

Noel Shore Bar - Figure 4.12 shows several time-velocity relationships for several locations on Noel Shore Bar. The form of the relationships is more variable over the bar than for those on Noel Bay Bar. The average maximum current speeds over the bar ranged from 0.98 m/s during the ebb to 1.00 m/s during the flood. In the channels, maximum speeds averaged 1.47 m/s during the ebb and 1.18 m/s during the flood. Current speeds were approximately 0.5 and 0.2 m/s greater in the channels than over the bar for the ebb and flood respectively. Figure 4.13 shows the areal distribution of the ebb and flood maximum mean current speeds over the bar, and the areas of ebb and flood dominance (based on maximum current speeds). Current speeds decreased towards the crest of the bar. The gentle sloping sides of the bar were flood dominant while the steep sides were ebb dominant (compare Figs. 3.37, 3.29 and 4.13).

Most of the time-velocity relationships indicate that the maximum current speeds occurred during the late ebb and early flood.

The average duration of flow over the bar was approximately 4.9 h during the ebb and 4.2 h during the flood. Channel locations averaged approximately 7.0 h and 5.5 h for the ebb and flood flow durations respectively. Flow durations are summarized in Table 4-8. The duration of flow over the west end of the bar was similar to that along the south side of the eastern part of the bar. Flow durations decreased towards the crest of the bar and the duration of the ebb was always longer than the flood.

Ebb and flood unit discharges (Table 4-9) at the west end of the bar averaged 8.57×10^4 m^3 and 8.59×10^4 m^3 respectively, (slightly flood dominant) while those at the east end of the bar averaged 3.35×10^4 m^3 and 3.48×10^4 m^3 for the ebb and flood respectively along the crest and 9.73×10^4 m^3 and 9.32×10^4 m^3 respectively along the southern side of the bar. Unit discharges in the channels were an order of magnitude larger (Table 4-9), but always ebb dominant (compare Fig. 4.13 and Table 4-9).

Great Village Bar - The time-velocity relationship near the crestline of Great Village Bar indicated that maximum flood velocities (1.14 m/s) were almost twice the magnitude of the maximum ebb velocities. Maximum speeds occurred during the middle of the ebb and flood respectively. The duration of the ebb (6.0 h) was slightly longer than the flood (5.5 h).

FIGURE 4.12: Representative time-velocity relationships (standardized mean velocities) from Noel Shore Bar. Station locations are shown in Figure 4.1.

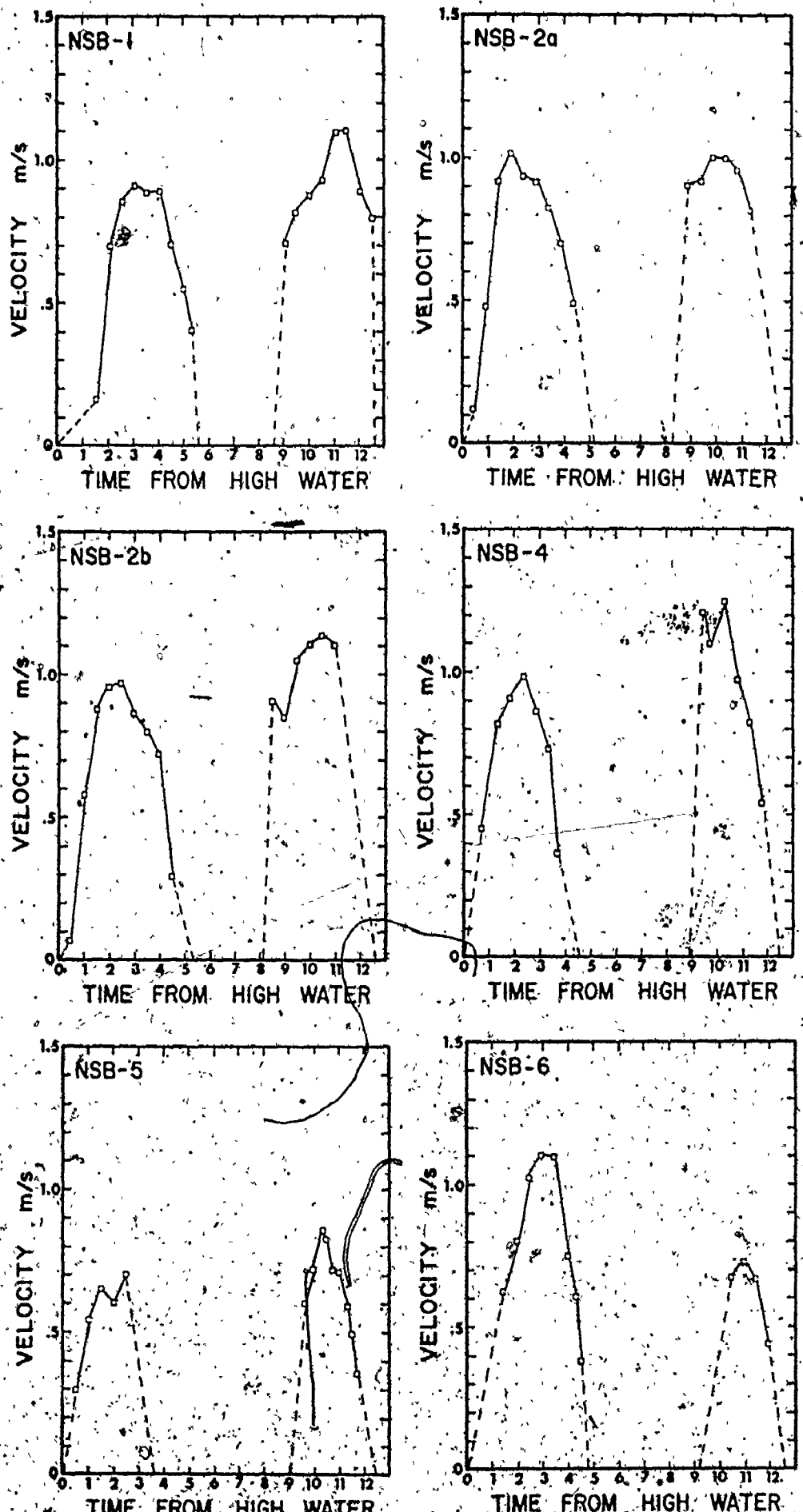
NSB-1
NSB-2a
NSB-2b
NSB-4
NSB-5
NSB-6
VELOCITY m/s
TIME FROM HIGH WATER
0
.5
1.0
1.5
0 1 2 3 4 5 6 7 8 9 10 11 12

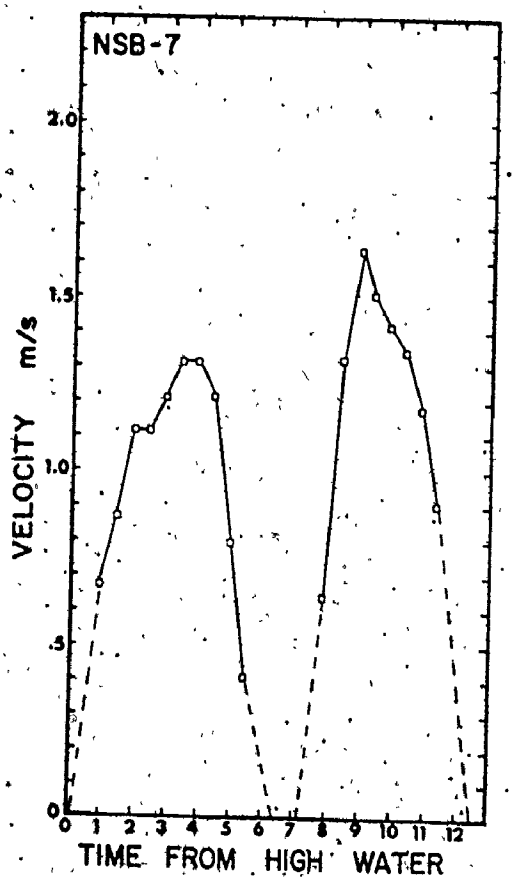

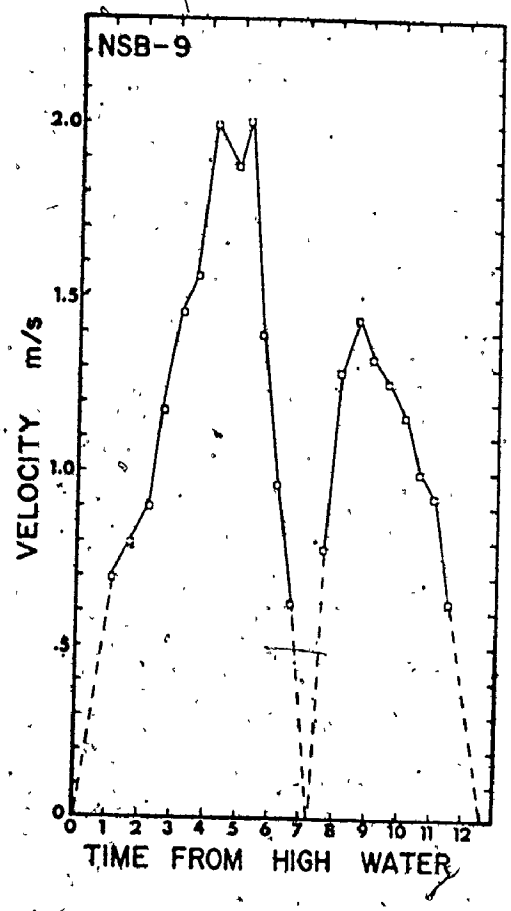

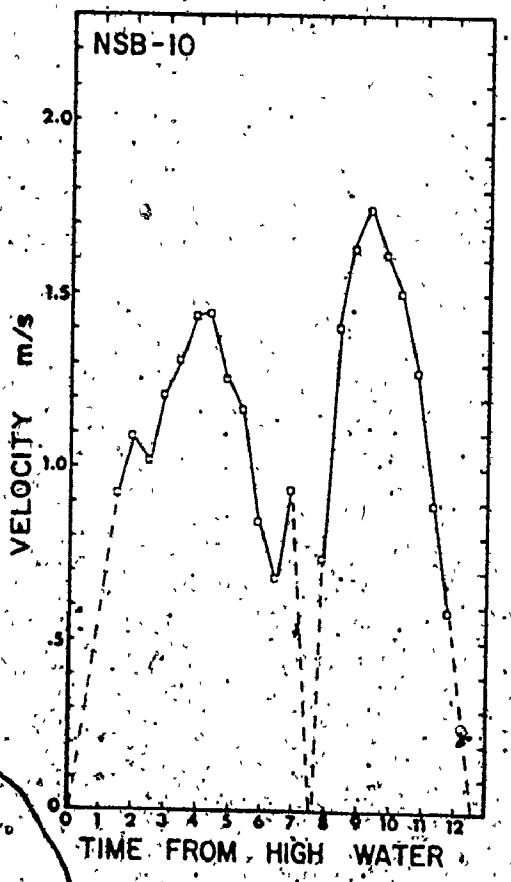

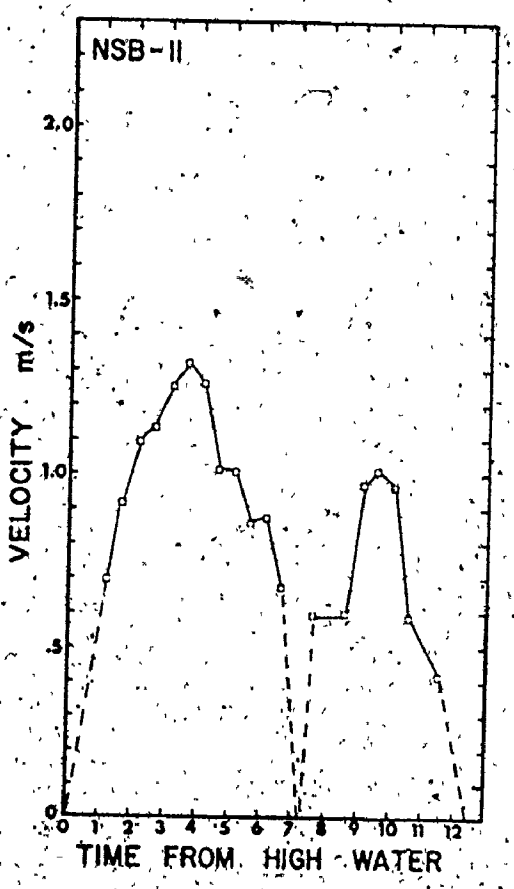

FIGURE 4.12 - cont'd.

FIGURE 4.13: The areal distribution of maximum mean current speeds (average of three maximum speeds) during the ebb and flood, and the areas of ebb and flood dominance on Noel Shore Bar. Current speeds used were standardized (see Appendix IV.1).

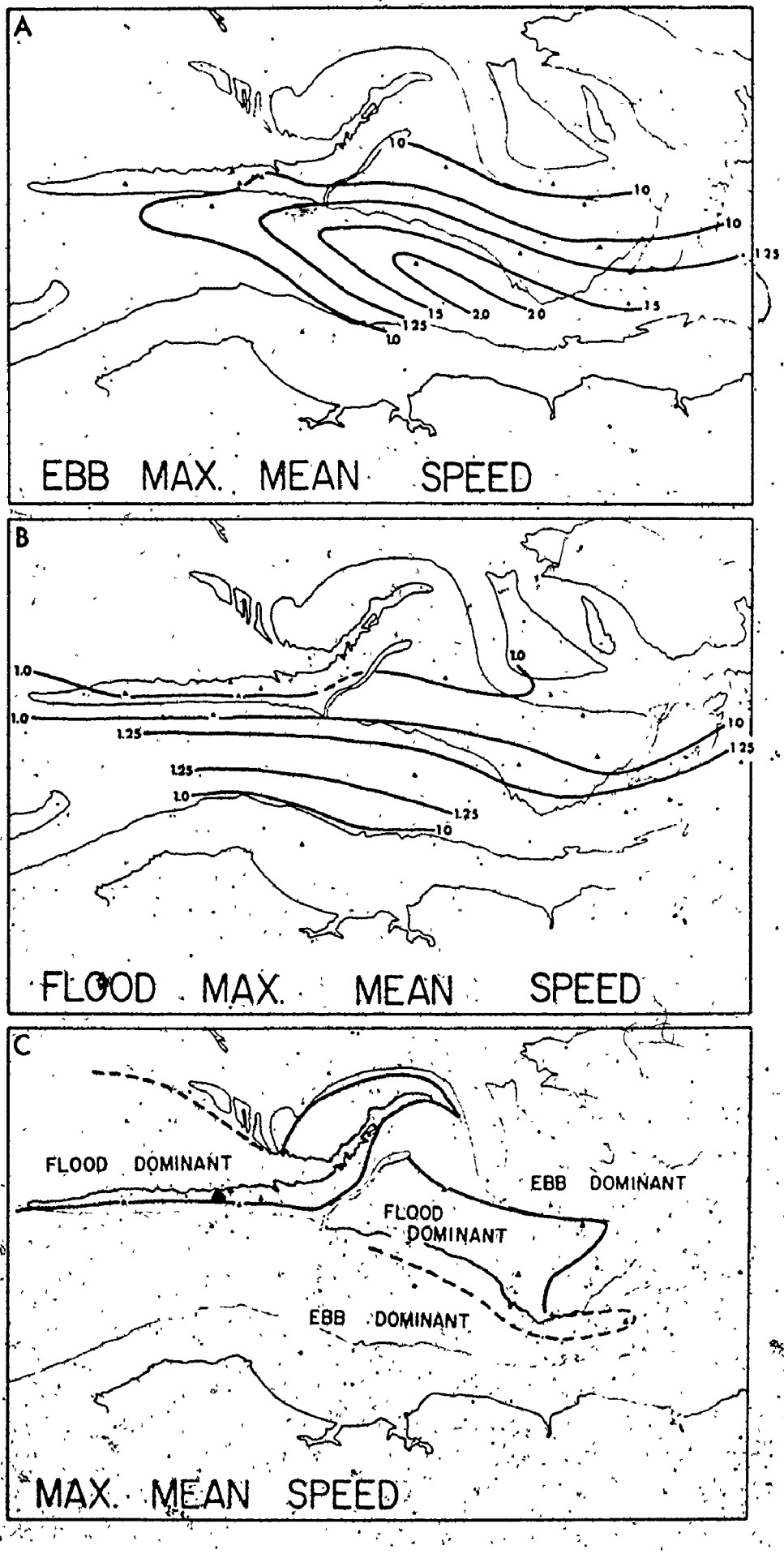
A
1.0
1.0
1.0
1.25
1.5
2.0
2.0
1.5
1.25
1.0
EBB MAX. MEAN SPEED
B
1.0
1.0
1.0
1.25
1.25
1.0
1.25
1.0
1.25
1.0
FLOOD MAX. MEAN SPEED
C
FLOOD DOMINANT
EBB DOMINANT
FLOOD DOMINANT
EBB DOMINANT
MAX. MEAN SPEED

TABLE 4-8

EBB AND FLOOD FLOW DURATIONS ON NOEL SHORE BAR, EAST NOEL BAR AND GREAT VILLAGE BAR (hours)

Location	Ebb	Low Tide Emergence	Flood	Difference Flood - Ebb
NOEL SHORE BAR				
1	5.12	3.00	4.30	- .82
2A	5.12	3.00	4.30	- .82
B	5.20 (5.16)[1]	2.75 (2.87)	4.33 (4.32)	- .87 (- .85)
3	4.62	3.00	4.97	.35
4	4.70	4.00	3.63	-1.07
5	3.45	5.50	3.47	.02
6	4.53	4.50	3.30	-1.23
7	6.37	.75	5.30	-1.07
8	6.25	--	6.08	- .17
9	7.12	--	5.38	-1.74
10	7.37	--	4.97	-2.40
11	7.12	--	5.38	-1.74
EAST NOEL BAR				
1	5.08	2.50	4.88	- .20
2	4.78	3.25	4.47	- .31
GREAT VILLAGE BAR	5.95	1.00	5.47	- .48

NOTE: 1. Station average.

T A B L E 4-9

EBB AND FLOOD DISCHARGE PER TIDAL CYCLE (m^3)[1]

Location	Ebb	Flood	Diff.[2]
NOEL SHORE BAR			
1	100302.884	82562.899	-17739.985
2A	96276.349	91542.751	- 4733.598
2B	77825.234	89636.404	11811.170
3	68578.688	79667.286	11088.598
4	48394.062	46762.193	- 1631.869
5	18616.225	22835.523	4219.298
6	60894.427	29891.843	-31002.584
7	133640.825	156544.455	22903.630
8	189663.437	111015.591	-78647.847
9	303466.331	216664.592	-86801.738
10	176538.510	198160.969	21622.459
11	143755.076	98925.586	-44829.490
EAST NOEL BAR			
EN1	58962.583	51360.146	- 7602.437
EN2	65759.919	50528.621	-15231.298
GREAT VILLAGE BAR			
GV1	51962.782	101834.371	49871.589

NOTE: 1. Data not standardized.
2. Negative sign indicates ebb dominance.

Middle Channel - The time-velocity relationship for the main channel in the middle of the sand-body complex (Fig. 4.1 B) indicated that: (i) maximum ebb speeds (1.20 m/s) were slightly greater than maximum flood speeds (1.14 m/s); (ii) maximum current speeds occurred during the early to middle part of the ebb and during the middle to late part of the flood; (iii) the duration of the ebb was approximately 7.1 h and for the flood, 4.3 h; and (iv) ebb and flood unit discharges were of the order of 2.51×10^5 m^3 and 2.25×10^5 m^3 respectively. These results suggest that the current flow in the channel was ebb dominant.

Selma Bar - The time-velocity relationships on Selma Bar are comparable to those on Noel Shore Bar in terms of variety, but current speeds are generally less. Figure 4.14 shows several time-velocity relationships from Selma Bar from measurements made with the direct recording current meter. Figure 4.15 shows some relationships recorded with one of the automatic recording current meters (Appendix III.1).

Average maximum current speeds were approximately 0.70 m/s and 0.90 m/s during the ebb and flood respectively over the bar. In the channels, maximum speeds averaged 1.07 m/s during the ebb and 1.07 m/s during the flood. Maximum flood speeds are generally larger than maximum ebb speeds. For the majority of the time-velocity relationships, maximum speeds occurred during the late ebb and early flood, both over the bar and in the channels.

Figure 4.16 shows the areal distribution of maximum ebb and flood current speeds, and the areas of ebb and flood dominance on Selma Bar. Flood velocities were generally greater along the south side and the exposed western and northwestern end of the bar. For example, maximum ebb velocities ranged from 0.37 to 1.15 m/s and maximum flood velocities ranged from 0.70 to 1.34 m/s along the south side of the bar (in an area with sand waves). In the flood dominated swatchway that bisects the bar from southwest to northeast, maximum ebb current speeds ranged from 0.67 to 0.83 m/s and maximum flood speeds from 1.02 to 1.04 m/s. Northeast of the swatchway (north of the bar crestline), maximum ebb and flood speeds were in the order of 1.08 and 1.13 m/s respectively. Current speeds decreased towards the bar crestline (s)

FIGURE 4.14: Representative time-velocity relationships (standardized mean velocities) from Selma Bar. Station locations are shown in Figure 4.1).

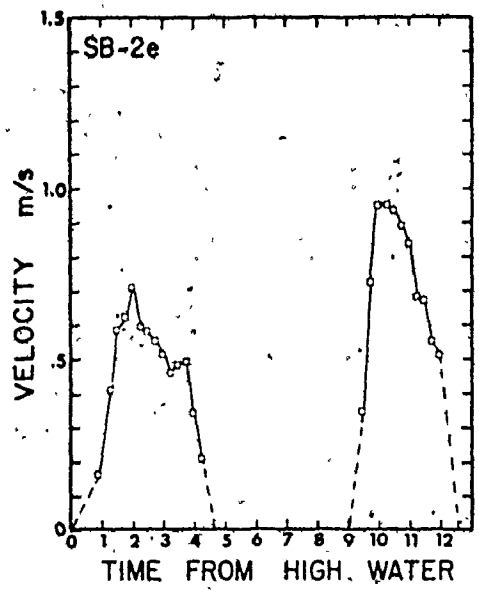
SB-2e
VELOCITY m/s
TIME FROM HIGH WATER

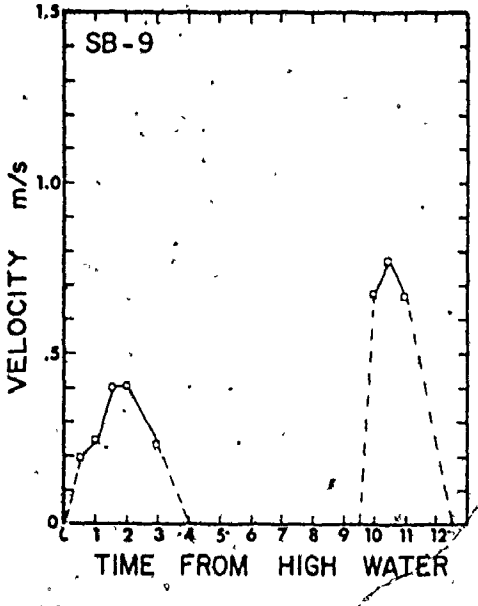
SB-9
VELOCITY m/s
TIME FROM HIGH WATER

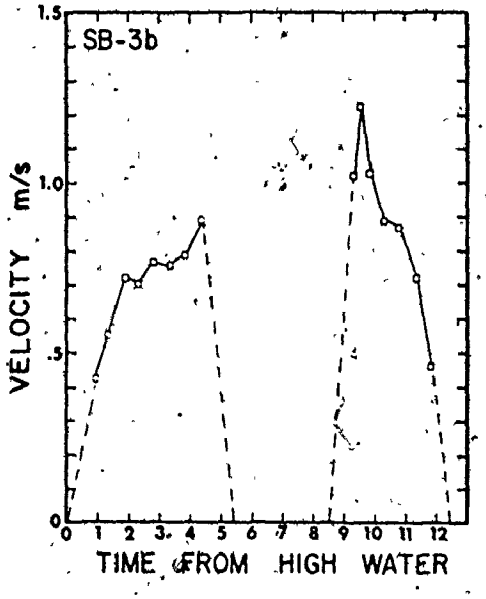
SB-3b
VELOCITY m/s
TIME FROM HIGH WATER

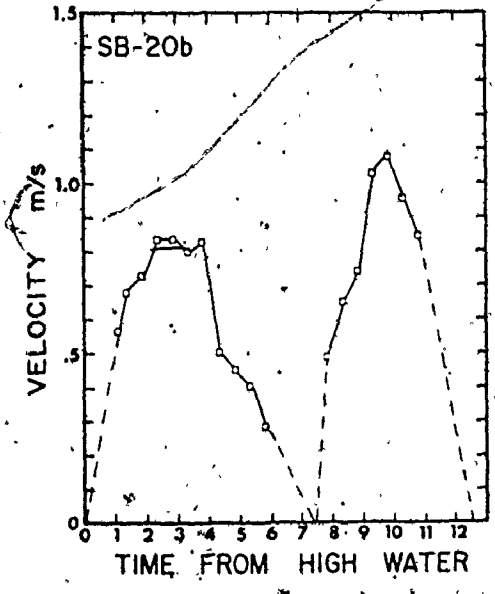
SB-20b
VELOCITY m/s
TIME FROM HIGH WATER

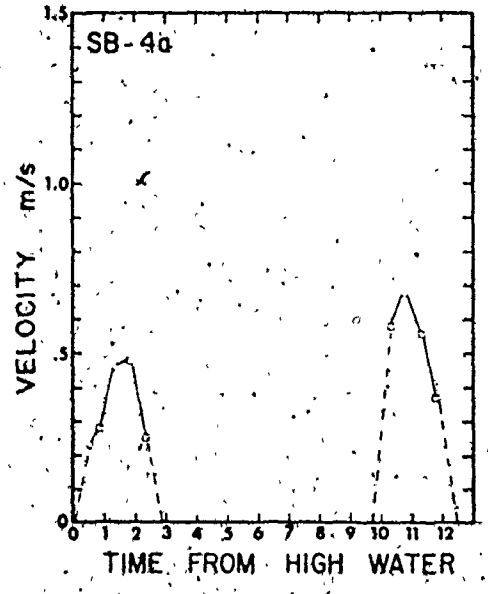
SB-4a
VELOCITY m/s
TIME FROM HIGH WATER

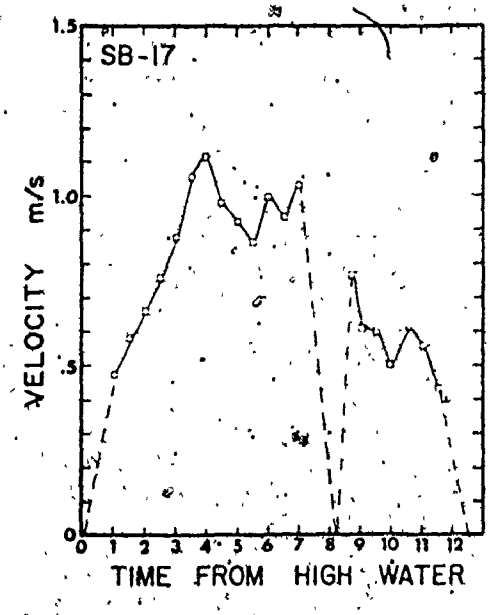
SB-17
VELOCITY m/s
TIME FROM HIGH WATER

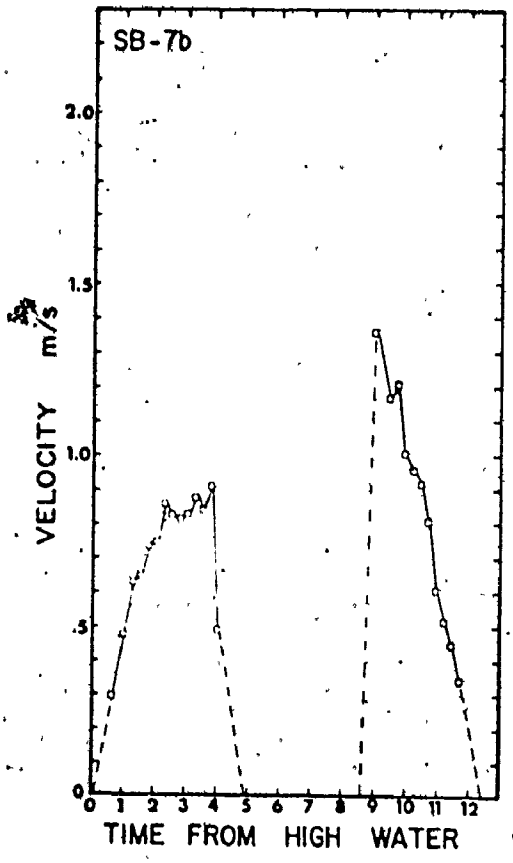
SB-7b
VELOCITY m/s
2.0
1.5
1.0
.5
0
0 1 2 3 4 5 6 7 8 9 10 11 12
TIME FROM HIGH WATER

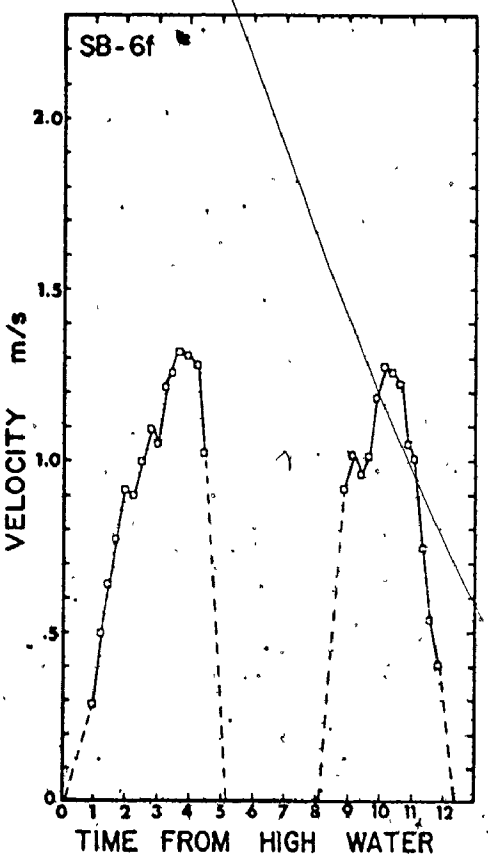
SB-6f
VELOCITY m/s
2.0
1.5
1.0
.5
0
0 1 2 3 4 5 6 7 8 9 10 11 12
TIME FROM HIGH WATER

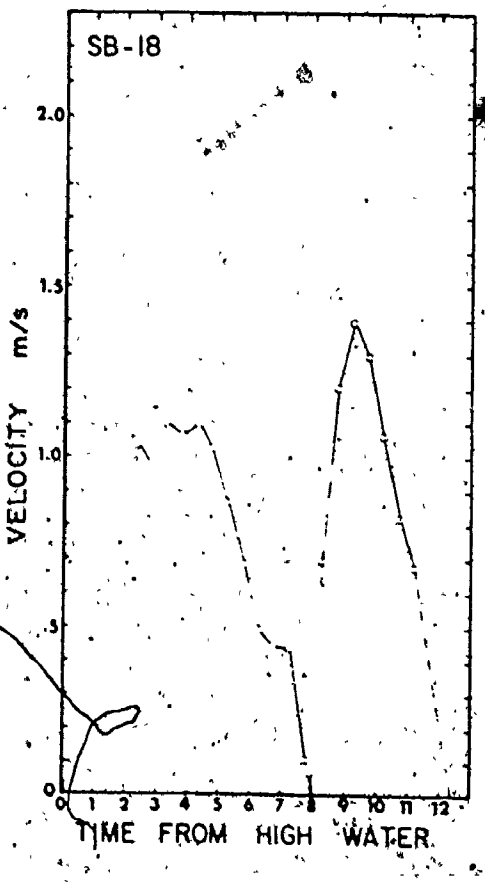
SB-18
VELOCITY m/s
2.0
1.5
1.0
.5
0
0 1 2 3 4 5 6 7 8 9 10 11 12
TIME FROM HIGH WATER

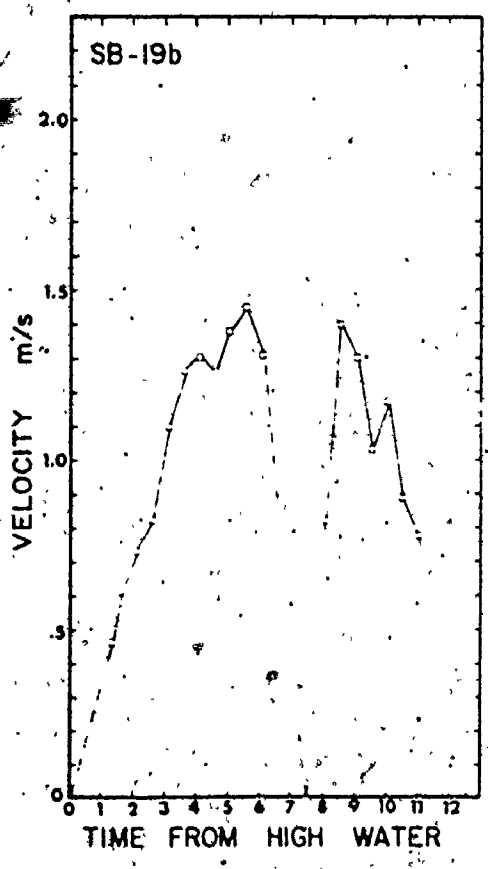
SB-19b
VELOCITY m/s
2.0
1.5
1.0
.5
0
0 1 2 3 4 5 6 7 8 9 10 11 12
TIME FROM HIGH WATER

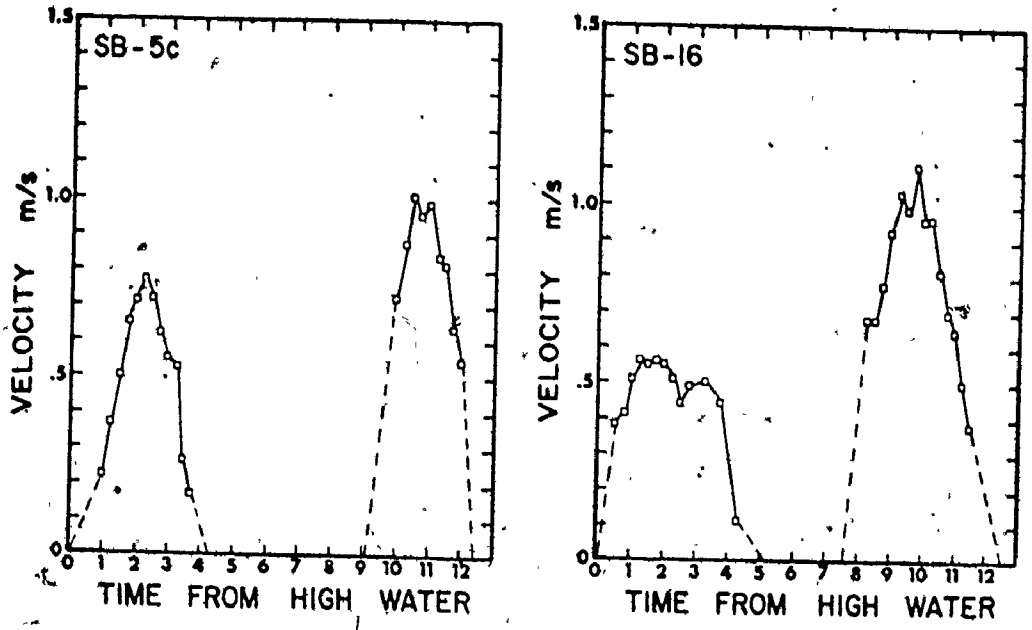

FIGURE 4.14 - cont'd.

FIGURE 4.15: Time-velocity relationships for two locations on Selma Bar from measurements made with an automatic recording current meter in 1972. Note reversal of current direction with each ebb and flood phase. See Appendix III.1 for operating dates.

A SELMA BAR 1

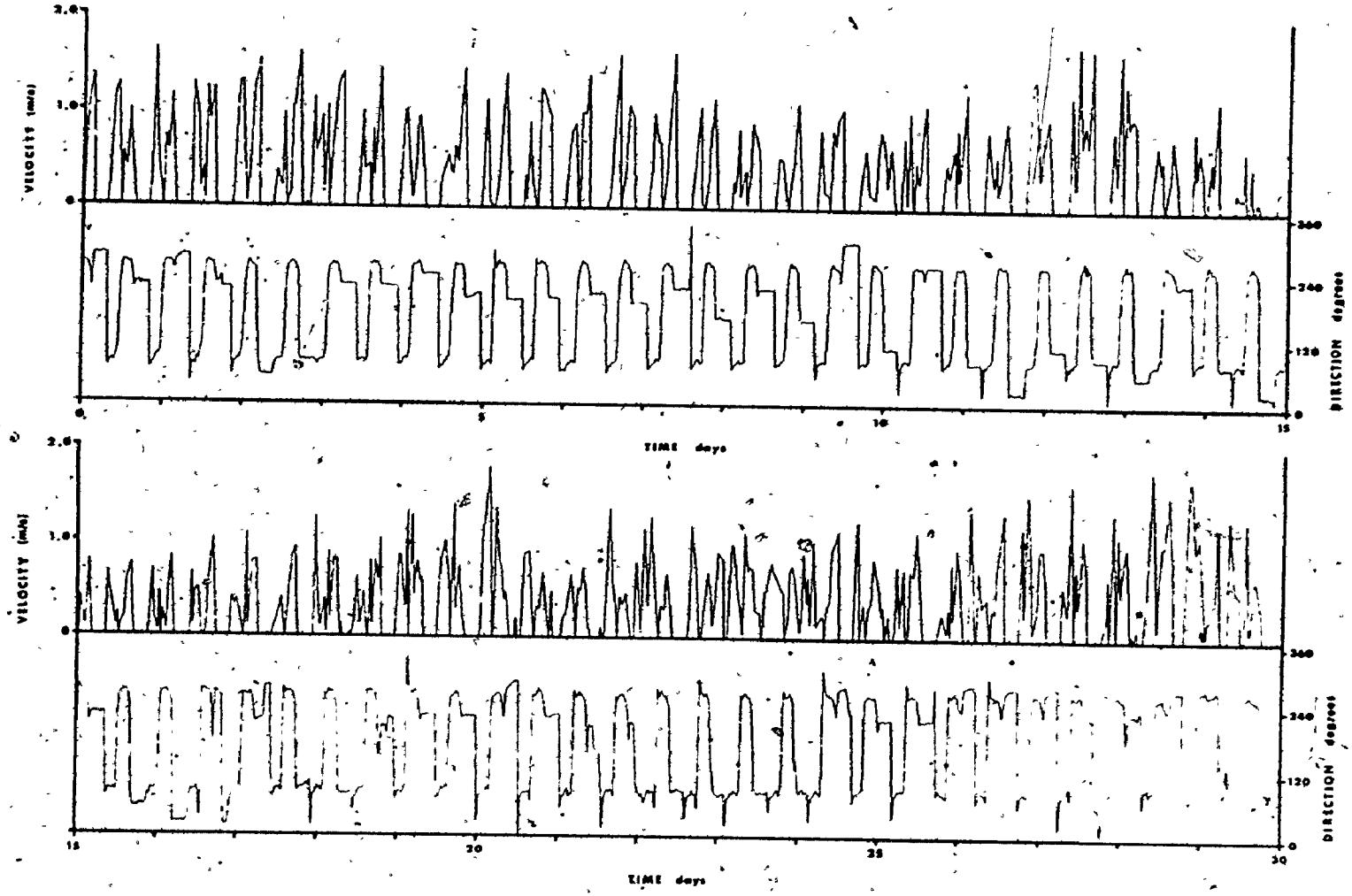
VELOCITY (m/s)
DIRECTION degrees
TIME days
VELOCITY (m/s)
DIRECTION degrees
TIME days

B SELMA BAR 3

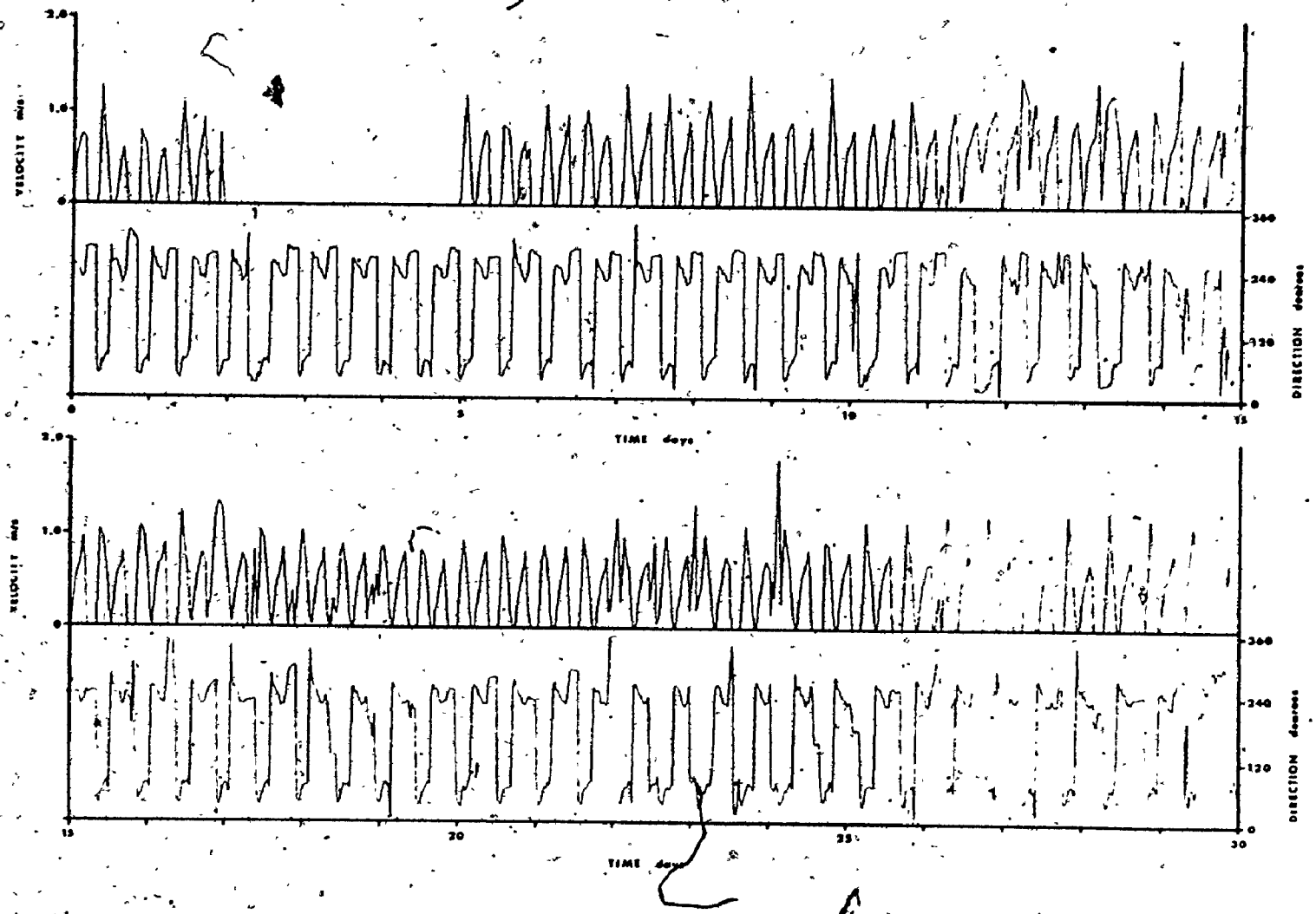

FIGURE 4.15 - cont'd.

FIGURE 4.16: The areal distribution of maximum mean current speeds (average of three maximum speeds) during the ebb and flood, and the areas of ebb and flood dominance on Selma Bar. Current speeds used were standardized (see Appendix IV.1).

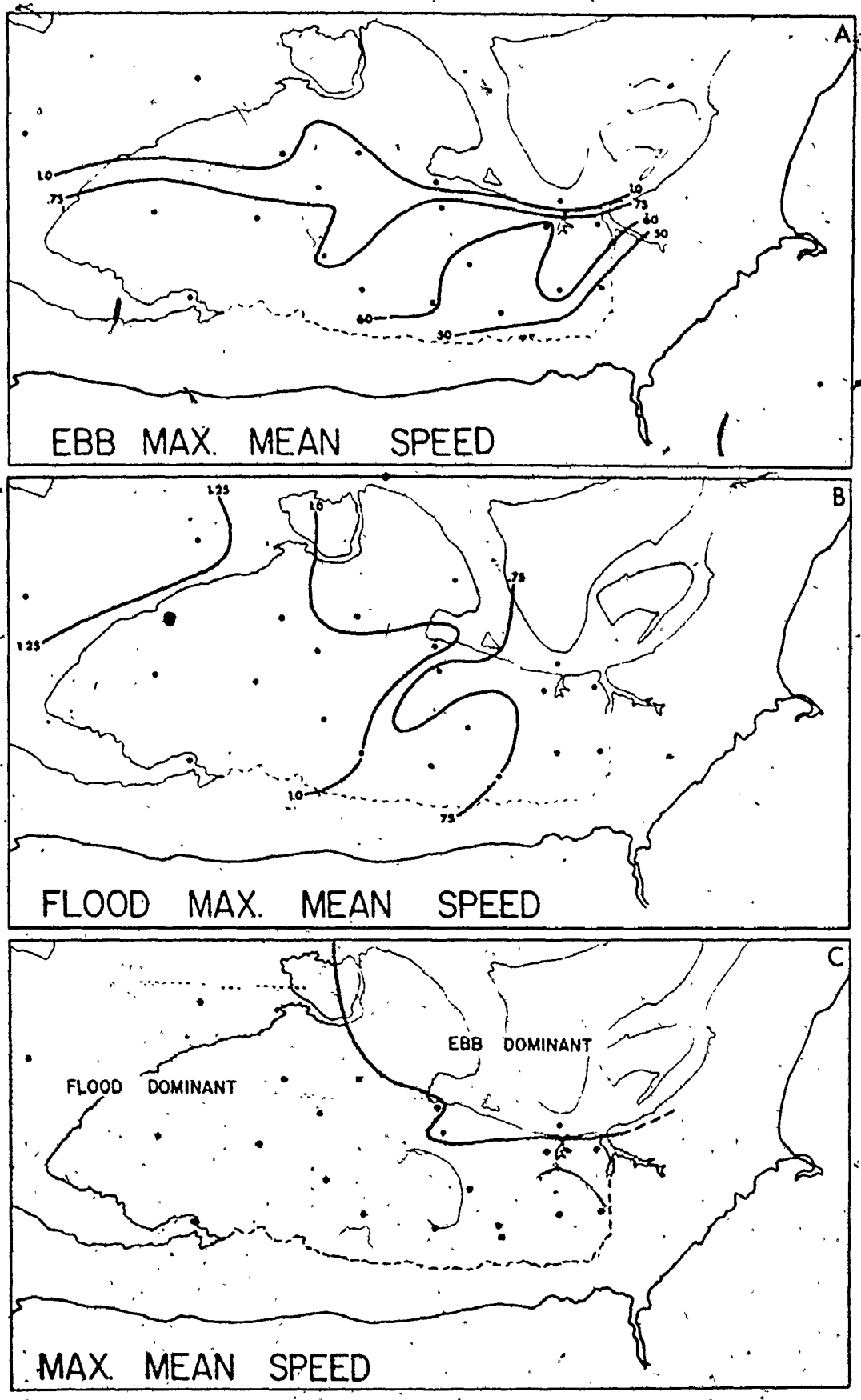
A
1.0
.75
1.0
.75
.60
.30
.60
.30
EBB MAX. MEAN SPEED
B
1.25
1.0
.75
1.25
1.0
.75
FLOOD MAX. MEAN SPEED
C
EBB DOMINANT
FLOOD DOMINANT
MAX. MEAN SPEED

TABLE 4-10

EBB AND FLOOD FLOW DURATIONS ON SELMA BAR (hours)

Location	Ebb	Low Tide Emergence	Flood	Difference Flood - Ebb
SELMA BAR				
1A	4.03	5.50	2.97	-1.06
B	4.37	4.50	3.55	- .82
C	4.03	4.75	3.55	- .48
D	4.28	4.00	3.22	-1.06
	(4.18)[1]		(3.32)	
2A	5.37	3.50	3.63	-1.74
B	4.87	4.00	3.63	-1.24
C	4.45	3.50	4.38	- .07
D	4.53	4.00	4.88	.35
E	4.53	4.50	3.47	-1.06
F	4.95	3.50	4.38	- .57
	(4.78)		(4.06)	
3A	4.95	3.00	4.55	- .40
B	5.37	3.00	3.97	-1.40
	(5.16)		(4.26)	
4A	2.87	6.75	2.80	- .07
B	2.55	7.00	3.22	.67
	(2.71)		(3.01)	
5A	3.70	6.00	2.80	- .90
B	4.03	4.00	4.30	.27
C	4.20	5.00	3.30	- .90
	(3.98)		(3.47)	
6A	2.92	7.28	2.47	- .45
B	4.20	3.50	3.80	- .40
C	4.95	3.00	4.47	- .48
D	5.03	3.50	3.88	-1.15
E	5.03	3.00	4.38	- .65
F	5.12	3.00	4.38	- .74
	(4.54)		(3.90)	
7A	5.20	3.00	4.22	- .98
B	4.95	3.50	3.88	-1.07
	(5.08)		(4.05)	

T A B L E 4-10 (cont'd)

Location	Ebb	Low Tide Emergence	Flood	Difference Flood - Ebb
SELMA BAR (cont'd)				
8A	3.28	5.92	3.47	.19
B	--	--	--	
9	4.03	3.50	2.80	-1.23
10	5.12	3.67	3.38	-1.74
11	3.37	5.63	3.33	- .04
12	3.87	6.00	4.63	- .76
13	4.20	4.50	3.55	- .65
14	4.20	5.00	3.30	- .90
15	3.45	4.50	3.30	- .15
16	5.03	2.50	4.72	- .31
17	8.12	--	4.22	-3.90
18	8.03	--	4.47	-2.73
19A	7.45	--	4.88	-2.57
B	7.87	--	4.55	-3.32
	(7.66)		(4.72)	
20A	7.20	--	5.05	-2.15
B	7.37		4.97	-2.40
	(7.29)		(5.01)	

NOTE: 1. Station average.

TABLE 4-11

EBB AND FLOOD DISCHARGE PER TIDAL CYCLE(m^3)[1]

SELMA BAR

Location	Ebb	Flood	Diff.[2]
1A	32649.789	37237.327	4587.530
1B	24030.800	26260.141	2229.340
1C	17528.664	28828.381	11299.717
1D	20816.685	22960.856	2144.181
2A	88767.558	88674.458	-93.099
2B	45990.328	40129.750	-5860.578
2C	29602.482	40242.329	10639.847
2D	30257.648	42069.758	11812.110
2E	42111.902	53596.071	11484.169
2F	25709.650	37455.476	11745.827
3A	35231.186	54600.729	19369.543
3B	58277.225	53240.022	-5037.203
4A	9020.678	13476.696	4456.017
4B	6777.956	11259.445	4481.489
5A	23330.867	38488.904	15158.037
5B	23177.811	42088.394	18910.583
5C	32057.142	35169.240	3112.098
6A	9982.588	-8811.472	-18794.059
6B	91155.728	85322.507	-5833.221
6C	50796.494	58728.035	7931.541
6D	44597.742	49610.509	5012.767
6E	52203.720	72353.019	20149.299
6F	49301.499	49251.944	-49.555
7A	67165.903	50858.268	-16307.635
7B	28217.488	29033.783	816.295
8A	20250.713	21387.180	1136.467

SELMA BAR

T A B L E 4-11 (cont'd)

Location	Ebb	Flood	Diff.
10	47631.640	53916.780	6285.139
11	13484.444	16693.083	3208.639
12	17508.986	17691.193	182.207
13	13743.271	21426.135	7682.864
14	26642.534	25668.745	-973.889
15	20480.519	23360.541	2880.021
16	30843.786	54649.320	23805.534
17	106875.424	53587.057	-53288.367
18	175534.568	150413.954	-25120.614
19A	126642.958	98049.046	-28593.912
19B	163716.755	122215.352	-41501.403
20A	77702.544		
20B	77877.247	73598.789	-4278.458

NOTE: 1. Data not standardized.
2. Negative sign indicates ebb dominance; positive is flood dominant.

Ebb and flood flow durations (Table 4.10) over the bar averaged approximately 4.1 and 3.7 h respectively. The duration of flow in the channels averaged 7.8 h for the ebb and 4.6 h for the flood. The ebb is significantly longer in duration than the flood.

Ebb and flood unit discharges are listed in Table 4-11.

Depth The variation of flow depths during ebb and flood can be depicted on a time-depth graph. Figure 4.17 shows two representative time-depth relationships from Selma Bar.

Time-depth relationships generally showed that water depth decreased (ebb) and increased (flood) almost as a linear function with respect to time. Some flattening of the curves occurred near high and low water (Fig. 2.19), but these regions of the curves represented only short time periods relative to the whole duration of the ebb and flood. The slope of the flood time-depth relationship is commonly much steeper than that for the ebb, indicating that water depths increase at a faster rate than the rate of water fall during the ebb.

The average rate of ebb (fall) and flood (rise) depth change can be determined by dividing the total measured depth change (m) by the duration of the flow (hours). Table 4.12 summarizes the average rates of ebb and flood depth change standardized on the mean tidal range (11.7 m) at Burntcoat Head from different parts of Cobequid Bay. Because the tidal range is of the same order for both the ebb and flood (Appendix III, Table III-1) and the duration of the ebb is generally greater than the flood duration, the flood rates of depth change are always greater than the ebb rates (i.e., the greater slope of the flood relationship relative to the ebb).

Figure 4.18 shows the average ebb and flood rates (standardized) for each of the different bars studied (bar and channel locations averaged together for each bar). The average ebb rates decrease by about 3 m/hr towards the head of the bay (i.e., from Noel Bay Bar to Selma Bar) while the flood rates increase from about 0.5 to 1.0 m/hr. The data for East Noel Bar is perhaps spurious.

Froude numbers (Appendix IV.2) increased gradually during the ebb to a maximum just before low water emergence of the sand bars. During the flood, Froude numbers decreased from a maximum right after submergence

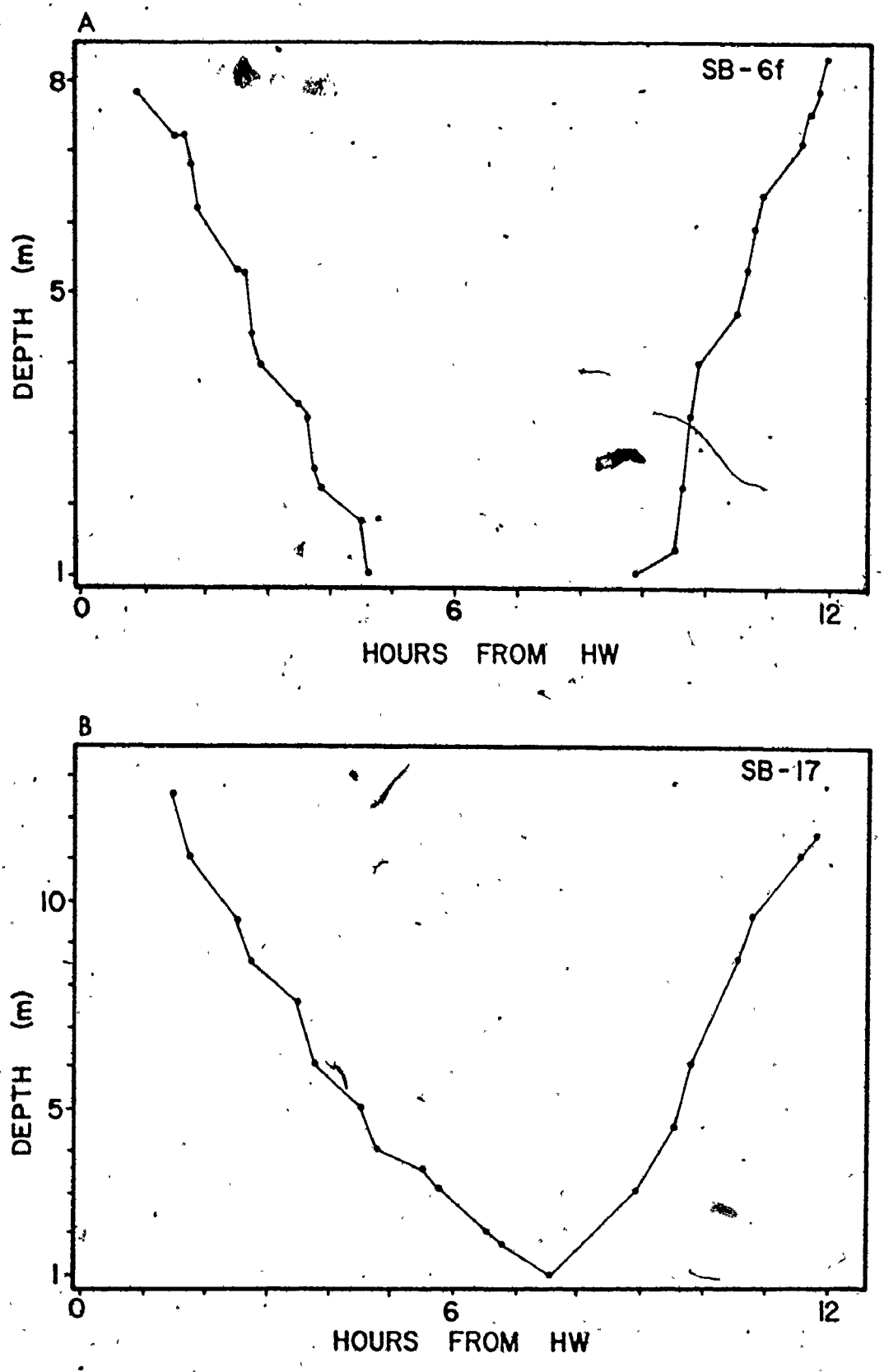

FIGURE 4.17: Representative time-depth relationships for two locations on Selma Bar. See Figure 4.1 for locations.

TABLE 4-12

RATES OF EBB AND FLOOD WATER LEVEL RISE AND FALL[1] (m/h)

Location[5]	Unstandardized Ebb Fall	Unstandardized Flood Rise	Standardized Ebb Fall	Standardized Flood Rise
NOEL BAY BAR				
1A	2.27	2.61	2.21	2.59
B	2.46	3.18	2.48	3.10
C	2.04	3.07	2.08	3.02
D	2.13	2.43	2.25	2.45
			(2.26)	(2.79)[4]
2A	1.99	2.62	1.97	2.58
B	2.55	3.50	2.41	3.28
			(2.18)	(2.93)
3A	2.04	2.25	2.51	2.66
B	2.22	2.67	2.65	3.00
C	2.11	3.00	2.20	3.03
			(2.45)	(2.90)
4	2.42	3.17	2.23	2.94
5	1.88	2.87	1.73	2.67
6A	2.21	3.27	2.39	3.36
B	2.49	2.26	2.65	2.30
			(2.52)	(2.83)
7	2.25	3.00	2.19	3.03
8	2.71	3.67	2.64	3.70
EAST NOEL BAR				
1	1.85	2.60	2.10	2.93
2	2.49	2.00	2.47	1.95
			(2.29)	(2.44)
GREAT VILLAGE BAR	2.20	2.57	2.32	2.61
MIDDLE CHANNEL	1.80	2.80	1.61	2.54

Continued.....

T A B L E 4-12 (cont'd)

Location	Unstandardized Ebb Fall	Unstandardized Flood Rise	Standardized Ebb Fall	Standardized Flood Rise
NOEL SHORE BAR				
1	2.88	4.05	2.53	3.56
2A	2.50	3.19	2.34	2.96
B	2.38	3.60	2.34	3.48
			(2.34)	(3.22)
3	2.29	2.83	2.41	2.88
4	2.33	2.31	2.29	2.29
5	2.00	2.10	2.11	2.08
6	2.33	3.13	2.27	3.08
7	2.38	3.14	2.42	3.11
8	2.00	3.20	2.25	3.47
9	2.09	2.88	2.20	2.96
10	1.96	2.63	1.98	2.65
11	1.91	3.13	2.07	3.18

Continued.....

T A B L E 4-12 (cont'd)

Location	Unstandardized Ebb Fall	Unstandardized Flood Rise	Standardized Ebb Fall	Standardized Flood Rise
SELMA BAR				
1A	2.44	2.80	2.15	2.58
B	2.22	2.50	2.52	2.79
C	2.40	3.35	2.42	3.14
D	2.29	3.14	2.16	3.01
			(2.31)	(2.88)
2A	2.27	4.50	2.09	4.25
B	2.70	2.75	2.43	2.55
C	2.00	2.11	2.44	2.47
D	2.00	2.50	2.09	2.66
E	2.66	3.40	2.32	3.06
F	2.07	2.57	2.45	2.89
			(2.30)	(2.98)
3A	1.80	2.76	1.83	2.76
B	2.51	3.40	2.49	3.29
			(2.16)	(3.03)
4A	2.00	2.33	2.05	2.25
B	1.70	2.61	2.05	2.99
			(2.05)	(2.62)
5A	1.86	2.60	1.93	2.56
B	1.69	2.00	2.08	2.34
C	2.65	3.35	2.42	3.11
			(2.14)	(2.67)
6A	2.24	2.25	2.54	2.66
B	2.80	2.55	2.48	2.35
C	1.88	2.15	2.22	2.47
D	1.95	3.20	2.11	3.31
E	2.08	3.27	2.15	3.19
F	1.99	2.50	2.28	2.79
			(2.30)	(2.80)
7A	2.00	3.08	2.15	3.28
B	1.56	1.93	1.74	2.07
			(1.95)	(2.68)
8A	2.00	3.33	2.07	3.30
B	2.00	1.80	2.07	1.90
			(2.07)	(2.60)

T A B L E 4-12 (cont'd)

Location	Unstandardized Ebb Fall	Unstandardized Flood Rise	Standardized Ebb Fall	Standardized Flood Rise
SELMA BAR				
9	2.20	3.50	2.11	3.30
10	2.22	4.00	2.15	3.97
11	1.60	2.33	2.01	2.75
12	1.28	1.75	1.30	1.84
13	1.38	1.65	1.52	1.74
14	2.18	2.65	2.26	2.77
15	1.40	2.96	1.55	3.12
16	2.40	2.55	2.84	2.87
17	1.83	2.91	1.89	3.01
18	1.77	3.50	1.71	3.28
19A	2.22	2.85	2.24	2.90
B	1.63	2.67	1.75 (2.00)	2.81 (2.86)
20A	2.00	--	2.17	--
B	1.88	2.50	2.06 (2.12)	2.71 (2.71)

NOTE: 1. Standardized Rates = $\frac{\text{Total water depth change}}{\text{flow duration}} \quad \frac{\text{Mean tidal range}^2}{\text{Daily Tidal range}^3}$

2. Mean tidal range = 11.7 m
(Canadian Tide and Current Tables, CHS, 1973)

3. See Table III-1 in Appendix III

4. Average values per station.

5. See Fig. 4.1 for locations.

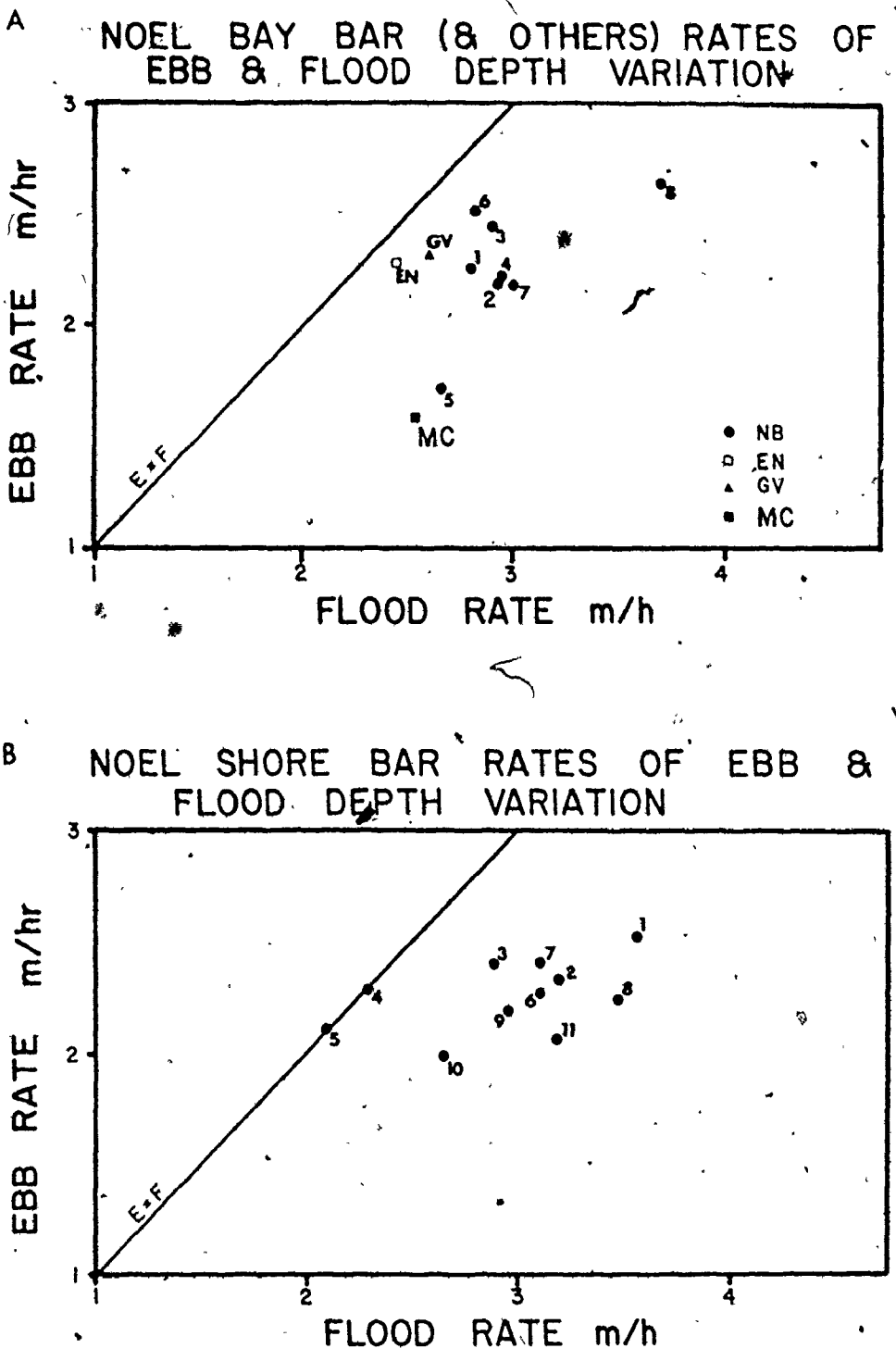

FIGURE 4.18: Ebb and flood rates of water level change per tidal cycle. Locations are shown in Figure 4.1.

C

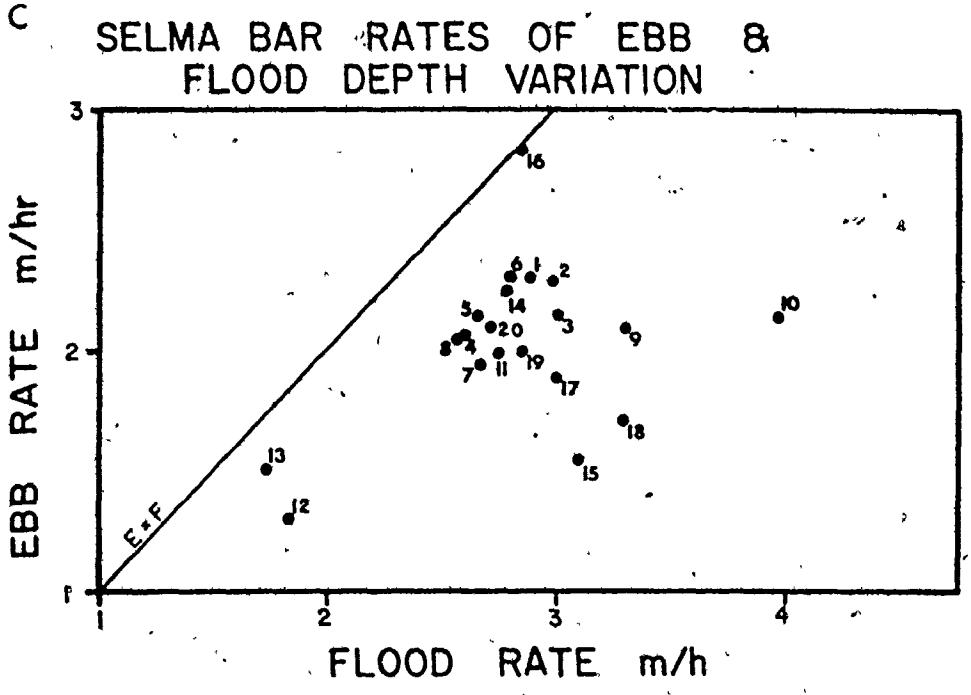

D

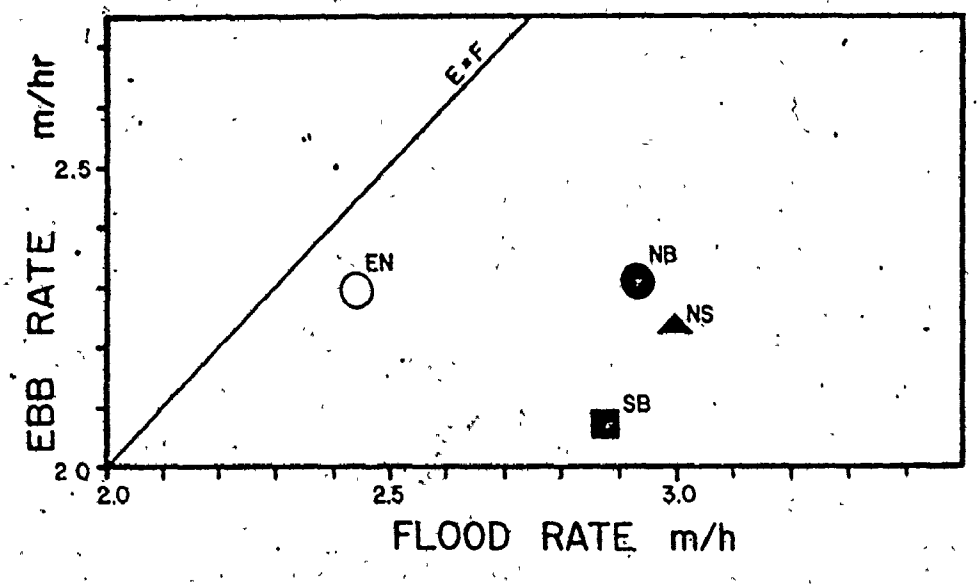

FIGURE 4.18 - cont'd.

of the bar surface to a minimum at high water. The magnitude of Froude numbers were generally larger towards the head of the bay (see Appendix IV.2).

Flow Directions - Current directions were measured at each point in the vertical velocity profiles. These measurements are listed in Appendix III.2 with the depth and current speed data.

The current direction data are important for two reasons: (i) to determine the existence or non-existence of secondary flow patterns; and (ii) to determine the mean directions of current flow and their relation to sediment transport patterns (the latter aspect is discussed in Chapter 6).

Figure 4.19 indicates the nature of a representative time-direction relationship in the study area using the flow direction one metre above the bottom. During the ebb, the tidal currents flow in a generally east to west direction across the bars at a slightly oblique angle to the orientation of the crestlines. As the water depths decrease, the oblique angle between the flow direction and the orientation of the bar crestlines increases (Fig. 4.19, i.e., the currents flow more toward the crestlines). Once the crestlines of the bars are emergent, tidal flow is confined to the interbar channels and flow directions are controlled by the channel pattern. Late stage ebb runoff from the bars is restricted to open channel flow in bedform troughs and bar swatchways, and some internal dewatering of the bars (e.g., Fig. 3.34 G).

During the flood, the tide first encroaches up the bar swatchways and bedform troughs until the crestlines of the bars are submerged. As the water depths increase, the oblique angle between the flow direction and the orientation of the bar crestline decreases, but the flow still continues to move generally across the bar's crestline (Fig. 4.19).

Figure 4.20 shows the general relationship between the mean near bottom (1 m above the bottom) current directions for the ebb and flood, and the orientation of the bar crestlines. The ebb generally flows up and across the steep side of the bars at an oblique angle to the crestlines while the flood generally flows up and across the gentle side of the bars at an oblique angle to the crestlines.

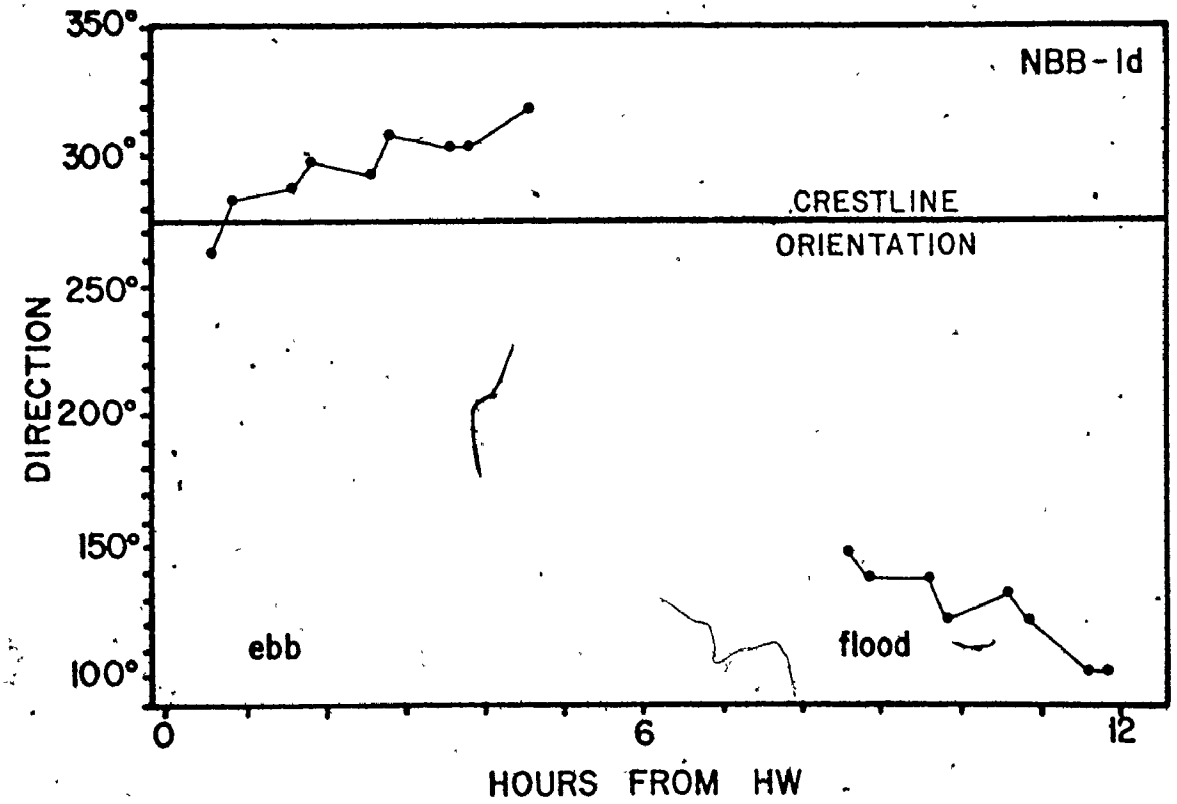

FIGURE 4.19: The variation of near bottom (1 m above the bottom) current directions during a tidal cycle relative to the orientation of the bar crestline.

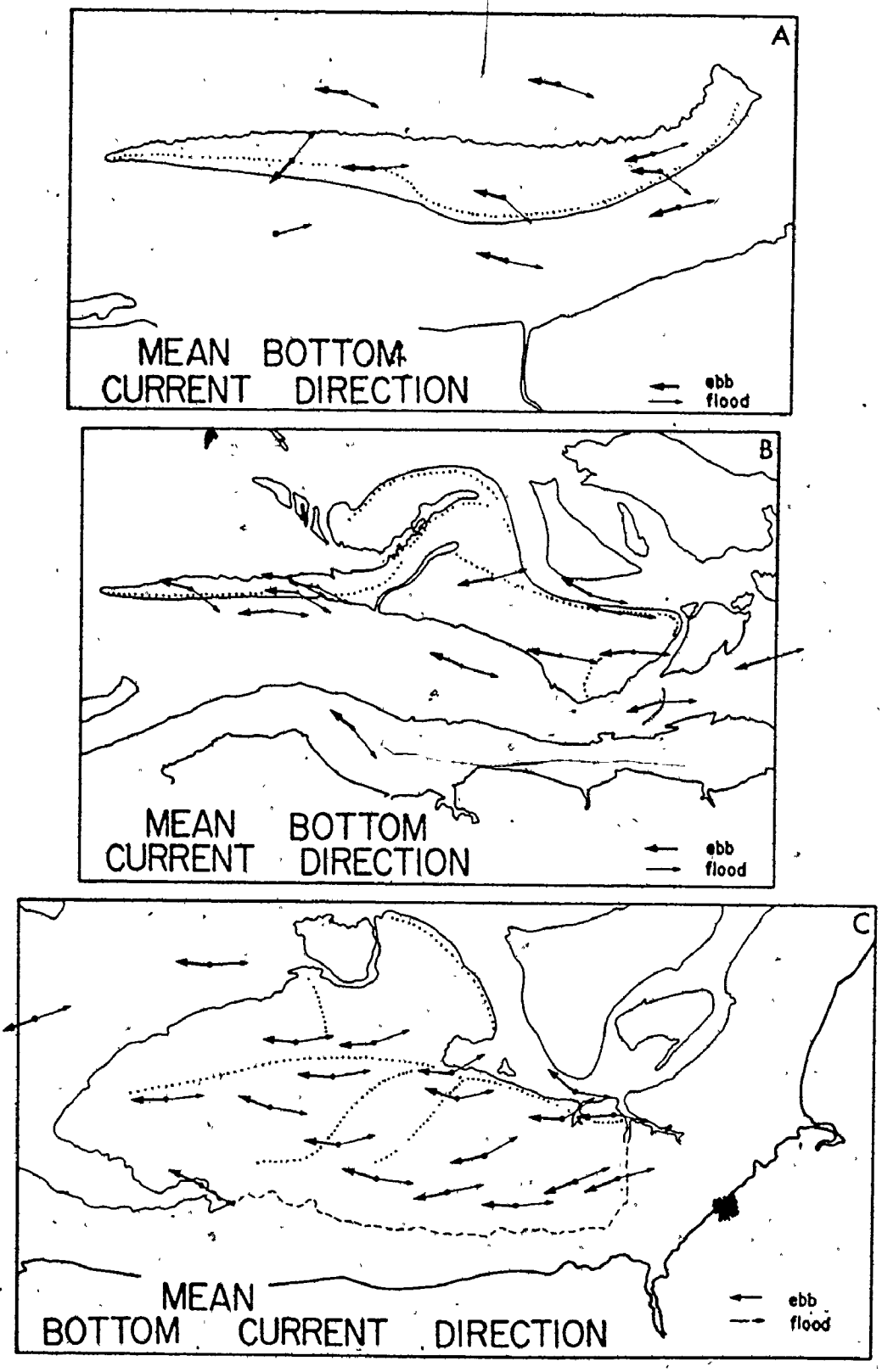

FIGURE 4.20: Mean bottom (1 m above the bottom) current directions for the ebb and flood at several locations on Noel Bay Bar, Noel Shore Bar and Selma Bar.

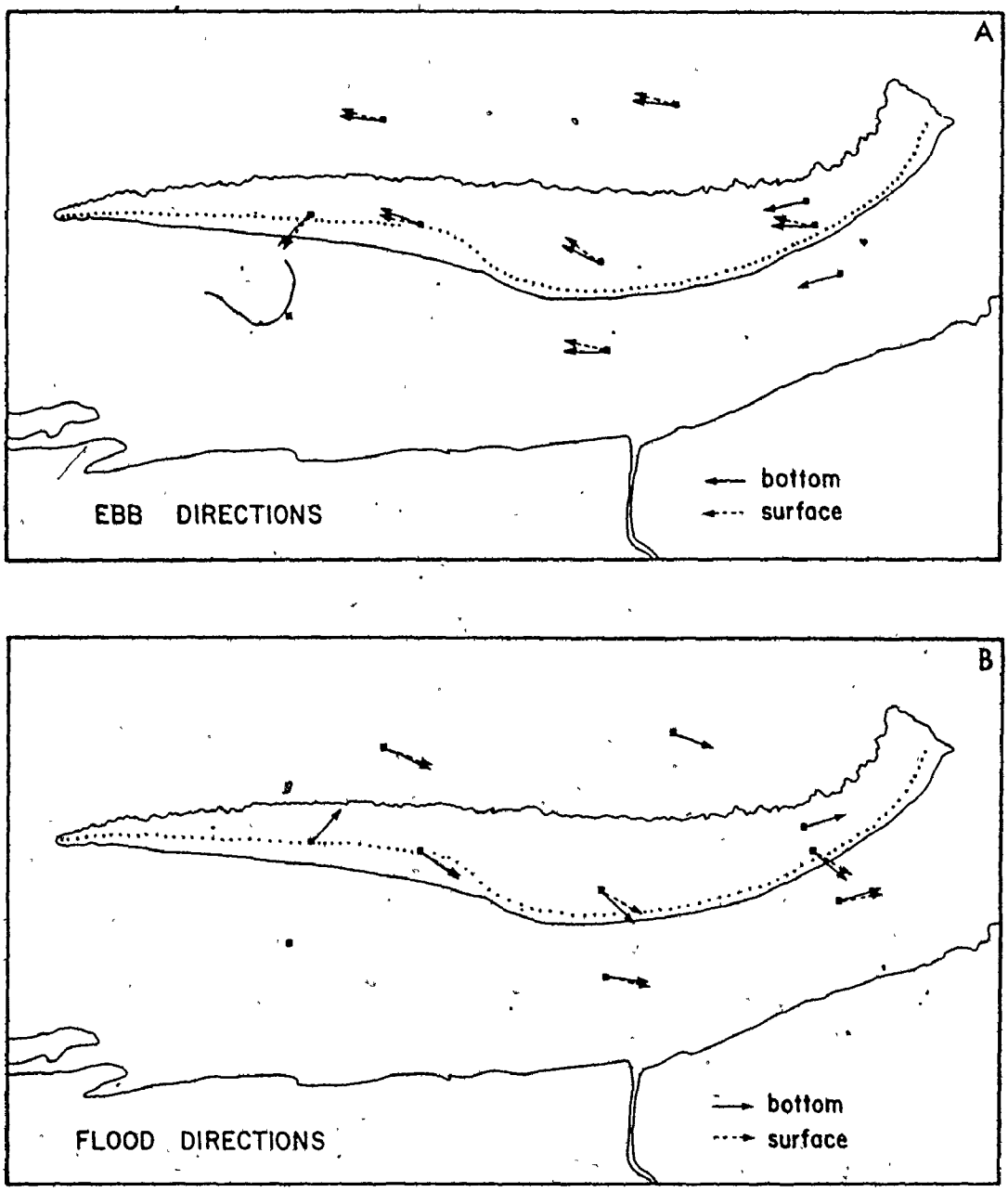

FIGURE 4.21: Mean bottom (1 m above the bottom) and surface (1 m below the surface) current directions during the ebb and flood over Noel Bay Bar

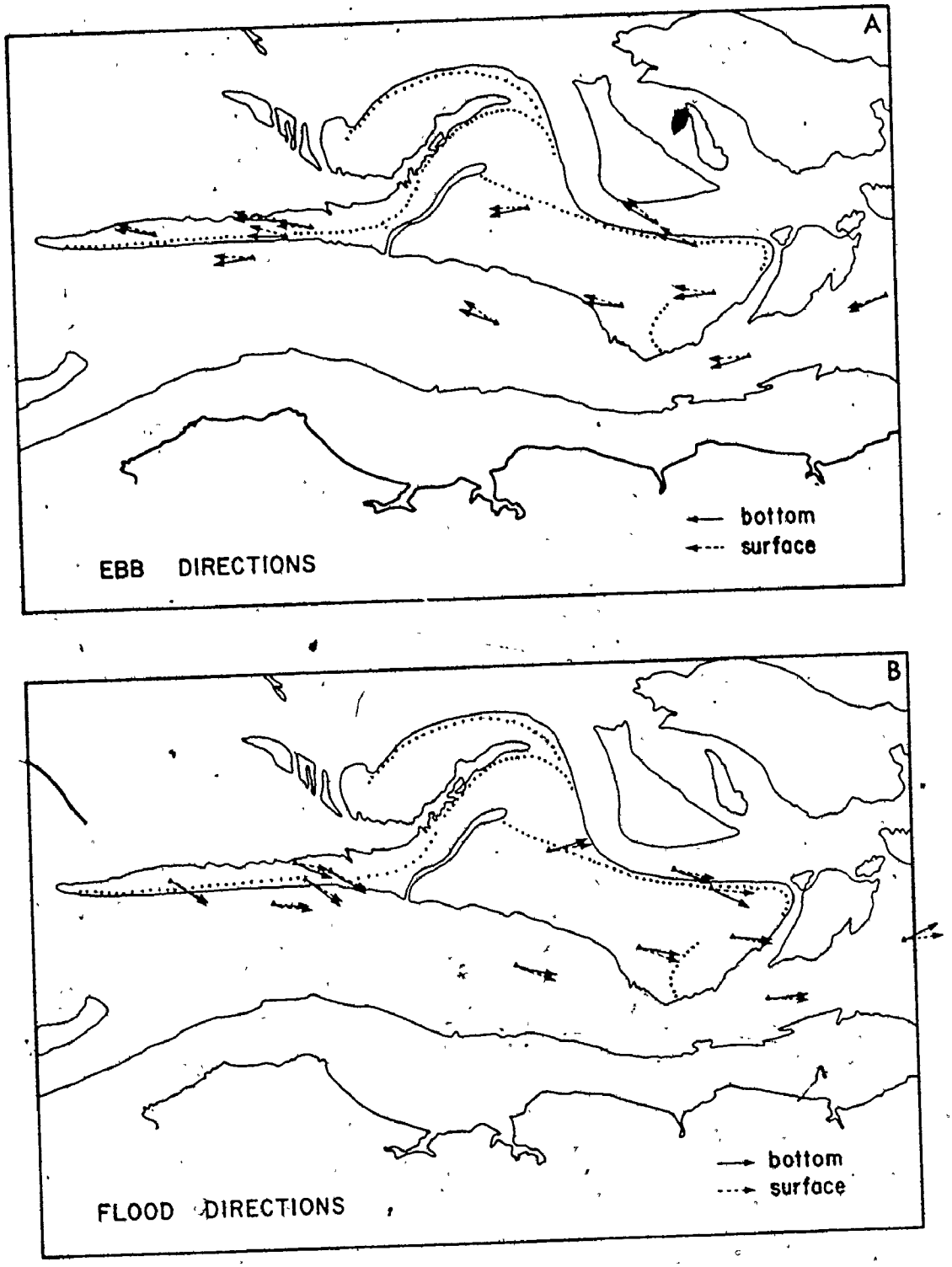

FIGURE 4.22: Mean bottom (1 m above the bottom) and surface (1 m below surface) current directions during the ebb and flood over Noel Shore Bar.

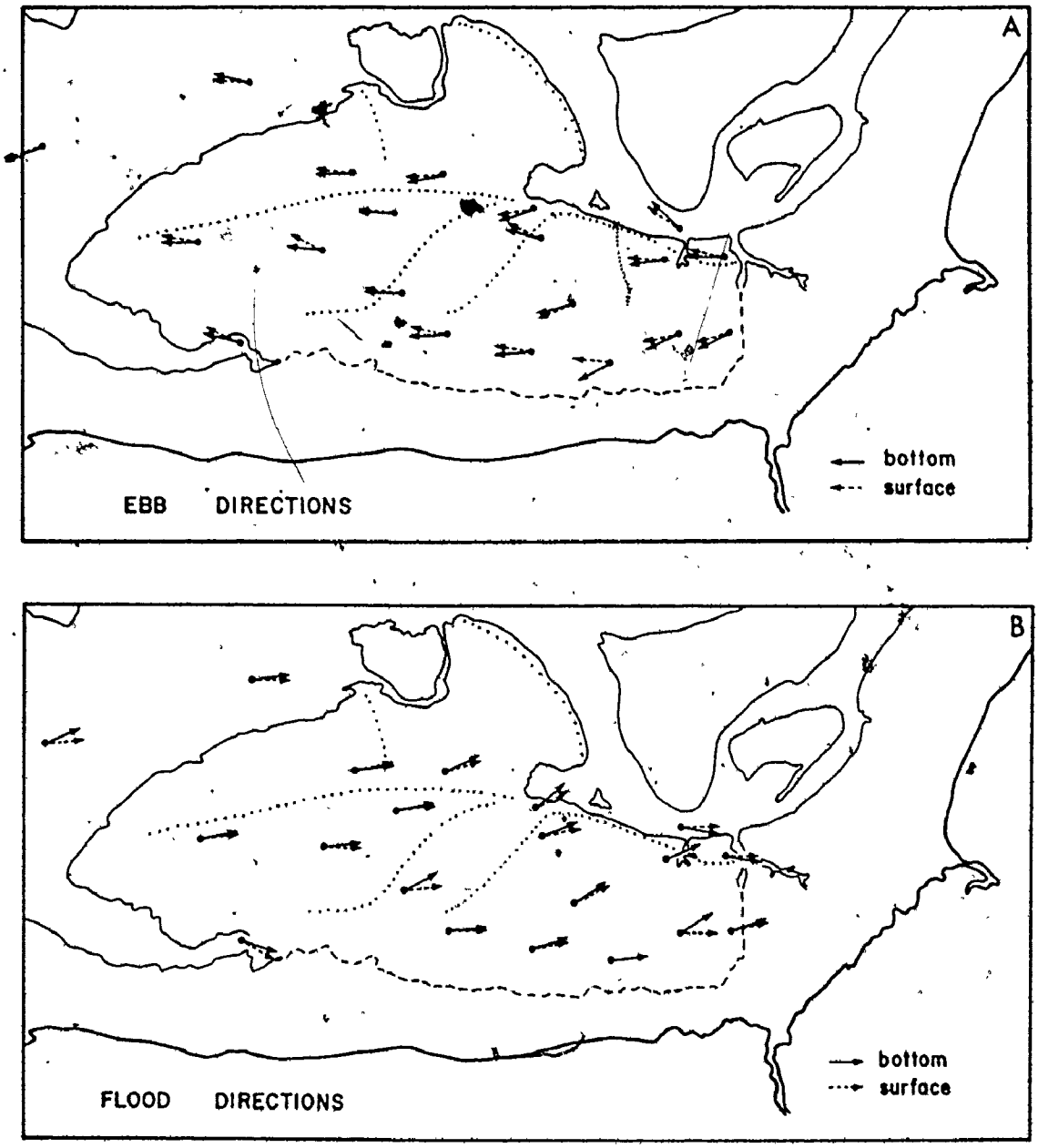

FIGURE 4.23: Mean bottom (1 m above the bottom) and surface (1 m below the surface) current directions during the ebb and flood over Selma Bar.

Figures 4.21, 4.22 and 4.23 show the ebb and flood mean bottom (1 m above the bottom) and surface (1 m below the surface) current directions relative to the orientation of the sand bar crestlines (e.g., Noel Bay Bar, Noel Shore Bar and Selma Bar). The mean current directions do not support the existence of a helicoidal pattern of flow in the channels to either side of the bar crestlines. Houbolt (1968) suggested that a helicoidal pattern of flow was necessary for the maintenance of linear tidal ridges in the North Sea. There is some evidence in the current direction data (Appendix III.3) that helicoidal flow may occur in the curved reaches of some channels, but only when water depths are relatively low.

Shear Velocity - The shear velocity (u_*) is an alternative to the mean velocity as a measure of the strength of flow. Shear velocity is directly related to the shear-stress on the bottom, but is expressed in units of velocity and is thus more readily meaningful than the shear-stress, which is expressed in units of force per unit area. Shear Velocity was determined from Equation 4.7 (Appendix IV.1) assuming that $\kappa = 0.4$ and using the slope of the linear regression line (Eqn. 4.18) fitted to the measured velocity distribution.

The shear velocity values obtained by this procedure showed some degree of random fluctuation with time during a tidal cycle from "expected reasonable values." These fluctuations of the time-shear-velocity relationship probably result from the non-systematic variation of the slopes of the regression lines fitted to the vertical profile data.

Sternberg and Ludwick (1975) suggested that a form of 'shear-stress' or 'shear velocity' can be determined from the mean flow velocity at one metre from the boundary (derived from the regression lines fitted to the vertical velocity profile or from a single velocity measurement at D = 1 m) by the relation

$$\tau_0 \propto \rho\, u_1^2$$

$$\text{or} \quad \tau_0 \propto u_* u_1$$

The proportionality in this relation is undefined and thus only approximate. Shear velocity (or shear-stress) derived in this manner does not give accurate results (i.e. absolute values) but does yield order of

magnitude values that have smaller time-shear velocity fluctuations. Because we know that

$$\frac{u}{u_*} \sim \frac{1}{f}$$

where f = Darcy-Weisbach friction factor

$$\text{or} \sim \log \frac{1}{k_s}$$

and ks = equivalent grain roughness of the boundary

we can hardly use the velocity one metre from the bottom to tell us what is happening to u_* and τ_0 if f or k_s are varying during a tidal cycle (see Chapter 5). As a result, shear velocities were determined directly from the vertical velocity profiles in this study. The data are a little 'noisy' but time-variant trends are still recognizable during the tidal cycle.

Shear velocities were generally of the order of 0.04 to 0.09 m/s at most locations (Appendix IV.2) during the ebb and flood. The largest values tended to occur during the flood rather than the ebb, and maximum values were often associated with maximum mean current speeds. Thus, the temporal variation of shear velocities generally had time asymmetries that were similar in form to the time-velocity relationships, and shear velocities tended to be less over the bars than in the channels. On Noel Bay Bar the average maximum shear velocities were approximately 0.08 and 0.07 m/s respectively during the ebb and flood and 0.08 and 0.06 m/s in the channel. Average values on Noel Shore Bar were 0.10 and 0.11 m/s respectively during the ebb and flood and 0.13 and 0.10 m/s in the channels, while on Selma Bar the average values were about 0.08 m/s for the ebb and flood, and 0.09 and 0.11 in the channels. The magnitude of shear velocities were about the same on all of the bars studied, but strengths increased towards the head of the bay in the channels (e.g., compare channel locations at Noel Bay Bar, Noel Shore Bar and Selma Bar). Average maximum shear velocities on the four sand bars studied ranged from 0.08 (NBB and SB) to 0.11 m/s (NSB) during the ebb and from 0.07 (NBB) to 0.10 (SB and NSB) during the flood.

Water Surface Slope - The theoretical water surface slope (S), determined from the shear velocity and the depth of flow (see Appendix IV.1), varies with time during the tidal cycle (Appendix IV.2). Slope values a ear igh to a maximum just

before low water during the ebb while the opposite trend occurred during the flood (i.e., the slope of the water surface decreased from a maximum just after the tide turned to a minimum at high water). During the ebb, the water surface steepens rapidly after the bar crestlines become exposed and the flow is confined to the relatively narrow interbar channel. Slopes are generally steeper over the bars than in the channels, thus possibly reflecting the influence of water depths and bottom topography. Surface slopes increase slightly towards the head of the bay, both for channel and bar locations (See Appendix IV.2).

'Recap' - The preceding results characterize some of the general aspects and time-variant properties of the semidiurnal tidal currents in Cobequid Bay, such as:

1. Current speeds are greater in the interbar channels of the sand-bar complex than over the sand bars; current speeds decrease towards the crestline of the bars; channel speeds increase slightly towards the head of the bay (i.e., from Noel Bay Bar to Selma Bar) while current speeds over the bars are similar throughout the bay; the asymmetry of the ebb time-velocity relationships increase towards the head of the bay, while the asymmetry of the flood relationships decrease; maximum speeds occur sooner over the sand bars than in the channels; and maximum flood speeds are generally larger than maximum ebb speeds.
2. The flow duration of the ebb is longer than the flow duration of the flood; the flow duration in the interbar channels is longer than that over the sand bars during both the ebb and the flood; and the difference between the channel and bar flow durations is greater during the ebb than during the flood.
3. The steep sides of the sand bars are ebb dominated while the gentle sides are flood dominated (with respect to maximum current speeds and unit discharges).
4. The rate of depth decrease during the ebb is less than the rate of depth increase during the flood; the rates of depth change for bar and channel locations are similar; the rate of depth decrease during the ebb is less towards the head of the bay, but the rate of depth increase during the flood is about the same throughout the bay; and Froude numbers are largest on either side of low water (late ebb and early flood) but less than 1.
5. The tidal currents flow across the sand bars at a slightly oblique angle to the orientation of the crestline of the bars; when water depths

are relatively deep, the angle between the current direction and the orientation of the bar crestline is small; when water depths are relatively shallow, the angle between the current direction and the orientation of the bar crestline is relatively large; both the mean bottom and surface current directions exhibit cross-bar components of flow during the ebb and flood; and, the tidal currents in the sand-body complex are reversing (i.e., not rotary).

6. Shear velocities show similar time asymmetries to the time-velocity relationships; and shear velocities are generally larger during the flood than during the ebb.

7. Water surface slopes steepen from high to low water (ebb) and flatten from low water to high water (flood).

Discussion - The tidal current regime of the sand-body complex in Cobequid Bay is characterized by two types of flow (Fig. 4.24): (i) a high-water 'sheet' flow phase (before the emergence of the sand bars); and (ii) a low water 'channel' flow phase (after the emergence of the sand bars). By continuity, discharge is the product of the cross-sectional area of the flow multiplied by the flow velocity. Current velocity is a function of depth, slope, boundary roughness and exposure.

At high tide slack-water, the intertidal zone (i.e., the foreshores and bars) is completely submerged and the flow cross-section available to the ebb currents is relatively large (because water depths are comparatively large). During the ebb, water levels are progressively drawn down from the east to the west (i.e., a diminishing negative wave) by the outgoing tide. The lowering of water levels causes the intertidal zone to gradually emerge and the cross-sectional area of the flow to be slowly reduced. Before the emergence of the sand-body complex, the tidal currents flow in a generally east to west direction, almost parallel to the shorelines of Cobequid Bay and at a slightly oblique angle to the crestline of the intertidal (now submerged) bars. As the time lag between the continued fall of the tide (water levels) and the sectional discharge per unit time increases (i.e., discharge is not able to keep up with the rate of water level drop), the slope of the water surface steepens and current speeds gradually increase. Current speeds and the gradient of the water surface continue to increase in the interbar channels until most of the intertidal zone area in the bay is emergent.

FIGURE 4.24: Summary of the tidal current flow regime in the Cobequid Bay sand-body complex during a tidal cycle.

A. High-water (ebb) 'sheet' flow phase; water depths are relatively deep; relative roughness is small; water surface slopes are small; current speeds are relatively weak; current flow is across the crestline of the bars at a small angle to the orientation of the bar axis.

B. Mid-ebb 'sheet' flow phase: water depths are relatively shallow over the crestline of the bars; relative roughness over the bars is large; water surface slopes across the bar are relatively steep; water levels on the upflow side of the bar are higher than those on the downflow side; current speeds over the bar are relatively high; current flow is across the crestline of the bars at a relatively steep angle to the orientation of the bar axis.

C. Late ebb 'channel' flow phase: flow in the interbar channels is confined by the emergent intertidal foreshore and/or the crestlines of adjacent sand bars; relative roughness is large; water surface slopes in the channels are steep; current speeds are relatively high; current flow is controlled by the hydraulic geometry and drainage pattern of the channel; some secondary flow may develop in the curved reaches of some channels; current flow is along the interbar channels.

E. Mid-flood 'sheet' flow phase: water depths are relatively shallow over the bars; relative roughness over the bars is large; water levels on the upflow side of the bars is higher than that on the downflow side; current speeds are relatively high over the bar; current flow is across the crestline of the bars at a relatively steep angle to the orientation of the bar axis.

F. High water (flood) 'sheet' flow phase: water depths are relatively deep; relative roughness is small; water surface slopes are small; current speeds are relatively weak; current flow is across the bars at a relatively small angle to orientation of the bar axis.

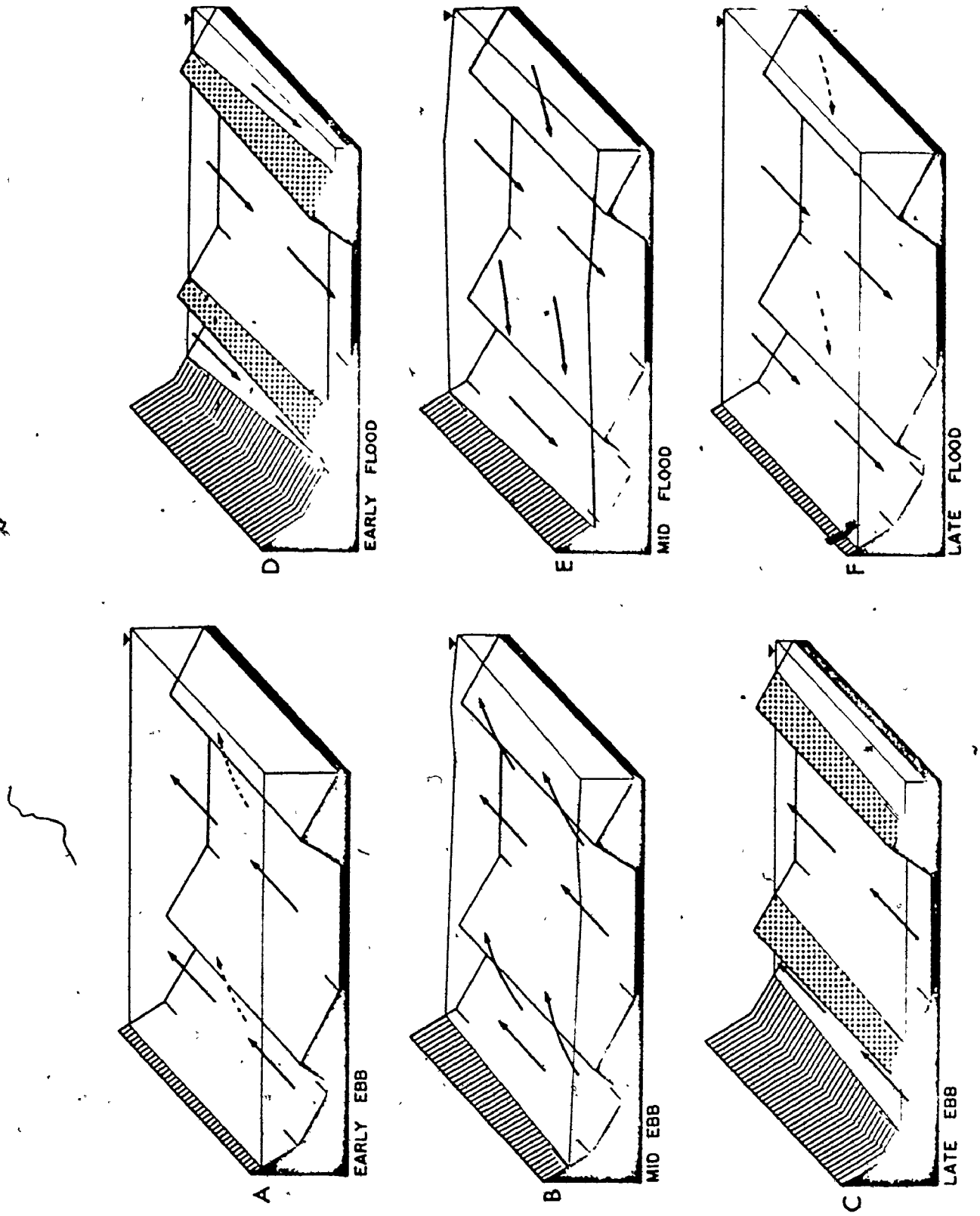
A
EARLY EBB
B
MID EBB
C
LATE EBB
D
EARLY FLOOD
E
MID FLOOD
F
LATE FLOOD

Current speeds over the sand bars continue to increase during the high-water, ebb 'sheet' flow phase until mid to late ebb when the lower water levels and increased bottom friction (i.e., reduced cross-sectional area of the flow and increased relative roughness) causes a steepening of the slope of the water surface slope between the bars and the channels, and increased deflection of the tidal currents across the crestline of the bars.

The development and pattern of the cross-bar flow during the high-water ebb 'sheet' flow phase is the result of several dynamic factors. Because the sand bars are elongate in outline and oriented at a small oblique angle to the flow, the cross-sectional flow over experimental slender bodies inclined at a small angle to the flow. During the ebb, the currents accelerate obliquely up the steep side and across the crestline of the bars, then decelerate down the gentle side because of the pressure differential and frictional drag across the bar (i.e., Bernoulli's principle). Maximum current speeds occur over the bar before the relative roughness of the boundary becomes too large (i.e., increased bottom friction from shallow flow depths).

The deflection of the currents across the bars results from the increased frictional drag over the bars, and a difference in water levels on either side of the bars. The difference of water levels on either side of the bar occurs because either: (i) there is less area to be drained from one side of the bar compared to the other side (e.g., on Selma Bar, the water levels on the south side of the bar would become lower faster because there is less area to be drained; so, flow on the north side of the bar would be deflected to the south); or (ii) the cross-sectional area of the channel flow is greater on one side of the bar than the other side (e.g., on Noel Bay Bar, the channel to the south of the bar has a relatively small cross-sectional area of flow compared with the channel to the north of the bar, thus water levels would be lower in the northerly channel and flow on the south side of the bar would be deflected across the bar to the northwest). This pattern of flow is supported by the fact that flow directions are deflected away from the crestline of the bars (e.g., Figs. 4.20, 4.21, 4.22, and 4.23) during the ebb.

As the bars become emergent, current speeds drop-off rapidly over the bars and both current speeds and directions are controlled by the hydraulic geometry and drainage pattern of the interbar channels. At some locations (e.g., Noel Bay Bar), current speeds do not decrease abruptly after the occurrence of maximum speeds during the ebb because additional water is released from late-stage ebb runoff from topographically higher positions on the same bar (e.g., via bedform troughs and swatchways across the bar) and from the delayed draining of intertidal areas located further towards the head of the bay. By comparison, current speeds drop off more rapidly during the late ebb on Selma Bar because: (i) the emergence of the bar's crestline cuts off current flow to the south side of the bar; and (ii) the area of the intertidal zone to the east of Selma (towards the head of the bay) is smaller (compared with that to the east of Noel Bay Bar), thus the amount of additional late-stage ebb runoff released by these areas is considerably less.

Maximum water surface slopes and current speeds occur later in the interbar channels relative to flow over the bars because: (i) the current flow is more effectively confined in the channels by the proximity of bounding intertidal zones (e.g., the crestline of bars and/or the foreshore); (ii) depths of flow in the channels are relatively deeper compared with bar locations, thus the relative increase of boundary friction with decreasing water levels is less; and (iii) the more effective confinement of the flow and concentration of the flow in channels results in a greater time lag between the progressive decrease of water depths and the cross-sectional discharge per unit time (i.e., the cross-sectional area of the channels is substantially smaller than the 'sheet' flow cross-section over the bars when maximum speeds occur).

During the 'channel' flow phase, secondary currents develop as they would in a fluvial open channel (e.g., the helicoidal flow pattern in the curved reach of a river -- see discussion in Graf, 1971, p. 260-269).

After peak current speeds and slopes are attained in the channels during the ebb, the flow gradually slows and the water surface gradually flattens because the amount of water entering the upflow end of the channels is reduced to just river and stream input, once the intertidal zone is completely emergent; and thus, the height of the hydraulic head is reduced.

The flow of the ebb from Cobequid Bay is basically a gravitational draining of the sand-body complex. It results from the time lag that develops between the drop of water levels and the volume of water that is able to leave the bay per unit time (which is controlled by the changing hydraulic geometry of the flow and the tidal range).

Confined to the interbar channels, the ebb currents continue to flow seaward out of the sand-body complex. Current speeds decrease slightly towards the west because the cross-sectional area of the channels increases in that direction and the flow becomes more dispersed. Speeds are less towards the shore because of rapid shoaling, thus increased boundary friction. At the western edge of the sand bar complex, the confined ebb currents are discharged into the relatively deep and wide entrance to Cobequid Bay as an 'expanding jet'. The abrupt increase in the cross-sectional area of the flow causes a rapid reduction in the speed of the currents.

When the flood tide begins to move up the bay, it has a relatively large cross-sectional area compared with the late stage ebb currents. The flood enters the sand-body complex along the paths of least resistance (i.e., where the speed of the ebb currents is relatively low or negligible -- see discussion in Chapter 6) e.g., along the northern and southern margins of the sand-body complex because the ebb currents are generally concentrated in the channels along the centre of the bay. Because there is less resistance to the flooding tide in the marginal channels (due to weaker ebb outflow and relatively larger cross-sectional areas), water depths increase more rapidly in these channels. The flood moves rapidly over the gentle side of the bars up bedform troughs and swatchways. Because water levels are again higher on one side of the bar compared with the other side (but in the opposite sense relative to the ebb situation), current flow takes place across the crestline of the bars once they are submerged. The angle between the direction of current flow and the orientation of the crestline of the bars decreases as water depths increase and boundary friction is reduced (i.e., relative roughness becomes less).

During the flood, the opposite conditions to the ebb generally prevail. Maximum current speeds and water surface slopes in the channels

occur during the early flood when the flow is still confined by the marginal intertidal zones (i.e., during the flood 'channel' phase of flow). Maximum speeds and slopes over the bars cannot occur until the crestlines are sufficiently submerged to overcome boundary resistance; hence maximum speeds occur later over the bars than in the channels during the flood tide. As water levels slowly rise during the flood, the cross-sectional area of the flow becomes larger and current speeds become less.

The difference between the flow duration of the ebb and flood reflects the time required for the flood tide to overcome the ebb currents. This difference becomes greater towards the head of the bay because the flood tide not only must overpower the momentum of the ebb outflow, but also the energy slopes of the intertidal foreshores and bars, and the channels. The rates of water level change during the ebb are less than during the flood because: (i) the length and tidal range of the semidiurnal tidal cycle is controlled primarily by the lunar cycle and the relative distance between the earth and moon; (ii) the tidal range for the ebb and flood are approximately the same; and (iii) the duration of the ebb is longer than the flood (controlled by the hydraulic regime in the bay).

The magnitude of current speeds during a tidal cycle (excluding the effect of variations in tidal range during the lunar month -- this is discussed in the next section) depends on: (i) the occurrence of ebb and flood shields (Fig. 4.25); and (ii) differences in topographic elevation in the intertidal zone.

The occurrence of ebb and flood shields control the exposure of different parts of the intertidal and subtidal system to the ebb and flood currents. An ebb (flood) shield (Coastal Research Group, 1969, p. 456) is a topographic high that protects parts of the intertidal-subtidal complex from modification by ebb (flood) currents. The west ends of Noel Bay Bar, Noel Shore Bar and Selma Bar are well-exposed to strong flood currents, but the topographically higher parts of the bars towards the east shield the western ends of the bars from strong ebb currents. The reverse is basically true for the opposite ends of the bars. The longitudinal topographic variations not only produce east-

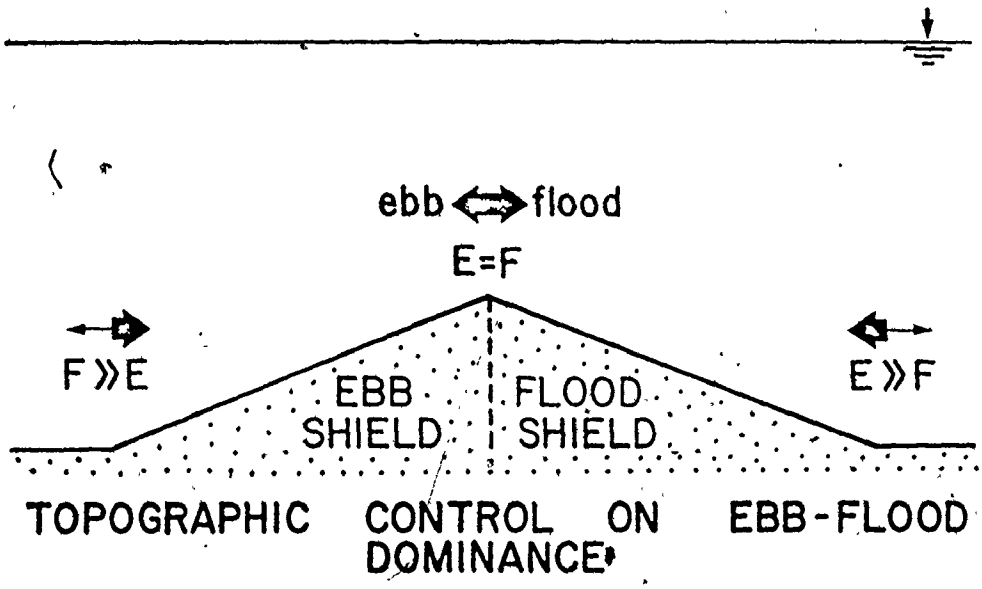

FIGURE 4.25: Diagram showing effects of bottom topograph in ebb and flood dominance (E = ebb; F = flood).

west shielding effects, but also north-south shielding from strong current flows across the bars. The south side of Selma Bar, for example, is protected from strong ebb currents because it is sheltered by Salter Head and the topographic crestline of the bar, but the south and west end of the bar are well-exposed to flood currents (and the north and eastern sides of the bar are flood shielded). This shielding results in flood-dominated time-velocity asymmetries along the south side and western end of the bar, and ebb dominated time-velocity asymmetries along the north-east side of the bar crestline. Thus, topographic shielding is an important factor controlling the areal distribution current strengths and the areas of ebb and flood dominance.

The topographic elevation of a location within the intertidal zone is also a significant factor controlling flow strengths and the degree of ebb or flood dominance. Current speeds are generally less and flow durations shorter along the crestline of the bars than for positions located in topographically lower areas to either side of the crestline. The lateral extent, relative height and orientation of a topographic shield affect the degree of ebb or flood dominance of an area (e.g., the larger and more extensive a shield, the greater the difference of current strengths on either side of the shield, hence the degree of ebb or flood dominance of an area).

Lunar Month Variation of the Tidal Currents

The variation of current strengths during the lunar-month (approximately 28 days) in response to variations of tidal range from neap and spring tides is an important aspect of tidal current analysis.

The time-velocity relationships of Figures 4.9 and 4.15, recorded with the automatic recording current meters, shows that there is some variation in the magnitude of the maximum current speeds during relatively long periods of measurement. The maximum near bottom current speeds for each ebb and flood phase monitored in these figures were converted to mean flow velocities (by determining the relation between the near bottom current speed and the mean flow speed from the measured vertical velocity profiles at NBB-1, NBB-6, NBB-8, SB-1 and SB-3) and plotted as a function of tidal range (determined from the Canadian Tide and Current Tables, C.H.S., 1971-73) at Burntcoat Head. Use of the predicted tidal

ranges at Burntcoat Head assumes that the level of the tide is same everywhere in the bay which should be good enough as an approximation (see discussion in Chapter 2.4).

Figures 4.26 and 4.27 show the relationship between the maximum mean velocities and tidal range for several locations on Noel Bay Bar and Selma Bar. These diagrams indicate that the relationship is not simple, and depends largely on the hydraulic characteristics of the particular location. Correlation coefficients of the plotted results decrease towards the head of the bay (ebb and flood).

Comparable results were found by plotting the average of the three maximum mean velocities (unstandardized) per ebb and flood (from the measured vertical velocity profiles) as a function of tidal range. The graphs, however, showed a large amount of scatter because the profile data used were from all of the measurement stations on each bar (Fig.4.28). Reasonable correlations were found for individual locations at which more than one tidal cycle was monitored (e.g., Appendix III, Table III-1). At several locations, the degree of ebb or flood dominance appeared to be dependent on the tidal range (e.g., SB-5 and SB-6 -- compare Table 4-11 and III-1).

The flow duration of the ebb and flood (Tables 4-6, 4-8 and 4-10) as a function of tidal range for individual locations were negatively correlated (i.e., flow durations were longer for neap tides and shorter for spring tides; conversely, the period of low tide emergence was longer during springs and shorter during neaps). Ebb and flood rates of depth change were positively correlated to tidal range (compare results of Table 4-12 with Table III-1). There were no apparent changes of ebb and flood current directions during the lunar tidal cycle (e.g., Fig. 4.15).

The lunar tidal variation of current speeds, durations of flow and rates of water depth change occur because: (i) the duration of the semidiurnal cycle (i.e., 12 h 25 min 14 s = ½ lunar day) is controlled primarily by the lunar cycle; and (ii) the tidal range is primarily a function of the distance between the earth and moon and this distance varies during the lunar month (i.e., the force of the moon's attraction increases during perigee and decreases by an equal proportion during

FIGURE 4.26: Maximum mean velocity as a function of tidal range (Burntcoat Head) at three locations on Noel Bay Bar. See Figure 4.1 for locations.

A

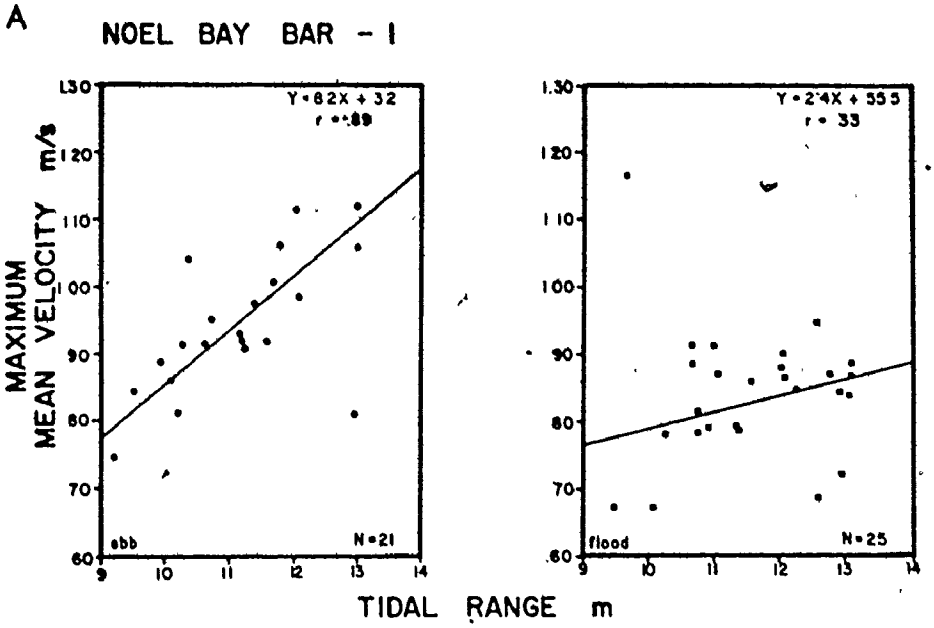
NOEL BAY BAR - 1
Y = 6.2X + 3.2
r = .89
ebb
N = 21
Y = 2.4X + 55.5
r = .33
flood
N = 25
MAXIMUM MEAN VELOCITY m/s
TIDAL RANGE m

B

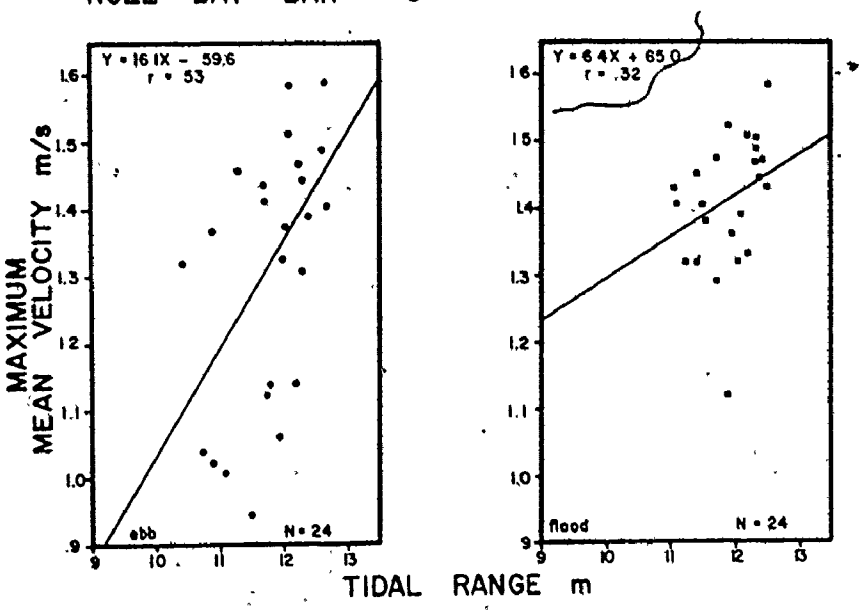
NOEL BAY BAR - 6
Y = 16.1X - 59.6
r = .53
ebb
N = 24
Y = 6.4X + 65.0
r = .32
flood
N = 24
MAXIMUM MEAN VELOCITY m/s
TIDAL RANGE m

C

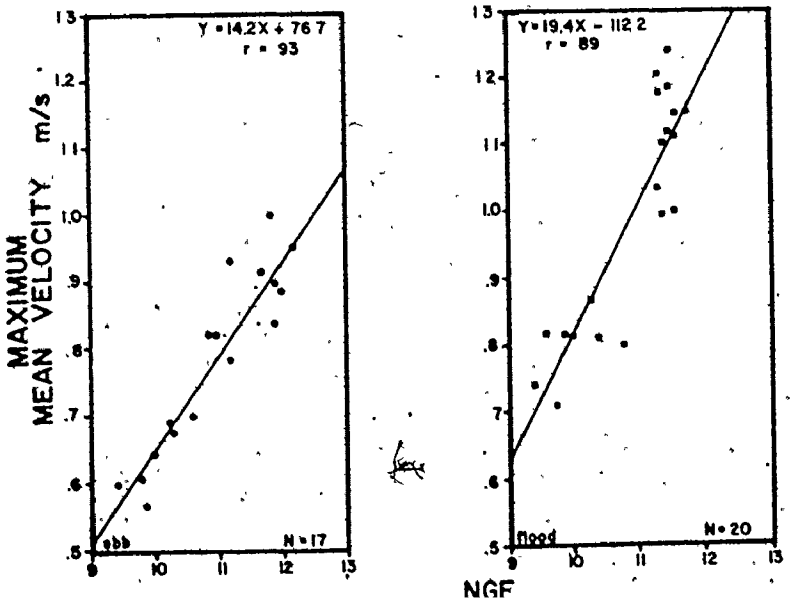
NOEL BAY BAR - 8
Y = 14.2X + 76.7
r = .93
ebb
N = 17
Y = 19.4X - 112.2
r = .89
flood
N = 20
MAXIMUM MEAN VELOCITY m/s
NGF

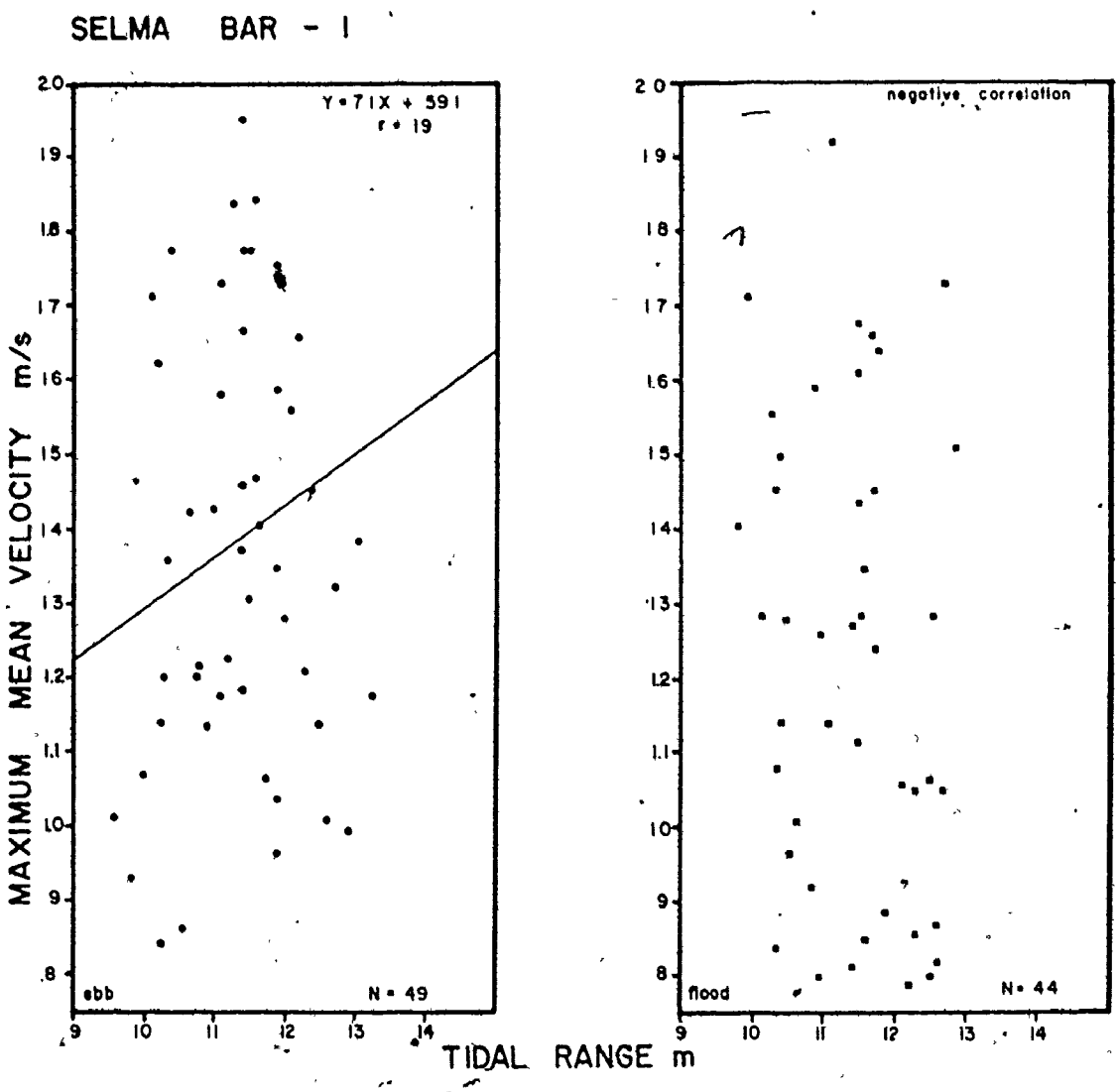

FIGURE 4.27: Maximum mean velocity as a function of tidal range (Burntcoat Head) at SB-1 and SB-3 See Figure 4.1 for locations.

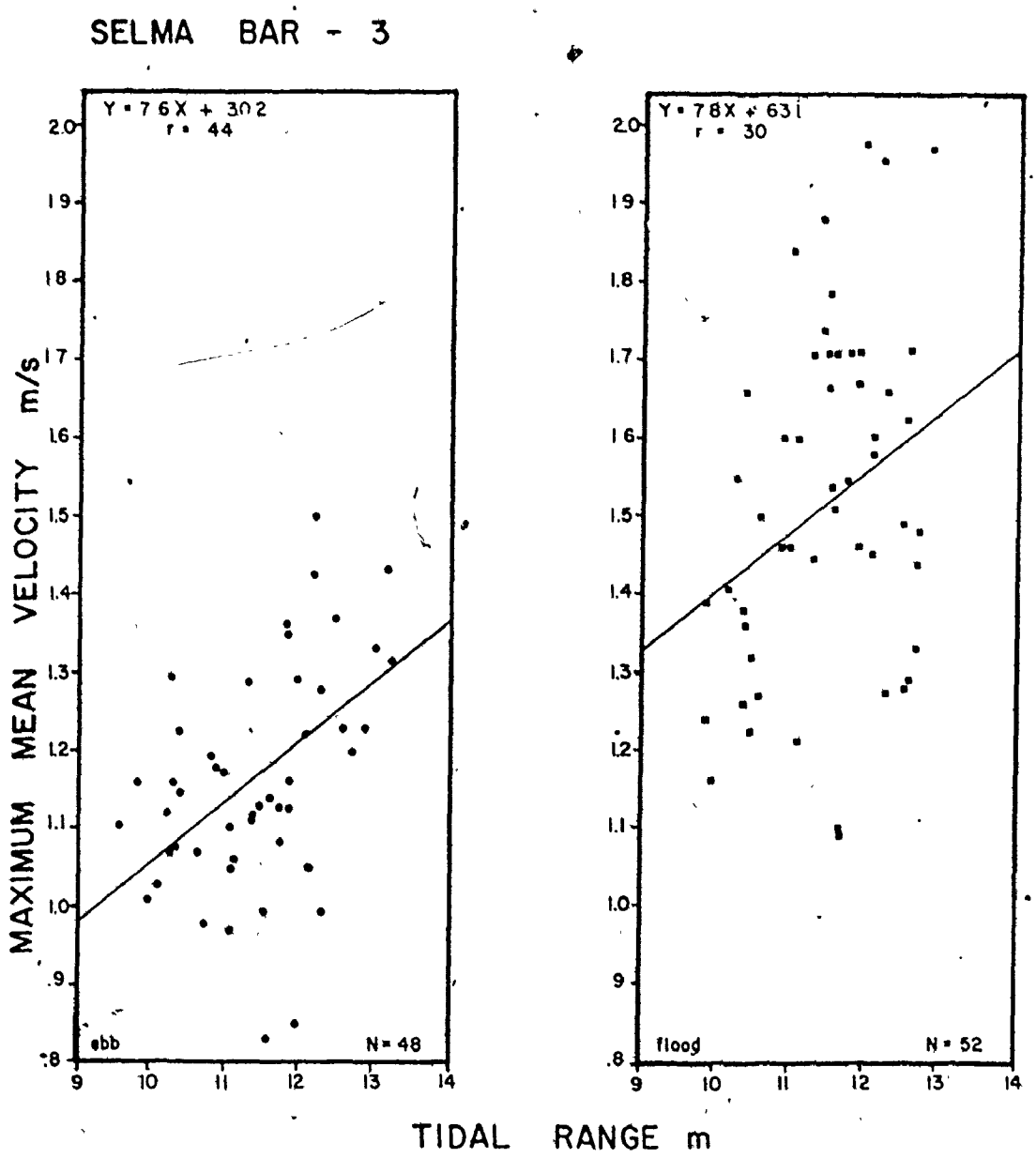

FIGURE 4.27: cont'd.

FIGURE 4.28: Average of three maximum mean velocities per tidal cycle as a function tidal range (Burntcoat Head). Current data from the measured vertical velocity profiles.

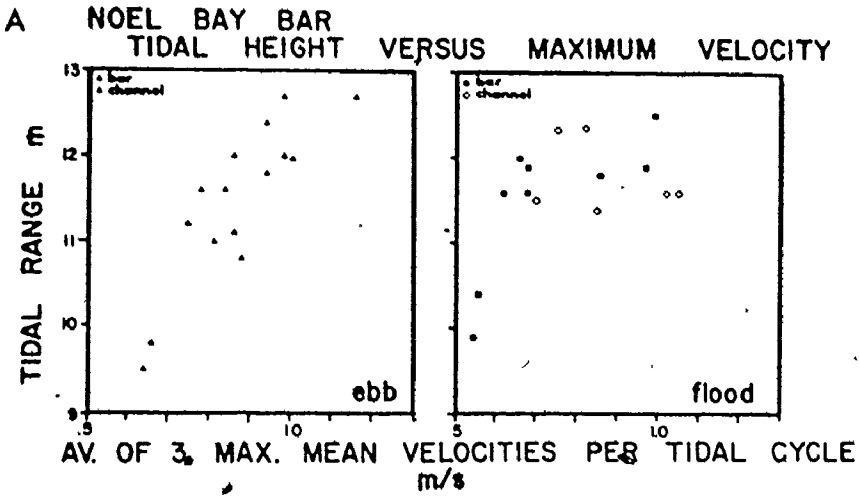
A NOEL BAY BAR
TIDAL HEIGHT VERSUS MAXIMUM VELOCITY
TIDAL RANGE m
ebb
flood
AV. OF 3 MAX. MEAN VELOCITIES PER TIDAL CYCLE
m/s

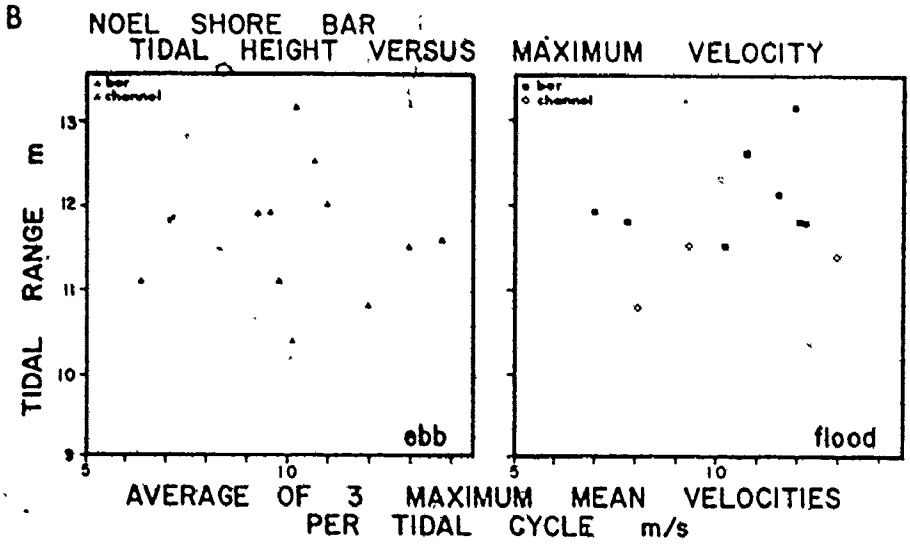
B NOEL SHORE BAR
TIDAL HEIGHT VERSUS MAXIMUM VELOCITY
TIDAL RANGE m
ebb
flood
AVERAGE OF 3 MAXIMUM MEAN VELOCITIES
PER TIDAL CYCLE m/s

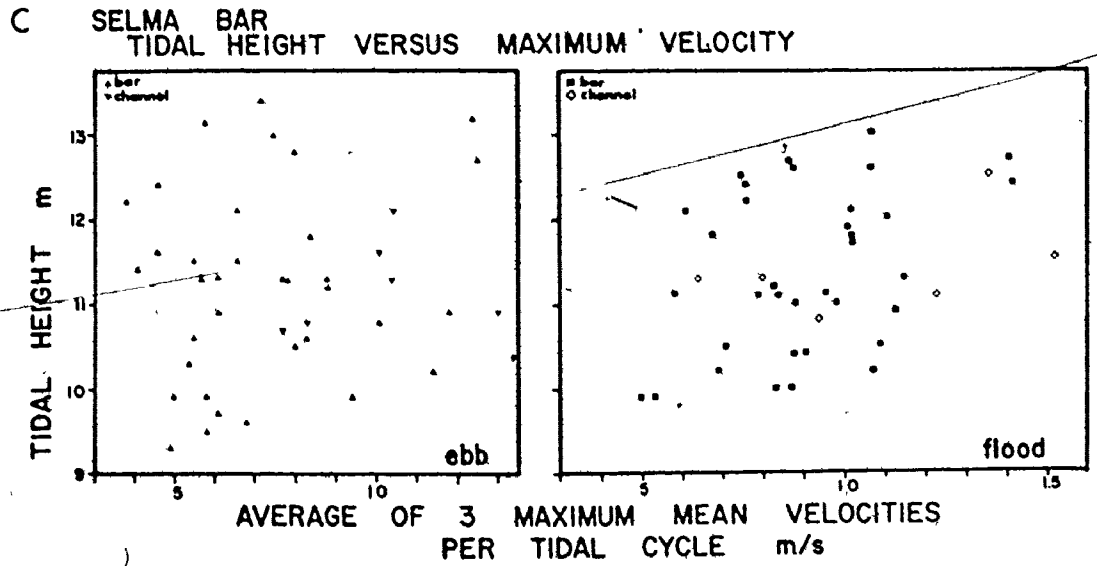
C SELMA BAR
TIDAL HEIGHT VERSUS MAXIMUM VELOCITY
TIDAL HEIGHT m
ebb
flood
AVERAGE OF 3 MAXIMUM MEAN VELOCITIES
PER TIDAL CYCLE m/s

apogee). During lunar perigee, larger tidal ranges occur which are reflected by: lower low water levels and higher high water levels; and thus, longer periods of intertidal emergence on the sand bars, greater current speeds and rates of water depth change, and generally shorter periods of flow duration during the ebb and flood. The converse occurs during lunar apogee (i.e., low water levels are relatively higher and high water levels relatively lower, thus, periods of emergence on the intertidal bars is shorter, current speeds and rates of water depth change are relatively lower, and the flow duration of the ebb and flood are relatively longer). It is, however, not possible to predict the strength of a current given only the tidal range (although tidal range is the primary control).

The difference in the correlation coefficients for current speed as a function of tidal range between Noel Bay Bar and Selma Bar (Figs. 4.26 and 4.27) may be a question of where the water is coming from and going to; near the head of the bay, sources and destinations are diverse (thus, the hypsometries of the flow are diverse), but near the mouth of the bay, sources and destinations are more uniform (i.e., all the water is going to or coming from some 'averaged' up-bay location).

The variation in the degree of ebb or flood dominance at a particular location may be a function of the bay s tidal balance (i.e., the net storage and loss of water) during a lunar month. As the moon approaches perigee, tidal ranges increase (springs) and there is a net loss of water from the bay. Conversely, as the moon approaches apogee, successive tidal ranges are smaller (neaps) and there is a net storage of water in the bay. This cyclic variation of the tidal water balance in the bay causes: (i) water temperatures to be warmer during lunar apogee (less cold water enters the bay during neap tides) and cooler during lunar perigee (more cold water enters the bay from the main Bay of Fundy during spring tides); and (ii) a flood dominated area will be slightly less flood dominant and an ebb dominated area will be slightly more ebb dominant during lunar perigee (spring tides) -- the converse occurs during lunar apogee (neap tides).

4.5 SUMMARY

Current measurements were made at more than 40 locations (Fig. 4.1) over a variety of bed configurations and in different parts of the sand-body complex in Cobequid Bay. The reported results are based on the measurement of more than 1200 vertical velocity profiles (representing over 11,000 individual readings of current speed and direction) and on more than 150 days of point velocity measurements made 0.5 m from the bottom with automatic recording current meters (see summaries in Appendix III.4).

The tidal currents in Cobequid Bay are semi-diurnal in period and reversing (Fig. 4.20 and 4.21) in character (i.e., the currents reverse their direction about 180 degrees every 6.3 h) as opposed to the rotary tidal currents of the open ocean.

The current measurements from Cobequid Bay show that the vertical distribution of velocity over relatively large-scale bedforms (i.e., megaripples and sand waves) and for relatively large depths of flow (compared to the height of the bedforms) could be estimated by a first-order linear regression model (i.e., the velocity measured is proportional to the logarithm of the depth). Of 1110 vertical profiles regressed by the linear model, almost 81% were statistically significant at the 95% level of confidence (Table 4-2). An attempt to use a second-order linear regression model to analyze the measured velocity profiles did improve some correlation coefficients, but did not produce a statistically significant improvement of fit compared with the results of the first-order linear model (Table 4-2). The improvement of fit with the second-order regression model was significant in only 44% of the profiles at the 95% confidence level. In fact, use of the second-order model reduced the number of vertical profiles that could be analyzed because a minimum of 5 measurement points per profile was required compared to only 3 (per profile) for the first-order model. The first-order linear model was subsequently used to analyze and summarize the vertical distribution of velocity from the measured profiles, and these results were used in all subsequent derivations of various hydraulic parameters (see Appendix IV).

Because the exact location of the measured vertical velocity profiles with respect to the bedforms on the boundary was unknown, analytic techniques involving the adjustment of the profile datums to compensate for bedform roughness (e.g., iteration of the linear regression model) were of little use (Table 4-1).

Although the vertical distribution of velocity in the measured profiles was statistically linear, comparison of the shape of the measured profiles with the fitted linear regression revealed that the data points of the measured profiles generally deviated to either side of the regression line in a regular manner. Three types of profiles were defined (Fig. 4.3): (i) Type 1 profiles were convex in shape relative to the regression line (i.e., measured velocities were larger near the bottom and surface, but smaller near mid-depths relative to the regression line); (ii) Type 2 profiles were concave in shape relative to the linear regression line (i.e., opposite trend of deviations compared to Type 1 profiles); and (iii) Type 3 profiles were essentially distributed in a random manner to either side of the regression line or linear. Almost 44% of the profiles were classified as Type 1, with about 20% as Type 2 and about 36% as Type 3 (from 1132 profiles; Table 4-3). Type 1 profiles were most common because most profiles were probably measured over the stoss-side of the bedforms in the region of accelerating flow. Similar results were found for flows over bedforms in experimental flumes (e.g., Fig. 4.7).

Profile shapes changed during the tidal cycle. Type 1 profiles were generally more common during the early ebb (Table 4-4) due to a drawdown of the water surface caused by the seaward retreat of the ebb tidal wave from the bay (i.e., the withdrawal of the ebb tidal wave generates a negative surface wave which causes velocities to be higher than expected in the near surface region of the flow; see Fig. 4.8). Such conditions did not develop during the early flood because the flood erters the bay as a positive wave.

The standard deviations of the observed profile velocity departures from the fitted regressions give an estimate of the magnitude of the horizontal turbulent velocity fluctuations of the flow. These values were in the order of 0.02 to 0.05 m/s, or about 60% of the derived values of shear velocity (typical mid-ebb and mid-flood shear velocities

ranged from about 0.02 to 0.09 m/s).

The semidiurnal, reversing currents in Cobequid Bay were time-velocity asymmetrical with respect both to the ebb and flood individually and also taken together to form a complete tidal cycle (Figs. 4.10, 4.12 and 4.14). Maximum mean profile speeds occurred during the middle to late part of the ebb and during the early to middle part of the flood. Near the western end of the sand-body complex (e.g., Noel Bay Bar and west end of Noel Shore Bar) maximum current speeds generally tend to occur near mid-ebb and during the early flood, while maximum current speeds tend to occur during the late ebb and near mid-flood towards the head of the bay (e.g., Selma Bar). Maximum mean velocities of the flood were about 10 to 20% larger than those of the ebb (Figs. 4.11, 4.13 and 4.16), for both flow over the intertidal sand bars and in the interbar channels. Maximum mean velocities for the ebb and flood averaged about 0.9 and 1.1 m/s respectively for Noel Bay Bar, and about 0.8 and 1.0 m/s respectively for Selma Bar. In the interbar channels, maximum mean speeds reached 2.0 m/s at some locations (and were always larger than current speeds over the sand bars). Current speeds generally decreased towards the crest of the bars, the shoreline and the head of the bay (compare Figs. 4.11, 4.13 and 4.16). During the lunar tidal month, maximum mean velocities varied about 0.1 to 0.2 m/s per metre of change in the tidal range (Figs. 4.26, 4.27 and 4.28).

The duration of flow was generally about 20 to 30% longer during the ebb than during the flood (Tables 4-6, 4-8 and 4-10), and shorter by about 10 to 15% during the ebb and 15 to 20% during the flood towards the head of the bay. The duration of the ebb and flood were averaged 4.5 hours and 3.5 hours respectively over the bars, and about 7.0 and 5.5 hours in the channels.

As a result of the variations in the flow duration of the ebb and flood, the rates of water level change were more rapid and current speeds faster during the flood than during the ebb (Fig. 4.18 and Table 4-12). Rates of depth change varied throughout the bay depending on the hydraulic geometry and hypsometry of the channels and the tidal range. During the ebb, water levels decreased at rates of about 2.25 m/h and during the flood, water levels rose at rates of about 295 m/h

The time-velocity asymmetry (i.e., the temporal variation of current strength, flow duration and rates of depth change) of the tidal currents measured both in the channels and over the sand bars was related to topographic shielding on and by the sand bars, the hydraulic geometry and hypsometry of the interbar channels, and the lunar month variation of the tidal range (hence, the current strength). The gently sloping side of the bars was generally dominated by flood currents and the steeply sloping side by the ebb currents. The degree of ebb or flood dominance on individual bars was determined to a large extent by the intertidal relief and topographic complexity of the intertidal bar surface (i.e., a larger difference between the ebb and flood resulted on bars with greater intertidal relief and topographic complexity than those that had relatively simple surface topographies. For example, on Noel Bay Bar (topographically simple, Fig. 3.18), (the maximum mean current velocity of the flood was generally about 0.1 m/s greater than the ebb while on Selma Bar (topographically complex, Fig. 3.35), the flood was generally about 0.25 m/s).

The pattern of ebb and flood dominance over the sand bars and in the interbar channels showed that the major ebb channels were located along the centre of the bay, and that two major flood channels were located along the north and south margins of the sand-body complex. The general circulation pattern in Cobequid Bay resembled that of a large ebb-tidal delta (see discussion in Chapter 6) following the model proposed by Hayes (1975) for the relatively smaller, mesotidal ebb deltas of tidal inlets through barrier bars along the east coast of the United States. There is no evidence to support the existence of a Coriolis force circulation pattern within the bay.

The flow regimes of the ebb and flood were divided into a high-water sheet-phase and a low-water channel-phase (Fig. 4.24). During the high-water sheet flow phase of both the ebb and flood, a component of flow developed across the sand bars (respectively in opposite directions) because the bars were aligned at a small angle of attack to the mean flow directions (Figs. 4.20 and 4.21) and because different interbar channels were characterized by different rates of drainage and flooding (Table 4-12)

due to their different hydraulic geometries and hypsometries, producing a difference in water levels on the two sides of the bars. Combined with the opposing ebb and flood current residuals on the two sides of the bars, the cross-bar component of flow produced a net flow circulation around the bars or parts of the bars (Figs. 4.11, 4.13, 4.16 and 4.24).

CHAPTER 5

BEDFORMS

5.1 INTRODUCTION

Geologists and engineers have been intrigued with flow-produced bedforms, particularly with those that develop transverse to the flow, for over a century. Some of the early workers on bedforms included Darwin (1892, cited in Raudkivi, 1967 a, p. 175-176); Deacon (1892, cited in Raudkivi, 1967 a, p. 176; Graf, 1971, p. 274; and Costello, 1974, p. 2); De la Beche (1834, cited in Harms, 1969), Dubuat (1786, cited in Graf, 1971, p. 14 and p. 274); Playfair (1802, cited in Harms, 1969) and Sainjon (1871, cited in Graf, 1971, p.274). Amongst these pioneer geologists and hydraulicians, Sorby (1853, 1859, 1908, cited in Potter and Pettijohn, 1963) was the first to interpret the sedimentary structures of sands and sandstones as the result of ripple migration, and to see the usefulness of the information for paleogeographic synthesis of sedimentary rocks.

The study of bedforms continued into the twentieth century with individuals such as Blasius (1910, in Graf 1971, p. 274); Bucher (1919); Cornish (1901 a, 1901 b, 1914), Gilbert (1914), Kindle (1917) and others. From this group of twentieth century investigations, the contributions of Blasius (1910, cited in Graf, 1971, p. 274) and Gilbert (1914) deserve particular note. Blasius recognized the importance of the relationship between the flow Froude number and the occurrence of different types of bedforms. Gilbert's early experiments made detailed descriptions of different bed configurations, the stages of bedform development and the different modes of sediment transport. The results from both of these studies were important to the recognition of a sequence of bedform development by Simons and Richardson (1962 b, 1963; Raudkivi, 1967 a, p. 195-197; Graf, 1971, p. 276-281; and others).

Interest in bedforms has intensified within the last few decades as the importance of bedforms, their sedimentary structures and mech-

anics, was realized with respect to the meaningful interpretation of 'modern' and ancient sediments and sedimentary sequences, and to engineering applications (e.g., sediment transport, erosion and flood control, channel and harbour maintenance, pollution control). Several text-books that summarize the important developments about bedforms include: Allen (1968 b), Graf (1971), Harms et al. (1975), Middleton (1965), Potter and Pettijohn (1963), Raudkivi (1967 a), and Yalin (1972).

There is a large literature on asymmetrical, current-produced bedforms and their cross-stratification covering several disciplines, and including descriptive, empirical and theoretical approaches. Much of the literature on alluvial bedforms (produced by unidirectional flow) can be readily extended to bedforms produced by bidirectional tidal currents because the latter bedforms are generally similar in appearance and behaviour to alluvial bedforms.

There is an almost equally large literature on tidal current-produced bedforms from estuaries (e.g., Boothroyd and Hubbard, 1975; Daboll, 1969; Green, 1975; Hartwell, 1970; Haynes & Dobson, 1969; McMullen, 1964; Robinson, 1960), from tidal channels and bars (e.g., Cornish, 1901 b; Kindle, 1917; Klein, 1970 a; Klein and Whaley, 1972; Ludwick, 1972; Swift and McMullen, 1968; Walton and Goodell, 1972) and from continental shelves (e.g., Belderson and Kenyon, 1969; Caston, 1972; Dyer, 1970; Houbolt, 1968; Jordan, 1962; Kenyon and Stride, 1970; McCave, 1971; Newton and Werner, 1970; Off, 1963; Smith, J. D., 1969; Stride, 1963; Swift, 1975; Swift et al., 1972; Werner and Newton, 1970. The bedforms, however, could only be observed directly at a few of these study locations. Most studies report results obtained indirectly by echo-sounder, side-scan sonar and shallow seismic systems. The large tides in Cobequid Bay and the emergence of most of the intertidal sand bars permitted direct observation of tide-produced bedforms during low tide periods. Subtidal bedforms were studied with an echo-sounder because water conditions were too turbid for SCUBA.

The purpose of this chapter is (i) to describe the geometrical and geomorphological characteristics of the different types of bedforms present in the areas studied and to map their occurrences; (ii) to relate the external morphological and dimensional properties of the bed-

forms to their internal cross-stratification; and (iii) to discuss the relationships between the bedforms and the sediment properties (scale, types, structures, grain size and sorting), the character of the flow (depth, flow strength and resistance), and the sediment transport mechanics. Field techniques and data are presented in Appendix V.

5.2 TERMINOLOGY

A bedform is "any bed feature whose elevation from the mean level of the bed exceeds one mean diameter of the grains on the bed" (Jackson, 1975, Appendix I). This, and other definitions of what is, or what is not, a bedform, and nomenclature to describe various bed geometries (e.g., Allen, 1963; 1968 b, p. 29-57; ASCE Task Force, 1966; Costello, 1974, p. 47; Raudkivi, 1967 a; Southard, p. 5-43, in Harms et al., 1975) were proposed to standardize terminology and to provide an unambiguous definition of terms used by various workers. However, a variety of terminologies are still used by different workers because each has a slightly different approach to the study of bedforms (e.g., geologists versus engineers), and there are differences of opinion on the meaning or interpretation of the various terms. The lack of uniformity of bedform nomenclature in the literature (e.g., Jackson, 1975, Table 2); Middleton, 1965, p. 2-3) makes it difficult to compare results from different studies unless the terms and the bedforms are themselves adequately and clearly defined.

Jackson (1975) pointed out that most bedform nomenclatures (e.g., ASCE Task Force, 1966,; Allen, 1963, 1968 a and b; Southard, p. 5-43 in Harms et al., 1975) proposed are based on "purely descriptive attributes" (e.g., size, superposition, etc.). The nomenclature used in this study (Fig. 5.1) is no different. Allen's (1963; 1968 b, p. 29-54 and p. 58-95) terminology for the external anatomy of bedforms, and Southard's (p. 19-23, in Harms et al., 1975) qualitative descriptions and nomenclature of bedforms are used throughout this study (Fig. 5.1).

In order of increasing size, the major bedforms found in the study area are ripples, megaripples (or dunes), sand waves and tidal bars (discussed in Chapter 3). Ripples are small-scale (with lengths less

than 0.25 m and heights less than 0.05 m; length/height ratios in the order of 10) asymmetrical (current) or symmetrical (wave) bedforms transversely oriented to the direction of the generating flow. In plan view, ripple crestlines vary from straight to linguoid.

Megaripples (or dunes) are transverse, asymmetrical bed features that are similar in appearance to ripples. The primary distinction is size. Lengths and heights of megaripples range from 1 to 12 m and from 0.1 to 0.7 m (length/height ratios in the order of 10 to 20). Crestline patterns are typically straight to slightly sinuous. Tidal megaripples are more nearly two-dimensional than alluvial dunes. Small ripples commonly occur on the stoss and lee-side slopes of the megaripples. Three main morphological types of megaripple are distinguished: "unmodified"(or linear), "scoured", and "planed-off". "Unmodified" megaripples are bedforms little altered by late-stage ebb flow or emergence. "Scoured" megaripples occur in areas where the mean current flow is oblique to the bedform crestlines formed earlier in the tidal cycle. A series of vortices are shed at more or less regular intervals from the megaripple crest (Allen, 1968 b, "swept catenary", p. 79-80, 271-275) and these erode deep scours into the surface of the downstream trough and lower stoss-side slope of the next bedform. "planed-off" megaripples (Boothroyd, 1969, p. 427) have a prominent flat crestal platform formed by late-(early-) stage, relatively high speed, shallow ebb (flood) flows during emergence (or submergence) of the bar.

Sand waves are larger asymmetrical to symmetrical shaped, composite bed features whose scale is different from that of ripples and megaripples (or dunes). Their lengths range from 12 to more than 30 m and heights from 0.4 to 1.5 m (ripple index commonly exceeds 40). Sand waves differ from megaripples in other respects than size. They lack a long avalanche lee-side slopes and scours in troughs, and megaripples (with superposed ripples) commonly occur on their stoss-side. The origin of sand waves is not yet well understood, but is probably different from that of ripples or megaripples (e.g., Costello, 1974). Figure 5.1 shows a typical flood oriented sand wave with superposed ebb-oriented megaripples.

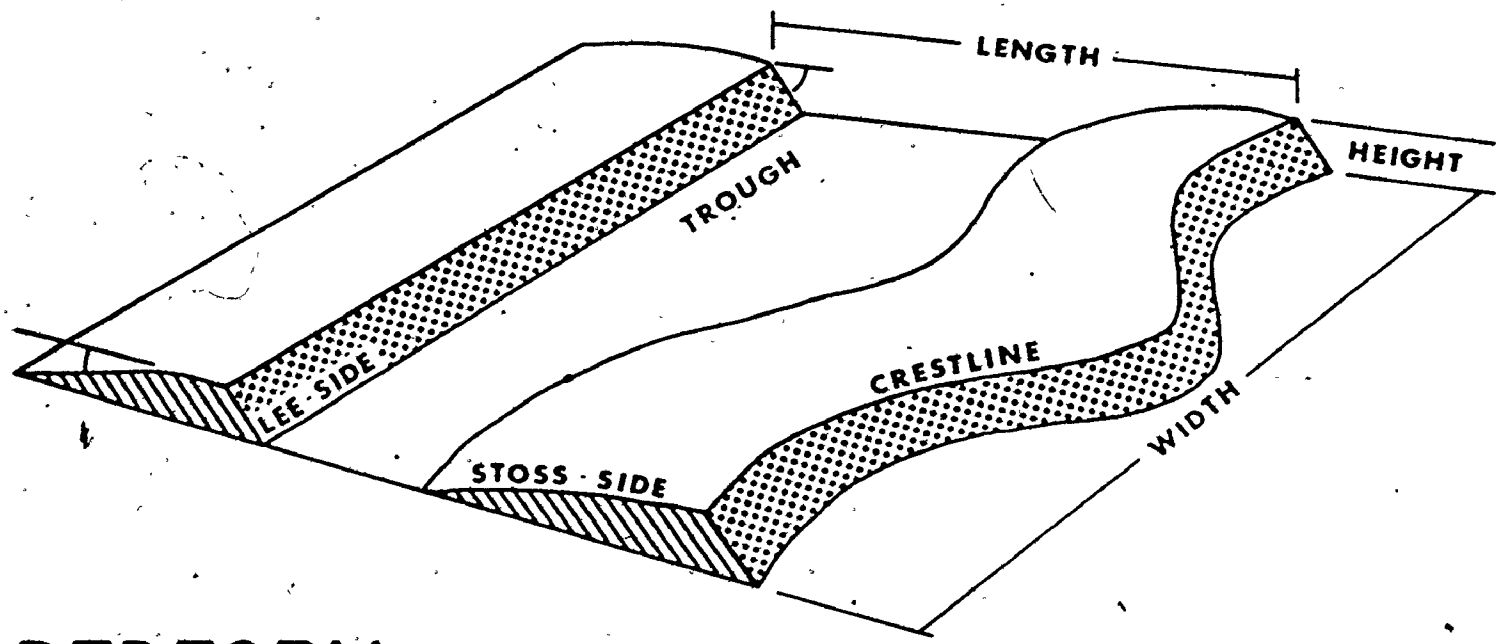

FIGURE 5.1: BEDFORM NOMENCLATURE

(See discussion in Appendix V.1)

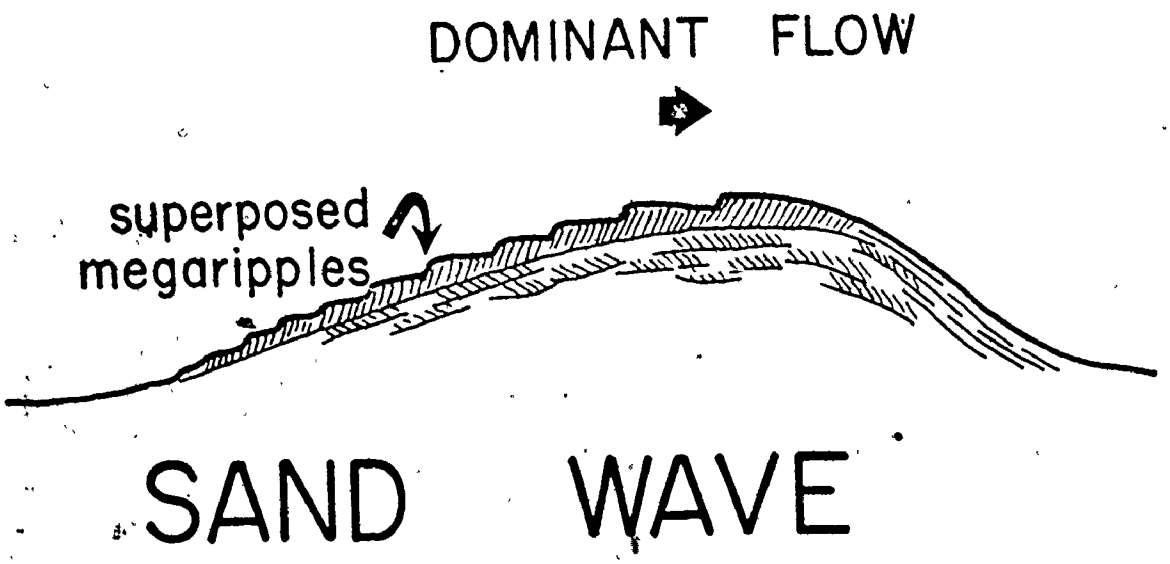

FIGURE 5.2: Ebb-oriented megaripples superposed on a flood-oriented sand wave. Note that internal structure of sand wave is composed of flood-oriented, megaripple cross-sets, and megaripple size decreases down the stoss-side of the sand wave.

5.3 EMERGENCE FEATURES

The bedforms directly observed on the intertidal bars at low tide following an ebb tide are either ebb-oriented or ebb-modified flood bedforms. These intertidal bedforms are modified during emergence and show features such as: falling water marks on bedform lee slopes (Fig. 5.21 A); small current ripples developed by shallow late stage ebb runoff across lee and lower stoss slopes of larger bedforms (Fig. 5.21 to 5.25); planed-off crestal platforms on larger bedforms (Fig. 5.22 E); flat-topped and ladder-back ripples (Fig. 5.3 D and E); liquefaction features; down slope braided and rippled channels within larger bedform troughs (Fig. 5.3 A and C); small micro-deltas built where late-stage ebb runoff has broken through a spur in a trough or through a low in a bedform crestline (Fig. 5.3 B); and rill erosion from dewatering of the bar at low tide (Fig. 3.34 G). Most of these features are destroyed by the succeeding flood tide, and thus have little potential of preservation.

Wave action is an important bedform modifying agent particularly at the west end of the bar complex (Fig. 2.26 F) and during stormy weather. During periods of strong wave activity, bedforms are completely obliterated on the exposed western ends of Noel Bay Bar and Noel Shore Bar leaving a plane, slightly undulating bed surface. Wave activity decreases eastwards where the bathymetry is shallower and more complex. On Selma Bar, for example, only the crests of larger bedforms are wave washed, (Fig. 2.16 G), obliterating superposed current ripples, and rounding brinklines even during very stormy conditions. For the most part, the tidal current-produced bedforms remains intact.

Figure 5.19 shows the difference between the relatively slow emergense of the intertidal sand bars during the late ebb, and their relatively rapid submergence during the early flood. As a result of this difference, late-stage ebb currents are only locally erosive compared with the early-stage flood currents which are erosive over the entire bed.

FIGURE 5.3: Emergence Features.

A. Late stage ebb run-off in bedform trough. Scale (centre) is 1 m long.

B. Small micro-delta built by late stage ebb run-off in a bedform trough. Scale is 1 m long. Note small current ripples that are almost buried by the delta.

C. Braided and linguoid rippled channel bottom produced by late stage ebb run-off in a bedform trough. End of scale is in decimetres and centimetres.

D. Current-wave produced ladder-back ripples near the crest of Selma Bar. Scale is 1 m long.

E. Planed-off, current-wave produced ladder-back ripples near the crest of Selma Bar. Scale is 1 m long.

F. Liquefaction of sediment on lower bedform stoss-sides in a topographically low area.

G. Sediment transport by wind on Selma Bar. Scale is 1 m long.

H. Sediment ventifacts produced by wind erosion near the crest of Selma Bar. Scale is 1 m long. Note obliteration of late stage ebb current ripples that are normally superposed on the megaripples.


A


B

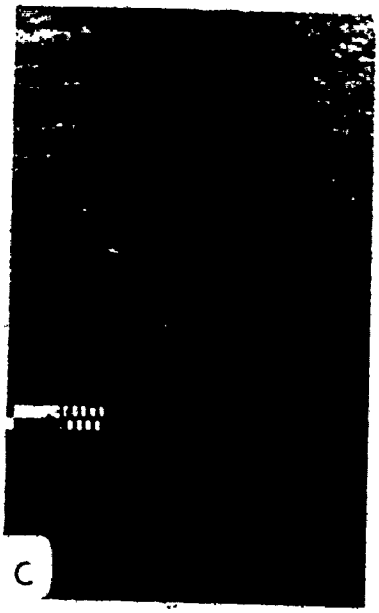
C

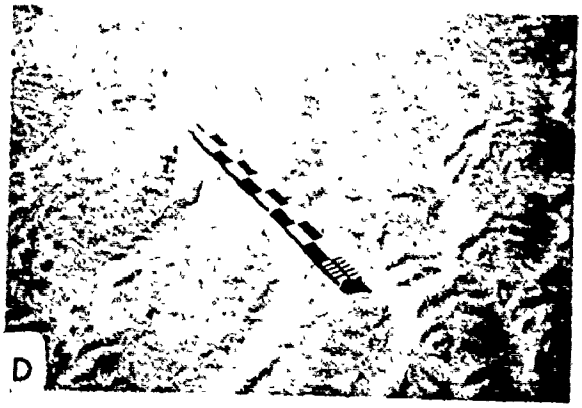
D


E


G


F


H

5.4 AREAL DISTRIBUTION

The areal variation of bedform characteristics and types on the intertidal sand bars is summarized in two ways: (i) quantitatively, i.e., the areal distribution of the measured bedform parameters such as, length, height, length/height, etc.; and (ii) qualitatively, i.e., the areal distribution of different morphological types or facies of bedforms such as ripples, 'unaltered' megaripples, 'scoured' megaripples, 'planed-off' megaripples, sand waves, etc.

The bedform data presented in the following sections were collected primarily during the 1971 and 1972 field seasons (Appendix V). The field techniques are discussed in Appendix V.1 and the field data are listed in Appendix V.2.

Lengths and Heights

Figures 5.4, 5.6, 5.8 and 5.10 show the areal variation of bedform length, height and length/height on four sand bars studied. The relation between bedform length and height, and the distribution of bedform lengths, heights and length/height ratios are summarized in Figures 5.5, 5.7, 5.9 and 5.11. These figures indicate that there is a reasonably good correlation between the length and height of bedforms, and that the contour patterns of bedform length and height generally tend to be elongate in the same direction as the axis of the bars.

On Noel Bay Bar (Fig. 5.4 and 5.5), the lengths and heights of bedforms ranged from 1 to 12 m, and from flat bed to more than 0.4 m respectively. The largest bedform lengths and heights occurred at the eastern end and along the south-central side of the bar. The shortest bedform lengths and smallest heights occurred primarily at the west end and along the northern side of the bar to about mid-bar. Figure 5.4 C shows that the areal variation of bedform length/height ratios are largest along the southwest side of the bar and generally decrease across the bar towards the northeast. The histograms of bedform length and height (Fig. 5.5 B) indicate that: (i) the heights are bimodal (dominant mode between 0.1 and 0.25 m); (ii) lengths are trimodal (dominant mode between 3 and 6 m); and (iii) length/height ratios are trimodal (dominant mode between 10 and 20 m).

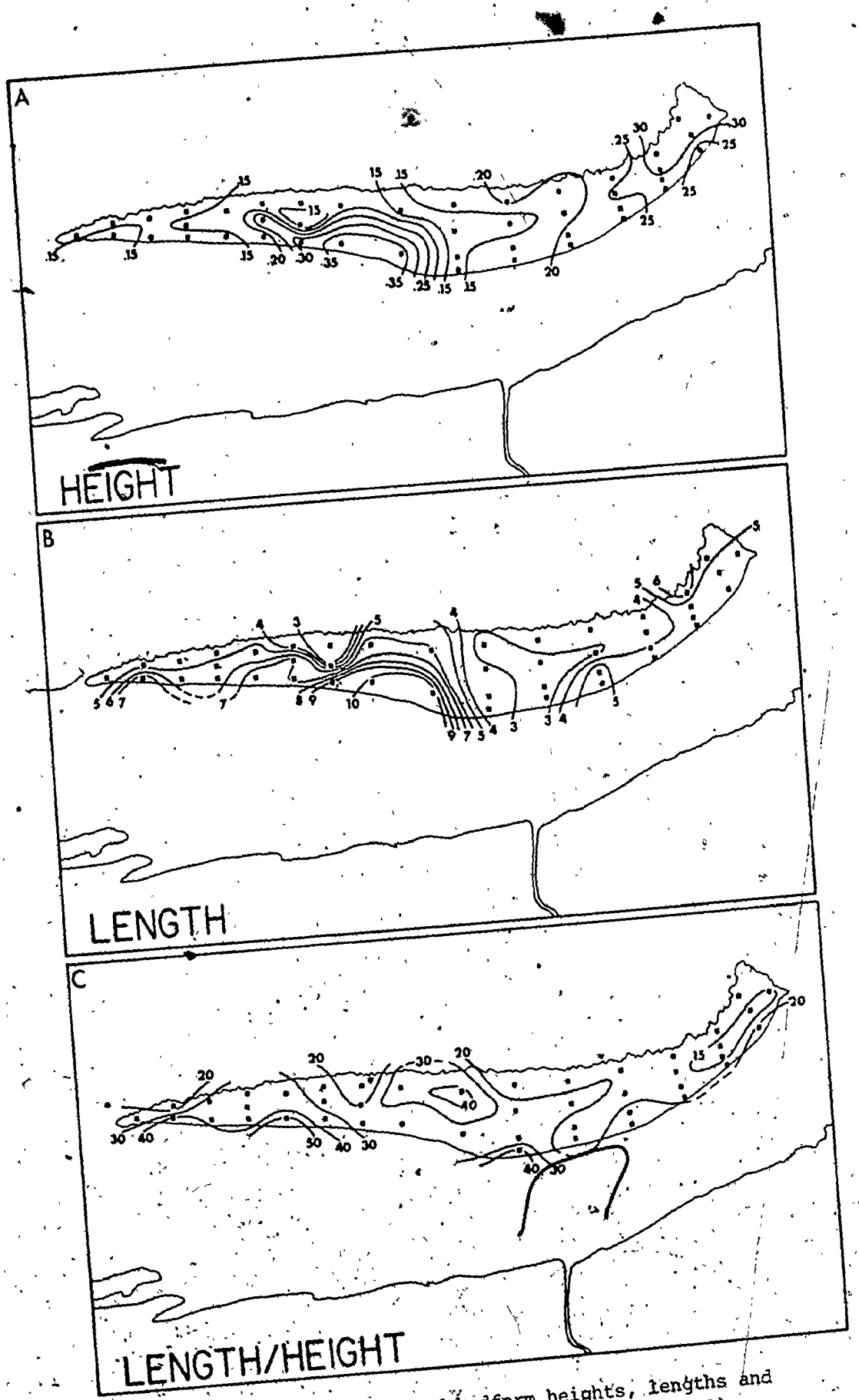

FIGURE 5.4: Areal variation of bedform heights, lengths and length/height ratios on Noel Bay Bar (1971).

FIGURE 5.5: Bedform characteristics on Noel Bay Bar -

A. Bedform height as a function of length;

B. Frequency histograms of bedform heights, lengths and length/height ratios.

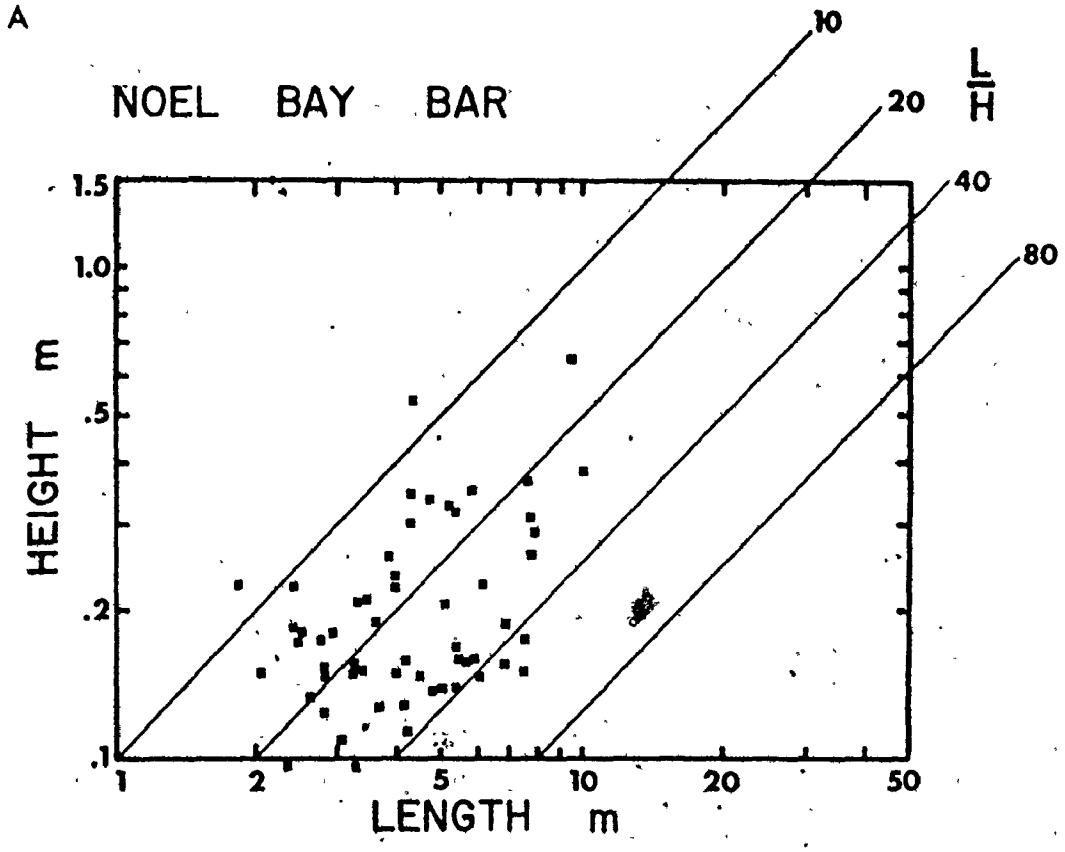
A
NOEL BAY BAR
L/H
10
20
40
80
HEIGHT m
1.5
1.0
.5
.2
.1
1
2
5
10
20
50
LENGTH m

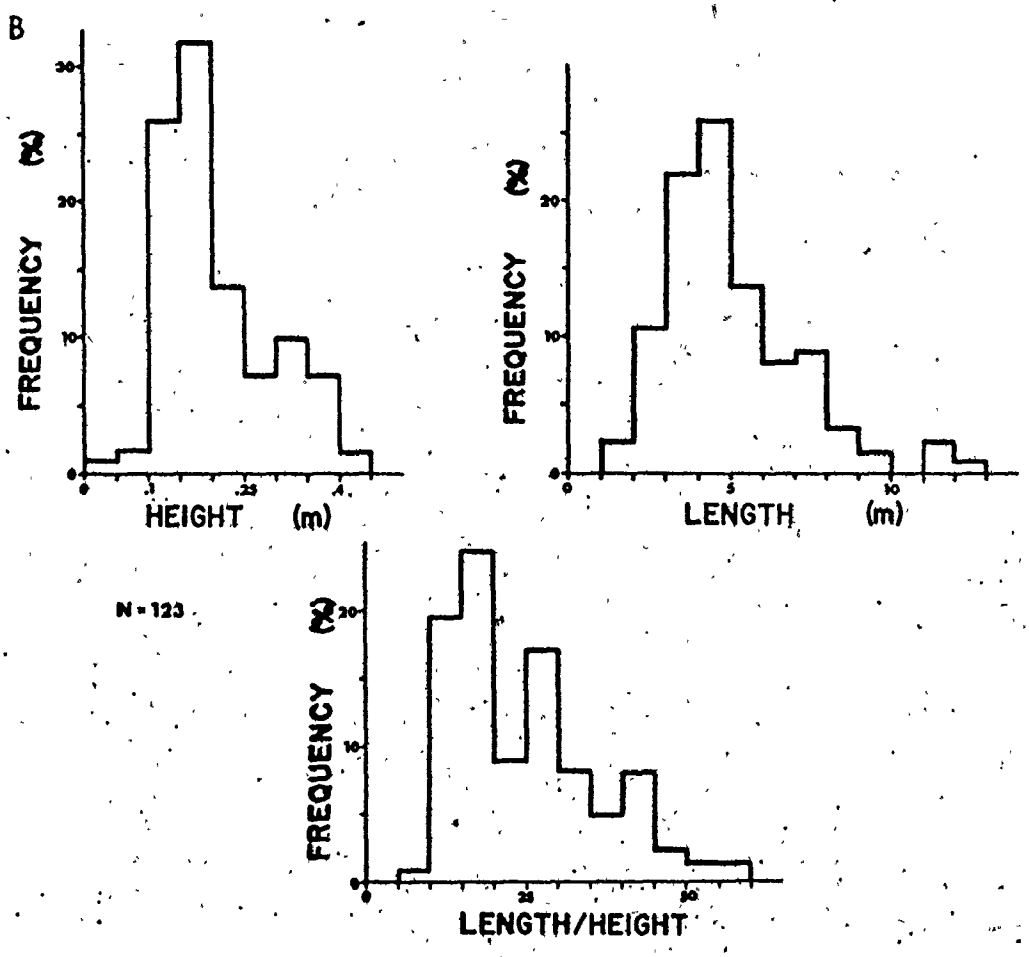
B
FREQUENCY (%)
HEIGHT (m)
LENGTH (m)
N = 123
LENGTH/HEIGHT

On East Noel Bar (Figs. 5.6 and 5.7), bedform lengths ranged from 1 to 16 m (with one exception at greater than 30 m near the northwest corner of the bar) and heights from 0.05 to 0.6 m. Bedform heights, lengths and length/height ratios generally decreased towards the centre of the bar (Fig. 5.6). The largest bedforms (length and height) occurred in the middle to northeastern part of the bar. Bedform heights were bimodal (dominant mode between 0.15 and 0.35 m) as were lengths (dominant mode between 4 and 6 m). Length/height ratios had a dominant mode between 20 and 35 m. The largest values of the ratio occurred at the west end of the bar.

Figures 5.8 and 5.9 summarize the characteristics of the bedforms on Noel Shore Bar. Lengths and heights range from 1 to 8 m and from 0.05 to 0.6 m respectively. As on the previous two bars, bedform height increases as a function of bedform length (Fig. 5.9 A). The largest bedforms (length and height) occurred along the southeastern, middle and northern parts of the bar (Fig. 5.8 A and B). Lengths and heights were generally smaller along the crestline of the bar, and larger in topographically lower parts of the bar (e.g., the southeast part of the bar; Fig. 3.27). The bedform population sampled is unimodally distributed with respect to length (dominant mode between 2 and 5 m) and slightly bimodal with respect to height (dominant mode between 0.15 and 0.3 m). The distribution of length/height ratios is unimodal (dominant mode between 5 and 15 m).

The frequency histograms of the bedform lengths and heights are not entirely representative of the bar because all parts of the bar were not visited, thus were not sampled. The deficiencies in sampling resulted from the lack of time during the field program and the shortness of the emergence periods over these parts of the bar. For example, the large bedforms on the southeast part of the bar (Fig. 3.27), with lengths in the order of 20 m and heights of about 0.6 m, were not sampled because the time during which this part of the bar was emergent was too short. Thus, the frequency histograms for bedform length and height should more realistically be bimodal to account for the larger bedforms from the topographically lower, unsampled parts of the bar.

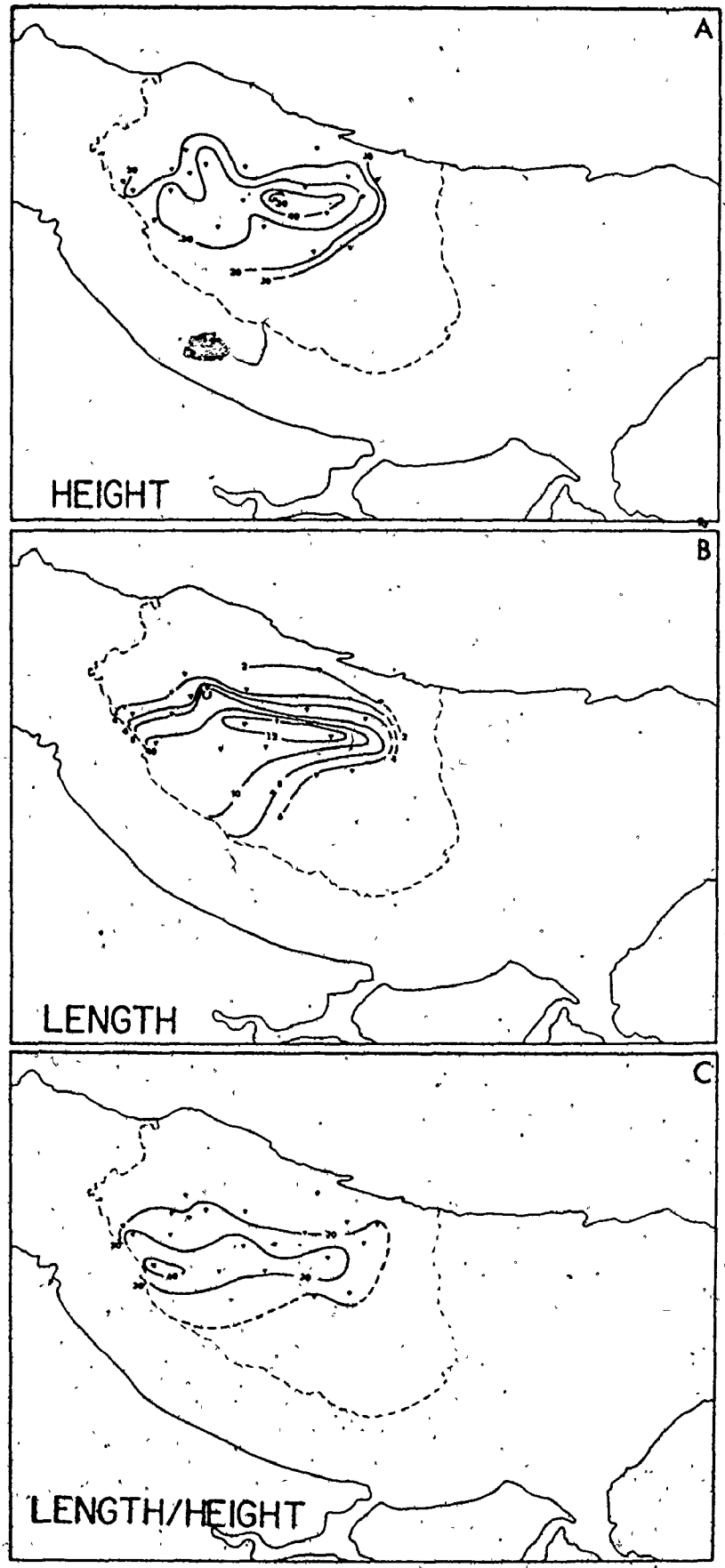

FIGURE 5.6: Areal variation of bedform heights, lengths and length/height ratios on East Noel Bar (1971).

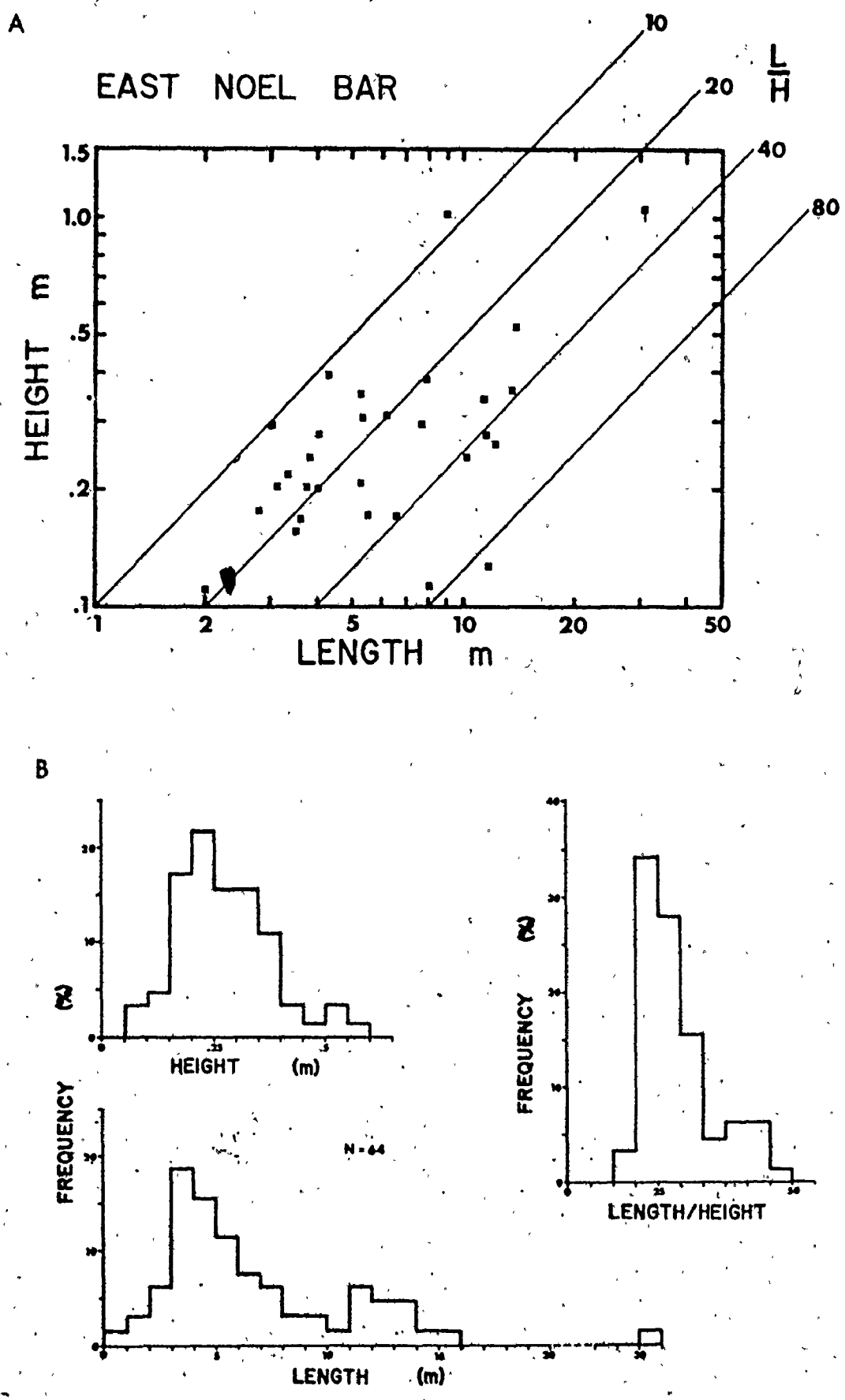

FIGURE 5.7: Bedform characteristics on East Noel Bar - A. Bedform height as a function of length; B. frequency histograms of bedform height, length and length/height ratios.

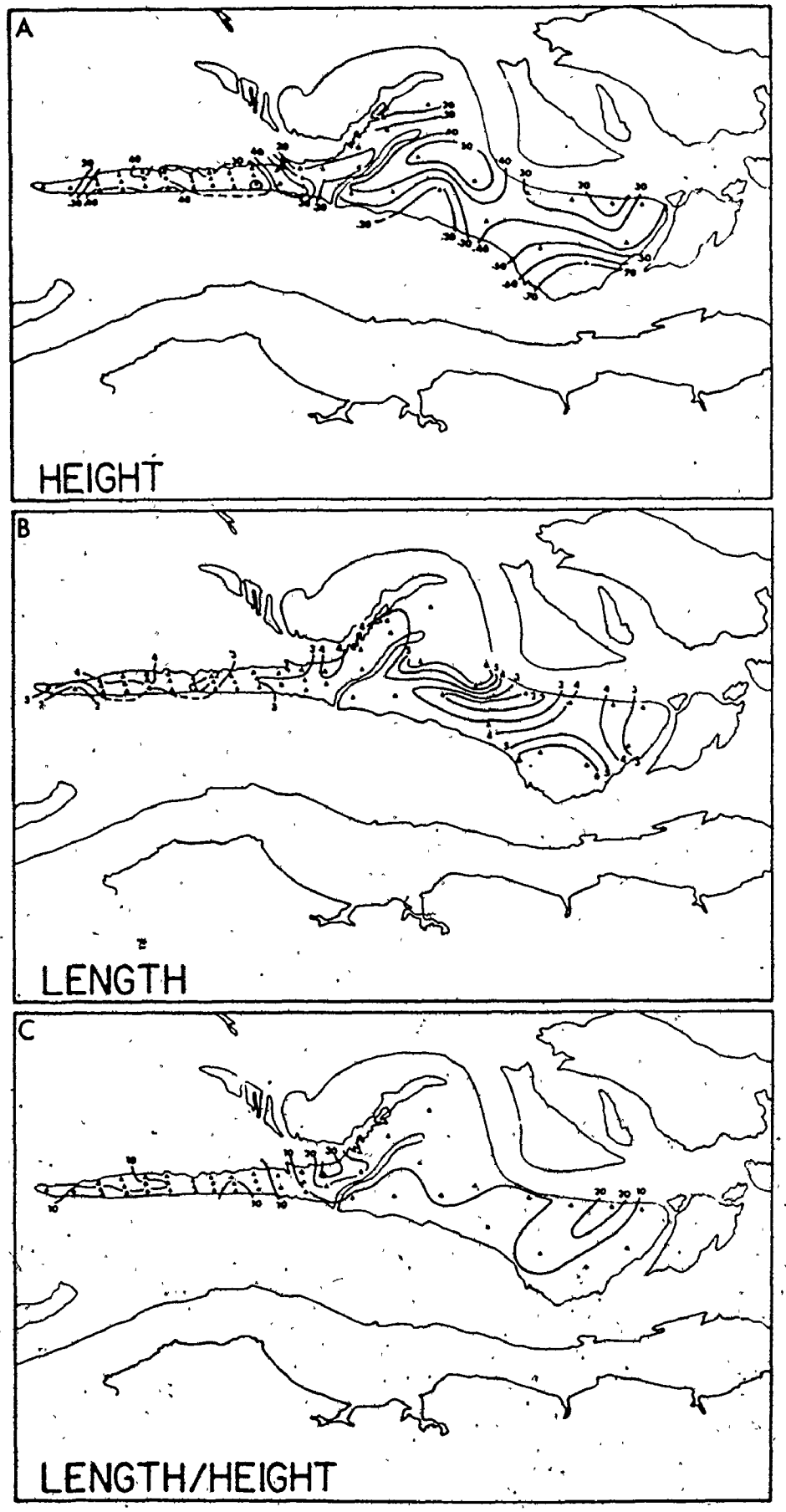

FIGURE 5.8: Areal variation of bedform heights, lengths and length/height ratios on Noel Shore Bar (1971-1973).

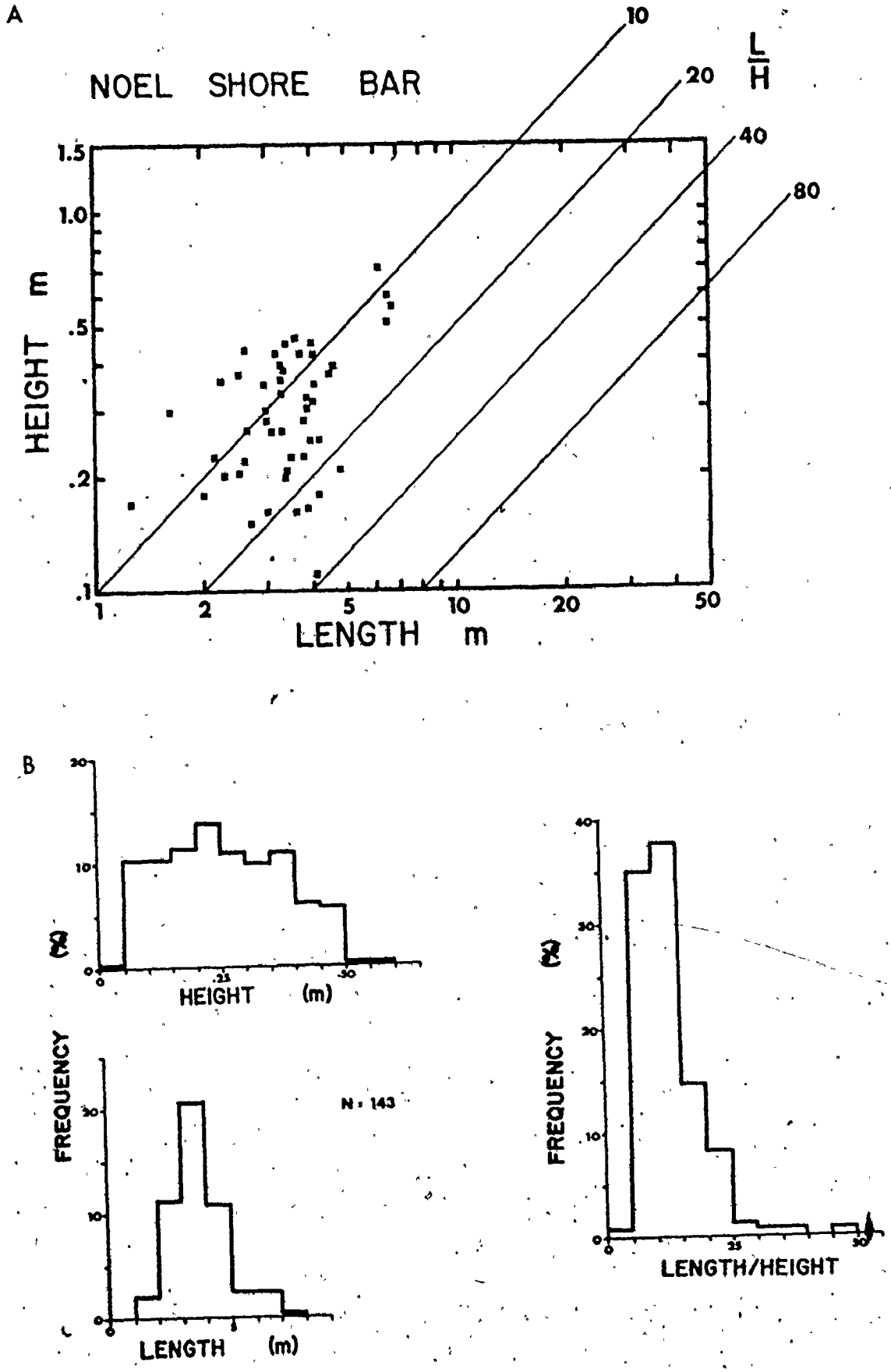

FIGURE 5.9: Bedform characteristics on Noel Shore Bar - A. Bedform height as a function of length; B. frequency histograms of bedform height, length and length/height ratios.

Large flood asymmetrical bed features with lengths in the order of 50 m and heights of about 1.5 to 2 m (length/height ratio of about 25 to 30) were apparent on the surface of the western part of the bar (Fig. 3.27). No detailed measurements were made of these features, and they are not included in the data of Figures 5.8 and 5.9.

On Selma Bar, bedform lengths and heights had the largest (measured) variation of scale compared to the other bars studied. Lengths ranged from 1 to more than 40 m, and heights from 0.1 to more than 1 m. Maximum lengths occurred along the southeast part of the bar (Figs. 3.32 and 5.10), and along the northwest side of the bar crestline. The length and height of bedforms over the remainder of the bar were fairly uniform. Bedform length and height generally increased away from the bar's crestline. The length and height distributions were polymodal (Fig. 5.11). The dominant modes for height and length were between 0.1 and 0.3 m, and between 2 and 5 m respectively. The dominant mode of the length/height ratio was between 10 and 25. The bedforms with the largest length/height ratios occurred in the extreme southeastern part of the bar. Ratio values generally decreased from here towards the northwest.

Figure 5.12 is a plot of all the averaged measurements of bedform length and height from Figures 5.4, 5.6, 5.8 and 5.10. The data represents 202 averages of bedform length and height from almost 600 individual measurements. The grouped data shows that length increased more rapidly than height, and that the relation could be expressed as a power function (a log-linear relation),

$$H = 0.124\ L^{0.44}$$

with a correlation coefficient of $r = 0.55$ that was statistically significant at better than the 99% level of confidence. This expression has a lower slope than the expression presented by Allen (1968 b, Fig. 4.10),

$$H = 0.074\ L^{0.77}.$$

The differences between the two relationships is primarily due to the nature of the bedform data plotted. Allen's data represents a wider range of bedform dimensions than found in the Cobequid Bay sand-body complex, and most of his measurements were derived from subtidal bed-

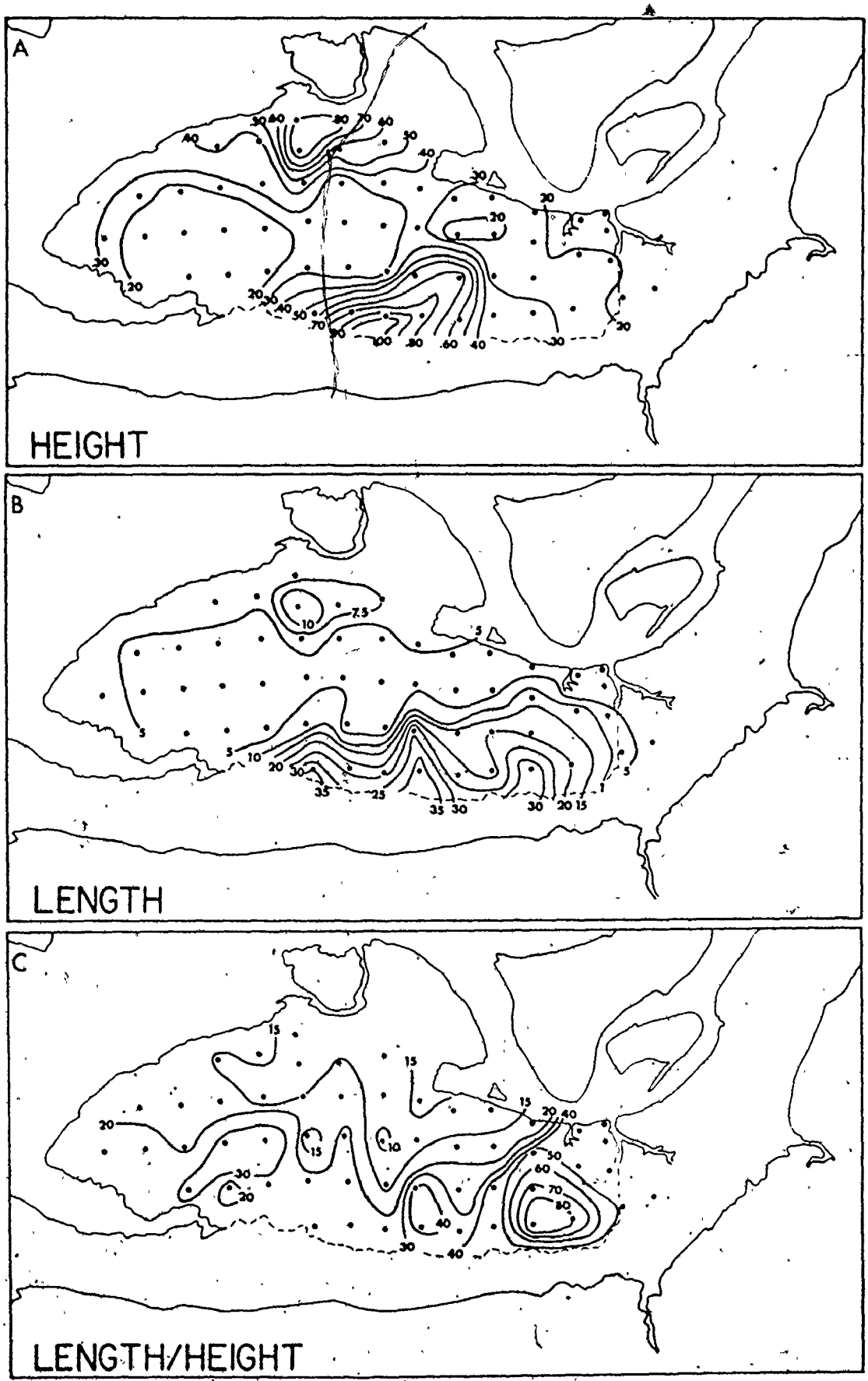

FIGURE 5.10: Areal variation of bedform heights, lengths and length/height ratios on Selma Bar (1972).

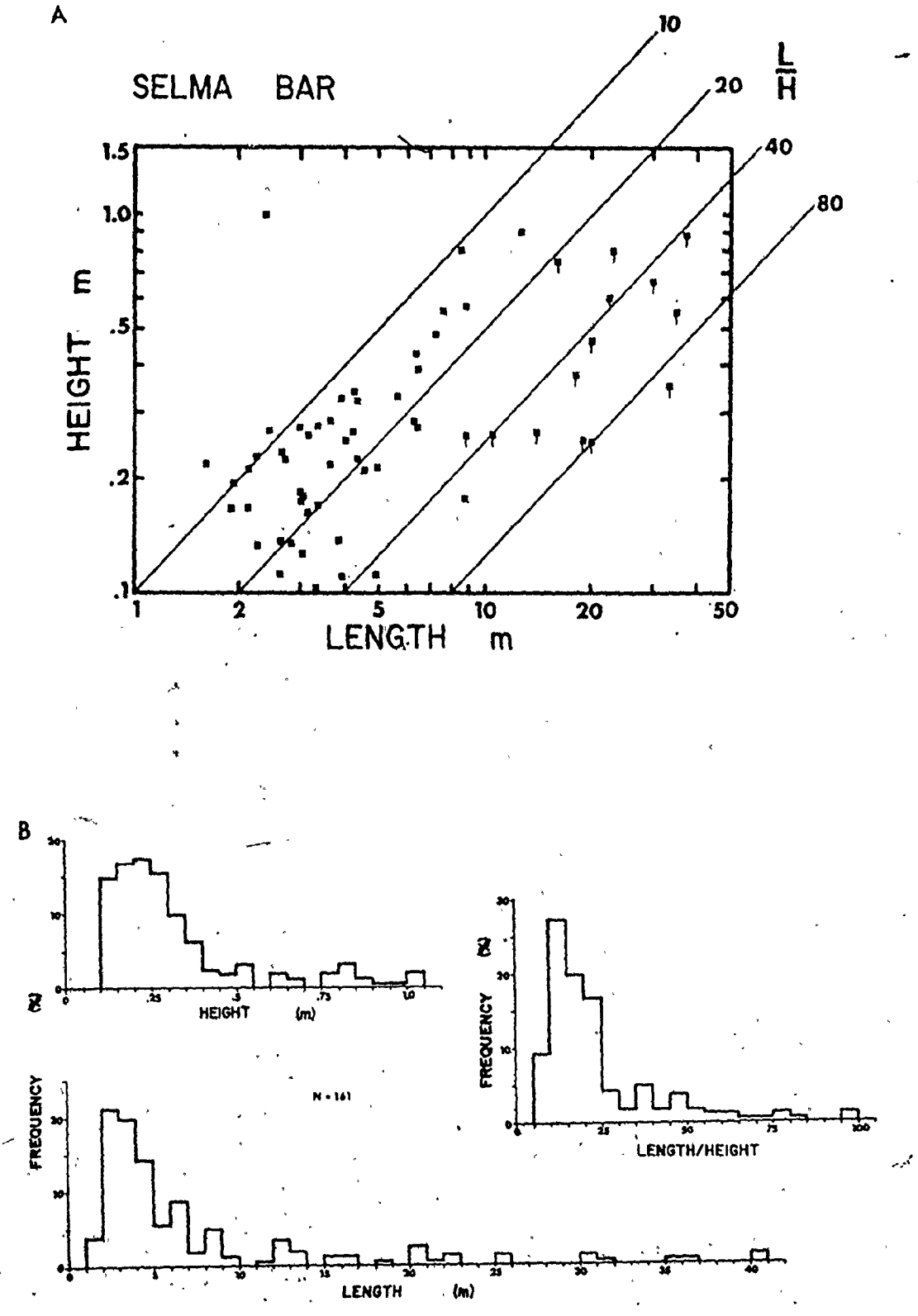

FIGURE 5.11: Bedform characteristics on Selma Bar - A. Bedform height as a function of length; B. Frequency histograms of bedform height, length and length/height ratios,

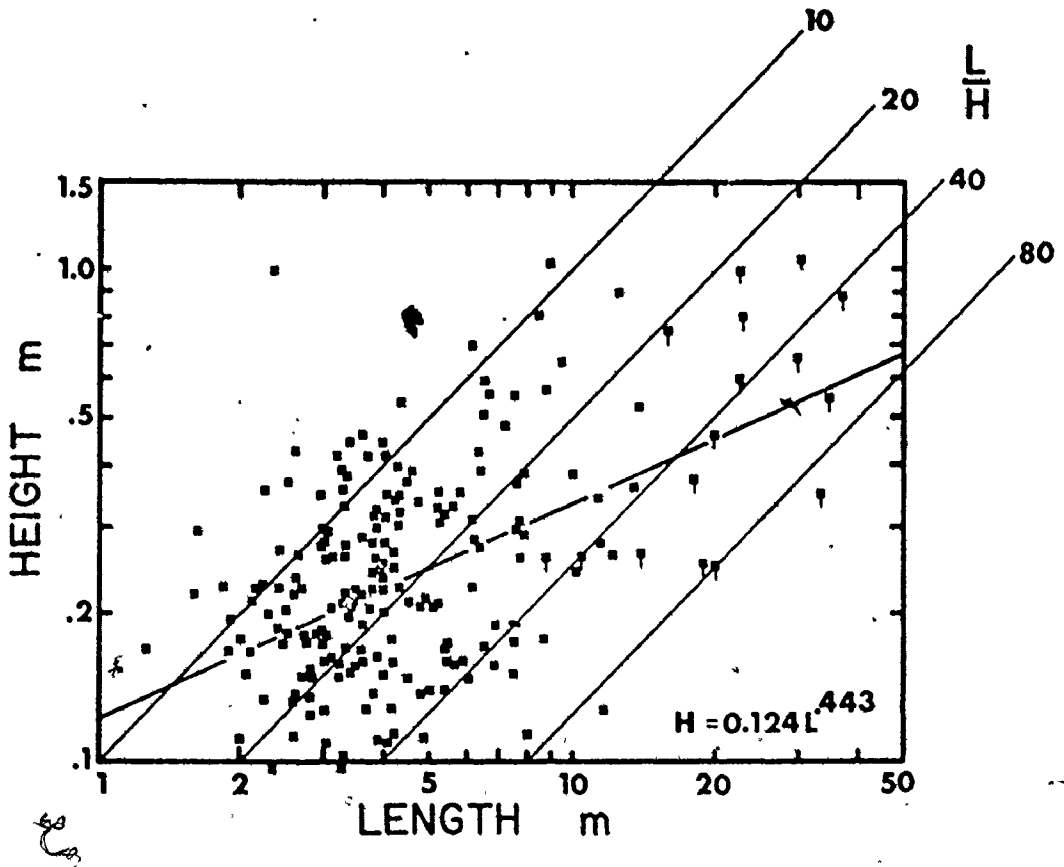

FIGURE 5.12: Bedform height as a function of length from the averaged bedform data of Noel Bay Bar, East Noel Bar, Noel Shore Bar and Selma Bar. Squares = megaripples; squares with ticks = sand waves (Selma Bar and East Noel Bar).

forms which tend to have larger length/height ratios compared to the ratios of bedforms from intertidal zones. (i.e., no late-stage ebb modification).

Figure 5.12 also shows that the average length/height ratio for megaripples was between 15 and 20, while that for sand waves is about 40. These values agree reasonably well with Allen's data (1968 b, p. 75-80) and those data points of comparable bedform scale in his Figure 4.10. Many of the bedforms that are intermediate to the megaripples and sand waves in Figure 5.12 are either planed-off megaripples or ebb modified flood bedforms.

Lee- and Stoss-side Slopes

Figures 5.13 to 5.16 show the areal variation of bedform lee- and stoss-side slopes on the four sand bars studied. Lee-side slopes were generally in the order of 25 to 30 degrees, thus at or near the angle of sediment repose. The angle of the bedform lee-side varied primarily as a function of sediment size (compare with Figs. 3.21, 3.26, 3.31 and 3.36) i.e., steeper with finer grain sizes.

The angle of bedform stoss-side slopes was much more variable. Slopes ranged from near zero to almost 15 degrees because bedform stoss-sides generally comprised a relatively flat crestal platform and a relatively steep stoss-side slope, upflow of the crestal platform (Allen, 1968 b, p. 61). The areal variation of stoss-sides slopes varied somewhat irregularly over the bars with respect to sediment size, but showed some correlation to bedform type (e.g., 'unmodified' megaripples versus 'planed-off' megaripples).

Orientation

Bedform orientations are an important indicator of directions of secondary flow and sediment transport. The areal variation of bedform orientations on the sand bars is best shown in Figures 3.16 and 5.19 (Noel Bay Bar), 3.24 (East Noel Bar), 3.27 (Noel Shore Bar) and 3.32 (Selma Bar). Figures 5.17 and 5.18 summarize the bedform orientation data measured on the bars (Appendix V). On Noel Bay Bar, the bedforms were oriented between 280 and 310° during the ebb (low tide emergence). A secondary mode is evident along the northwest part of the bar where some ebb modified flood megaripples occurred (note smaller arrows in

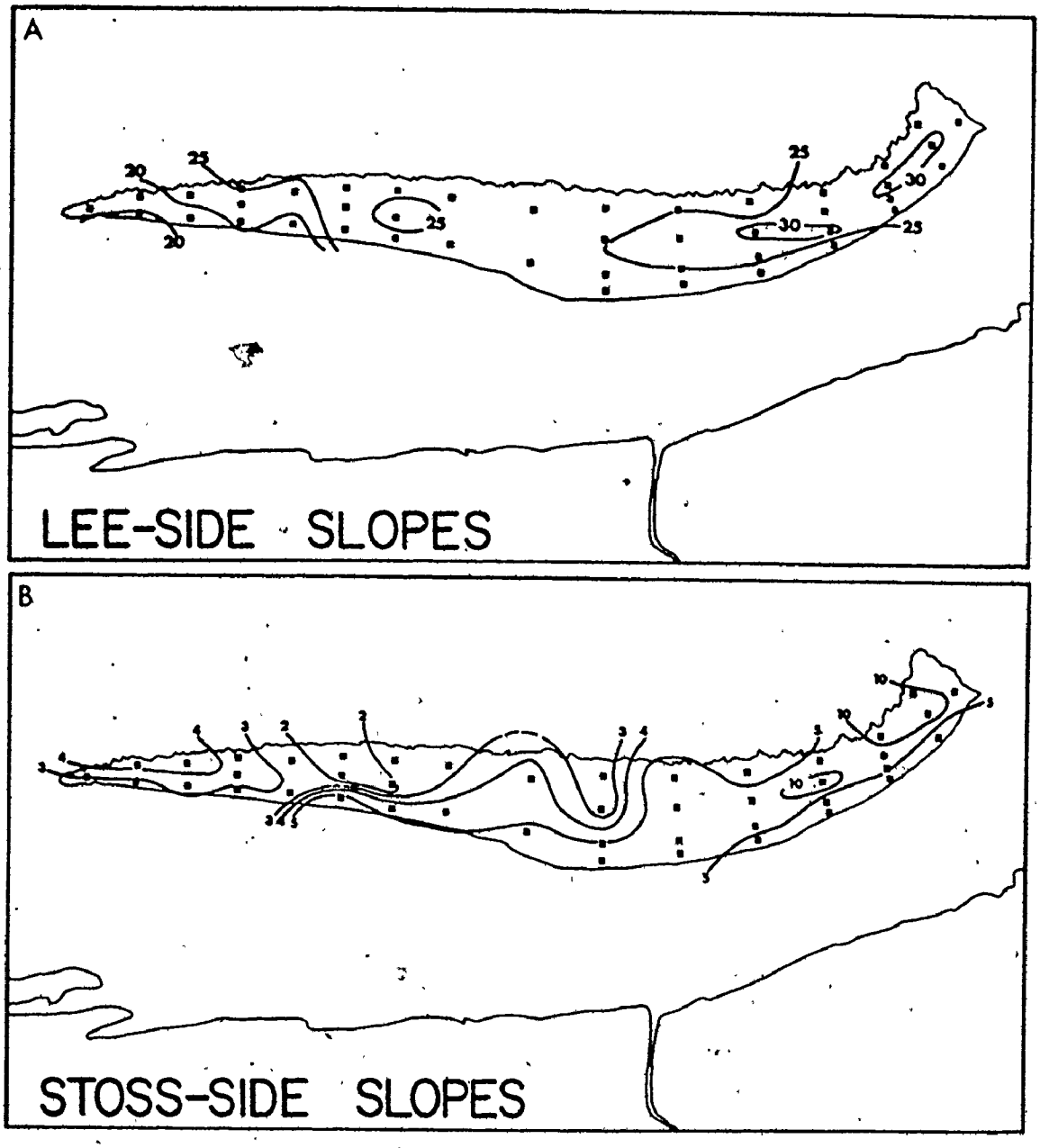

FIGURE 5.13: Areal variation of bedform lee- (A) and stoss-side (B) slopes on Noel Bay Bar.

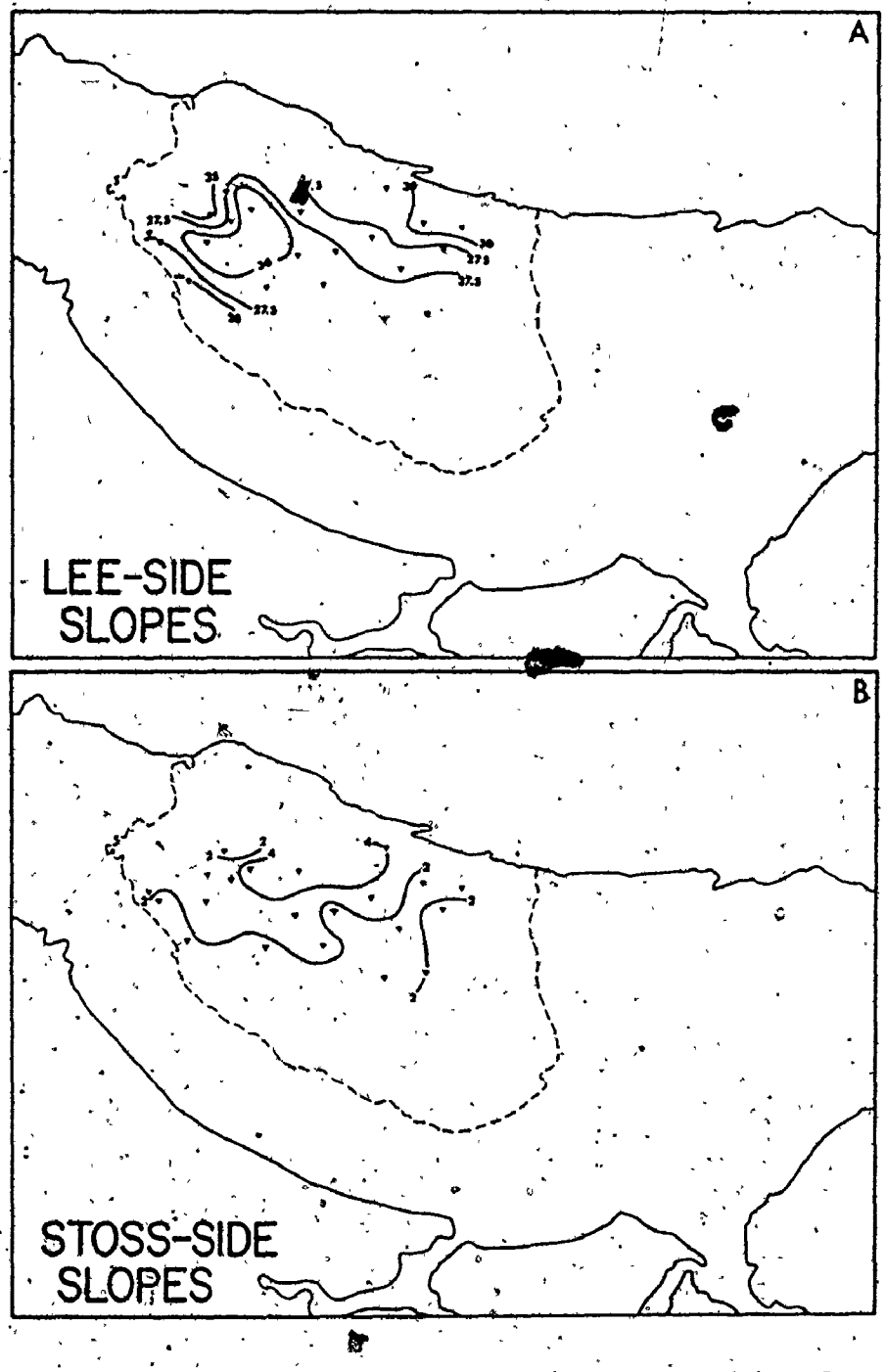

FIGURE 5.14: Areal variation of bedform lee- (A) and stoss-side (B) slopes on East Noel Bar.

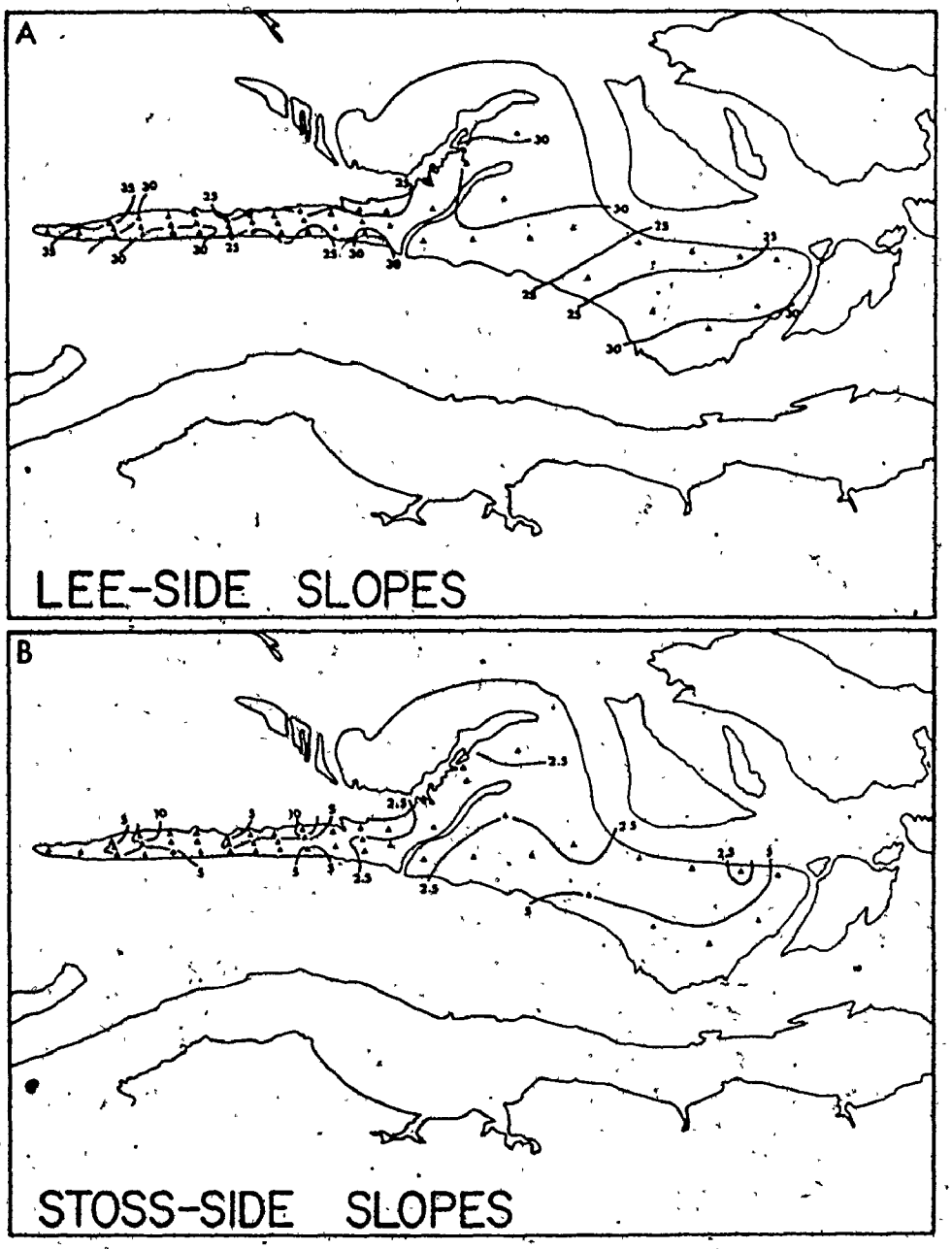

FIGURE 5.15: Areal variation of bedform lee- (A) and stoss-side (B) slopes on Noel Shore Bar.

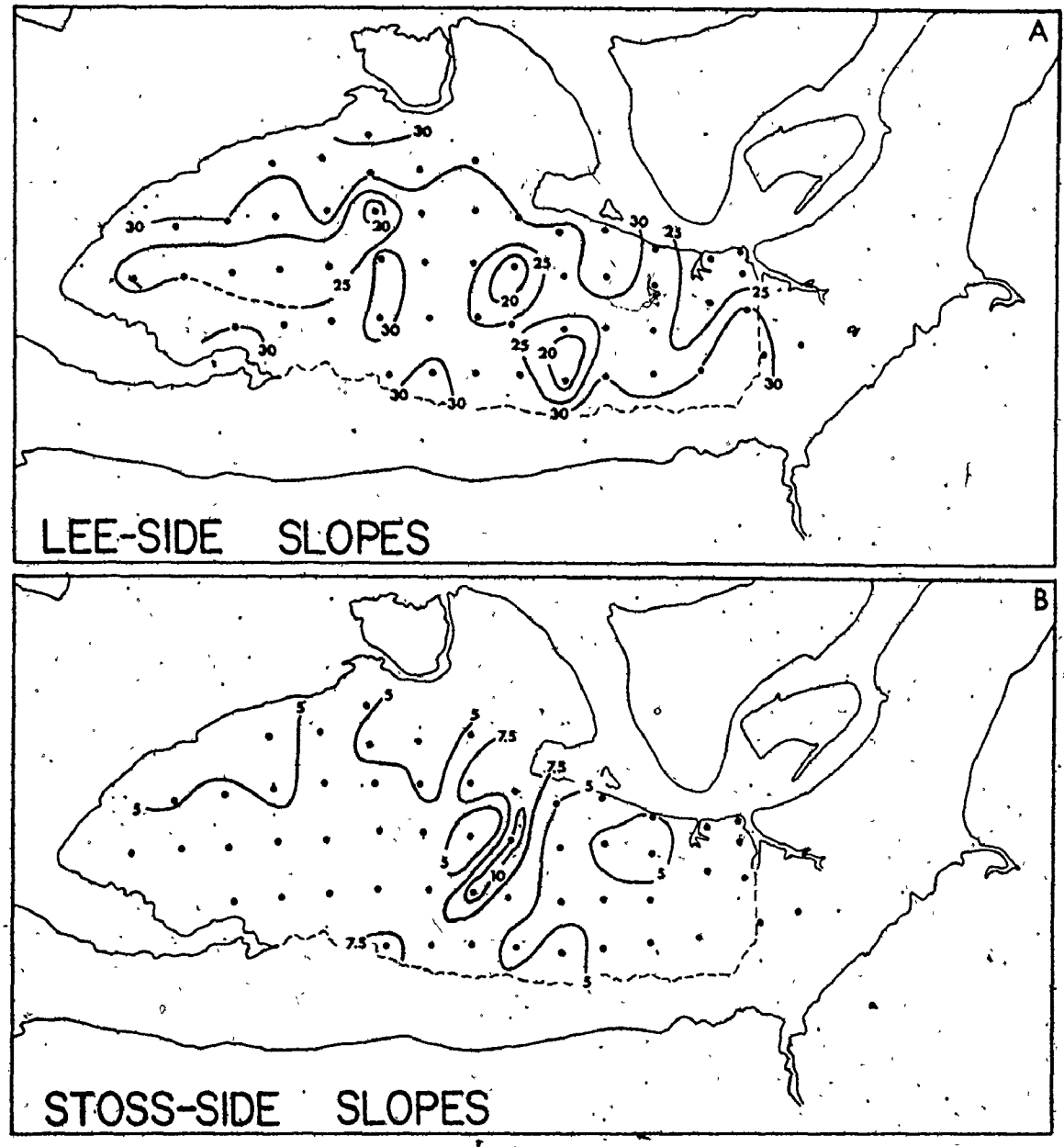

FIGURE 5.16: Areal variation of bedform lee- (A) and stoss-side (B) slopes on Selma Bar.

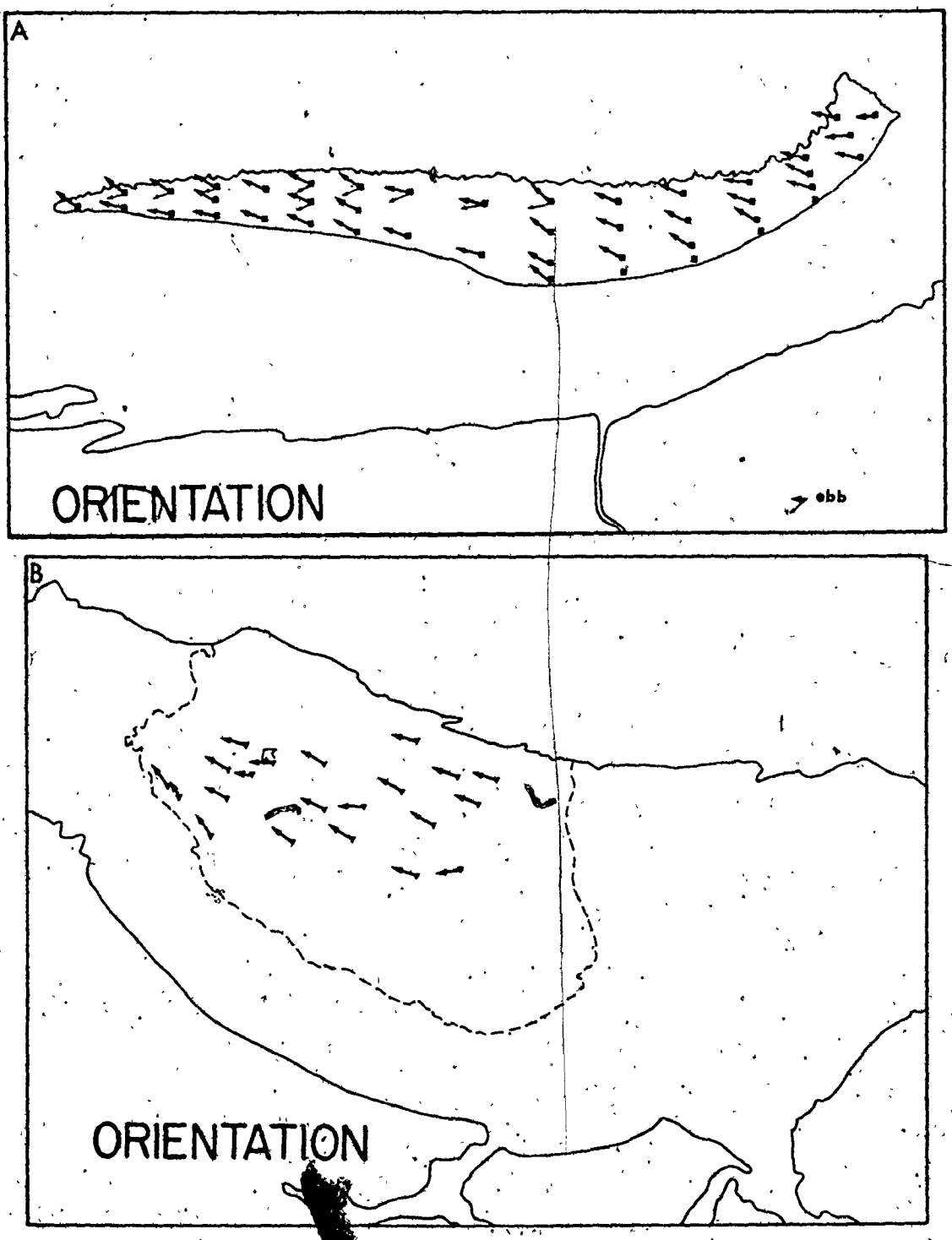

FIGURE 5.17: Areal variation of bedform orientations on Noel Bay Bar (A), East Noel Bar (B), Noel Shore Bar (C) and Selma Bar (D). Bedform orientation is the direction perpendicular to the lee-side slope of the ebb bedform (or flood bedform as noted).

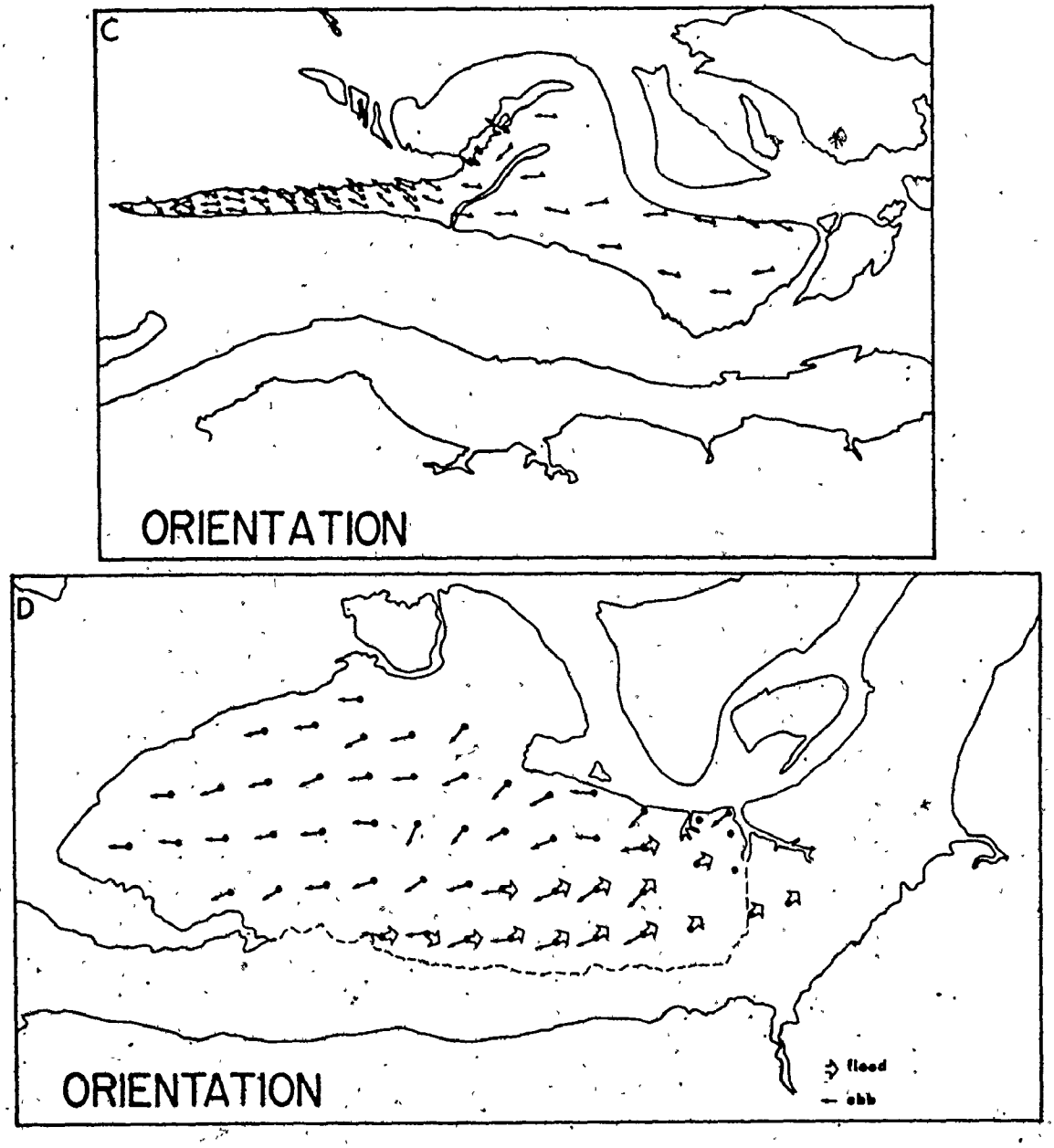

FIGURE 5.17 - cont'd.

FIGURE 5.18: Frequency histograms of bedform orientations on Noel Bay Bar (A), East Noel Bar (B), Noel Shore Bar (C) and Selma Bar (D)

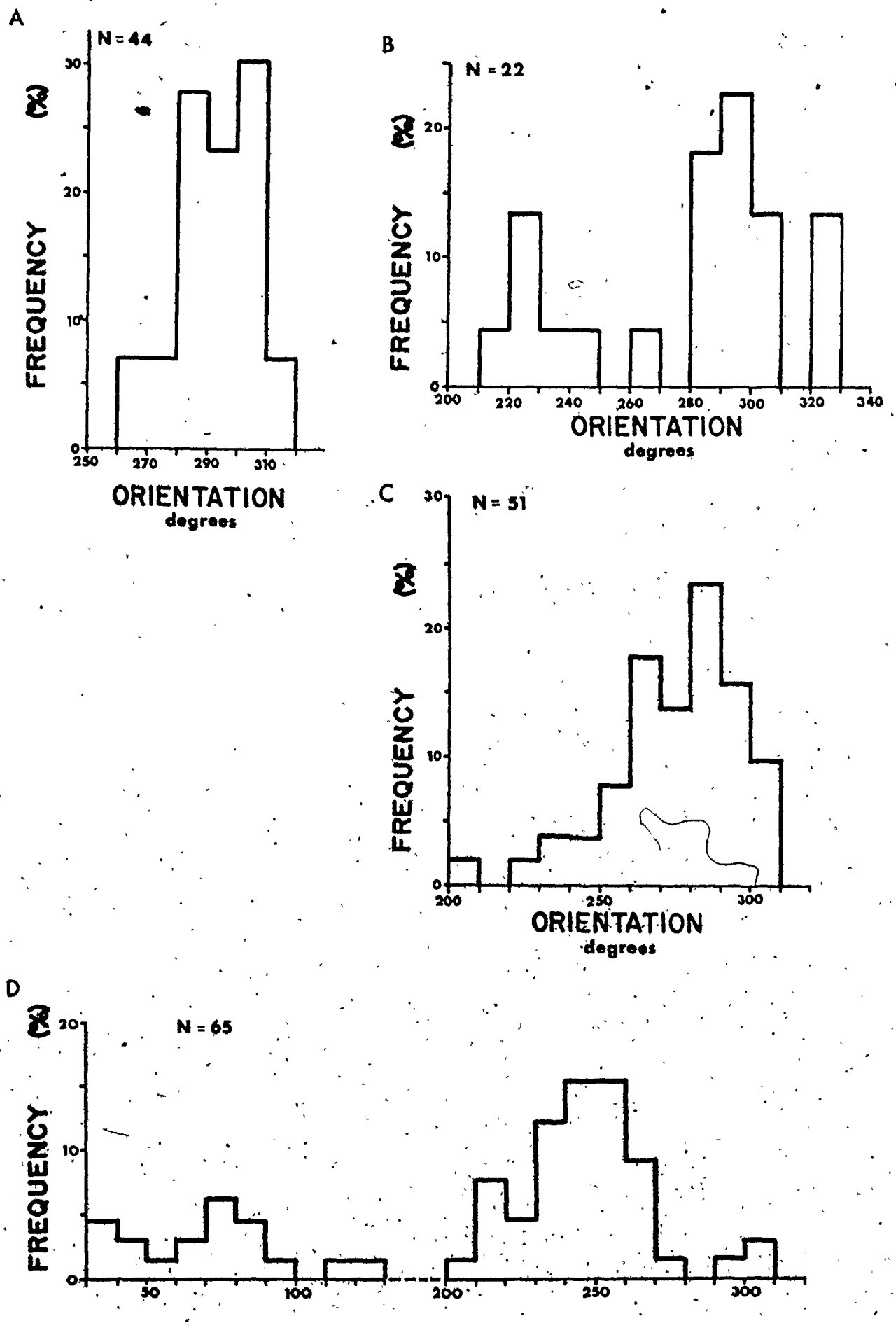
A
N = 44
FREQUENCY (%)
30
20
10
0
250
270
290
310
ORIENTATION
degrees
B
N = 22
FREQUENCY (%)
20
10
0
200
220
240
260
280
300
320
340
ORIENTATION
degrees
C
N = 51
FREQUENCY (%)
30
20
10
0
200
250
300
ORIENTATION
degrees
D
N = 65
FREQUENCY (%)
20
10
0
50
100
200
250
300

FIGURE 5.19: Photos of bedform orientations and emergence-submergence characteristics on sand bars.

A. Orientation of ebb-megaripples on the west end of Noel Bay Bar. Note the different orientations of the bedform crestlines across the bar. Ebb currents flowed from right to left (east to west).

B. Orientation of ebb-megaripples on the middle part of Noel Bay Bar. See above. Note smooth southern edge of bar relative the bar's northern edge.

C. Slow emergence of sand bar (Noel Bay Bar) during the late ebb. Arrow points to emergent megaripple crestline. View is to the south across the crest of Noel Bay Bar.

D. Rapid submergence of sand bar (Selma Bar) during the early flood. View is to the south from the north side of Selma Bar.

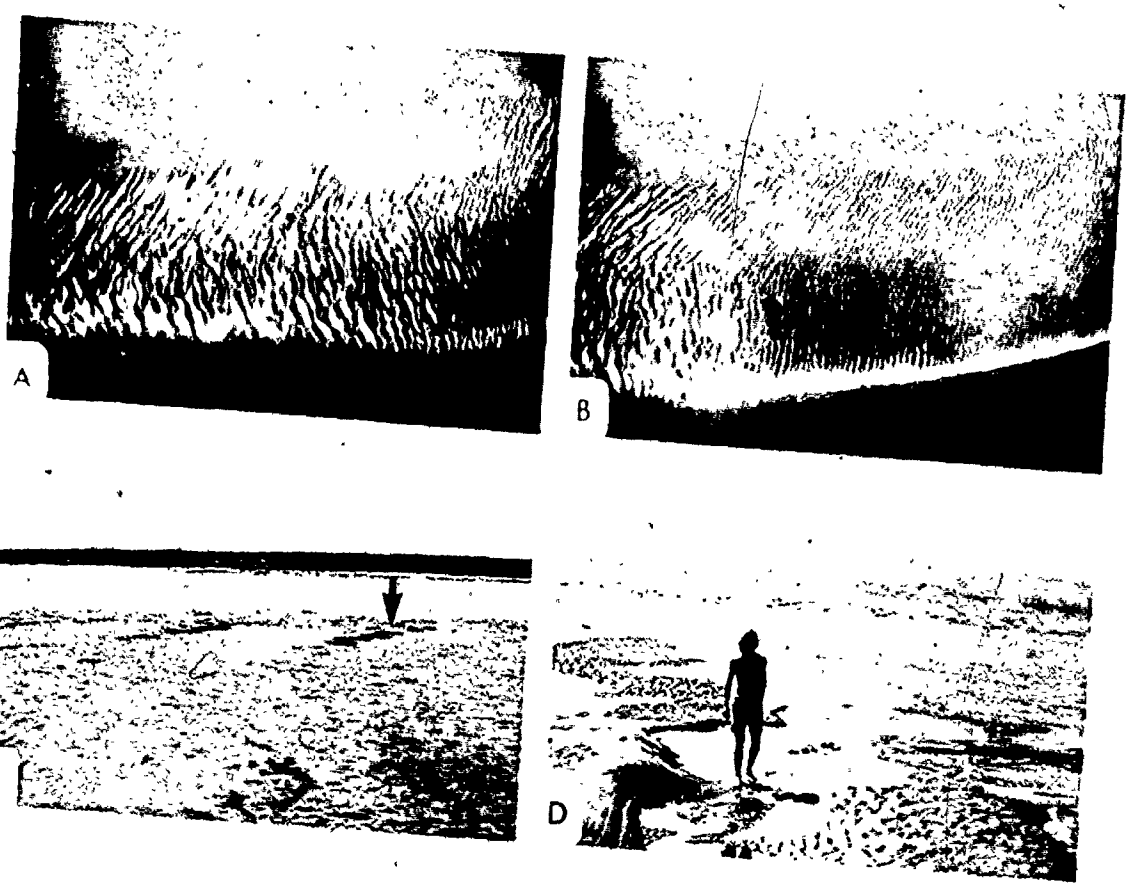
A
B
C
D

Fig. 5.17). These bedforms were oriented at about 260° during the ebb, or at about 80° during the flood. Bedforms to the north of the bar's crestline were generally oriented towards the northwest, while those to the south of the crestline were oriented more to the west. Note bedform orientations in Figure 2.19.

The bedform orientations on East Noel Bar showed a wider range of dispersion (i.e., from 210 to 330°) compared to bedforms on Noel Bay Bar. The major mode was around 290 to 300°.

On Noel Shore Bar, the predominant bedform orientation was between 260 and 310° which was similar to the bedforms on Noel Bay Bar. Orientations to the south of the bar's crestline face more westerly than those to the north of the crestline which faced more north-westerly. The very large bed features were oriented primarily to the east-northeast (flood oriented).

Bedform orientations on Selma Bar were strongly bimodal because both ebb and flood features were preserved at low tide. The ebb features had a dominant mode between 240 and 260°, while the flood features, from the south side of the bar had a dominant mode of about 70 to 80°. The large arrows in the southeast part of the bar (Fig. 5.17D) reflect the orientation of flood oriented sand waves; the smaller arrows reflect the orientation of the smaller, ebb-oriented megaripples superposed on the sand waves. The orientation of the ebb features generally converged towards the crestline of the bar from the north, and diverged away from it to the south. The bedforms in the main swatchway across the bar were oriented to the south along its axis. Over the remainder of the bar, the bedforms were oriented in a generally east-west direction.

Bedform Facies

The ebb oriented or ebb modified flood asymmetrical bed features exposed on the bars at low tide can be grouped into a number of bedform facies based on the foregoing quantitative results from the external geometry and scale of the bedforms and from the qualitative morphological properties of the bedforms (e.g., crestline continuity and sinuosity, scours, planed-off crestal platforms, superposed bed features) observed in the field and from air photographs.

The bedforms on the bars are grouped into seven facies (with sub-facies): (i) Facies A = [illegible] or [illegible] bed; (ii) [illegible] = rip

beds; (iii) Facies C = linear megaripples; (iv) Facies D = sinuous megaripples; (v) Facies E = irregular megaripples; (vi) Facies F = catenary megaripples; and vii) Facies G = ebb modified flood bedforms (including sand waves). The areal distribution of the different facies on each bar is summarized in Figures 5.20.

Facies A - (plane or flat bed) - Facies A occurs along the steep slopes of bars (e.g., southern margin of Noel Bay Bar, northeastern margins of Noel Shore and Selma Bars). The slopes (Fig. 5.21 A) range in steepness from about 5 to 18 degrees. The bed surface is generally featureless except where late-stage ebb runoff or dewatering of the bar during low tide has produced small ripples, small braided rills (Fig. 3.34 G and 5.21 D) and/or larger late-stage ebb surface runoff channels. This facies, although relatively consistent in occurrence on nearly all bars in Cobequid Bay, represents only a very small area of the bars. Other features of this facies are shown in Figure 5.21 A to D. Sometimes remnants of 'scoured megaripples were observed on the lower slopes (Fig. 5.21 B).

Facies B - (rippled bed) - Facies B (Fig. 5.21 E to H) generally occurs adjacent to Facies A, i.e., next to steep bar slopes and/or in areas where the sediments are relatively fine grained (e.g., northeast corner of Selma Bar, southeast corner of East Noel Bar). Facies B includes the occurrence of current ripples superposed on megaripples. Both current (asymmetrical) and wave (symmetrical) produced ripples characterize this facies. The current ripples are typically linear to slightly sinuous crested. Lengths and heights are commonly in the order of 0.10 to 0.15 m and 0.02 to 0.05 m. Crestlines are laterally continuous and uniform in height. In fine grained sediments, mud pellets are frequently found in current ripple troughs.

Wave produced ripples are uncommon. They usually occur as a superimposed bed feature on current ripples (e.g., ladden back ripples; Fig. 5.3 D and E)) and very rarely as the only bed feature. Wave ripples are smaller than current ripples and are generally symmetrical in cross-section.

Facies C - (linear megaripples) - Facies C (Fig. 5.22) bedforms are straight crested megaripples that are laterally continuous and uniform

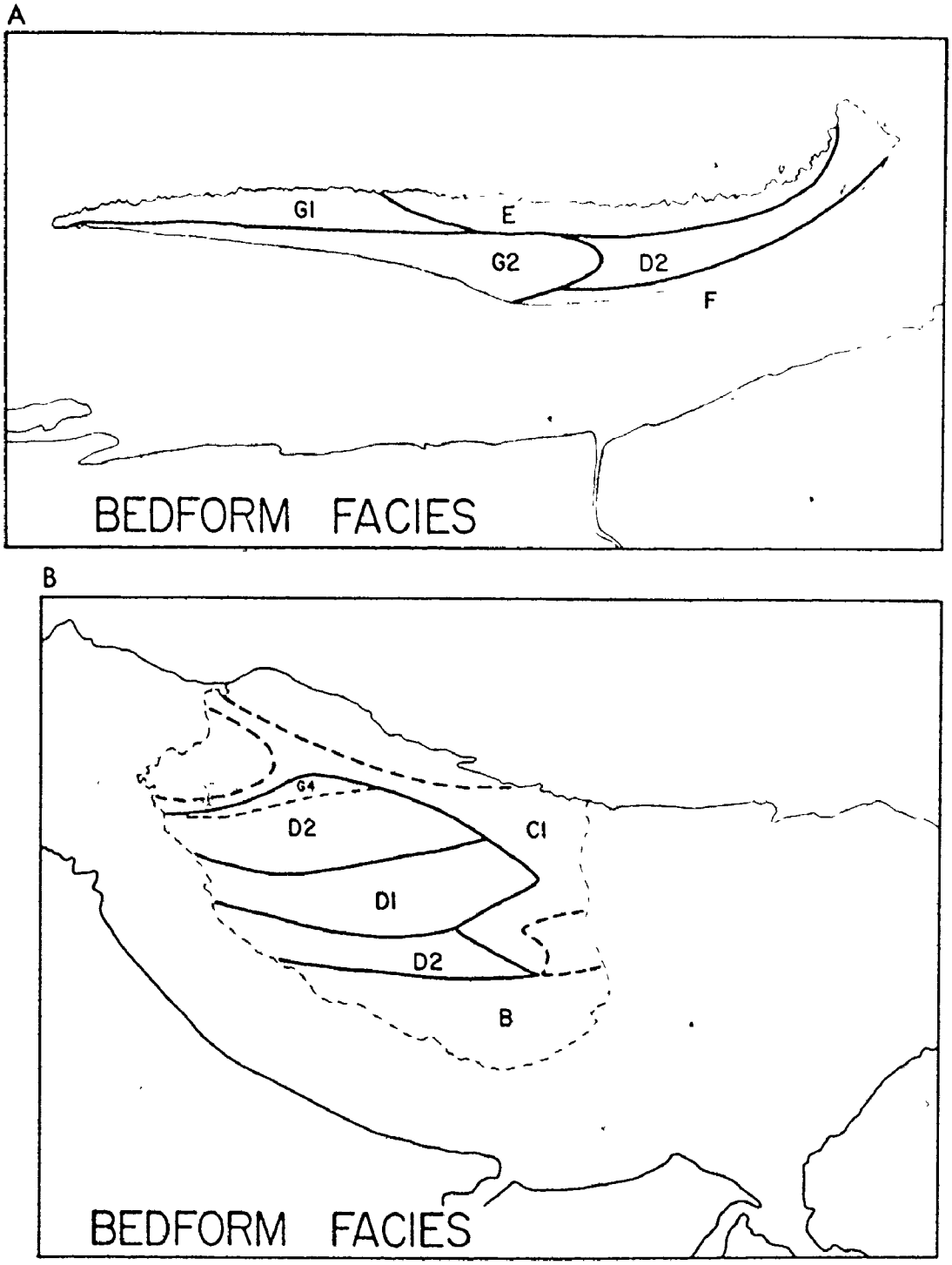

FIGURE 5.20: Areal variation of bedform facies on Noel Bay Bar (A), East Noel Bar (B), Noel Shore Bar (C) and Selma Bar (D). The facies are described in the text.

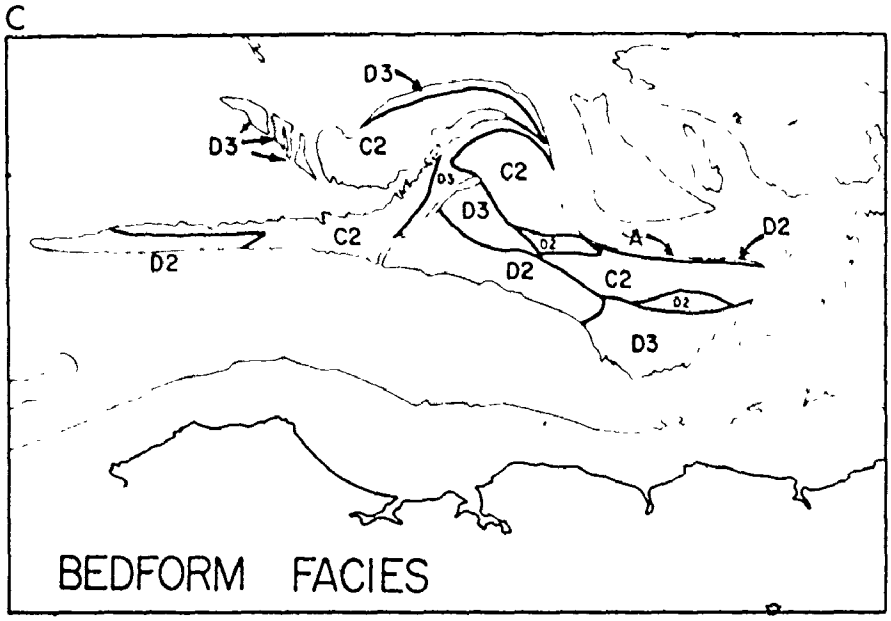

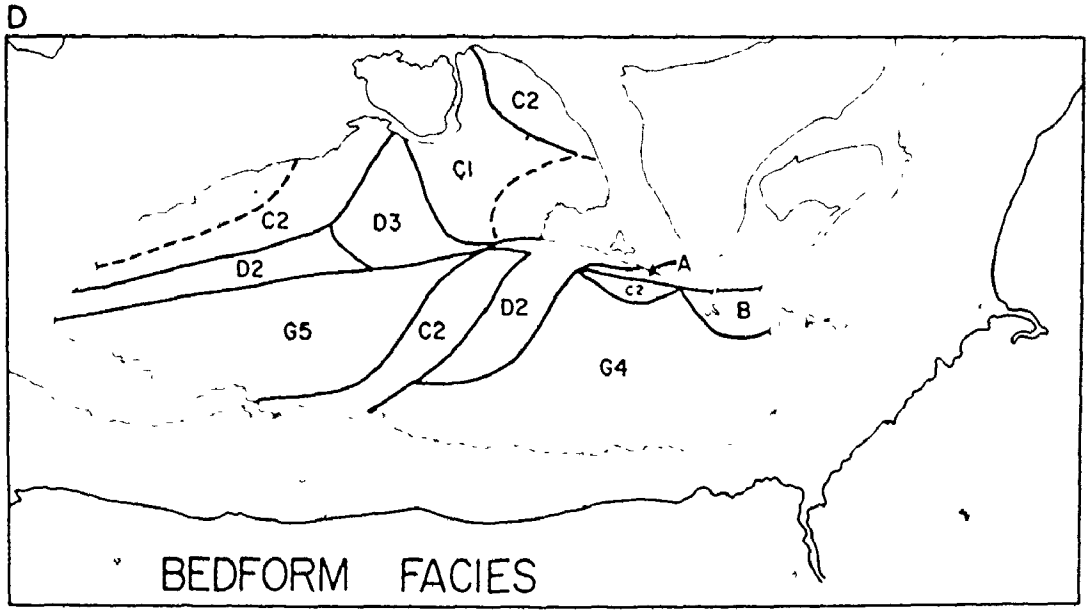

FIGURE 5.20 - cont'd.

FIGURE 5.21: Facies A (plane or flat bed) and Facies B (rippled bed) bedforms:

A. Relatively steep flat bed along the north side of Selma Bar, looking east. Scale is 1 m long. Small surface irregularities are primarily late stage ebb runoff features.

B. Lower part of flat bed on Noel Bay Bar showing the occurrence of 'nearly' obliterated, scoured megaripples. Scale is 1 m long. Note the small late stage ebb runoff rills in the remnant megaripple troughs.

Pebbled-sand near the crest of Selma Bar. This feature is common near the crest of the steep side on each of the bars. Lens cap is 0.05 m in diameter.

D. Rill erosion developed during the low tide dewatering of groundwater from the steep side of Selma Bar. Scale is 1 m long.

E. Linear crested current ripples on the crest of Selma Bar. Note tape measure for scale.

F. Linguoid current ripples on the stoss-side of megaripples Scale is 1 m long.

G. Sinuous crested current ripples with falling water marks. Ripple height is approximately 0.05 m.

H. Current ripples with mud drapes in their troughs. Scale is in centimetres and decimetres.


A


B

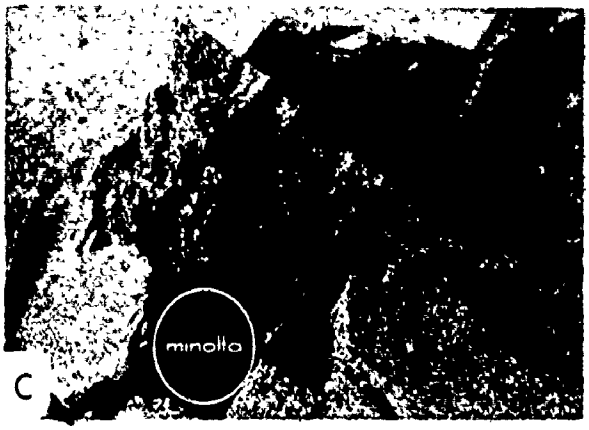
minolta
C


D


E

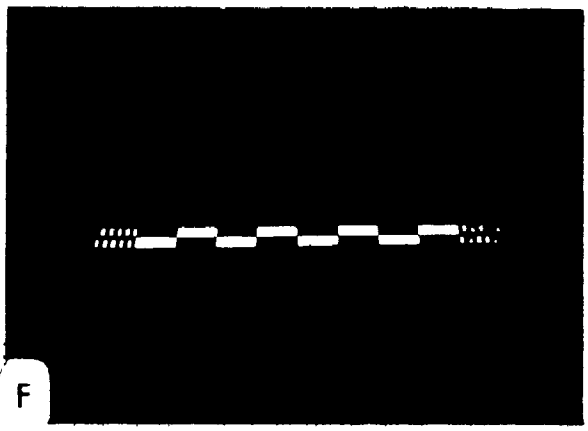
F

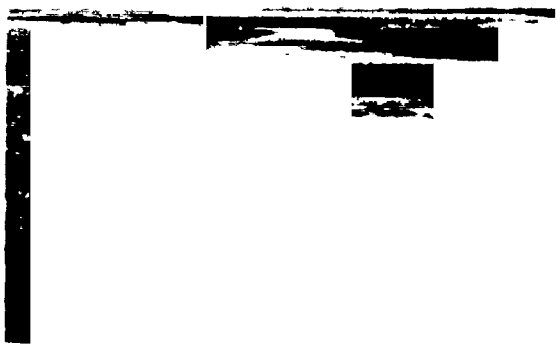

FIGURE 5.22: Facies C bedforms (linear crested megaripples).

A. Falling water marks on megaripple lee-side slopes and superposed late-stage emergent run-off linguoid and straight current ripples. Megaripple crest is slightly 'planed-off'. Scale is 1 m long.

B. View of lower part of a megaripple lee-side slope showing an avalanche deposit (grades from fine to coarse downslope). Scale (sitting in the megaripple trough) is 1 m long.

C. Linear crested megaripple in gravelly sands and with pebble and cobbe sized sediments exposed in the troughs (Facies C1). View is to the northeast, near the northeast side of East Noel Bar. Scale is 1 m long.

D. Close-up view of a linear crested megaripple with pebble and cobble sized sediments in the trough (Facies C1). Note: The pebble streaks and current ripples on the stoss-sides, and the falling water marks on the lee-sides of the megaripples. Scale is 1 m long.

E. Linear crested megaripple with sand sized sediments in the troughs (Facies C2). Note: Superposed current ripples; late stage ebb runoff features and absence of scours in trough. View is to the south across the crest of Noel Shore Bar. Scale is 1 m long.

F. Close-up view of linear crested megaripple with sand-sized sediments in the trough. Note: Current ripples on stoss-sides and falling water marks on the lee-sides of the megaripple; rill erosion features near the base of the megaripple from low tide dewatering of the bedform; and absence of scours in the megaripple trough. Shovel is approximately 1 m long.


A


B


C


D

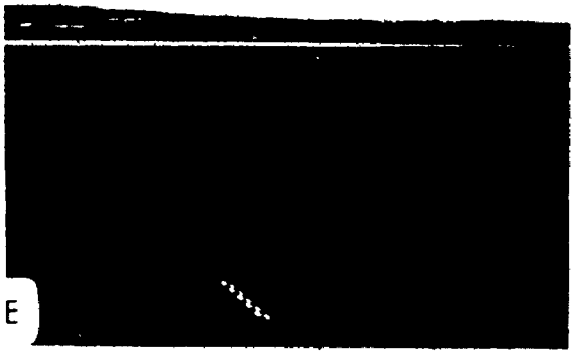
E

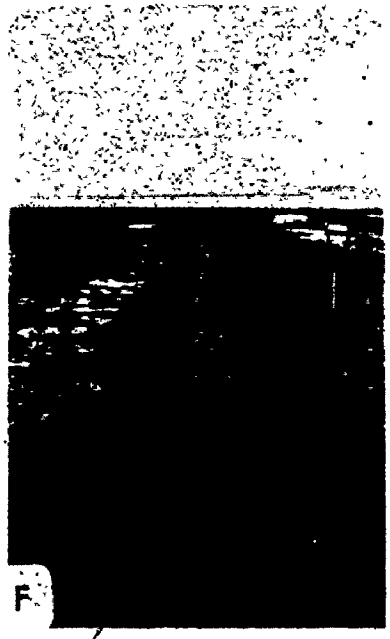
F

in height. The crestal platform is usually very small and the brinkline relatively sharp. Lee slopes are very close to the angle of repose for unconsolidated sediment. Often an avalanche or gravity shear type of deposit occurs at the base of the lee face (Fig. 5.22 A). Stoss-sides are long, gentle (less than 5 degrees), slightly convex, upward slopes and commonly superposed with linear to sinuous crested ripples. Length/height ratios for this facies range from 10 to 20.

There are two subfacies to Facies C: (C1) linear megaripples with pebble and cobble sized sediments exposed in the troughs (e.g., East Noel Bar) and (C2) linear megaripples with sand-sized sediment in the troughs. Facies C1 bedforms occur in slightly coarser sands (1.5Ø) than those of C2 (1.75 to 2.00 Ø). The presence of pebble and cobble-sized sediments in the troughs of C1 bedforms precludes the development of scours in the troughs. Scours are uncommon with C2 bedforms, and if present, are laterally small (0.1 to 0.2 m) and shallow (0.02 to 0.05 m). Linear ripples are usually superposed on the troughs of C2 megaripples.

Facies C megaripples are commonly found near the bar crestlines in areas where the topography is relatively flat-lying. C1 megaripples occur where sediment supply is small, i.e., not enough to cover the troughs.

Facies D - (sinuous megaripples) - Facies D (Fig. 5.23 and 5.24) megaripples are sinuous crested bed features that are laterally continuous and slightly uneven in height which varies up to 0.05 m along crest. Many of these bedforms grade laterally into Facies C. Morphologically, the bedforms of Facies D are more three-dimensional compared with Facies C bedforms (two dimensional).

This facies is subdivided into: (D1) sinuous megaripples with pebble and cobble-sized sediments in the troughs (e.g., East Noel Bar, Selma Bar) and (D2) sinuous megaripples with sand-sized sediments in the troughs (e.g, Selma Bar, Noel Shore Bar, Noel Bay Bar). With D1 type megaripples, the bedform troughs are flat and featureless. The troughs of D2 megaripples have well-developed spurs and scours. Both D1 and D2 types have an alternating saddle lobe crestline configuration which is out-of phase in the downcurrent direction. Bedform height is greatest

FIGURE 5.23: Facies D bedforms (sinuous crested megaripples).

A. Sinuous crested megaripples with pebble and cobble sized sediments exposed in the trough on East Noel Bar (Facies D1). Scale is 1 m long.

B. Close-up view of some larger, sinuous crested megaripples with coarse sediments exposed in the troughs (Facies D1). Scale is 1 m long. View is to the southwest on East Noel Bar.

C. Sinuous crested megaripples with sand-sized sediments in the troughs (Facies D2) on Noel Shore Bar. Note the occurrence of broad, shallow scours in the troughs of the megaripples. Scale is 1 m long.

D. Sinuous crested megaripples with sand-sized sediments in the troughs (Facies D2) on the north side of Selma Bar. View is to the south-southeast. Note the well-developed scours and lee-side spurs. Some crestal platforms are planed-off. Note the people (centre background) for scale.

E. Planed-off crestal platform of a Facies D3 megaripple. Scale is 1 m long. Note heavy mineral streaking on platform.

F. Irregular crestal elevation of a sinuous crested megaripple (Facies D2) with well-developed spurs and scours. View is to the north, towards the crestline of Noel Shore Bar. Scale is 1 m long.

G. Planed-off megaripples (Facies D3) near the crestline of Noel Shore Bar. Note well-developed catenary spurs and elongate scours in the trough of the megaripple. Scale is 1 m long.

H. Swept caternary crestline of Facies D3 megaripples on Noel Shore Bar. View is to the southwest from the bar crest. Scale is 1 m long. Note the current ripples superposed on the megaripple spurs and lee-side slopes.


A


B


C


D


E


F

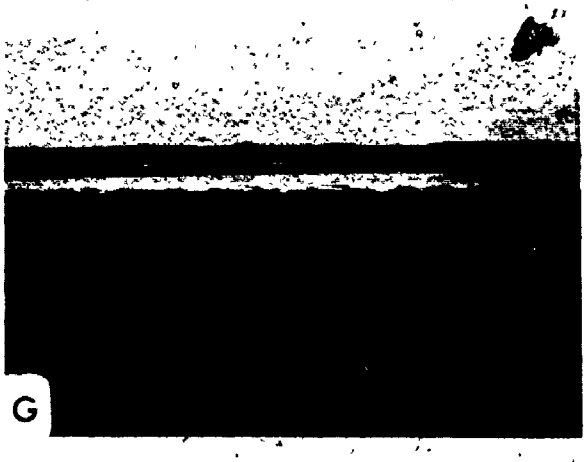
G

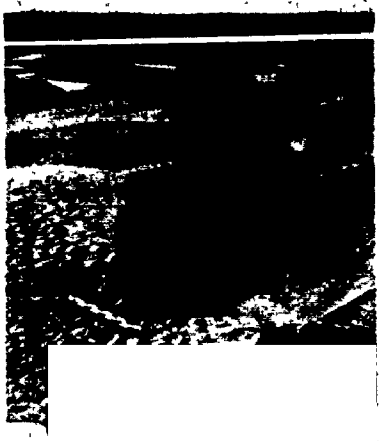

FIGURE 5.24: Facies D2 (sinuous crested megaripples with scours), Facies E (irregular megaripples) and Facies F (catenary megaripples) bedforms.

A. Sinuous crested megaripples (Facies D2) with regularly spaced scours in the troughs. View is to the northeast, near the crest of Selma Bar. Scale is 1 m long.

B. Close-up view of sinuous crested, scoured megaripples (Facies D2). Note: Spur and scour development and ripple fans. Hammer is approximately 0.3 m long.

C. Sinuous crested megaripples (Facies D2) with well-developed scours and spurs, but an irregular crestal elevation. Note packsack for approximate scale (about 0.5 m high).

D. Large scour into the stoss-side of a Facies D2 megaripple on the southeast side of Noel Shore Bar. Scale is 1 m long.

E. Irregular crested megaripple with numerous small scours in the stoss-side of the bedform (Facies E). View is to the northeast, near the north side of Noel Bay Bar. Scale is 1 m long.

F. Facies E megaripple near the north side of Noel Bay Bar. Note the irregularity of the megaripple outline with respect to elevation and plan, and the small scours on the stoss-side. Scale is 1 m long.

G. Remnant catenary megaripples (Facies F) along the southeast end of Noel Bay Bar. Crestlines have been disrupted by late stage ebb runoff and falling water levels. Scale is 1 m long. View is to the southwest.


A


B


C


D


E


F


G

of the saddles (by about two-thirds the height). The scours of the D2 megaripples are generally covered with ripplefans (Allen, 1968 b, p. 84-87). Linear ripples are superposed on the spurs of both types. Stoss-sides have short, crestal platforms and laterally uneven lower stoss-side slopes. The latter result from reattachment and scouring of the flow from the upflow bedform crestline.

A third subfacies (D3), of Facies D, are megaripples similar to D2 bedforms but with a broad, near-horizontal planed-off crestal platform up to several meters in width and laterally continuous. D3 megaripples are laterally uniform in crestline elevation, but trough levels vary from saddles to lobes depending the extent of scour and spur development (which is generally good). Lee-slopes are near the angle of repose as with D1 and D2 megaripples, and lower stoss-side morphology is similar to the other Facies D subfacies. Morphologically, the lower stoss-side slopes of the D3 subfacies bedforms are steeper (8 to 10 degrees versus 5 degrees). In some areas, the megaripple is almost completely planed-off (e.g., southeast corner of Noel Shore Bar); thus, there is little or no evidence of a lower stoss-side surface. As a result of the planing-off of the megaripple crests, subfacies D3 features have large and a wide range of length/height ratios (15 to 40), compared with 15 to 20 for subfacies D1 and D2.

The stoss-side surfaces of the Facies D megaripple are covered with sinuous and linguoid current ripples (including some planed-off crestal platforms). Ripples in the scours are generally linear to sinuous crested.

Facies D megaripples are found in areas that are topographically sloping along the sides of the bars or along sides of and over secondary bar crestlines (e.g., Noel Shore Bar, Selma Bar).

Facies E - (irregular megaripples) - The megaripples of Facies E (Fig. 5.24 E and F) are extremely sinuous to irregular crested and laterally discontinuous. Crestline elevations are very irregular, varying several tenths of a meter in height laterally. Many lee slopes are poorly developed and at about 25 degrees. The stoss-sides are covered with small, 0.20 to 0.30 m wide by 0.20 m deep scours, irregularly

are evident in the bedform troughs but these have generally been completely destroyed by late-stage ebb runoff in the troughs. Bedform crestlines extend laterally for only a few meters before being disrupted by crestline bifurcation, scours and/or late-stage ebb runoff channels that have eroded through low areas in the crest. Sinuous and linguoid current ripples are superposed on the stoss-sides.

Compared with Facies C and D megaripples, the features of Facies E have steeper length/height ratios (e.g., 15 to 20).

Facies E megaripples occur in the lee of an ebb shield but where currents can flow around the shield (e.g., north-east side of Noel Bay Bar).

Facies F - (catenary megaripples) - Facies F (Fig. 5.24 G) megaripples are transverse catenary bedforms with out-of-phase saddles and lobes in direction of flow. The saddles are slightly rounded, possibly due to late-stage ebb flow modification. The crestline elevation varies only a few tenths of a metre laterally. Bedform heights are greatest opposite the megaripple lobes in the scours. Lee slopes are less than the angle of sediment repose and the brinklines are rounded. Stoss sides are uneven laterally because they are part of spur and scour development from the upflow bedform, i.e., stoss-sides on downflow megaripple are slightly concave upwards opposite a scour and slightly convex upward opposite a spur. Length/height ratios are 15 to 20.

Bedforms belonging to Facies F are found only along the southeastern margin of Noel Bay Bar, south of the bar crestline and on the steepest bar slopes (12 to 15 degrees). Towards the west within this area, the catenary megaripples gradually diminish in height and are almost completely obliterated at mid-bar. Within the western half of this area, the presence of isolated scours (Fig. 5.21 B) and somewhat catenary shaped undulations is the only evidence to support extension of Facies F to include the whole southeastern margin of Noel Bay Bar.

Facies G - (ebb modified flood bedforms) - This facies includes four subfacies of bedforms which can be described as ebb-modified flood bedforms and which occur only in the specific locations noted below.

Subfacies G1 (Fig. 5.25 A and B) is found along the northwestern margin of Noel Bay Bar and consists basically of low amplitude linear to sinuous crested megaripples with length/height ratios ranging from 20 to 20. The bedform troughs are broad and flat, and there are few scours. Where scours occur, they are small in areal extent (a few tenths of a metre) and shallow (a few hundredths of a metre). Crestlines are fairly uniform in height where no superposed bedforms are present. Lee slopes have relatively low angles (compared with the bedforms of Facies C and D) and stoss sides are gently sloping (5 degree angle), but the latter tend to be somewhat chaotic in morphology due to the superposition of small megaripples. The dominant megaripple is oriented generally towards the northwest while the superposed asymmetrical features face almost due west. The superposed megaripples are particularly evident on air photographs but difficult to perceive on the bar. Their lengths are of the order of 2 m and heights of 0.10 to 0.12 m (ripple index = 20). These superposed megaripples resemble an ebb cap in many ways; thus the large bed feature on which they are superposed may be an ebb-modified flood feature.

Since the west end of Noel Bay Bar is exposed to the strongest wave activity, bedforms located here show the greatest degree of wave modication, which is usually a rounding and smoothing of the bedform crestlines and brinklines.

Subfacies G2 (Fig. 5.25 C and D) is found along the southwestern edges of Noel Bay Bar and extends from the western end of the bar, eastwards to midbar. Bedforms in this area are large with ripple indices from 30 to 50. These bedforms appear to be large ebb capped (thus ebb modified) megaripples. Crestlines are fairly uniform in elevation and laterally continuous within the narrow width of the zone. There are no scours, either in the troughs on stoss-sides. Lee-side angles are lower than those from Facies C and D and the lee slopes are characterized by two segments: a long upper slope at about 25 degrees, and a short lower slope at about 5 to 8 degrees (as high as 12 degrees). The low lee-side slope possibly represents the ebb-modified flood bedform stoss side. The ebb bedform stoss-sides are convex upwards and covered with primarily linguoid ripples. There is some evidence of smaller megaripples climbing

FIGURE 5.25: Facies G bedforms (ebb modified flood megaripples).

A. Low amplitude, linear to sinuous crested megaripples with broad flat troughs and few scours (Facies G1). View is to south across the west end of Noel Bay Bar. Scale is 1 m long.

B. Facies G1 megaripples with superposed ebb bedforms. View is the southwest, across the west end of Noel Bay Bar. Scale is 1 m long.

C. Large ebb capped megaripples (Facies G2) with relatively uniform crestal elevations and linear to sinuous crestlines. View is to the north-northeast across the west end of Noel Bay Bar (from the south side). Scale is 1 m long.

D. Facies G2 megaripple showing a small megaripple climbing the stoss-side slope of the larger bed feature. View is to the north across the west end of Noel Bay Bar (from the south). Scale is 1 m long.

E. Small ebb-capped megaripples (Facies G5) near the crest of the western part of Selma Bar. Left end of scale rests on ebb cap; right end rests on remnant flood stoss side. View is to the southeast. Scale is 1 m.

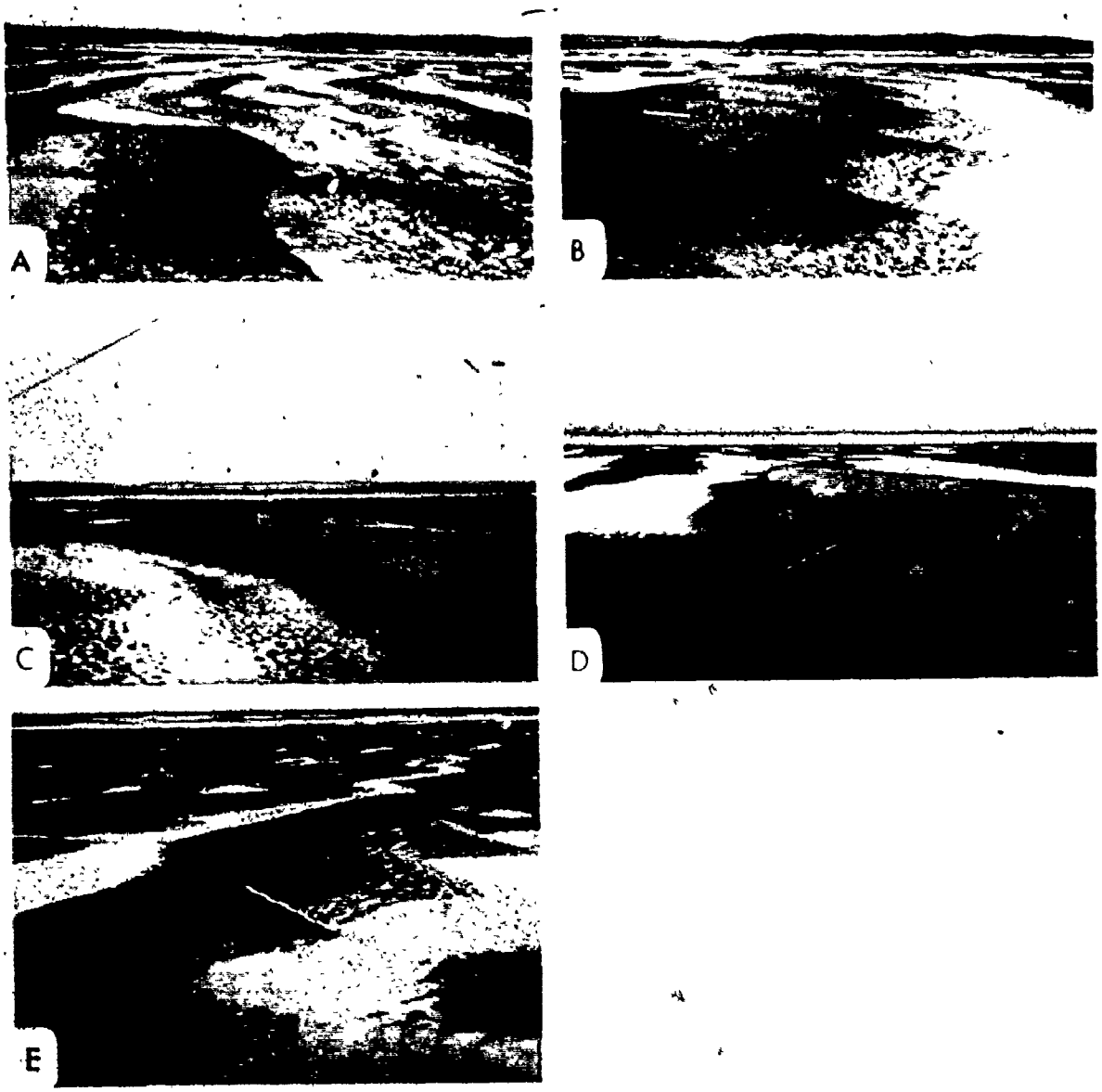
A
B
C
D
E

up the stoss-side of the large ebb feature (Fig. 5.25 D). Late stage ebb runoff and wave action generally have very little effect on these bedforms.

Subfacies G3 is found along the western part of Noel Shore Bar (see air photo, Fig. 3.27) and consists of very large flood asymmetrical sand waves with lengths of 35 to 55 m and height in the order of 1.5 to 2.0 m (length/height ratios = 25 to 30). These large bed features are lunate crested and continuous over the width of this part of the bar. Linear and scoured megaripples previously discussed under Facies C and D are superposed obliquely on the large bed features.

Subfacies G4 (Fig. 5.26) includes the sand waves described by Knight 1971, 1972, 1973) and Dalrymple et al. (1975), and defined earlier in this chapter under terminology. On Selma Bar, these bedforms are large flood asymmetrical bed features (length/height ratios are generally greater than 30 and as large as 80). The flood lee slopes are not at the angle of repose but at about 12 to 15 degrees. The crestlines are straight to sinuous and continuous across the bar from the southern margin towards the bar crest. Small, ebb-oriented megaripples are superposed obliquely on the flood features at low tide. The soundings at high slack water show that the sand waves have superposed flood megaripples.

The superposed megaripples are straight to slightly sinuous. Megaripples at the crest of the sand wave are commonly planed-off. Some megaripple troughs are weakly scoured. Megaripple heights (Fig. 5.2) and length decrease down the sand wave stoss side (in the ebb flow direction). Lee slopes are avalanche faces close to 30 degrees and stoss-slopes are gently sloping, convex upwards, planar to rippled surfaces. Heights are uniform laterally.

A single, similar sand wave, but ebb-oriented occurs on East Noel Bar (Fig. 5.26 E and F) in the northwest corner of the bar. This sand wave has superimposed ebb oriented megaripples obliquely oriented to the sand wave orientation.

Sand waves seem to occur typically in coarse-grained sands (0.5 to 1.5 Ø) compared with megaripples (1.0 to 2.0 Ø) and in areas that are very strongly ebb or flood dominant.

FIGURE 5.26: Facies G4 bedforms (ebb modified flood features = sand waves).

A. Large sand wave on the southeast side of Selma Bar with obliquely superposed megaripples. View is to the southwest. Scale (in person's hand) is 1 m long.

B. Close-up view of megaripples that cap sand waves. Sand wave crestline is to the left; view is to the south along the crestline of the sand wave. Note presence of superposed megaripples and ripples on the sand wave. Scale is 1 m long.

C. Straight to sinuous crested, simple sand waves with only a single ebb megaripple cap near the sand wave brinkline. View is to the northwest across Selma Bar. Note people (right centre) for scale.

D. Close-up view of single ebb megaripple cap developed along sand wave brinkline. Scale is 1 m long.

E. Ebb oriented sand wave near the northeastern edge of East Noel Bar. Note composite nature of lee-sides slope and various late ebb runoff features.

F. Trench through sand wave on East Noel Bar showing successive cross-sets and reactivation surfaces. Note scale at bottom of trench.

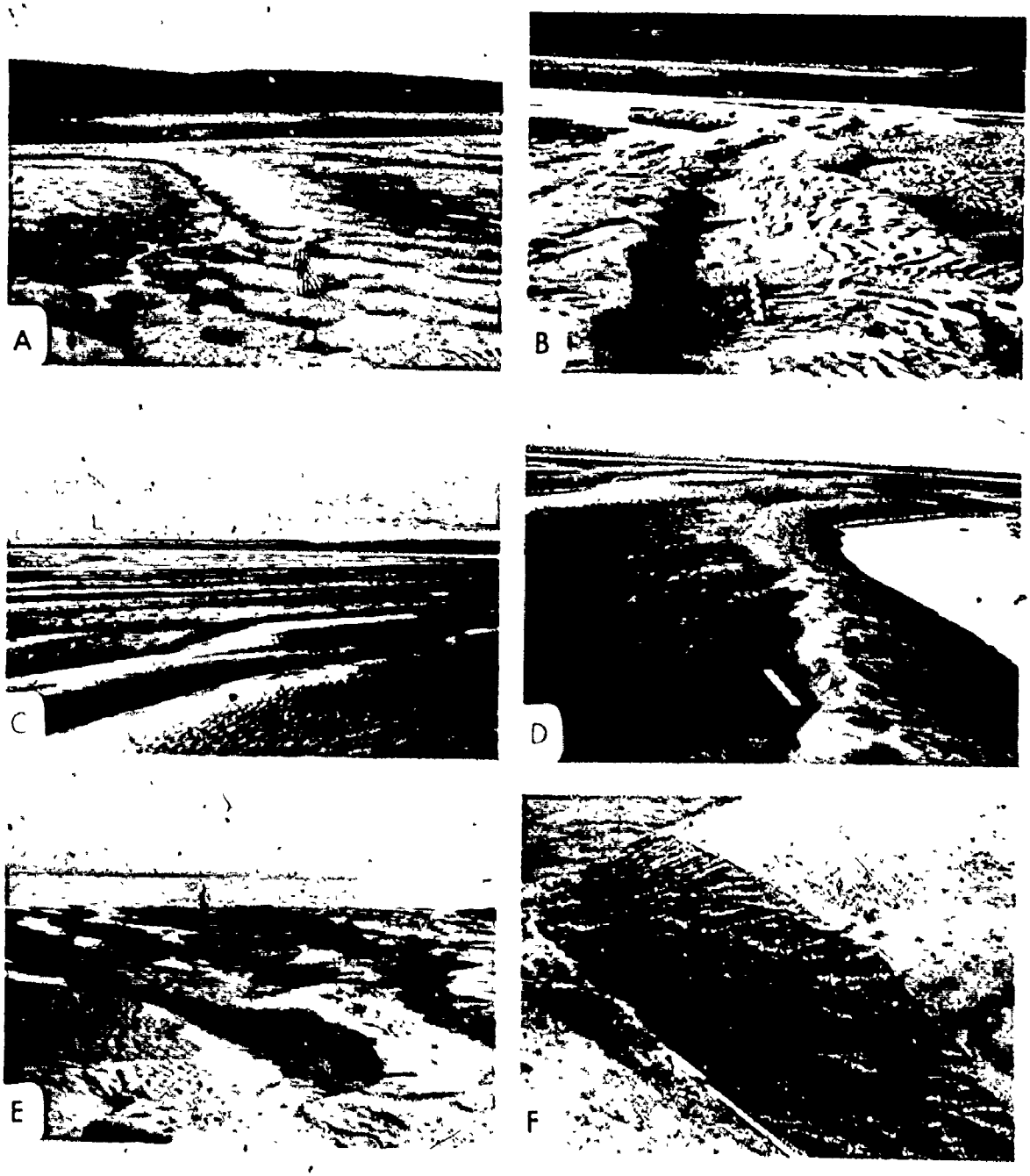
A
B
C
D
E
F

Subfacies G5 (Fig. 5.25E) occurs on the western part of Selma Bar and is characterized by ebb capped flood megaripples. Lee slopes consist of a short (0.10 to 0.15 m)slope at about 25 degrees and a relatively long lower slope at 6 to 8 degrees which is the remnant flood stoss side. The ebb stoss slope has a low angle (zero to 3 degrees) crestal platform and a 12 to 14 degree lower stoss-slope. Crestlines are laterally straight to sinuous in plan. Some shallow depressions along the bedform trough may be remnant flood trough scours. The bedforms of subfacies G5 have length/height ratios ranging from 20 to 30.

Recap and Discussion

The analysis of the areal variation of the dimensions and types of bedforms on the intertidal sand bars reveals that: (i) bedform heights vary as a function of the bedform length; (ii) bedform size and three-dimensionality increase down the gentle side, away from the crestline of the bars; (iii) the steep side of the bars are characterized by a relatively smooth intertidal shoreline and a plane or nearly-plane bed; (iv) sand waves occur only in areas where the ebb or flood currents are substantially dominant; (v) the angle of the bedform lee-side slopes is controlled by the sediment grain size and the degree of late-stage ebb modification; (vi) the stoss-side slopes of the bedforms are a function of the bedform type; and (vii) bedform crestlines are oriented obliquely to the axis of the bars and generally diverge away from the crestline of the bars.

A comparison of the dimensional and morphological properties of the intertidal bedforms relative to the sediment characteristics (Fig. 3.21, 3.26, 3.31 and 3.36) and the current strengths and durations (Figs. 4.11, 4.13 and 4.16; Tables 4-6, 4-8 and 4-10) indicates that: (i) bedform size and type are determined by the current strength and flow duration (i.e., stronger and longer flows produce larger and more three-dimensional bedforms), and sediment size to some extent (i.e., larger bedforms generally occur with coarser grain sizes); and (ii) current flow generally occurs at an oblique angle to the orientation of the bedform crestlines, but sand waves are usually less oblique to the currents than megaripples. The areal pattern of bedform crestline orientations generally supports the model for tidal current flow over and the

discussed in Section 4.4 (Fig. 4.24).

Facies C, D and G are the most common types of bedforms on the sand bars. For a typical intertidal sand bar located away from the shore, the areal distribution of bedform facies might be as follows: Facies A is restricted to the steeper, ebb-dominated side of the bar; Facies A grades upslope into Facies B near the crest of the bar and(or) laterally in Facies F near the exposed ends of the bar's steeper side (Facies F bedforms reflect directions of current flow across the bar crestline before emergence and parallel to the bar crestline after emergence); Facies C typically occurs along the upper part of the gently sloping side of the bar near the bar crest; Facies C bedforms grade laterally downslope into Facies D bedforms which commonly occur along the intertidal margin of the sand bars; Subfacies D3 bedforms are a modification of Subfacies D2 bedforms and generally occur on the topographically higher parts of the sand bar crestline or flanks of the crestline; Facies E bedforms, although relatively uncommon, occur in the lee of a topographic shield where the currents develop a horizontal eddy; and finally, Facies G bedforms are restricted to areas of the bar that are straongly ebb- or flood-dominant, e.g., at the exposed ends of the sand bar or on the flanks of a topographic shield. The distribution of the bedform facies and subfacies is primarily the result of the interaction between the areal and temporal variations of the current properties (strength, depth, duration and direction), the grain size of the sediments, and the topgraphy of the sand bars.

5.5 TIME VARIABILITY

Simons, Richardson and Nordin (1965) determined that different bed configurations succeeded one another in a definite sequence as the hydraulic conditions were changed (i.e., each bedform type occurred under a definite range of hydraulic conditions). Some of the beform properties, such as dimensions and orientations were largely dependent on the flow variables (e.g., current strength and direction, depth and duration). Allen and Friend (1976), Jain and Kenedy (1974) and Raichlen and Kennedy

(1965), for example, found that the height and length of bedforms (specifically ripples and dunes) was dependent on the duration of the flow at or above the threshold of the bedform's "existence-field" (Allen and Friend, 1976). Thus, ripples and dunes (or megaripples) have a complex time - hydraulic dependency. The purpose of this section is to discuss some of the time-variant properties of the intertidal bedforms in Cobequid Bay.

Semidiurnal Tidal Cycles

Van Veen (1935) was one of the first to demonstrate the reversal of bedforms during a tidal cycle and that the asymmetry of the bed features was related to the relative strengths of the ebb and flood currents. More recent discussions on the reversal of tidal bedforms included Boothroyd and Hubbard (1975), Jones et al. (1965), Klein, (1970a) and McCave (1971).

Echo soundings made during periods of high slack water over the bars indicated that many of the bedforms which were ebb oriented at low water became flood-oriented during the flood phase of the tide. The degree of reorientation and reworking of the bedforms depended on the time-velocity asymmetry and flow duration of the tidal currents (both of which were dependent on the degree of topographic exposure or shielding, the local bed elevation and flow cross-sectional area), and to the time in the lunar monthly cycle (because current strength is partially a function of the tidal range). Bedform reversal and reworking varied from complete reorientation to only slight reworking and modification.

Successive modification of tidal bedforms in Cobequid Bay were observed by echo sounding during the ebb and flood. In areas where the ebb and flood currents were almost equal in strength and duration (e.g., SB-6; Table 4.10; Figure 4.14), the bedforms reversed completely with each phase of the tide (Figure 5.27). At low tide, the ebb oriented megaripples at SB-6 (Fig. 5.23 D and E) had a double-angled stoss side (i.e., a crestal platform with a slope of 4 to 5 degrees and a lower slope at 12 to 14 degrees, both of which were covered with current ripples). The lower stoss slope represents a reworked lee slope of a flood megaripple. The echograms in Figure 5.27 indicate the serial modification and reversal of megaripples during the ebb and flood at SB-6.

FIGURE 5.27: Sequential reversal of megaripples (Facies D) during the ebb and flood along the northwest side of Selma Bar (near SB-6). Times (T) are from high water. The sounding line extends to the west of SB-6.

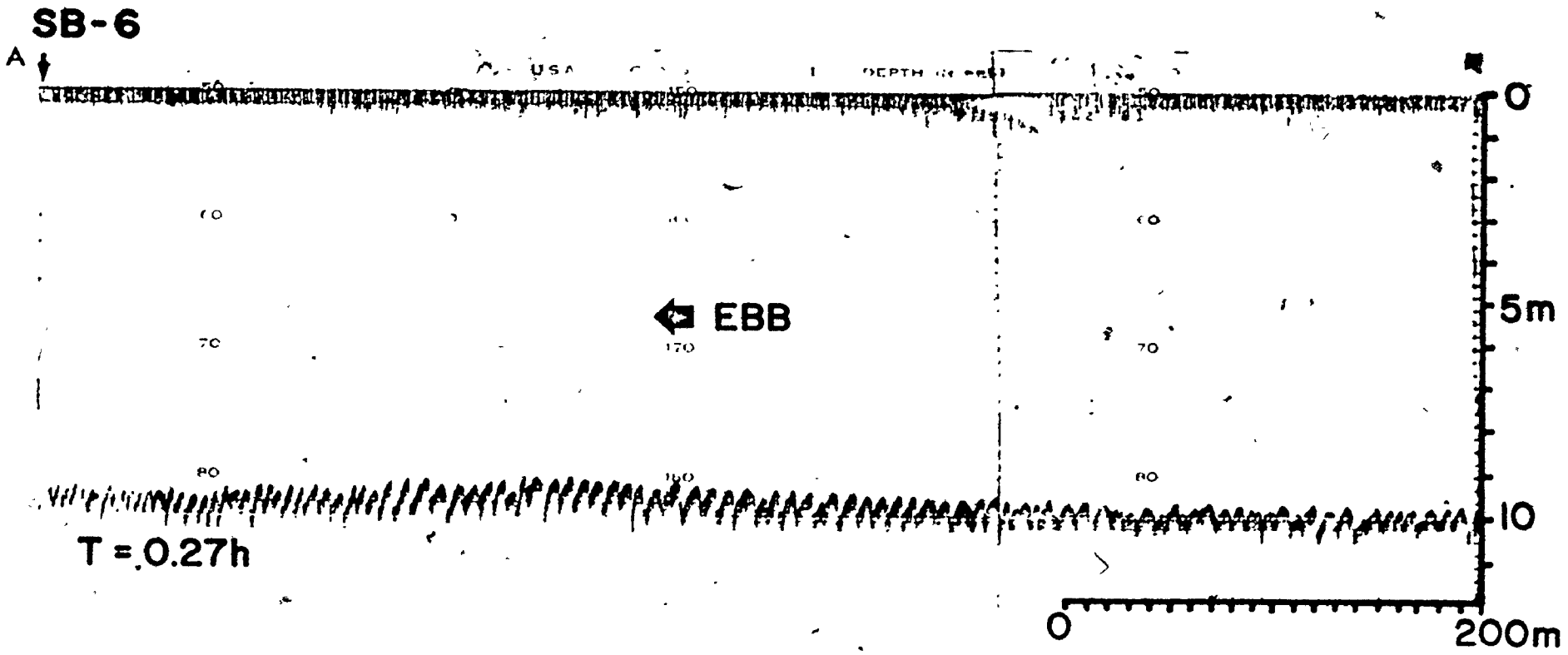
SB-6
A
EBB
T = 0.27h
0
5m
10
0
200m

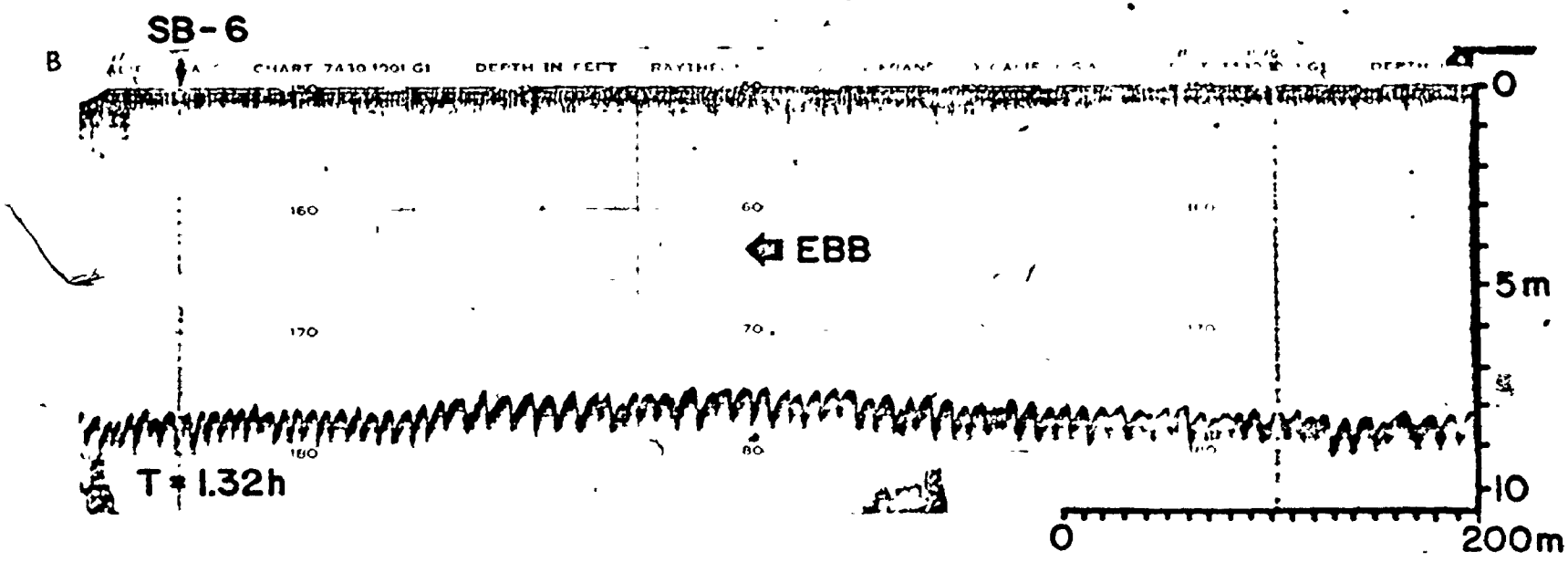

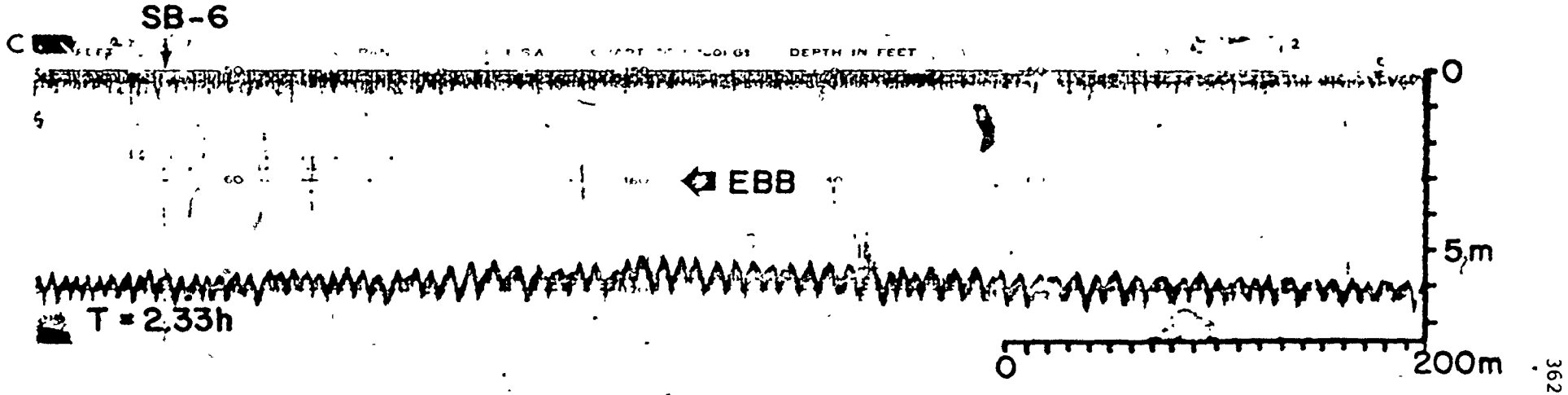

FIGURE 5.27 cont'd

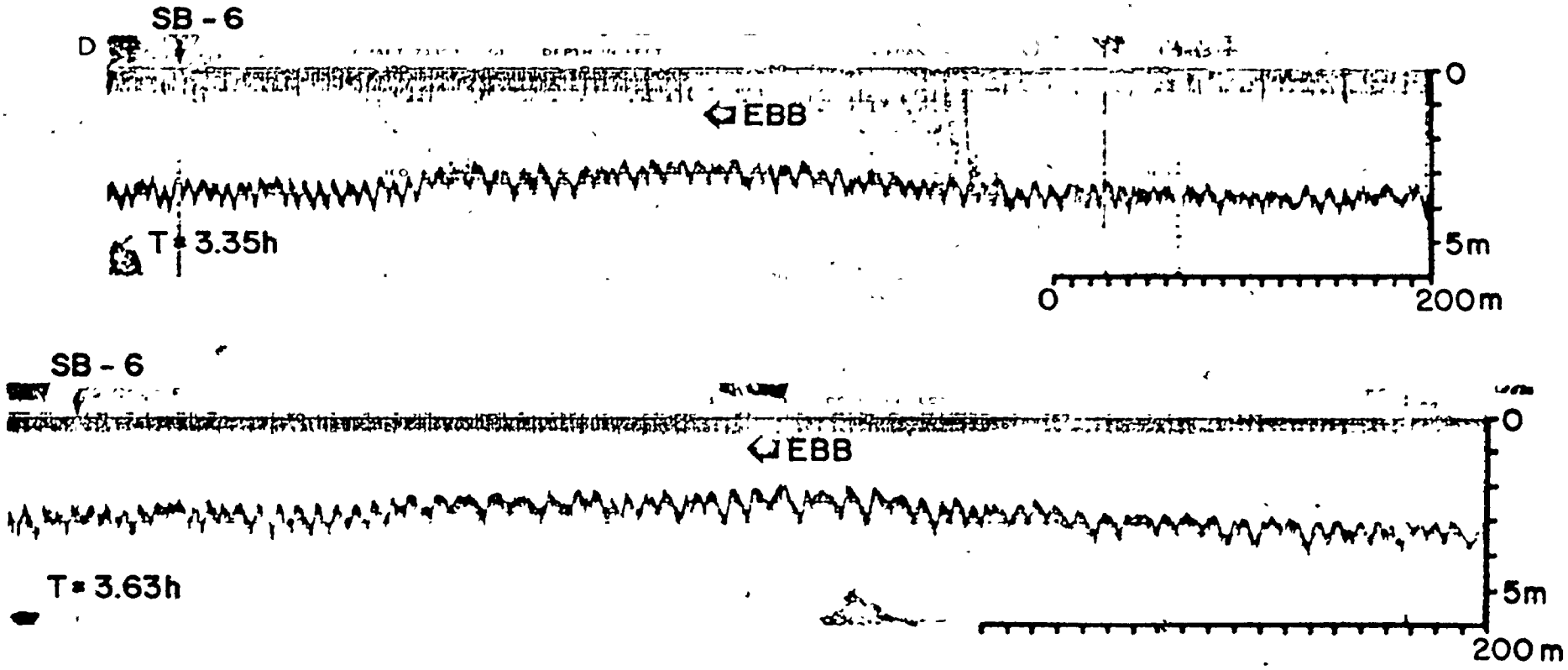

FIGURE 5 27 - cont'd

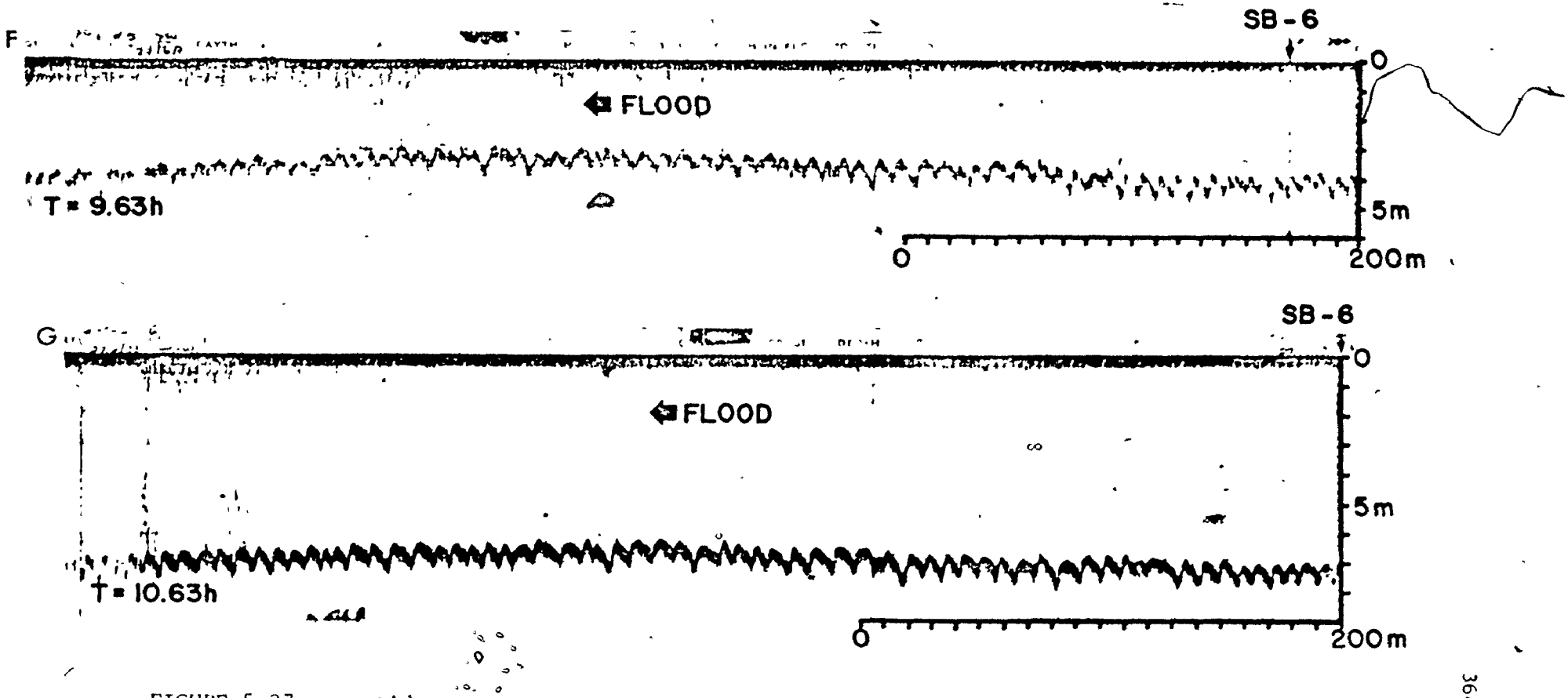

FIGURE 5.27 - cont'd

In areas where the shielding of tidal currents produced a significant inequality of the ebb and flood current strengths (e.g., western ends of Noel Bay Bar, Noel Shore Bar and Selma Bar, and south of the Selma Bar crestline), only partial reversal of bedforms occurred. The bedforms at the west end of Selma Bar, for example, were regular crested megaripples (comparable to Facies D2 bedforms) with lengths and heights in the order of 5 m and 0.2 m (ripple index = 25) at high slack water following a flood tide (Figre 5.28). At low tide, following an ebb these same bedforms are only partially obliterated because the ebb currents have only the duration and strength to produce small, superposed ebb-caps on the modified flood megaripples (Facies G5, Fig. 5.25 E).

Figure 5.29 shows the stages of megaripple reversal and the development of reactivation surfaces during the ebb and flood.

In areas where the time-velocity relation was strongly asymmetrical, such as the area south of the Selma Bar crestline (ebb shield) which was strongly flood dominant, flood oriented sand waves (Facies G4) occurred with obliquely superposed megaripples (Fig. 5.26 A to D) during the ebb and flood. The sand waves did not reverse during a semidiurnal tidal cycle (Fig. 5.30). The superposed megaripples either changed direction or were obliterated and reconstructed during each ebb and flood tide. The echograms in Figure 5.30 show the succession changes in the cross-sectional shape of sand waves during the ebb and flood between SB-2 and SB-13. Note the progression rounding of the sand wave brinkline during the ebb and the presence of superposed megaripples during the ebb and flood.

Areas of small megaripples are usually destroyed and reconstructed with each ebb and flood, thus are impossible to maintain.

Lunar-Month Tidal Cycle

The effect of tidal height and current velocity on the dimensions and characteristics of intertidal bedforms is imperfectly known. Some observations have been made by Allen, G.P. et al. (1969), Allen and Friend (1976), Cornish (1901 b), Hartwell, (1970), Ludwick (1972) and Nasner (1974, cited by Allen, 1976 b). Allen, G. P. et al. (1969) found that dune height varied on about the same period as the tidal range,

FIGURE 5.28: Flood oriented megaripples on the western part of Selma Bar (A) and along the major swatchway across Selma Bar (B). Both areas are flood dominant. Compare (A) with ebb megaripples Facies in Figure 5.25 E (SB-5) and (B) with the Facies C and D megaripples in Figure 5.22 E and 5.24 C.

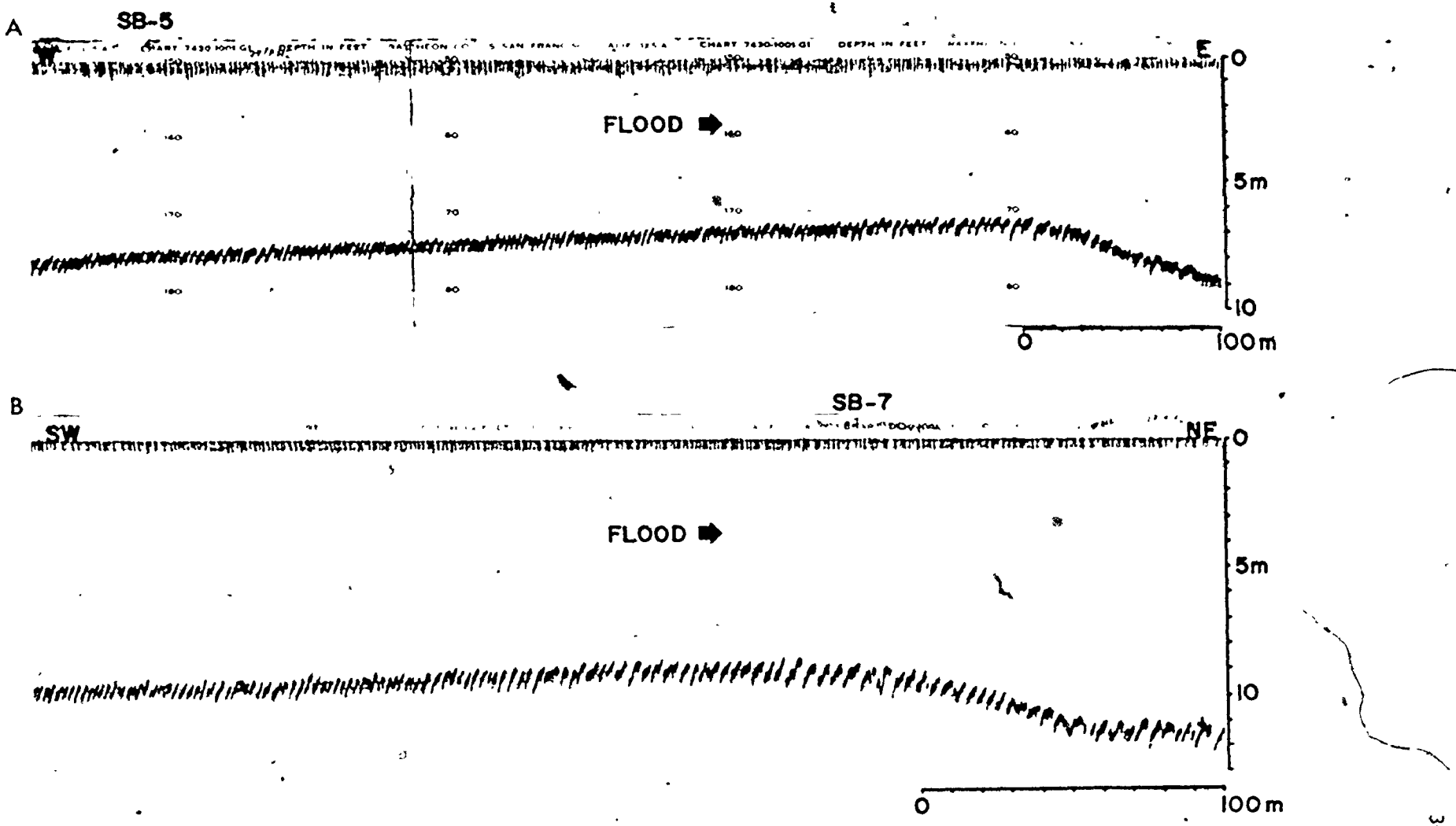
A
SB-5
E
FLOOD
0
5m
10
0
100m
B
SB-7
SW
NE
FLOOD
0
5m
10
0
100m

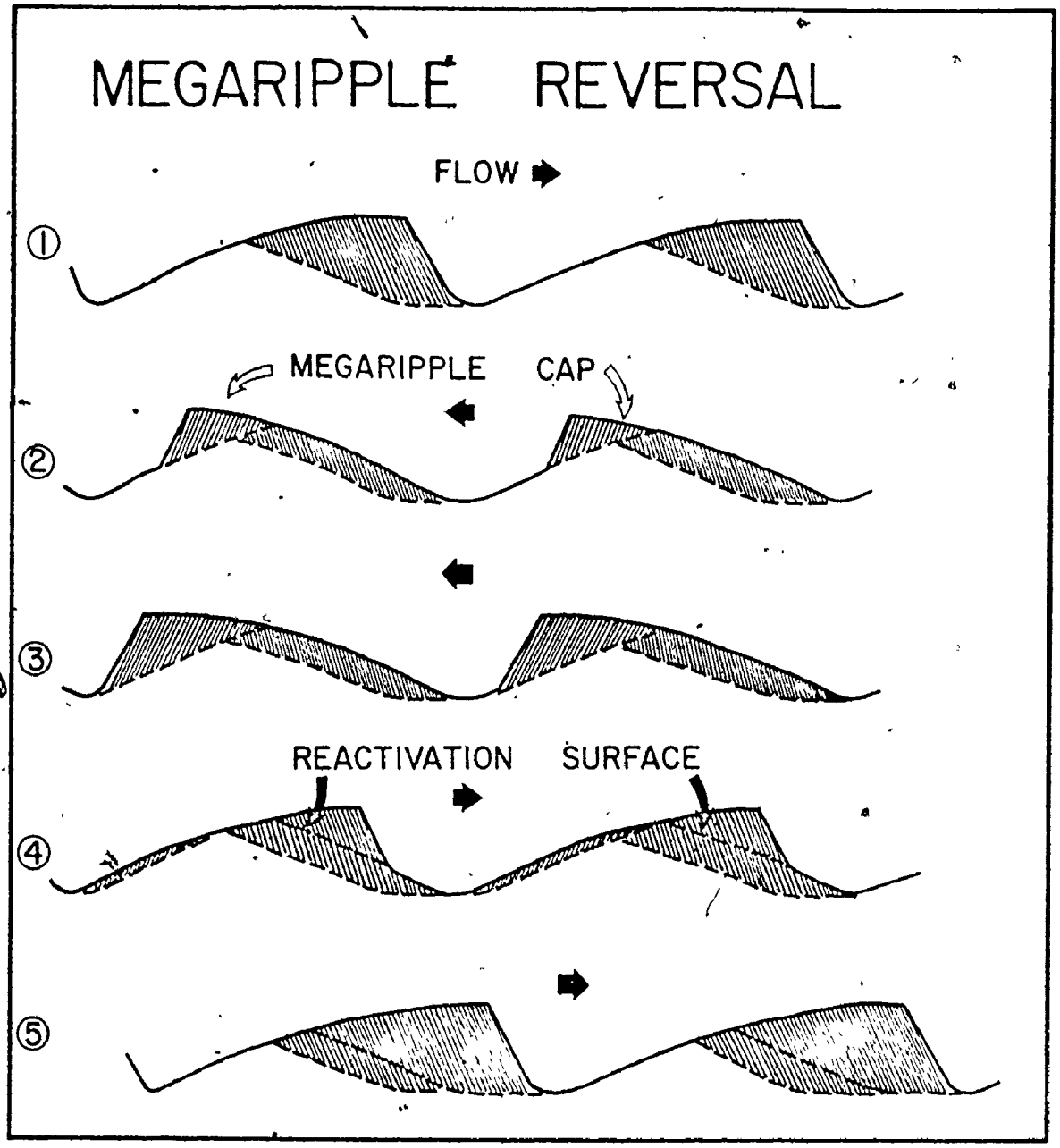

FIGURE 5.29: Stages of megaripple reversal and the development of reactivation surfaces during a tidal cycle.

(1) Megaripple constructed by tidal current flow
(2) Current flow reverses: Crest of original megaripple is eroded and a megaripple cap develops on the remnant megaripple stoss-side.
(3) New megaripple is fully developed.
(4) Current flow reverses to original direction (in 1 above). Crest of reversed megaripple is eroded and a megaripple cap develops in the opposite direction on reactivation surface.
(5) Megaripple is completely reversed and fully developed, but has migrated downflow relative to the direction of dominant flow.

FIGURE 5.30: Sequential changes of the sand waves and the reversal of the small megaripples superposed on the sand waves during the ebb and flood along the south side of Selma Bar. Times (T) are from high water. The sounding line extends to the east of SB-2.

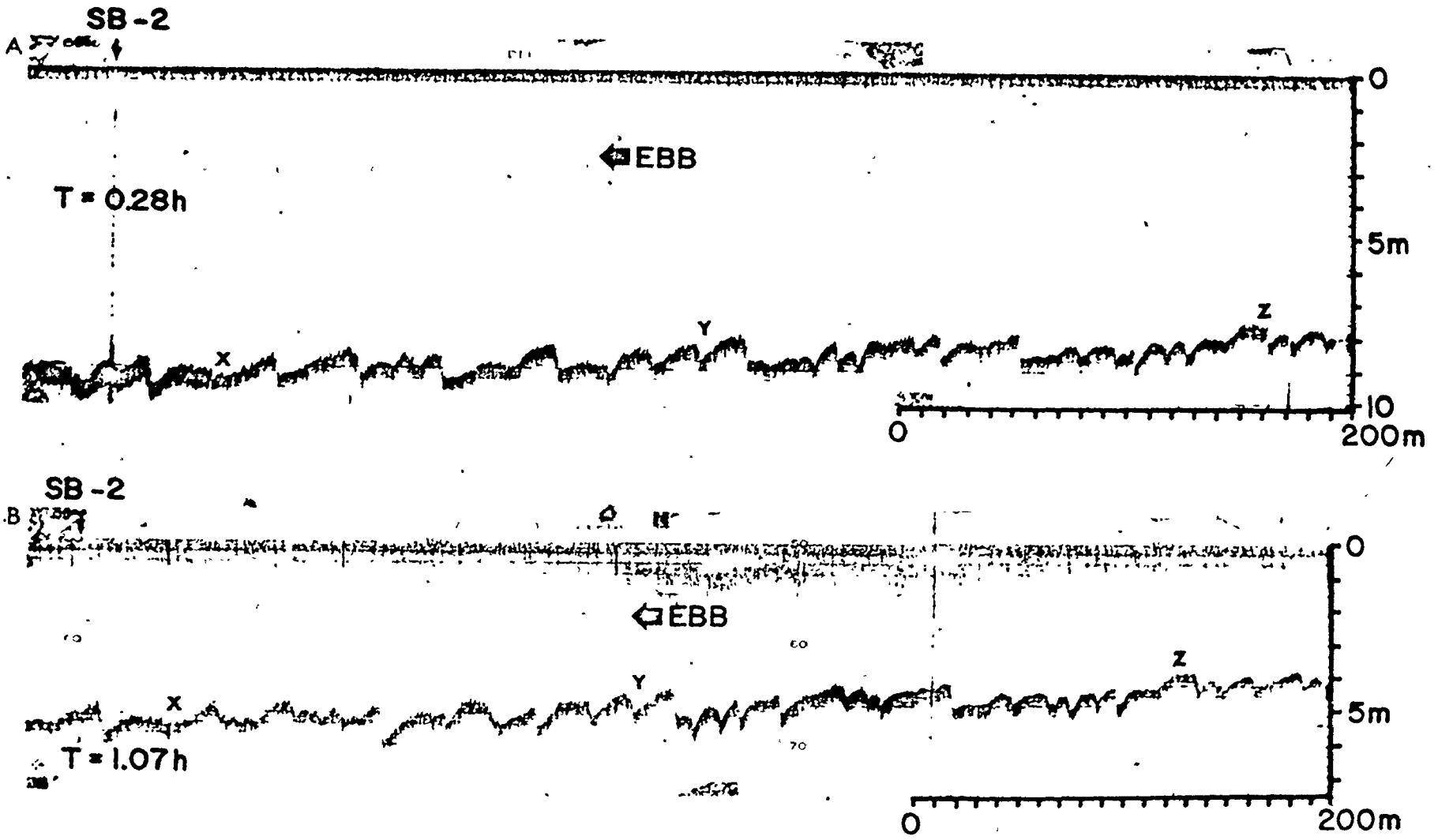
SB-2
A
EBB
T = 0.28h
X
Y
Z
0
5m
10
0
200m
SB-2
B
EBB
X
Y
Z
T = 1.07h
0
5m
0
200m

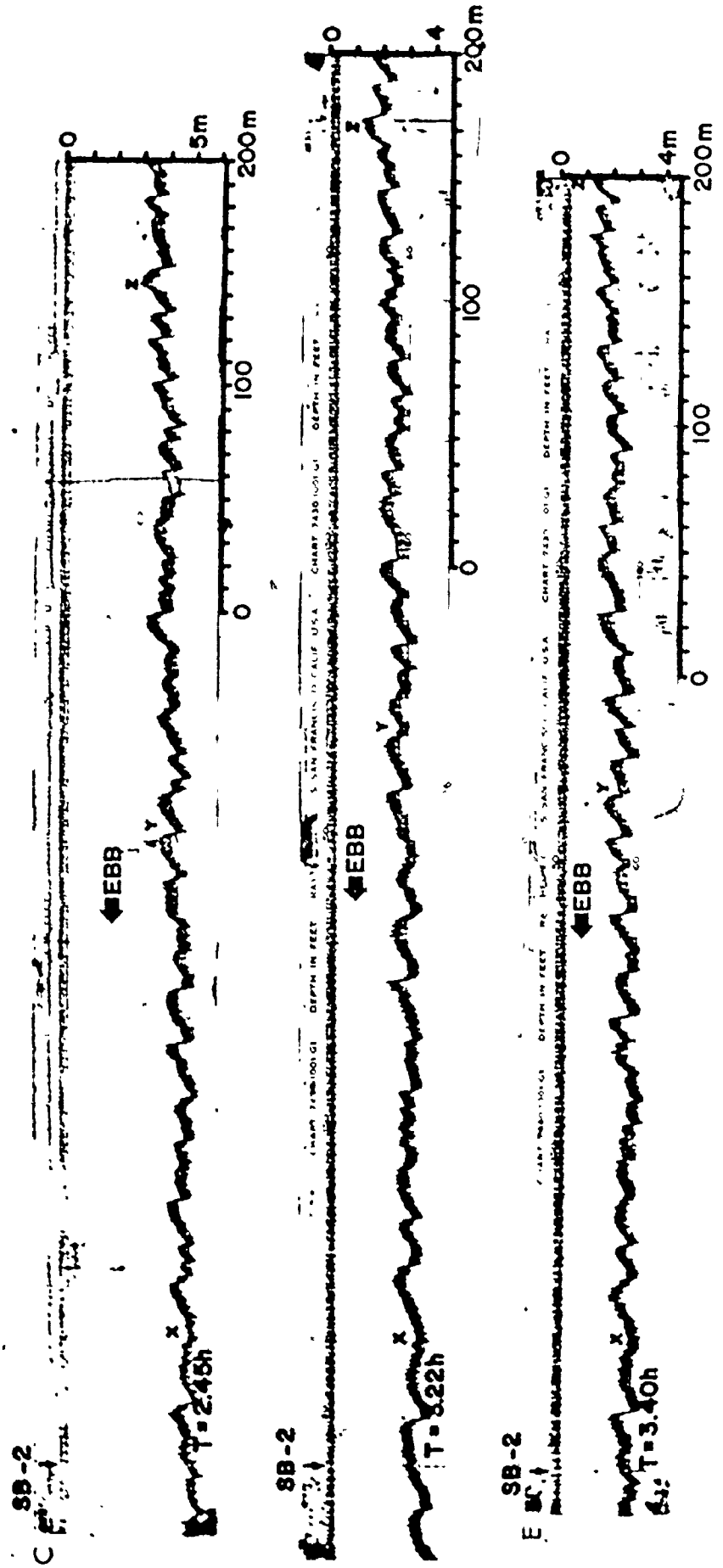

FIGURE 5.30 - cont'd

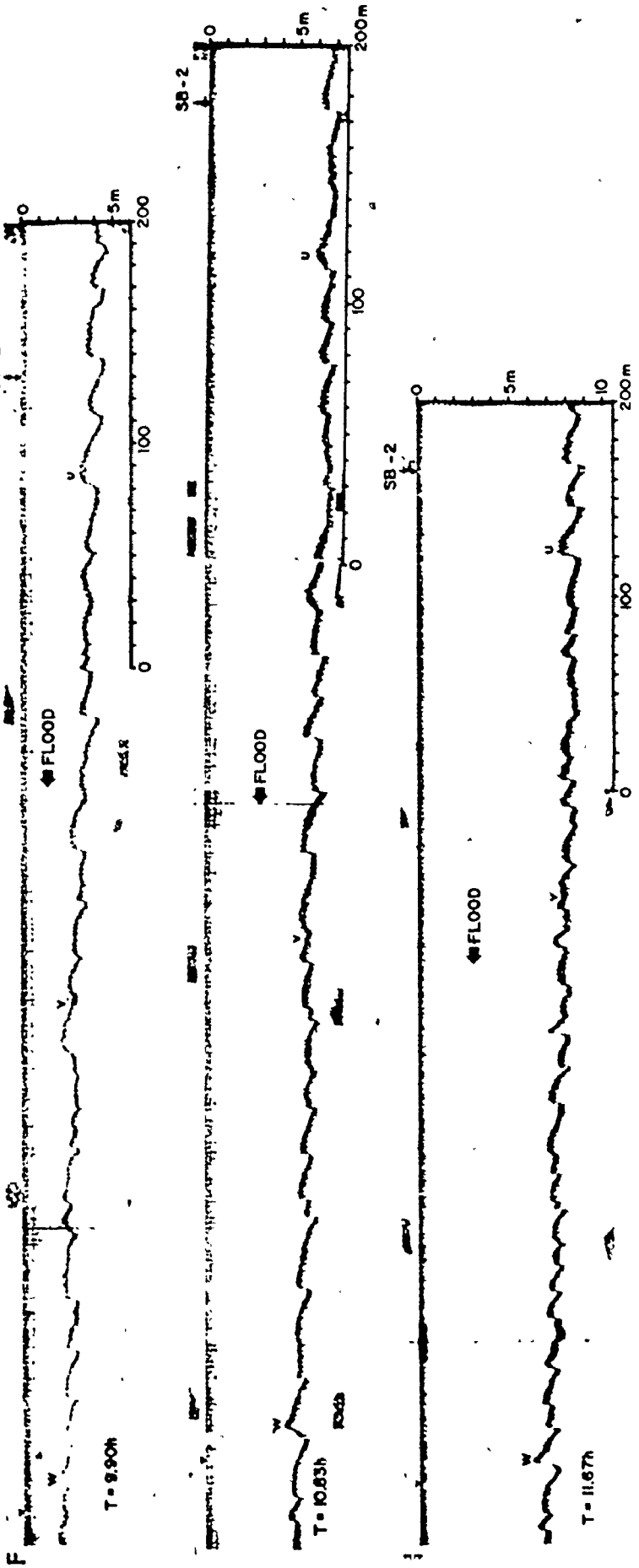

FIGURE 5.30 - cont d.

but with a short lag behind the change of range. Cornish (1901 b) and Hartwell (1970) described the growth of dune height during spring tides and the decrease of height or disappearance of dunes during neap tides. Nasner (1974, cited in Allen, 1976 b) found that dune height and length varied on the same period as the flow discharge from tidal reaches of the River Weser, Germany, and that dune height varied about twice as much as bedform length.

Net migration rates, depth of scour, bed elevation, and the length and height of megaripples and sand waves were monitored at selected locations during the lunar-month tidal cycle. Figures 5.31, 5.32 and 5.33; Table 5-1 summarize some of the results for different bedform types. The average migration rate was determined by measuring the advance (or retreat) of bedform brinklines at several locations along the same or an adjacent brinkline and averaging the migration distance and dividing the average by the number of elapsed tidal cycles since the last measurement date. The plotted value is the average rate of net migration (for the ebb and flood tides combined) since the individual ebb and flood components of migration could not be separated.

The graphs indicate that: (i) the variation of the measured bedform properties (length, height, scour depth, bed elevation, and net migration rate) varied on about the same period as the tidal range during the lunar-month tidal cycle; (ii) megaripples generally moved faster than sand waves or ebb modified flood bedforms (Facies G), i.e., megaripples = 0.2 to 0.8 m per tidal cycle, and sand waves = 0.1 to 0.3 m per tidal cycle; (iii) migration rates, scour depths, bed elevations, lengths and heights for sand waves were more uniform than for megaripples (i.e., the measured properties varied less for sand waves than for megaripples); (iv) a lag occurred between the occurrence of the maximum and minimum migration rates and the occurrence of spring and neap tides; and (v) there is some suggestion that the maximum and minimum bedform heights and lengths lagged behind the occurrence of the spring and neap tides respectively. Unfortunately, the bedform time series measurements are too infrequent and not sufficiently extensive to allow further conclusions with respect to the properties of bedform lag and relaxation times (Allen, 1973, 1974, 1976 a and b).

FIGURE 5.31: Variation of bedform properties at three locations on Noel Bay Bar during a lunar month tidal cycle,
Open Triangles = average net migration rate;
Closed circles = average bedform height.
See Figure 4.1 for locations.
Vertical lines indicate time of spring and neap tides.

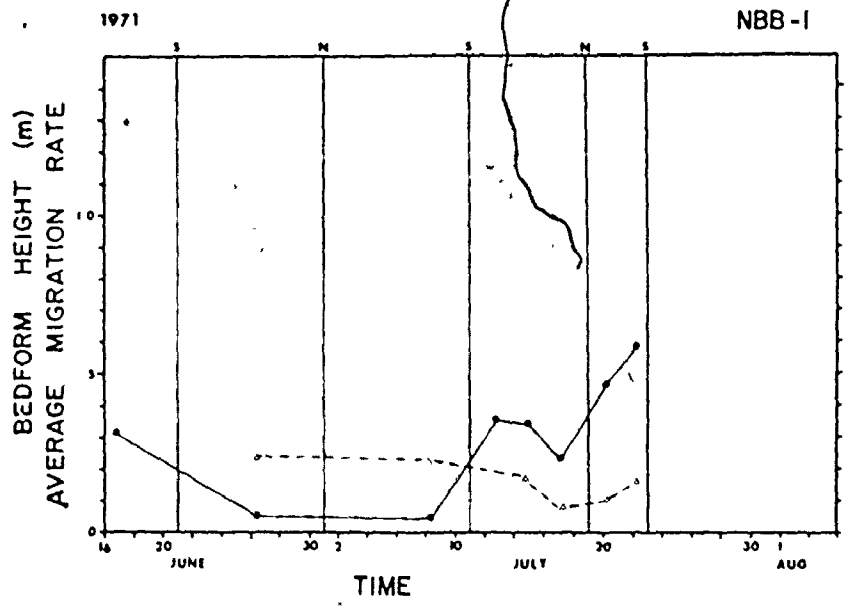
1971
NBB-1
BEDFORM HEIGHT (m)
AVERAGE MIGRATION RATE
S
N
S
N
S
JUNE
JULY
AUG
TIME

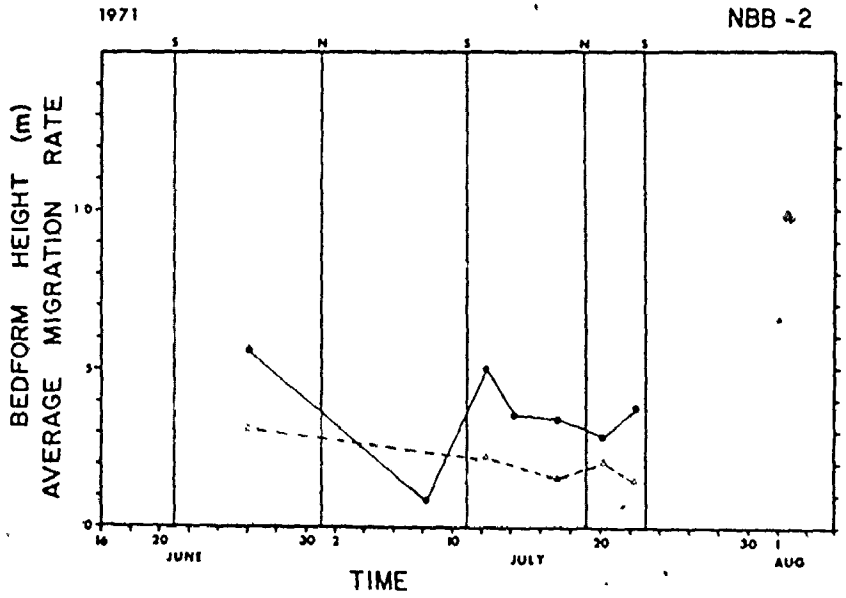
1971
NBB-2
BEDFORM HEIGHT (m)
AVERAGE MIGRATION RATE
S
N
S
N
S
JUNE
JULY
AUG
TIME

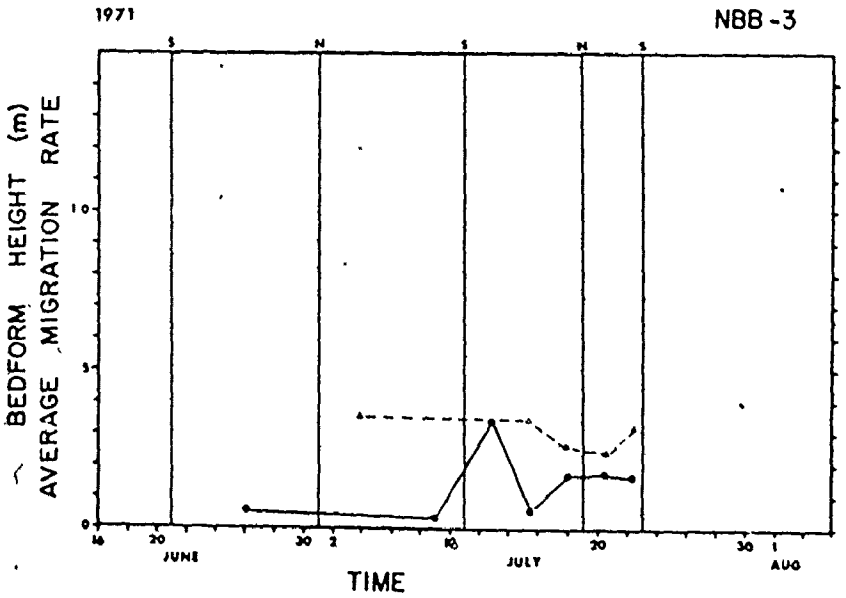
1971
NBB-3
BEDFORM HEIGHT (m)
AVERAGE MIGRATION RATE
S
N
S
N
S
JUNE
JULY
AUG
TIME

FIGURE 5.32: Variation of bedform properties at three locations on East Noel Bar during a lunar month tidal cycle.
Open triangles = average net migration rate;
Closed circles = average bedform height.
See Figure 4.1 for locations.
Vertical lines indicate time of spring and neap tides.

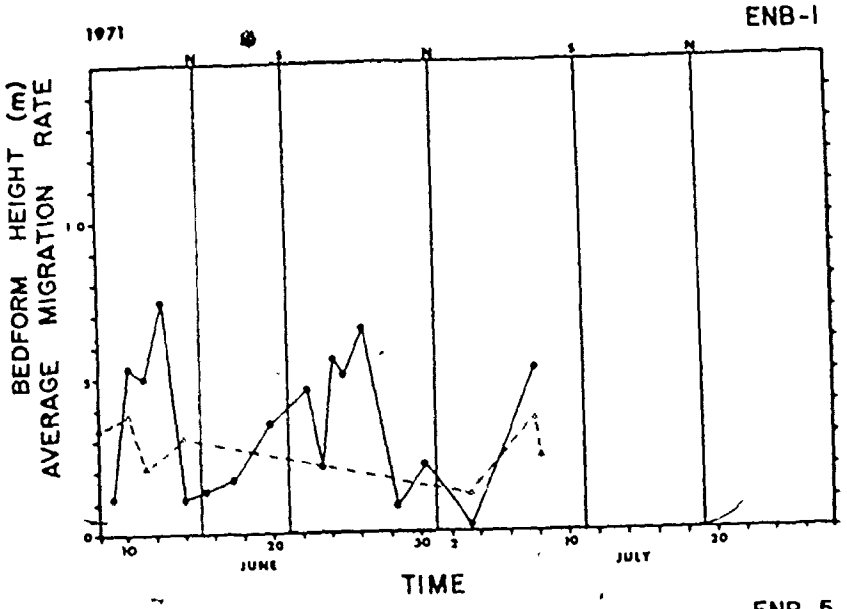
ENB-1
1971
BEDFORM HEIGHT (m)
AVERAGE MIGRATION RATE
JUNE
JULY
TIME

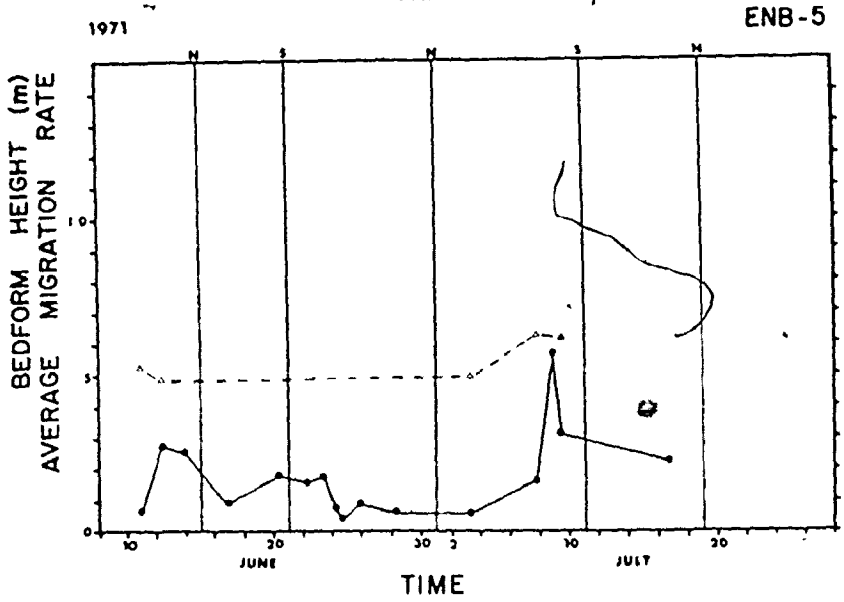
ENB-5
1971
BEDFORM HEIGHT (m)
AVERAGE MIGRATION RATE
JUNE
JULY
TIME

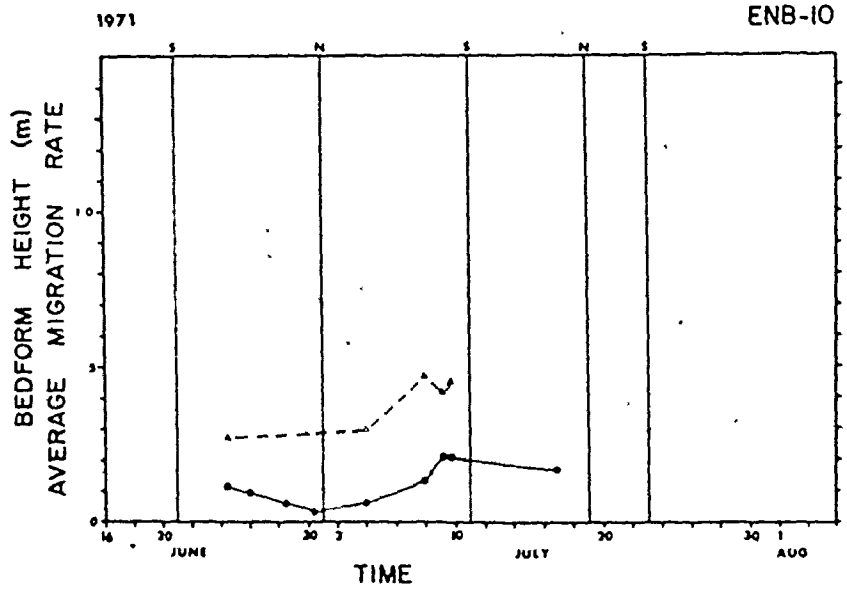
ENB-10
1971
BEDFORM HEIGHT (m)
AVERAGE MIGRATION RATE
JUNE
JULY
AUG
TIME

FIGURE 5.33: Variation of bedform properties at four locations on Selma Bar during a lunar month tidal cycle.
Open square = average bedform length;
Closed triangles = average depth of scour;
Closed squares = average relative bed elevation;
See Figure 4.1 for locations.
SB-5 = Facies S3; SB-6 = Facies D2 and D3;
SB-1 and SB-2 = Facies S4.

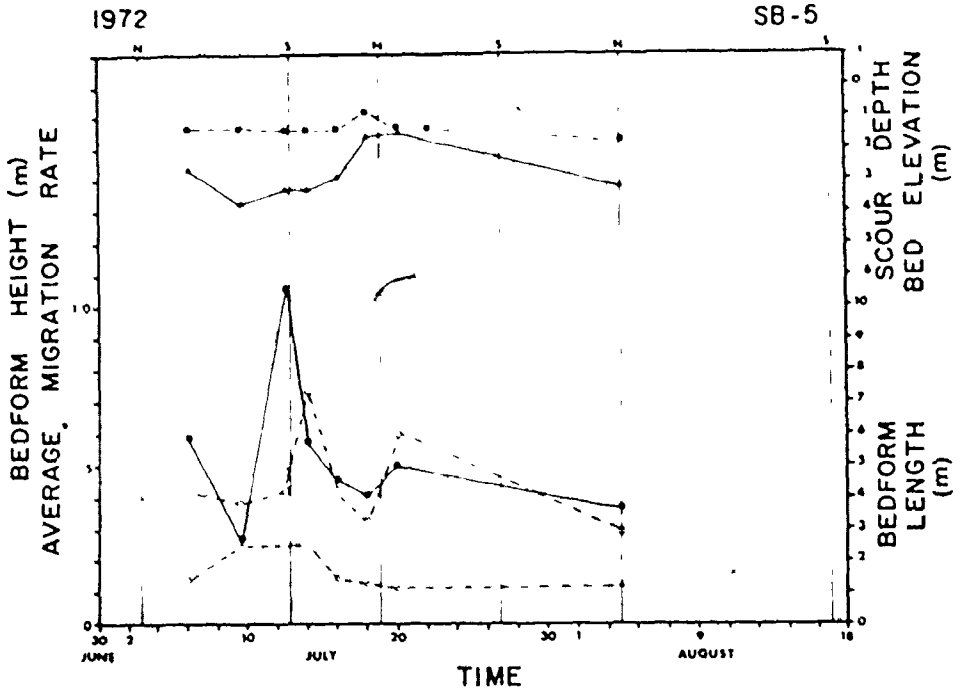
1972
SB-5
BEDFORM HEIGHT (m)
AVERAGE MIGRATION RATE
SCOUR DEPTH
BED ELEVATION (m)
BEDFORM LENGTH (m)
JUNE
JULY
AUGUST
TIME

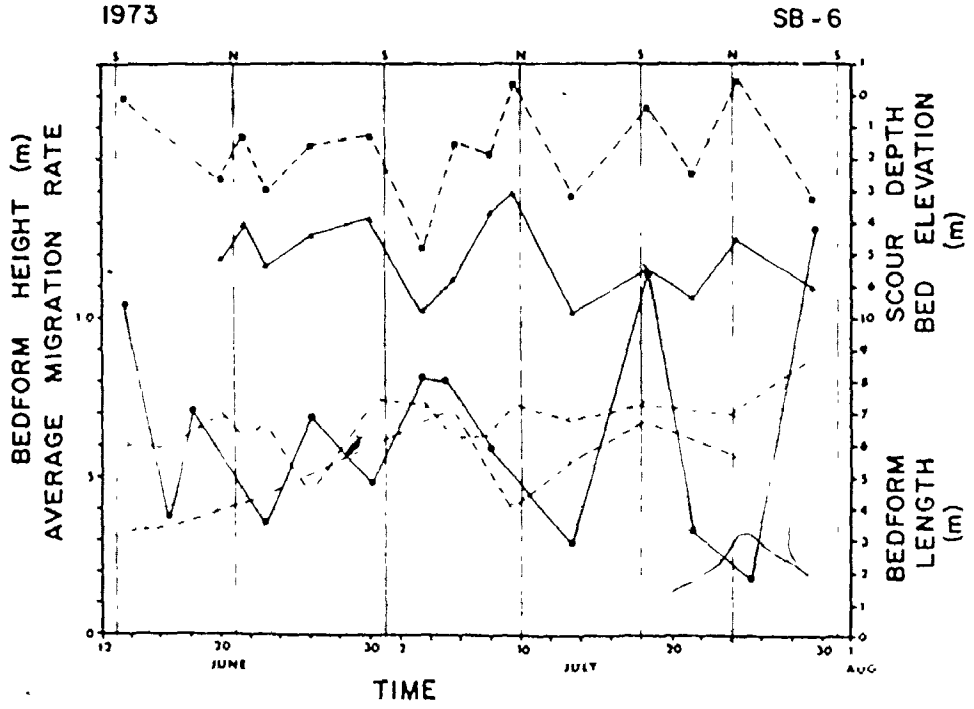
1973
SB-6
BEDFORM HEIGHT (m)
AVERAGE MIGRATION RATE
SCOUR DEPTH
BED ELEVATION (m)
BEDFORM LENGTH (m)
JUNE
JULY
AUG
TIME

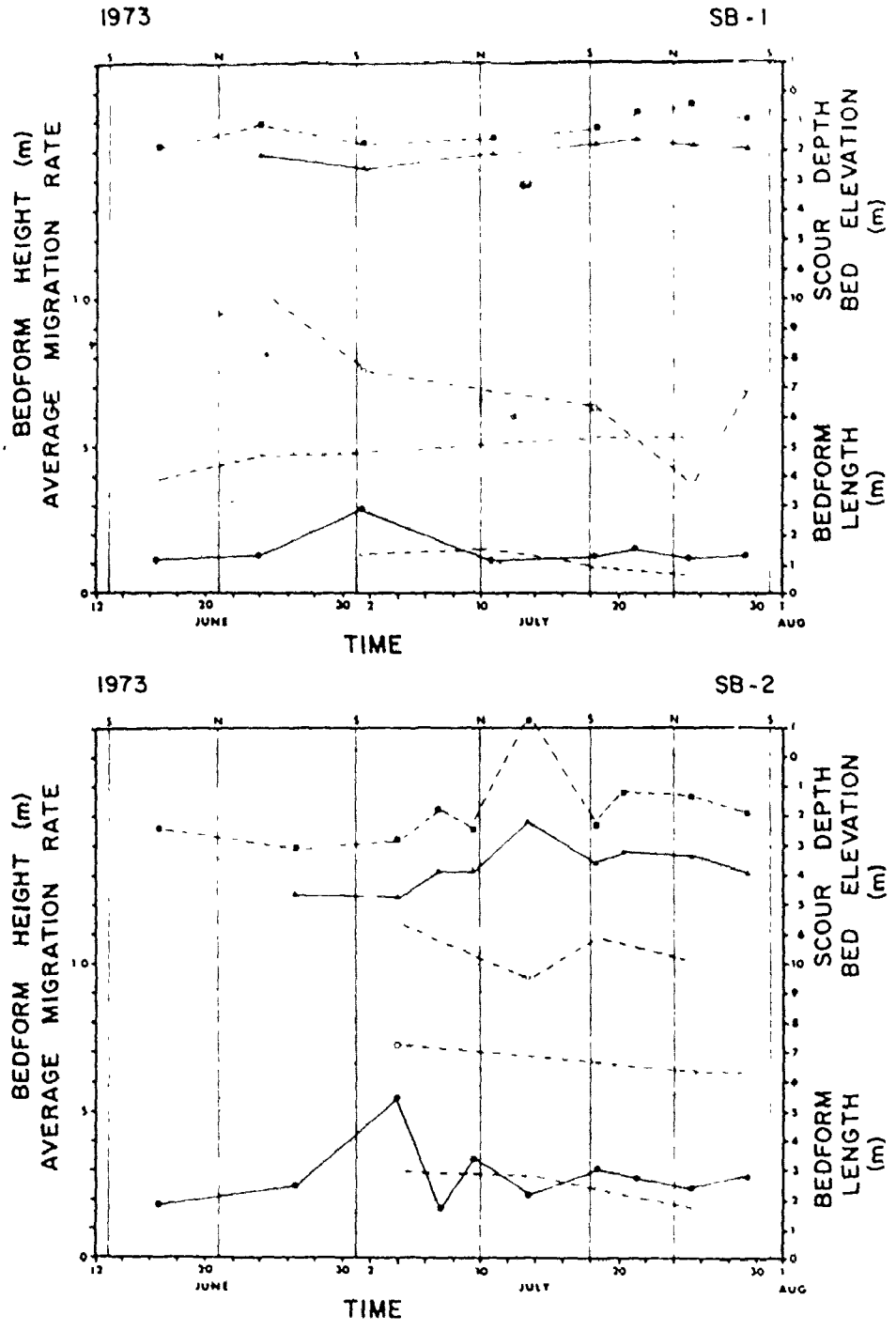

FIGURE 5.33 - cont'd.

TABLE 5-1

AVERAGE RATES OF NET BEDFORM MIGRATION

Location[1]	Replicates per Location (no. of stakes)	Number of Measurements per Location	Average Rate of Net Migration (metres tidal cycle)[3]
NOEL BAY BAR (1971)[1]			
1	3	8	0.31 ± 0.18
2	2	7	0.35 ± .15
3	2	7	0.15 ± 0.11
EAST NOEL BAR (1971)[2]			
1	1	17	0.35 ± 0.23
2	1	16	0.20 ± 0.15
3	1	14	0.22 ± 0.16
4	1	16	0.22 ± [illegible]
5	1	16	0.17 ± 0.14
6	1	9	0.20 ± 0.09
10	1	9	0.12 ± 0.09
12	1	8	0.13 ± 0.07
14	1	9	0.38 ± 0.19
20	1	7	0.28 ± 0.23
SELMA BAR (1972)[1]			
1	5	4	0.31 ± [illegible]
2	5	4	0.31 ± 0.07
4	5	6	0.16 ± 0.07
5	5	8	0.53 ± 0.24
6	5	6	0.74 ± 0.23
8	5	5	0.47 ± 0.13

T A B L E 5-1 (cont'd)

Location[1]	Replicates per Location (no. of stakes)	Number of Measurements per Location	Average Rate of Net Migration (metres/tidal cycle)[3]
SELMA BAR (1973)[1]			
1	11	8	0.14 ± 0.06
2	11	10	0.28 ± 0.11
6	5	14	0.65 ± 0.34

NOTE: 1 For locations see Fig. 4.1 (current meter stations).

2 For locations see Fig. V.1 (bedform stations).

3 Average over the period of a lunar month.

The bedform migration data from the same brinkline indicated that differences up to ±50% of the mean could occur. The average difference of brinkline migration for sand waves was +39% and -49% for megaripples on Selma Bar. Differences of migration rates for different brinklines in the same area were about the same order of magnitude. There was some tendency for the differences to be slightly larger during periods of neap tides than during springs but more detailed field observations are really required to substantiate the reality of this trend.

Table 5-1 summarizes the average net migration rates for bedforms at the different sites monitored. Migration rates in areas of strong current speeds (e.g., SB-5, -6 and -8) were substantially larger than in areas with lower velocities (e.g., East Noel Bar). Bedforms moved faster at the east end of the Noel Bay Bar than at the west end. On East Noel Bar, the net migration rates of bedforms generally increased from east to west across the bar.

The net rates of migration per tidal cycle determined from this study generally agree with results found in other tidal estuaries. Hartwell (1970), for example, reported a net migration of 8.5 m during a 54-day period (average of 0.08 m/tidal cycle) for sand waves. Boothroyd and Hubbard (1975) determined rates of between .05 to .1 m per tidal cycle and .4 m per tidal cycle during neap and spring tides respectively for sand waves and 0.6 m per tidal cycle for megaripples in the Parker and Essex estuaries along the northeast coast of the United States. Ludwick (1972) reported sand wave (lengths = 85 m; heights = 1.4 m) migration rates of 0.4 to 0.5 m/tidal cycle and 0.3 to 0.4 m/tidal cycle during the ebb and flood respectively in the entrance to Chesapeake Bay.

5.6 HYDRAULIC RELATIONSHIPS

The morphology and scale of tidal bedforms, as with fluvial bed features, changes with variation of the energy input, usually with some degree of lag (Allen, 1973, 1974, 1976 a and b). Several attempts have been made by different workers to establish the relationship between bedform morphology and scale, and flow conditions. Simons et al. (1963, 1965 a, 1966) recognized a sequence of occurrence of transverse bed

configurations from flume experiments with increasing flow velocity at a given depth of flow:

ripples → ripples on dunes → dunes → washed-out dunes → upper plane bed

Boothroyd and Hubbard (1975) described a sequence of intertidal estuarine bedforms which developed as the flow strength or mean velocity of the flow increased:

ripples → linear megaripples → cuspate megaripples → planed-off megaripples → rhomboid megaripples → flat beds
↓
sand waves

This sequence is similar to that of Simons et al. (1965) except for sand waves. Boothroyd and Hubbard believed that sand waves were a completely different bed feature and as such did not belong in the ripple and dune sequence. Pratt and Smith (1972), Pratt (1973) and Costello (1974) recognized intermediate flattened dunes or bars between ripples and dunes in flume experiments which Costello (1974) and Southard (p. 17 and 25 in Harms et al., 1975) believed were equivalent to sand waves observed in natural environments. Costello (1974) suggested that Boothroyd and Hubbard's linear megaripples were "dwarfed sand waves", thus their sequence of bedforms should be:

ripples → sand waves → cuspate dunes → planed-off dunes

i.e., similar to the sequence of transverse bed features observed in flume experiments.

Other studies have attempted to relate bedform length and height to flow strength, specifically discharge (e.g., Allen, 1974, 1976 a and b, Pretious and Blench, 1951), tidal coefficient (e.g., Allen, G. P., et al., 1969), the ratio of the tidal range in any semidiurnal cycle to the range at the largest spring tide on which flow strength on discharge is largely dependent in tidal systems and stream power (Simons et. al., 1965 a).

Yalin (1964, p. 111 and 113; 1972, p. 217-249) argued on a semi-empirical basis that ripple wavelength (L_R) was independent of flow depth but directly proportional to grain size,

$$L_R \approx 1000D$$

and that ripple height (H_R) should not exceed one-sixth of the flow depth, i.e.

$$H_R \leq 0.17d$$

He also proposed that the wavelength of dunes (L_D) were dependent on the depth of flow,

$$L_D = 5d$$

and that dune heights (H_D) were less than one-sixth the depth

$$H_D \leq 0.17d$$

Allen (1968 c, 1970), using the data of Guy et al. (1966) and field results, partially confirmed Yalin's results for ripples and dunes. He proposed that dune wavelength (L_D) and height (H_D) were dependent on the scale of the generating flow system.

$$L_D = 1.16d^{1.55}$$

and

$$H_D = 0.086d^{1.19}$$

where $0.1 \leq d \leq 100$ m. These results generally agree with the occurrence of bedforms in natural systems reported by Allen and Friend (1976), Lonsdale et al. (1972), McCave (1971) and Znamenskaya (1963, Fig. 7), and in flume studies (e.g., Kennedy, 1969). Allen (1969, Fig. 29), however, found that three-dimensional current ripples could reach heights comparable to the flow depth, and that the degree of ripple three-dimensionality depended on both depth and velocity (e.g., Froude number). Ripples and dunes vary from simple, long-crested two-dimensional forms (e.g., linear crestlines in plan) to short-crested, three-dimensional forms (e.g., linguoid or lunate). The factors controlling the dimensionality are poorly understood, but Allen (1968 b, 1969), Harms (1969) and Yalin (1972, p. 226) proposed that there might be some relation between the increase of flow strength, duration and relative roughness, and greater three-dimensionality of the bedforms.

According to Allen and Friend (1976), Jain and Kennedy (1974) and Raichlen and Kennedy (1965), the length and height of a bedform is dependent on the duration of the flow at or above the hydraulic threshold for the initiation of the particular bedform type.

Nevertheless, there does appear to be a reasonable correlation between the scale of bedforms and the generating flow system, albeit the relationships of bedform height and length (e.g., Allen, 1968 b, Fig. 6.1; 1968 c, Fig. 7) show appreciable scatter. Allen (1974) noted that this might be due to "lag effects rather than observational errors." Such lag effects are particularly evident in tidal systems because both depth and velocity change relatively rapidly with time (compared with the temporal variation of the flow conditions in a fluvial system) and bedform development cannot change that quickly. Klein and Whaley (1972), for example, reported that the megaripples generated by tidal currents on an intertidal sand bar near Five Islands were much smaller than those that could potentially exist in the available flow depth according to the empirical relationships of Allen (1968 c) and Yalin (1972).

Furthermore, the lag between bedform development and changing flow conditions is indicated by the occurrence of relatively unaltered megaripples and sand waves on the intertidal sand bars, rather than current ripples or plane beds as predicted by Simons et al. (1965 a) and Allen (1968 b) for decelerating flows. There is insufficient time to destroy or substantially alter the large-scale bedforms as the flow scale is reduced during the late ebb just before emergence of the sand bar (Allen, 1974). Such lag effects are common to most intertidal sand bars and sand flats with large bedforms (e.g., Allen, 1968 c, 1974 and 1976 a and b; Boersma, 1969; Cornish, 1901 a; Daboll, 1969; Farrell, 1972; Gellatly, 1970; Harwell, 1970; Kindle, 1917; Newell and Rigby, 1957; Terwindt, 1971 b, and Tucker, 1973).

The depth-velocity-size diagrams of Southard (1971) are a relatively simple means of characterizing the occurrence of different bed configurations and the mean hydraulic properties. Southard and Boguchwal (1973) and Costello (1974) extended Southard's graphical approach by examining the nature of bedform transitions from ripples to lower flat bed and the development of bedforms in medium to coarse grained sands. These data, however, were observed in experimental flumes with uniform flow conditions, sand-sized beds and most flow depths less than 1 metre. Few field studies have attempted to determine if Southard's approach can be extended to natural flows, where flow conditions are unsteady and/or nonuniform, e.g., Klein and Whaley (1972), Boothroyd and Hubbard (1975) and Jackson

Klein and Whaley (1972) reported that "the distribution of dunes and sand waves on a depth-velocity diagram is identical to the occurrence of dunes plotted on a similar diagram by Southard (1971, [illegible]) for sands with a median diameter of 0.45 mm". This comment is interesting for two reasons: (i) Southard did not differentiate between dunes and sand waves; and (ii) Costello (1974) found that sand wave (on bar) and dune (or megaripple) phase fields were differentiated on the basis of depth and velocity rather than just depth as suggested by the data of Klein and Whaley. Their sand wave data agrees with Southard's empirical stability fields only with respect to the relative position (i.e., intermediate between ripple and transition-flat bed stability fields).

Boothroyd and Hubbard's (1975) data for sand sizes of 0.35 and 0.40 mm in a tidal estuary showed that the position of megaripples and sand waves agreed fairly well with Costello's (1974) predicted dune and bar phase fields. The sand waves distinguished from dunes by Jackson (1975) in the Lower Wabash River both plotted within Southard's dune field, but did not show any appreciable separation of position on depth-velocity-size diagrams. Jackson does, however, find some suggestion that the transverse bar stability field correspond to Costello's barlike bedforms. Thus, Southard's approach does appear to have some limitations on field application, but the nature of the restrictions is not known.

Vanoni (1974) presented a similar procedure for predicting bedforms. He found that d/D_{50} (flow depth to median size of bed sediment), Froude number and $R_g = d_{50}\frac{\sqrt{d_{50}}}{\nu}$ were the important variables for predicting the occurrence of bedforms (i.e., essentially a dimensionless depth, velocity and sediment size which is fundamentally similar to Southard's graphical approach). Vanoni's analysis was based on both laboratory and field studies from several investigations. He, however, recognized only a ripple to dune transition with no evidence of an intermediate bar or sand wave bed phase (Costello, 1974).

Other studies have attempted to explain the occurrence of bedforms by hydrodynamic analysis. These attempts are summarized in Allen (1968 b), Costello (1974), Graf (1971), Raudkivi (1967 a) and Yalin (1972). Still other studies have approached the problem of bedform development as a

stochastic process, (e.g., Allen, 1969; Ashida and Tanaka, 1967; Crickmore, 1970; Nordin, 1971; Nordin and Alger, 1966; Pratt and Smith, 1972; Squarer, 1970). Both types of approaches were considered to be beyond the intended scope of this study.

The purpose of this section is to relate some of the bedform properties seen and measured directly at low low with the mean hydraulic characteristics of the flow.

Bedform Scale

Further to the analysis of Section 5.4, the average length and height of bedforms were graphed as a function of: (i) the average of the two maximum mean current speeds determined from the vertical velocity profiles per phase of the tide and (ii) the depth of flow at the time that the maximum mean flow velocity occurred during the ebb and flood phases of the tide.

Figure 5.34 shows the graphed relationships of the height, length and length/height ratios of the bedforms exposed at low tide on the sand bars as a function of maximum ebb current speeds (see above). Both the length and height of the bedforms are positively correlated with velocity. Length/height ratios were negatively correlated to current speed. Correlation coefficients of the three relationships explain only about 25% of the variance about the linear regression (i.e., $r^2 \approx 0.5$) but the results are statistically significant at the 99% level of confidence for bedform length and height, and at the 95% level for length/height ratios.

Bedform length and height were negatively correlated, and length/height ratios positively correlated to depth, but all three relationships explained only a small part of the variance (e.g., values of $r^2 = -0.06$, -0.04 and 0.05 respectively).

As a simple test of whether or not the scale of the ebb bedforms seen at low tide had any relationship to the hydraulic conditions (and bedform development) during the flood, the dimensions of the ebb bedforms (and some flood bedforms, e.g., sand waves) were graphed as a function the maximum flood speeds and mid-flood flow depths (e.g., Fig. 5.35). The relationships generally had a large amount of scatter with low correlation coefficients (e.g., length and height versus velocity, and height versus depth). The length/height ratios as a function of

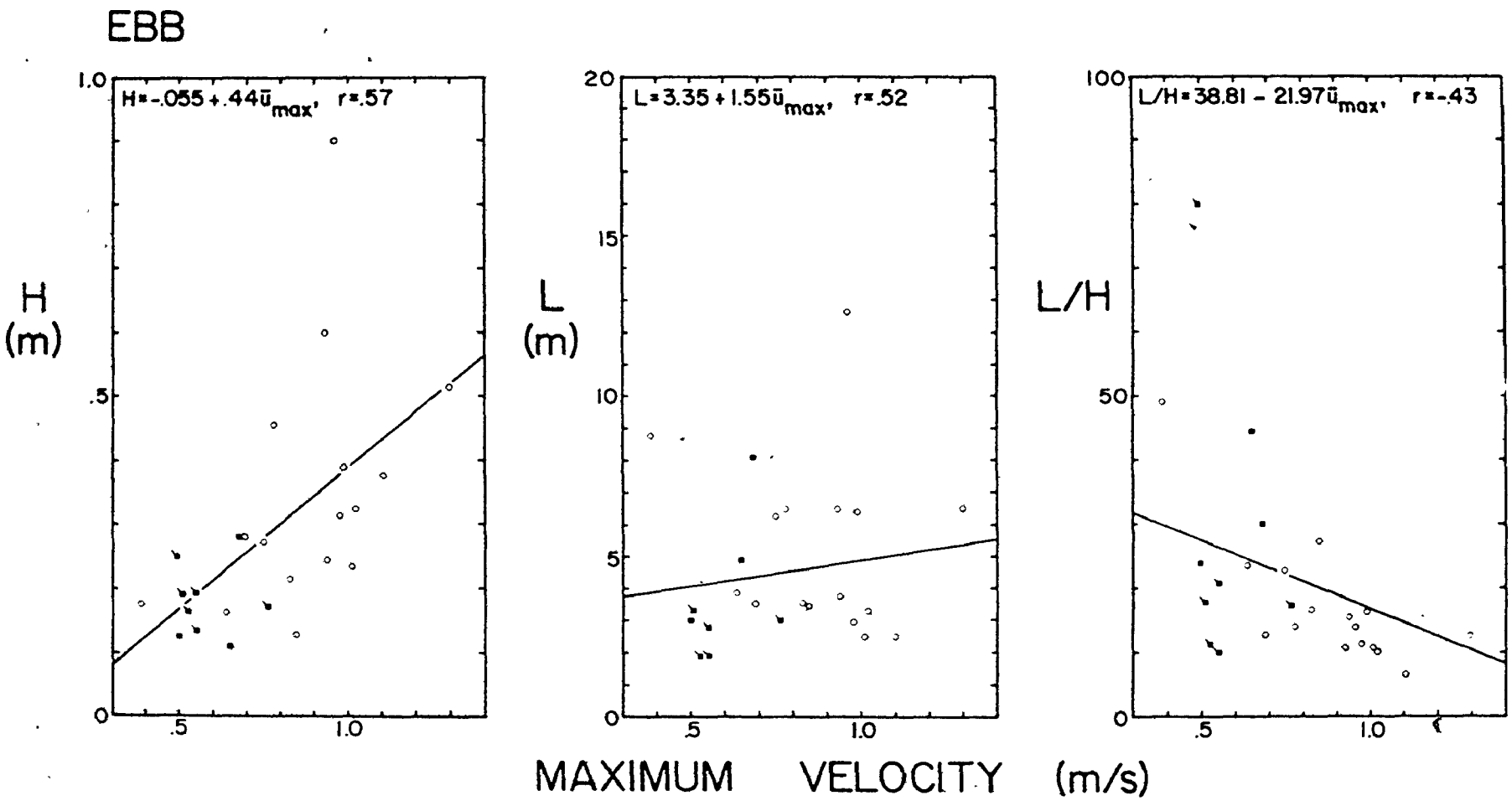

FIGURE 3.34: Height, length, and length/height ratios of ebb bedforms as a function of the average maximum ebb current velocity. Open circles = megaripples; closed squares with ticks = sand waves; closed squares = ebb modified flood bedforms.

FIGURE 5.35: Flood bedform dimensions as a function of the average maximum flood velocity and mid-flood flow depth. Open circles = megaripples; closed squares with ticks = sand waves; closed squares = ebb modified flood bedforms.

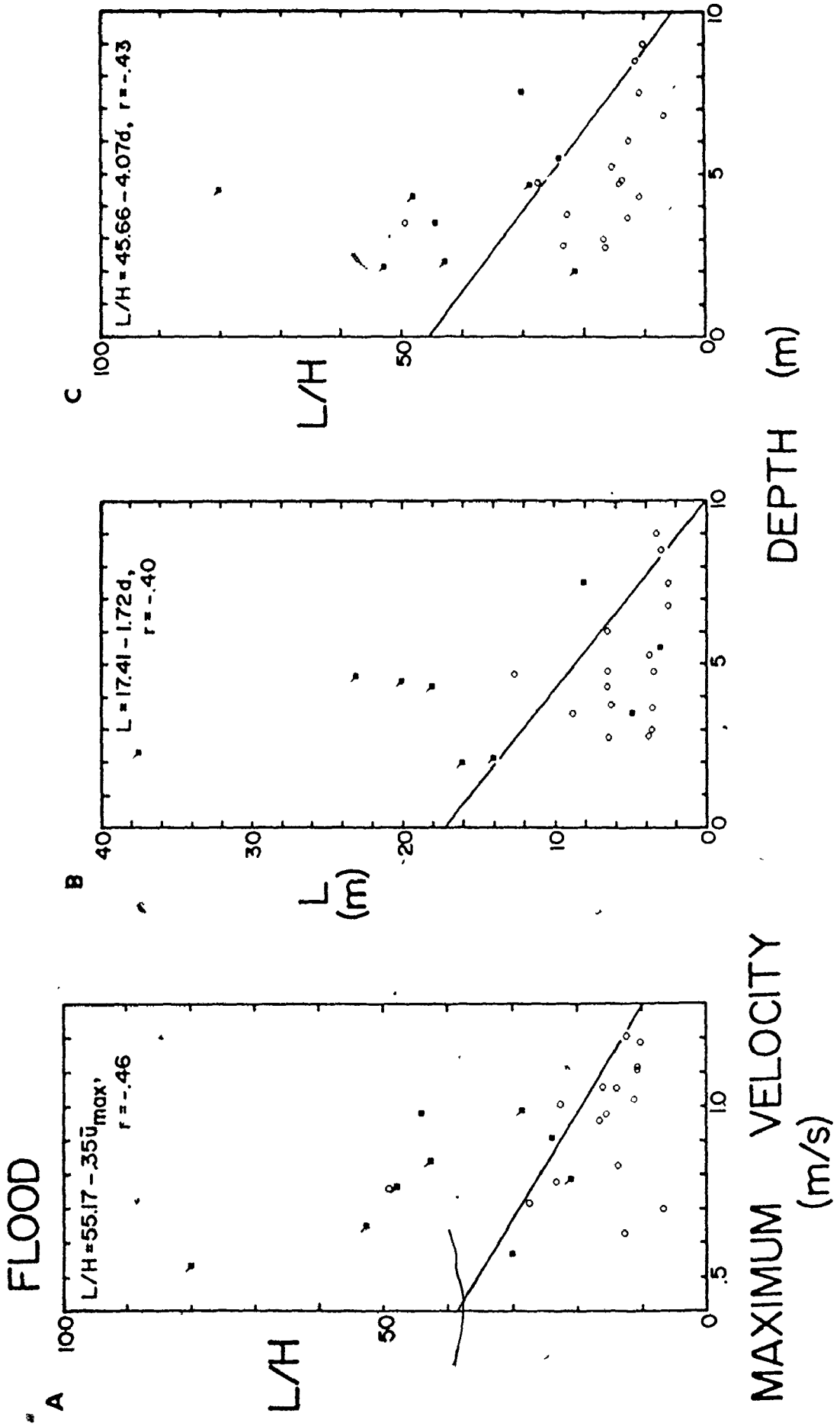
FLOOD
A
L/H=55.17-35ū max,
r=-.46
L/H
100
50
0
.5
1.0
MAXIMUM VELOCITY (m/s)
B
L=17.41-1.72d,
r=-.40
L (m)
40
30
20
10
0
0
5
10
C
L/H=45.66-4.07d, r=-.43
L/H
100
50
0
0
5
10
DEPTH (m)

FIGURE 5.36: Bedform dimensions as a function of the ebb and flood flow durations. Open circles = megaripples; closed squares with ticks = sand waves; closed squares = ebb modified flood bedforms.

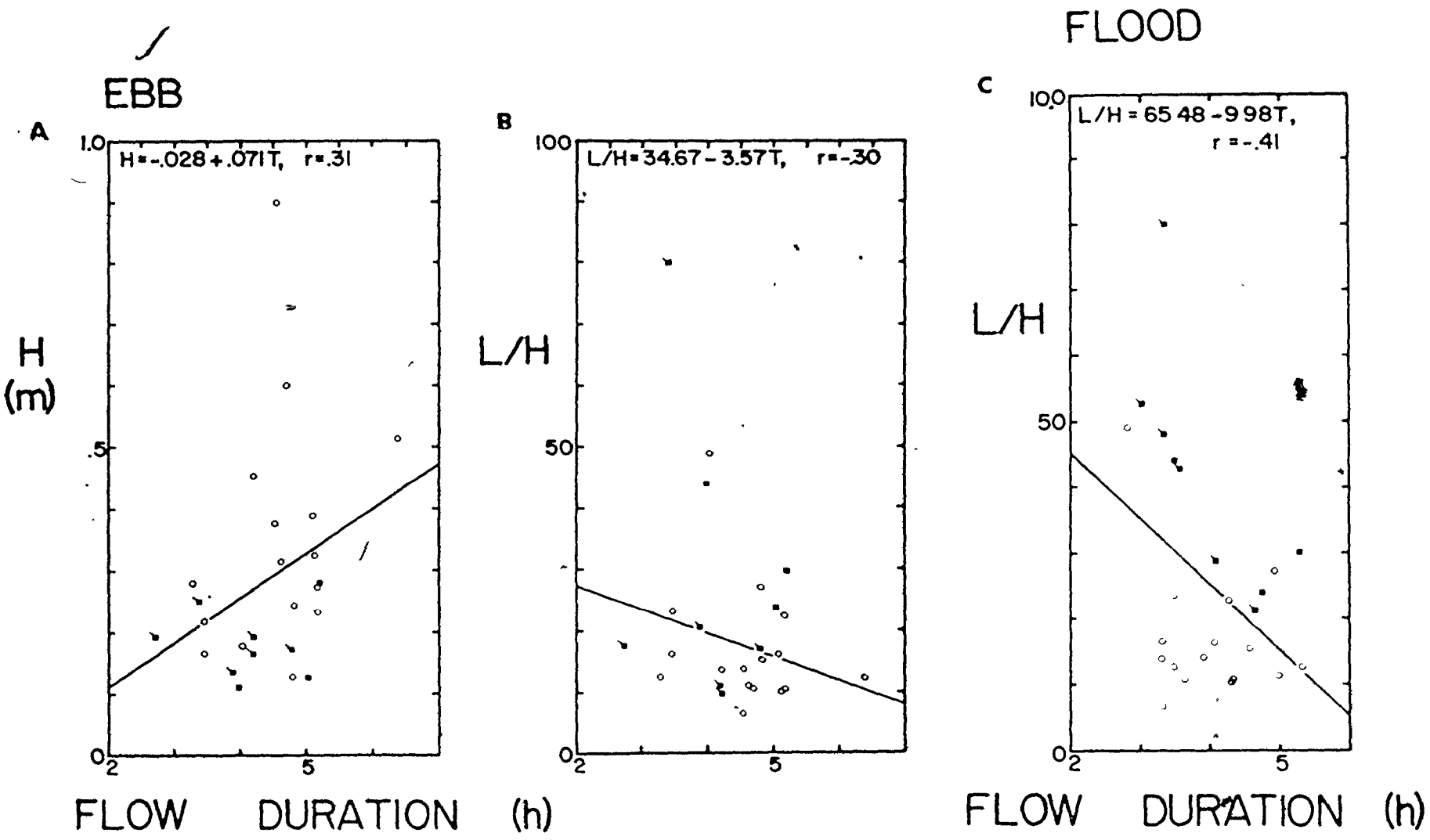
EBB
FLOOD
A
B
C
H=-.028+.071T, r=.31
L/H=34.67-3.57T, r=-.30
L/H = 65 48 -9 98T,
r = -.41
H
(m)
L/H
L/H
1.0
.5
0
100
50
0
100.0
50
0
2
5
2
5
2
5
FLOW DURATION (h)
FLOW DURATION (h)

velocity and depth, and length as a function of depth were statistically significant at the 95% level of confidence. The other relationships examined had correlation coefficients that were less than 0.27 (e.g., H versus $\bar{u}_{max\ f}$, r = 0.27; L versus $\bar{u}_{max\ F}$, r = -0.24; H versus D_f, r = -0.17; L versus D_f, r = -0.40).

Lastly, the spatial properties of the bedforms were examined as a function of the duration of the ebb and flood. The results generally showed a fairly large amount of scatter (e.g., Fig. 5.38), but it appeared that bedform size increased with longer durations of flow (e.g., H versus t_e, r = 0.33; L versus t_e, r = 0.17; H/L versus t_e, r = -0.33; H versus t_f, r = 0.38; L versus t_f, r = -0.24; and L/H versus t_f, r = -0.41). Only the relationship in Figure 5.38 C was statistically significant at the 95% level of confidence.

The foregoing results suggest that the scale of bedforms generated by tidal currents is controlled primarily by: the strength and duration of the ebb currents for bedform heights (ebb); the mid-flood depth (and possibly the duration of the ebb and flood currents) for the lengths of bedforms (primarily ebb); and the ebb and flood current speeds and flow durations, and mid-flood depths for the length/height ratios of the intertidal bedforms.

The relatively large degree of scatter in Figures 5.34, 5.35 and 5.36, and in Allen's (1968 b) Figure 4.10 is likely related to: (i) the effect of mean grain size and grain size distribution on bedform lengths and heights, e.g., Simons et al. (1965 a) found that bedform lengths decreased with increased sediment size; (ii) the net effects of the ebb and flood currents and bedform reversal; (iii) the alteration of bedform dimensions by shallow late-stage ebb currents (e.g., bedform crests are planed-off, thus measured bedform height is low relative to length, and length/height ratios are larger than for an unaltered bedform); and (iv) the lag of bedform development behind the time-varying flow conditions (Allen, 1974) which prevents bedforms from achieving equilibrium with the flow and maximum dimensions (relative to the maximum velocity and given depths). Nevertheless, these data presented in this study are useful as a comparison to Allen's data (1968 b, p. 75-80 and Fig. 4.10 and Fig. 6.4) and for approximate predictions and interpretation of

bedforms and sedimentary structures in Holocene and ancient clastic sediments.

Compared with the results of other investigations, the bedform data from this study showed both similarities and differences. Allen's (1968 b, Fig. 6.4) graph of bedform height as a function of depth had a steeper slope, a reversed correlation (i.e., bedform heights increased at greater depths; in this study, heights were found to decrease with relatively larger depths of flow) and less scatter (i.e., a larger correlation coefficient). These differences can be attributed partly to points listed in the preceding paragraph and to the fact that Allen's data are primarily from subtidal bedforms which were unaltered by shallow, late-stage ebb currents.

As in this investigation, Klein and Whaley (1972) found that the empirical relationships of Yalin (1964) and Allen(1968 b) for bedform length and height as a function of depth, although positively correlated, overestimated the actual scale of the bedforms that existed. Allen (1974) believed that the difference was due to bedform lag effects (relative to changing flow conditions) resulting from rapid emergence and differences of subtidal and intertidal bedform development and modification (e.g., late-stage ebb and early-stage flood). McCave (1971), for subtidal sand waves in the North Sea, reported a general agreement with Allen's relationships. Smith (1968), however, found that Yalin's (1964) H/D value of 1/6 was incorrect for the occurrence of subtidal sand waves on Middle Ground in Vineyard Sound (H/d = 1/2.2), and Terwindt (1971 b, Fig. 4) reported that small dunes superposed on sand waves and banks in the North Sea were inversely related to the flow depth. Thus, there is little agreement between workers on the form of the relationship of bedform height as a function of depth. This suggests that each relationship is possibly unique to the system in which the data was collected and therefore reduces usefulness of this sort data correlation for predictive and interpretive purposes in the analysis of Holocene and ancient sedimentary bedforms and structures.

Flow Regimes

There have been many different attempts to forumlate a relationship between the occurrence and development of bedforms and the mean hydraulic

properties of the generating flow. Some of the different approaches are summarized in Allen (1968 b, p. 138-148) and in Southard (p. 5-43, in Harms et al., 1975. Of the many possible relationships, only three are examined here: (i) depth-velocity-size (Southard, 1971; Southard and Boguchwal, 1973; Costello, 1974); (ii) mean velocity and grain size (Southard, 1971; Costello, 1974); and (iii) stream power and grain size (Simons et al., 1965 a and 1966.

Depth-Velocity - The variation of depth and velocity with time during the ebb or flood phases of a tidal cycle graphed as a continuous curve on a depth-velocity diagram. Figures 5.37, 5.38 and 5.39 are several examples of this type of diagram from different parts of the intertidal bars studied using the total flow depth and the mean flow velocity determined from the vertical velocity profiles. During the ebb, flow depths gradually decrease while current velocities initially increased rapidly, then remained fairly uniform until the late ebb when velocities dropped off quickly. A similar depth-velocity relationship occurred during the flood, but during this phase of the tidal cycle, water depths slowly increased.

The bed phase boundaries shown in Figures 5.37, 5.38 and 5.39 were extrapolated from Costello's (1974) Figures 5.2 and 5.4 for a sediment size of 0.49 mm (somewhat coarser than the sediments in this study). The time history of the flow depth and velocity during the ebb and flood indicated that the current velocities generally level off within one bed phase. Thus, these measurements should predict the resulting bed configuration.

Figure 5.37 shows the time history of the flow depth and velocity at three locations on Noel Bar: NBB-1c and 2 a (sinuous crested megaripples at low tide) and NBB-3a (ebb-modified flood bed features at low tide). At all three locations, there is a small ebb-flood inequality (with respect to maximum velocity) (slight ebb dominance) and all measurements fall within Costello's 'bar' phase. The measurements at NBB-1c and 2 a show only a small inequality between the ebb and flood, and plot within the middle to upper part of Costello's 'bar' phase. At low tide, the bedforms are sinuous crested megaripples (Facies D2) at both locations. Since there is only a small difference between the ebb and

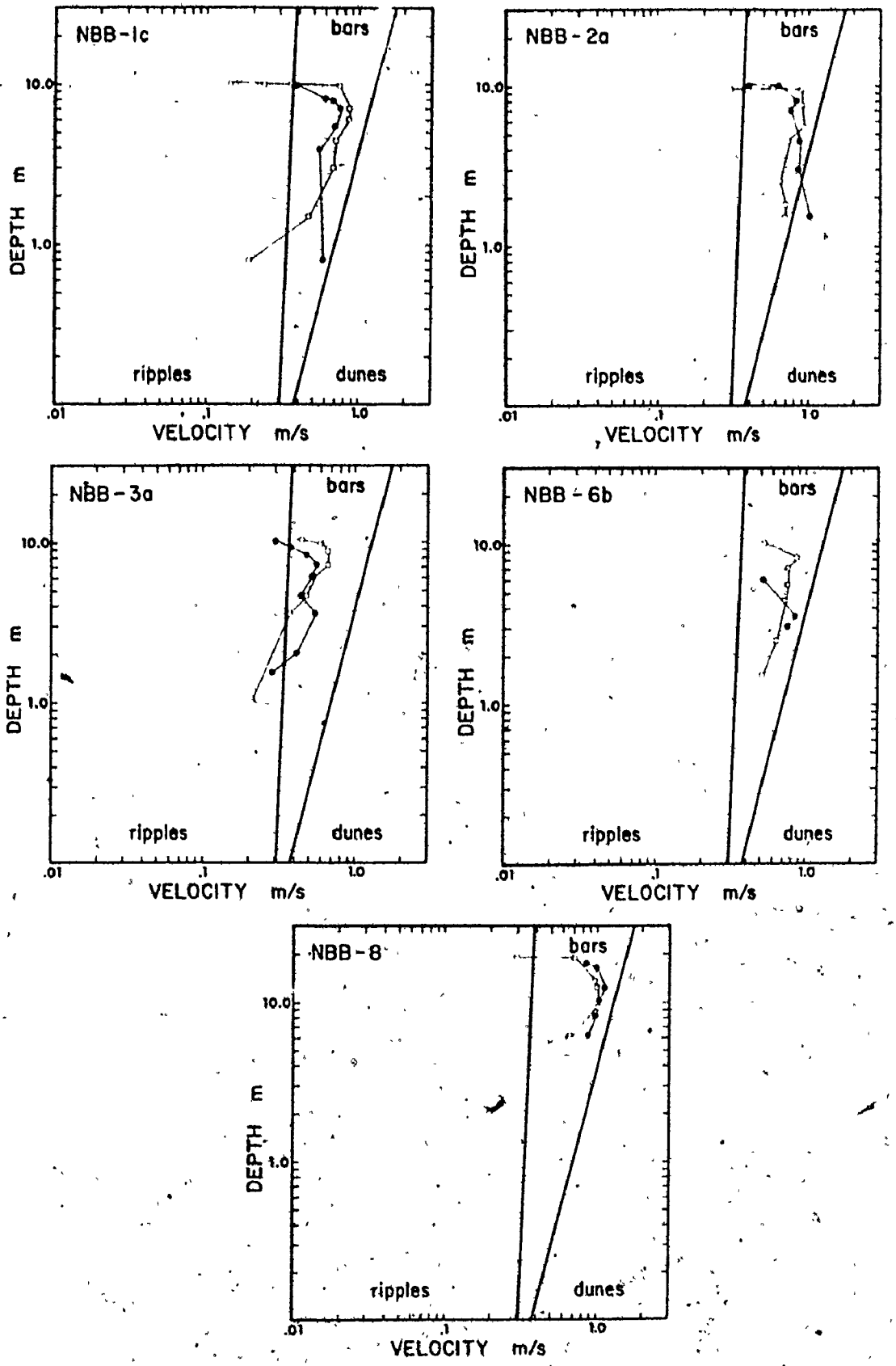

FIGURE 5.37: Depth-velocity diagrams for several locations on Noel Bay-Bar. See Figures 4.1 for locations and 5.20 for bedform types. Open squares = ebb; closed circles = flood.

flood, the flood bedforms are likely similar to the ebb features. At NBB-3a, the measurements plot within the lower to middle part of the bar phase. Relatively large ebb-capped bed features (Fig. 5.25 C and D) occurred in this area at low tide, and showed little similarity to the megaripples at NBB-1c and -2a in terms of scale and morphology (e.g., Figure 5.23 C).

Figure 5.38 indicates some representative depth-velocity diagrams from Noel Shore Bar. The current velocities are generally larger over Noel Shore Bar than over Noel Bay bar, and most of the measurements fall very close to the bar-dune phase boundary or just slightly over it. The flood is dominant at each location (Figure 5.38) by about 0.1 to 0.2 m/s with respect to the maximum mean velocities. Traversing the bar from NSB-5 to NSB-1 to NSB-4 to NSB-7, the depth-velocity measurements of both the ebb and flood progressively shift from the 'bar' phase into the dune phase and the ebb bedform types change from Facies C2 to Facies D2 to Facies D3, i.e., from linear crested to sinuous crested (with scours) to planed-off megaripples (with scours) with increasing velocity (Figure 5.38). The results predict that the flood bedforms should be megaripples (or dunes) and the ebb bed features should be ebb-modified flood megaripples or bedforms transitional between the 'bar' and 'dune' phases. Echo sounding clearly indicated the presence of flood oriented megaripples at NSB-1, -4 and -7 (bedforms at NSB-5 are too small to be reliably detected by echo sounding) during the flood. At low tide, the exposed megaripples were ebb oriented, i.e., the asymmetry of the flood megaripples was completely reversed. Although the ebb velocities generally did not reach as far as the flood velocities into the 'dune'phase, the longer duration of the ebb currents compensated for the velocity difference, giving the ebb enough time to completely rework the flood features.

Figure 5.39 shows some representative depth-velocity diagrams from Selma Bar (e.g., SB-2f, -5b, -6e). Each location was flood dominant in the order of 0.1 to 0.25 m/s with respect to the maximum mean velocities. From SB-2f to SB-3a to SB-5c to 6e, maximum ebb and flood velocities were progressively larger and the ebb bedform types changed from megaripples superposed on flood sand waves (Facies G4), to linear to slightly sinuous crested megaripples (Facies C2), to ebb capped (linear to sinuous crest-

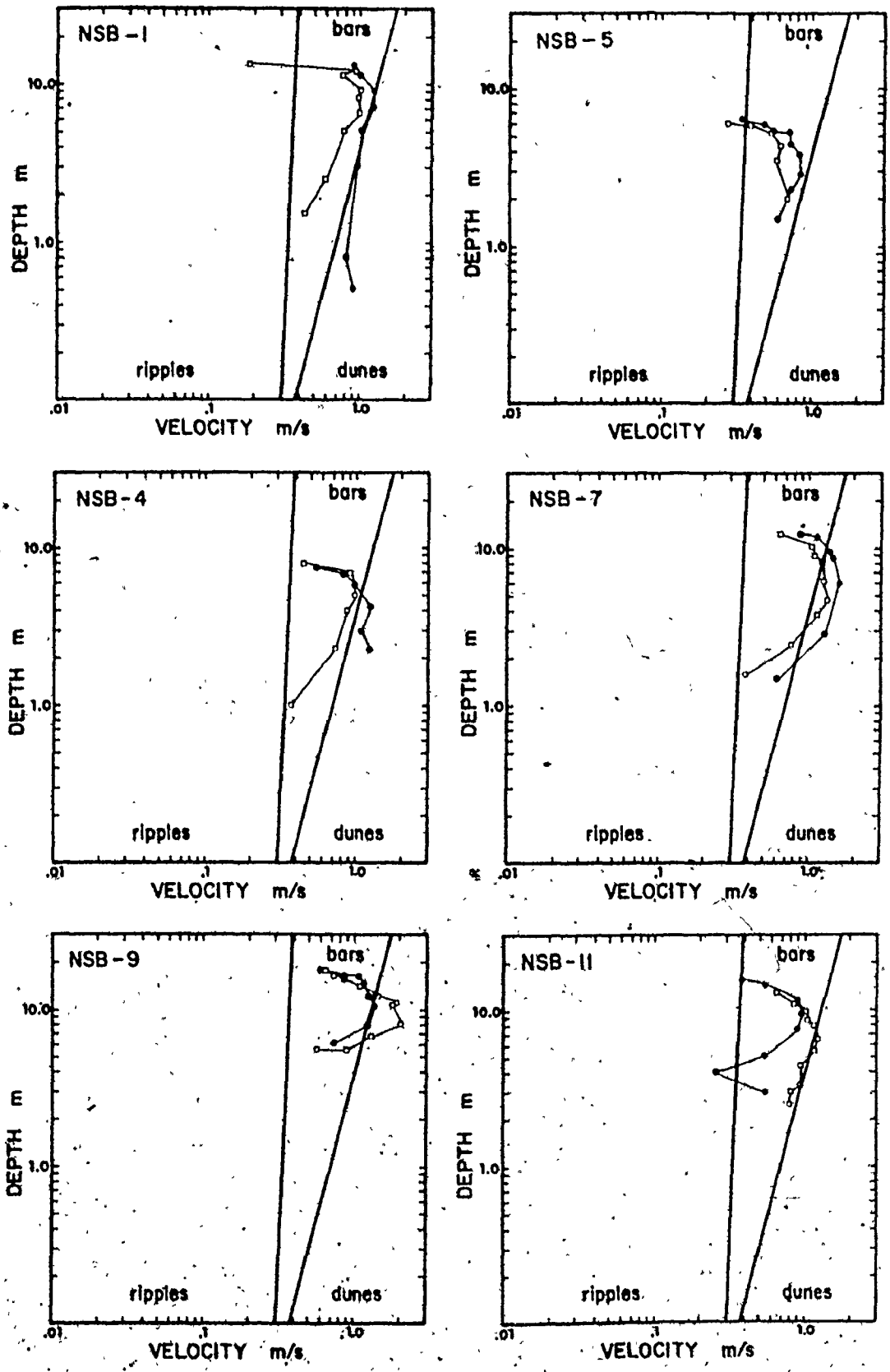

FIGURE 5.38: Depth-velocity diagrams for several locations on Noel Shore Bar. See Figures 4.1 for locations and 5.20 for bedform type. Open squares = ebb; closed circles = flood.

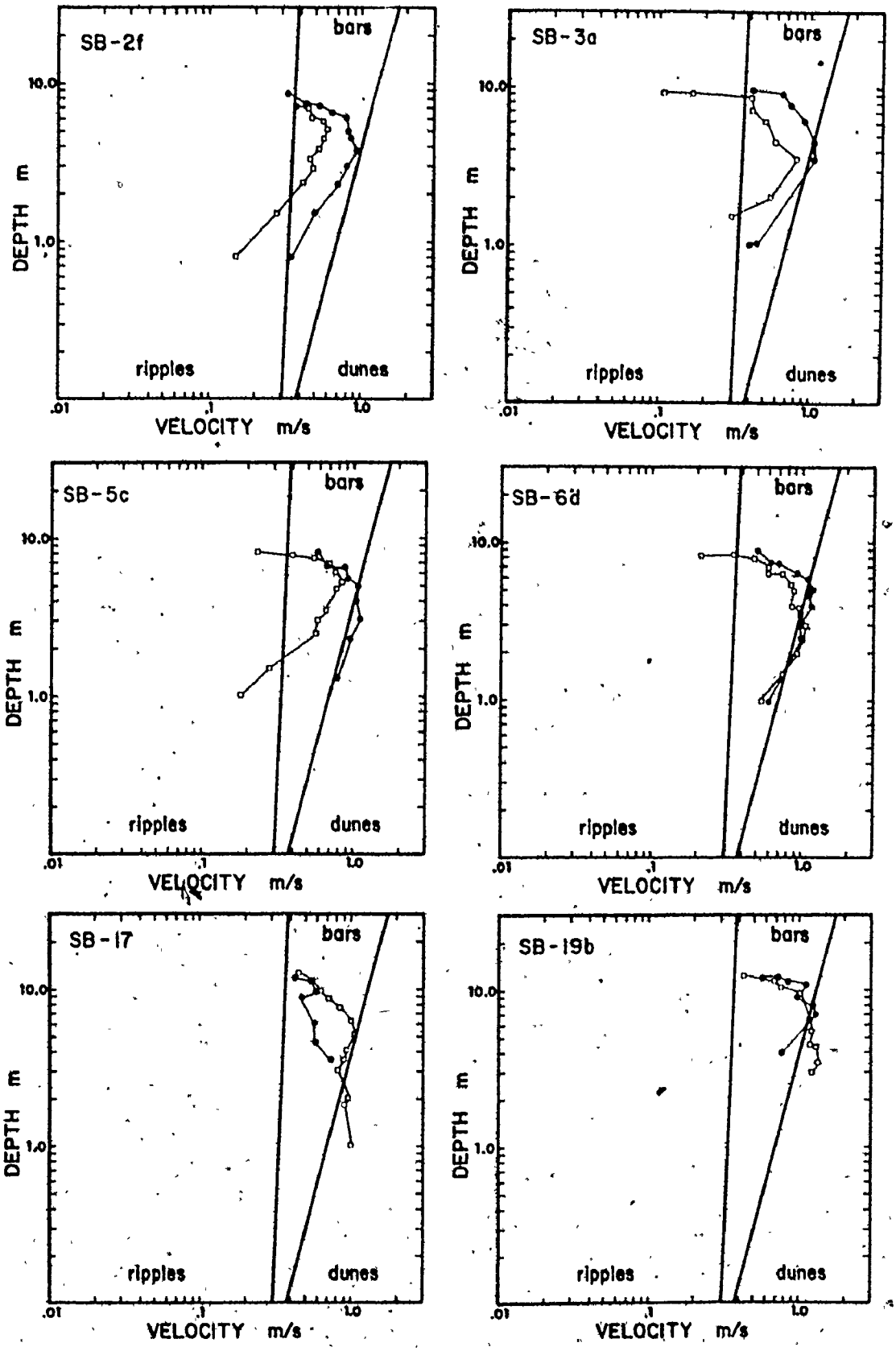

FIGURE 5.39: Depth-velocity diagrams for several locations on Selma Bar. See Figures 4.1 for locations and 5.20 for bedform types. Open squares = ebb; closed circles = flood.

lines) flood megaripples (Facies G5) to large planed-off megaripples with deep scours (Facies D3). This ordering does not imply a proposed sequence of bedform development.

The sand waves (Facies G4) at SB-2f were flood asymmetrical features with superposed megaripples during the ebb and flood. Velocities remained in the 'bar' phase during both the ebb and flood, but flood velocities came very close to the bar-dune transition. Thus, the superposed megaripples should not be in equilibrium with the flow during the ebb and flood, particularly during the ebb because the velocities are not large enough. Costello (1974) believed that the superposed megaripples were "a metastable, secondary form, ... initiated by the large sand waves." He also believed that the sand waves were his bar-type of bedform. The strong flood dominance of this area on Selma Bar accounts for the flood asymmetry of the sand waves.

The currents at SB-5 c were stronger (Fig. 5.39) but had a similar ebb-flood asymmetry to those at SB-2 f. The relatively larger velocities of both the ebb and flood and small sediment size (Fig. 3.36) (relative to SB-2 f) must account for the marked difference in bedform type (Facies G4 versus G5) since both the flow depth and duration were comparable at the two locations.

The depth-velocity relationship (flood dominant) and sediment size were similar at SB-3 a and -5 c, but the maximum ebb speeds at SB-3 a were slightly larger and occurred at shallower depths than at SB-5 c (Fig. 5.39). As a result, the ebb bedforms (Facies C2) exposed at low tide were completely reversed at SB-3 a, even though the area was flood dominant with respect to maximum ebb and flood current speeds.

At SB-6, the ebb and flood currents were almost identical with respect to speed, depth and duration. The depth-velocity relationship predicts the occurrence of megaripples (Fig. 5.39). At low tide, this area of the bar had Facies D2 and D3 megaripples (sinuous crested) that reversed their asymmetry with each ebb and flood respectively.

Figures 5.37, 5.38 and 5.39 also show several depth-velocity diagrams for some channel locations. Both depths and velocities were relatively larger and durations longer compared to the flow conditions over the sand bars. Few bedforms occurred on the channel bottoms, however, be-

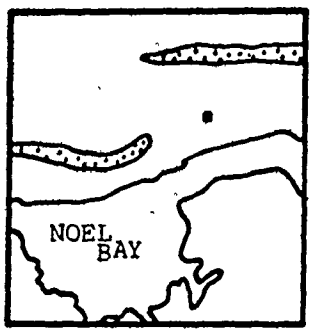

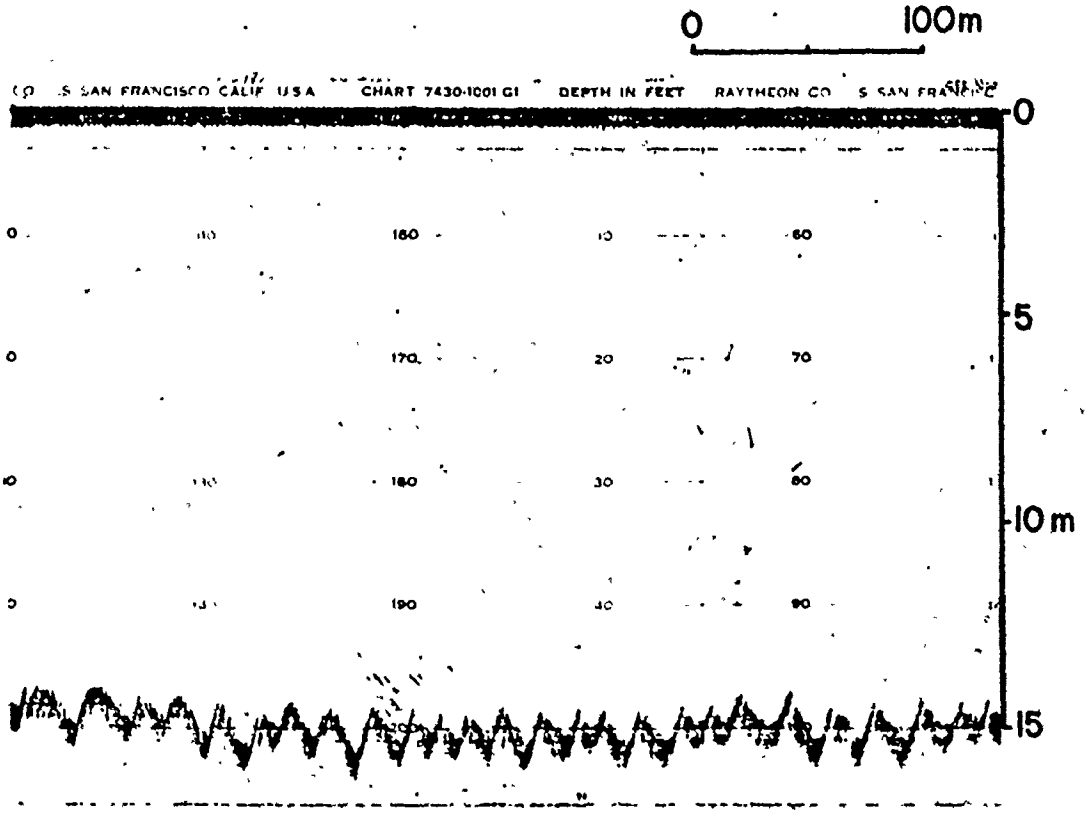

FIGURE 5.40: Bedforms on channel bottom to the north of Noel Head along the south shore of Cobequid Bay (during ebb).

FIGURE 5.41: Depth-velocity diagrams of average maximum current speeds and flow depths for each current station (Fig. 4.1) in terms of the bed configuration during the ebb (A) and flood (B) respectively.

Open triangles = ripples
Closed circles = linear megaripples
Open circles = sinuous megaripples
Inverted, open triangle = disorganized megaripples
Closed square = ebb modified flood bedforms
Closed square with tick = sand/waves
Open diamond = channel location (no bedforms)

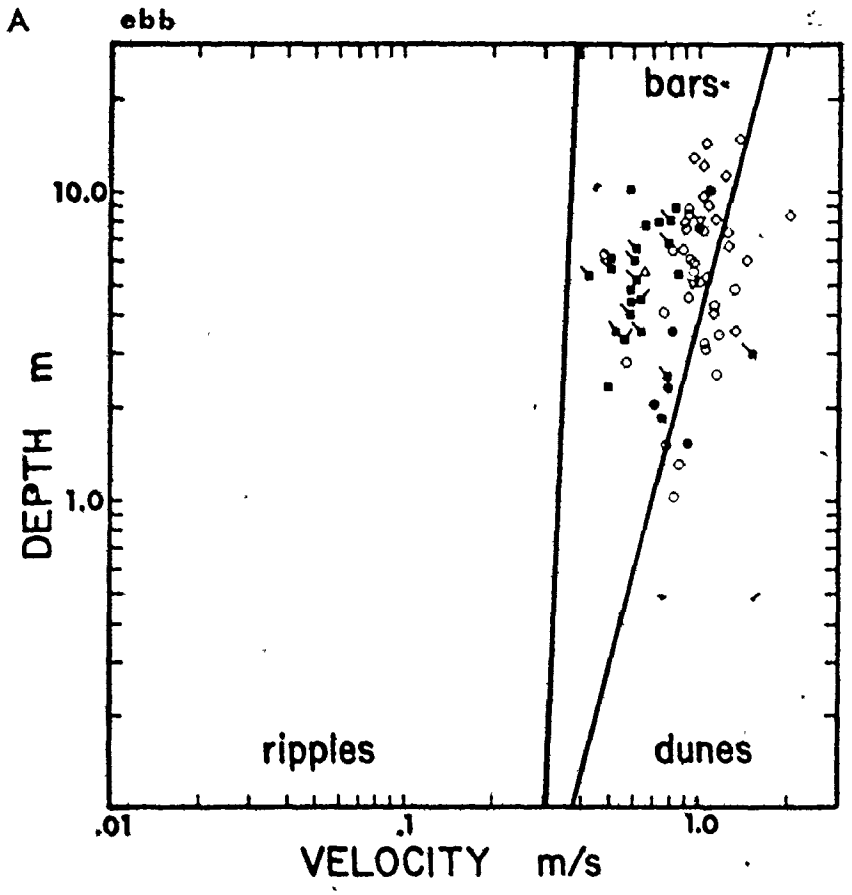
A
ebb
bars
10.0
1.0
DEPTH m
ripples
dunes
.01
.1
1.0
VELOCITY m/s

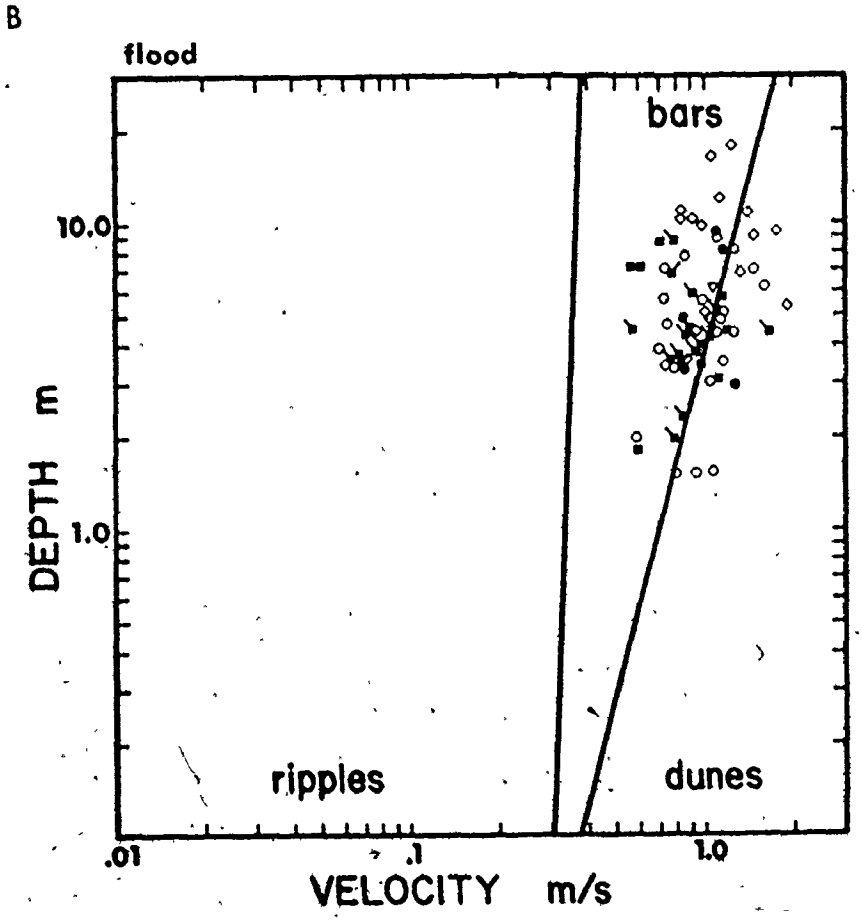
B
flood
bars
10.0
1.0
DEPTH m
ripples
dunes
.01
.1
1.0
VELOCITY m/s

cause the sediments were too coarse, or the bottom was scoured to bedrock. Figure 5.40 shows the occurrence of some large, ebb oriented bedforms in the channel to the south Noel Shore Bar. The bottom sediments were pebbly coarse-sized sands. The depth-velocity relation at NSB-9 (Fig. 5.38), although located further east (Fig. 4.1), gives some impression of the flow characteristics in the channel relative to the development of the bedforms in Figure 5.40.

From each depth-velocity diagram, the maximum mean velocity and flow depth were plotted separately for the ebb and flood (Figure 5.41). The ebb depth-velocity diagram (Fig. 5.41 A) shows a fairly clear distinction between Facies G (sand waves and other ebb-modified flood bed configurations) and Facies C, D and E (megaripples) bedform types even though grain size is not considered as a third controlling parameter (i.e., the phase boundaries are for 0.49 mm bed material (Costello, 1974, Fig. 5.2 and 5.4) but the sediment size on the sand bars ranges from 0.2 to 0.5 mm). The position of the data points on the graph relative to bedform phase boundaries and the bedform types observed at low tide in the field (and the results of Figures 5.37, 5.38 and 5.39) indicate that the bar-dune boundary should be shifted to the left for the ebb data. This is quite reasonable considering that the mean grain size of the bar sediments is about 0.28 mm and that Southard's (1971) depth-velocity-size phase boundaries shift to the left for finer sediment sizes. The disregard for grain size in Figure 5.41 accounts for some of the point scatter.

The separation of Facies G4 and Facies, C, D, E bedforms suggests that sand waves and megaripples possess different hydrodynamic regimes. This result supports Costello's (1974) argument. Facies C megaripples (linear crested) also appear to be a transitional bedform between sand waves (Facies G4) and sinuous crested megaripples (Facies D).

The depth-velocity diagram for the flood relative to the bedform facies for the ebb (Fig. 5.41 B) shows that there is a greater degree of overlap of the bedform facies (e.g., particularly sand waves and megaripples) and that flood current speeds are generally faster. This diagram indicates the relative differences between the ebb and flood currents with respect to bedform phase boundaries.

Flow Strength-Grain Size - The separation of sand waves from megaripples on the basis of flow strength and grain size is evident in Figures 5.42 (maximum mean velocity versus grain size) and 5.43 (stream power at the time of the maximum mean velocity versus grain size). The ebb velocity-grain size relation separates the bedform types into three phases: sand waves, ebb-modified flood bed features and megaripples. The position of the phase boundaries is different from those fields defined by Southard (1971, Fig. 4) and Costello (1974, Fig. 3.13) because maximum mean velocities are used as opposed to mean flow velocities and neither of the flume-based diagrams includes a separate phase for sand waves (bars) or ebb modified flood features.

Figure 5.42 shows a flow power ($\tau_o \bar{u}_{max}$) as a function of mean sediment size with the bedform phase boundaries of Simons and Richardson (1966), Simons et al. (1965 a), Allen (1968 b, Fig. 6.9), Harms (1969) and Blench (1969). Flow power is proportional to the sediment transport rate and equal to the rate at which the flow does work per unit area of the boundary. The plotted data show a considerable degree of scatter outside the experimental bedform phase boundaries because $\bar{u}_{max}$ and σ_{max} were used rather than an ebb time averaged $\bar{u}$ and τ_o, and there is considerable variation in the magnitude of the derived shear stress (i.e. because $\tau_o = u_*^2 \rho$, thus any error in the determination of u_* will be amplified in the value of τ_o). Nevertheless, the diagram shows a separation of megaripples and sand waves, not on the basis of flow power as much as on grain size.

In both Figures 5.42 and 5.43, grain size is the most important variable for differentiating the megaripples from the sand waves; the ebb modified flood bedforms occur in an intermediate position between the two.

Discussion

The data presented within this section generally supports Costello's (1974) argument that: (i) a 'bar' bedform occurs between ripples and dunes; and (ii) the 'bar' bedform is the same bed phase as sand waves in natural systems (e.g., Boothroyd and Hubbard, 1975; this study). The main difference between megaripples and sand waves is size. There is no evidence to suggest that sand waves actually overtake one another from field

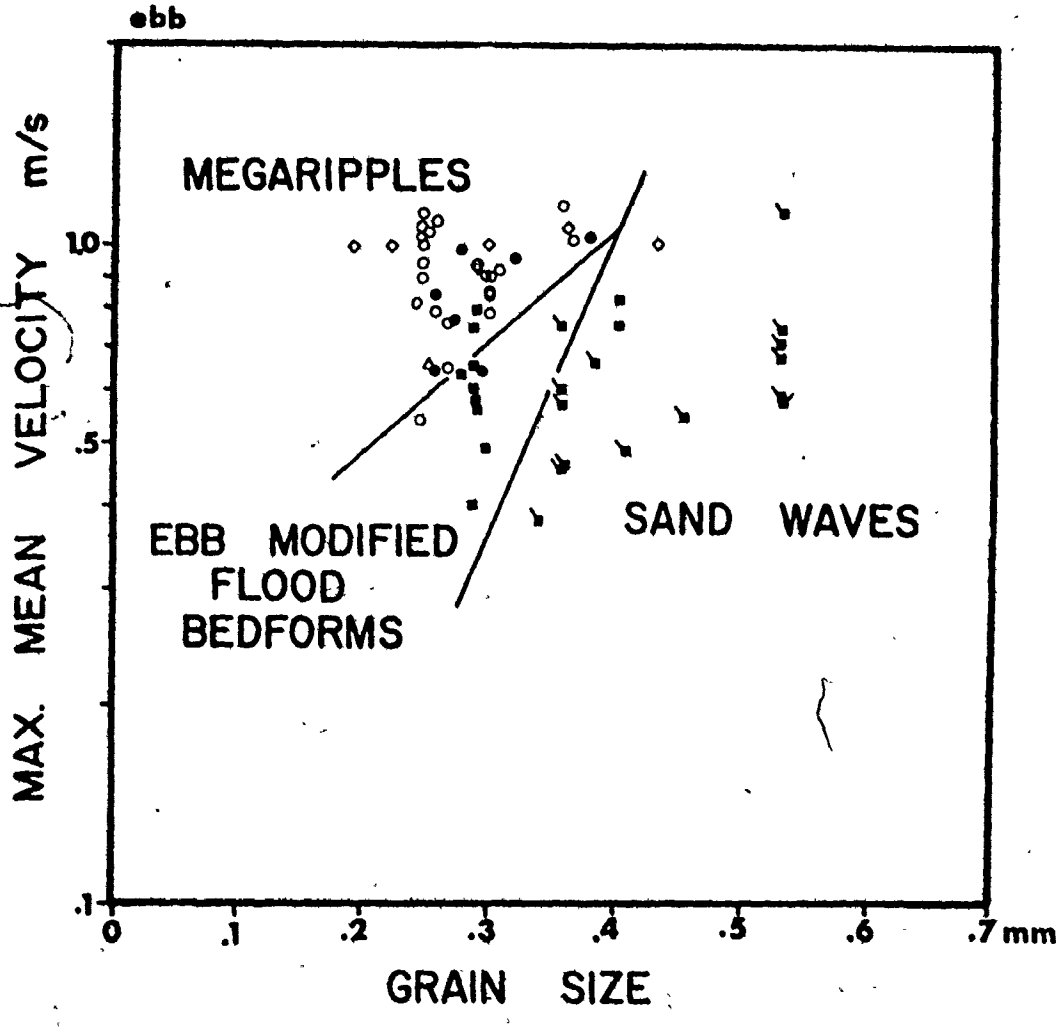

FIGURE 5.42: Bedform stability fields as a function of grain size and maximum mean velocity. See Fig. 5.41 for symbol description.

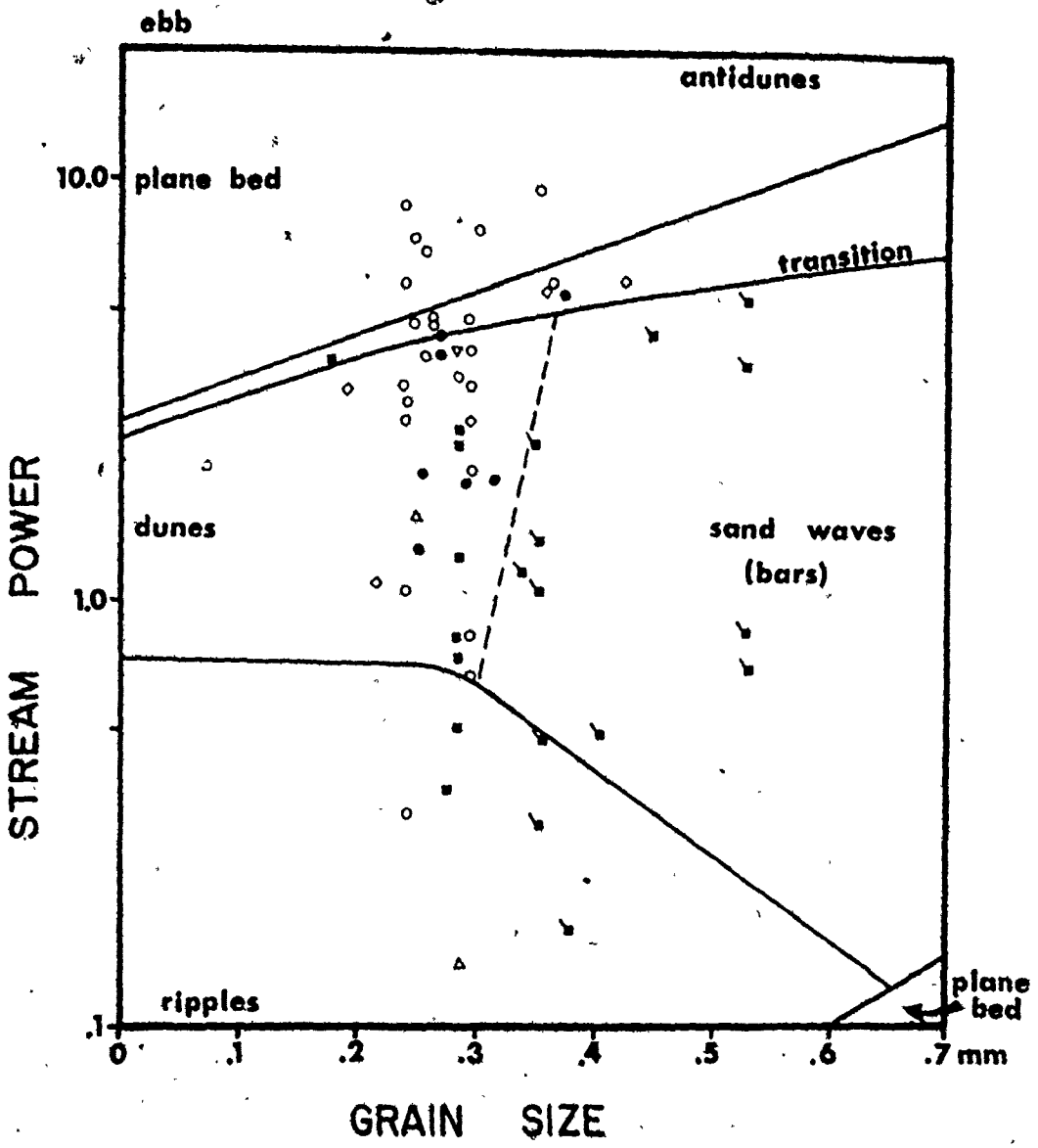

FIGURE 5.43: Bedform stability fields (after Simons, et al., 1965 a) as a function of grain size and stream power. See Fig. 5.41 for symbol description.

observations and collected data. According to Costello (1974), the mechanics of sand wave formation require a coalescence of faster moving smaller bars and ripples (e.g, possibly Fig. 5.25 b). The lack of evidence for the merging of sand waves may be because of the bidirectional tidal currents.

The results indicate that megaripples form in finer sediment sizes and greater flow strength than sand waves. This is the opposite to Klein and Whaley's (1972) findings. The ebb modified flood bedforms occur with intermediate grain sizes and flow strength relative to conditions of megaripple and sand wave development. A generalized sequence of bedform development with increasing flow strength is:

ripples→sand waves→ebb modified flood megaripples→linear megaripples→sinuous megaripples→planed-off megaripples→plane bed

This sequence is similar to the observed sequence in experimental flumes (Costello, 1974) and tidal estuaries (Boothroyd and Hubbard, 1975).

This sequence and the diagrams (Figs. 5.41, 5.42 and 5.43) offer a graphical means of predicting the approximate bed configuration during the ebb and gives some information about the relative occurrence and development of bedforms and the mean hydraulic conditions of the generating flow.

5.7 FLOW RESISTANCE

Flow resistance is related to the boundary roughness, and the flow velocity and depth, and is a measure of the energy loss in a flow. Knowledge about the variation of flow resistance with different bed configurations and flow conditions is important for: (i) the reliable prediction of the particular hydraulic properties of a flow, and the occurrence and development of bedforms in open channel flows; and (ii) the reconstruction of the paleohydraulic conditions associated with the deposition of various cross-stratification types that are recognized in ancient sedimentary rock sequences.

There is a large volume of literature on the subject of bedforms and flow resistance, much of it by hydraulic engineers. The current status

of the subject is reviewed in A.S.C.E. Task Committee, (1963 a), A.S.C.E. Task Force, (1971), Graf (1971, p. 303-320), Khanna (1970), Meliavsky (1965, p. 87-101), Raudkivi (1967 a, p. 222-252) and Yalin (1972, p. 262-286). Most of studies have been carried out in experimental flumes with artificial roughness elements (e.g., Koloseus and Davidian, 1966; O'Loughlin and Macdonald, 1964; Morris, 1955; Raju and Garde, 1970; Robinson and Albertson, 1952; Sayre and Albertson, 1961) and in alluvial channels with natural bedforms (e.g., Chang, 1970; Einstein and Barbarossa, 1952; Engelund, 1966; Garde and Raju, 1966; Herbich and Shulits, 1964; Nordin, 1964; Raudkivi, 1967 b; Rouse, 1965; Shen, 1962; Simons and Richardson, 1966; Smith, K.V.H., 1968; Squarer, 1970; and Vanoni and Hwang, 1967 and 1968). Few studies have attempted to ascertain resistance in reversing flows, e.g., in experimental flumes (Bayazit, 1969) and in natural systems (Charnock, 1959; Ludwick, 1975; Sternberg, 1968, 1970 and 1976). No one has studied the resistance of intertidal bedforms.

Chezy's C, Darcy-Weisbach's friction factor (f), $\bar{u}/u_*$ and the drag coefficient (C_D) are all measures of the boundary roughness and are equivalent to each other by the following relation:

$$\frac{C}{\sqrt{g}} = \sqrt{\frac{8}{f}} = \frac{\bar{u}}{u_*} = \frac{1}{\sqrt{C_D}}$$

The Darcy-Weisbach f, used in this study is derived from:

$$f = \frac{8u_*^2}{\bar{u}^2}$$

where u_* and $\bar{u}$ are determined for each vertical velocity profile measured.

For open channel flows over cohesionless sediment boundaries, the flow resistance is divided into two parts (Einstein and Barbarossa, 1952): (i) the grain roughness of the bed surface; and (ii) the form roughness of the bedforms (ripples, megaripples and sand waves), i.e.,

$$f = f' + f''$$

where f = total resistance, f' = grain roughness and f'' = form roughness. This relation was discussed by A.S.C.E. Task Committee (1963 a) and has been studied by Vanoni and Hwang (1967). Lovera and Kennedy (1969) and Alam and Kennedy (1969) suggested that the grain roughness

could be determined from a graph of the Darcy-Weisbach friction factor as a function of the Reynolds number for flat bed flows in sandy channels. The value of f'' could be derived by

$$f'' = f - f'$$

For boundaries covered with bedforms, form roughness comprises the largest part of the total flow resistance. Using Lovera and Kennedy's (1969, Fig. 2) graph, the magnitude of grain roughness for the Cobequid Bay sediments is negligible relative to the large flow Reynolds numbers (Appendix IV).

There are several methods for estimating flow resistance (e.g., Einstein and Barbarossa, 1952; Engelund, 1966; Simons and Richardson, 1966; Smith, 1968 and 1970), but none assesses form roughness in terms of the length, height and planimetric-shape of the bedforms. Chang (1970, O'Loughlin and MacDonald (1964, cited in Bayazit, 1969), Squarer (1970) and Vanoni and Hwang (1967, 1968) have studied the effects of the length and height of roughness elements (current ripples and artificial roughness) on flow resistance. Resistance is generally larger for increased relative roughness and with increased two dimensionality of the roughness elements. Most studies on flow resistance have been done in experimental flumes at a relatively small scale or in rivers (Annambhotla et al., (1972) with unidirectional flows. Few investigations have been made of the resistance characteristics of bedforms constructed by reversing tidal currents, either in experimental flumes or natural systems.

Semidiurnal Variation

Several representative diagrams of the Darcy-Weisbach friction factor (f) as a function of time during a tidal cycle are shown in Figures 5.44 and 5.45 for different bed configurations. The diagrams indicate that f increases very rapidly during the early part of the ebb then decreases to a minimum about mid-ebb and then quickly increases during the late ebb. During the flood, f-values increase rapidly to a maximum shortly after submergence of the bar surfaces and then gradually diminish towards high slack water.

Ludwick (1975, Table III) reported comparable values for the bed friction factor from flows over ripples, dunes and sand waves from

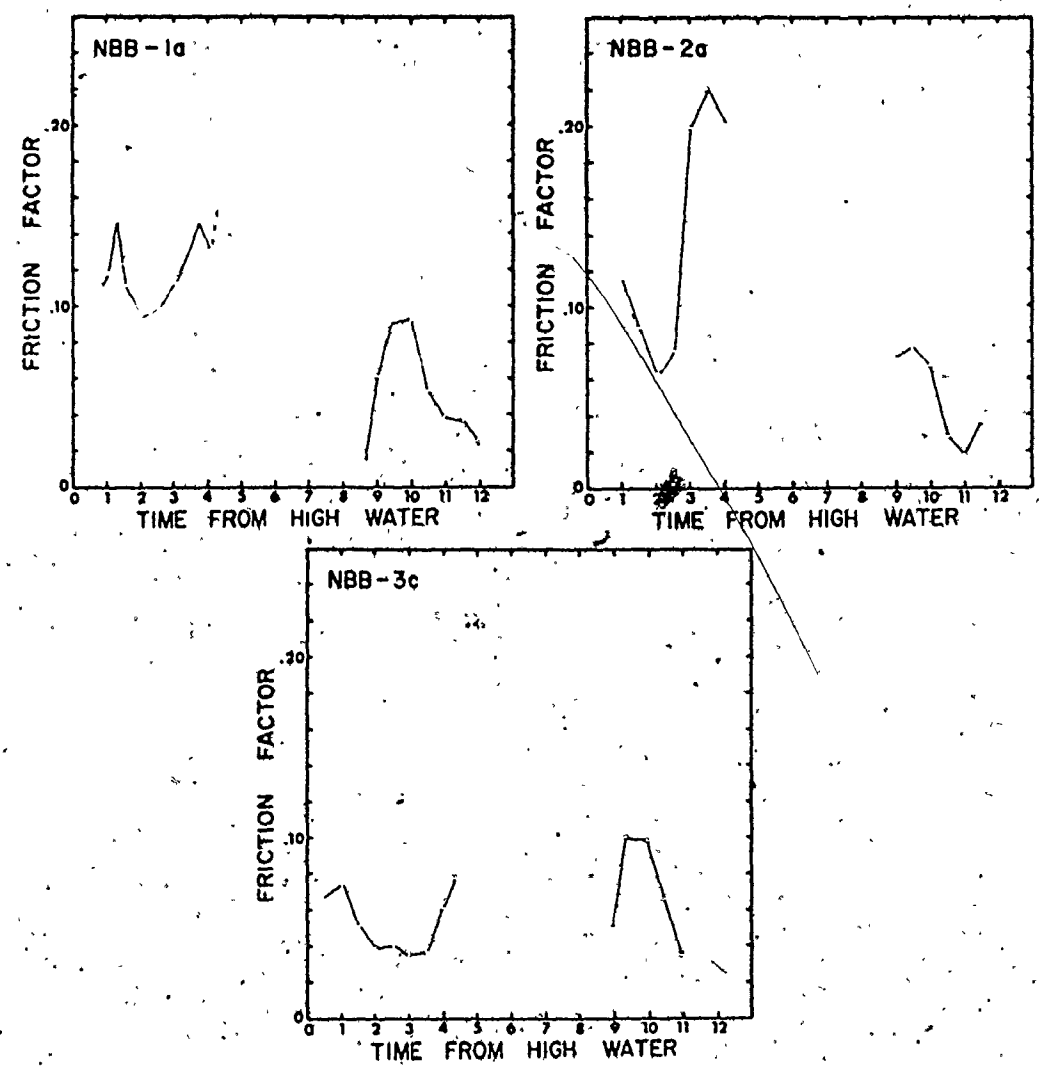

FIGURE 5.44: Temporal variation of the Darcy-Weisbach friction factor during a tidal cycle at several locations on Noel Bay Bar. See Figures 4.1 for locations and 5.20 for bedform types.

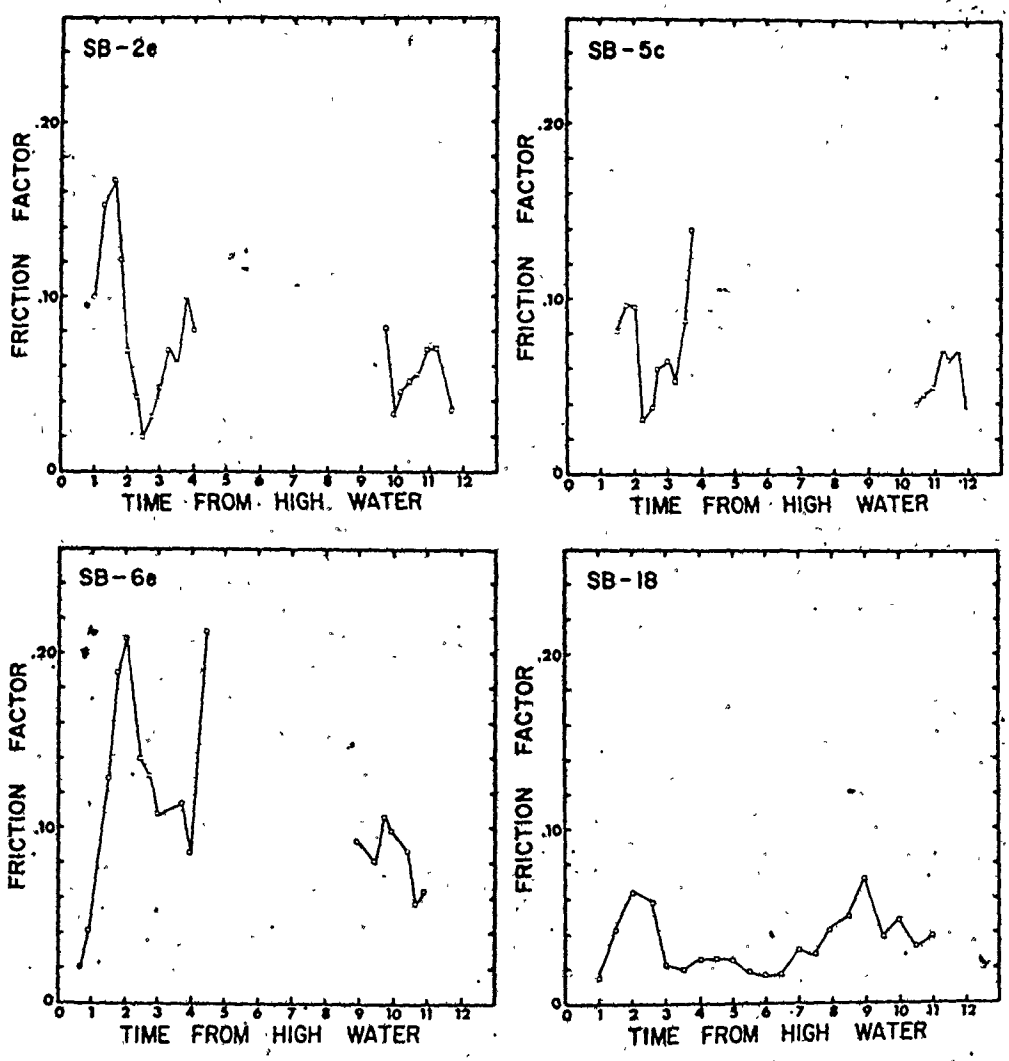

FIGURE 5.45: Temporal variation of the Darcy-Weisbach friction factor during a tidal cycle at different locations on Selma Bar. See Figures 4.1 for locations and 5.20 for bedform types.

Raudkivi's (1963) experimental results. He attributed the increase in friction factor to the hierarchy of bedforms and their sequence. The friction factor (or C_D) does not take on a constant value as suggested by the data of Sternberg (1968, 1972) and McCave (1973), but it does reach a maximum (Figs. 5.44 and 5.45) with varying flow strength (e.g., $\bar{u}$ or u_*) then falls off as does Raudkivi's (1963) data. See discussion by Komar (p. 91-106, in Stanley and Swift, 1976) and Ludwick (1975).

A possible hypothesis (Fig. 5.46) to explain the variation of f-values during a tidal cycle in areas with large bedforms is related to the ebb and flood reversal of bedforms. Following high slack water, early ebb currents have relatively large depths and bedforms are well-developed flood features and any flow separation is small, thus f-values are initially low to moderate. As the flow strength gradually increases, the flood bedforms are progressively reworked and the large f-values correspond to a maximum of bedform steepness (i.e., lower values of L/H). By mid-ebb, the bedforms are well-developed ebb features with fully developed flow separation but slightly lower and flatter (i.e., larger values of L/H); the amount of sediment in suspension is increased (McCave, 1973); thus f-values are smaller. As the flow depths continue to decrease, the relative roughness of the bedforms (H/d) increases and Froude numbers become larger, thus f-values are high just before emergence of the bar surface.

During the flood, f-values are initially low until flow separation becomes well developed. Between early to middle flood, the ebb bedforms are reworked and reversed. Bedform steepness reaches a maximum and f-values are high. From mid-flood to high slack water, f-values decrease as the depth of flow increases. Where there is a large ebb-flood asymmetry, mid-phase f-values are commonly larger on the dominant part of the tidal cycle, because this is when the flow separation will be best developed.

Bayazit (1969) suggested a similar explanation for the variation of resistance in experimental reversing flows over cohesionless sediments. However, he did not observe an increase of f-values during the late ebb because flow depths were kept constant, thus not affected by increased bedform relative roughness.

SB-18 in Figure 5.45 is a representative time-friction factor diagram for a channel location. The boundary is composed primarily of pebble and

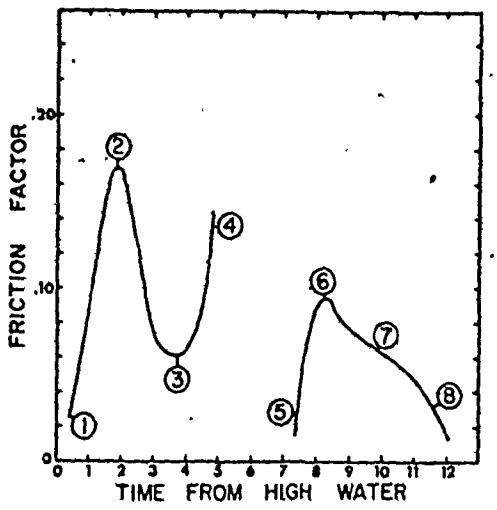

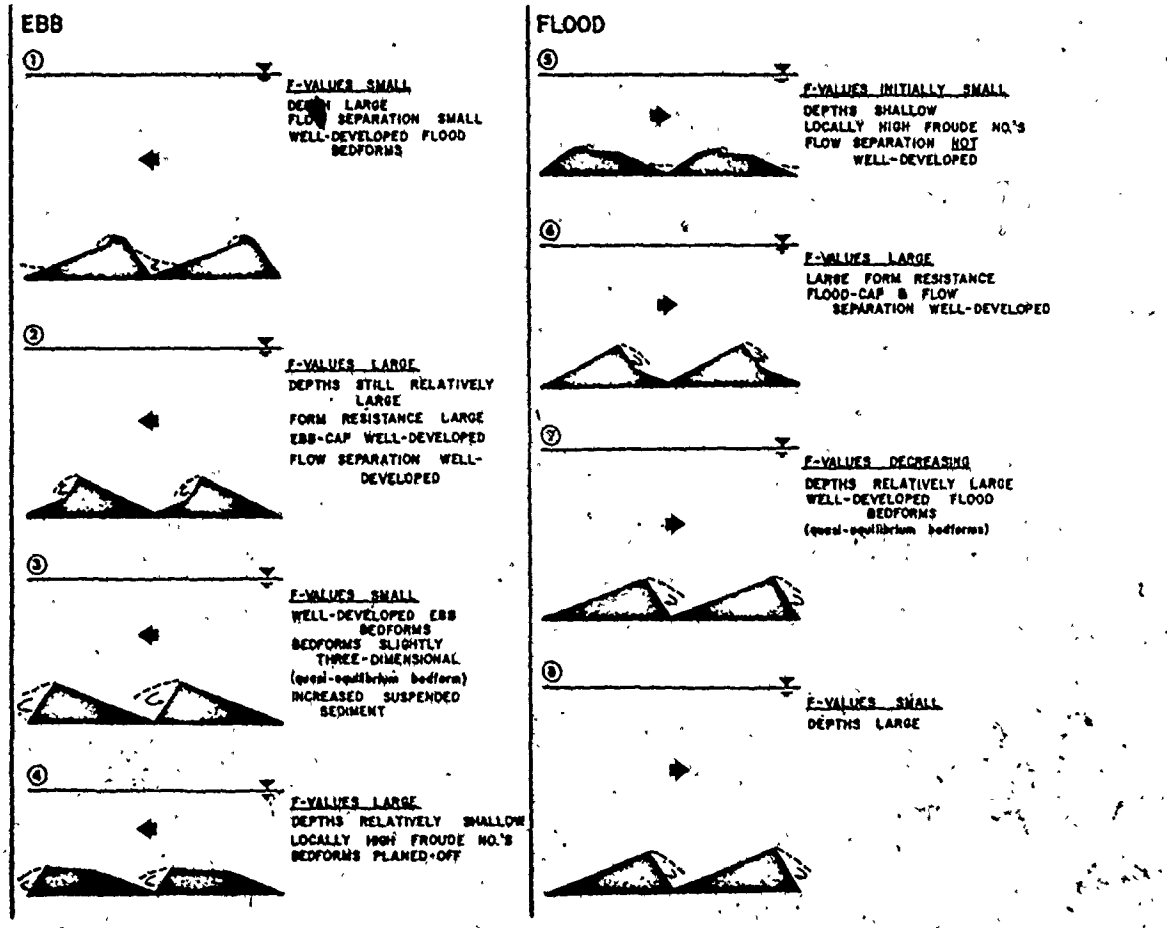

FIGURE 5.46: Hypothetical model depicting variation of the Darcy-Weisbach friction factor during a tidal cycle for flow over megaripples.

cobble sized sediments, i.e., the roughness height is smaller compared with bedform heights, thus f-values are lower. The absence of relatively shallow flow depths at low tide explains why there is no increase in f-values during the late ebb.

Friction Factor and Bedform Roughness

Several investigations have found that flow resistance is a function of the size and geometry of bedforms. Vanoni and Hwang (1967, 1968) showed that eH (exposure parameter times bedform height) is a better length measure of hydraulic roughness than H/L or an equivalent sand grain roughness (e.g., k_s). The value of 'e' is, however, difficult to determine accurately in the field. Chang (1970); Raju and Garde (1970); Robinson and Albertson (1952) and Sayre and Albertson (1961) have reported a good correlation between flow resistance and relative roughness, d/H. Morris (1955) suggested that the longitudinal spacing of boundary roughness elements and depth (d/L = relative roughness spacing) is related to flow resistance because the main source of friction loss is turbulence from the wake and separation zones behind bed roughness elements. Thus, roughness element spacing should be correlated to friction loss.

Bayazit (1969) found that the roughness of a reversing flow in an experimental flume was characterized by the value of the friction factor at the time of the maximum mean flow velocity per ebb and flood. The same procedure for selecting representative f-values was used in this study. Because bedforms changed early in the ebb and flood and there were changes produced by late stage deflection of flow and large relative roughness values, the most reliable and consistent f-values were found in mid-ebb and in mid to late flood. This agreed with the occurrence of peak current velocities during the ebb and flood.

These f-values were graphed as a function of bedform height, length and ripple index. Figure 5.47 shows the results for ebb bedforms and f-values. Bedform height and length were positively correlated with f-values, and ripple index is inversely related to friction factor. None of the correlations was statistically very convincing because they had low correlation coefficients. Nevertheless, the results indicate that f-values increased with increasing bedform length and height, and decreasing ripple index. Although these results are statistically insigni-

FIGURE 5.47: Darcy-Weisbach friction factor as a function of bedform dimensions.
Open circles = megaripples;
Closed squares = ebb modified flood bedforms;
Closed Squares with ticks = sand waves

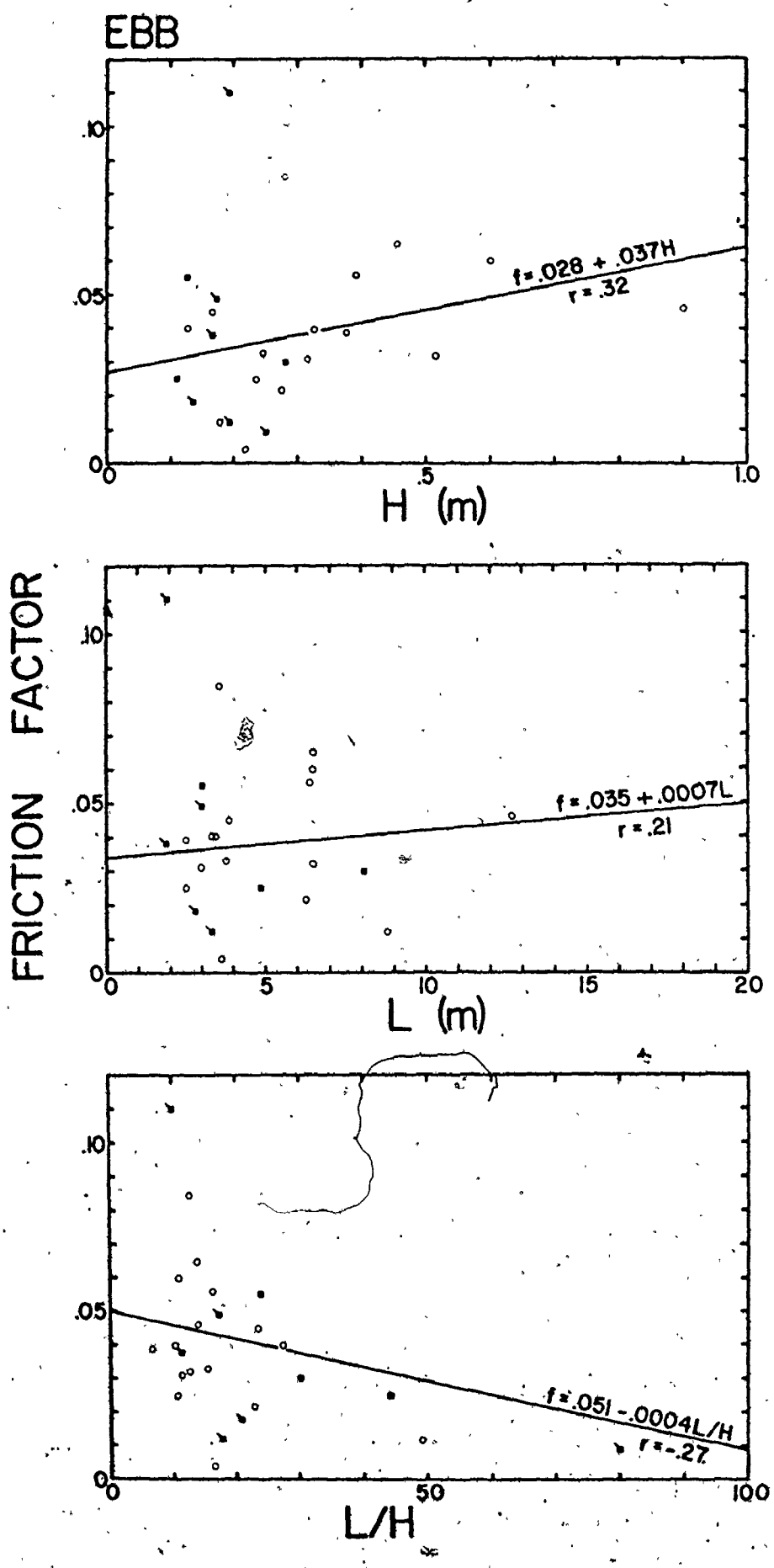
EBB
FRICTION FACTOR
.10
.05
0
0
.5
1.0
H (m)
f=.028 + .037H
r=.32
5
10
15
20
L (m)
f=.035 + .0007L
r=.21
50
100
L/H
f=.051 - .0004L/H
r=-.27

ficant, they are meaningful because a lot of the point scatter is due to modification of the bedform dimensions by late-stage ebb currents, and variability in the value of the Darcy-Weisbach friction factor which is calculated from u_*.

A graph of friction factor $\frac{1}{f}$ versus D/H and D/L showed little (r=0.18) to no correlation respectively.

The f-values for intertidal bedforms are comparable to those determined from velocity profiles of Dyer (1970) from a tidal channel and of Jordan (1965) and Scott and Stephens (1966) from the Missouri River. The maximum friction factor is larger for intertidal bedforms than for corresponding bedforms in unidirectional flows. This may be due to the tendency for fluvial bedforms to be more three-dimensional in form than intertidal bedforms.

Allen (1976 b) concluded that there was "... no acceptably reliable way of calculating the flow resistance of a large stream from the properties of its bedforms, ...". The results reported here partly support that conclusion.

5.8 SEDIMENTARY STRUCTURES

The migration of bedforms and accumulation of bed sediment produces a diverse variety of sedimentary structures in terms of size and geometry. From the extensive literature on stratification types, the following authors present a general review of the subject: Allen (1963; 1968 b, p. 96-129); Blatt et al. (1972, p. 111-158); McKee and Weir (1953); Pettijohn et al. (1973, p. 102-127); and Potter and Pettijohn (1963).

Sedimentologists working on tidally deposited sediments have concentrated their efforts in two areas; (i) the identification and description of characteristic primary sedimentary structures produced by tidal currents in Holocene clastic sediments (e.g., Boersma, 1969; Boersma et al., 1968; Ginsburg, 1975; Houbolt, 1968; Klein, 1970 a; Oomkens and Terwindt, 1960; de Raaf and Boersma, 1971; Reineck, 1963, 1967; Reineck and Singh, 1967, 1972, 1973; Reineck and Wunderlich, 1968; van Straaten, 1953 and Terwindt et al. 1968 and 1972; etc.); and (ii) the identification and reconstruction of the tidal nature of ancient clastic sediments (e.g.,

Bosence, 1973; Ginsburg, 1975; Klein, 1967, 1970 b, 1971, 1972; de Raaf et al., 1971; van Straaten, 1954; Swett et al., 1971; etc.) Results from the latter area have met with varied success.

The purpose of this section is to describe the internal cross-stratification of the intertidal bedforms examined in this study and to discuss their origins. The trenching and peel techniques used are described in Appendix V.3.

Results and Discussion

The sedimentary structures produced by the migration of bedforms on the intertidal bars have either simple or complex internal organization depending on the bedform type. Essentially two dimensional bedforms such as ripples and linear megaripples are characterized by a simple internal geometry. Sand waves and sinuous megaripples are distinguished by complex cross-stratification. Reineck (1963), Klein (1970 a) and Boersma (pers. comm., February, 1973) recognized a similar relation between bedding and bedform type. Some examples of primary sedimentary structures megaripples and sand waves are shown in Figures 5.48 to 5.53.

Facies C2 Megaripples - (linear crestlines) are characterized by tabular cross-stratified sets (Figure 5.48 A). These bedforms have a single unimodal (ebb) cross-stratified set whose length and maximum thickness are comparable to the scale of the megaripple. The sets have fairly sharp bounding surfaces which dip at about 5 degrees in the ebb direction. Individual cross-strata are tangential to the lower erosional surface. The upper, steep part of the cross-strata dip downcurrent between 25 and 30 degrees. There is some indication of simple ripple cross-lamination near the upper surface of the bedform, but much of this has been disrupted by the peel technique.

Facies D2 Megaripple - Figure 5.48 B shows the internal structures a Facies D2 megaripple on Selma Bar. The internal organization is similar to the Facies C2 megaripple (above). The cross-stratified set last deposited by the ebb has a maximum thickness of about two-thirds of the bedform's height. Individual sets are separated by ebb and flood planar to concave erosional surfaces with dips ranging from 5 to 10 degrees. These surfaces truncate the upper parts of cross-stratified sets within the bedform. Some herringbone cross-stratification is evident below (Fig. 5.48 B2) the last deposited ebb sets. Ebb and flood cross-strata dip

FIGURE 5.48: Peels from Facies C2 (A) and D2(B) megaripples on Selma Bar. Photos are numbered consecutively upflow from the megaripple brinkline.
A & B - 13/8/73

SB - 8

13/8/73

1 of

B2

EBB

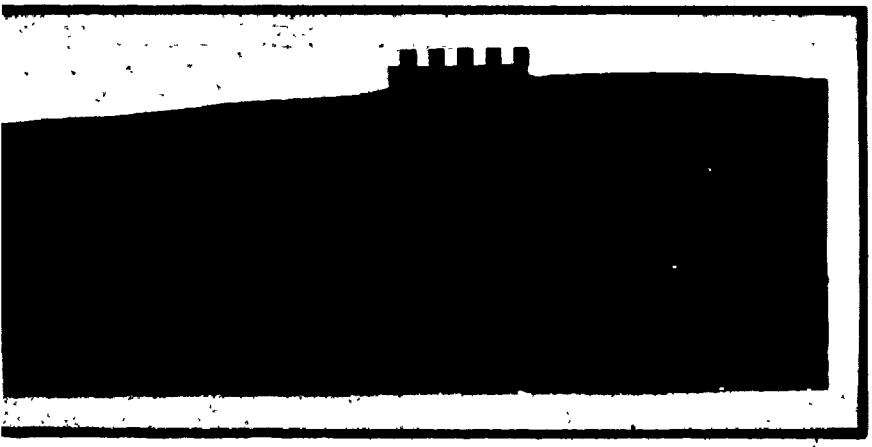

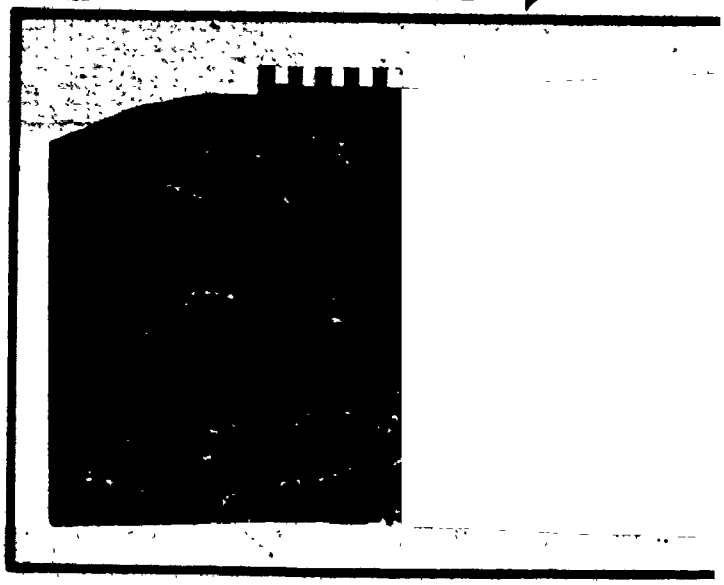

A

EBB

BB

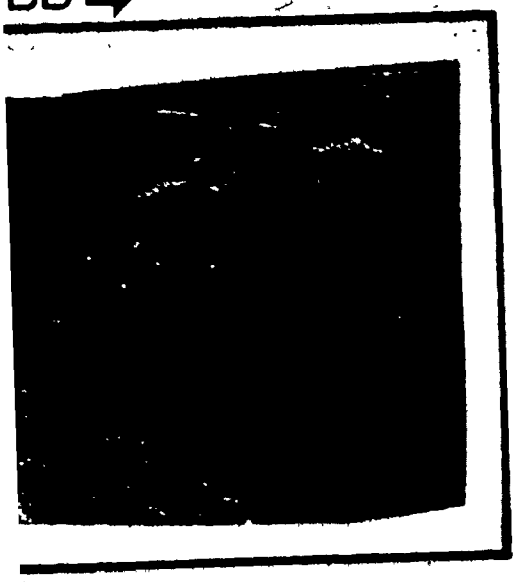

BI

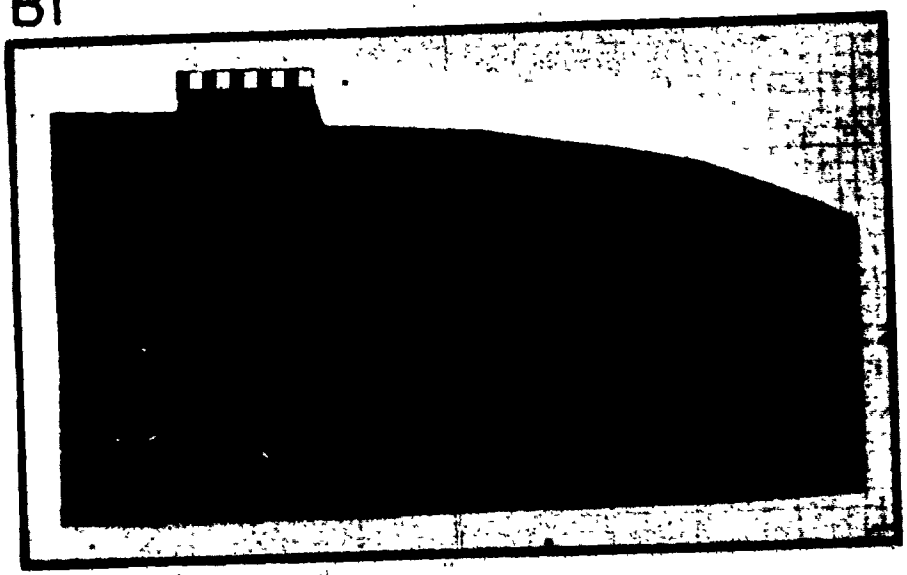

downcurrent at about 25 degrees and contact the lower bounding surfaces tangentially. Beneath the uppermost ebb set, there seems to be an equal proportion of ebb and flood sets in terms of frequency and thickness. Sinuous megaripples are trough cross-stratified and are more complex internally than linear megaripples (Facies C).

The herringbone cross-stratification observed in Figure 5.48 B2 results because the currents of the ebb and flood are nearly equal. Echo sounding during submerged periods and direct observation at low tide show that the megaripples in this area completely reverse their asymmetry with each phase of the semidiurnal tidal cycle. With each phase of the tide, the currents erode some of the existing cross-strata before depositing cross-strata of its own. In this manner, parts of cross-stratified sets generated by ebb and flood currents are preserved. If either the ebb or flood were dominant, then only one orientation of cross-stratification would likely be preserved.

Facies D3 Megaripples - The internal structures shown in Figures 5.49 and 5.50 are from Facies D3 megaripples (planed-off crestal platforms); two examples are from Selma Bar and two from Noel Shore Bar (NSB-4 and -6). The most distinctive sedimentary structure in these megaripples is the parallel bedding (0.1 to 0.15 m thick) overlying trough to planar cross-stratification (0.1 to 0.15 m thick). Note the different types of cross-stratification deposited during the ebb through the megaripple and the absence of an ebb cap, typical of Facies C and other Facies D megaripples. The ebb cross-stratification was deposited initially on either a reactivation surface (Collinson, 1970; Klein, 1970 a, Boersma, 1969) dipping in the ebb direction (Fig. 5.29) or on the remnant flood stoss-side, then into the trough of the developing ebb megaripples. The ebb trough cross-stratification dip at 25 to 28 degrees down current and have tangential contacts with the lower bounding surface. The concordant bedding that truncates the upper parts of the cross-stratification dips downcurrent at less than 5 degrees. The planar foresets near the megaripple lee side dip at 20 to 25 degrees. The thickness of the planar foresets is comparable to the height of the bedform. The periodic truncation of the parallel bedding and planar foresets indicates the random behaviour of the bedfor mo

FIGURE 5.49: Two sets of peels from Facies D3 megaripples on the northwest side of Selma Bar. Photos are numbered consecutively from the megaripple brinkline.

A. - 27/6/73

B. - 9/7/73

SB - 6

27/6/73

A3

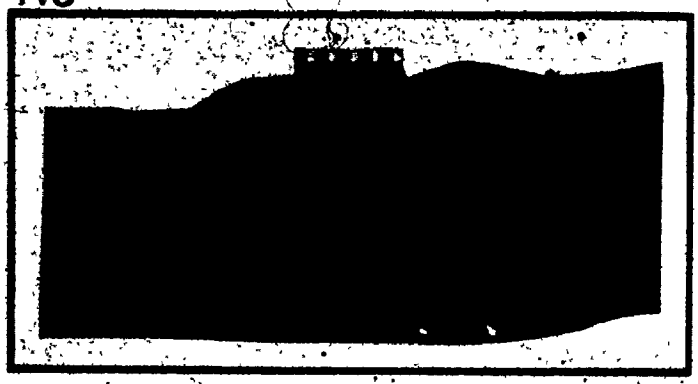

A2

B3

B2

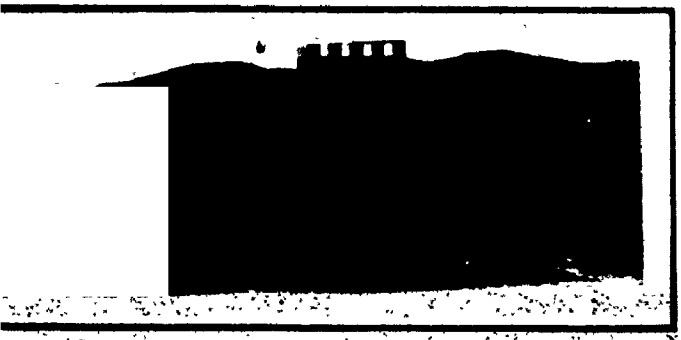

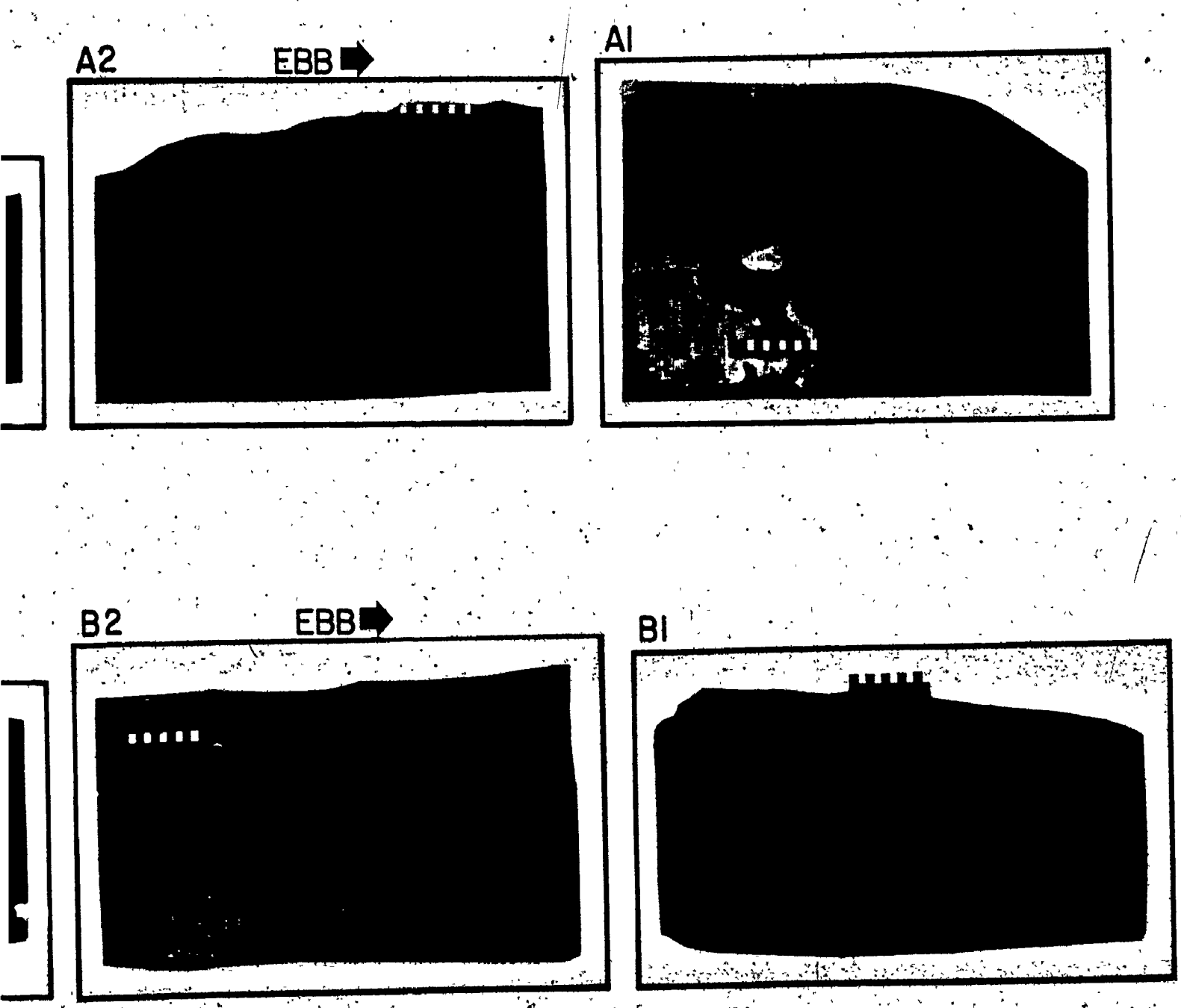
A2
EBB
A1
B2
EBB
B1

FIGURE 5.50: Two sets of peels from Facies D3 megaripples on Noel Shore Bar. Photos are numbered consecutively from the megaripple brinkline.

A. - 17/8/73

B. - 15/8/73

NSB - 6

17/8/73

A1

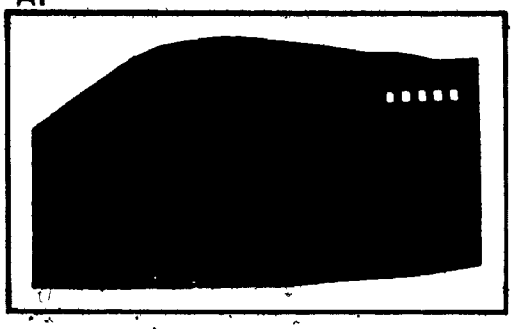

A2

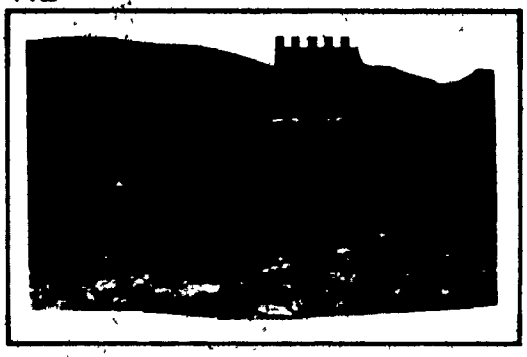

A3 ⬅EBB

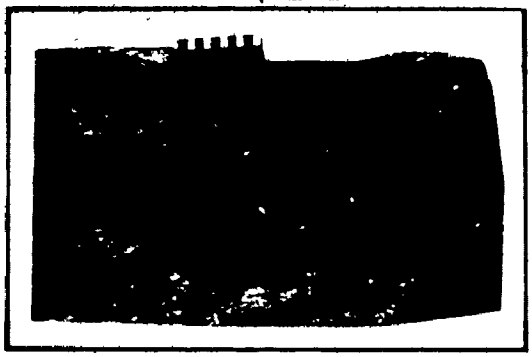

NSB - 4

15/8/73

B1

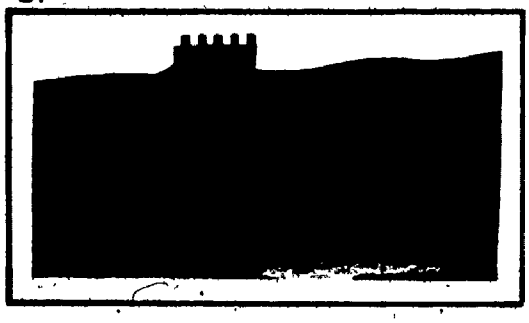

B2

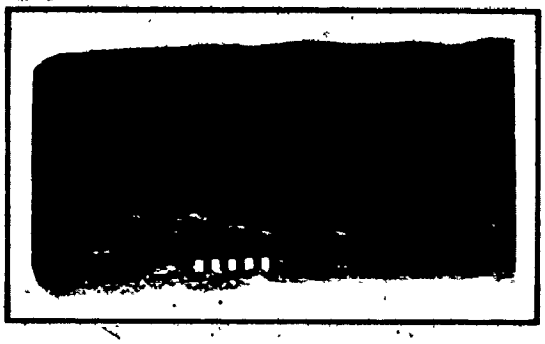

B3 EBB➡

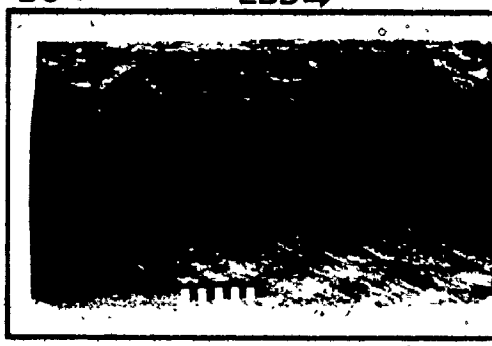

EBB

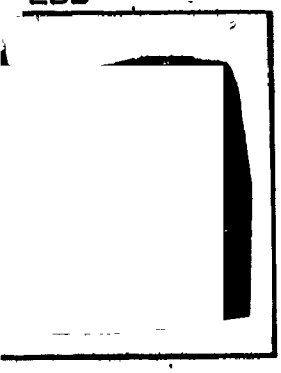

A4

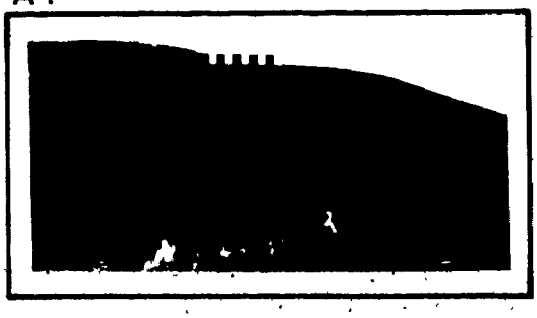

A⊥

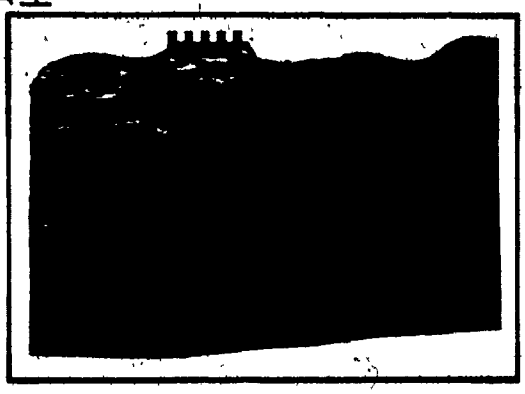

EBB➡

B4

B⊥

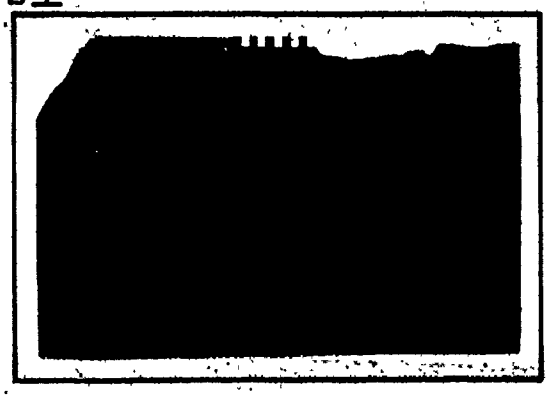

features associated with the ebb cross-stratification, show some similarity to small-order reactivations (Allen, 1973, his Fig. 3) caused by random fluctuations in the flow velocity. The frequency and relative complexity of such discontinuity planes increases upcurrent from the lee-slope.

The deposition of the parallel bedding and planar foresets (Jopling, 1965) is associated with the planing-off phase of megaripple crests just before low tide emergence. During the late ebb, current flow becomes shallow and rapid, i.e., the flow Froude number increases over the bedform crest causing the sediment to move as a sheet (upper plane bed phase of Simons et al., 1965 a).

Although it is not clear from current measurements (Fig. 4.14) whether SB-6 is ebb or flood dominant and echo-sounding indicates that the megaripples at SB-6 reverse their orientation with each ebb and flood (Fig. 5.27), there is no herringbone cross-stratification preserved in the bedform. It is possible that flood cross-stratification was not found because: (i) the peels were not taken deep enough (e.g., maximum depth of about 0.35 to 0.40 m); or (ii) ebb erosion and bedform migration completely destroyed or reworked any flood cross-stratification produced. If the latter is true, it is difficult to explain the occurrence of parallel bedding within the megaripple. It may be the result of deposition from shallow (high Froude number) flows during the early flood (Fig. 5.19 D).

The sedimentary structures at NSB-6 (Fig. 5.50 A) are similar to those at SB-6, but the former location is ebb dominated (Fig. 4.13). Beneath the brinkline of the megaripple, the sedimentary structures are characterized by parallel bedding and planar foresets. Towards the stoss-side of the megaripple, these structures gradually disappear as they are replaced by ebb trough cross-stratification (with dips of 6 to 15 degrees) that are deposited on concave (upwards) reactivation or discontinuity surfaces.

Figure 5.50 B, from NSB-4, shows that the planed-off megaripples here are similar to the bedform described above, except for the thick (about .20 m+) unit of low angle (approximately 8 to 10 degrees) flood dipping cross-stratification. The upper bounding surface of the flood set is slightly undulating and it dips at about 5 (the

Figures 5.50 A and B show the nature of the sedimentary structures transverse to the direction of flow and beneath the bedform crestal platform at NSB-4 and -6. The geometry of the stratification indicates the occurrence of tabular and trough cross-stratification within the bedform.

The sequence of sedimentary structures shown in Figure 5.51 are from Facies G5 megaripples (ebb capped flood megaripples). The superposed cap on the remnant flood megaripples is a composite ebb cap, i.e., composed of more than one ebb cross-stratified set. The ebb cross-strata dip down current at about 28 to 30 degrees and the intervening reactivation surfaces are inclined downcurrent at 10 and 15 degrees (convex upwards). The remnant flood megaripple stoss-side is covered with a cross-laminated 'ripple-roof' that is about 4.5 cm thick. Reactivation planes separating the ripple cross-lamination and some parallel bedding dip downcurrent (ebb) at about 5 degrees. The cross-laminated sets result from late-stage ebb runoff in the trough of the megaripple which generate linear and linguoid ripples and some parallel lamination. These structures are destroyed by the succeeding tide. Beneath the ebb cap, flood cross-stratified sets are the dominant sedimentary structure. Sets are separated by planar to slightly undulating discontinuities (or reactivation surfaces) which dip to the east at 10 and 12 degrees. The flood cross-strata dip at about 30 degrees and have tangential contacts with the lower bounding surface. Some of the cross-stratified sets have low angle planar bedding (about 10 to 12 degrees) that is slightly convex upwards. It may represent the initial phases of flood reworking and reversal of the ebb bed feature during the early flood by rapid, shallow flows (relatively large Froude number). The preserved flood cross-stratified sets are thicker than the individual ebb sets in the megaripple cap (17 to 12 cm versus 4 to 6 cm) and represent deposition after the bedform is reversed sufficiently and flow separation is well-developed.

Facies G4 Sand Waves - The internal sedimentary structures of some sand waves (Facies G4) are shown in Figures 5.52 and 5.53. from two locations on Selma Bar. These bed features are similar to Klein's (1970a) complex sand waves. Their internal organization is more complex than that of the megaripples. Surfaces of discontinuity are numerous and are generally curved (as opposed to planar). They truncate the cross-stratified

FIGURE 5.51: Peels from Facies G5 (ebb capped flood megaripples) bedforms near SB-5 on Selma Bar.
A & B - 4/7/73

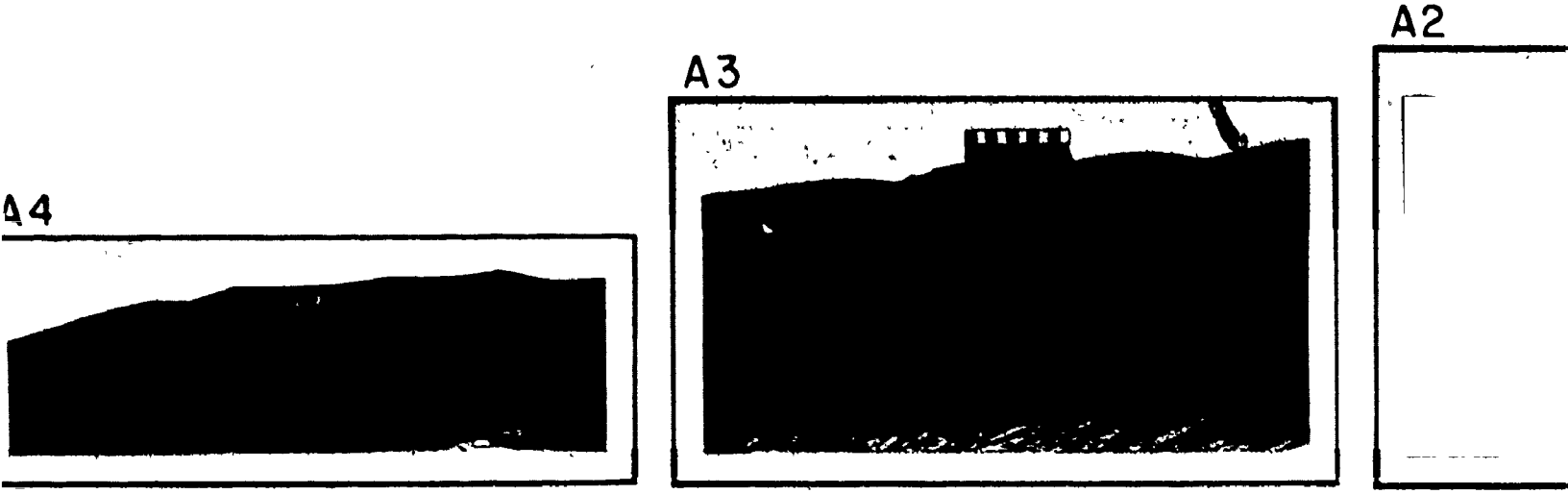

SB-5

4/7/73

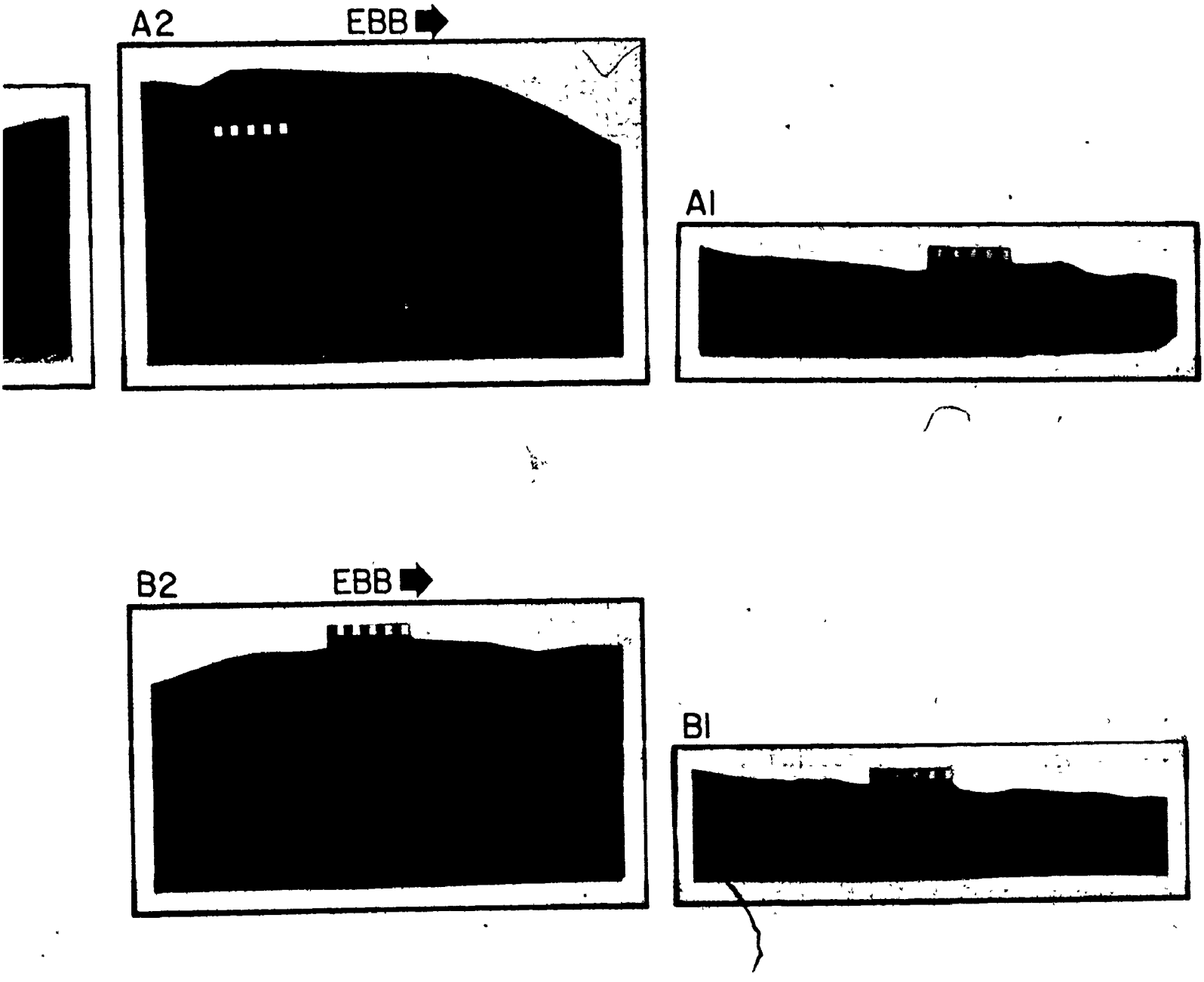
A2
EBB
A1
B2
EBB
B1

FIGURE 5.52: Peels from Facies G4 (sand waves) bedforms near SB-1 on Selma Bar.

A. 28/6/73

B. 5/7/73

SB-1

28/6/73

A1

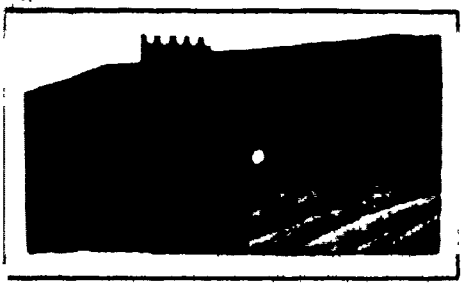

A2

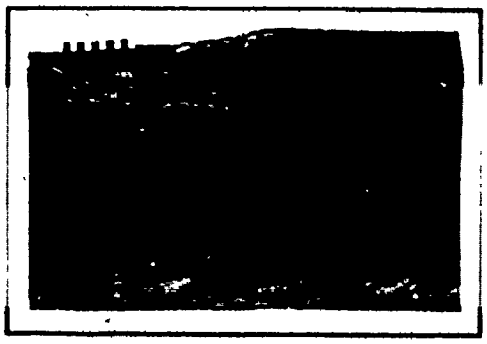

A3 ⬅FLOOD

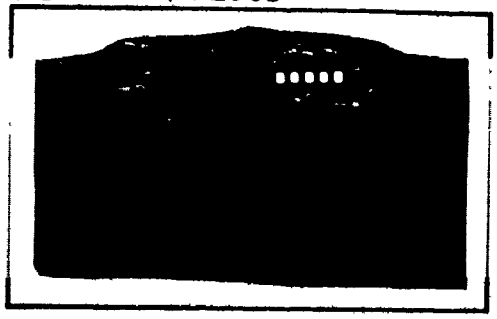

A4

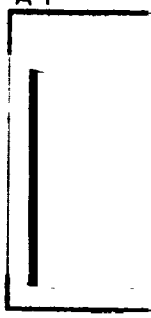

5/7/73

B1

B2

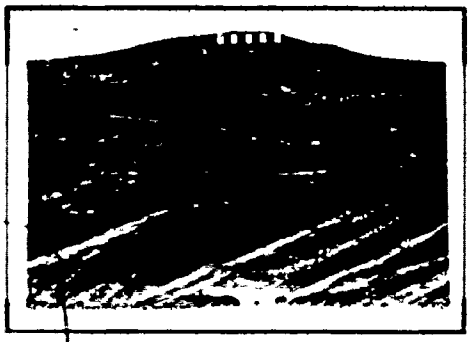

B3 ⬅FLOOD

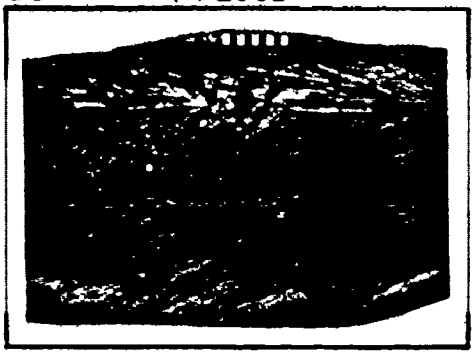

B4

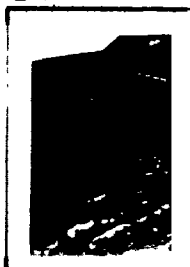

1 of 1

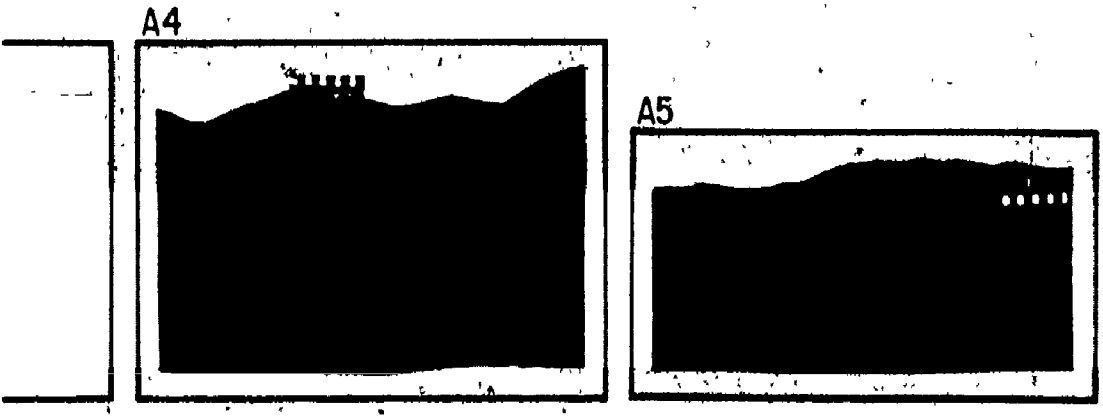
A4
A5

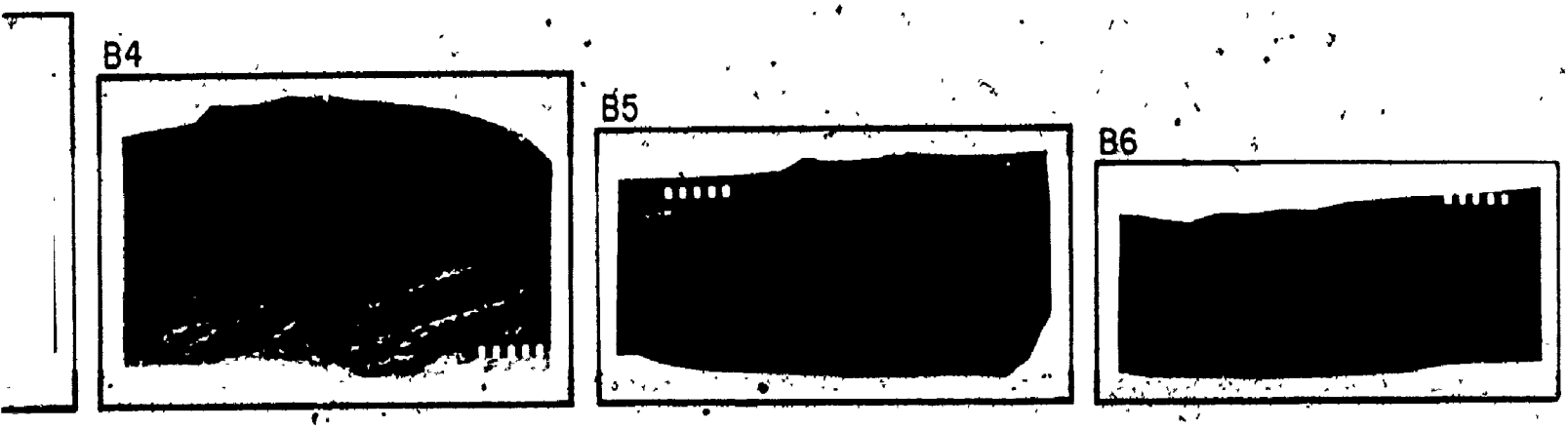
B4
B5
B6

FIGURE 5.53: Peels from Facies G4 (sand waves) bedforms near SB-2 on Selma Bar.

A. 3/7/73.

B. 10/7/73.

SB-2

3/7/73

A1

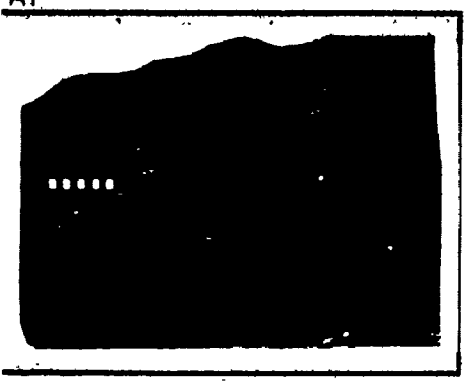

A2

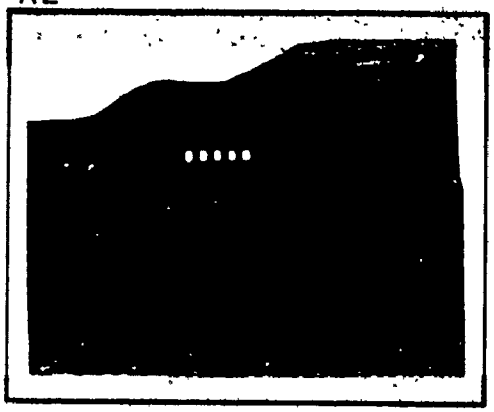

A3

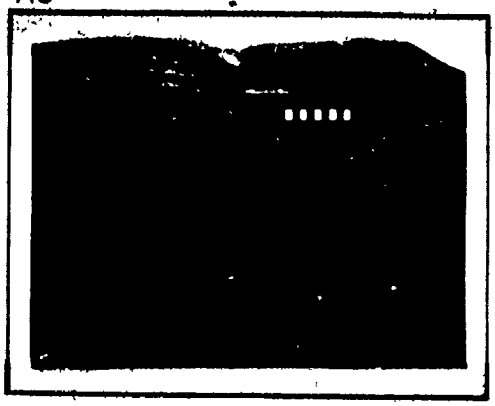

A4

10/7/73

B1

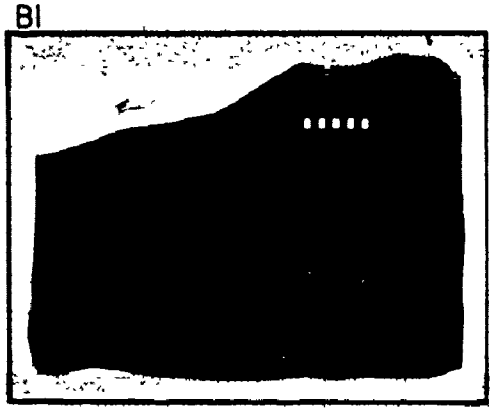

B2

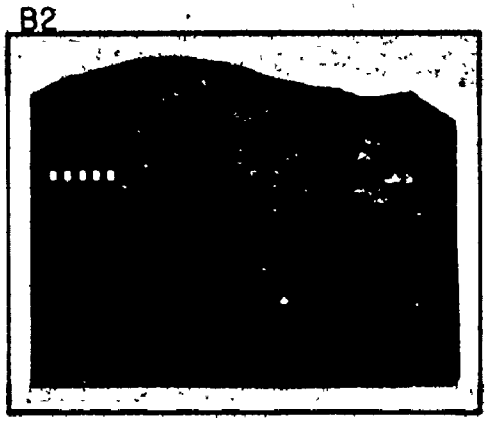

B3

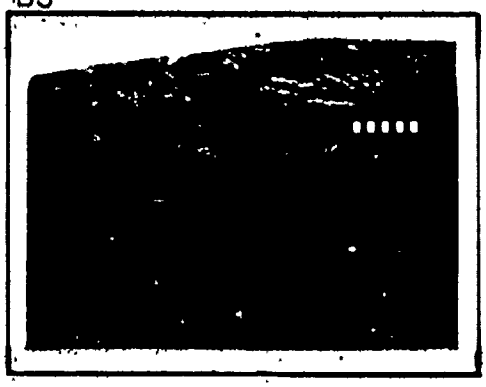

B4

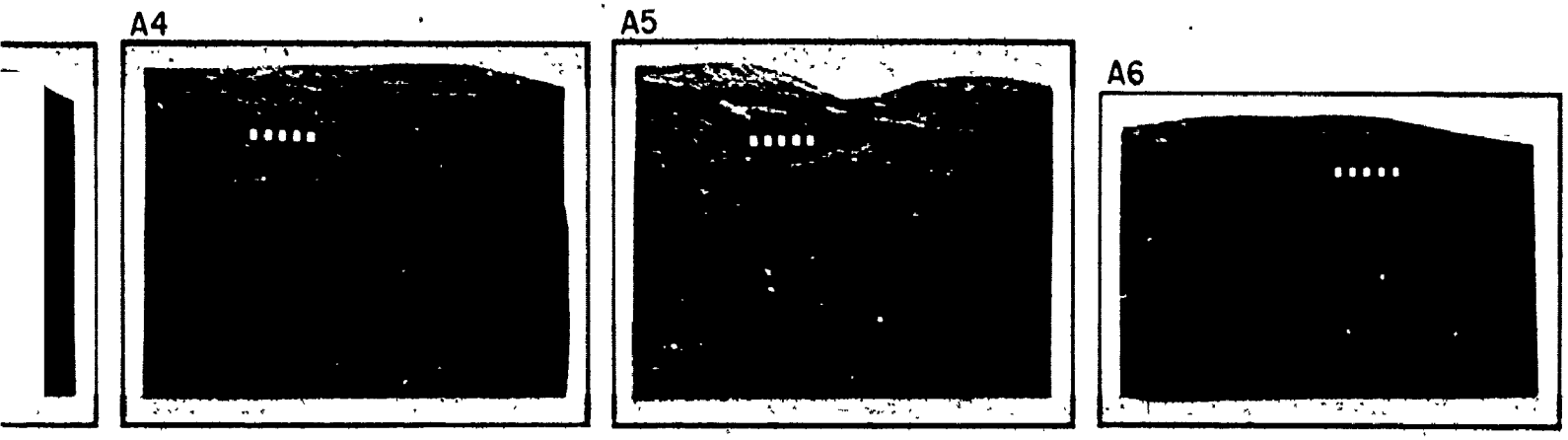
A4
A5
A6

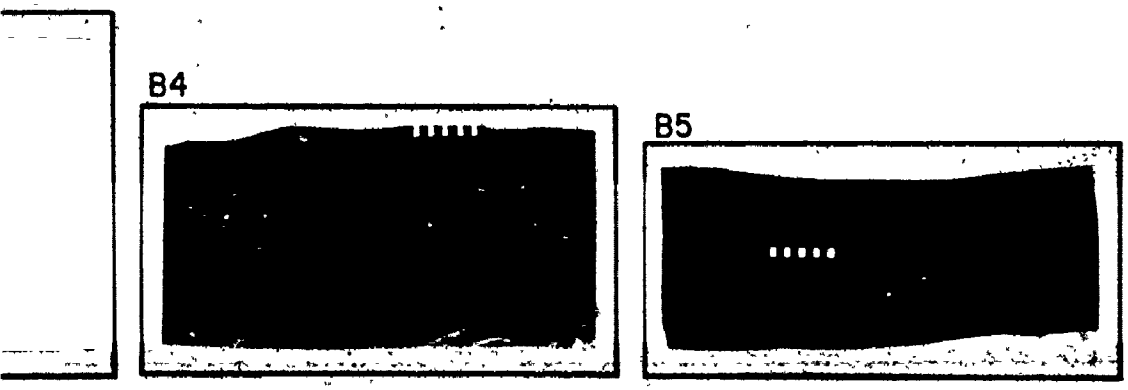
B4
B5

sets at oblique angles without any regular organization. The sand waves have a megaripple 'roof' during both the ebb and flood (Fig. 5.3C). Migration of these superposed bed features accounts for most of the internal sedimentary structures.

At SB-1, the sand waves are capped by only one or two ebb megaripples when viewed at low tide (Fig. 5.26 C and D). The cross-stratification of the megaripples dips to the west at 25 to 28 degrees and laminae are concave upwards. Ebb laminae are tangential to the lower bounding erosional surface. The thickness of the ebb sets range from .06 to .12 m, which is generally less than the actual height of the ebb megaripple. There is very little preservation of the ebb sets because the subordinate flood currents erode and rework the surface of the sand waves to depth of about .20 m (Fig. 5.33). Most of the preserved structures in the sand waves is flood trough cross-stratification and eastward dipping (between 10 and 22 degrees) flood reactivation surfaces. There are two types of discontinuity planes separating the flood sets: (i) low angle reactivation surfaces that are convex upwards and dip towards the east; and (ii) erosional surfaces which are concave upwards. The first type occurs near the lee slopes of the sand wave and are similar to those described by Klein (1970 a) that result from the process of bedform reversal. The trough-like erosional surfaces that are more common within the core of the sand waves may be attributable to changes in bedform movement caused by random fluctuations in current velocity (Allen, 1973, his Fig. 3 and 4). Some ripple trough cross-lamination occurs at the tops of the large flood sets and beneath some of the erosional reactivation surfaces. These structures may represent preserved ripple features that were constructed by low tide open channel flow in the troughs of the sand waves.

The two series of sand wave peels at SB-1 were collected on June 28 and July 5 (1973) with mean tidal ranges of 12.20 and 11.85 m respectively (at Burntcoat Head). The first sequence was taken about one or two tidal cycles before maximum spring tides and the second example was taken about seven or eight tidal cycles after spring tides. Although the primary structures were fundamentally the same in the two series, there were some differences, such as: (i) the flood sets were generally thinner on July 28 than on July 5 near the sand wave lee-slope; and (ii) there were more reactivation surfaces and erosional planes on

June 28 than on July 5. The differences possibly reflect the effect of tidal range on current strength and thus on the erosion potential of the currents. The thickness and length of the cross-stratified sets deposited should increase towards spring tides, but the stronger currents cause greater erosion. As a result, only part of the total set thickness is preserved. Towards neap tides, successive cross-stratified sets deposited should show a decrease in thickness and a greater chance of total preservation because current velocities are less during this period. This hypothesis is only partially supported by peels collected at SB-2 (i.e., post spring tide structures are only slightly more complex and thinner than near neap peels).

Figure 5.53 shows two series of peels from a sand wave at SB-2. The sand waves here are very similar to those at SB-1. The major differences are: (i) the stoss-side of sand waves at SB-2 are completely covered with superposed megaripples (Fig. 5.26 A and B) compared with only one or two at SB-1; and (ii) the ebb and flood cross-stratified sets are thicker at SB-2 (the superposed megaripples have larger heights) than at SB-1. The superposed ebb megaripples at SB-2 decrease in height and length away from the sand wave crest and disappear in the troughs. Costello (1974) suggested that "the presence of dunes on sand waves indicates either a nonequilibrium condition in which sand waves are being altered to dunes, or an equilibrium sand-wave state with dunes being a minor bed configuration that is developed only locally." He concluded that "the dunes are a metastable, secondary form superimposed on, and initiated by, the large sand waves."

The internal structures of the ebb dominated sand wave (Fig. 5.26 E and F) is less complex than a flood dominated sand wave. The structures consist of successive ebb cross-sets and ebb reactivation surfaces.

5.9 WINTER CONDITIONS

Although drift ice and the ice-foot produce impressive and conspicuous sights during the winter in Cobequid Bay, their geological significance appears to be smaller than that of the frozen ice-sediment crust.

The presence of the frozen crust protecting the intertidal zone sediments is the change of greatest sedimentological importance produced by winter conditions. The crust essentially immobilizes and protects all of the intertidal sediments from the "normal" (summer) entrainment and transport processes and leaves almost no free sediment in the intertidal zone. Areas with standing or running water where the crust did not form, or places where the crust was removed, and the subtidal area are the only places where sediment is still mobile. This effect is most significant in the non-cohesive sediments of the intertidal sand bars where sediment is extensively moved as bed load by traction and intermittent suspension during most of the year. On the mudflats, the frozen crust does not appear to play as significant a role in arresting sediment transport because the transport of sediment by suspension is more important than bed load movement. The presence of the crust does, however, inhibit resuspension of sediment.

The observed decrease in the amount of bed load is in contrast to that expected if the frozen crust were not present. With lower winter water temperatures (-0.5°C in winter versus 15 to 20°C in summer), the water viscosity increases, producing a decrease in the settling velocity and an increase in the amount of material being transported both by bed-traction and by suspension. The presence of the ice-sediment crust clearly offsets these factors with respect to transport of bed materials. At present, no data exist from Cobequid Bay to allow further comment concerning the amount of suspended sediment in the water during the winter.

Winter Bedforms

During the winter, the sand waves and megaripples which cover the sand bars in summer are not present in the same form, but are replaced by the smooth and rounded surface of the ice-sediment crust. All bedform amplitudes are reduced with megaripples commonly being obliterated and sand waves greatly subdued. Sand waves show symmetrical cross-sections and have rounded to flat crestal platforms (Fig. 5.54 B) which contain lenticular scours and grooves up to 2 m in length and 10 cm in depth (Fig. 5.54 C).

These modifications result from the combined presence of the crust and drift ice. Prior to the of the ice

FIGURE 5.54: Winter bedforms and late stage runoff features.

A. Small linear and barchanoid ripples on the surface of the frozen crust showing sediment scarcity. Shovel is about 1 m long.

B. Modified sand waves in winter showing diminished heights, symmetrical cross-sections, and relatively flat crestal platforms. Shovel (right foreground) is about 1 m long.

C. Ice-made gouges and tidal scours on the crestal platform of modified sand waves in winter. Shovel is 1 m long.

D. Limited winter development of megaripples within the lower part of the intertidal zone along the north side of Selma Bar with grounded drift ice on the bedform crests. Shovel is 1 m long.

E. Late stage ebb runoff in a bedform trough. Shovel is 1 m long.

F. Rapid local erosion by undercutting along the edges of a lateral channel on Selma Bar by late stage runoff. Note antidunes.

G. Depositional lobe at the terminus of one of the lateral channels along the north side of Selma Bar. Note person for scale.

H. Same lateral channel (F above) during the summer showing a generally depositional regime.

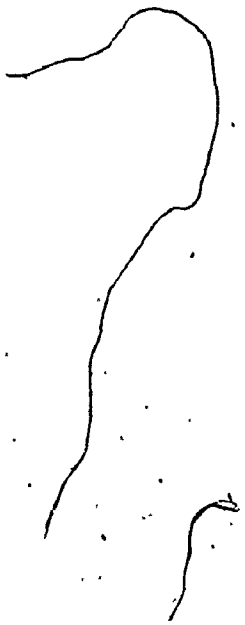

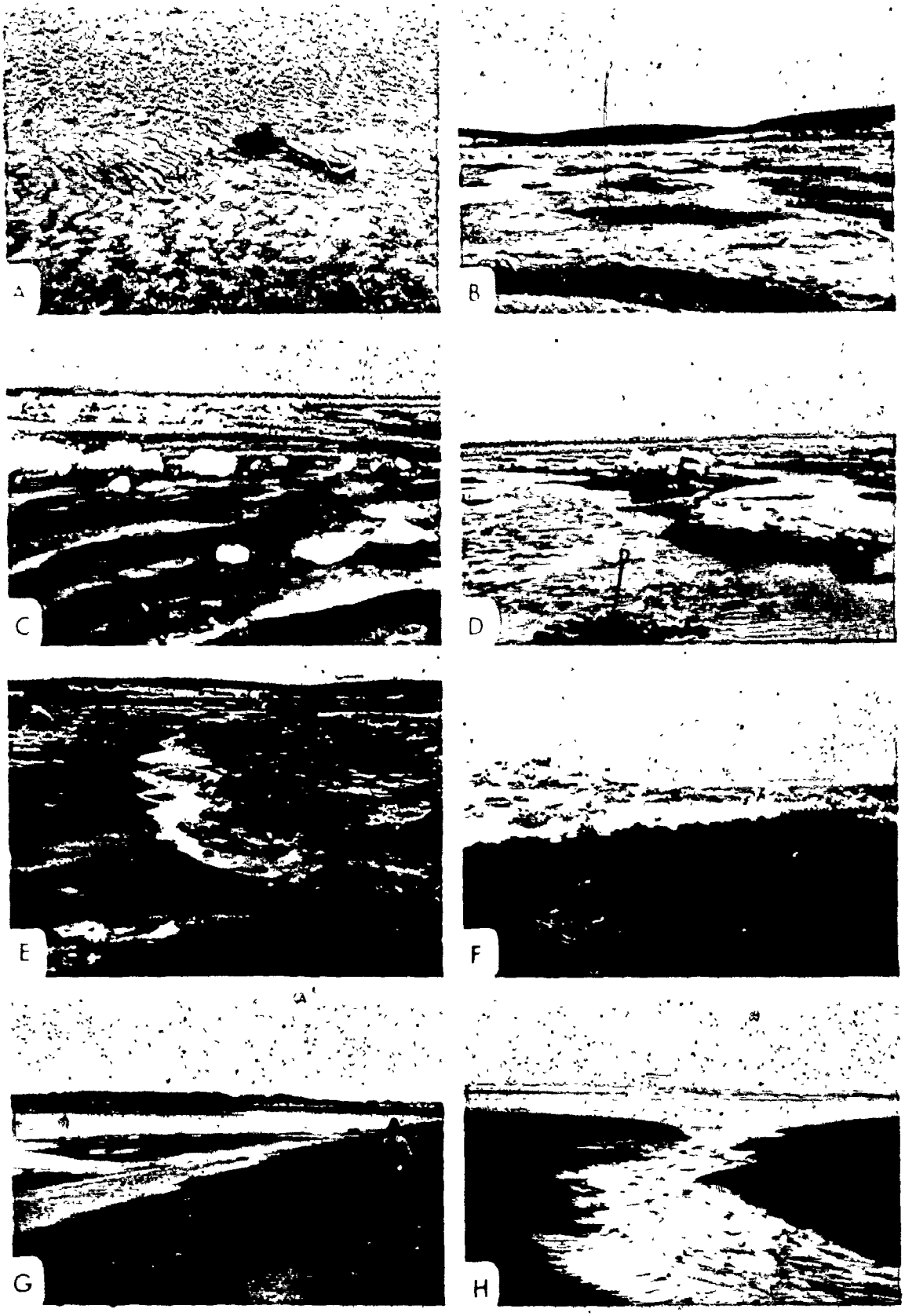
A
B
C
D
E
F
G
H

which are present plane off the crests of bedforms by the intermittent dragging and grounding of their keels when water depths are shallow. Current scour and redistribution of unfrozen sediment during and after the formation of the frozen crust further subdue the bedform morphology.

On much of the higher portions of the sand bars, the only active bedforms observed in winter were small isolated linear and barchanoid ripples (Fig. 5.54 A) generally less than 0.01 m in height. The linear ripples formed in small depressions on the frozen crust where slightly larger amounts of sediment collected. On warm sunny days, the low albedo produced by the sand in the ripples caused the ripples to melt into the frozen crust, further reducing the already scarce supply of available sediment.

The only large active bedforms seen during the winter were megaripples which formed in the lower intertidal zone, and presumably also in the subtidal, where the frozen crust did not form (Fig. 5.54 D). These bedforms were strongly asymmetric in the ebb direction, sharp crested, and very similar to those megaripples which form on the surfaces of the intertidal sand bars during the summer. They showed some effect of the dragging of ice block keels over their crests.

Shortly after break-up, both sand waves and megaripples resume their summer form and remain this way until the following freeze-up.

Sediment Circulation

A further consequence of the presence of the frozen crust on the intertidal sand bars is the significant change in the relative importance of the various elements of the total sediment transport pattern. During the summer, movement of sand by tidal currents through alternate zones of ebb and flood dominance, on the north and south side of Selma Bar respectively, produces a net "elliptical racetrack" transport pattern (Fig.5.55) (Dalrymple et. al, 1976). Lateral transport of sediment along bedform troughs and gullies by ebb runoff current component. In summer, the runoff channels have rounded, depositional sides (Fig. 5.55), indicating the lack of erosive power of the lateral flows.

During the winter, the relative importance of tidal current counter-clockwise sediment (and tra are 55)

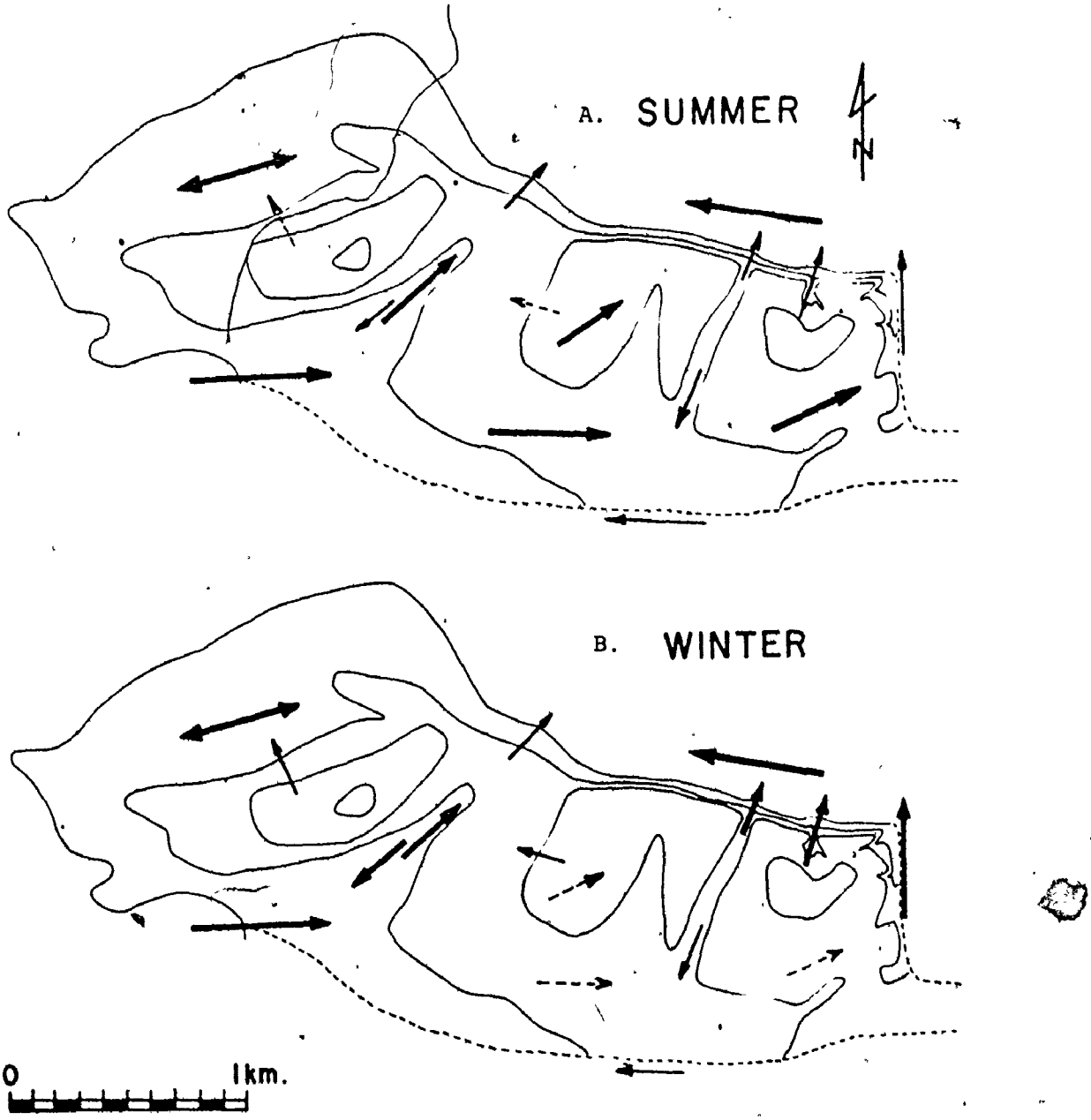

FIGURE 5.5: Sketches illustrating sediment circulation on Selma Bar. (Arrow lengths and weight have relative significance only). A. Summer circulation pattern showing a strong circular or elliptical transport of sediment which moves by intermittent suspension and traction over the whole bar surface. B. Winter sediment movement showing a decrease in the relative amount of circular transport as bedload processes are greatly reduced by the presence of the frozen ice crust. Lateral [illegible] is

The zones of ebb and flood dominance persist through both summer and winter, because they are primarily the result of the large scale topographic form of the sand bar. In winter, the presence of the ice-sediment crust immobilizes sediment, leaving very little for tidal current transport, thus significantly reducing the effective net elliptical circulation of sediment. Lateral movement by late stage ebb runoff, however, is enhanced during the winter because the frozen crust greatly reduces downward percolation of water, thus forcing the water to flow laterally or collect in depressions on the surface. Late stage ebb runoff which occurs along the troughs of remnant bedforms is not everywhere continuous (Fig. 5.54 E) because the troughs are often made up of a series of disconnected tidally scoured depressions separated by areas of unbroken crust (Fig. 5.56). Lateral runoff from these depressions occurs to a certain extent by percolation beneath the crust, but mainly by thin, sheet overflows with low erosive potential. Where lateral troughs are larger and more continuous, there is significant channelization of the flow. If the gradient in the channels is steep, there is downcutting and erosion by undercutting and collapse of the frozen crust (Fig. 5.54 F), and relatively large amounts of sediment are moved in a lateral direction across the sand bar. In 1974, the increased amount of lateral drainage and sediment transport was evidenced by the occurrence of a large deltaic fan (Fig. 5.54 G) at the terminus of one of these lateral runoff channels on the north side of Selma Bar. The fan measured approximately 20 by 25 meters in area, and 3 m in height at the apex. A much smaller deltaic lobe is present during the summer.

Frozen Crust Removal

Although the frozen crust probably forms at the onset of extended periods of subfreezing temperatures, and remains until March or April, its presence is not continuous everywhere for the entire winter. In both muddy and sandy areas, the frozen crust is removed or breached locally (Fig. 5.57 A and B), leaving unfrozen sediment exposed to current scour and transport. Sections of the crust were observed in the bases of large blocks of drift ice grounded in the intertidal zone at low tide. It is believed that the ice blocks were at one time rooted and when they became buoyant enought to break loose, they took with them a portion of the

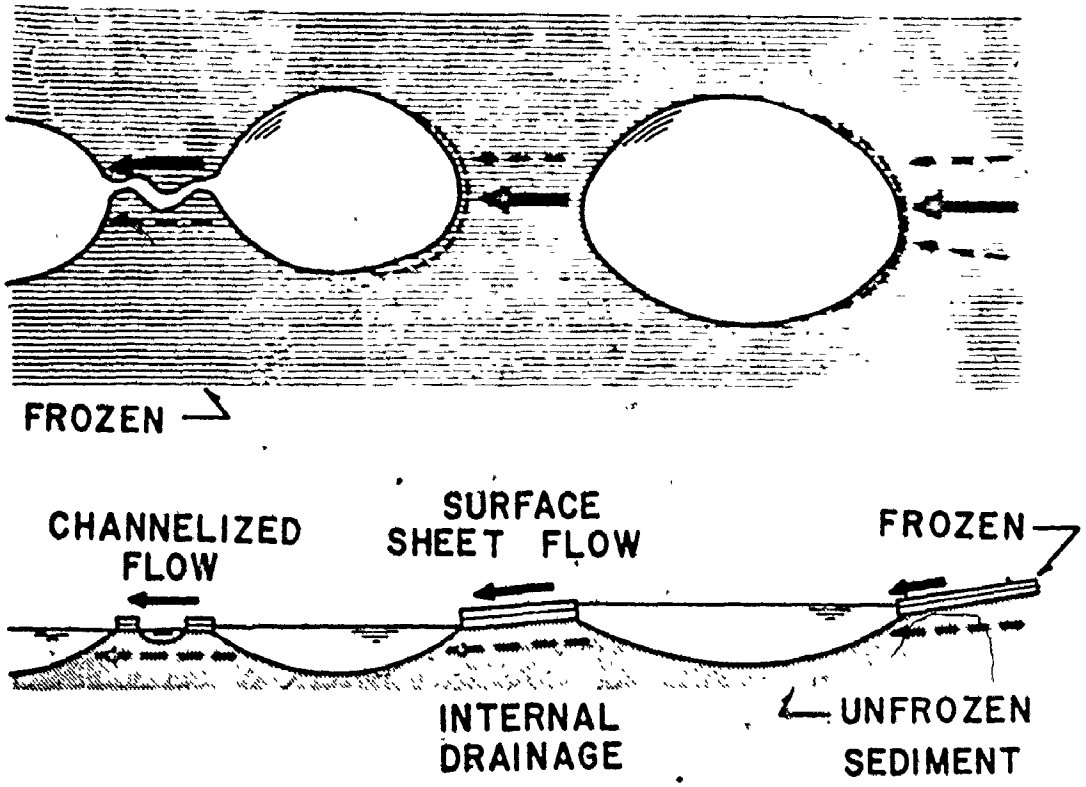

FIGURE 5.56: Schematic diagram showing the discontinuous nature of lateral drainage through scour-pits which occur along the axis of remnant bedform troughs. They are formed by tidal current erosion rather than by the late stage runoff.

FIGURE 5.57: Frozen crust removal, scour-pits on intertidal sand bars and mudflats in winter, Cobequid Bay.

A. Fragment of the ice crust frozen to the base of a composite ice block in the intertidal zone. Shovel (arrow) measures one meter.

B. Sections of the frozen crust removed and transported by tidal scour. Shovel is about 1 m long.

C. View looking longitudinally across a scour-pit on Selma Bar. Breaching of the frozen crust exposes unfrozen non-cohesive sand to extensive erosion by tidal currents. The shovel (arrow) measures one meter.

D. Ice rafted sediments on Selma Bar: Two large sandstone blocks in right foreground about 1 m in length, and a fragment of salt marsh in middle background. View is to the east.

E. A general view of the Selma mudflat with broad steep-sided depressions where the frozen crust has been removed. Shovel is 1 m long.

F. Sediment frozen to the underside of the frozen crust on a mudflat near Five Islands. Trowel is 0.2 m long.

G. Pseudo-monroes on the mudflat near Five Islands in areas where the frozen crust has been removed.

H. Close-up view of pseudo-monroes. Scale is 0.01 m in width.

I. Discontinuities on mudflat surface during summer months. Compare with E. Scale is 1 m long.

J. Scratching of the surface of the frozen ice crust by drift ice. Shovel is 1 m long.

K. Extensive ice gouging in exposed unfrozen muddy sediments. Shovel is about 1 m long.

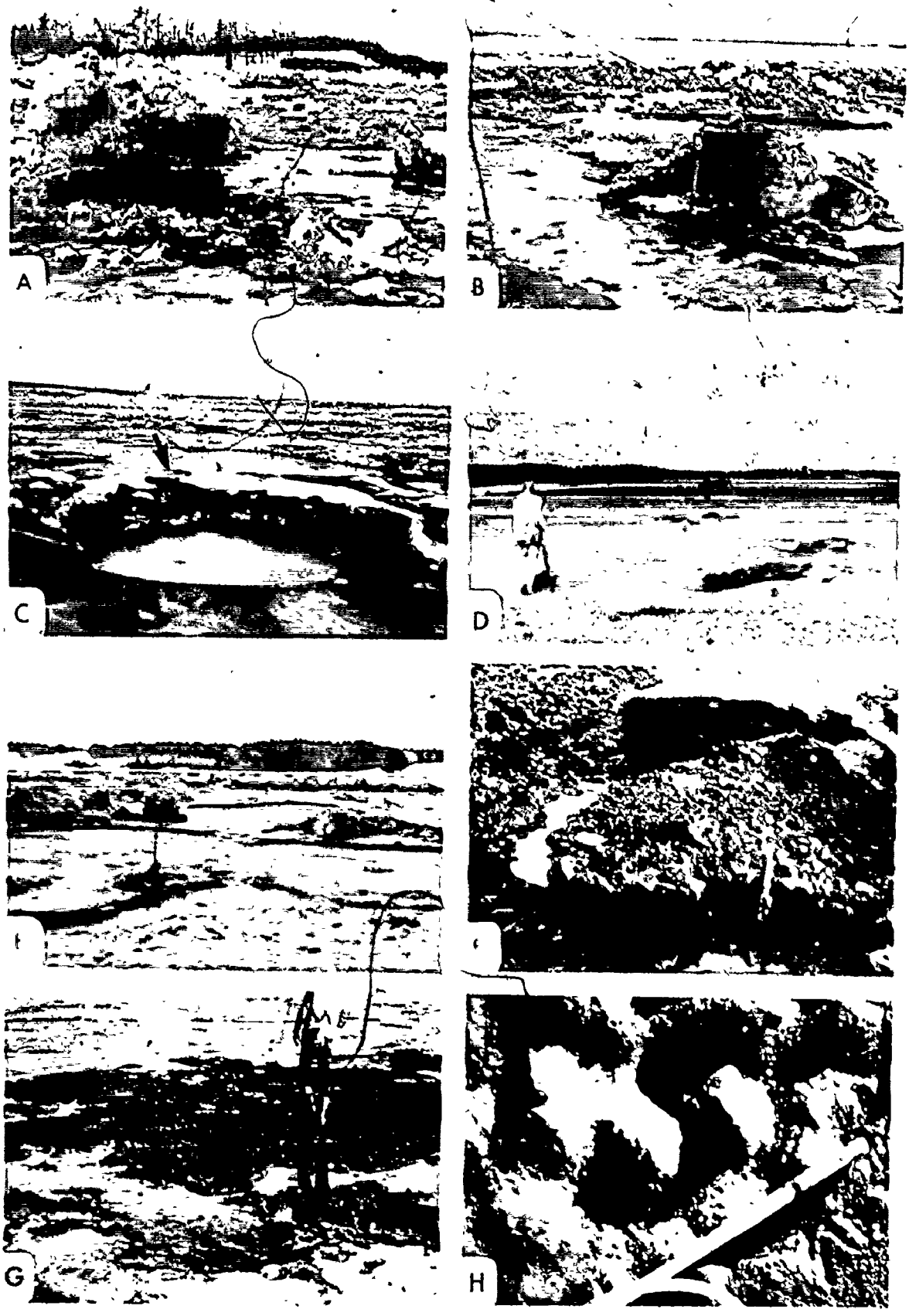
A
B
C
D
G
H


I


J


K

to which they had been frozen. Another mechanism for crust removal is scour and undercutting along the edges of previously breached crust, or in unfrozen areas, by tidal currents or lateral flows. Hydrostatic pressure from groundwater draining beneath the crust and freeze-thaw mechanisms may be a further aid in removing sections of the ice-sediment crust from intertidal areas.

Once freed from the bottom, sections of the crust can be moved by tidal currents or drift ice. Depending on the density of the crust relative to seawater, the size of the crust fragment, and the current strength, intermittent and possibly even rapid transport of the crust pieces of crust could take place over variable distances.

The removal or lack of the ice-sediment crust produces several sedimentologically and geologically important features. Current scour and undercutting along the sides of ebb runoff channels in both mudflats and sand bars produces vertical-sided gullies. In the geological record, this should be evident as truncated internal sedimentary structures. Other effects resulting from the removal of the crust are unique to either the mudflats or the sand bars, and depend on the cohesiveness of the sediments, and relative current strengths.

On the intertidal sand bars where the sandy sediments are non-cohesive, the unfrozen sediment exposed by the removal of isolated pieces of crust are rapidly scoured by tidal currents forming deep depressions (Fig. 5.57 C and 5.58). Observed scoured holes had dimensions up to 10 m across and maximum probed depths up to 75 cm. Some scours may have been deeper but often the centers could not be reached due to the water filling them. The scours were roughly circular to elliptical in shape; some show a preferred orientation, but most did not. On the ebb downstream side, the frozen crust was undercut by current erosion. Sediment transported by the ebb currents was deposited as large, planar to gently curved foreset beds on the ebb upstream side of the scour depression (Fig. 5.58). With the sub-freezing temperatures prevalent during periods of emergence, a 5 to 15 mm thick frozen crust formed at the surface of these deposits in the scour lee by the freezing of interstitial pore water. The thickness of this frozen crust was sufficient to protect the unfrozen sediments beneath from erosion by the ood

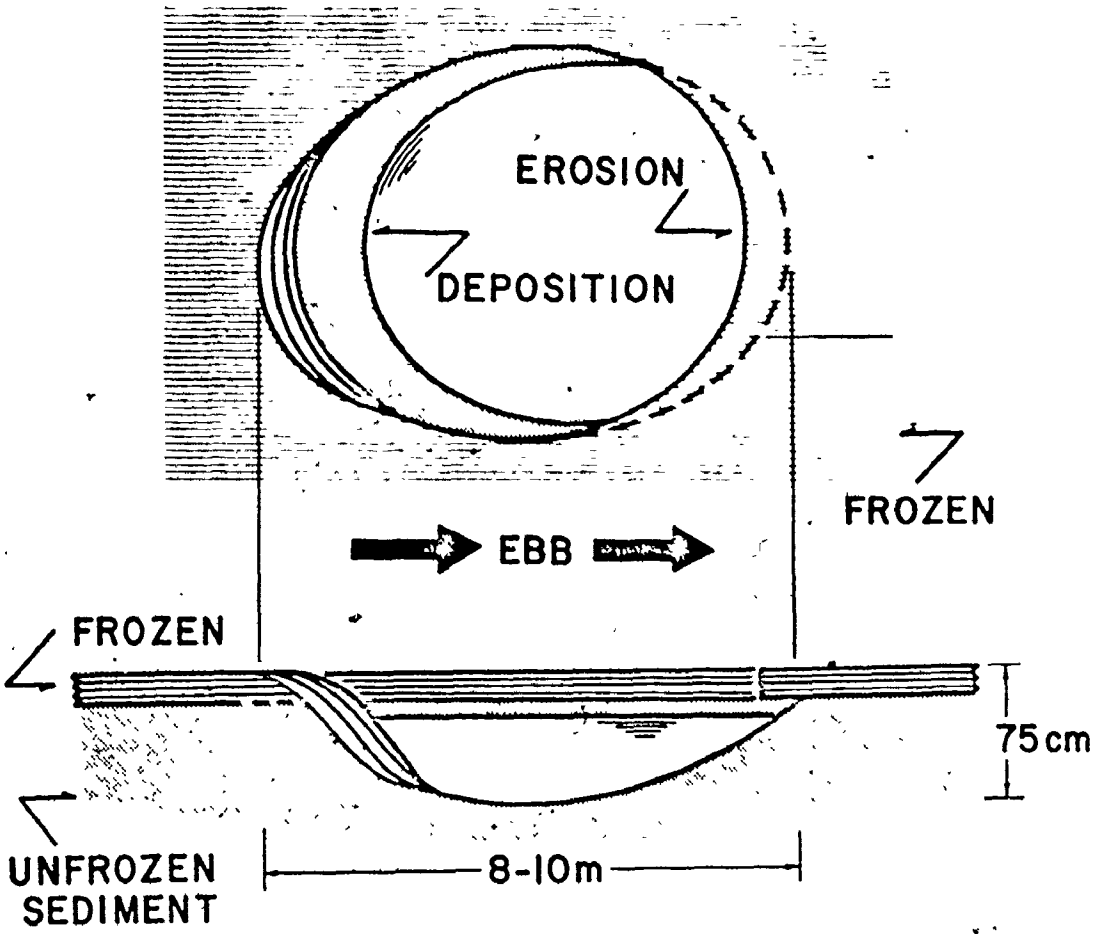

FIGURE 5.58: Schematic cross-section and plan view of a typical scour. Note deposition in the ebb lee of the scour and erosion in the flood lee side.

erosion by ebb currents because these sediments have not been exposed to subfreezing temperatures and therefore cannot form a protective crust. In this way, the scour holes, and lateral runoff channels can be progressively filled from the ebb-upstream direction and extended in the downstream ebb direction. This ebb migration probably occurs in both ebb and flood dominated areas. The preservation potential of these scour holes and their fill, in the form of truncated internal stratification and large planar or trough cross-bedded sets, is considered to be relatively high as the depth of scour (up to 0.8 m) extends well below the 0.3 to 0.7 m thick active layer which is involved in bed load transport during the summer.

In contrast to the above, on the cohesive mudflat sediments the removal of the crust left broad, shallow, steepsided depressions that were generally less than 0.08 m deep and up to 30 m across (Fig. 5.57 E). It is not expected that sections of crust up to 30 m in diameter were removed as one piece, but rather as a progressive detachment of smaller fragments of the crust from the intertidal surface. Each piece of frozen crust removed took with it 10 to 20 mm of muddy sediment which was frozen to the underside of the crust (Fig. 5.57 F). The removal of sediment in this manner leaves surfaces of discontinuity and/or abrupt terminations of mudflat stratification which could possibly be preserved in the geological record. In summer, numerous shallow depressions (Fig. 5.57 I)occur on the mudflat surfaces which might perhaps be related to the removal of sediment by ice rafting of the ice-sediment crust.

Another feature which can be attributed to the removal of the ice crust on the mud is the occurrence of pseudo-monroes, similar in morphology to the monroes reported by Dionne (1973 b). The forms reported here were smaller in size than Dionne's, with heights ranging from 0.02 to 0.04 m and diameters from 0.04 to 0.08 m. These features were observed on a mudflat near Five Island (Figs. 5.57 G and H) and occurred in localized fields where the crust had been removed. Although the expulsion mechanism of formation proposed by Dionne for his larger features cannot be ruled out, it is believed that these small conical mounds were the result of suction deformation during the removal of the ice-sediment crust.

Ice-Rafted Sediment

The dislodgement and transport of the frozen crust removes significant amounts of sediment incorporated directly within the crust and adhering to its base. Much sediment, up to boulder size, is also contained within drift ice. Using an average concentration fo 3.7 gm/m^3, Hind (1875) estimated that the total quantity of mud carried by drift ice in the Avon River estuary amounted to just less than 85 million kg Based on the highest sediment concentrations measured in their samples (18%), ATPEMC (1969) calculated that 32.6 billion kg of sediment were trapped in the ice present in the Salmon River estuary at the time of their sample collection.

Occurrences of ice-rated sediments are common on many of the intertidal areas in Cobequid Bay and the material transported by ice can be deposited anywhere that a particular piece of drift ice grounds or melts. Scattered patches of gravel, cobbles, boulders and pieces of salt marsh are common on the mudflats, foreshores and sand bars (Fig. 5.57 D). On some mudflats, areas of hummocky topography a few centimeters in height and a meter or so across represent deposition of large quantities of poorly sorted sediment from drift ice.

Ice Gouging

The presence of the frozen crust over much of the intertidal zone limits the extent and degree of ice gouging. Faint scratches due to the dragging of drift ice across the bottom were observed on the surface of the crust (Fig. 5.57 J). In areas where the frozen crust had been removed, in both mudflat and sandy area, the frozen sediments exposed were gouged by ice (Fig. 5.57 K), which produced features similar to those described by Dionne (1969, 1971, 1974) and others. Although field observations were restricted to mid-winter when the crust was at its maximum development, it is expected that ice gouging might be more important during break-up with the melting and removal of the crust.

Although no remnant ice gouges have been observed during the summer in Cobequid Bay, it is expected that the preservation potential of these features might be fairly good in mudflat areas where currents and the resulting scour are minimal. In contrast, one would not expect to see preservation of any ice gouge marks in areas of non-cohesive sandy sediments. In summer, the strong tidal currents in these areas produce

megaripples which migrate and scour the sediment to depths of 30 to 70 cm.

Tidal Channel Erosion by Drift Ice

Drift ice has one further effect which might be of geological significance. The rise and fall of drift ice with the tide in the tidal channels that cut across the salt marshes erodes the channel sidewalls, producing a slickensided surface, and increases the width of these channels (Fig. 2.28 G). This erosive action is another way in which drift ice may pick up sediment.

Recap and Discussion

During the summer months, Minas Basin and Cobequid Bay sediment dynamics are controlled primarily by tidal currents with a minor input from wave activity. During the winter months (from December to March, when the mean daily temperatures are below freezing) ice becomes an active and significant sedimentological agent, but it does not outweigh the long-term dominating effect of the tides.

The grounding and stranding of drift ice on the intertidal and supratidal zones of Minas Basin-Cobequid Bay, and the formation of the ice-foot presents a spectacular sight in winter, but it is possible to acquire a false sense of its sedimentological significance. The presence of drift ice damps wave activity, and this combined with the formation of the ice-foot substantially protects the shoreline from erosion in winter, except from the small amount of erosion due to freeze-thaw activity at the sediment-ice contact along the shore. Drift ice plays an important role in sediment pickup and transport, in ice gouging and in removal of the ice-sediment crust overlying many of the intertidal zone sediments.

Although much less conspicuous and certainly less spectacular, the frozen crust covering much of the intertidal zone sediments is of greater sedimentological significance. This crust is considered to form primarily by the upward accretion of materials, such as snow, slush ice, water and small amounts of sediment, freezing on the sediment surface. The relatively low specific gravity, low sediment content, lack of sedimentary structures, and the slow observed rate of downward freezing tend to favour the accretionary buildup origin for the ice-sediment crust. Other factors favouring the development of the crust are:

extended periods of cold weather, snowfall, long exposure at low tide, and high sediment porosity. This last factor suggests that downward freezing may be of greater significance than the other evidence would indicate.

The major result of the formation of the frozen crust is the almost complete immobilization of the sediment surface in the intertidal zone. This is particularly significant in areas of the intertidal zone which have sandy sediments and relatively strong current velocities, such as the intertidal sand bars. Some of the sedimentological effects that the frozen crust has on the intertidal sediments and sedimentation are:

1) The movement of sediment by tidal currents as bed load is almost completely stopped, despite the hydrodynamic factors of increased viscosity and reduced settling velocity which should result in increased sediment transport rates. Essentially the elliptical circulation of sediment around the intertidal sand bars ceases.

2) Lateral transport of sediment by channelized late stage ebb runoff is increased in absolute amount and relative to bed load transport by tidal currents, due to the decreased internal drainage. Runoff channels and gulleys are deepened and widened by the concentrated runoff flow and by tidal currents.

3) Localized removal of the frozen crust on the sand bars initiates deep scouring by tidal currents into the underlying unfrozen sediments. These scours subsequently become infilled with large scale ebb oriented trough and planar cross-stratification.

4) Removal of the crust over muddy areas produces abrupt terminations of sediment laminae where sediment has been removed.

5) The sediment frozen to the base of the crust, plus material incorporated within the crust, are removed and transported by tidal currents and drift ice.

6) The bedforms that cover the intertidal sand bars during the summer are greatly subdued (sand waves) or completely obliterated (megaripples) during the winter as a result of the combined effects of grounding drift ice and the formation of the frozen crust.

7) The presence of the frozen ice-sediment crust protests the unfrozen sediments beneath from ice gouging, at least during the mid-

Almost no visible surface evidence of the effects of winter ice action remain within a few weeks after break-up. However, certain features, although not volumetrically significant, do stand a reasonable chance of geological preservation: (1) Large scale ebb cross-bedding infilling scour pits on the intertidal sand bars; (2) Partial infilling of steep walled runoff channels; (3) Ice rafted boulders and poorly sorted coarse debris redistributed into areas of finer sediments. Lag gravels in tidal channels draining mudflat areas may include terrigenous pebbles as well as soft sediment pebbles and biogenic materials; (4) Abrupt discontinuities in mudflat laminae; (5) Ice gouging features in mudflat areas and some soft sediment deformation; and (6) Reactivation surfaces in sandy strata resulting from bedform rounding and modification. These features could provide valuable environmental clues (if recognized) for complete understanding of the sedimentary dynamics in ancient sedimentary environments.

5.10 SUMMARY

The surface of the intertidal sand bars were covered with a variety of small and large scale bedforms (e.g., ripples, megaripples and sand waves) that were generated by the tidal currents. The major bedforms, in order of increasing size, were: (i) ripples, with lengths generally less than 0.15 m and heights less than 0.05 m; (ii) megaripples, with lengths from 1 to 12 m and heights from 0.1 to 0.7 m; and (iii) sand waves, with lengths from 10 to 30 m and heights from 0.4 to 1.5 m. The linear sand bars are themselves a major bed feature.

The bedforms produced by tidal currents are similar in many respects to the bedforms found in sandy river channels. Thus, despite the relative unsteadiness of the tidal currents, it seems that they can be treated as though they were steady, at least as far as the fields of stability of the different bedforms is concerned.

Seven different intertidal bedform facies were recognized on the sand bars, based on scale and external morphology: (i) plane bed (Facies A; Fig. 5.21); (ii) ripples (Facies B; Fig. 5.21); (iii) linear crested megaripples (Facies C; Fig. 5.22); (iv) sinuous crested megaripples

(Facies D; Figs. 5.23 and 5.24); (v) disorganized megaripples (Facies E; Fig. 5.24); (vi) catenary megaripples (Facies F; Fig. 5.24); and (vii) ebb modified, flood oriented megaripples and sand waves (Facies G; also includes ebb oriented sand waves; Figs. 5.25 and 5.26). For a hypothetical sand bar, Facies A bedforms occur along the steeply sloping, ebb dominated side of the bar, Facies B bedforms near the crest of the bar's steep slope and superposed on larger bedforms, Facies C bedforms on the middle to upper part and Facies D bedforms on the middle to lower part of the gently sloping, flood dominated side of the bar. Facies E, F and G bedforms occur in localized areas near the ends of the bars and/or associated with a particular topographic feature on the surface of the bar (e.g., a swatchway, a secondary bar crestline that causes the development of a counter-current in its lee, or an area that is strongly dominated by the ebb or flood).

The bedforms observed directly on the sand bars at low water, following an ebb tide were either ebb-oriented or ebb-modified, flood-oriented features, often showing some modification due to low tide emergence (e.g., superposed ripples, late stage runoff features in the troughs of the bedforms; Fig. 5.3). The orientation of megaripple and sand wave crestlines (i.e., the direction perpendicular to the strike of the bedform brinklines) were generally oriented at a small oblique angle to the crestlines of the bars (Figs. 5.17 and 5.18). Megaripple crests were generally oriented at a steeper angle than sand wave crests with respect to the mean direction of the ebb and flood tidal currents (compare Figs. 4.20 and 5.17), i.e., the difference between the mean direction of flow and the orientation of the bedform crest varied from 10 to 30 degrees for megaripples, and from 5 to 20 degrees for sand waves.

Bedform scale and morphology varied over the bars in response to differences in sediment size and flow characteristics (Figs. 5.34, 5.35 and 5.36). Megaripples were larger and more three-dimensional in areas where the flow strength was stronger and the flow duration longer, e.g., Facies C bedforms (linear crested megaripples) occurred nearer to the crestline of the bars where current strengths and flow durations were relatively less and sediment size somewhat finer than Facies D bedforms (sinuous crested megaripples) which occurred in the lower part of the

4.11, 4.13 and 4.16 with Figures 5.4, 5.8, 5.10 and 5.20 shows the interrelation between the areal distributions of flow strength and bedform development (scale and morphology). Sand waves generally occurred in slightly coarser (mean grain size about 0.42 mm) and poorer sorted medium grained sands than the sediments (mean grain size about 0.26 mm) where megaripples were found.

Net rates of bedform movement varied with bedform type and current strength (e.g., compare results in Table 5-1 with Fig. 4.1 for location and Figs. 4.11, 4.16, 5.4, 5.8, 5.10 and 5.20). Megaripples generally moved faster than sand waves or ebb modified flood bedforms (e.g., megaripples = 0.2 to 0.8 m per tidal cycle, and sand waves = 0.1 to 0.3 m per tidal cycle). Both migration rates and bedform scale (and morphology to some extent) vary during the lunar tidal month (Fig. 5.31, 5.32 and 5.33) as current strengths vary from neap to spring tides. Some lag occurred in the adjustment of bedform dimensions to changing flow conditions from neaps to springs, but the time interval between field observations were too long and infrequent to establish the exact nature of the lag effects. Substantial relaxation effects between the temporal variations of the flow and bedform development were apparent by the presence of the large bedforms (e.g., megaripples and sand waves) on the intertidal sand bars at low tide, i.e. without lag effects, the emergent surface should have only current ripples or 'lower flow regime' plane bed.

Echo sounding over and epoxy peels from the bedforms on the sand bars indicated that megaripples reversed their asymmetry with each ebb and flood (Figs. 5.27, 5.28 and 5.29). The extent of reorientation and reworking (and the net migration rates) of the megaripples was determined by the strength of the currents and the degree of ebb or flood dominance. The sand waves (Fig. 5.28), which occurred in strongly flood (or ebb) dominant areas of the bars (e.g., Figs. 4.11 and 5.20), did not reverse their asymmetry with each ebb or flood, but their superposed megaripples were reoriented and reworked with each tide.

The sequence of bedforms with increasing flow strength was similar to that described from flume observations, rivers and other tidal environments:

plane bed → ripples → sand waves → linear megaripples → sinuous megaripples → planed-off megaripples → upper flow plane bed

The various bed phase boundaries, particularly those for megaripples and sand waves (Figs. 5.41, 5.42 and 5.43), with respect to depth, velocity and grain size were comparable to those reported in other studies (e.g., Costello, 1974). The tidal bedforms, however, were not as three dimensional in form as those bedforms reported from flumes and rivers because the duration of tidal flow was relatively shorter (Allen, 1968 b). The tidal megaripples are analogous to dunes found in rivers, and were the most common bedform on the sand bars. The tidal sand waves may be comparable to Costello's (1974) 'bars', but are different with respect to morphology and superposed bedforms. Costello's 'bars' are simple, two-dimensional bedforms without superposed bed features (except where a bar front overrides the stoss-side of a downflow bar), rather complex, composite bed features such as the sand waves on the tidal sand bars. The differences may be due to the flow scale and the bimodality of the tidal currents, compared with unidirection flows in Costello's experimental flume. The superimposition of ripples on megaripples and sand waves probably developed during relatively short periods of time immediately prior to the low tide emergence of the bars. The presence of megaripples is more difficult to explain in as much as the mechanism of sand wave formation is not clearly understood. Costello (1974) proposed that the megaripples could be "a metastable, secondary form" initiated by the sand waves. Upper flow regime bed features were uncommon on the sand bars and restricted to localized areas on the crests of some megaripples and sand waves, and in some of the late-stage ebb-runoff channels.

The magnitude of the flow resistance or friction factor varied with bedform scale (Fig. 5.47) and during the semidiurnal tidal cycle (Figs. 5.44, 5.45 and 5.46). The alteration of the flow friction factor (at time of maximum ebb velocity) with bedform scale typically varied from about 0.032 for smaller bedforms to 0.050 for larger bedforms (Fig. 5.47). As the current velocity increased during the ebb, the friction factor first showed a sudden increase to a maximum value (typical values ranged from $f = 0.10$ to 0.18) during the period of bedform reversal, then steadily decreased (to about $f = 0.04$) as the bedforms reached a quasi-equilibrium state with the flow (Fig. 5.46), and increased (to about $f = 0.10$ to 0.20) during the late ebb due to the shallow depths of flow and increased con-

cen of in the During the flood, the

friction factor increased rapidly (to about f = 0.10) at first during the period of bedform reversal and relatively large concentrations of suspended sediment, then decreased towards high water as the bedforms became flatter and the depth of flow larger. Sketches and photographs of more than 20 trench faces, and more than 60 epoxy peels were made from trenches at several locations on the sand bars to examine the internal sedimentary structures of the intertidal bedforms. Most of the preserved sedimentary structures were produced by the migration of megaripples (Figs. 5.48 through 5.53). Because the surfaces of the bars were characterized by currents that were either ebb or flood dominant, it was common to find only ebb or flood sets of cross-bedding preserved in the bedforms. In other words, "herringbone" cross-stratification which has often been used by other workers as a distinguishing criteria of tidal deposits was extremely uncommon. The absence of "herringbone" cross-bedding in an ancient sedimentary deposit does not necessarily eliminate the possibility that the sediment was deposited by tidal processes.

The thickness of the preserved cross-bedding sets in megaripples were commonly about the same height as the bedform. The longitudinal extent of the cross-bedding in the current direction was variable, depending upon the degree of ebb or flood dominance at a particular location (compare Figs. 5.50 and 5.51). Laterally (perpendicular to the current direction) and in plan, the cross-bedding was either planar or trough-shaped (Fig. 5.50) depending on the three-dimensionality of the megaripples (e.g., linear versus sinuous crested megaripples).

The sand waves migrated primarily from the movement of megaripples superposed on their stoss-side (Figs. 5.52 and 5.53). As a result, the internal structure of sand waves consisted of composite sets of megaripple cross-bedding that were oriented in either the ebb or flood direction depending upon the asymmetry of the sand wave's external geometry. Cross-bedding deposited by the subordinate tidal current was rarely preserved. Some of the variation in the thickness and preservation potential of deposits from the subordinate current were possibly related to changes in current strength during the lunar tidal month, i.e., erosion potential, and set thickness and height appeared to decrease during neap tides, and to increase during springs.

During the process of bedform reversal, the upper part of the sediment surface (on previously deposited lee face laminae) were eroded producing a surface of discontinuity or "reactivation surface" (Boersma, 1969; Collinson, 1970, Klein, 1970 a), which separated individual sets of cross-bedding deposited during the locally dominant part of the tidal cycle. Some of the surfaces of discontinuity between sets, however, resulted from the random scour and migration of the megaripples (Allen, 1973).

During the winter months, the frozen crust on the sand bars caused almost complete immobilization of the intertidal sediment surface preventing the development of large bedforms. The combined effects of grounding drift ice (Fig. 5.54) and the formation of the frozen crust subdued or completely obliterated pre-existing sand waves and megaripples. Because internal drainage of the sand bars was decreased and surface runoff was effectively concentrated in swatchways and gulleys, lateral transport of sediment and downcutting in the channelized late stage ebb runoff was increased (Figs. 5.54 and 5.55). Localized removal of the frozen crust on the sand bars exposed the unfrozen sediments to deep scouring by the tidal currents (Figs. 5.57 and 5.58). The scours were eventually infilled with large ebb oriented trough to planar cross-stratification.

CHAPTER 6

SEDIMENT TRANSPORT AND CURRENT PATTERNS

6.1 INTRODUCTION

A number of people (e.g., Balaz and Klein, 1972; Caston, 1972; Caston and Stride, 1970; Houbolt, 1968; James and Stanley, 1968; Klein, 1970 a; Ludwick, 1974; Reineck, 1963; Robinson, 1960, 1966; Smith, 1968, 1969; Stride, 1963; Swift, 1975; Swift and Ludwick, p. 159-196, in Stanley and Swift, 1976; van Veen, 1950) who have studied subtidal and intertidal sand bars (or ridges) have indicated that the ridges are commonly separated by either interdigitating or alternating ebb- and flood-dominated channels and that sediment movement is usually characterized by a "circular" or "elliptical" pattern of transport around individual bars or groups of bars. A variety of techniques have been used to establish the directions and rates of sediment transport and current velocities including: bedform asymmetry and their internal sedimentary structures (Houbolt, 1968; Klein, 1970 a; Reineck, 1963; Stride, 1963); direction and strength of currents (Ludwick, 1974; Robinson, 1960, 1966; Smith, 1968, 1969; Sternberg, 1967; Walton and Goodell, 1972); empirical and semi-empirical sediment transport equations (Ackers and White, 1973; Biswas and Chakrabarti, 1974; Kachel and Sternberg, 1971; Sternberg, 1967, 1972; White, 1972); textural and mineralogical trends (James and Stanley, 1968); and fluorescent tracers (Oertel, 1972; Sandusky, 1968, reported in Klein, 1970 a and Balaz and Klein, 1972). Most of these studies have been carried out in areas with tidal ranges less than 5 m. Similar studies in macrotidal areas are uncommon.

The purpose of this chapter is to discuss the gross sediment transport and current patterns on the individual intertidal sand bars studied and in the sand-body complex in order to formulate a general model for the evolution and maintenance of the modern sand deposit in Cobequid Bay.

6.2 SEDIMENT TRANSPORT

The mechanisms and rates of sediment transport are an important aspect of the interaction between the flow and the bed properties. Both geologists and engineers have been interested in the movement of sediments by flowing water as shown by the large number of studies on this subject in the literature. Recent reviews on the theory and measurement of sediment transport include those of A.S.C.E. Task Committee (1971 a and 1971 b), Graf (1971, p. 123-242, 357-384), Raudkivi (1967 a, p. 39-135) and Yalin (1972, p. 111-164). Briggs and Middleton (1965) and Brush (1965) reviewed some of the sedimentological consequences of sediment movement.

It is apparent from these reviews that a large number of variables can be related to sediment discharge (e.g., slope, shear stress, fluid discharge, turbulence intensity, water temperature, and bed configuration), but all of these variables have not yet been interrelated in one simple sediment discharge formula. Thus, many of the formulae and techniques developed have met with only limited success because no one procedure accounts for all the significant parameters that may affect sediment transport. Most approaches assume conditions of flow that are seldom, if ever, found in natural flow systems (e.g., steady-uniform flow) and/or that depend on hydraulic parameters which are difficult to determine or are determined with uncertain accuracy (e.g., shear stress, energy slopes). It is also impractical to apply and compare the results of every empirical relationship published in the literature because there is no objective means of evaluating which method gives a correct or near-correct result. It is, therefore, best to select those hydraulic relationships or procedures that have been developed and(or)tested under conditions comparable to those in the field situation and that will give results suitable to the needs of the study.

The transport of noncohesive sediments by a flow is a complex process that is incompletely understood. It is usual to distinguish between three mechanisms of sediment transport in a flow: solution load (not discussed here), wash load (which comprises the finest sediment that is held almost continuously in suspension) and bed material load (which consists of the coarser material forming the bed, and is moved along or close to the bed). The of is

is difficult to estimate. Bed material is always available for transport depending on the competence of the flow.

The bed material is moved by two different mechanisms of transport, generally called suspension and traction (of bed load). The 'suspended load' refers to the movement of bed material in such a way the weight of the sediment is supported by the vertical component of turbulence in the flow (see discussion by Middleton, 1976). The 'traction load' is that part of the bed material load that moves within a relatively thin "bed layer" (two grain diameters thick - Einstein, 1950) by rolling, sliding and saltation along the bed (i.e., the weight of the sediment is supported primarily by the solid bed of the flow and grain-to-grain collisions). The size distribution of the bed material and the competence of the flow governs what material actually makes up the suspended load and the traction load (Middleton, 1976). The distinction between the suspended and traction loads is, however, an arbitrary division. According to Einstein(1950), 'bed load' occurs within two grain diameters of the bed. By his definition, almost certainly most of the sediment transport on the bars is not 'bed load' because under conditions of dune movement, there is much transport in suspension.

Bedform Migration

The distance and direction of net migration of a bedform brinkline gives a simple, but minimum estimate of the direction and net rate of bed material transport by assuming that the volume of sediment deposited on or eroded from the lee-slope of a bedform during a tidal cycle (ebb and flood) is equal to the net rate of sediment movement. Not all sediment eroded from the stoss-side of a bedform is, however, deposited on its lee-side. Some sediment is transported down current to the next bedform(s). The net distance of migration, therefore, reflects only part of the total net sediment transport. Furthermore, the lee-side orientation of the bedform (i.e., the inferred net migration direction) does not necessarily coincide with the true transport direction. Measurements of current directions and bedform orientations in this study (compare Figures 4.20 and 5.17) and those of Allen (1968 b) indicated that directions of transport depended largely on the local bar topography and the three-dimensionality of the bedforms. For the above reasons, it was concluded that a

better estimate of the rates and directions of sediment transport could be obtained by other means, so this procedure was not attempted.

Empirical Relationships

Many empirical techniques have been developed that relate the rate of sediment transport to some form of flow strength (e.g., mean flow velocity, boundary shear stress or shear velocity, stream power). Two simple empirical relationships that assess the relative rates and directions of sediment transport were suggested by Biswas and Chakrabarti (1974) and Ludwick (1974; also discussed in Swift and Ludwick, p. 186-190, in Stanley and Swift, 1976). Biswas and Chakrabarti suggested that the total sediment transport rate was proportional to the sixth power of the mean flow velocity as an approximation. They determined the ebb or flood 'predominance' of a given location from the following expression:

$$P_F = \frac{\int_0^{T_1} V_F^6 \, dt}{\int_0^{T_1} V_F^6 \, dt + \int_0^{T_2} V_E^6 \, dt}$$

where P_F = flood predominance (transport seawards if $P_F < 0.50$); V_F = average flood velocity; V_E = average ebb velocity; and T_1 and T_2 = times of high and low water slacks (average ebb and flood velocities determined from integration of the time-velocity curves).

Ludwick used the relationship that the total sediment transport was proportional to the flow power per unit area of bed (Bagnold, 1956; Inman, p. 141, in Shephard, 1963).

$$\omega = \tau_o \bar{u} \propto q_{st}$$

where ω = flow power per unit area of bed; τ_o = boundary shear stress; $\bar{u}$ = profile mean velocity (Ludwick actually used the average velocity measured one metre above the bed); and q_{st} = total sediment transport rate per unit time and unit width. The tidal flow power was integrated over each ebb and flood cycle, corrected to the mean tidal range and the threshold of sediment movement, and averaged for each station. The net sediment transport was determined by taking the vector sum of the time integrated, ebb and flood flow power values.

Both of the above-mentioned techniques give relative estimates of

as absolute measures because they are not expressed in absolute units of sediment transport (e.g., $m^3/s/m$). An alternative approach is to select a single empirical bedload equation already tested in a tidal system which gives absolute transport values. Two such examples are the 'modified Einstein method' (Colby and Hembree, 1955) used by Biswas and Chakrabarti (1974) in the tidal estuary of the River Hooghly (India), or the general transport function developed and tested by Ackers and White (1973) in both experimental flumes and natural systems (Paraguay River and Thames Estuary). Both techniques estimate the total sediment load of the flow. Because only gross estimates of the rates and directions of sediment transport were required in this study, it made little difference which of the two procedures was selected.

The Ackers and White (1973; White, 1972) technique was chosen because: (i) it was simple to use; and (ii) there were test results available from the Thames Estuary for comparison (White, 1972). The transport function is based on three dimensionless parameters: grain size (D_{gr}); particle mobility (F_{gr}) and sediment transport (G_{gr}). For relatively fine grain sizes (D_{gr} = 1 to 60, i.e., grain sizes = 0.04 to 2.5 mm), total transport is related to the total flow power (primarily shear velocity). For coarser sediment sizes (D_{gr}>60, i.e., grain sizes = 2.5 to 4.0 mm), the rate of transport is related to flow power per unit area of bed (product of mean flow velocity and net grain shear). The transport function cannot be used for grain sizes less than 0.04 mm (silt; D_{gr}<1) because such sediments have cohesive properties. If bedforms are present, it is assumed that the relationship between the mean flow velocity and the effective shear stress is similar to that of a plane sand-grain roughened boundary. The sediment mobility (F_{gr}) and sediment transport (G_{gr}) parameters depend on the sediment grain size and the characteristics of the flow, e.g., whether the sediment is moved primarily as a suspended or traction load. A summary of the equations and calculation procedures is given in Appendix IV.1.

The derived rates of sediment transport (non-standardized), using the Ackers and White empirical total-load formula, are listed in Appendix IV.2 with the other derived hydraulic parameters. The rate and direction of sediment movement for each ebb and flood cycle, and for the net tran[illegible] per [illegible] at each [illegible] was

determined by taking the time-integrated vector sums of the respective derived transport rates and directions (near bottom current directions). The results are shown in Table 6.1 Figures 6.1, 6.2 and 6.3 show the areal patterns of transport vectors for the sand bars studied.

Discussion

The sediment transport results listed in Table 6-1 and shown in Figures 6.1, 6.2 and 6.3 suggest that the pattern of sand circulation on and around the sand bars is similar to that indicated by the current measurements (Figs. 4.11, 4.13, 4.15, 4.20, 4.21, 4.22 and 4.23) and the bedform observations (Fig.5.17; see also Figs. 3.16, 3.24, 3.27 and 3.32). The ebb and flood transport vectors are directed generally across the bars in opposite directions, but at an oblique angle to the crestline of the bars (see Fig. 6.4). The net transport vectors on the bars and in their adjoining channels are predominantly flood oriented and show that sediment is moved up the gently sloping side of the bars at an oblique angle to the crestline. Along the steeply sloping sides of the bars and their adjoining channels, net transport occurs parallel to subparallel to the crestline of the bars towards the west, i.e., ebb dominant.

Although the channels typically attain higher current speeds than over the sand bars, the sediment transport rates are lower in the channels than over the bars (Table 6-1). This result is misleading because the mean grain size of the bed material in the channels was used in the initial calculation of the total sediment load rather than the average mean grain size of the bar sediments. Most of the channel beds have little or no sediment (sand sized sediment) from the scouring action of the tidal currents, thus most of the sand sized sediments moved into the channels from the bars or from upflow, particularly during the flood, must be bypassed along the channels out of the sand-body complex during the ebb. In reality, the rate of sediment transport is related to the flow strength (i.e., velocity or shear velocity), therefore, for sand grain sizes, transport rates (i.e., capacity and competence) within the channels are really larger than over the bars. Table 6-1 (bracketed values) shows the recalculated transport rates in the channels using the average mean sediment size on the adjacent sand bars (based on recalculated values in Appendix IV.3).

T A B L E .6 - 1

TIME INTEGRATED VECTOR SUMS OF THE EBB, FLOOD AND VECTOR MEAN SEDIMENT TRANSPORT RATES PER TIDAL CYCLE[1]

Station[2]	Ebb Vector Sum Rate Kg/m	Ebb Vector Sum Direction	Flood Vector Sum Rate Kg/m	Flood Vector Sum Direction	Vector Mean Rate Kg/m	Vector Mean Direction
NOEL BAY BAR						
1A	4093	276	562	137	4133	270
B	1094	278	313	133	1138	266
C	1339	280	274	140	1368	271
D	738	287	54	133	742	285
2A	4856	278	3218	128	5825	240
B	2588	255	4586	73	5261	70
3A	65	210	7	53	65	207
B	425	253	58	55	428	256
C	565	286	306	118	643	261
4	2009(2542)	249(249)[3]	468(565)	74(74)	2063(2604)	247(248)
5	7110(3676)	255(255)	705(461)	74(74)	7146(3705)	225(255)
6A	230(2426)	276(277)	104(529)	95(96)	252(2483)	277(277)
B	54(688)	292(291)	18(68)	99(100)	58(691)	281(282)
7	4313(1944)	280(280)	5706(2502)	112(112)	7153(3168)	143(146)
8	3182(3150)	282(282)	3366(3334)	118(108)	4633(4587)	167(167)
EAST NOEL BAR						
1	590	300	673	118	896	104
2	1429	322	353	167	1472	314
GREAT VILLAGE BAR						
	673	271	10440	94	10462	94
MIDDLE CHANNEL						
	30808	248	5915	68	31356	248

T A B L E 6 - 1 (Cont'd)

TIME INTEGRATED VECTOR SUMS OF THE EBB, FLOOD AND VECTOR MEAN SEDIMENT TRANSPORT RATES PER TIDAL CYCLE[1]

Station[2]	Ebb Vector Sum Rate Kg/m	Ebb Vector Sum Direction	Flood Vector Sum Rate Kg/m	Flood Vector Sum Direction	Vector Mean Rate Kg/m	Vector Mean Direction
NOEL SHORE BAR						
1	2347	281	3636	122	4327	152
2A	3679	275	4709	115	5962	160
B	1958	278	3409	107	3931	119
3	3337	278	5544	118	6469	143
4	4000	269	7798	73	8762	57
5	389	286	778	102	868	98
6	10066	274	176	95	10066	274
7	10249	278	15523	99	18601	101
8	2786	273	313	94	2804	273
9	1411(68612)	307(303)	(6397)	(106)	(68910)	(305)
10	54(14040)	264(261)	454(32166)	88(89)	457(35097)	89(95)
11	(12838)	(292)	(1498)	(98)	(12925)	(294)
SELMA BAR						
1A	79	284	284	83	295	75
B	32	283	76	88	83	77
C	14	257	670	74	670	74
D	22	250	274	80	274	81
2A	5803	272	6980	84	5803	92
B	140	292	479	101	500	97
C	101	291	572	95	580	92
D	140	264	882	87	893	88
E	274	270	1508	92	1534	92
F	50	270	529	83	533	82
3A	338	254	7099	71	7106	71
B	1141	266	3708	64	3881	55
4A	14	280	263	72	263	70
B	86	269	43	68	97	288

T A B L E 6 - 1 (Cont'd)

TIME INTEGRATED VECTOR SUMS OF THE EBB, FLOOD AND VECTOR MEAN SEDIMENT TRANSPORT RATES PER TIDAL CYCLE[1]

Station[2]	Ebb Vector Sum Rate Kg/m	Ebb Vector Sum Direction	Flood Vector Sum Rate Kg/m	Flood Vector Sum Direction	Vector Mean Rate Kg/m	Vector Mean Direction
SELMA BAR (cont'd)						
5A	112	292	2200	102	2303	101
B	50	292	673	113	677	113
C	580	280	3643	91	3690	93
6A	256	236	29	67	256	235
B	6880	295	18619	92	19850	80
C	1595	288	1386	87	2113	347
D	7096	272	6602	82	9691	335
E	6894	273	17248	72	19857	59
F	11912	269	6768	76	13702	285
7A	5512	287	2142	72	5915	305
B	3114	253	4421	55	5407	22
8A	1822	279	680	80	1944	290
B	522	256	101	53	533	261
9		278	83	75	83	75
10	392	273	4738	92	4756	92
11	4	259	86	59	86	58
12	61	262	151	58	162	43
13	83	261	569	77	576	76
14	2794	267	1321	68	3089	283
15	680	270	3852	81	3910	79
16	58	271	1217	84	1217	84
17	5972(4306)	311(312)	58(50)	106(107)	5972(4306)	311(312)
18	(5072)	(285)	18(11934)	77(80)	(12967)	(64)
19A	(15138)	(257)	587(3542)	75(258)	(15467)	(77)
B	36(18968)	240(240)	(8640)	(63)	(20843)	(238)

TABLE 6 - 1 (Cont'd)

TIME INTEGRATED VECTOR SUMS OF THE EBB, FLOOD AND VECTOR MEAN SEDIMENT TRANSPORT RATES PER TIDAL CYCLE[1]

Station[2]	Ebb Vector Sum		Flood Vector Sum		Vector Mean	
	Rate Kg/m	Direction	Rate Kg/m	Direction	Rate Kg/m	Direction
SELMA BAR (cont'd)						
20A	580(846)	297(297)				
B	281(436)	293(292)	1292(2178)	123(123)	1321(2271)	176(136)

NOTE: 1. Rates computed using d_{50} of bed material.

2. See Figure 4.1.

3. Bracketed values are the rates recomputed for channel locations assuming a d_{50} of adjacent bar sediments rather than d_{50} of actual bed materials (from recomputed values listed in Appendix IV.3).

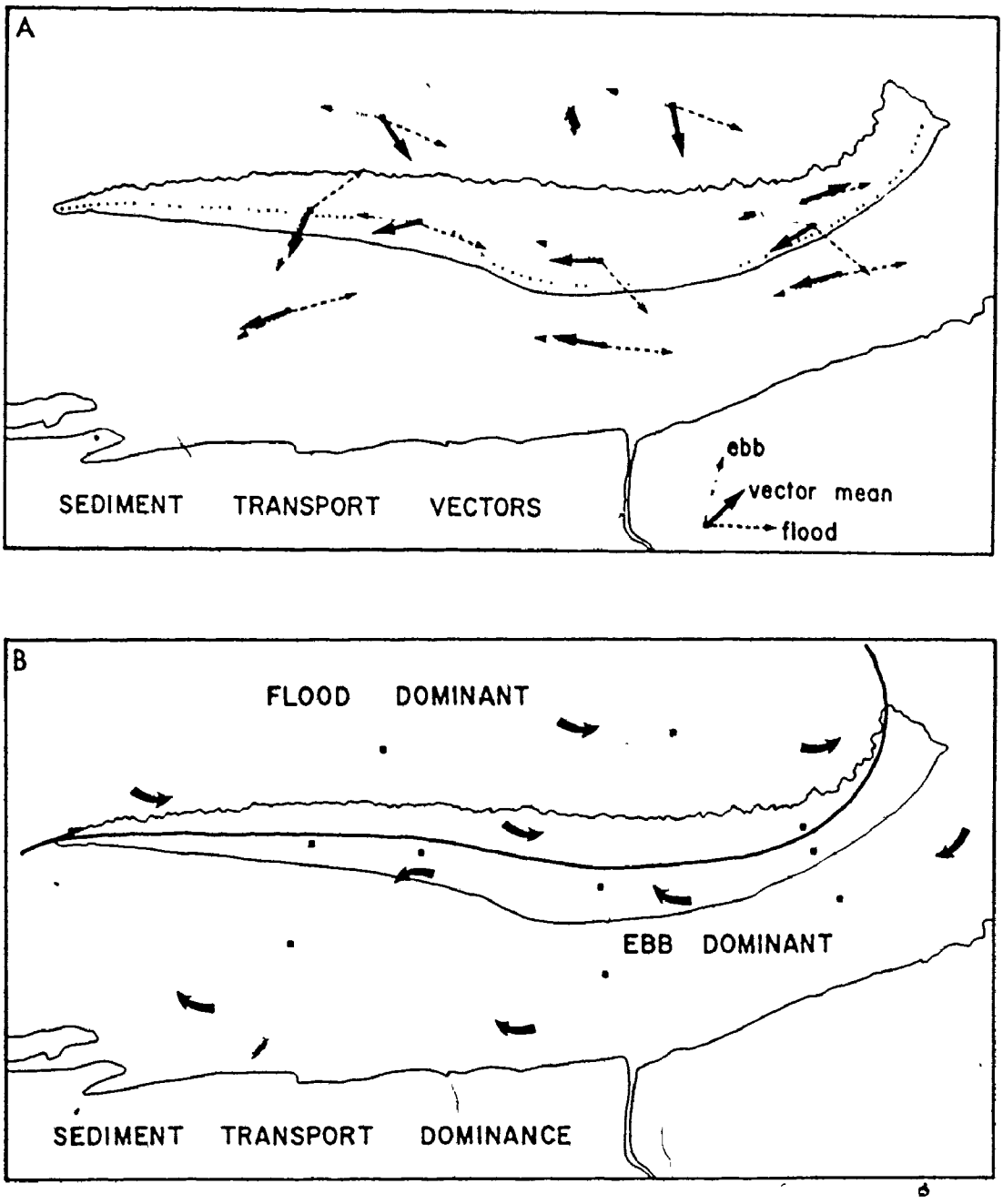

FIGURE 6.1: Sediment transport vectors (direction only) on Noel Bay Bar for the ebb-flood and ebb-flood vector means (A) and the areal patterns of sediment transport dominance for the ebb and flood (B).

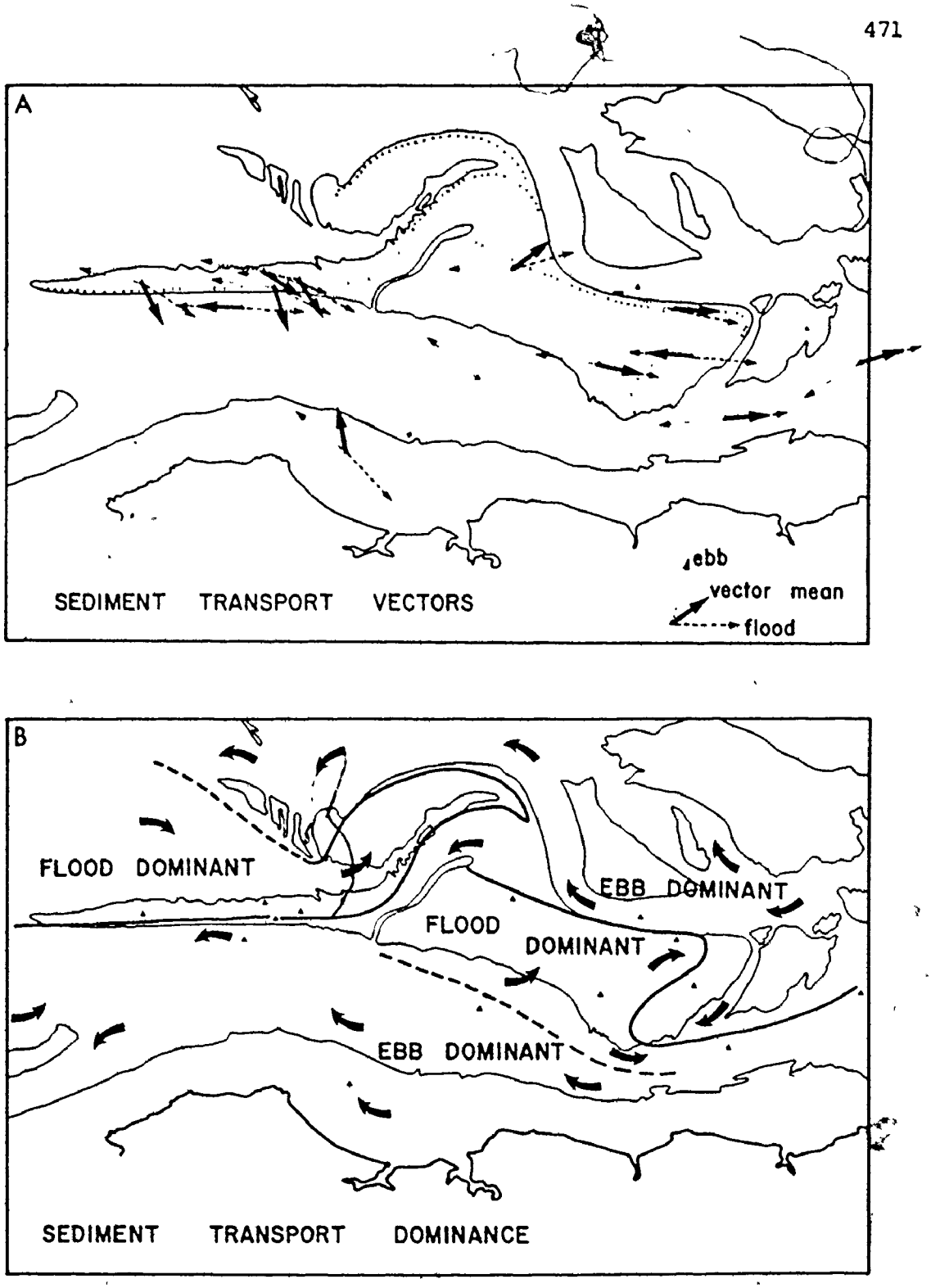

FIGURE 6.2: Sediment transport vectors (direction only) on Noel Shore Bar for the ebb-flood and ebb-flood vector means (A) and the areal patterns of sediment transport dominance for the ebb and flood (B).

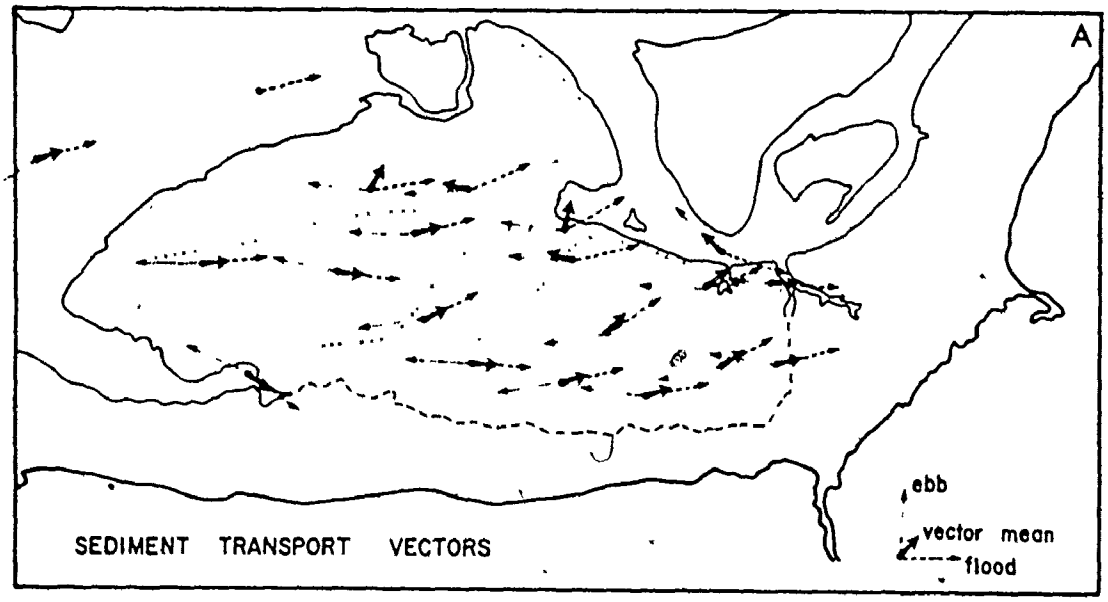

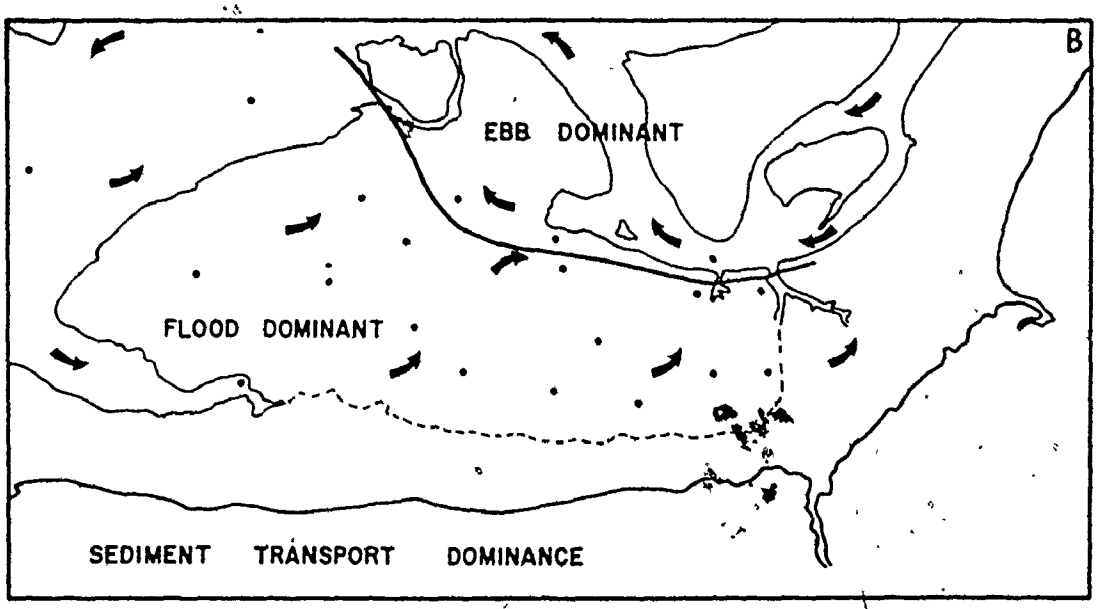

FIGURE 6.3: Sediment transport vectors (direction only) on Selma Bar for the ebb-flood and ebb-flood vector means (A) and the areal patterns of sediment transport dominance for the ebb and flood (B).

The sediment transport patterns show that the gently sloping side of the bars and their adjoining channels are generally dominated by the flood while the steeply sloping side of the bars and their adjacent channels are generally dominated by the ebb. This pattern is supported by fluorescent tracer studies carried out by Dalrymple (1973 b; and pers. comm.) on Noel Bay Bar, Selma Bar and Diamond Bar.

The nature of the sediment dispersal patterns on the bars reflects the importance of shielding and the distribution of ebb-and flood dominated areas that were determined from the study of bedforms and tidal currents. The strongly flood dominant transport on the surfaces (gently sloping sides) clearly indicates the extent to which the ebb-oriented megaripples seen at low tide reverse their asymmetry.

The tidal current measurements (strength and direction), bedform measurements and observations (morphological asymmetry, scale, internal structures), and sediment transport results (net bedform migration, empirical transport equations) from the sand bars investigated strongly supports the existence of some sort of residual "circular" to "elliptical" circulation of currents and sand around individual bars, parts of, or groups of bars. On Noel Bay Bar, Fig. 6.1), the net transport of sand is to the southeast up the gently sloping side of the bar (flood dominant) at a slightly oblique angle to the bar crestline, and to the west along the steeply sloping side of the bar and in the adjacent channel (ebb dominant). On East Noel Bar (Fig. 6.2), net sediment movement occurs in a northwesterly direction across the bar (ebb dominant) and to the east in the channel along the north side of the bar. On Noel Shore Bar (Fig. 6.2), sediment moves around the bar within one of three cells: (i) a clockwise transport system on the west part of the bar; (ii) an anticlockwise transport system on the eastern part of the bar, and (iii) an anticlockwise transport system on the northern part of the bar (inferred from bedforms and bar topography because there were no current measurements taken here). The net pattern of sand circulation on Selma Bar (Fig. 6.3) is anticlockwise. Sediment is transported to the east and northeast along the flood dominated, south-side of the bar (gently sloping side) somewhat obliquely towards the bars crestline, and to the north along the large swatchway that crosses the bar and along the channel separating the bar from the at the end of the

the bar (steeply sloping side) is generally ebb-dominant with net transport to the west. Thus, the sand bars are hydraulically maintained sand traps that result from the opposed current and transport residuals on the two sides of the bars, or parts of the bars.

The calculated sediment transport rates are large compared with maximum rates of movement established from air photos confirming that sand is moved around the bars more rapidly than the net lateral migration rates of the bars because the bars are relatively stable in position over a period of three to five years. Major changes in the positions of some bars, as recorded on older air photos and maps result from localized rapid migration or avulsion (into bar swatchways) of the interbar channels. It is possible to estimate the expected rate of lateral migration of the steeply sloping side of a bar knowing the net transport rate and direction (relative to the orientation of the bar crestline) across the gently sloping side of the bar.

As a hypothetical example, consider a sand bar with a net flood-oriented transport rate of 3000 kg/m per tidal cycle at angles of 10, 20 and 50 degrees to the bars crestline up the gently sloping side of the bar. The net upslope component of transport for these three hypothetical vectors would be about 91, 351 and 1761 kg per metre of crestline per tidal cycle (or 34, 132 and 662 m^3 per metre of crestline per tidal cycle, assuming a sediment density of 2.65 kg/m^3). Assume that the sediment transport rate per tidal cycle on the gently sloping side of the bar represents the amount of sediment actually deposited on the bar's steep side, and that no vertical accretion occurs along the bar's crestline. If the bar has a steep slope of five degrees and a vertical elevation difference of ten metres (from the bar's crestline to the adjacent channel bottom), then the crestline would migrate laterally at about 0.3, 1.2 and 5.8 m per metre of crestline per tidal cycle for the assumed hypothetical transport rate and directions.

These rates are, of course, much too large relative to reality. Major movement of the position of the sand bars occurs about every 3 to 5 years as recorded in old air photos and maps. Furthermore, five degrees for the slope of the steep side of a bar is conservative. The steep side of some of the bars are often as high as ten degrees which would give larger rates of lateral migration for the above hypothetical

example. The results, nevertheless, indicate that sand must be removed from the steeply sloping sides of the bars almost as fast as it is deposited, otherwise the bars could not maintain their relatively stable positions. To maintain a relatively constant surface elevation, and balance sediment removal on the steep side of the bars, sand must also be renewed on the gently sloping sides of the bars.

The net transport rates along the steep sides of the bars (i.e., ebb dominated channels) are generally an order of magnitude larger (bracketed values in Table 6-1) than net rates across the bars. Thus, there is a considerable volume of sand leaving the sand-body complex (e.g., for a net transport rate of 1.0×10^5 kg/m per tidal cycle, this would represent about 7.3×10^6 kg/m/y or 2.75×10^6 m^3/m/y). However, because the sand-body complex is neither increasing nor decreasing in size, and there are no large accumulations of sand in Minas Basin, sand must be circulated around the ends of the bars (or parts of the bars), producing an essentially closed, but continuous "circular" to "elliptical" transport system(s). Observations by Dalrymple (1973 b; and pers. comm. 1976) on other bars in Cobequid Bay also confirm the existence of some sort of an "elliptical" transport pattern. Swift and McMullen (1968) surmised that the pattern of flood dominance on the gently sloping sides of the bars and of ebb dominance along the steeply sloping sides "provides a possible mechanism for the localization and growth of the sand-body complex" from their reconnaissance study of the sand bars in Cobequid Bay.

During the winter, the relative importance of tidal current sediment circulation and lateral transport are decreased. The zones of ebb and flood dominance persist through both summer and winter, because they are primarily the result of the local bar topography. The ice-sediment crust on the bars in winter immobilizes the sediment surface, thus significantly reducing the "elliptical circulation" of sediment around the bars or parts of bars (e.g., compare diagrams in Fig. 5.55). Lateral transport of sediment by channelized late stage runoff is increased in absolute amount and relative to bed load transport, due to the decreased internal drainage of the sand bars.

Similar examples of this pattern of sediment transport have been reported by Allen (1968 b), Caston and Stride (1970), Houbolt (1968), James and Stanley (1968), Klein (1970 a), Reineck (1963) and Smith (1969). Balaz and Klein (1972) and Klein (1970 a) believed that sand was circulated in some sort of elliptical pattern around each bar as en equilibrium system because the sedimentary facies and morphology of the bars in their study area remained relatively unchanged over a period of 20 years. Klein's results from Big Bar, a somewhat unrepresentative bar located near Five Islands along the north shore of Minas Basin, indicated that the gentle side of the bar was dominated by the ebb and the steep side by the flood (the opposite relationship to that found on the bars in Cobequid Bay). Balaz and Klein (1972) believed that 'supermature quartzites' could be produced by the continuous movement of sand grains around intertidal and subtidal sand bars with such essentially closed transport systems. Their findings were, however, inadequately compared to the characteristics of the source materials, and the roundess determinations were made by subjective visual comparisons, which makes their findings somewhat inconclusive.

6.3 CIRCULATION PATTERNS

The gross circulation patterns of the currents and sediments associated with tidal sand ridges (or bars) and their evolution and maintenance on continental shelves and in tidal estuaries has been discussed by several workers. Swift (1975) and Swift and Ludwick (p. 169-184, in Stanley and Swift, 1976) have summarized the current state of the subject.

Three hydraulic mechanisms are frequently used to explain the occurrence of tidal sand ridges: (i) the development of double helical flow cells in the intervening channels between the sand ridges (Allen, 1968 b; Caston and Stride, 1970; Houbolt, 1968; and Off, 1963); (ii) the interdigitation of ebb- and flood-dominant flows separated by discontinuous zigzag ridge systems (Caston, 1972; Ludwick, 1974; Robinson, 1956); and (iii) the development of a reversing cross-ridge component of flow generated by a cross-ridge pressure gradient (Huthnance, 1973; Smith, 1968, 1969).

Swift and Ludwick (p. 175-176, in Stanley and Swift, 1976) and Swift (1975) briefly reviewed the nature of double and single helicoidal flow cells associated with experimental and natural straight and curved channels respectively. They pointed out that such flow cells have long been recognized in open channel flows, but that flume and experimental studies have not completely supported the development of double helical flow cells in straight channels. Off (1963), Houbolt (1968) and Allen (1968 b), however, argued that the linear tidal ridge systems in the North Sea were due to two helicoidal spirals that converged at the surface along the channel axis and diverged at the surface along the crestline of the ridges. Their evidence for this conclusion included the occurrence of foam-lines and flotsam along the axis of the channel and bedforms that climbed up both sides of the sand bars towards the crestline of the bars (and migrated in opposite directions on either side of the bar's crestline).

Bedform observations and near-bottom current measurements, however, by various workers (e.g., Caston, 1972) have suggested that the sand ridges actually separate ebb and flood dominant tidal currents to either side of the ridges which does not support the helicoidal flow hypothesis. The inequality and opposite directions of the residual tidal currents on either side of the linear ridges causes sand to be circulated within closed or nearly closed transport systems around the ridges and for the ridge to migrate laterally in the direction of the stronger net sediment transport (or current) residual. As a result, the ridges are commonly asymmetrical in cross-section. Caston (1972, his Fig. 11) believed that the progressive lateral migration of the linear ridges would eventually deform into a "sigmoid" pattern and finally in three separate ridges from the differential rates of migration of the ridge crestline.

Ludwick (1974) proposed that sand ridge formation at the entrance to Chesapeake Bay resulted from retardation of the estuarine tide relative to the shelf tide. The increased friction in the shallower and relatively more complex nearshore waters of the estuary caused the estuarine tide to lag behind the tide on the shelf. During the ebb, the estuarine tide apparently continued to drain at low water while the shelf tide had already begun to flood. The relatively strong ebb flow passed out of the

inlet as an expanding 'jet' and the incoming flood tide which was relatively weak and dispersed was deflected to either side of the ebb-outflow. As a result of this flow pattern (interdigitation of ebb and flood dominant areas), a series of discontinuous "zigzag" ridges developed along the irregular junction or interface of the ebb and flood currents with opposite flow residuals on either side of the ridges. Each linear segment of the ridge system acted as a closed or nearly closed sand circulation cell because of the ebb and flood residual flows on either side. The channel-ridge pattern of the outer Thames Estuary (Robinson, 1960, his Fig. 2) is similar to the "zig zag" shoals at the entrance to Chesapeake Bay, but is more extensively developed because the tidal range is larger and wave activity relatively less. According to Oertal (1972), the amount of vertical buildup of the ridges into the intertidal zone is controlled primarily by the depth of the wave base and the wave climate (assuming a continuous supply of sand).

Huthnance (1973) and Smith (1968, 1969) proposed a different hydraulic mechanism to explain the occurrence of linear sand ridges. In their model, the ridges were oriented at a small angle to the direction of the flow and maintained by a cross-ridge component of flow. They believed that a ridge behaved somewhat like a two-dimensional slender body or half-hydrofoil inclined at small angle of attack to the flow. As the tidal flow encountered the sand ridge, the flow streamlines were deflected over, along and around the sand body. The potential flow solution for flow, past such an object predicts that the pressure will be less over the front (upflow) portion of the sand body and larger over the rear (downflow) portion (i.e., Bernoulli principle) and the flow will be skewed along the body because there is a pressure differential between the upflow and downflow ends of the inclined body. For a tidal sand ridge, sand is moved first up one side, then up the other as the currents are reversed (or rotated). Robinson (1960, his Fig. 7) considered a similar explanation for the current flow and sediment transport around a sand bank in the outer Thames Estuary. Figure 6.4 depicts a simplified diagram of Smith's model showing the relationship between a bar's orientation and the orientation of the crestlines of its superposed bedforms and the net current directions of the ebb and flood.

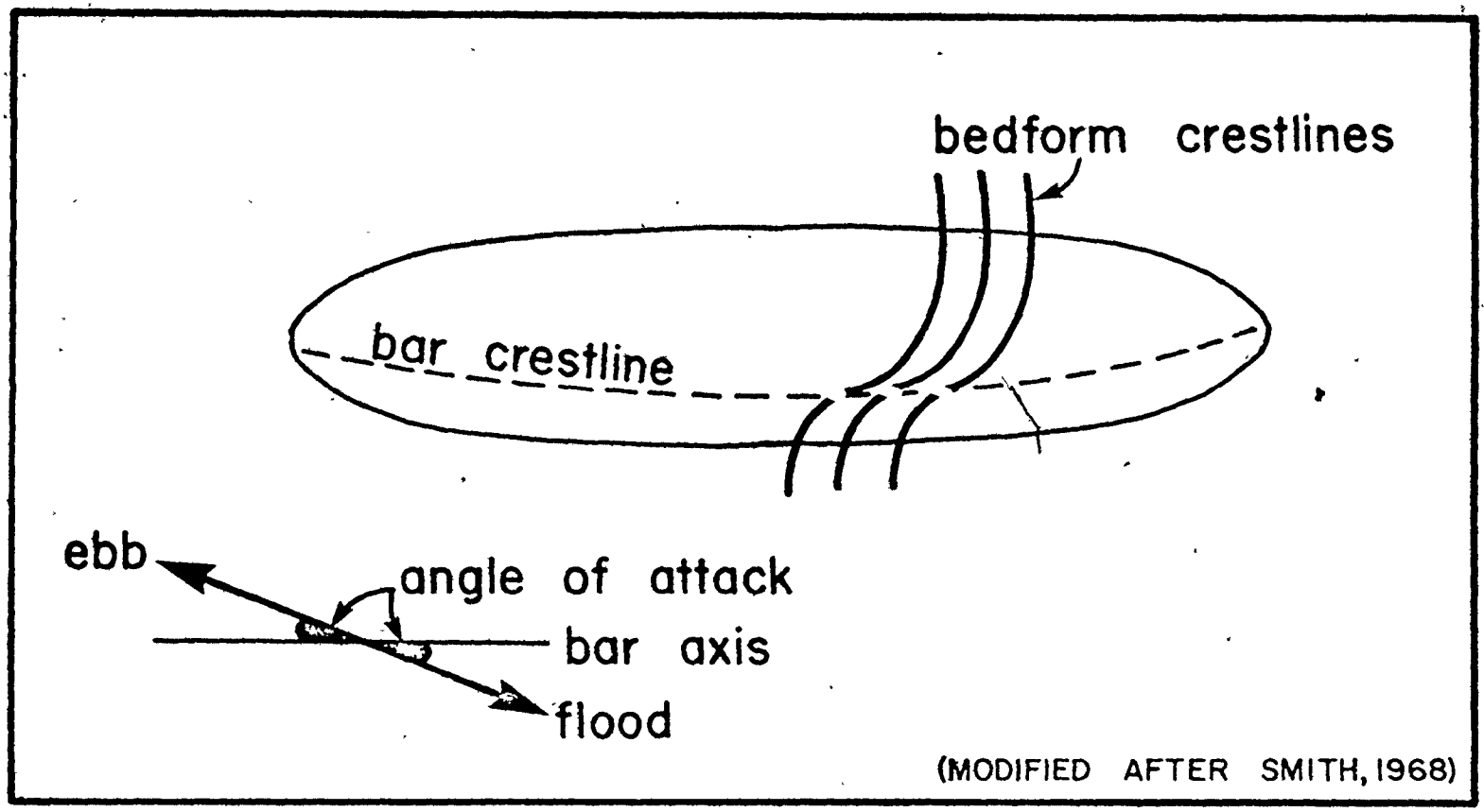

FIGURE 6.4: Hypothetical sand bar showing the relationship of the bar orientation to the mean flow directions of the ebb and flood, and the orientation of bedform crests on either side of the bar crestline.

Swift (1975) argued that Huthnance's explanation required the existence of the ridges first and the flow pattern second, and thus did not explain the actual initiation or origin of the ridges. He proposed (Swift, 1975, his Fig. 16), that the oblique alignment of linear sand ridges relative to the long axis of the tidal ellipse for a rotating tide might be the result of a retardation in the initiation of sediment movement (Postma, 1967), thus a delay in "the period of maximum sand transport" behind maximum ebb and flood flow, and from the development of an Ekman flow structure (i.e., boundary flows are "upward expanding Ekman spirals, as a consequence of frictional retardation of the flow by the sea floor"). Smith (1968, 1969) suggested that the origin and orientation of a ridge were a response to deposition along the long axis of the tidal ellipse for a rotating tide on an open shelf. Both explanations (i.e., Smith, 1968, 1969; Swift, 1975) are possible, but neither one has been confirmed with field data.

Although not considered by the above-mentioned workers, Smith's explanation for the origin and orientation of sand ridges from a rotating tide might hold for linear sand bars in a tidal estuary with a reversing tide. Whatever the case, it is possible that all three of the mechanisms discussed above might have some influence on the development and maintenance of the sand ridges (or bars) both on the open shelf with rotary tides or in estuaries with reversing tides. The only factors of generally common agreement about linear sand ridges is that: (i) the ridges are tide-maintained; and (ii) their height is controlled by the wave climate (strength, direction, frequency) and the depth of the wave base.

Ebb-Flood Channel Systems in Cobequid Bay

A generalized circulation model for the sand-body complex in Cobequid Bay, based on the gross patterns of sediment transport and current flow over and around individual sand bars is shown in Figure 6.5. The dominant flow directions and the distribution of ebb and flood dominant areas depicted in Figure 6.5 indicates that the general circulation pattern in Cobequid Bay is: (i) comparable to Swift's (1975, his Fig. 10 c) tidal channel complex situated at the head of a large bay into which there is relatively little fluvial input; and (ii) similar to the ebb tidal delta proposed for tidal inlets by Hayes et al. (1970, 1973) and Hayes (1975; see 66)

The flow patterns indicated in Figure 6.5 show the occurrence of the major ebb-dominated channels in the centre of the bay (always adjacent to the steeply sloping sides of the bars) and the major flood dominated channels along the north and south margins of the complex. (always adjacent to the gently sloping, flood dominated sides of the bars). The linear sand bars at the west end of the sand-body complex and the small irregular shaped bars at the seaward end of the ebb dominated channels are comparable to the "channel-margin linear bars" and the "terminal sediment lobe" of the ebb tidal delta model proposed by Hayes (1975) for mesotidal inlets through barrier islands along the east coast of the United States (Fig.6.6).

The areal pattern of suspended sediment content and the position of foam lines in the waters of the bay recorded in air photographs (Figure 6.7) taken shortly after the tide began to flood at the western end of the channel-bar complex clearly shows a partitioning of the ebb and flood currents by the sand bars, and the continued drain of the ebb from the sand-body complex after the tide has already begun to flood from the main bay. A similar pattern of flow is suggested by the ATPEMC (1969) seawater and current data shown in Figure 2.3.

Discussion

The actual geometry and morphology of the channel-bar complex is the result of the repeated interaction and interdigitation of the ebb and flood tides. The sand-body complex is in a state of dynamic equilibrium with the tidal regime because the sand bars have changed little near the shore or are changing slowly offshore with time (see Section 3.3).

Although the ebb and flood phases of the tidal cycle are both characterized high-water sheet-flow and low-water channel-flow phases (Fig. 4.24), their respective hydrodynamics and hydraulics are different. The ebb tide is basically a "tidal drain" (Price, 1963) or gravitational drain of the intertidal zone that is initiated by the relatively rapid retreat of the tidal wave from Cobequid Bay, with the subsequent 'drawdown' of the water surface (gravitational energy slope) towards the continental shelf. The flood tide, on the other hand, begins to move landward only when the energy slope of the flood near the entrance to the bay is sifficient to overcome the gravitational energy slope of the ebb tide.

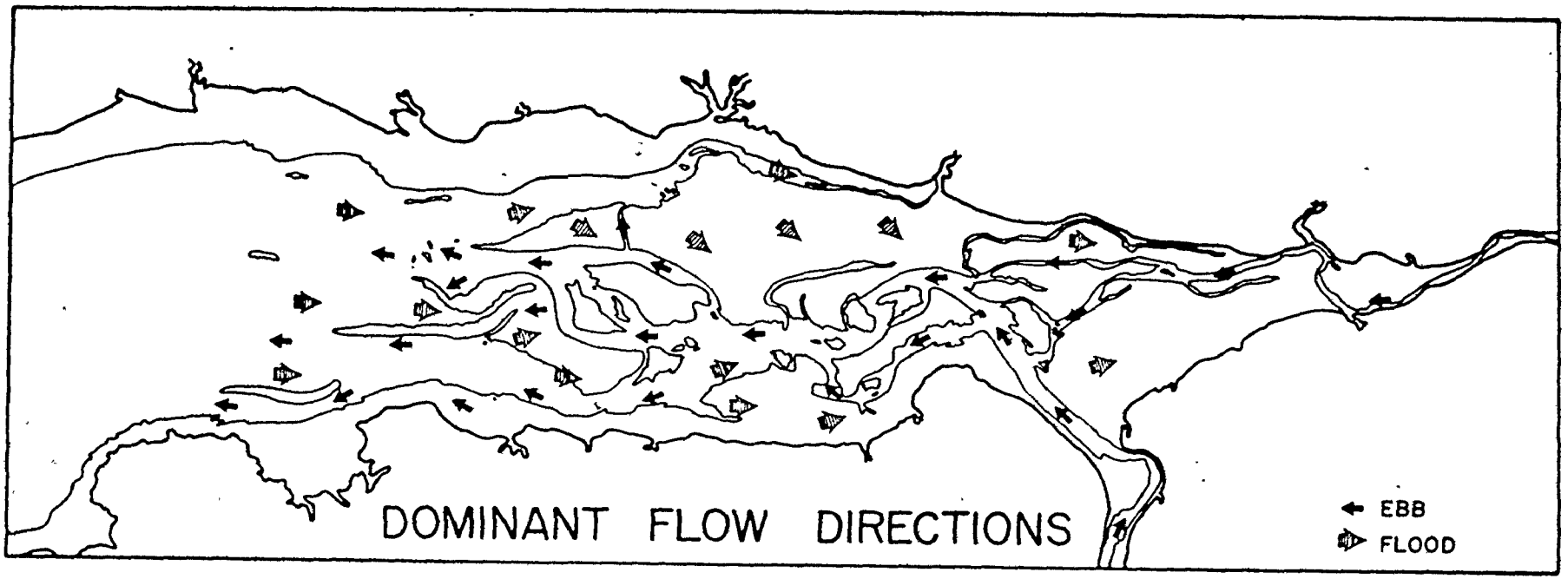

FIGURE 6.5: Directions of dominant tidal currents and sediment transport vectors in the sand-body complex.

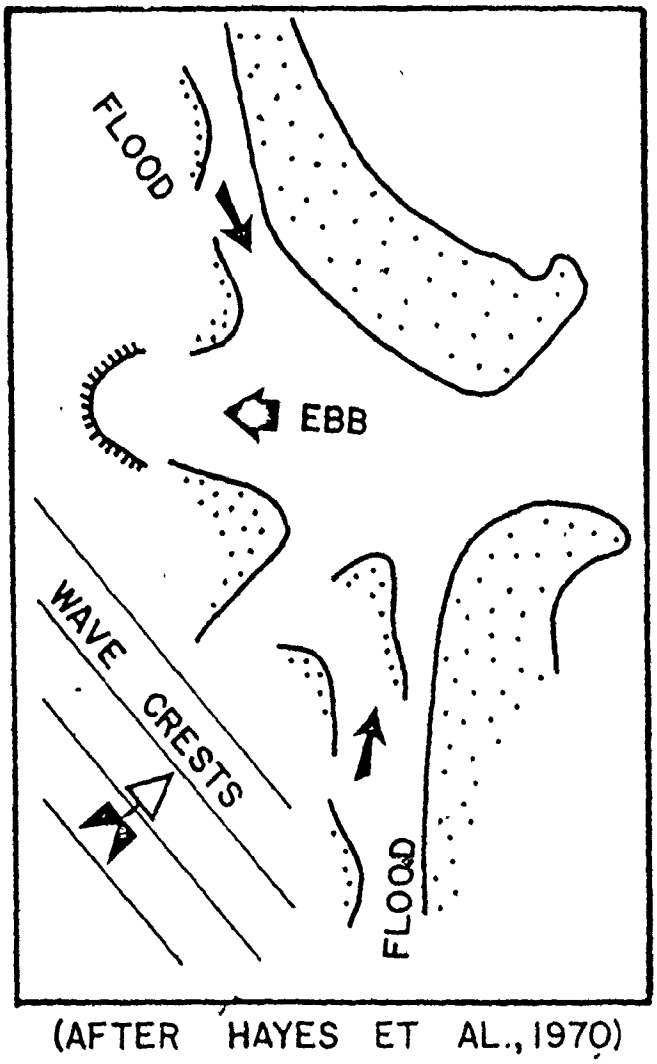

FIGURE 6.6: Ebb tidal delta model proposed for a tidal inlet with a mesotidal range.

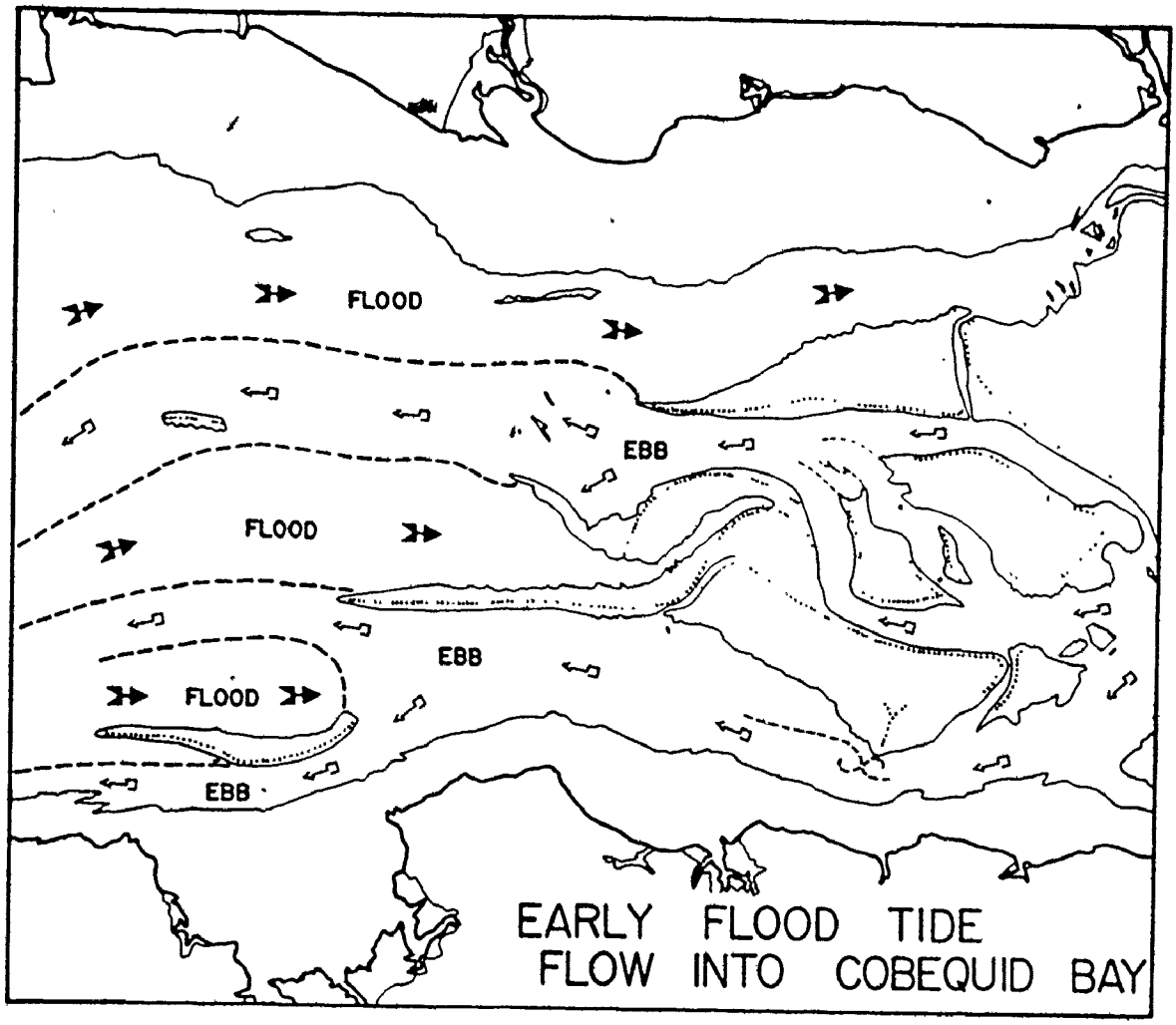

FIGURE 6.7: Early flood tide flow intb Cobequid Bay showing the partitioning of the ebb and flood by the sand bars. Diagram is based on the areal patterns of suspended sediment content and the position of foam lines recorded in air photographs.

During the ebb, the properties of the tidal drain or the ebb currents are controlled by the rate of drawdown of the water surface (i.e., the gradient of the gravitational energy slope) and the hydraulic geometry of the interbar channels. The rates of water level change (Fig. 4.18, Table 4-12) vary along and between the interbar channels due to differences in the hydraulic geometry and hypsometry of the channels (i.e., water levels decrease more rapidly in channels that are relatively wider and deeper, compared with the relatively slower rates of water lowering in those channels with slightly smaller wetted perimeters, e.g. ebb (small) versus flood (large) dominant channels. As the water levels decrease at different rates in adjacent channels, a component of flow across the bars at an oblique angle to the long axis of the bar with the currents flowing from the channels with the relatively higher water levels (i.e., those with relatively small wetted perimeters) to those with lower water levels (i.e., those with slightly larger wetted perimeters). The cross-bar component of flow develops in response to the mechanism proposed by Smith (1968, 1969).

As soon as the crestlines of the bars become emergent, the ebb tide changes to a low-water channel-flow phase and the cross-bar component of flow stops. The emergence of Selma and Great Village Bars which are connected to the shoreline (Figs. 3.2 and 6.5) deflects the ebb towards the centre of the bay where the flow follows the shortest path(s) of least resistance to the western edge of the sand-body complex. The steeply sloping sides of the bars and the major channels in the centre of the bay are dominated by the ebb and are maintained by erosion resulting from the effective concentration and downcutting of the late-stage, channellized currents when maximum current velocities occur during the late ebb. The low-water, channellized-flow of the late ebb in the centre of the bay and the relatively high rates of sediment transport to the west along the ebb dominant channels produces much of the east-west elongation of the sand bars (and thus, the relatively pointed planimetric shape of the western ends of the bars).

Current measurements indicated that single helicoidal flow cells developed in the curved reaches of the ebb-dominated channels only during the late-ebb, low-water channel-flow phases of the ebb tide. None of the current measurements the of

flow cells' in the channels, either during the high-water sheet-flow phase or the low water channel flow phase.

The low-water, channellized-flow of the ebb discharges from the seaward edge of the sand-body complex as a "spreading jet" into the open bay. As the ebb-jet flow westward, shear occurs along the edges of the jet, causing the formation of turbulent eddies and lateral mixing of the jet. The jet is slowed and its volume increased as the surrounding water is entrained and accelerated.

The ebb tide draining the sand-body complex is retarded by friction (i.e., large relative roughness), thus the gradient of the gravitational energy slope is relatively steep making it more difficult for the incoming flood tidal wave to overcome the ebb outflow. As a result, the ebb continues to flow out of Cobequid Bay after the ocean tide has already begun to flood from the west.

When the incoming flood wave encounters the outflow of the ebb-jet(s), it is deflected to either side of the ebb (dynamic diversion of Todd, 1968) because the energy slope of the flood is not sufficient to overcome that of the ebb. The flood enters Cobequid Bay around the margins of the sand-body complex where there is little or no ebb flow. As a result, water levels increase more rapidly in the marginal channels than in the ebb dominant channels in the centre of the bay and a component of flow develops across the bars in the opposite direction to that during the ebb, after the flood tide submerges the crestline of the bars.

Some interdigitation of the ebb and flood occurs in the centre of the bay (Figs. 6.5 and 6.7), but the ebb tends to predominate. When the energy slope of the flood is almost sufficient to overcome the ebb in the centre of the bay, water levels begin to rise for a short period of time (i.e., 5 to 10 minutes) just before the tide actually turns.

Once the flood tidal wave has overcome the ebb gravitational drain from the complex, its rate of advance is controlled by the hydraulic geometry or water depth in the interbar channels, particularly the channels that are exposed to the flood. The effect of water depth on the rate of advance (or retreat) on the tidal wave can be shown by a simple calculation. The celerity (c) of the tidal wave is equal to

$$c = \sqrt{gD}$$

where g =

depth of 10 m, the celerity of the tidal wave would be about 10 m/s and the wave would take about half an hour to travel the length of Cobequid Bay (assuming a length of 20 km). For a water depth of 5 m, the wave would travel at only 7 m/s and would take almost 0.8 h to travel the bay's length. This partly explains why the duration of the ebb is longer than the flood, i.e., because depths are increasing and relative roughness is decreasing during the flood, the flood wave requires less time to advance up the bay, while the reverse is true during the ebb.

According to Robinson (1960), the flood tide should be more erosive because it tends to flow as a bottom current, being more saline and colder (thus denser) than the ebb tide which is more a surface current in the Thames Estuary. Although the flood dominated marginal channels tend to be deeper and broader than the ebb channels in the centre of Cobequid Bay, suggesting that the flood is more capable of scouring the bed than the ebb, Robinson's explanation cannot be completely accepted. It appears that the ebb currents are generally more erosive than the flood currents in Cobequid Bay because maximum velocities of the ebb occur during the low-water, channel phase of flow (see Chapter 4) when depths are relatively shallow, while maximum velocities of the flood occur during the early part of the high-water sheet phase of flow when depths are relatively deeper. The erosive properties of the late-ebb causes extensive downcutting in the channels dominated by the ebb, maintenance of the steeply sloping sides of the bars, and elongation of the bars in an east to west direction. The relatively denser waters of the flood are capable of scouring the beds of the flood-dominated channels for a short period when water depths are not too great and maximum velocities occur during the latter part of the low-water channel-phase and early part of the high-water sheet-phase of flow (i.e., just after the crests of the bars are submerged). The relative depth of the ebb when maximum velocities occur are shallower than that during the flood when maximum velocities occur (perhaps a relative depth difference of about 1.0 to 1.5 m). As a result, the ebb tends to be more erosive (although its capacity is less) than the flood. The ebb removes the sand deposited on the steep sides of the bars during the flood and the flood replenishes the sand removed during the ebb.

Thus, the general sediment and circulation pattern in Cobequid Bay resembles a large ebb tidal delta that is characterized by three components: (i) the erosive, gravitational drain of the ebb currents in the centre of the bay; (ii) the relatively constructive flood currents around the north and south margins of the sand-body complex with some interdigitation with ebb in the centre of the bay; and (iii) the opposing cross-bar components of flow during the high-water sheet-flow phases of the ebb and flood respectively. The interaction of these three components, averaged over a tidal cycle, causes an elliptical pattern of residual sediment and current circulation around individual sand bars or parts of bars. Circulation is generally clockwise on those bars that are located to the north of the major ebb dominated channel in the centre of the bay, and anti-clockwise on the bars to the south of it. The sense of circulation on the bars is determined by the angle of attack the bar crestline relative to the direction of the reversing currents, and the local bar topography.

6.4 Evolution of the Channel-Bar Complex

The modern tidal regime in Cobequid Bay explains the maintenance and the observed geometry and morphology of the sand-body complex, but it does not account for the source of the sand or the initial localization of the sand bars. Swift and McMullen (1968) suggested that the Holocene sand-body originated from the erosion of materials, primarily Triassic sandstones, in the shoreline of the bay during the post-Pleistocene marine transgression. Glacial sediments already in and(or)around the bay should also be considered as an equally important source of the sediments in the sand bars. Both sources of sediment were substantiated to some extent with field observations and sparker records (see Section 3.3), but the relative volumes of sediment from each source were not determined.

According to Prest and Grant (1969), the sea invaded the Bay of Fundy about 13,200 y B.P. after the ice retreated to the highlands. Emergent banks at the entrance to the bay, however, effectively separated the Gulf of Maine and the Bay of Fundy system from the tidal dynamics of the Atlantic Ocean until about 8000 y B.P. (Grant, 1970). As a result, Grant believed that the proto- Bay of Fundy system was a tideless sea and that tidal conditions evolved since that time. The bay apparently did not

reach resonant dimensions until about 6000 y B.P., and only since then has the tidal range been amplified, with most of the increase occurring within the last 3000 to 4000 y B.P. The rate of amplification of the tidal range has decreased within the last 500 y B.P. (Grant, 1970, his Fig. 15).

During the period following the retreat of the ice from Minas Basin-Cobequid Bay, considerable volumes of sediment were discharged into the bay from glacio-fluvial processes or eroded from the bottom and flanks of the bay due to rising sea levels (resulting from the eustatic rise of sea level, tidal range amplification and isostatic sinking of the earth's crust to compensate for Pleistocene ice-loading).

Swift and McMullen (1968) proposed that early sand-body in Cobequid Bay was a tabular "sand sheet", implying that more sand was dumped into the bay than could initially be redistributed by the proto-tidal currents in the system. As amplification of the tidal range occurred, the sand-body was progressively altered to accommodate the increased tidal discharge, perhaps in a manner similar to the development and adjustment of the sand bars and channels in a braided-fluvial system to different discharges, e.g., see discussions by Cant (1975), Collinson (1970, Smith, N.D., (1970) and Walker (1976).

The evolution of the major ebb channels in the centre bay were most likely the key to the development of the ebb tidal delta morphology and general circulation in the Cobequid Bay sand-body complex. Because the ebb is primarily a gravitational drain of the bay's intertidal zone following the retreat of the ebb tidal wave, the ebb channels selected their location in the centre of the bay, as this was the most direct seaward route through essentially homogeneous sediments. The depression on the bedrock surface extending up the centre of the bay may also have been important in determining the location of the ebb channels.

As the tidal discharge increased through time and sea levels rose, the early sheet-flood phase which characterized the proto-tidal regime became less important, and the low-water channel phases became more important, particularly the ebb channels for the recirculation of sand out of the bay that was deposited at the head of the bay during the flood. The repeated action of the ebb and flood sheet-flow and channel-flow phases initiated and developed individual san as

traps, and with opposing flow residuals on the two sides, each bar developed a closed or nearly closed elliptical sand transport system, the long axis of which aligned with the long axis of the sand bar and the tidal ellipse of the reversing currents.

With time, the supply of sediment gradually decreased as the volume of fluvial input was reduced with the disappearance of ice from the area, and a reduction in the rates of sea level rise and tidal amplification within the 500 y B.P. (Grant, 1970, his Fig. 15), the sand-body complex has probably attained some degree of dynamic equilibrium with the tidal regime in the system. As a result, the position of the bars has remained relatively stable, and in the past 100 y of historic records there is no evidence of any major erosion or accretion in the amount of sand in the bay. The present circulation patterns and calculated sediment transport rates confirm that sand is moved more rapidly around individual bars, parts or groups of bars than the rates of movement of the bars established from air photos.

Although there is a net ebb outflow of the tidal prism through Minas Channel (because the ebb is augmented by some fluvial input into the bay; see Table 2-3), the sand-body persists at the head of Cobequid Bay because sediment transport during the flood is slightly larger (volumetrically) than that during the ebb (result of higher flood transport rates and the effect of such depositional mechanisms as those discussed by Postma, 1967) and because wave action is dominant from the west. Strong wave activity from the west controls the surface elevation of the sand bars.

6.5 STRATIGRAPHIC IMPLICATIONS

Tidal deposits possibly represent an important part of the geologic record particularly because some workers believe that the moon was much closer to the earth during early geologic history (e.g., Klein, 1971 and 1972; Merifield and Lamar, 1968 and 1970; and Olson (1970 and 1972) because clastic tidal deposits could form potentially important hydrocarbon reservoirs.

The recognition of ancient tidal deposits, however, has been limited to only a relatively small number of stratigraphic sequences (e.g., Bosence, 1973; several examples in Ginsburg, 1975; Klein, 1970 b, 1971,

1972; and de Raaf and Boersma, 1971) primarily due to problems of identifying distinctly tidal sedimentary characteristics. Many sedimentary features are representative of more than one sedimentary environment, although they may result from different processes. Klein (1971) pointed out that "great care must be exercised in recognizing the combination of features present, and interpreting the flow processes responsible for them."

Klein (1971, his Table I; also see Klein, 1970 a, his Table 8) tabulated a list of criteria for the recognition of ancient tidal deposits and proposed "a sedimentary model for determining the paleotidal range." Although his model has been criticized for not synthesizing all of the most important characteristics of clastic tidal deposits, particularly with respect to differentiating intertidal and subtidal sediments, it certainly identifies some of the problems of distinguishing tidal sequences from vertical sequences laid down in other sedimentary environments. For example, the fining-upward paleotidal sequence in Klein (1972, his Fig. I) is very similar to Allen's (1970 b; Klein, 1972, his Fig. 2; also see Walker, 1976) fining-upward for a meandering alluvial channel. Klein (1967 and 1972) believed that the only way to distinguish between a "migrating estuarine, fluvial and tidal channel" sequence was to examine the channel lag deposits, i.e., tidal channels should be floored by a shell lag, estuarine channels with a mixture of clay chips and shells, and fluvial channels with gravel, clay pebbles and possibly organic remains (e.g., logs).

Figure 6.9 (symbol key in Fig. 6.8) shows a hypothetical regressive and transgressive vertical section from Cobequid Bay that could conceivably result if a relative rise or fall of sea level changed the present resonant dimensions of the Bay of Fundy system, causing a decrease in the tidal range. If emergence took place, or subsidence was particularly slow, the sedimentary facies near the head of bay would prograde over those of the outer bay. The resulting vertical sequence would begin with an erosional surface overlain by lag deposits and pass up into cross-bedded subtidal and intertidal bar sands, then cross-rippled flat sands, interbedded sand and mud from the "mixed flats", mud deposits from intertidal mudflats, and finally into supratidal saltmarsh and fluviatile deposits. If, however, relatively rapid subsidence occurred, the sand-

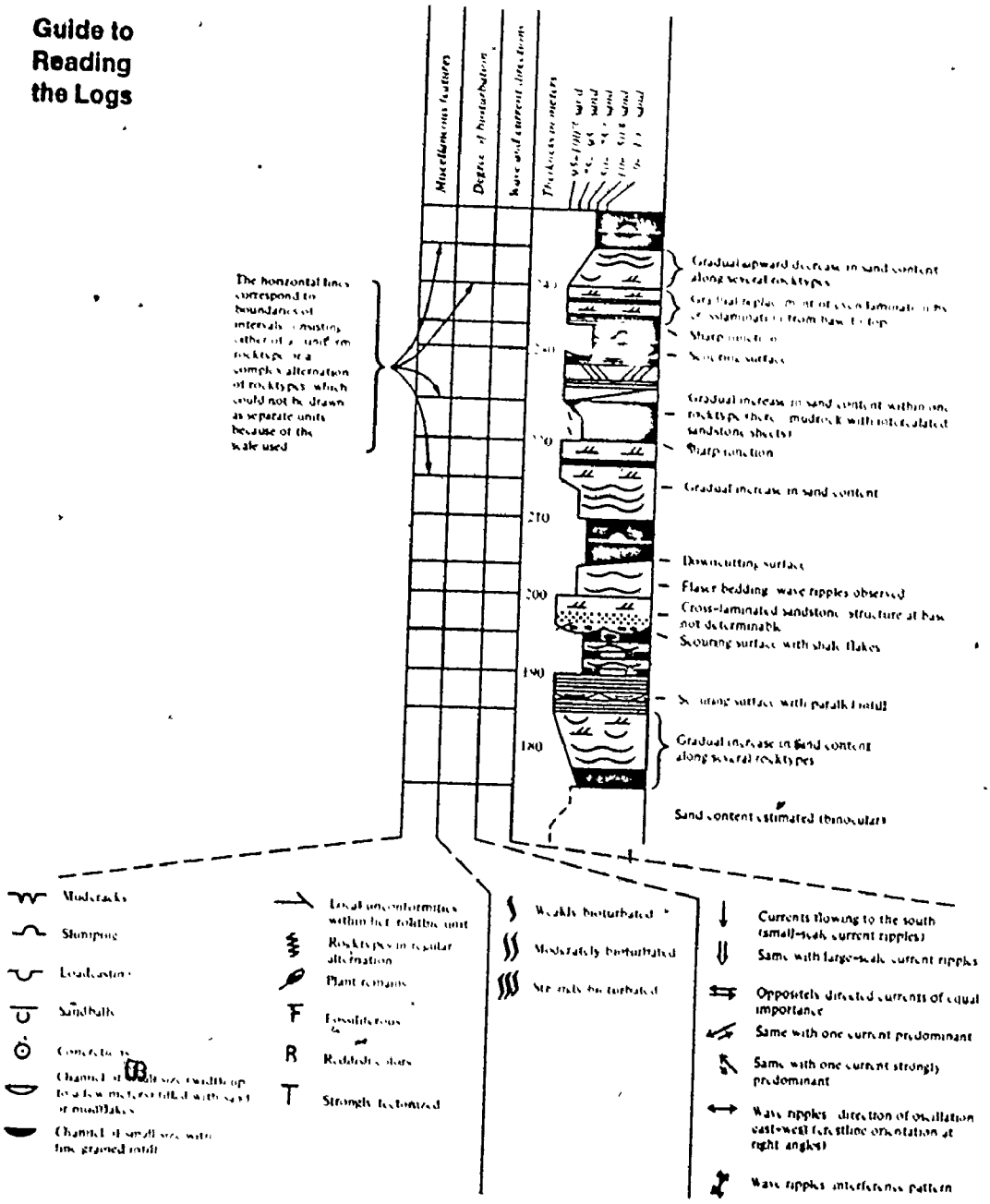

FIGURE 6.8: Stratigraphic key to Figure 6.9 (from Ginsburg, 1975).

Basic Rock Types

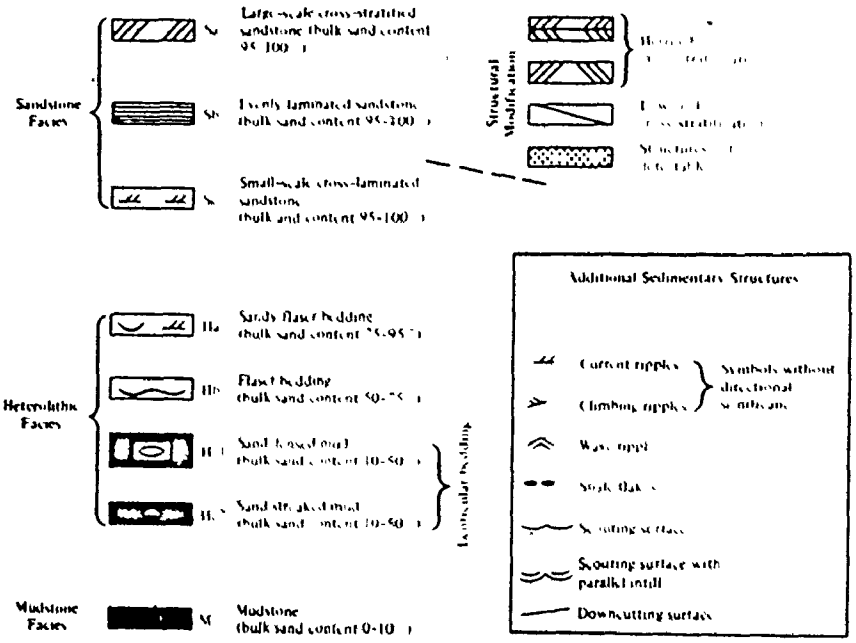

Composite Rock Types

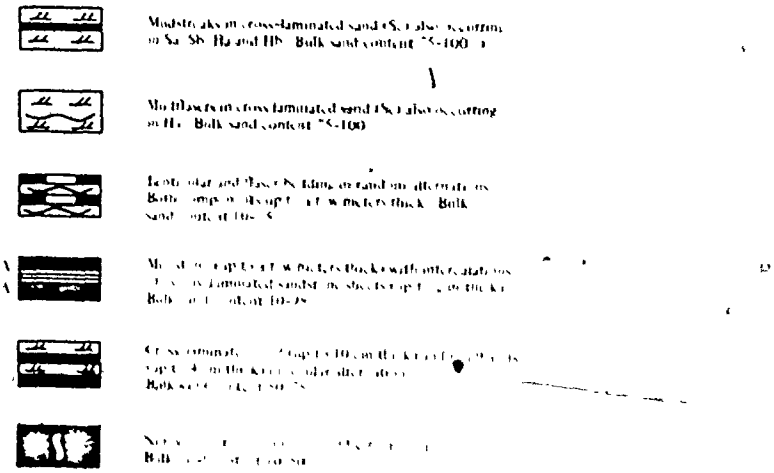

FIGURE 6.8 - cont'd.

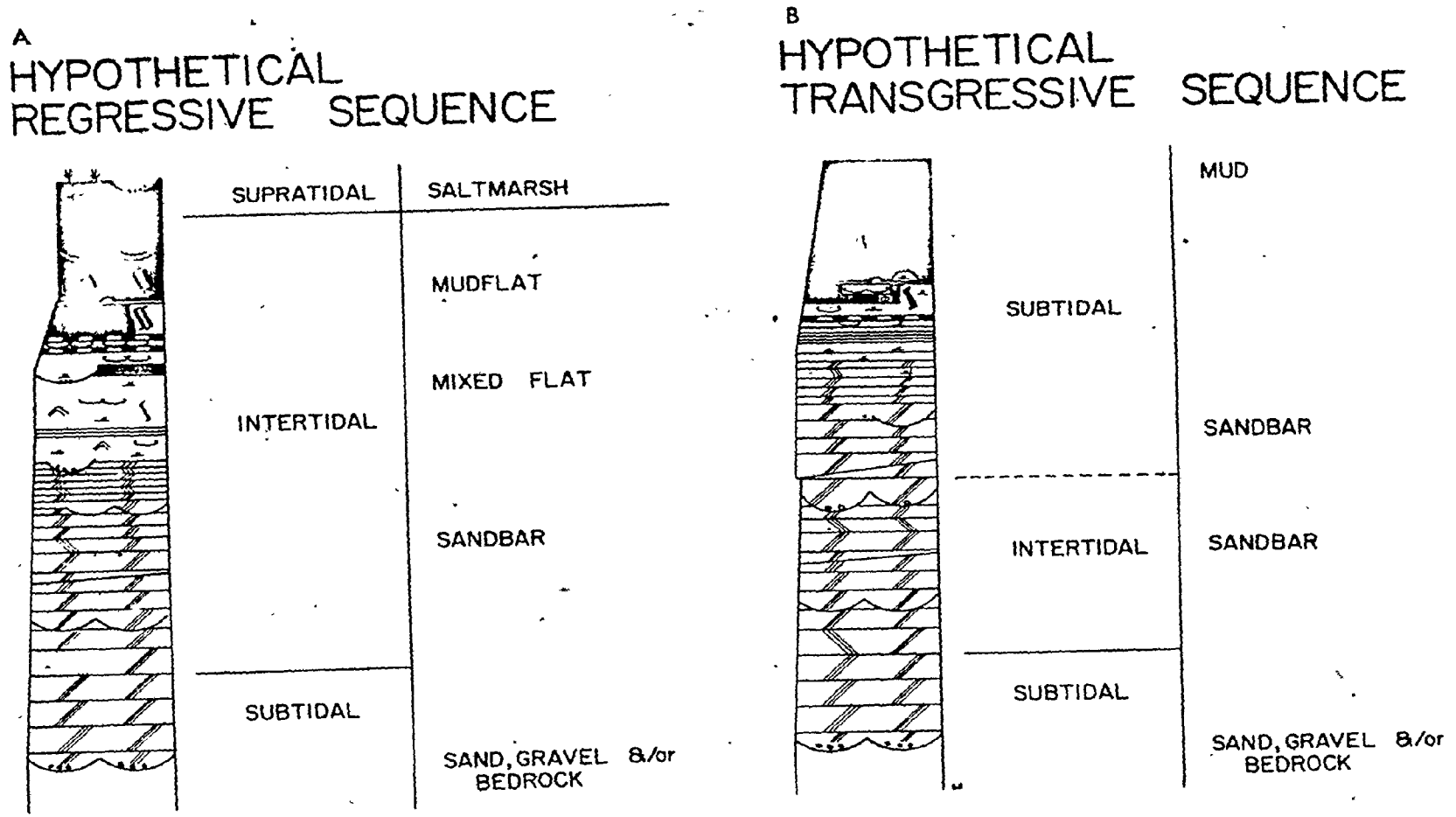

FIGURE 6.9: Hypothetical regressive (A) and transgressive (B) vertical sections of the sedimentary facies in Cobequid Bay.

body complex would be submerged, and the cross-bedded bar sands would pass up into rippled sand and subtidal muds. Both sections fine upwards.

Because bi-modal cross-stratification is relatively uncommon in the sand bars in Cobequid Bay, it is of little use as an identifying feature of tidal deposition in ancient sedimentary deposits. Examination of the channel lag deposits is also a tenuous criteria to identify tidal deposition because some tidal systems are strongly influenced by fluvial input. Because macrotidal deposits are similar to many mesotidal deposits, there are further problems of distinguishing paleotidal ranges from ancient sedimentary sequences. Thus, both the reliable recognition of ancient tidal deposits and their paleotidal range are to some extent unsolved problems in sedimentology.

6.6 SUMMARY

As a result of the time velocity asymmetry of the tidal currents in the channels and over the bars, residual current and sand circulation occurred within closed or nearly closed elliptical loops (Fig. 6.1, 6.2 and 6.3) around individual bars, parts or groups of bars. Each bar or part of a bar behaved as a hydraulic sediment trap between opposing directions of residual current flow, i.e., the gently sloping sides of the bars were dominated by the flood, and the steeply sloping sides by the ebb. Rates of sediment transport estimated by an empirical total-load equation (Ackers and White, 1973) indicated that rates of movement varied considerably over different parts of the sand bars and at different times (Table 6-1). Typical transport rates on the gently sloping, flood dominated sides of the bars were generally less than 5.0×10^2 kg/m per ebb and 3.5×10^3 to 7.5×10^3 kg/m per flood for the ebb dominant channels and along the steeply sloping sides of the bars, transport rates were generally between 4.0×10^3 and 1.5×10^4 kg/m per ebb and less than 3.0×10^2 kg/m per flood. The vector mean of the ebb and flood transport rates indicated that a considerable volume of sediment was moved across the bars in the flood direction (Figs. 6.1, 6.2 and 6.3) at an oblique angle to the crestline of the bars and seaward along the ebb dominated channels. The calculated sediment transport rates are high compared with maximum rates of lateral movement of the bars established from air

photos (i.e., the bars are relatively stable in position over a period of 3 to 5 years) confirming that sand is moved around the bars more rapidly than the net lateral migration rate of the bars. Major changes in the positions of some bars, as recorded in older air photos and maps from the last 100 years seem to result from localized rapid migration of the bar crestlines, or evulsion into swatchways by the interbar channels.

There was no indication that Coriolis effects were important in termining the patterns of current or sediment circulation, on the position of the sand bars and channels in the sand-body complex. Circulation patterns on sand bars along the north side of the bay were generally clockwise, and those to the south were generally anti-clockwise.

The asymmetry of the tidal currents and sediment transport vectors, and the occurrence of megaripples and sand waves (i.e., their orientation, net migration rates, internal structures) indicated that sand-body complex on Cobequid Bay resembled a large 'ebb-tidal delta' (Figs. 6.5 and 6.7) with the main ebb channels in the centre of the bay and flanked by 'channel margin linear bars built by the interaction of the ebb and flood, and flood dominated marginal channels to the north and south of the complex. This observed geometry and morphology of the sand-body complex resulted primarily from the time-velocity asymmetry of the tidal currents. Maximum ebb currents occurred during the late, low-water channel-flow phase of the ebb tide. As the tide turns at low water, strong ebb currents were still flowing seaward out of the major ebb channels. With the advance of the flood tidal wave, water levels began to rise and the flood currents were deflected to either side of the complex. The cross-bar components of sediment transport developed because the bars were oriented at a small angle of attack to the mean current direction (i.e., both ebb and flood) and the interbar channels had different hydraulic geometris and hypsometries producing different rates of drainage or flooding and thus differences in water levels on the two sides of the same bar.

The surface level of the bars was controlled by the wave climate and areal variation of the base level of wave activity in the complex. Because the largest waves and most frequent wave activity originated from the west, most of the wave energy was dissipated near the seaward edge of the sand-body complex on the exposed western ends of the sand bars and adjacent headlands. The effectiveness of wave action decreased towards the head of

the bay due to shoaling and increased complexity of the seabed, allowing the sand bars to build higher into the intertidal zone near the head of the bay than those near the exposed seaward edge of the complex.

The sediment and geometry of the present sand-body complex originated from the erosion and reworking of Pleistocene sediments and Triassic bedrock in and around the bay during the last 3000 years as sea level rose from the combined effects of eustatic sea level rise, land subsidence and increasing amplitude of the tidal range as the Bay of Fundy System reached resonant dimensions. If the sedimentary facies in Cobequid Bay were preserved in the ancient record, as a result of either a marine transgression or regression, a fining-up sequence would be preserved (Fig. 6.9). The major difference between the transgressive and regressive sequence is that the latter would be topped by a intertidal mudflat and supratidal marsh facies, while the former would pass up into subtidal muds.

The morphology, distribution of sediments and bedforms, current strengths and general circulation patterns of the sand-body complex in Cobequid Bay resembled the model proposed for "ebb-tidal deltas" of tidal inlets through barrier islands with mesotidal ranges (Fig. 6.6). The sand-body complex differed mainly with respect to tidal range, and the scale, relief and topographic complexity of the sand bars, the latter indicating the importance of tidal range in controlling the geometry of a tide-maintained sedimentary deposit. Nevertheless, the general properties of the sediments, bedforms and current hydraulics are similar between different tidal environments, despite dissimilarities of tidal range.

CHAPTER 7

SUMMARY AND CONCLUSIONS

7.1 SETTING

Cobequid Bay is located at the eastern end of the Bay of Fundy (Fig. 1.4) and is reputed to have the largest tides in the world (Fig. 2.16; Table 2-1). At Burntcoat Head (Fig. 1.5), the mean tidal range is 11.7 m (spring tides at lunar apogee and perigee average 12.3 m and 15.4 respectively). The tides are semidiurnal with a small diurnal inequality (maximum of about 0.8 m). The large tides are apparently caused by the resonant amplification of the semidiurnal tidal component of the oceanic tide as it moves across the continental shelf southeast of Nova Scotia. The development of the large tides occurred only during the last 4000 years as the bay reached resonant dimensions from a combination of rising sea level, isostatic rebound and erosion of the shoreline and seabed.

The tidal currents are reversing. Ebb and flood directional modes are separated by about 180 degrees. Current speeds, measured 0.5 m from the bottom, reach speeds up to 2.0 m/s in some channels and in the range of 0.3 to 1.25 m/s over intertidal areas.

The predominant wind direction is from the west with an average speed of about 16 km/h. This direction coincides with the maximum over-water fetch distance (about 50 km) in Minas Basin- Cobequid Bay (Fig. 2.15). Waves, are, however, generally less than 1 m height because of the relatively small size and restricted nature of the bay. Most wave energy from the west is dissipated on the bedrock headlands (e.g., Economy Point, Burntcoat Head), the broad intertidal zone along the shoreline and at the western end of the sand-body complex in Cobequid Bay. The morphology and distribution of sediment and bedform facies in the complex is almost entirely the result of the tide and tidal currents.

The climate of the study area is strongly influenced by continental air masses from the west, thus the mean annual temperature is only about 6°C. Summer and winter temperatures are moderated to some degree by marine influences. The mean annual precipitation, including rain and

snow, totals about 1.2 m. From December to March, there is drift ice in the bay, an ice-foot (Fig. 2.27) around the shoreline and an ice-sediment crust (Fig. 2.28) over many of the intertidal areas. The presence of drift ice and the formation of the ice-foot greatly reduces erosion of the shoreline by wave action. The frozen crust on many of the intertidal areas decreases the amount of sediment movement ~~in the intertidal~~ zone. Some sediment is, however, transported by drift ice and eroded remnants of the frozen crust, and in the subtidal channels. Sediment concentrations reach up to 68% by weight in the frozen crust and up to 23% in the drift ice.

The modern sediments in the bay were derived primarily from the erosion of Triassic sandstones and Pleistocene tills and outwash exposed in and around the bay. The rivers, most of which have drainage areas of less than 300 km^2, are presently contributing little water or sediment to the bay, but were important sources of sediment and freshwater discharge during the post-Pleistocene retreat of the continental ice-sheets.

Figure 2.6 summarizes the lateral relationship of sediment facies in the bay with respect to exposure to wave and current action and to position in the intertidal-subtidal zones. The bay is bordered by cliffs of Triassic sandstone and Pleistocene sediments that reach up to 30 m in height at some locations. The intertidal shore is characterized by a bedrock platform that is either exposed (e.g., adjacent to bedrock headlands) or covered with a veneer of sediments. Mud accumulates only in areas that are sheltered from wave and current activity (e.g., around the margins of the bay, in small bays and estuaries) forming mudflats. The mudflats are backed by a supratidal marsh. As in macrotidal estuaries elsewhere, sand deposition is concentrated in the centre (Fig. 3.3), away from the shore. The sand has been moulded into an extensive intertidal to subtidal channel-bar complex (Figs. 3.2 and 3.5). The sand bars are elongate features, 1 to 5 km long, oriented parallel to the reversing tidal currents, and covered with megaripples and sand waves.

Suspended sediment concentrations (from 77-1 litre water samples collected during several tidal cycles) in the bay ranged from 70 to over 2700 mg/l which was several orders of magnitude larger than the concentrations in the local rivers above any tidal influence. The largest concentration in the open bay occurred during the late ebb and early

flood when water depths were relatively shallow. Maximum concentrations lagged the occurrence of the maximum ebb and flood speeds by up to 30 minutes. Flood concentrations were about 50% higher than those during the ebb due to "scour and settling lag effects" (Postma, 1967). Most of the suspended sediments were clay and silt, not sand-sized.

Fresh water input to the bay by rivers lowered salinities to 25 to 30 o/oo. The large tidal prism, however, caused the fresh and saline waters in the bay to be well-mixed. Vertical temperature and salinity gradients were generally less than 0.5°C and 0.02 o/oo respectively. The temperatures and salinities of the flood were about 2 to 3°C and 1 to 2 o/oo lower than those of the ebb. Water temperatures, during the summer, averaged about 16°C, and during the winter, just below 0°C. Water temperatures and salinities varied both during the semidiurnal tidal cycle and during the lunar tidal month in the order of 1 to 2°C and 2 to 3 o/oo. (i.e,, temperatures and salinities were lower during spring tides than neaps and during early ebb and late flood). Areal variations of tidal current directions, and water temperatures and salinities (Fig. 2.23) do not support the existence of a Coriolis circulation pattern in the bay.

7.2 SAND-BODY COMPLEX

The sand-body complex in the centre of Cobequid Bay comprises two subfacies (Fig. 3.3): (i) the broad, intertidal sand flats situated near the head of the bay that are composed of fine-grained silts and sands, covered with ripples and a few large bedforms, and crossed by a braided pattern of tidal channels; and (ii) the elongate, intertidal to subtidal sand bars situated in the middle to western parts of the bay that are composed of medium grained sands, covered with megaripples and sand waves and cut by swatchways and relatively few, but deep tidal channels. Detailed examination of four sand bars (i.e., Noel Bey Bar, East Noel Bar, Noel Shore Bar and Selma Bar) from the latter subfacies represented the main study areas of this research project (Fig. 3.2).

Thirteen transects of the sand-body complex (totalling more than 100km of survey line) and numerous individual surveys of the four bars mentioned above (echo sounding and level surveying) were made to determine the bathymetric configurations of the sand bar and channels (Fig. 3.4 and 3.5). The sand bars were separated from the intertidal shore and each other by tidal channels ranging from 5 to 15 m deep below the tops of the bars (Fig. 3.6). The bars were about 3 km long, 1 km wide and 5 to 15 m in relief. In plan, the bars were relatively blunt-shaped at their eastern ends, and relatively pointed at their western ends. The gentle sides of the bars sloped at 3 to 5 degrees and the steep sides sloped at 4 to 12 degrees. The steep sides of the sand bars located in the northern half of the bay generally faced to the south, while those of the bars along the southern half of the sand-body complex faced to the north. The maximum relief of the bars decreased from about 25 m near the western end of the complex to less than 5 m near Salter Head (Figs. 3.5 and 3.6). The duration of intertidal exposure increased from about 2.5 hours to over 4 hours towards the head of the bay, because the sand-body complex became increasingly intertidal from west to east at high water. Bars near the mouth of the bay were coverd by about 10 m of water, but those near Salter Head were covered with less than 5 m.

The relief and relative level of the bar surfaces was controlled by the base level of strong wave activity from the west. Large waves approached from the west but most of the wave energy was dissipated at or near the seaward edge of the complex. Because wave energy decreased towards the head of the bay, the surface of the bars were built higher into the intertidal zone near the head of the bay than those at the exposed seaward edge of the complex (Fig. 3.6). The western ends of the bars were as much as 2 to 3 m lower in surface elevation than the eastern ends.

The geometry and structure of the sand-body complex was determined from more than 100km of continuous sparker survey (Fig. 3.4). The sand bars ranged from 5 to 15 m thick (Fig. 3.12), or roughly equivalent to the maximum bathymetric relief of the bars. The thickness of the bars decreased towards the head and sides of the sand-body complex. The bars were underlain by Triassic bedrock and(or) Pleistocene sediments (Figs. 3.7). The premodern Pleistocene sediments generally comprised elongate deposits up to 10 m thick (Fig. 3.10) beneath the sand bars. The topo-

graphy of the bedrock surface formed a broad, shallow depression along the longitudinal axis of the bay, shallows and decreases in relief towards the east. In stratigraphic cross-section, the sand-body complex resembled a clastic wedge that had prograded over the bedrock surface from the head of the bay.

The historical record of air photos and charts (Figs. 3.14 and 3.15) from the past 100 years indicated that the position of the sand bars near the shore were relatively stable, but those offshore had moved, primarily by lateral migration of the sand bars and avulsion of the interbar channels into intertidal swatchways, significantly about every 5 years. Although the surface topography and outline of the bars has changed within the last 40 years, there was no evidence of a major change in the volume of sand in the bay or in the types of large bedforms on the bars.

The bar sediments (from the mechanical analysis of more than 250 sediment samples from the bars and channels) were primarily well-sorted, medium grained sands (i.e., about 0.34 mm). Grain size decreased and sorting improved away from the shore and towards the head of the bay and the bar crests. The best sorted and finest grained sands were found along the bar crests. There was some tendency for sediment size distribution to be negatively skewed on the gentle, flood dominated sides of the bars, and positively skewed on the steep, ebb dominated sides of the bars.

7.3 TIDAL CURRENTS

Current measurements were made at more than 40 locations (Fig. 4.1) over a variety of bed locations and in different parts of the sand-body complex. Most of the thesis results were based on the measurement of more than 1200 vertical velocity profiles with a direct reading current meter. Further results were based on more than 150 days of point velocity measurements made 0.5 m from the bottom with automatic recording current meters.

The tidal currents were semidiurnal in period, reversing (Figs. 4.20 and 4.21) in character, and time-velocity asymmetrical (Figs. 4.10, 4.12 and 4.14). Maximum mean profile speeds occurred during the late to middle part of the ebb and during the early to middle part of the flood. There was some tendency for maximum ebb and flood velocities to occur slightly

later towards the head of the bay. Maximum flood speeds were about 10 to 20% greater than ebb speeds (Figs. 4.11, 4.13, and 4.16) for flow over the sand bars and in the channels. Maximum mean profile velocities averaged about 0.9 and 1.0 m/s for the ebb and flood near the western end of the complex and about 0.8 and 1.0 m/s near Selma Bar, towards the head of the bay. Maximum mean channel speeds were as high as 2.0 m/s. Current speeds decreased towards the shoreline, the head of the bay and the bar crests (compare Figs. 4.11, 4.13 and 416). During the lunar tidal month, maximum speeds varied by about 0.1 to 0.2 m/s per one metre change in the spring to neap tidal ranges.

The vertical distribution of current velocity over the relatively large-scale bedforms (i.e., megaripples and sand waves) and for relatively large depths of flow (compared to bedform heights) could be fitted with a first-order linear regression model (i.e., measured current speeds were proportional to the logarithm of the depth), thus agreeing with the results of experimental steady-uniform flows. Almost 81% of 1110 profiles (Table 4-2) that were regressed were statistically linear at the 95% level of confidence. The use of a second-order linear regression model did not produce a statistically significant improvement of fit compared to the results of the first-order model (i.e., the improvement of fit with the second-order model was significant in only 44% of the profiles, and fewer profiles could be analysed with the second-order regression model because it required a minimum of 5 measurement points per profile compared to 3 (per profile) for the first-order model). The first-order regression model was used throughout the data analysis.

Adjustment of the datums of the vertical velocity profiles to compensate for the presence of the large bed roughness elements (e.g., megaripples and sand waves) were of little use because the exact position of the measured profiles over the bedforms was unknown. Iteration of the linear regression model, for example, produced highly variable results (Table 4-1).

A comparison of the shape of the measured vertical velocity profiles relative to the fitted linear regression lines showed that the measured velocity points generally deviated from the fitted line in a regular pattern. Three profile types (Fig. 4.3) were defined: (i) convex relative to the regression line (Type 1 - speeds near surface and bottom were greater, and those at mid depth were lower than estimated by

the regression model); (ii) concave relative to the fitted line (Type 2); and (iii) linear or randomly distributed to either side of the regression line (Type 3). Almost 44% of the measured profiles (from 1132 profiles; Table 4-3) were Type 1, with about 20% as Type 2 and 36% as Type 3. Type 1 profiles were most common because most profiles were measured over the stoss-side of the bedforms within the region of accelerating flow (Fig. 4.8). Similar results were found for flows over bedforms in experimental flumes.

Profile shapes changed during the tidal cycle. Type 1 profiles were more common during the early ebb as a result of the negative surface wave produced by the retreat of the ebb tide from the bay. Similar conditions did not occur during the flood because it advanced as a positive surface wave.

The standard deviations of the observed profile velocity departures from the fitted linear regression model gave an estimate of the magnitude of the horizontal turbulent velocity fluctuations in the flow. These ranged from about 0.02 to 0.05 m/s or about 60% of the derived shear velocity values (which generally ranged from 0.02 to 0.09 m/s).

The duration of ebb and flood flows averaged about 4.5 h and 3.5 h over the sand bars and about 7.0 h and 5.5 h in the channels. The duration of the ebb was typically about 20 to 30% longer than the flood (Tables 4-6, 4-8 and 4-10). Ebb durations were 10 to 15% shorter and flood durations about 15 to 20% shorter from the mouth of the bay to Selma Bar. As a result of the variation of ebb and flood durations, the rates of water level change were more rapid and current speeds faster during the flood than during the ebb (Table 4-12 and Fig. 418). Rates of depth change varied from about 2.25 m/h during the ebb and about 2.95 m/h during the flood, and varied throughout the bay as a result of differences in hydraulic geometry and hyposometry of the interbar channels and the tidal range.

The time-velocity asymmetry and strength of the tidal currents (Figs. 4.10, 4.12 and 4.14) was related to topographic shielding on and by the sand bars (Fig. 4.25), the hydraulic geometry and hypsometry of the channels and the lunar tidal month variation of tidal range. The gently sloping sides of the bars were generally dominated by the flood (Figs. 4.11, 4.13 and 4.16) and the steeply sloping sides of the ebb.

The relative strength of the ebb or flood dominance was determined by the intertidal relief and topographic complexity of the bar surfaces. For example, the difference of maximum current strength on either side of Noel Bay Bar, a topographically simple bar of relatively small intertidal relief, was about 0.1 m/s, but on Selma Bar, a relatively complex bar with a somewhat larger maximum relief, was about 0.25 m/s.

The pattern of dominance by the ebb and flood over the sand bars (Figs. 4.11, 4.13 and 4.16) and in the channels indicated that the main ebb channels were located along the longitudinal axis of the bay (Fig. 6.5) and that two major flood channels were located along the north and south margins of the bay. As a result of the interdigitation of the ebb and flood channels, the general circulation of the bay resembled a large ebb tidal delta, similar in many respects to the ebb tidal delta model for tidal inlets with mesotidal ranges (Fig. 6.6), but different with respect to tidal ranges and dimensions of the sedimentary deposits.

The ebb and flood flow regimes each consisted of a high-water sheet-flow phase and a low-water channel-flow phase (Fig. 4.24). During the high-water sheet-flow phase when the bar crests were submerged, a component of flow developed across the bars in opposing directions during the ebb and flood because the bars were aligned at a small angle of attack to the flow (Figs. 4.20 and 4.21) and because the different hydraulic geomtries and hypsometries of the channels produced different rates of drainage and flooding and subsequently different water levels on the two sides of the bars. The combined effects of the ebb and flood current residuals on either side of the bars and the cross-bar components of flow produced a net flow circulation around the bars (Figs. 4.11, 4.13, 4.16 and 4.24).

7.4 BEDFORMS

The surface of the intertidal sand bars were covered with a variety of small and large scale bedforms (e.g., ripples, megaripples and sand waves) that were generated by the tidal currents. The major bedforms, in order of increasing size, were: (i) ripples, with lengths generally less than 0.15 m and heights less than 0.05 m; (ii) megaripples, with lengths from 1 to 12 m and heights from 0.1 to 0.7 m; and (iii) sand

waves, with lengths from 10 to 30 m and heights from 0.4 to 1.5 m. The linear sand bars are themselves a major bed feature.

The bedforms produced by tidal currents are similar in many respects to the bedforms found in sandy river channels. Thus, despite the relative unsteadiness of the tidal currents, it seems that they can be treated as though they were steady, at least as far as the fields of stability of the different bedforms is concerned.

Based on their external morphology and scale, seven different intertidal bedform facies were differentiated on the sand bars (Fig. 5.2): (i) plane bed (Facies A); (ii) ripples (Facies B); (iii) linear crested megaripples (Facies C); (iv) sinuous crested megaripples (Facies D); (v) disorganized megaripples (Facies E); (vi) catenary crested megaripples (Facies F); and (vii) ebb-modified, flood-oriented megaripples and sand waves (Facies G; also includes ebb oriented sand waves). Facies A (plane bed) bed features occurred along the steeply sloping, ebb dominated, sides of the bars and frequently passed up into Facies B (ripples) bedforms near the crest of the bars. Facies B bedforms also occurred as superposed bed features on megaripples and sand waves. On the gently sloping, flood dominated sides of the bars, Facies C (linear megaripples) bedforms occurred on the middle to upper part and Facies D (sinuous megaripples) bedforms on the middle to lower part of the bars. Facies E, F and G bedforms typically occurred in localized areas near the ends of the bars and (or) associated with a particular topographic feature on the surface of the bar (e.g., a swatchway, a secondary crestline on the bar that caused the development of a counter-current flow around the bar, or an area that was strongly dominated by the ebb or flood).

The intertidal bedforms on the bars at low tide following an ebb tide were either ebb-oriented or ebb-modified, flood-oriented features with some modification due to low tide emergence. The bedform crests were generally aligned at a small oblique angle to the bar crests. Megaripple crests were oriented at a steeper angle to the mean flow direction (10 to 30 degrees) than the crests of the sand waves (5 to 20 degrees).

The scale and morphology of the bedforms (from measurements made on almost 600 bedforms) varied over the bars with respect to differences in sediment size and flow properties (i.e., strength, asymmetry and duration). Megaripples were larger and more three-dimensional in areas where the flow

strength was stronger and the flow duration longer. For example, the linear crested megaripples (Facies C) occurred nearer the bar crests where current strengths were relatively less and flow durations shorter than the sinuous crested megaripples that occurred down the side of the bars when current strengths were relatively stronger (maximum speeds about 0 15 m/s stronger) and flow durations longer (about 0.5 h longer). Comparison of Figures 4.11, 4.13 and 4.16 with Figures 5.4, 5.8, 5.10 and 5.20 shows the interrelation between current strength and bedform development. Sand waves typically occurred in poorer sorted sediments with a mean grain size of about 0.42 mm than megaripples that occurred in better sorted sands with a mean grain size of about 0.26 mm (Fig. 5.42).

The net rates of bedform movement differed with the bedform type and the current strength. Megaripples moved faster (0.2 to 0.8 m per tidal cycle) than sand waves (about 0.1 to 0.3 m per tidal cycle). Both the net rates of migration and the scale of the bedforms (and morphology to some extent) changed during the lunar tidal month (Figs. 5.31, 5.32 and 5.33) from neap to spring tides as current strength varied. Field observations were too infrequent to establish the exact form of the lag effects between the adjustment of the bedforms to the changing flow conditions. Substantial relaxation effects were, however, apparent from the presence of large bedforms on the intertidal bedforms on the bars at low tide (i.e., without lag effect, the emergent features should only have been ripples on 'lower flow regime' plane bed.

Echo soundings made during the semidiurnal tidal cycles over bedforms and epoxy peels (and trenches through) from bedforms exposed at low tide indicated that many of the bedforms that were ebb-oriented at low water reversed their asymmetry and became flood-oriented during the flood (Figs. 5.27, 5.28 and 5.29). The extent of reorientation and reworking (and their net migration rates) of megaripples was determined by the relative strength of the ebb and flood (i.e., the degree of ebb or flood dominance). Sand waves occurred only in strongly flood or ebb dominated areas on the bars and did not reverse their asymmetry with each ebb and flood, but their superposed megaripples were reoriented and reworked with each tide.

The sequence of bedforms with increasing flow strength was similar to that described from flume observations, rivers, and other tidal environments:

plane bed → ripples → sand waves → linear megaripples → sinuous megaripples → planed-off megaripples → upper flow regime plane bed

The bed phase stability fields for megaripples and sand waves with respect to depth, velocity and grain size (Fig. 5.41) were comparable to those proposed by Costello (1974) from flume experiments. The tidal bedforms were, however, not as three-dimensional as the river and flume bed features because the durations of flow were relatively shorter. Tide produced megaripples were analogous to the dunes found in rivers, and were the most common bedform on the bars. The tidal sand waves may be comparable to Costello's (1974) bars, but further work is required on such features.

The friction factor (i.e., Darcy-Weisbach friction factor), derived from the flow properties, varied with bedform scale (Fig. 5.47) and during the semidiurnal tidal cycle (Fig. 5.46). The magnitude of the flow friction factor at the time of the maximum ebb velocity varied from 0.032 for smaller megaripples to 0.050 for larger megaripples. Both bedform length and height were related to the value of the friction factor (Fig. 5.47). As current speeds increased during the ebb, the friction factor first showed a rapid increase to a maximum value ($f \sim 0.10$ to 0.18) during the period of bedform reversal, then steadily decreased ($f \sim 0.04$) as the bedforms reached a quasi-equilibrium state with the flow (Fig. 5.46), and increased ($f \sim 0.10$ to 0.20) during the late ebb when flow depths were relatively shallow and suspended sediment concentrations large. During the flood, the value of the friction factor increased rapidly ($f \sim 0.10$) at first as the bedforms were reversed, and the flow was relatively shallow and had relatively high concentrations of suspended sediment; then decreased towards high water as the bedforms became flatter and the flow depths larger.

The internal sedimentary structures of the intertidal bedforms was determined from sketches and photographs of more than 20 trenches through bedforms, and from more than 60 epoxy peels from trench faces at several locations on the sand bars. Most of the preserved sedimentary structures were produced by the migration of ripples and small to medium

scale megaripples. Most of the preserved cross-bedding sets were flood oriented because the gently sloping sides of the bars were dominated by the flood. Some ebb sets were preserved on the steep sides of the bars. "Herringbone cross-stratification" was uncommon due to the effective segregation of the ebb and flood dominated areas on the bars. Thus, an ancient tidal deposit from the geologic record need not have bimodal cross-stratification (i.e., "herringbone cross-stratification") to be tidal in origin.

The thickness of the preserved cross-bedding sets in megaripples were about the same height as the bedforms. The longitudinal extent of the cross-bedding in the current direction was variable, depending upon the degree of ebb or flood dominance at a particular location (compare Figs. 5.50 and 5.51). Laterally and in plan, megaripple cross-stratification was planar to trough-shaped depending on the three-dimensionality of the bedform (e.g., linear versus sinuous crested megaripples).

The sand waves migrated primarily by the movement of a superposed layer of megaripples and ripples. The internal structures of the sand waves consisted of composite sets of megaripple cross-bedding (Fig. 5.2) oriented in the direction of the dominant current. Cross-bedding deposited by the subordinate tidal current was rarely preserved. Some of the variation of set thickness and length was possibly related to variations of sediment transport rates and erosion potential during the lunar tidal month.

In the winter, the frozen crust and the grounding of drift ice (Fig. 5.54) on the sand bars effectively stopped the development of large bedforms, and either reduced the size or obliterated the large bedforms developed during the summer. Because the internal drainage of the bars was decreased during the winter, lateral surface runoff and concentration of late-stage runoff in low areas on the bar surfaces (e.g., swatchways and remnant bedform troughs) was increased (compared with summer conditions), producing relatively deep lateral runoff channels from the bars. Localized removal of the frozen crust from the bars during the winter exposed the underlying unfrozen sediments to deep tidal scouring (Figs. 5.57 and 5.58) which were progressively infilled with ebb-oriented trough to planar cross-stratification.

7.5 SEDIMENT TRANSPORT AND CURRENT PATTERNS

The result of the pattern of tidal current asymmetry was that residual current and sediment transport occurred around the individual bars, parts of or groups of bars within closed or nearly closed "elliptical loops". Each bar or part of a bar behaved as a hydraulic sand trap between opposing directions of residual current flow. The gently sloping sides of the bars were dominated by the flood, and the steeply sloping sides of the ebb.

Rates of sediment transport were estimated with an empirical total-load equation (Ackers and White, 1973). The results (Figs. 6.1, 6.2 and 6.3, and Table 6-1) indicated that rates of movement varied considerably over the bars and in the channels and that the areal pattern of transport was comparable to that of the tidal currents (Figs. 4.11, 4.13, 4.16 and 4.20). Typical transport rates on the gently sloping, flood dominated sides of the bar were commonly less than 5.0×10^2 kg/m per ebb and 3.5×10^3 to 7.5×10^3 kg/m per flood. Along the steep, ebb dominated sides of the bars, transport rates ranged from 4.0×10^3 to 1.5×10^4 kg/m per ebb and were less than 3.0×10^2 kg/m per flood. Ebb and flood vector means were oriented at an oblique angle to the bar crests. The calculated net transport rates and vectors indicated that large amounts of sediment were moved across the bar towards the head of the bay during the flood, and out of the bay along the ebb dominated channels and steep sides of the bars during the ebb. The relative transport rates on either side of the bar crests were high compared to the maximum rates of lateral movement of the bars established from historical air photos and charts confirming that sand must be circulated around the bars or parts of the bars. Major changes in the position or outline of the bars occurred about every 3 to 5 years by lateral migration or avulsion of interbar channel flows into swatchways across the bars.

Coriolis effects were unimportant with respect to the general circulation patterns in the bay or on the bars. Circulation was generally clockwise on bars in the northern half of the complex, and anti-clockwise on bars in the southern half. The asymmetry of the currents and sediment transport vectors, and bedform properties (e.g., orientation, net migration rates and internal structures) showed that the general circulation

in the sand-body complex was similar to the "ebb tidal delta" (Figs. 6.5 and 6.7) of a tidal inlet with a mesotidal range. The main ebb channels were located in the centre of the bay and the complex was flanked by flood channels to the north and south. The overall morphology of the complex resulted primarily from the interaction and asymmetry of the ebb and flood currents. Maximum ebb currents occurred during the late, low-water channelized phase of the ebb. As the tide turned at low water, the strong ebb currents continued to flow seaward out of the main ebb channels. With the advance of the flood wave, water levels rose and the flood currents were deflected into the channels along the north and south margins of the complex, following the paths of least resistance. During the high-water sheet-flow phases of the ebb and flood, components of flow developed across the bars (dominantly flood) because the bars were oriented at a small angle of attack to the mean ebb and flood flow directions and because the different hydraulic geometries and hypsometries of the inter-bar channels produced different water levels on the two sides of the bars as the tide drained or flooded. The surface level of the bars was controlled by the base level of strong wave activity. Wave action was strongest at the mouth of the bay and decreased to the east, thus the surface level of the bars increased from west to east.

The sediment and geometry of the modern sand-body complex originated from the erosion and reworking of Pleistocene sediments and Triassic bedrock in and around the bay during the last 3000 years as sea level rose and the Bay of Fundy reached resonant dimensions. If the modern sedimentary facies in the bay were preserved in the geologic record, as a result of either a marine transgression or regression, a fining-upward vertical section of cross-stratified bar sands would results (Fig. 6.9), capped by subtidal muds or intertidal muds and saltmarsh deposits respectively.

The morphology, distribution of sediments and bedforms, current strengths and general circulation patterns of the sand-body complex in Cobequid resembled the model proposed for "ebb-tidal deltas" of tidal inlets through barrier islands with mesotidal ranges (Fig. 6.6). The sand-body complex differed mainly with respect to tidal range, and the scale, relief and topographic complexity of the sand bars; the latter indicating the importance of tidal range in controlling the geometry of a tide-maintained sedimentary deposit. Nevertheless, the general properties of

of the sediments, bedforms and current hydraulics are similar to those of other tidal environments, despite differences of tidal range and the scale, relief and topographic complexity of the elongate sand bars in the macrotidal sand-body complex of Cobequid Bay.

REFERENCES

Ackers, P. and White, W.R. (1973) Sediment transport: new approach and analysis. Proc. Am. Soc. Civ. Eng., 99(HY 11):2041-2060.

Admiralty Tide Tables (1976) Volume I. European waters including Mediterranean Sea. Hydrographer of the Navy, 1975.

Alam, A.M.Z. and Kennedy, J.F. (1969) Friction factors for flow in Sand-Bed channels. Proc. Am. Soc. Civ. Eng., 95(HY 6):1973-1992.

Allen, G.P., Castaing, P. and Klingebiel, A. (1972) Distinction of elementary sand populations in the Gironde estuary (France) by R-mode factor analysis of grain size data. Sedimentology, 19:21-35.

_____, Derresequier, A. and Klingebiel, A. (1969) Evolution des structures sedimentaires sur un banc sableux d'estaire en fonction de l'amplitude des marées. Acad. Sci., C.R., Sér. D, 269:2167-2169.

Allen, J.R.L. (1963) The classification of cross-stratified units with notes on their origin. Sedimentology, 2:93-114.

_____ (1968a) On the character and classification of bed forms. Geol. Mijnbouw, 47(3):173-185.

_____ (1968b) Current ripples. Amsterdam: North-Holland Publishing Co., p. 433.

_____ (1968c) The nature and origin of bed form hierarchies. Sedimentology, 10:161-182.

Allen, J.R.L. (1969) On the geometry of current ripples in relation to stability of fluid flow. Geogr. Ann., Ser. A., 51:61-96.

_____ (1970a) Physical processes of sedimentation. Allen & Unwin, London, 248 p.

_____ (1970b) Studies in fluviatile sedimentation: a comparison of fining upward cyclothems, with special reference to coarse-member composition and interpretation. J. Sed. Pet., 40:298-323.

_____ (1973) Features of cross-stratified units due to random and other changes in bedforms. Sedimentology, 20:189-202.

_____ (1974) Reaction, relaxation and lag in natural sedimentary systems: General principles, examples and lessons. Earth-Sci. Rev. 10:263-342.

_____ (1976a) Computational models for dune time-lag: General ideas, difficulties and early results. Sed. Geol., 15:1-53.

_____ (1976b) Time-lag in dunes in unsteady flows: an analysis of Nasner's data from the River Weser, Germany. Sed. Geol., 15: 309-321.

_____ and Collinson, J.D. (1974) The superimposition and classification of dunes formed by unidirectional aqueous flows. Sed. Geol., 12: 169-178.

_____ and Friend, P.F. (1976) Changes in intertidal dunes during two spring-reap cycles, Lifeboat Station Bank, Wells-next the Sea, Norfolk (England). Sedimentology, 23(3):329-346.

Annambhotla, V.S.S., Sayre, W.W. and Livesey, R.H. (1972) Statistical properties of Missouri River bedforms. Proc. Am. Soc. Civ. Eng., 98(WW4):489-510.

Anonymous (1966) Bay of Fundy, data report on tidal and current survey, 1965. Bedford Inst. Oceanogr. Data, Series 66-2-D, 53 p.

Arkin, H. and Colton, R.R. (1963) Tables for statisticians. New York: Barnes & Noble, Inc., 168 p.

A.S.C.E. Task Committee (1963a) Friction factors in open channels. Proc. Am. Soc. Civ. Eng., 89(HY 2):97-143.

_____ (1963b) Sediment transportation mechanics: suspension of sediment. Proc. Am. Soc. Civ. Eng., 89(HY 5):45-76.

A.S.C.E. Task Force (1966) Task force on bed forms in alluvial channels, 1966. Nomenclature for bed forms in alluvial channels. Proc. Am. Soc. Civ. Eng., 92(HY 3):51-64.

_____ (1971a) Sediment transportation mechanics: H. Sediment discharge formulas. Proc. Am. Soc. Civ. Eng., 97(HY 4):523-567.

_____ (1971b) Sediment transportation mechanics: F. Hydraulic relations for alluvial streams. Proc. Am. Soc. Civ. Eng., 97(HY 1): 101-141.

Ashida, K. and Tanaka, Y. (1967) A statistical study of sand waves. Proc. 12th Congr. Int. Assoc. Hydraul. Res., 2:103-110.

ATPEMC (1969) Report to Atlantic Tidal Power Programming Board on the feasibility of tidal power development in the Bay of Fundy. Atlantic

Tidal Power Engineering and Management Committee, Halifax, Nova Scotia, 189 p, plus 11 appendices.

Bagnold, R.A. (1956) The flow of cohesionless grains in fluids. Roy. Soc. London, Phil. Trans., Ser. A, 249:235-297.

_____ (1966) An approach to the sediment transport problem from general physics. U.S. Geol. Surv., Prof. Paper 422-I, 37 p.

Bailey, W.B., MacGregor, D.G. and Hackey, H.B. (1953) Annual variations of temperature and salinity in the Bay of Fundy. J. Fish. Res. Bd. Can., 11:33-44.

Bajard, J. (1966) Figures et structures sedimentaires dans la zone intertidale de la partie orientale de la Baie du Mont-Saint Michel. Rev. Géogr. Phys. Géol. Dyn., 8(1):39-111.

Balaz, R.J. and Klein, G. de Vries (1972) Roundness-mineralogical relations of some intertidal sands. J. Sed. Pet., 42(2):425-433.

Barr, J.L., Dinkelman, M.G. and Sandusky, C.L. (1970) Large epoxy peels. J. Sed. Pet., 40(1):445-449.

Bauer, H.A. (1933) A world map of tides. Geogr. Rev., 23:259-270.

Bayazit, M. (1969) Resistance to reversing flows over movable beds. Proc. Am. Soc. Civ. Eng., 95(HY 4):1109-1127.

Bazin, H. (1865) Recherches hydrauliques. Mém. divers savants, Sci. Math. et Phys., V.19, Paris.

Belderson, R.H. and Kenyon, N.H. (1969) Direct illustration of one way sand transport by tidal currents. J. Sed. Pet., 39:1249-1250.

Bell, W.A. (1929) Horton-Windsor District, Nova Scotia. Geol. Surv. Can. Mem. 155, 268 p.

_____ (1960) Mississipian Horton Group of type Windsor-Horton District, Nova Scotia. Geol. Surv. Can. Mem. 314, 112 p.

Belt, E.S. (1964) Revision of Nova Scotia middle carboniferous units. Amer. J. Sci., 262:653-673.

_____ (1965) Stratigraphy and palaeogeography of Mabou Group and related middle Carboniferous facies, Nova Scotia, Canada. Geol. Soc. Amer., Bull. 76:777-802.

Berner, R.A. (1970) Sedimentary pyrite formation. Amer. J. Sci., 268: 1-23.

_____ (1971) Principles of chemical sedimentology. McGraw Hill Book Co., Toronto, 240 p.

Biswas, A.N. and Chakrabarti, A.K. (1974) Sediment transport in a tidal river. Proc. Am. Soc. Civ. Eng., 100(HY 11):1677-1683.

Blatt, H., Middleton, G.V. and Murray, R. (1972) Origin of sedimentary rocks. Prentice-Hall Inc., Englewood Cliffs, N.J., 634 p.

Bleakney, J. Sherman (1972) Ecological implications of annual variation in tidal extremes. Ecology, 53(5):933-938.

Blench, T. (1969) Mobile-bed fluviology. Univ. Alberta Press, Edmonton, Canada, 168 p.

Blinco, P.H. and Partheniades, E. (1971) Turbulence characteristics in free surface flows over smooth and rough boundaries. J. Hydraul. Res., 9(1):43-69.

Boersma, J.R. (1967) Remarkable types of mega cross-stratification in fluviatile sequence of a subrecent distributary of the Rhine Amerogen; The Netherlands. Geol. Mijnbouw, 46(6):217-235.

_____ (1969) Internal structure of some tidal mega-ripples on a shoal in the Westerschelde estuary, the Netherlands. Report of Preliminary Investigation. Geol. Mijnbouw, 48(4):409-414.

_____, Van de Meene, E.A. and Tjalsma, R.C. (1968) Intricated cross-stratification due to interaction of a mega-ripple with its leeside system of backflow ripples. Sedimentology, 11:147-162.

Boothroyd, J.C. (1969) Hydraulic conditions controlling the formation of estuarine bedforms in Hayes, M.O. (ed.) Coastal environments of northeastern Massachusetts and New Hampshire. Soc. Econ. Paleontol. Mineral. (Eastern Section) Guidebook, 462 p.

_____ and Hubbard, D.K. (1975) Genesis of bedforms in Mesotidal Estuaries in [illegible]nin, L.E. (ed.), Estuarine Research, Vol. II, Academic Pres[illegible]nc., New York, 587 p.

Borns, Harold W. and Swift, D.J.P. (1966) Surficial geology, northshore of Minas Basin, Nova Scotia. Reprinted from Guidebook, Geology and Parts of the Atlantic Prov., Geol. Assoc. Can. and Mineralogical Assoc. Can., pp. 81-85.

Bosence, D.J.W. (1973) Facies relationships in a tidally influenced environment: a study from the Eocene of the London Basin. Geol. Mijnbouw, 52(2):63-67.

Bostock, H.S. (1970) Physiographic subdivision of Canada in Douglas, R.J.W. (ed.) Geology and Economic Minerals of Canada, Dept. of Energy, Mines and Resources, Canada, 838 p.

Bousfield, E.L. and Leim, A.H. (1959) The fauna of the Minas Basin and Minas Channel. Can. Nat. Mus. Bull., No. 166:1-30.

Bowden, D.F. and Fairbairn, L.A. (1952) A determination of the frictional forces in a tidal current. Proc. Roy. Soc. London, Ser. A, 214:371-392.

_____ and _____ (1956) Measurements of turbulent fluctuations and Reynolds stresses in a tidal current. Proc. Roy. Soc. London, Ser. A, 237:422-438.

_____, _____ and Hughes, P. (1959) Distribution of shearing stresses in a tidal current. Geophys. J.R. Astron. Soc., 2:288-305.

_____ and Howe, M.R. (1963) Observations of turbulence in a tidal current. J. Fluid Mech., 17:271-284.

Briggs, L.I. and Middleton, G.V. (1965) Hydromechanical principles of sediment structure formation in Middleton, G.V. (ed.) Primary sedimentary structures and their hydrodynamic interpretation. Soc. Econ. Paleontologists & Mineralogists, Spec. Publ. 12, 265 p.

Brisbin, D. (1974) A comparison of Pleistocene source material sands and intertidal sands, Minas Basin, Bay of Fundy. Tech. Memo. 74-5 (unpublished), Department of Geology, McMaster University, 36 p.

Brooks, N.H. (1958) Mechanics of streams with movable beds of fine sand (with discussions). Trans. Am. Soc. Civ. Eng., 123: 526-594.

Brush, L.M., Jr. (1965) Experimental work on primary sedimentary structures in Middleton, G.V. (ed.) Primary sedimentary structures and their hydrodynamic interpretation. Soc. Econ. Paleontologists & Mineralogists, Spec. Publ. 12, 265 p.

Bucher, W.H. (1919) On ripples and related sedimentary surface forms and their paleographic interpretations. Amer. J. Sci., 47(4):149-210, 241-269.

Bumpus, D.F. (1959) Sources of water in the Bay of Fundy contributed by surface circulation. Washington & Ottawa, Intern. Passamaquoddy Fish. Board, App. I, C.6, 11 p.

_____ and Lauzier, L.M. (1965) Surface circulation of the continental shelf off eastern North America between Newfoundland and Florida. Serial Atlas of the Marine Environment: New York, Am. Geogr. Soc., Folio 7.

Cameron, H.L. (1961) Interpretation of high attitude, small-scale photography. Can. Surveyor, 15:567-573.

Canadian Hydrographic Service (1971, 1972, 1973) Canadian Tide and Current Tables, Ottawa.

Cannon, G.A. (1971) Statistical characteristics of velocity fluctuations at intermediate scales in a coastal plain estuary. Amer. Geophys. Union, Trans., 76:5852-5858.

Cant, D.J. (1975) Sandy braided stream deposits in the South Saskatchewan River. Geol. Soc. Am., Abstr., 7(6):731.

Carver, R.E. (ed.) (1971) Procedures in sedimentary petrology. Wiley-Interscience, John Wiley & Sons, Inc., New York, 653 p.

Caston, V.N.D. (1972) Linear sand banks in the Southern North Sea. Sedimentology, 18:63-78.

_____ and Stride, A.H. (1970) Tidal sand movement between some linear sand banks in the North Sea off Northeast Norfolk. Mar. Geol., 9:M38-M42.

Chang, F.F.M. (1970) Ripple concentration and friction factor. Proc. Am. Soc. Civ. Eng., 96(HY 2):417-430.

Charlier, R.H. (1969a) Harnessing the energies of the oceans; a review and bibliography, part I. Mar. Technol. Soc. J., 3(3):13-32.

_____ (1969b) Harnessing the energies of the oceans; part II. Mar. Technol. Soc. J., 3(4):59-81.

Charnock, H. (1959) Tidal friction from currents near the seabed. J. Geophys. Res., 2:215-221.

Chow, V.T. (1959) "Open-channel hydraulics". McGraw-Hill, New York, 680 p.

Church, M. and Gilbert, R. (1975) Proglacial fluvial and lacustrine environments in Jopling, A.V. and McDonald, B.C. (eds.), Glaciofluvial and glaciolacustrine sedimentation. Soc. Econ. Paleontol. Mineral. Spec. Publ. No. 23, 320 p.

Churchill, F.J. (1924) Recent changes in the coastline in the county of Kings. Proc. Trans. Nova Scotia Inst. Sci., 16:84-86.

Clancy, E.P. (1969) The Tides - Pulse of the Earth. Anchor Books, Doubleday & Comp. Inc., Garden City, N.Y., 228 p.

Clarke, R.H. (1972) Energy from Fundy tides. Can. Geogr. J., LXXXV(5): 150-163.

Clauser, F.H. (1956) The turbulent boundary layer. Advances in Fluid Mech., 4:1-51.

Clifton, H.E. (1969) Beach lamination: nature and origin. Mar. Geol., 7:553-559.

Coastal Research Group (1969) Coastal Environments - Northeastern Massachusetts and New Hampshire. Soc. Econ. Paleontol. Mineral. Field Trip, May 9-11, 1969. Coastal Research Group Contrib. No. 1-CRG, Univ. Mass., Amherst, 462 p.

Colby, B.R. (1964) Discharge of sands and mean velocity relationships in sand-bed streams. U.S. Geol. Surv., Prof. Paper 462-A, 47 p.

_____ and Hembree, C.H. (1955) Computations of total sediment discharge, Niobrara River near Cody, Nebraska. U.S. Geol. Surv., Water-Supply Pap. 1357, 187 p.

Collinson, J.D. (1970) Bedforms of the Tana River, Norway. Geogr. Ann., Ser. A., 52(1):31-55.

Cornish, V. (1901a) The formation of wave surfaces in sand. Scot. Geogr. J., 17:1-11.

_____ (1901b) On sand waves in tidal currents. Geogr. J., 18:170-200.

_____ (1914) Waves of sand and snow and the eddies which make them. London: F. Fisher Unwin, 383 p.

Costello, W.R. (1974) Development of bed configurations in coarse sands. Unpublished Ph.D. Thesis, Mass. Inst. Techn., Cambridge, Mass. (Report 74-1), 119 p.

Craig, H.D. (1973) Biofacies and biogenic structures of Cobequid Bay. Tech. Memo. 74-1, Dept. Geol., McMaster University, 29 p.

Crickmore, M.J. (1970) Effect of flume width on bedform characteristics. Proc. Am. Soc. Civ. Eng., 96(HY 2):473-496.

Cronin, L.E. (ed.) (1975) Estuarine research. Vol. II, Academic Press, Inc., New York, 587 p.

Crosby, D.G. (1962) Wolfville Map Area, Nova Scotia. Geol. Surv. Can. Mem. 325, 62 p.

Culbertson, J.K. and Dawdy, D.R. (1964) A study of fluvial characteristics and hydraulic variables, Middle Rio Grande, New Mexico. U.S. Geol. Surv., Water-Supply Pap., 1498-F, 74 p.

_____, Scott, C.H. and Bennett, J.P. (1972) Summary of alluvial-channel data from Rio Grande Conveyance channel, New Mexico, 1965-69. U.S. Geol. Surv., Prof. Paper, 562-J, 49 p.

Daboll, J.M. (1969) Holocene sediments of the Parker River Estuary, Massachusetts. Coastal Research Group Contrib. No. 3-CRG, Dept. Geol., University of Massachusetts, Amherst, 138 p.

Dalrymple, R.W. (1973a) Preliminary study of an intertidal sand body, Cobequid Bay, Bay of Fundy, Nova Scotia. Maritime Sediments, 9(1): 21-28.

_____ (1973b) Sediment texture and transport studies in an intertidal environment: a progress report. Maritime Sediments, 9(2):45-58.

_____ (1974a) Factor analyses of grain-size data from Cobequid Bay, Bay of Fundy, Nova Scotia. Geol. Soc. Amer., Abstr., 5(1):17.

_____ (1974b) Field studies on intertidal sand bars (1973), north shore of Minas Basin, Bay of Fundy, Nova Scotia. Unpub. Tech. Memo. 73-5, Department of Geology, McMaster University, 21 p.

_____ (1975) Sediment transport in Cobequid Bay with special reference to sediment tracer experiments. Proc. Mathematical Aspects of Fundy Tidal Power, Canadian Mathematic Congress, Summer Research Institute, Halifax, Nova Scotia, pp. 3-4.

Dalrymple, R.W. (1976) Sediment transport in a macro-tidal environment (Bay of Fundy). Amer. Geophys. Union, Trans., 57(4):268.

_____, Knight, R.J. and Middleton, G.V. (1975) Intertidal Sand Bars in Cobequid Bay (Bay of Fundy) in Cronin, L.E. (ed.) Estuarine Research, Vol. II, Academic Press Inc., New York, 587 p.

Davies, J.L. (1964) A morphogenic approach to world shorelines. Z. Geomorphol., 8:127-142.

Davis, J.C. (1973) Statistics and data analysis in geology. John Wiley & Sons, Inc., New York, 550 p.

Davis, R.A. (1973) Coastal ice formation and its effects on beach sedimentation. Shore and Beach, 41(1):3-9.

Dawson, W. Bell (1917) Tides at the Head of the Bay of Fundy. Department of Naval Service, Ottawa, 34 p.

Defant, A. (1958) Ebb and flow. The tides of earth, air and water. Ann Arbor, Univ. Michigan Press, 121 p.

_____ (1961) Physical oceanography, Vol. II, Pergamon Press, N.Y. 570 p.

Dickson, M. (1974) The sieve method of size analysis: an instruction manual. McMaster Univ., Dept. Geology, Tech. Memo. 74-3, 17 p.

Dionne, J.C. (1969) Tidal flat erosion by ice at La Pocatière, St. Lawrence Estuary. J. Sed. Pet., 39(3):1174-1181.

Dionne, J.C. (1970) Aspects morpho-sédimentologiques du glaciel, en particulier des côtes du Saint-Laurent, Qué. Lab. Rech. For. Rapp. Infor. Q-F-X-9, 324 p.

_____ (1971) Érosion glacielle de la silkke, Estuaire du Saint-Laurent. Rev. Géomorph. Dyn., 20(1):5-21.

_____ (1973a) La motion de pied de glace (icefoot), en particulier dans l'estuaire du Saint-Laurent. Cah. Géogr. Qué., 17(41):221-250.

_____ (1973b) Monroes: a type of so-called mud volcanoes in tidal flats. J. Sed. Pet., 43(3):848-856.

_____ (1974) Polished and striated mud surfaces in the St. Lawrence tidal flats, Quebec. Can. J. Earth Sci., 11(6):860-866.

Dohler, G. (1966) Tides in Canadian Waters. Canadian Hydrographic Service, Ottawa, 19 p.

_____ (1970) Hydrographic Tidal Manual. Dept. Energy Mines & Resources, Ottawa, 143 p.

Duff, G.F.D. (1970) Tidal resonance and tidal barriers in the Bay of Fundy System. J. Fish. Res. Bd., Can. 27:1701-1728.

Dyer, K.R. (1970) Current velocity profiles in a tidal channel. Geophys. J.R. Astron. Soc., 22:153-161.

Einstein, H.A. (1950) The bed-load function of sediment transportation in open channel flows. U.S. Dept. Agric. Tech. Bull. No. 1026, 102 p.

Einstein, H.A. and Barbarossa, N.L. (1952) River channel roughness. Trans. Am. Soc. Civ. Eng., 117:1121-1126.

_____ and Chien, N. (1955) Effects of heavy sediment concentration near the bed on velocity and sediment distribution. Univ. Calif. Inst. Eng. Res., No. 8, 99 p.

Engelund, F. (1966) Hydraulic resistance of alluvial streams. Proc. Am. Soc. Civ. Eng., 92(HY 2):315-326.

Evans, G. (1965) Intertidal flat sediments and their environments of deposition in the Wash. Geol. Soc. London, Quart. J., 121: 209-245.

Environment Canada (1970) Temperature and precipitation 1941-1970, Atlantic Provinces. Environment Canada and Atmospheric Environment, Downsview, Ontario, 55 p.

_____ (1975) Canadian Normal: - Wind. Environment Canada, and Atmospheric Environment, Downsview, Ontario, 3, 144 p.

Farrell, S.C. (1970) Sediment distribution and hydrodynamics: Saco River and Scarboro estuaries. Coastal Research Group Contrib. No. 6-CRG, Dept. Geol., Univ. Massachusetts, Amherst, 129 p.

Forrester, W.D. (1958) Current measurements in Passamaquoddy Bay and the Bay of Fundy, 1957-1958. Can. Hydrog. Surv. Tidal Publ. No. 40, 73 p.

Garde, R.J. and Raju, K.R. (1966) Resistance relationships in alluvial channel flow. Proc. Am. Soc. Civ. Eng., 94(HY 4):77-100.

Garrett, C. (1972) Tidal resonance in the Bay of Fundy and Gulf of Maine. Nature, 238:441-443.

_____ (1974a) Normal modes of the Bay of Fundy and Gulf of Maine. Can. J. Earth Sci., 11(4):549-556.

_____ (1974b) Ocean tides. Geosci. Can., 1(4):8-14.

Gellatly, D.C. (1970) Cross-bedded tidal megaripples from King Sound (northwest Australia). Sediment. Geol., 4:185-191.

Gierloff-Emden, H.G. (1961) Nehrungen und Lagunen. Pet. Geogr. Mitt., 105:81-82, 161-176.

Gilbert, G.K. (1914) The transportation of debris by running water. U.S. Geol. Surv., Prof. Paper 86, 263 p.

Ginsburg, R.N. (ed.) (1975) Tidal deposits: A casebook of recent examples and fossil counterparts. Springer-Verlag, New York, 428 p.

Glass, D.J. (ed.) (1972) Quaternary geology, geomorphology and hydrogeology of the Atlantic provinces. XXIV Int. Geol. Congr. Excursion, A61-C61, Montreal, Quebec, 76 p.

Godin, G. (1968) The 1965 current survey of the Bay of Fundy - a new analysis of the data and an interpretation of the results. Marine Sciences Branch MS Dept. Ser. No. 8, 97 p. Dept. Energy, Mines & Resources, Ottawa.

Goldthwait, J.W. (1924) Physiography of Nova Scotia. Geol. Surv. Can., Mem. 140, 179 p.

Gordon, C.M. (1975) Sediment entrainment and suspension in a turbulent tidal flow. Mar. Geol., 18:M57-M64.

_____ and Dohne, C.F. (1973) Some observations of turbulent flow in a tidal estuary. J. Geophys. Res., 78(12):1971-1978.

Graf, W.H. (1971) Hydraulics of sediment transport. McGraw-Hill Book Co. Montreal, 513 p.

Grant, D.R. (1970) Recent coastal submergence of the Maritime Provinces, Canada. Can. J. Earth Sci., 7(2):676-689.

Grant, H.L., Stewart, R.W. and Moilliet, A. (1962) Turbulence spectra from a tidal channel. J. Fluid. Mech., 12:241-263.

Grass, Anthony J. (1970) Initial instability of fine bed sand. Proc. Am. Soc. Civ. Eng., 96(HY 3):619-632.

Gray, D.M. (ed.) (1970) Handbook on the Principles of Hydrology. Nat. Res. Council Canada and Water Information Centre, Inc., Port Washington, N.Y.

Gray, T.J. and Gashus, O.K. (eds.) (1972) Tidal power. Plenum Publ. Corp., New York 630 p.

Green, C.D. (1975) A study of hydraulics and bedforms at the Mouth of the Tay Estuary, Scotland, in Cronin, L.E. (ed.), Estuarine Research, Vol. II. Academic Press, Inc., New York, 587 p.

Greenwood, B. and Davidson-Arnott, R.G.D. (1972) Textural variation in the sub-environments of the shallow-water wave zone, Kouchibouguac Bay, New Brunswick. Can. J. Earth Sci., 9:679-688.

Gross, M.G. (1972) Oceanography: a view of the earth. Prentice-Hall Inc., Englewood Cliffs, New Jersey, 581 p.

Guttman, I. and Wilks, S.S. (1965) Introductory engineering statistics. New York, John Wiley & Sons, Inc., 340 p.

Guy, H.P., Simons, D.B. and Richardson, E.V. (1966) Summary of alluvial channel data from flume experiments, 1956-1961. U.S. Geol. Surv. Prof. Paper 462-I, 185 p.

Hama, F.R. (1954) Boundary-layer characteristics for smooth and rough surfaces. Trans. Soc. Naval Architects and Mar. Eng., 62:333-358.

Häntzschel, W. (1939) Tidal flat deposits (Hattenschlich) in Trask, P.D. (ed.) Recent Marine Sediments, Dover Publications, Inc., New York.

Harms, J.C. (1969) Hydraulic significance of some sand ripples. Geol. Soc. Amer., Bull., 80:363-396.

_____, Southard, J.B., Spearing, D.R. and Walker, R.G. (1975) Depositional environments as interpreted from primary sedimentary structures and stratification sequences. Soc. Econ. Paleontol. Mineral., Short Course No. 2, Dallas, Texas, 161 p.

Harris, I. McK. (1975) Soc. Econ. Paleontol. Mineral. (Eastern Section) Field Trip: Introduction; Itinerary. Maritime Sediments, 11(1): 9-15.

_____ and Schenk, P.E. (1975) The Megume Group. Maritime Sediments, 11(1):25-46.

Hartwell, A.D. (1970) Hydrography and holocene sedimentation of the Merrimack River estuary, Massachusetts. Coastal Research Group Contrib. No. 5-CRG, Dept. Geol., Univ. Massachusetts. Amherst, 166 p.

Harvey, J.G. (1966) Large sand waves in the Irish Sea. Mar. Geol., 4: 49-55.

Hayes, M.O. (1975) Morphology of sand accumulation in Estuaries: An introduction to the Symposium in Cronin, L.E. (ed.), Estuarine Research, Vol. II, Academic Press Inc., New York, 587 p.

_____, Goldsmith, V. and Hobbs, C.H. (1970) Offset coastal inlets. Proc. 12th Coastal Eng. Conf., Sept. 1970, Washington, D.C. pp. 1187-1200.

_____, Owens, E.H., Hubbard, D.K. and Abele, R.W. (1973) Investigation of form and processes in the coastal zone in Coates, D.R. (ed.), Coastal Geomorphology, Proc. 3rd Ann. Geomorphology Symp., Ser., Binghamton, New York, Sept. 1972, 404 p.

Hayes, J. and Dobson, M. (1969) Physiography, foraminifera, and sedimentation in the Dovey Estuary (Wales). Geol. J., 6(2): 217-256.

Henderson, F.M. (1966) Open channel flow. MacMillan Co., Toronto, 406 p.

Hennigar, T.W. (1972) Hydrogeology of the Truro Area, Nova Scotia. Dept. Mines, Groundwater Section, Report 72-1, 127 p.

Herbich, J.B. and Shulits, S. (1964) Large-scale roughness in open channel flow. Proc. Am. Soc. Civ. Eng., 90(HY 6):203-230.

Hind, H.Y. (1975) The ice phenomena and the tides of the Bay of Fundy. Can. Monthly Nat. Rev., 8(3):189-203.

Houbolt, J.J.H.C. (1968) Recent sediments in the Southern Bight of the North Sea. Geol. Mijnbouw, 47(4):245-273.

Huntec (1966) Report on geological-geophysical study of Minas Basin, Bay of Fundy, N.S. Unpublished report to Atlantic Development Board of Canada, Huntec Ltd., Toronto, 58 p.

Huthnance, J.M. (1973) Tidal current asymmetries over the Norfolk Sandbanks. Estuarine Coastal Mar. Sci., 1:89-99.

Inman, D.L. (1949) Sorting of sediments in the light of fluid mechanics. J. Sed. Pet., 19(2):51-70.

_____ (1963) Sediments: physical properties and mechanics of sedimentation in F.P. Shepard (Ed.), Submarine Geology, 2nd ed.,

Ippen, A. T. and Harleman, D.R.F. (1966) Tidal dynamics in Estuaries in Ippen, A. T. (ed.), Estuary and Coastline Hydrodynamics, McGraw Hill, New York, 744 p.

Jackson, R.G. II (1975) Hierarchical attributes and a unifying model of bed forms composed of cohesionless material and produced by shearing flow. Geol. Soc. Amer., Bull., 86:1523-1533.

Jacob, A.F. (1973) Descriptive classification of cross-stratification. Geology, pp. 103-106.

Jain, S.C. and Kennedy, J.F. (1974) The spectral evolution of sedimentary bedforms. J. Fluid Mech., 63:301-314.

James, N.P. and Stanley, D.J. (1968) Sable Island Bank off Nova Scotia: sediment dispersal and recent history. Amer. Ass. Petrol. Geol. Bull., 52:2208-2230.

Johnson, D.W. (1925) The New England-Acadian Shoreline. John Wiley & Sons, New York, 608 p.

Johnson, M.A. and Belderson, R.H. (1969) Tidal origin of some vertical sedimentary changes in Epicontinental Seas. J. Geol., 77:353-357.

Jones, T.A. (1970) Comparison of the descriptors of sediment grain-size distributions. J. Sed. Pet., 40:1204-1215.

Jones, N.S., Kain, J.M. and Stride, A.H. (1965) The movement of sand waves on Warts Bank, Isle of Man. Mar. Geol., 3:329-336.

Jopling, A.V. (1965) Hydraulic factors controlling the shape of laminae in laboratory deltas. J. Sed. Pet., 35:777-791.

Jordan, G.F. (1962) Large submarine sand waves. Science, 136:839-848.

Jordan, P.R. (1965) Fluvial sediment of the Mississippi River at St. Louis, Missouri. U.S. Geol. Surv., Prof. Paper 1802, 89 p.

Kachel, N.B. and Sternburg, R.W. (1971) Transport of bedload as ripples during an ebb current. Mar. Geol., 10:229-244.

von Kármán, T. (1930) Mechanische aehnlichkiet und turbulenz. Nachr. Ges. Wiss. Göttingen, Math-Phys. Klasse, V.58.

Kaye, C.A. and Stuckey, G.W. (1973) Nodal tidal cycle of 18.6 yr. Geology, pp. 141-144.

Kennedy, J.F. (1969) The formation of sediment ripples, dunes and antidunes. Ann. Rev. Fluid Mech., 1:147-168.

Kenyon, N.H. (1970) Sand ribbons of European tidal seas. Mar. Geol. 9:25-39.

_____ and Stride, A.H. (1970) The tide swept continental shelf sediments between the Shetland Isles and France. Sedimentology, 14:159-173.

Keulegan, G.H. (1938) Laws of turbulent flow in open channels. U.S. Nat. Bur. Stand. J. Res., 21:707-741.

Khanna, S.P. (1970) Experimental investigations of the form of bed roughness. Proc. Am. Soc. Civ. Eng., 96(HY 10):2029-2040.

Kindle, E.M. (1917) Recent and fossil ripple marks. Geol. Surv. Can., Mus. Bull. 25, 121 p.

King, L.H. and MacLean, B. (1974) Geology of the Scotian Shelf and adjacent areas, Map 812H. Mar. Sci. Pap. Ser. No. 7, Geol. Surv. Can., Pap. 74-31, Ottawa.

Klein, G. de V. (1962) Triassic sedimentation, Maritime Provinces. Geol. Soc. Amer., Bull., 73:1127-1146.

_____ (1964) Sedimentary facies in the Bay of Fundy intertidal zone, Nova Scotia in van Straaten, L.M.J.U. (Ed.), Deltaic and shallow marine deposits, Developments in Sedimentology, Vol. I, Elsevier, Amsterdam, 464 p.

_____ (1967) Comparison of recent and ancient tidal flat and estuarine sediments in Lauff, G.H. (ed.) Estuaries. Am. Assoc. Adv. Sci. Publ. No. 83, Washington, D.C. 757 p.

_____ (1968a) Intertidal zone sedimentation, Minas Basin, northshore, Bay of Fundy, Nova Scotia in Margulies, A.E. and Steere, R.C. (eds.), National Symposium on Ocean Science and Engineering of the Atlantic Shelf, Mar. Tech. Soc. Trans, 366 p.

_____ (1968b) Report on Advanced Science Seminar on intertidal zone sedimentation, Minas Basin, Bay of Fundy, Nova Scotia, July 6 to August 7, 1968. Maritime Sediments, 4(2):52-56.

_____ (1970a) Depositional and dispersal dynamics of intertidal sand bars. J. Sed. Pet., 40(4):1095-1127.

Klein, G. de V. (1970b) Tidal origin of a Precambrian quartzite - the lower fine-grained quartzite (Dalradian) of Islay, Scotland. J. Sed. Pet., 40:973-985.

_____ (1971) A sedimentary model for determining paleotidal range. Geol. Soc. Amer. Bull., 82:2585-2592.

_____ (1972) Sedimentary model for determining paleotidal range: reply. Geol. Soc. Amer. Bull., 83:539-546.

_____ and Sanders, J.E. (1964) Comparison of sediments from Bay of Fundy and Dutch Wadden Sea tidal flats. J. Sed. Pet., 34(1):18-24.

_____ and Whaley, M.L. (1972) Hydraulic parameters controlling bedform migration on an intertidal sand body. Geol. Soc. Amer., Bull., 83:3465-3470.

Knight, R.J. (1971) Cobequid Bay sedimentology project. A progress report. Maritime Sediments, 7(1):1-18.

_____ (1972) Cobequid Bay sedimentology project. A progress report. Maritime Sediments, 8(2):45-60.

_____ (1973a) Intertidal sedimentation in Cobequid Bay, Nova Scotia. Fluvial Processes and Sedimentation Proceedings - Hydrology Symposium, Univ. Alberta, Edmonton, pp. 639-650.

_____ (1973b) Intertidal fluid-sediment relationships in Cobequid Bay of Minas Basin, Nova Scotia in Report of Activities, Geol. Surv. Can. Paper 74-1, Part A, 119 p.

Knight, R.J. and Dalrymple, R.W. (1975) Intertidal sediments from the south shore of Cobequid Bay, Bay of Fundy, Nova Scotia, Canada in Ginsburg, R.N. (ed.), Tidal Deposits, A casebook of recent examples and fossil counterparts, Springer-Verlag New York Inc., New York, 428 p.

_____ and _____ (1976) Winter conditions in a macrotidal environment, Cobequid Bay, Nova Scotia. Rev. Géogr. Montréal, XXX(1-2): 65-86.

Koloseus, H.J. and Davidson, J. (1966) Roughness-concentration effects on flow over hydrodynamically rough surfaces. U.S. Geol. Surv., Water-Supply Paper 1592-D, 21 p.

Koons, E.D. (1941) The origin of the Bay of Fundy and associated submarine scarps. J. Geomorphol., 4:237-249.

_____ (1942) The origin of the Bay of Fundy, a discussion. J. Geomorphol., 5:143-150.

Lambiase, J.J. (1974) Avon River estuary sedimentology study: initial report. Tech. Memo. 74-7, Dept. Geol., McMaster University, Hamilton, 24 p.

Leliavsky, S. (1965) River and canal hydraulics. Design textbooks in civil engineering: Vol. 4, Chapman & Hall, Ltd., London, 228 p.

Leopold, L.B., Wolman, M.G. and Miller, J.P. (1964) Fluvial processes in Geomorphology. W.H. Freeman & Co., San Franc., 522 p.

Lesser, R.M. (1951) Some observations of velocity profiles near the sea floor. Am. Geophys. Union, Trans., 32:207-211.

Lonsdale, P., Normark, W.R. and Newman, W.A.. (1972) Sedimentation and erosion on Horizon Guyot. Geol. Soc. Amer., Bull., 83: 289-316.

Lovera, F. and Kennedy, J.F. (1969) Friction-factors for flat-bed flows in sand channels. Proc. Am. Soc. Civ. Eng., 95(HY 4):1227-1234.

Ludwick, J.C. (1970a) Sand waves in the tidal entrance to Chesapeake Bay: preliminary observations. Chesapeake Science, 11:98-110.

_____ (1970b) Sand waves and tidal channels in the entrance to Chesapeake Bay. Virginia J. Science, 21:178-184.

_____ (1972) Migration of tidal sand waves in Chesapeake Bay entrance in Swift, D.J.P., Duane, D.B. and Pilkey, O.H. Shelf Sediment Transport. Dowden, Hutchinson and Ross, Inc., 756 p.

_____ (1974) Tidal currents and zig-zag sand shoals in a wide estuary entrance. Geol. Soc. Amer. Bull., 85:717-726.

_____ (1975) Variations in the boundary-drag coefficient in the tidal entrance to Chesapeake Bay, Virginia. Mar. Geol., 19:19-28.

Mahmood, K. and Blinco, P.H. (1972) Flow of triangular elements simulating dunes, discussion of paper by Rifai and Smith. Proc. Am. Soc. Civ. Eng., 98(HY 3):571-577.

Mahmood, K. and Simons, D.B. (1975) Flow and resistance characteristics of sand bed channels. Int. Assoc. Hyd. Res., Int. Symp. River Mech., 1:317-323, January 1973, Bangkok, Thailand.

Mathieu, R., (1966) Structures sedimentaires des depots de la zone intertidale dans la partie occidentale de la Baie du Mont-Saint-Michel. Rev. de Géogr. Phys. et de Géol. Dynamique, 8(1):113-122.

McCann, S.B. and Carlisle, R.J. (1972) The nature of the icefoot on the beaches of Radstock Bay, southwest Devon Island, N.W.T., Canada in the spring and summer of 1970. Inst. British Geogr., Spec. Publ. No. 4, pp. 175-186.

McCave, I.N. (1969) Deposition of fine-grained sediment from tidal currents. Nature, 224(5226):1288-1289.

_____ (1970) Deposition of fine grained suspended sediments from tidal currents. J. Geophys. Res., 75(21):4151-4159.

McCave, I. (1971) Sand waves in the North Sea off the coast of Holland. Mar. Geol., 10:199-225.

McCave, I.N. (1973) Some boundary-layer characteristics of tidal currents bearing sand in suspension. Mém. Soc. Roy. Sci. Liège, 6^{e} Série, 6:107-126.

McClellan (1965) Elements of physical oceanography. Pergamon Press Inc., Edinburgh, 151 p.

McKee, E.D. and Weir, G.W. (1953) Terminology for stratification and cross-stratification in sedimentary rocks. Geol. Soc. Amer., Bull., 64:381-390.

McMullen, R.M. (1964) Modern sedimentation in the Mawddach Estuary, Barmouth, North Wales. Unpublished Ph.D. thesis, University of Reading, England, 399 p.

McQuivey, R.S. (1973a) Principles and measuring techniques of turbulence characteristics in open channel flow. U.S. Geol. Surv. Prof. Pap. 802-A, 82 p.

_____ (1973b) Summary of turbulence data from rivers, convergence channels and laboratory flumes. U.S. Geol. Surv. Prof. Pap. 802-B, 66 p.

_____ and Richardson, E.V. (1969) Some turbulence measurements in open-channel flow. Proc. Am. Soc. Civ. Eng., 95(HY 1): 209-223.

McWhirter, N. and McWhirter, R. (1972) The Guinness Book of Records. London, Guinness Superlatives Ltd., 19th edition, 317 p.

Merifield, P.M. and Lamar, D.L. (1968) Sand waves and early-moon history. J. Geophys. Res., 73:4767-4774.

_____ and _____ (1970) Paleotides and the geologic record in Palaeogeophysics, S.K. Runcorn (ed.), Academic Press, New York, 518 p.

Middleton, G.V. (ed.) (1965) Primary sedimentary structures and their hydrodynamic interpretation. Soc. Econ. Paleontol. Mineral. Spec. Publ. 12, 265 p.

_____ (1972) Brief field guide to intertidal sediments, Minas Basin, Nova Scotia. Maritime Sediments, 8(3):114-122.

_____ (1976) Hydraulic interpretation of sand size distributions. J. Geol., 84:405-426.

_____, Knight, R.J., Dalrymple, R.W. and Lambiase, J.J. (1975) Intertidal sand bodies in the Minas Basin, Bay of Fundy. Geol. Soc. Am., Abstr., 7(6):82.

_____, _____ and Dalrymple, R.W. (1976) A facies model for a macrotidal environment -- Cobequid Bay, Nova Scotia. Amer. Assoc. Petrol. Geol., 60:697-698. AAPG-SEPM Annual Convention Program, New Orleans.

Miller, J. (1966) The suspended sediment system in the Bay of Fundy. Unpublished M.Sc. thesis, Univ. Dalhousie, Halifax, 100 p.

Miyake, Y. and Koizumi, M. (1948) The measurement of the viscosity coefficient of sea water. J. Mar. Res., 7(2):63-66.

Morris, H.M. (1955) Flow in rough conduits. Trans. Am. Soc. Civ. Eng., 120(HY 2):373-398.

_____ and Wiggert, J.M. (1972) Applied hydraulics for engineering. The Ronald Press Co., New York, 629 p.

Oertel, G. F. (1972) Patterns of sediment transport at nearshore zones influenced by wave and tidal currents: A study utilizing fluorescent tracers. Georgia Marine Science Center, Univ. System of Georgia, Skidaway Is., Georgia. Tech. Report Series 72-7, 28 p.

Off, T. (1963) Rhythmic linear sand bodies caused by tidal currents. Amer. Assoc. Petrol. Geol., Bull. 47:324-341.

O'Loughlin, E. M. and Macdonald, E. G. (1964) Some roughness-concentration effects on boundary resistance. La Houille Blanche, No. 7, pp. 773-782.

Olson, W. S. (1970) Tidal amplitudes in geological history. New York Acad. Sci. Trans., Ser. 2, 32:220-233.

_____ (1972) Sedimentary model for determining paleotidal range: Discussion. Geol. Soc. Amer., Bull., 83:537-538.

Oomkens, E. and Terwindt, J. H. J. (1960) Inshore estuarine sediments in the Haringoliet (Netherlands). Geol. Mijnbouw, 39:701-710.

Pelletier, B. R. and McMullen, R. M. (1972) Sedimentation patterns in the Bay of Fundy and Minas Basin in Gray, T. J. and Gashus, O. K. Tidal Power, Plenum Publishing Corp., New York, 630 p.

Pettijohn, F. J., Potter, P. E. and Siever, R. (1973) Sand and sandstone. Springer-Verlag, New York, 618 p.

Nece, R.E. and Smith, J.D. (1970) Boundary shear stress in rivers and estuaries. Proc. Am. Soc. Civ. Eng., 96(WW 2):335-358.

Newell, N.O. and Rigby, J. (1957) Geological studies on the Great Bahama Bank in R.J. LeBlanc and J.C. Breeding (eds.) Regional Aspects of Carbonate Deposition, Soc. Econ. Paleontol. Mineral. Spec. Publ. No. 5:15-72.

Newton, R.S. and Werner, F. (1970) Form und schichtungsgefuge periodischen sandkorpen im Stromungsfeld des Außenelbewatts. Geol. Rundsch. 60(1):321-330.

Nikuradse, J. (1933) Laws of flow in rough pipes. Nat. Advisory Comm. Aeronautics, Tech. Mem. 1292:1-62 (translation from German, 1950).

Nordin, C.F. (1964) Aspects of flow resistance on sediment transport, Rio Grande near Bernallilo, New Mexico. U.S. Geol. Surv. Water Supply Pap. 1498-H.

_____ (1971) Statistical properties of dune profiles. U.S. Geol. Surv. Prof. Pap., 562-F, 41 p.

_____ and Algert, J.H. (1966) Spectral analysis of sand waves. Proc. Am. Soc. Civ. Eng., 92(HY 5):95-114.

_____ and Dempster, G.R. (1963) Vertical distribution of velocity and suspended sediment, Middle Rio Grande, New Mexico. U.S. Geol. Surv. Prof. Pap. 462-B, 21 p.

Phlipponeau, M. (1956) La Baie du Mont-Saint-Michel. Étude de morphologie littorale. Mém. Soc. Géol. et Min. Bretagne, tome XI.

Postma, H. (1954) Hydrography of the Dutch Wadden Sea. Arch. Neerl. Zool., 10:405-511.

_____ (1957) Size frequency distributions of sands in the Dutch Wadden Sea. Arch. Neerl. Zoologie, 12:319-349.

_____ (1961) Transport and accumulation of suspended matter in the Dutch Wadden Sea. Neth. J. Sea Res., 1:148-190.

_____ (1967) Sediment transport and sedimentation in the estuarine environment in Lauff, G.H. Estuaries, Am. Assoc. Adv. Sci., Washington, D.C. 757 p.

Potter, P.E. and Pettijohn, F.J. (1963) Paleocurrents and basin analysis. New York, Springer-Verlag, 296 p.

Powers, S. (1916) The Acadian Triassic. J. Geol., 24:1-26, 105-122, 254-268.

Prandtl, L. (1926) Über die ausgebildete turbulenze. 2nd Internat. Congr. Applied Mech., Zurich, 62 p.

Pratt, C.J. (1973) Bagnold approach and bed-form development. Proc. Am. Soc. Civ. Eng., 99:121-137.

_____ and Smith, K.U.H. (1972) Ripple and dune phases in a narrowly graded sand. Proc. Am. Soc. Civ. Eng., 98(HY 5):859-874.

Prest, V.K. (1970) Quaternary geology of Canada in R.J.W. Douglas (ed.), Geology and Economic Minerals of Canada, Queen's Printer, Ottawa, pp. 677-764.

_____, Grant, D.R. and Rampton, V.N. (1968) Glacial map of Canada. Geol. Surv. Can., Map 1253A.

_____ and Grant, D.R. (1969) Retreat of the last ice sheet from the Maritime Provinces - Gulf of St. Lawrence Region. Geol. Surv. Can. Paper 69-33, 15 p.

Pretorius, E.S. and Blench, T. (1951) Final report on special observations of bed movement in Lower Fraser River at Badner Reach during 1950 Freshet. Nat. Res. Council Can. Rept., Fraser River Model, Vancouver, Can., 12 p.

Price, W.A. (1963) Patterns of flow and channeling in tidal inlets. J. Sed. Pet., 33(2):279-290.

Proudman, J. (1953) Dynamical oceanography. John Wiley & Sons, Inc., New York, 409 p.

de Raaf, J.F.M. and Boersma, J.R. (1971) Tidal deposits and their sedimentary structures (seven examples from Western Europe). Geol. Mijnbouw, 50(3):479-504.

Raichlen, F. and Kennedy, J.F. (1965) The growth of sediment bed forms from an initially flattened bed. Proc. Int. Ass. Hydraul. Research, 11th Congr., pp. 1-8.

Raju, K.G.R. and Garde, R.J. (1970) Resistance to flow over two dimensional strip roughness. Proc. Am. Soc. Civ. Eng., 96 (HY 5):815-834.

Rao, D.B. (1968) Natural oscillations of the Bay of Fundy. J. Fish. Res. Bd. Canada, 25:1097-1114.

Raudkivi, A.J. (1963) Study of sediment ripple formation. Proc. Am. Soc. Civ. Eng., 89(HY 6):15-33.

_____ (1966) Bed forms in alluvial channels. J. Fluid Mech., 26(3): 507-514.

_____ (1967a) Loose boundary hydraulics. Pergamon Press, Toronto, 331 p.

_____ (1967b) Analysis of resistance in fluvial channels. Proc. Am. Soc. Civ. Eng., 93(HY 5):73-84.

Redfield, A.C. (1950) The analysis of tidal phenomena in narrow embayments. Papers Phys. Oceanog. Meteorol., M.I.T. and Woods Hole Oceanog. Inst., 11(4):36 p.

Reineck, H.I. (1963) Sedimentgefuge im Bereich der Sudlichen Nordsee. Abl. Senckenbergischen Naturfor. Gesells., 505:1-138.

_____ (1967) Layered sediments of tidal flats, beaches and shelf bottoms of the North Sea in Lauff, G.H. (ed.), Estuaries. Am. Assoc. Adv. Sci. Publ. No. 83, Washington, D.C. 757 p.

Reineck, H.E. (1972) Tidal flats in Rigby, J.K. and Hamblin, W.K. (eds.) Recognition of ancient sedimentary environments. Soc. Econ. Paleontol. Mineral. Spec. Publ. 16.

_____ and Singh, I.B. (1967) Primary sedimentary structures in the recent sediments of the Jade, North Sea. Mar. Geol., 5:227-235.

_____ and _____ (1973) Genesis of laminated sand and graded rhythmites in storm-sand layers of shelf mud. Sedimentology, 18:123-128.

_____ and _____ (1973) Depositional sedimentary environments. Springer-Verlag, New York, 439 p.

_____ and Wunderlich, F. (1968) Classification and origin of flaser and lenticular bedding. Sedimentology, 11:99-104.

Richards, A.F. (1976) Extracting energy from oceans: a review. Maine Techn. Soc. Journal, 10(2):5-24.

Richardson, E.V. and McQuivey, R.S. (1968) Measurement of turbulence in water. Proc. Am. Soc. Civ. Eng., 94(HY 2):411-429.

Rifai, M.F. and Smith, K.V.H. (1971) Flow over triangular elements simulating dunes. Proc. Am. Soc. Civ. Eng., 97(HY 7):963-976.

Riley, J.P. and Skirrow, G. (eds.) (1965) Chemical Oceanography. Academic Press, New York.

Robinson, A.H.W. (1960) Ebb-flood channel systems in sandy bays and estuaries. Geography, 45:183-199.

Robinson, A.H.W. (1966) Residual currents in relation to shoreline evolution of the East Anglian Coast. Mar. Geol., 4:57-84.

Robinson, A.R. and Albertson, M.L. (1952) Artificial roughness standard for open channels. Amer. Geophys. Union, Trans., 33(6): 881-888.

Rouse, H. (ed.) (1950) Engineering Hydraulics. Wiley, New York, 1033 p.

_____ (1965) Critical analysis of open-channel resistance. Proc. Am. Soc. Civ. Eng., 91(HY 4):1-25.

Salsman, G.G., Tolbert, W.H. and Villars, R.G. (1966) Sand-ridge migration in St. Andrew Bay, Florida. Mar. Geol. 4:11-19.

Savini, J. and Bodhaine, G.L. (1971) Analysis of current-meter data at Columbia River Gaging stations, Washington and Oregon. U.S. Geol. Surv. Water Supply Pap. 1869-F, Washington, 31 p.

Sayre, W.W. and Albertson, M.L. (1961) Roughness spacing in rigid open channels. Proc. Am. Soc. Civ. Eng., 87(HY 3):121-150.

Schenk, P.E. (1975) A regional synthesis. Maritime Sediments, 11(1): 17-24.

Schlee, J. and Webster, J. (1967) A computer program for grain-size data. Sedimentology, 8:45-53.

Schlichting, H. (1968) Boundary layer theory. McGraw-Hill Book Co., Toronto, 747 p.

Scott, C.H. and Stephens, H.D. (1966) Special sediment investigations: Mississippi River at St. Louis, Missouri, 1961-63. U.S. Geol. Surv. Water-Supply Pap. 1819-J, 35 p.

Shen, H.W. (1962) Development of bed roughness in alluvial channels. Proc. Am. Soc. Civ. Eng., 88(HY 3):45-58.

_____(ed.) (1971) River Mechanics - Volume I. Water Resources Publication, Fort Collins.

_____ (1975) Hans A. Einstein's contributions in sedimentation. Proc. Am. Soc. Civ. Eng., 101:469-488.

Shepard, F.P. (1930) Fundian faults or Fundian glaciers. Geol. Soc. Amer., Bull., 41:659-674.

_____ (1942) Origin of the Bay of Fundy: a reply. J. Geomorphology, 5:137-142.

Shields, A. (1936) Anwendung der Aehnlichkeitsmechanik und der turbulenzforschung auf die Geschiebebewegung. Mitteilungen der Preussischen Versuchsanstalt für Wasserbau and Schiffau, Berlin, Helft 26.

Simons, D.B. and Richardson, E.V. (1962a) The effect of bed roughness on depth-discharge relations in alluvial channels. U.S. Geol. Surv., Water-Supply Pap. 1498-E, 26 p.

_____ and _____ (1962b) Resistance to flow in alluvial channels. Trans. Am. Soc. Civ. Eng., 1(1):927-1006.

Simons, D.B. and Richardson, E.V. (1963a) Forms of bed roughness in alluvial channels. Proc. Am. Soc. Civ. Eng., 87(HY 3): 87-105.

_____ and _____ (1966) Resistance to flow in alluvial channels. U.S. Geol. Surv., Prof. Pap. 422-J, 61 p.

_____, Richardson, E.V. and Hausild, W.L. (1963b) Some effects of fine sediment on flow phenomena. U.S. Geol. Surv., Water-Supply Pap. 1498-G, 47p.

_____, _____ and Nordin, C.F. (1965a) Sedimentary structures generated by flow in alluvial channels in Middleton, G.V. (ed.) Primary sedimentary structures and their hydrodynamic interpretation. Soc. Econ. Paleontol. Mineral. Spec. Publ. No. 12, 265 p.

_____, _____ and _____ (1965b) Bedload equation for ripples and dunes. U.S. Geol. Surv., Prof. Pap. 462-H, 9 p.

Skinner, Brian J. and Turekian, K.K. (1973) Man and the Ocean. Prentice-Hall Inc., Englewood Cliffs, 149 p.

Smith, J.D. (1968) The dynamics of sand waves and sand ridges. University of Chicago Photoduplication Thesis No. T16801, 78 p.

_____ (1969) Geomorphology of a sand ridge. J. Geol., 77:39-55.

Smith, K.V.H. (1968) Alluvial channel resistance related to bedforms. Proc. Am. Soc. Civ. Eng., 94(HY 1):59-69.

Smith, K. V. H. (1970) The Einstein-Barbarossa diagram for computing bedform resistance in alluvial channels. Proc. Inst. Civ. Eng., 46: 169-184.

Smith, N. D. (1970) The braided stream depositional environment: comparison of the Platte River with some Silurian clastic rocks, north-central Appalachians. Geol. Soc. Amer., Bull., 81:2993-3014.

Smith, R. S. (1969) Sedimentology of the deltas of the Moose and Diligent Rivers, Minas Basin, Bay of Fundy, Nova Scotia. Unpublished M.Sc. thesis, University of Pennsylvania, Philadelphia, 112 p.

Smitheringale, W. G. (1960) Geology of Nictaux-Torbrook map area, Annapolis and Kings Counties, Nova Scotia. Geol. Surv. Can., Pap. 60-13, 32 p.

Southard, J. B. (1971) Representation of bed configurations in depth-velocity-size diagrams. J. Sed. Pet., 41(4):903-915.

_____ and Boguchwal, L. A. (1973) Flume experiments on the transition from ripples to lower flat bed with increasing sand size. J. Sed. Pet., 43:1114-1121.

Spencer, L. J. (1957) Obituary of Rudolf Richter. Proc. Geol. Soc. London (1956-1957), No. 1554, pp. 137-138.

Squarer, D. (1970) Friction factors and bedforms in fluvial channels. Proc. Am. Soc. Civ. Eng., 36(HY 4):995-1017.

Stanley, D.J. and Swift, D.J.P. (eds.) (1976) Marine sediment transport and environmental management. John Wiley & Sons (AGI), 602 p.

Sternberg, R.W. (1965) Observations of boundary-layer flow in a tidal current. Unpublished Ph.D. thesis, Dept. Oceanogr., University of Washington, Seattle, 72 p.

_____ (1966) Boundary layer observations in a tidal current. J. Geophys. Res., 71:2175-2178.

_____ (1967) Measurements of sediment movement and ripple migration in a shallow water marine environment. Mar. Geol., 5:195-205.

_____ (1968) Friction factors in tidal channels with differing bed roughness. Mar. Geol., 6:243-260.

_____ (1970) Field measurements of the hydrodynamic roughness of the deep-sea boundary. Deep-Sea Res., 17:413-420.

_____ (1971) Measurements of incipient motion of sediment particles in the marine environment. Mar. Geol. 10:113-119.

_____ (1972) Predicting initial motion and bedload transport of sediment particles in the shallow marine environment in Swift, D.J.P., Duane, D.B. and Pilkey, O.H. Shelf Sediment Transport. Dowden, Hutchinson and Ross, Inc., 756 p.

_____ (1976) Measurements of boundary-layer flow and boundary roughness over Campeche Bank, Yucatan. Mar. Geol., 20:

Sternberg, R.W. and Kachel, N.B. (1971) Transport of bedload as ripples during an ebb current. Mar. Geol. 10:229-244.

Stevenson, I.M. (1958) Truro map area, Colchester and Hants Counties, Nova Scotia. Geol. Surv. Can., Mem. 297, 124 p.

Stewart, H.B. and Jordan, G.F. (1965) Underwater sand ridges on Georges schoal in Miller, R.L. (ed.) Papers in Marine Geology, MacMillan, New York, 531 p.

Stichling, W. (1974) Sediment loads in Canadian rivers. Inland Waters Directorate, Tech. Bull. 74, Environment Canada, 27 p.

Van Straaten, L.M.J.U. (1953) Megaripples in the Dutch Wadden Sea and in the Basin of Arcachon (France). Geol. Mijnbouw, 15(1): 1-11.

_____ (1954) Sedimentology of recent tidal flat deposits and the Psammites du Condroz (Devonian). Geol. Mijnbouw, 16(2):25-47.

_____ (1961) Sedimentation in tidal flat areas. J. Alberta Soc. Petrol. Geol., 9:203-226.

_____ and Kuenen, Ph.H. (1957) Accumulation of fine grained sediments in the Dutch Wadden Sea. Geol. Mijnbouw, 19:329-354.

_____ and _____ (1958) Tidal action as a cause of clay accumulation. J. Sed. Pet., 28:406-413.

Stride, A.H. (1963) Current-swept sea floors near the southern half of Great Britain. Quart. J. Geol. Soc. London, 119:175-200.

Stride, A.H., Belderson, R.H. and Kenyon, N.H. (1972) Longitudinal furrows and depositional sand bodies of the English Channel. Mem. Bur. Rech. Geol. Min., 79:233-240.

Sverdrup, H.U., Johnson, M.W. and Fleming, R.H. (1942) The Oceans, their physics, chemistry and general biology. Prentice Hall Inc., Englewood Cliffs, N.J., 1087 p.

Swett, K., Klein, G. de V. and Smit, D.E. (1971) A Cambrian tidal sand body - the Eriboll Sandstone of northwest Scotland: An ancient-recent analog. J. Geol., 79:400-415.

Swift, D.J.P. (1966) Bay of Fundy in Fairbridge, R.W. (ed.), Encyclopedia of Oceanography. Van Nostrand, New York.

_____ (1975) Tidal sand ridges and shoal-retreat massifs. Mar. Geol., 18:105-134.

_____ and Borns, H.W. Jr. (1967a) A raised fluviomarine outwash terrace, north shore of the Minas Basin, N.S. J. Geol., 75:633-711.

_____ and _____ (1967b) Genesis of the raised fluviomarine outwash terrace, North Shore of the Minas Basin, Nova Scotia: A preliminary report. Maritime Sediments, 3:17-23.

_____, Duane, D.B. and Pilkey, T. (eds.) (1972) Shelf sediment transport: Process and Pattern, Dowden, Hutchinson and Ross, Inc., Stroudsburg, Pa. 756 p.

Swift, D.J.P. and Lyall, A. (1968) Origin of the Bay of Fundy, and interpretation from sub-bottom profiles. Mar. Geol., 6:331-343. 343.

_____ and McMullen, R.M. (1968) Preliminary studies of intertidal sand bodies in the Minas Basin, Bay of Fundy, N.S. Can. J. Earth Sci., 5:175-183.

_____, Pelletier, B.R., Lyall, A.K. and Miller, J.A. (1973) Quaternary sedimentation in the Bay of Fundy in Hood, P.J., Earth Science Symposium on Offshore Eastern Canada, Geol. Surv. Canada, Paper 71-23, 652 p.

Tanner, W.F. (1967) Ripple mark indices and their uses. Sedimentology, 9:89-104.

Terwindt, J.H.J. (1967) Mud transport in the Dutch Delta Area and along the adjacent coastline. Netherlands Jour. Sea Res., 3:505-531.

_____ (1970) Observation on submerged sand ripples with heights ranging from 30 to 200 cm occurring in tidal channels of S.W. Netherlands. Geol. Mijnbouw, 49(6):489-501.

_____ (1971a) Litho-facies of inshore estuarine and tidal-inlet deposits. Geol. Mijnbouw, 50(3): 515-526.

_____ (1971b) Sand waves in the Southern Bight of the North Sea. Mar. Geol., 10:51-67.

_____ (1973) Sand movement in the in-and offshore tidal area of the S.W. part of the Netherlands. Geol. Mijn[illegible] 69-77.

Terwindt, J.H.J. and Breusers, H.N.C. (1972) Experiments on the origin of flaser, lenticular and sand-clay alternating bedding. Sedimentology, 19:85-98.

_____, Breusers, H.N.C. and Svasek, J.N. (1968) Experimental investigation of the erosion-sensitivity of a sand-clay lamination. Sedimentology, 11:105-114.

_____, de Jong, J.D. and van der Wilk, E. (1963) Sediment movement and sediment properties in the tidal area of the Lower Rhine. Verh. Kon. Ned. Geol. Mijnbouw. Gen., Geol. Serie, 2(2):243-258.

Thompson, R.W. (1968) Tidal flat sedimentation on the Colorado River delta, northwestern Gulf of California. Geol. Soc. Am. Mem. 107, 133 p.

Todd, T.W. (1968) Dynamic diversion: influence of longshore current-tidal flow interaction on Chenier and Barrier Island Plains. J. Sed. Pet., 38(3):734-746.

Toffaleti, F.B. (1965) Deep river velocity and sediment profiles and the suspended sand load. Proc. Federal Inter-agency Sedimentation Conf., Misc. Publ. 970 (1963), U.S. Dept. Agric., pp. 207-228.

Tucker, M.E. (1973) The sedimentary environments of tropical African estuaries: Freetown Peninsula, Sierra Leone. Geol. Mijnbouw, 52:203-15.

U.S. Army Coastal Engineers (1973) Shore Protection Manual, U.S. Army Coastal Engineering Res. Center, Fort Belvoir, Va. 3 volumes.

Vanoni, V.A. (1974) Factors determining bed forms of alluvial streams. Proc. Am. Soc. Civ. Eng., 100(HY 3):363-377.

_____ and Hwang, Li-San (1967) Relation between bed forms and friction in streams. Proc. Am. Soc. Civ. Eng., 93(HY 3):121-144.

_____ and _____ (1968) Relation between bed forms and friction in streams (Closure). Proc. Am. Soc. Civ. Eng., 94(HY 6):1524-1527.

_____ and Nomicos, G.N. (1959) Resistance properties of sediments laden streams. Proc. Am. Soc. Civ. Eng., 85(HY 5):77-107.

Van Veen, J. (1950) Eb- en vloedschaarsystemen in de Nederlandse getijwateren. Wadden-symposium-Tijdschr. Koninkl. Ned. Aardrijkskundig Genoot., 67:45-65.

Visher, G.S. (1969) Grain size distributions and depositional processes. J. Sed. Pet., 39:1074-1106.

Walker, R.G. (1976) Facies Models 3. Sandy fluvial systems. Geosci. Can., 3(2):101-109.

Walton, F.D. and Goodell, H.G. (1972) Sedimentary dynamics under tidal influences, Big Grass Island, Taylor County, Florida. Mar. Geol., 13:1-29.

Weeks, L. J. (1948) Londonderry and Bass River map areas, Colchester and Hants Counties, Nova Scotia. Geol. Surv. Can., Mem. 245, 86 p.

Wehrfritz, N. (1973) A study of the surface texture of intertidal sand grains with a scanning electron microscope. Tech. Memo. 73-8, Department of Geology, McMaster University, 25 p.

Werner, F. and Newton, R.S. (1970) Riesenrippeln im Fehmambelt. Meyiana, 20:83-90.

White, W.R. (1972) Sediment transport in channels: a general function. Hydraulics Research Station Rept. No. INT-104, Wallingford, England.

Wightman, D.M. (1975) Paleotidal range and Pleistocene sea-level changes at Cape d'Or of Fundy, N.S. Geol. Soc. Amer., Abstr. 7(6):880-881.

Wiseman, W.J. (1969) On the structure of high frequency turbulence in a tidal estuary. Chesapeake Bay Inst. Rept. 69-12, Johns Hopkins University, Baltimore, Md., 74 p.

Wolman, M.G. (1955) The nature channel of Brandywine Creek, Pennsylvania. U.S. Geol, Surv., Prof. Pap. 271, 56 p.

Wright, L.D., Coleman, J.M. and Thom, B.G. (1975) Sediment transport and deposition in a macrotidal river channel: Ord River, Australia in Cronin, L.E. (ed.), Estuarine Research, Vol. II, Academic

Yalin, M.S. (1964) Geometrical Properties of sand waves. Proc. Am. Soc. Civ. Eng., 90(HY 5):105-119.

_____ (1972) Mechanics of sediment transport. Pergamon Press, Toronto, 290 p.

Yuen, K.B. (1969) Effect of tidal barriers upon the M_2 tide in the Bay of Fundy. J. Fish. Res. Bd. Can., 26:2477-2492.

Znamenskaya, N.S. (1963) Experimental study of the dune movement of sediment. Soviet Hydrology Selected Papers, No. 3:253-275.

A P P E N D I X I

GENERAL METHODS AND EQUIPMENT

I.1 SEAWATER PROPERTIES

Water temperatures were recorded with two pairs of reversing thermometers mounted on the outside of a Knudsen bottle during the first summer field season. Measurements were made at frequent intervals during individual tidal cycles at three locations above the seabed: 0.5 metres, mid-depth, and 0.5 metres from the surface. During the subsequent field seasons, additional water temperatures were obtained from a thermistor on one of the recording current metres (0.5 m from the bottom) and from an ordinary Taylor thermometer suspended from the side of the boat to measure surface water temperatures.

Water samples were collected with a 1-litre Knudsen bottle at the same time as water temperature measurements during the first summer. Samples were filtered through ashless filter paper at the end of each collection-day. Unfortunately, an asher could not be found to oxidize the filter papers for the determination of suspended sediment concentrations. As a result, approximately 139 filtered samples could not be analyzed.

Following the outcome of the water sampling program from the first field season, a different approach was made during the second year. A 1-litre 'instantaneous' water sampler (Fig. I.1 F) was borrowed from the Applied Hydrology Division, Inland Waters Directorate, Ottawa (pers. comm. with E. R. Peterson and P. I. Campbell, 1972). As this sampler was suspended with its sampling orifice oriented into the current flow, a more representative sample could be collected than with Knudsen bottles (which were suspended vertically). Seventy-seven water samples of approximately 750 ml volume each were collected at 0.5 m from the bottom, mid-depth and 0.5 m from the surface at regular intervals of time through semidiurnal tidal cycles on five different occasions. The samples were stored in glass salinity-bottles and injected with a solution of $NaNO_3$

FIGURE I.1: Field equipment.

A. Seagull: 7.3 m long, wooden-hulled boat that was used during the 1971 summer field season. Powered by single-cylinder 'make-and' break' engine.

B. Mallard: 9.5 m long, wooden-hulled sounding launch that was used during the 1972 summer field season. Powered by six-cylinder Perkins diesel.

C. Hudson Barge (alias 'The Barge"): 9.8 m long, aluminium hulled boat that was used during the 1973 summer field season. Powered by six-cylinder Perkins diesel.

D. Plessey current meter (automatic recording) suspended from tubular steel davit (0.5 m from the bed) and supported by a 200 kg concrete base.

E. Kelvin-Hughes 'direct-reading' current meter suspended over the side of the boat. The meter is about 0.7 m long.

F. 'Instantaneous' 1-litre water sampler used for the collection of suspended sediment samples. Sampler is about 0.5 m long.

G. Trench through a megaripple showing the position of three peels relative to the bedform cross-sectional shape and the method of burying the peels during the low tide period when the epoxy was hardening. Scale is 1 m long.

A

B

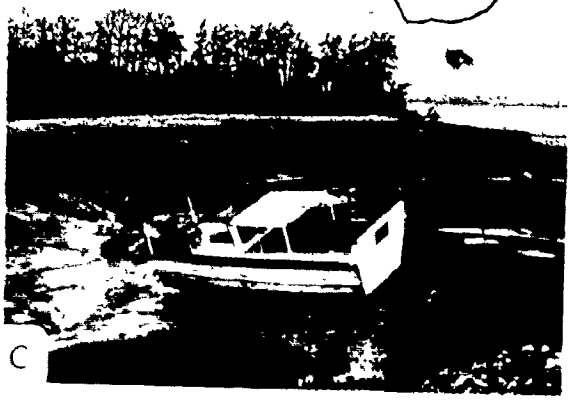

C

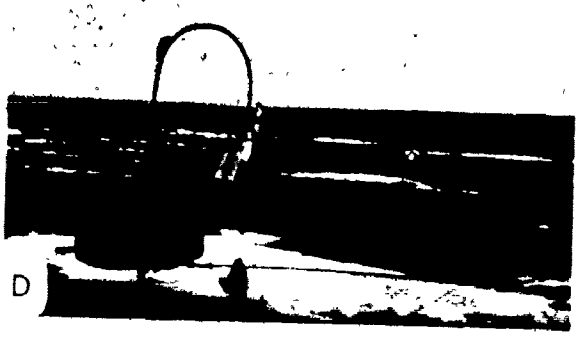

D

F

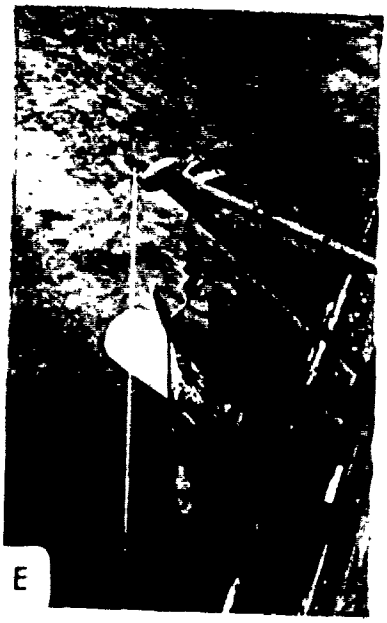

E

G

to prevent algal growth. The bottles were placed in styrofoam containers and left in a cool, dark location until analysis.

At first, size analysis of the suspended sediments in the water samples was attempted, but the sample volume proved to be inadequate for most techniques and (or) there was a large and inconsistent amount of dissolved solids present in the form of marine salts. The salts could only be removed by thorough washing of the concentrated materials, and as the sample size was small, this method could not be used.

Suspended sediment concentrations from the water samples were finally made by vacuum filtering the samples through preweighed, 0.22 μ cellulose fibre Millipore filters. The filters were thoroughly washed with distilled water to remove any dissolved salts, oven dried and reweighed. Visual estimation of the coarseness of some of the suspended sediments was made from the filters with the aid of a binocular microscope.

I.2 BOATS

All survey and station work were done from small boats (Fig. I.1A A, B and C), 7 - 10 m in length, either rented locally, e.g., Seagull (rented from Mr. Aubrey Scott, Noel), or loaned from the Atlantic Oceanographic Laboratory, Bedford Institute of Oceanography (Dartmouth), e.g., Mallard and Hudson Barge. As a working boat, the Seagull was seaworthy, but too small to accommodate equipment, samples and personnel, and very uncomfortable during marginal weather since it did not have a cabin. The Mallard, although more practical for long work periods (up to 15 hours) and somewhat rougher conditions out on the bay, had some problems similar to those of the Seagull. Specifically, these two boats were constructed of wood which restricted grounding on the offshore intertidal zones only during fair to moderate weather, i.e., relatively calm sea conditions. The V-hull design of these boats caused further difficulties. To keep the boats upright during grounded-out periods at low tide, either a beam was secured against the side (Seagull), or two wedge-shaped chocks were fastened against the keel (Mallard) prior to grounding.

The Hudson Barge solved all the problems experienced during the

earlier field seasons concerning boats. The barge was spacious, (relatively) seaworthy, flat-bottomed with a shallow keel, and constructed of reinforced aluminum.

I.3 NAVIGATION

Field work requiring absolute fixes and locations were restricted to daylight hours. Station locations and position fixes along survey lines were determined from sightings made to predetermined shore reference locations with a Brunton compass and a Kelvin-Hughes telescopic sextant. A minimum of three reference locations were necessary to position each offshore station. Positions were plotted on base maps using the angular displacement between the reference locations for a given set of sightings, and a three-arm protractor (Davis Instrument Corp.). The positions determined by sextant were sighted and reduced more rapidly, and were more reliable than comparable compass measurements and results.

Relative positions for day and night, and marginal weather (e.g. fod) work periods were found by line-of-sight and dead-reckoning, and with the aid of topographic maps, air photos and echo sounder.

I.4 BATHYMETRIC SURVEY AND REDUCTION

Because the field work was concentrated in the area between Burntcoat Head and Salter Head, only this area was surveyed. The survey was undertaken during August 6, 8 and 9, 1973, using a model DE-719, Raytheon Fathometer. The sounder operated with sounding rate of 9 pulses per second at a frequency of 200kHz. The power of the sounder was too low, and the frequency too high to pick up any subsurface horizons. Accuracy of the sounder was 0.5% ± 25 mm of the indicated depth.

Survey lines were oriented diagonally across the bay (Fig. 3.4) because tidal currents prevented the running of lines perpendicular to the shore. The lines were kept relatively straight by using arbitrary shore and horizon features as range markers, and by keeping the boat angled slightly into the current to compensate for down-drift. Boat speed was kept as slow as possible without losing steerage-way (about 1.0 to 1.6 m/s.

Thirteen transects of the bay, totalling about 110 km were made at spacings of about 1.5 km. Position fixes were determined with two simultaneous sextant readings, and times were recorded for each of the fixes periodically along and at the ends of the survey lines. The times of surveying during the semidiurnal tidal cycle were restricted to periods near high water while water depths were still sufficient to cross the bay and before the tidal currents reached maximum speeds. Fortunately, conditions remained calm throughout most of the survey.

Water depths were read from the sounding records at regular intervals. These values were reduced and corrected to a high water sounding datum of 12.4 m, the mean high water level during the survey period. This level is the elevation above the internationally agreed-upon chart datum (Dohler, 1970). Corrections due to the variation in tidal level during the survey were determined from survey fix times and from a tabulation of the predicted hourly heights of the tide at Burntcoat Head (G.C. Dohler, Canadian Hydrographic Service, pers. comm., 1973) assuming that high water occurs at the same time everywhere in Cobequid Bay, and that water levels are approximated by a horizontal plane throughout the bay.

The corrected depths from the sounding records were plotted on a base map of the bay and contours were extrapolated at 5 m intervals with the aid of air photographs. The contours were extended beyond the western end of the surveyed area by making use of information from the Huntec (1966) survey of the bay.

I.5 STRUCTURE AND GEOMETRY

The structure of the intertidal-subtidal sedimentary body in Cobequid Bay, between Burntcoat Head and Salter Head, was obtained with a Huntec 'Hydrosonde 2A' sparker, a continuous seismic profiler with a penetration capability of up to 100 m. The profiler consisted of a spark source, a hydrophone, a transmitter, a receiver (comprising of a signal processor, helix recorder, keying programmer and D.C. Power supplies), and an A.C. generator.

Two different sound sources were used at the beginning of the survey: (i) an ED-10 'Boomer" (Huntec Ltd.); and (ii) a two-electrode sparker

with concentric configuration (Huntec Ltd.). Although the catamaran-mounted 'Boomer' was supposed to give greater record resolvability, it gave consistently poor records. As well, the unit submerged while under way which caused towing problems in the tidal currents. Use of the 'Boomer' was discontinued.

The sparker was then used for the entire survey. It was trailed five to seven metres astern of the boat and outside the wake at the end of a three meter long wooden beam. The hydrophone , a M-35 magnetostrictive velocity sensitive type (Harris Division of General Instrument Corp.), was streamed 12 to 15 metres behind the boat. A sweep time of 125 milliseconds was used and the high/low filters were set at 3027 and 1153 cycles per second. The maximum power output of the sparker was 165 Joules.

Because there was no drilling data from the bay to determine seismic wave velocities through different sub-bottom materials, the average velocities reported by Huntec (1966) were used to convert the hydrosonde travel times to depths. The seismic velocities for unconsolidated sediments and bedrock were 1.0 and 1.5 m/ms (one-way times).

Depth and thickness times were read from the profiles at spacings of 100 to 125 m depending on the length of the survey line. These times were used to construct contour and isopach maps of the major sub-bottom reflectors and units interpreted from the profiles. All depths are relative to the sounding datum (12.4 m above chart datum) established for the bathymetric survey.

Without borehole data, identification and correlation of the major units was done by examination of outcrops exposed in the shoreline and intertidal foreshore. In areas where there was no lateral exposure of an unidentified unit, geological and pedological maps and reports, and sedimentological 'insight' were used. Once the true reflections are separated from the multiples, interpretation of the profiles becomes a question of making geological sense out of the seismic events.

Because the hydrophone is more responsive to energy arriving from the side than along its axis (to cut down towing noise), the bottom echo or 'bubble' pulse (5 - 7 ms) is a little longer than the direct arrival pulse (5 ms) at the water surface. The width of the 'bubble' pulse more or less determines the resolution limits of the profile records, because any

sub-bottom reflector is going to return a signal that is about 5 ms long. For a seismic velocity of approximately 1 m/ms for unconsolidated sediments, this makes the absolute thickness of the 'bubble' pulse and the sub-bottom reflector about 5 m. The relatively thick reflecting pulse is recorded as two parallel lines, the width of which is approximately equal to 5 ms.

Much of the sparker energy is generally lost in unconsolidated sediments; nevertheless, a good bedrock surface underlying the sediments is indicated in most of the profiles (Fig. 3.7). The bedform surface is commonly lost in the 'bubble' pulse where the water depths shallow near shore, or parts of the surface may show here and there within the span of the bottom arrival. In this situation, it is best to place the bedrock surface somewhere within the 'bubble' pulse and to compare the result with direct field observation (e.g., in the intertidal zone).

APPENDIX II

SEDIMENT SAMPLES

II.1 SAND BARS

The first objective on each of the sand bars was to collect comprehensive information on topography, bathymetry, sediment textures, bedforms and currents. The topography of the upper, intertidal portions of the sand bars and the subtidal bathymetry was mapped with a Zeiss Ni-2 level and a model DE-719 Raytheon Fathometer respectively. The 1973 air photographs were used to delineate the outline of the bars at low tide, and to give a preliminary impression of the distribution of bedform types and relative sizes.

Sediment samples (Fig.II.1) were collected on a regular grid, with lines running approximately north-south and east-west. Grid spacing varied from about 250 to 300 metres depending on the size of the bar. Orientation and spacing of the grid lines was maintained by pace and compass (Brunton), and positions were determined from compass azimuths and (or) sextant readings to reference locations on shore. All samples were collected from the upper 2 centimetres of bedform crests or plane bed surface to avoid local variations.

A few subtidal sediment samples (Fig. II.1) were collected with a Dietz-Lafond or a Van Veen grab sampler from some of the channel bottoms adjacent to the bars. This part of the sediment sampling program was generally unsuccessful. Strong tidal currents made operation of the grab samplers difficult and it was almost impossible to maintain a stationary position while the position was fixed. The relatively coarse sediments in the channel bottoms usually prevented the samplers from closing completely, thus the fine-grained fraction of the grab sample was lost as the sampler returned to the surface. As a result, the bottom grab samples are probably not very representative. They do, however, provide some generalized information about the nature of the channel bottom sediments relative to the intertidal zone sediments.

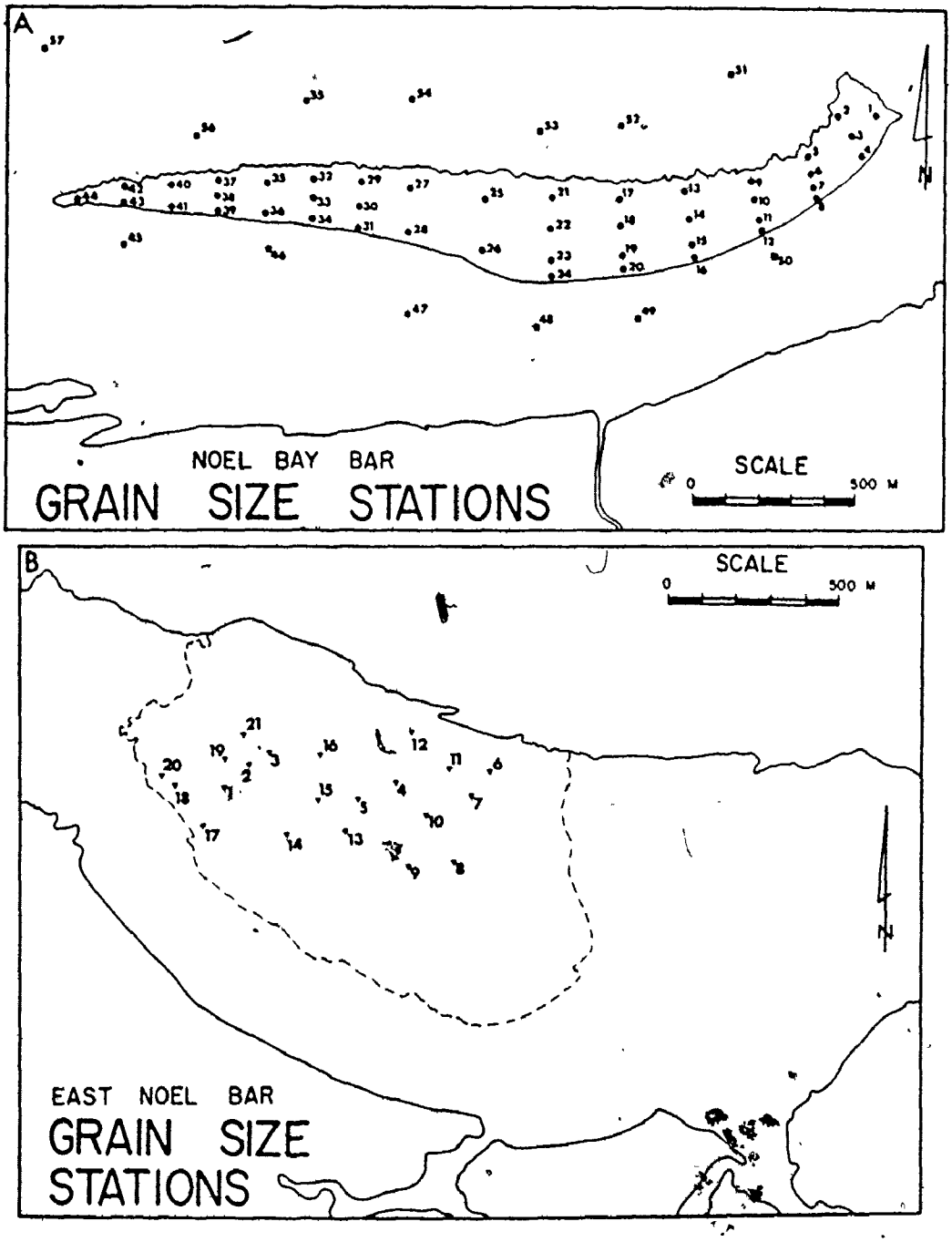

FIGURE II.1: The location of sediment samples on Noel Bay Bar (A), East Noel Bar (B), Noel Shore Bar (C) and Selma Bar (D).

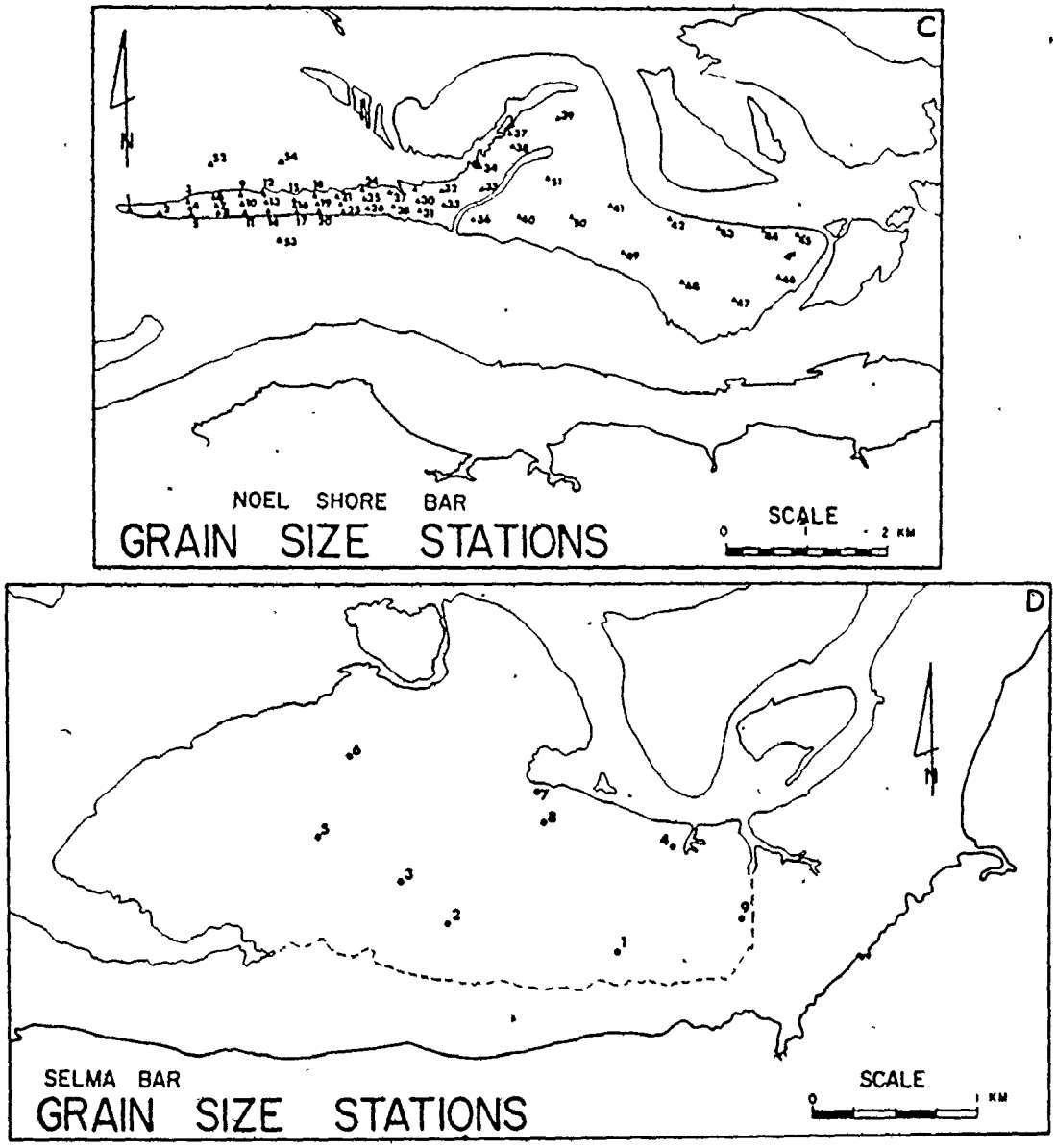

FIGURE II.1 - cont'd.

II.2 GRAIN SIZE ANALYSIS

The sediment samples were analyzed mechanically using the method outlined by Dickson (1974).

After drying, the samples were hand-sieved through a -1.0 phi (2.0 mm opening) sieve. The material not passing through this sieve was sieved at ½ phi intervals by hand. The material finer than -1.0 phi was split to give a sample weight of about 50 to 75 grams with a riffle splitter. This representative sample was wet sieved through a 4.0 phi (0.0625 mm) sieve to separate the mud fraction from the sand. The material retained on the 4.0 phi sieve was oven dried and sieved for 10 minutes at ½ phi intervals in a Ro-Tap Sieve Shaker. The material passing the 4.0 phi sieve was added to the mud fraction. The mud fraction separated by wet sieving was filtered through preweighed, 9.0 phi (0.0020 mm) Millipore filters to determine the total fines fraction.

The grain size distribution of the sediment samples were plotted as cumulative frequency curves of sediment size (in phi units) on arithmetic probability paper, to allow visual examination of their size distributions. The study of particle size distributions is based on the idea that the characteristics of the sediment population reflect some aspects of the processes active during their deposition (Middleton, 1976; Visher, 1969). Grain size is measured on a negative logarithmic scale so that the cumulative frequency curve plotted on probability paper can be considered a log-probability plot. In many cases, it is possible to dissect the curve into a limited number of straight line segments, suggesting that the whole sediment sample population is actually composed of several truncated or overlapping normal distributions. Grain size distributions generally exhibit three or more straight line segments which can be interpreted in terms of an assumed mechanism of sediment transport; (i) traction; (ii) intermittent suspension; and (iii) suspension. The finest population is carried by suspension; the coarsest population is interpreted as those grains transported by rolling or sliding, i. e., traction or "bedload". The intermediate population between suspension and traction are the grains that move by saltation and intermittent suspension. Middleton (1976) discussed the hydraulic criterion for separ-

the ent sus ion and tra ion ons.

Subsequent analysis of the grain size data was made by calculating moment measure statistics from a program developed by R. W. Dalrymple. The program uses a direct integration of the linear approximations between points on the cumulative frequency curve, apparently giving a closer estimation of mean, standard deviation (sorting), skewness and kurtosis than from the continuous parabolic interpolation used in the program by Schlee and Webster (1967). Samples that were open ended by more than 5% in either the fine or coarse tail were accepted by Dalrymple's program, e.g., channel bottom samples (fines lost through inability of grab sampler to close properly). Jones (1970, p. 1205) found that moment statistics calculated on samples that were open ended by more than 5% in either tail differed significantly from their true values.

II.3 SIEVE FRACTIONS AND STATISTICS

The following is a listing of the sediment sieve data from the field samples, including: sieve sizes and cumulative percents, moment statistics, and percentages of granules, sand and silt-clay. Sample locations are shown in Figure II.1.

All samples were collected from bedform crests or plane beds, except those designated with a number and letter. These latter samples were collected to show the variation of textures over bedforms. On East Noel Bar (at locations 1 to 5 only), the letters refer to: (a) the bottom of the lee-slope; (b) the middle of the lee-slope; (c) the crest of the bedform; and (d), (e)....at equidistant intervals to the trough of the upcurrent bedform. On Noel Shore Bar, sediment samples were collected at the bottom (a) and crest (b) of the bedforms only at locations 41, 42, 45, 46, 47, 48 and 49. On Selma Bar, the sample letters refer to the same positions over a bedform as on East Noel Bar.

The sediment samples from 'Crowe's foreshore' were collected at approximately 5 m intervals up the intertidal foreshore (north-south) to the south of Selma Bar from the mud veneer.

Note: Only those samples from the crests of bedforms or plane sand beds [illegible] sed to [illegible] the [illegible] dis[illegible]ion of grain size [illegible] in

Noel Bay Bar

SIEVE SIZE	1 CUMULATIVE PERCENT	2	3	4	5	6	7	8 SIEVE SIZE
-2.00	3.6[illegible]	0.00						-2.00
-1.50	.65	.00						-1.50
-1.00	.18	.13	0.00	0.00	0.00			-1.00
-.50	.22	.16	.17	.02	.03	0.00	.03	-.50
0.00	.51	.33	.23	.06	.14	.03	.01	0.00
.50	1.02	.95	.32	.37	.02	.28	.01	.50
1.00	2.22	1.54	.64	.58	1.09	3.05	.21	1.00
1.50	25.32	24.39	35.26	11.09	19.22	24.38	12.04	1.50
2.00	98.15	83.12	99.67	99.70	96.03	97.99	99.97	2.00
2.50	99.28	98.12	99.97	99.26	96.32	99.14	99.86	2.50
3.00	99.93	99.86	99.97	99.82	99.70	99.13	99.93	3.00
3.50	99.98	99.97	99.95	99.92	99.98	99.98	99.98	3.50
4.00	100.00	99.97	100.00	100.00	100.00	100.00	99.98	4.00
4.50		100.00					100.00	4.50

MOMENT STATISTICS

	1	2	3	4	5	6	7
MEAN SIZE	1.00	1.70	1.73	1.70	1.72	1.69	1.77
STANDARD DEVIATION	.59	.39	.34	.33	.37	.48	.32
SKEWNESS	-1.23	-.91	-.68	-.24	-.19	.28	.47
KURTOSIS	18.99	11.93	16.18	3.72	9.14	9.61	9.1
PERCENT GRAVELS	.18	.13	0.00	0.00	0.00	0.00	.28
PERCENT SAND	99.99	99.84	100.00	100.00	100.00	100.00	99.48
PERCENT SILT AND CLAY	0.00	.04	0.00	0.00	0.00	0.00	.62

SIEVE SIZE	8 CUMULATIVE PERCENT	9	10	11	12	13	14	15 SIEVE SIZE
-2.50	0.00	0.00	0.00	0.00	0.00	0.00		-2.00
-2.00	.00	.00	.00	.00	.00	.00		-1.50
-1.50	.12	.13	.35	.14	.02	.71	0.00	-1.00
-1.00	.27	.32	1.50	.29	.04	.97	.02	-.50
-.50	.90	.67	2.85	.55	.14	1.94	.00	0.00
0.00	1.23	2.07	5.01	1.38	0.00	4.12	.10	.50
.50	13.92	23.10	26.06	10.26	14.00	24.47	1.55	1.00
1.00	83.06	99.07	99.00	60.29	83.21	99.03	39.92	1.50
1.50	98.35	99.98	99.35	99.57	99.55	99.92	99.74	2.00
2.00	99.83	99.76	99.76	99.83	99.98	99.98	99.60	2.50
2.50	99.92	99.91	99.94	99.94	99.98	99.99	99.89	3.00
3.00	99.95	99.96	100.00	100.00	99.99	99.97	99.93	3.50
3.50	100.00	100.00			100.00	100.00	100.00	4.00
4.00								4.50

MOMENT STATISTICS

	8	9	10	11	12	13	14
MEAN SIZE	1.77	1.67	1.63	1.87	1.76	1.62	1.68
STANDARD DEVIATION	.38	.38	.37	.43	.33	.47	.37
SKEWNESS	-.07	-.57	-1.20	-.68	.06	.00	.00
KURTOSIS	9.86	8.64	8.67	8.77	5.75	10.11	7.35
PERCENT GRAVELS	.23	.06	.16	.03	.01	.00	.00
PERCENT SAND	99.62	99.62	99.90	99.97	99.98	99.98	100.00
PERCENT SILT AND CLAY	.00	.04	0.00	0.00	.01	.03	0.00

Noel Bay Bar (cont'd)

	15	16	17	18	19	20	21	
SIEVE SIZE	CUMULATIVE PERCENT							SIEVE SIZE
-1.50	0.00	0.00		0.00				-2.50
-1.00	.06	.06	0.00	.17				-2.00
-.50	.16	.16	.03	1.39	0.00	0.00		-1.50
0.00	.41	.36	1.97	1.91	.07	.02	3.33	-1.00
.50	.97	.75	3.87	1.97	.21	0.93	.01	-.50
1.00	1.69	2.73	10.91	1.99	.44	0.61	.01	0.00
1.50	9.93	23.38	66.26	1.99	.84	0.62	.16	.50
2.00	80.21	83.00	90.00	3.27	2.81	5.42	2.36	1.00
2.50	97.47	97.53	98.03	14.88	18.55	9.78	19.61	1.50
3.00	99.83	99.87	99.75	89.89	73.05	75.00	87.65	2.00
3.50	99.96	99.99	99.92	98.81	96.99	94.85	96.91	2.50
4.00	100.00	99.99	99.97	99.78	99.80	99.84	99.84	3.00
		100.00	100.00	99.93	99.97	99.97	99.99	3.50
				99.97	99.99	99.99	99.99	4.00
				100.00	100.00	100.00	100.00	4.50

MOMENT STATISTICS

MEAN SIZE	1.00	MEAN SIZE 1.10	MEAN SIZE 1.71	MEAN SIZE 1.71	MEAN SIZE 1.62	MEAN SIZE 1.76	MEAN SIZE 1.71
STANDARD DEVIATION	.87	STANDARD DEVIATION .62	STANDARD DEVIATION .37	STANDARD DEVIATION .30	STANDARD DEVIATION .41	STANDARD DEVIATION .47	STANDARD DEVIATION .34
SKEWNESS	-.00	SKEWNESS -.31	SKEWNESS -.28	SKEWNESS -3.34	SKEWNESS -.05	SKEWNESS -2.19	SKEWNESS -.16
KURTOSIS	18.22	KURTOSIS 7.87	KURTOSIS 6.00	KURTOSIS 24.54	KURTOSIS 9.56	KURTOSIS 16.12	KURTOSIS 6.00
PERCENT GRAVELS	.0%	.3%	0.00	1.4%	.07	.02	0.00
PERCENT SAND	99.9%	99.9%	99.97	99.3%	99.92	99.98	99.99
PERCENT SILT AND CLAY	0.00	.01	.03	.4%	.01	.01	.01

	22	23	24	25	26	27	28	
SIEVE SIZE	CUMULATIVE PERCENT							SIEVE SIZE
-2.00		0.00	0.00					
-1.50	0.00	.01	.03	0.00		0.00		-1.00
-1.00	.04	.62	.05	.01	0.00	.01		-1.00
-.50	.19	.83	.09	.01	.01	.07		-.50
0.00	.47	.87	.12	.05	.04	.14	3.66	0.00
.50	1.01	.22	.22	.28	.06	.00	.02	.50
1.00	2.07	1.33	.01	1.15	.02	1.05	.16	1.00
1.50	24.06	11.36	7.00	13.07	0.00	10.84	.05	1.50
2.00	91.07	82.01	87.00	00.10	83.05	82.36	76.00	2.00
2.50	96.93	97.05	94.33	99.26	99.49	97.92	93.04	2.50
3.00	99.98	99.00	99.32	99.81	99.57	99.88	99.32	3.00
3.50	100.00	100.00	99.93	99.94	99.91	99.96	99.98	3.50
4.00			99.97	99.99	99.99	99.97	99.99	4.00
4.50			100.00	100.00	100.00	100.00	100.00	4.50

MOMENT STATISTICS

MEAN SIZE	1.00	MEAN SIZE 1.20	MEAN SIZE 1.18	MEAN SIZE 1.74	MEAN SIZE 1.01	MEAN SIZE 1.79	MEAN SIZE 1.94
STANDARD DEVIATION	.83	STANDARD DEVIATION .85	STANDARD DEVIATION .41	STANDARD DEVIATION .34	STANDARD DEVIATION .34	STANDARD DEVIATION .36	STANDARD DEVIATION .33
SKEWNESS	-1.02	SKEWNESS -.10	SKEWNESS -.01	SKEWNESS .14	SKEWNESS .04	SKEWNESS -.10	SKEWNESS 1.10
KURTOSIS	9.32	KURTOSIS 6.02	KURTOSIS 7.00	KURTOSIS 6.90	KURTOSIS 7.71	KURTOSIS 6.71	KURTOSIS 6.3
PERCENT GRAVELS	.0%	.0%	.05	.01	0.00	.01	0.00
PERCENT SAND	99.0%	99.0%	99.92	99.9%	99.9%	99.9%	99.9%
PERCENT SILT AND CLAY	1.0%	0.00	.03	.0%	.0%	.03	.1%

Noel Bay Bar (cont'd)

	29	30	31	32	33	34	35	
SIEVE SIZE	CUMULATIVE PERCENT							SIEVE SIZE
-2.00				0.00	0.00		0.00	-2.00
-1.50	0.00	0.10		.02	.01	0.00	.01	-1.50
-1.00	.06	.01		.06	.01	.04	.12	-1.00
-.50	.11	.04	0.00	.13	.04	.10	.20	-.50
0.00	.26	.14	.01	.20	.06	.34	.34	0.00
.50	.56	.36	.01	.08	.22	.73	.61	.50
1.00	2.03	1.04	.11	2.77	1.23	1.00	1.23	1.00
1.50	10.03	6.27	3.02	10.01	11.20	9.25	17.50	1.50
2.00	60.50	72.15	72.20	58.97	62.06	70.38	62.84	2.00
2.50	90.81	96.02	96.16	96.79	97.71	96.00	97.72	2.50
3.00	99.00	99.79	99.02	99.08	99.74	99.50	99.77	3.00
3.50	99.94	99.94	99.93	99.93	99.96	99.91	99.93	3.50
4.00	99.98	99.97	99.97	99.98	99.99	99.97	99.98	4.00
4.50	100.00	100.00	100.00	100.00	100.00	100.00	100.00	4.50

MOMENT STATISTICS

	MEAN SIZE 1.73	MEAN SIZE 1.62	MEAN SIZE 1.69	MEAN SIZE 1.69	MEAN SIZE 1.79	MEAN SIZE 1.61	MEAN SIZE 1.76
	STANDARD DEVIATION .37	STANDARD DEVIATION .37	STANDARD DEVIATION .36	STANDARD DEVIATION .37	STANDARD DEVIATION .36	STANDARD DEVIATION .38	STANDARD DEVIATION .39
	SKEWNESS -.06	SKEWNESS -.24	SKEWNESS .06	SKEWNESS -.06	SKEWNESS -.01	SKEWNESS -.03	SKEWNESS -.73
	KURTOSIS 3.70	KURTOSIS 7.61	KURTOSIS 5.15	KURTOSIS 11.16	KURTOSIS 7.22	KURTOSIS 18.38	KURTOSIS 11.39
PERCENT GRANULE	.04	.01	0.00	.04	.01	.04	.12
PERCENT SAND	99.96	99.99	99.97	99.96	99.98	99.91	99.84
PERCENT SILT AND CLAY	.02	.03	.03	.04	.01	.03	.04

	36	37	38	39	40	41	42	
SIEVE SIZE	CUMULATIVE PERCENT							SIEVE SIZE
-2.00			0.01					
-1.50	0.00	0.00	.10	0.00	0.00		0.00	-1.50
-1.00	.01	.03	.32	.02	.07		.02	-1.00
-.50	.01	.21	.92	.03	.27		.07	-.50
0.00	.04	.53	.71	.05	.68	0.00	.16	0.00
.50	.31	.96	1.69	.10	1.08	.03	.35	.50
1.00	.99	1.89	2.85	.57	0.78	.39	.99	1.00
1.50	9.27	10.22	19.96	6.82	00.00	00.33	1.03	1.50
2.00	60.02	65.07	68.08	99.04	97.33	91.97	99.33	2.00
2.50	90.00	97.36	98.07	97.04	97.04	97.09	98.00	2.50
3.00	99.70	99.00	99.79	99.00	99.72	99.04	99.59	3.00
3.50	99.94	99.96	99.96	99.99	99.94	99.99	99.87	3.50
4.00	99.99	99.99	99.98	99.99	99.97	100.00	99.97	4.00
4.50	100.00	100.00	100.00	100.00	100.00		100.00	4.50

MOMENT STATISTICS

	MEAN SIZE 1.68	MEAN SIZE 1.77	MEAN SIZE 1.66	MEAN SIZE 1.70	MEAN SIZE 1.66	MEAN SIZE 1.66	MEAN SIZE 1.76
	STANDARD DEVIATION .36	STANDARD DEVIATION .36	STANDARD DEVIATION .36	STANDARD DEVIATION .33	STANDARD DEVIATION .30	STANDARD DEVIATION .36	STANDARD DEVIATION .36
	SKEWNESS -.36	SKEWNESS -.69	SKEWNESS -.04	SKEWNESS -.04	SKEWNESS -	SKEWNESS .01	SKEWNESS -.3
	KURTOSIS 12.06	KURTOSIS 10.96	KURTOSIS 10.96	KURTOSIS 9.72	KURTOSIS 7.29	KURTOSIS 7.61	KURTOSIS 7.1
PERCENT GRANULE	.01	.01	.02	.02	.01	.01	.01
PERCENT SAND	99.99	99.99	99.98	99.98	99.98	99.91	99.9
PERCENT SILT AND CLAY	.00	.03	.02	.01	.01	.07	.1

Noel Bay Bar (cont'd)

43	44	45	46	47☆	48	49☆
CUMULATIVE PERCENT						SIEVE SIZE
	0.00				0.00	-3.00
	.05	0.00	0.00		10.11	-2.00
	.09	.48	1.06		39.08	-1.50
	.05	.57	1.57		90.33	-1.00
0.00	.11	.65	2.04		93.07	-.50
.01	.23	.08	2.63		96.83	0.00	
.01	.58	1.53	4.86		98.02	.50
.16	1.36	4.34	10.13		99.29	1.00
12.00	10.11	10.37	23.76		99.86	1.50
89.93	63.36	67.77	98.59		99.98	2.00
97.84	97.84	93.11	99.83		99.99	2.50
99.88	99.83	98.96	99.97		99.99	3.00
100.00	99.99	99.88	99.91		99.99	3.50
	99.99	99.99	99.97		99.99	4.00
	100.00	100.00	100.00		100.00	4.50
STATS						
MEAN SIZE 1.78	MEAN SIZE 1.76	MEAN SIZE 1.84	MEAN SIZE 1.97		MEAN SIZE -.00	
STANDARD DEVIATION .38	STANDARD DEVIATION .37	STANDARD DEVIATION .57	STANDARD DEVIATION .63		STANDARD DEVIATION 2.31	
SKEWNESS .00	SKEWNESS -.73	SKEWNESS -1.51	SKEWNESS -1.92	GRAVEL	SKEWNESS .29	GRAVEL
KURTOSIS 9.00	KURTOSIS 14.53	KURTOSIS 10.91	KURTOSIS 11.00	ONLY	KURTOSIS 1.54	ONLY
GRAVELS 0.00	.05	.57	1.97		51.00	
SAND 100.00	99.94	99.87	98.06		47.77	
SILT AND CLAY 0.00	.01	.05	.03		.22	

50	51	52	53	54☆	55	56	57
CUMULATIVE PERCENT							SIEVE SIZE
				32.05			
				32.05			0.00 -3.50
				32.05			77.00 -3.00
				32.05			76.01 -2.50
	0.00	0.00	0.00	32.05		0.00	76.00 -2.00
0.00	.20	.02	.04	44.16		.07	80.06 -1.50
.02	.09	.03	.03	98.89		.24	81.00 -1.00
.13	.01	.03	.79	99.18		.51	82.05 -.50
.24	.07	.16	1.09	98.24	0.00	.00	84.75 0.00
.02	2.23	.01	2.06	99.16	.02	1.74	88.20 .50
9.05	7.05	9.06	9.39	63.01	.19	.01	93.07 1.00
35.02	99.02	38.74	14.99	99.97	.72	17.32	99.19 1.50
21.01	91.78	79.06	77.00	99.21	1.00	96.12	99.87 2.00
1.07	93.19	97.05	97.18	99.36	1.00	97.07	99.81 2.50
99.26	99.07	99.96	99.08	99.18	1.00	99.02	99.95 3.00
99.81	99.19	99.02	99.96	99.02	1.00	99.14	99.95 3.50
99.91	99.97	99.99	100.00	99.51	1.00	99.96	99.99 4.00
100.00	100.00	100.00		100.00	1.00	100.00	100.00 4.50
STATS							
MEAN SIZE 2.19	MEAN SIZE 1.98	MEAN SIZE 1.97	MEAN SIZE 1.78		MEAN SIZE 2.36	MEAN SIZE 1.00	MEAN SIZE -1.00
STANDARD DEVIATION .61	STANDARD DEVIATION .00	STANDARD DEVIATION .00	STANDARD DEVIATION .62		STANDARD DEVIATION .63	STANDARD DEVIATION .00	STANDARD DEVIATION 1.00
SKEWNESS -1.00	SKEWNESS -1.00	SKEWNESS -.07	SKEWNESS -2.01		SKEWNESS .28	SKEWNESS -1.02	SKEWNESS 0.00
KURTOSIS .00	KURTOSIS 10.01	KURTOSIS 8.11	KURTOSIS 15.09		KURTOSIS .22	KURTOSIS 10.07	KURTOSIS .00
GRAVELS .32	.30	.03	.03	98.84	.00	.24	0.00
SAND 99.61	99.62	99.97	99.37	.00	99.92	99.76	100.00
SILT AND CLAY .07	.08	.00	0.38	.00	.00	.00	.00

moment statistics cannot be computed, distribution too open ended at coarse tail.
incomplete grab sample

EAST NOEL BAR

SIEVE SIZE	1a CUMULATIVE PERCENT	1b	1c	1d	1e	SIEVE SIZE
-3.50	0.00					-3.00
-3.00	1.00		0.00			-2.50
-2.50	2.10	0.00	.07			-2.00
-2.00	2.00	.02	.29	0.00	0.00	-1.50
-1.50	2.00	.00	.37	.04	.04	-1.00
-1.00	2.99	.05	.09	.10	.09	-.50
-.50	3.33	.5.	.62	.38	.19	0.00
0.00	3.50	.59	.79	.39	.38	.50
.50	3.97	.96	1.19	.64	.52	1.00
1.00	4.01	1.30	2.31	1.09	1.19	1.50
1.50	7.02	4.73	8.04	7.76	7.32	2.00
2.00	54.00	23.22	74.94	62.92	61.94	2.50
2.50	84.59	99.07	99.78	99.59	92.36	3.00
3.00	97.00	99.00	99.87	99.88	98.75	3.50
3.50	99.35	99.91	99.94	99.76	99.74	4.00
4.00	99.76	99.96	99.92	99.87	99.89	4.50
4.50	100.00	100.00	100.00	100.00	100.00	5.00

MOMENT STATISTICS

	1a	1b	1c	1d	1e
MEAN SIZE	1.00	2.92	1.03	1.00	1.04
STANDARD DEVIATION	.96	.08	.99	.00	.00
SKEWNESS	-1.08	-1.20	-2.08	-.01	-.26
KURTOSIS	14.23	29.99	26.37	12.50	8.73
PERCENT GRANULE	2.95	.05	.09	.10	.09
PERCENT SAND	99.78	99.93	99.93	99.78	99.88
PERCENT SILT AND CLAY	.26	.06	.08	.13	.11

SIEVE SIZE	2a CUMULATIVE PERCENT	2b	2c	2d	2e	SIEVE SIZE
-2.00	0.03		0.00			-2.00
-1.50	.05	0.00	.01	0.00	0.00	-1.50
-1.00	.07	.01	.03	.04	.04	-1.00
-.50	.12	.04	.23	.14	.07	-.50
0.00	.16	.15	.38	.32	.16	0.00
.50	.21	.36	.53	.67	.34	.50
1.00	.73	.84	1.94	2.85	.93	1.00
1.50	6.73	12.40	14.01	17.48	11.75	1.50
2.00	78.00	99.04	68.37	68.49	77.00	2.00
2.50	93.14	99.93	97.23	96.98	99.67	2.50
3.00	98.72	99.91	99.81	99.91	99.82	3.00
3.50	99.76	99.97	99.97	99.93	99.98	3.50
4.00	99.98	99.99	99.98	99.96	99.91	4.00
4.50	100.00	100.00	100.00	100.00	100.00	4.50

MOMENT STATISTICS

	2a	2b	2c	2d	2e
MEAN SIZE	1.00	1.03	1.77	1.77	1.03
STANDARD DEVIATION	.93	.06	.92	.92	.91
SKEWNESS	.20	.29	-.78	-.29	.22
KURTOSIS	6.93	6.98	12.20	8.59	7.05
PERCENT GRANULE	.07	.01	.15	.06	.06
PERCENT SAND	99.83	99.93	99.78	99.87	99.91
PERCENT SILT AND CLAY	.10	.06	.07	.08	.03

East Noel Bar (cont'd)

3a	3b	3c	3d	3e	3f
SIEVE SIZE	CUMULATIVE PERCENT				
-3.50		0.00			0.00
-3.00		1.16			.03
-2.50	.00	1.00		0.00	1.12
-2.00	.1	1.00	.00	.00	1.00
-1.50	.1.	2.00	.00	.00	2.10
-1.00	.03	2.00	.00	.00	2.97
-.50	.07.	2.07	.00	.00	4.33
0.00	1.7.	2.22	.02	1.10	39.95
.50	2.58	2.22	5.40	7.00	11.09
1.00	10.10	47.20	82.03	21.7.	72.10
1.50	90.01	63.00	99.00	62.00	90.62
2.00	91.20	90.00	99.78	1.00	97.00
2.50	99.05	99.09	99.95	99.00	99.78
3.00	99.00	99.09	99.00	99.00	99.92
3.50	99.00	99.00	99.97	99.00	99.96
4.00	99.92	99.00	99.00	99.00	99.99
4.50	100.00	100.00	100.00	100.00	100.00

MOMENT STATISTICS					
MEAN SIZE	1.02	1.03	1.23	1.2.	1.
STANDARD DEVIATION	.07	.03	.00	.00	.00
SKEWNESS	-.06	-.01	-3.30	-.35	-1.1.
KURTOSIS	6.33	9.10	28.78	6.01	9.27
PERCENT GRANULES	.10	.02	.04	.21	.04
PERCENT SAND	99.90	99.99	97.92	99.77	99.96
PERCENT SILT AND CLAY	.00	.10	.13	.00	.00

3g	3h	3i	4a	4b	4c
SIEVE SIZE	CUMULATIVE PERCENT				
-3.50	0.00	0.00			
-3.00	.06	.00			
-2.50	.06	.79.			
-2.00	.16	1.20			
-1.50	.36	1.73			
-1.00	.00	2.20			
-.50	1.32	3.10			
0.00	3.20	3.22			
.50	3.72	3.31			
1.00	90.90	70.01			
1.50	99.00	97.10			
2.00	99.00	99.00			
2.50	99.00	99.00			
3.00	99.00	99.00			
3.50	99.00	99.00			
4.00	100.00	100.00			

MOMENT STATISTICS					
MEAN SIZE	1.16	1.02	1.38	2.09	1.0.
STANDARD DEVIATION	.13	.11	.02	.00	.01
SKEWNESS	-.70	-1.73	-1.11	.10	.10
KURTOSIS	6.87	1.00	1.00	9.23	9.1.
PERCENT GRANULES	.06	.03	2.20	8.31	.04
PERCENT SAND	99.32	99.00	99.00	99.00	99.00
PERCENT SILT AND CLAY	.04	.12	.11	.10	.10

East Noel Bar (cont'd)

4d	4e	4f	4g	4h	
SIEVE SIZE CUMULATIVE PERCENT					SIEVE SIZE
-2.00	0.00	0.00	0.00	0.00	-2.00
-1.50	0.00	.00	.00	.00	-1.50
-1.00	.03	.03	.10	.11	-1.00
-.50	.06	.07	.26	.27	-.50
0.00	.13	.23	.75	1.11	0.00
.50	.24	.66	1.77	3.21	.50
1.00	.89	1.08	3.81	5.80	1.00
1.50	6.49	10.06	12.62	20.15	1.50
2.00	49.24	63.16	69.86	81.53	2.00
2.50	96.49	96.86	96.73	98.91	2.50
3.00	99.06	99.79	99.01	99.55	3.00
3.50	99.81	99.94	99.92	99.86	3.50
4.00	99.96	99.98	99.98	99.91	4.00
4.50	100.00	100.00	100.00	100.00	4.50

MOMENT STATISTICS

MEAN SIZE 1.02	MEAN SIZE 1.77	MEAN SIZE 1.75	MEAN SIZE 1.73	MEAN SIZE 1.77
STANDARD DEVIATION .37	STANDARD DEVIATION .45	STANDARD DEVIATION .36	STANDARD DEVIATION .46	STANDARD DEVIATION .41
SKEWNESS .19	SKEWNESS -2.86	SKEWNESS -1.66	SKEWNESS -2.48	SKEWNESS -.01
KURTOSIS 9.17	KURTOSIS 27.99	KURTOSIS 16.76	KURTOSIS 19.38	KURTOSIS 13.48
PERCENT GRAVELS .01	.04	.16	.57	.33
PERCENT SAND 99.91	99.35	99.79	99.37	99.46
PERCENT SILT AND CLAY .08	.61	.04	.07	.09

5a	5b	5c	5d	5e	5f	
SIEVE SIZE CUMULATIVE PERCENT						SIEVE SIZE
-2.00	0.00	0.00			0.00	-2.00
-1.50	.07	.03	0.00	.04	.04	-1.50
-1.00	.26	.06	.08	.21	.11	-1.00
-.50	.63	.23	.18	.23	.22	-.50
0.00	.93	.91	.14	.25	.36	0.00
.50	.73	.76	.26	.27	.67	.50
1.00	1.31	1.00	.76	.06	.92	1.00
1.50	2.03	2.26	1.94	2.03	3.29	1.50
2.00	24.29	28.33	24.56	29.99	48.07	2.00
2.50	96.98	96.21	92.01	96.29	96.36	2.50
3.00	99.80	99.20	99.80	98.53	99.66	3.00
3.50	99.96	99.76	99.85	99.84	99.89	3.50
4.00	99.99	99.95	99.98	99.96	99.91	4.00
4.50	100.00	100.00	100.00	100.00	100.00	4.50

MOMENT STATISTICS

MEAN SIZE 1.00	MEAN SIZE 1.00	MEAN SIZE 1.00	MEAN SIZE 1.00	MEAN SIZE 1.00	MEAN SIZE 1.00
STANDARD DEVIATION .41	STANDARD DEVIATION .43	STANDARD DEVIATION .38	STANDARD DEVIATION .44	STANDARD DEVIATION .37	STANDARD DEVIATION .41
SKEWNESS -1.76	SKEWNESS -.32	SKEWNESS -.05	SKEWNESS -.20	SKEWNESS .01	SKEWNESS -.27
KURTOSIS 17.08	KURTOSIS 11.37	KURTOSIS 7.02	KURTOSIS 13.07	KURTOSIS 5.04	KURTOSIS 12.20
PERCENT GRAVELS .25	.05	.01	.21	.11	.11
PERCENT SAND 99.71	99.77	99.84	99.74	99.85	99.85
PERCENT SILT AND CLAY .03	.18	.07	.04	.04	.03

East Noel Bar (cont'd)

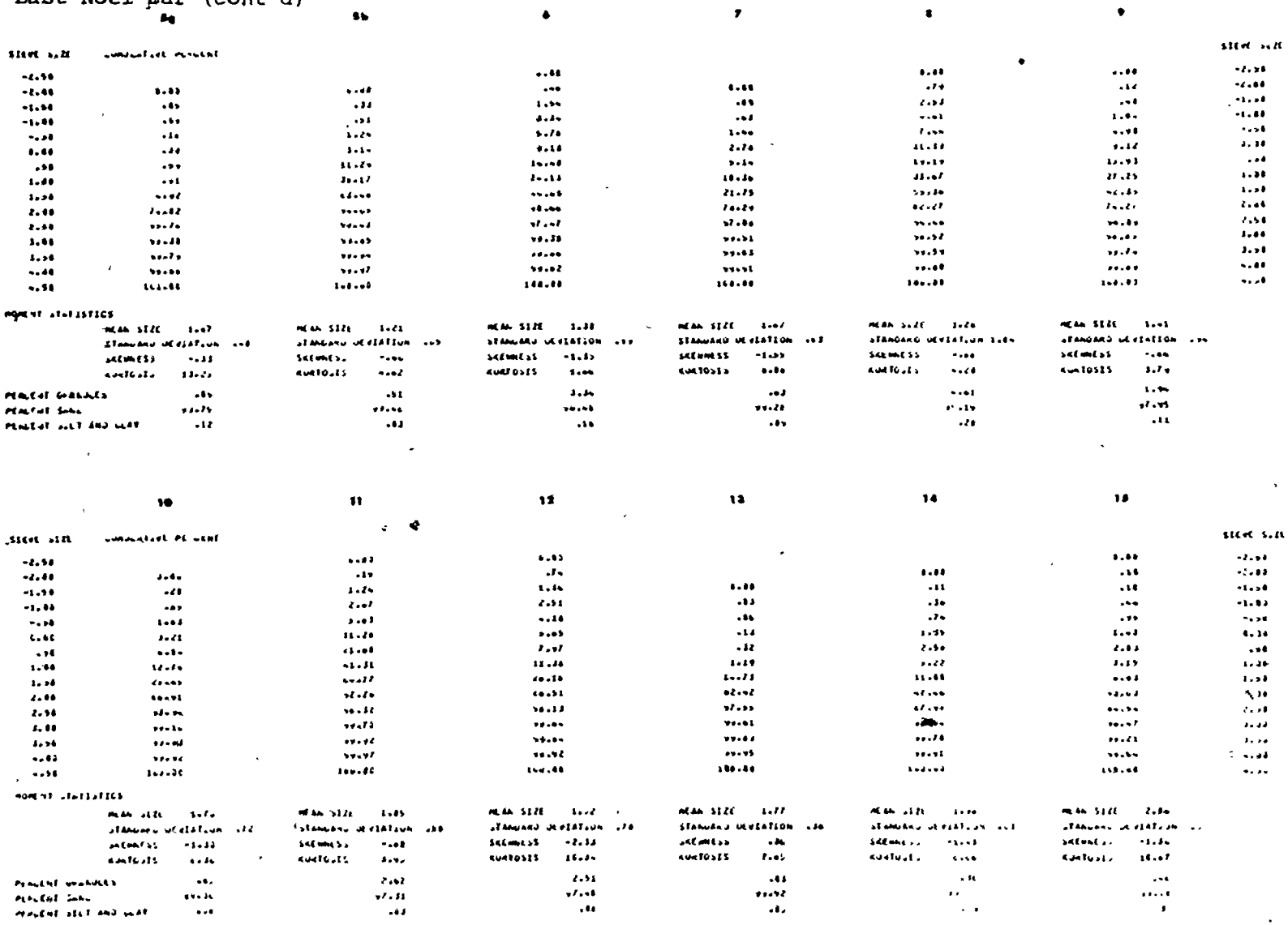

East Noel Bar (cont'd)

	16	17	18	19	20	21
SIEVE SIZE	CUMULATIVE PERCENT					
-5.00	0.00					
-2.50	.27					
-2.00	.27	0.00	0.00	0.00	0.00	0.00
-1.50	.27	.04	.15	.16	.29	.59
-1.00	.42	.03	.01	.24	.07	1.04
-.50	.55	.99	2.02	.58	5.38	2.53
0.00	1.04	1.52	3.76	.99	2.11	5.21
.50	2.55	2.99	9.99	1.13	3.73	9.05
1.00	12.07	11.13	9.17	9.19	8.08	17.29
1.50	41.35	6.99	19.36	23.09	12.99	33.99
2.00	83.18	83.00	99.12	88.38	21.03	91.04
2.50	97.98	97.07	98.19	97.35	93.19	99.59
3.00	99.49	99.99	99.92	99.59	99.37	99.73
3.50	99.79	99.78	99.99	99.79	99.87	99.99
4.00	99.86	99.99	99.99	99.89	99.99	99.99
4.50	100.00	100.00	100.00	100.00	100.00	100.00

MOMENT STATISTICS

MEAN SIZE	1.99	1.50	1.00	1.71	1.07
STANDARD DEVIATION	.77	.99	.93	.98	.93
SKEWNESS	-1.71	-1.11	-2.23	-1.84	-1.65
KURTOSIS	11.06	9.04	11.97	11.12	9.04
PERCENT GRAVELS	.02	.03	.01	.04	.03
PERCENT SAND	99.99	99.21	99.31	99.95	99.31
PERCENT SILT AND CLAY	.14	.11	.08	.11	.64

	22
SIEVE SIZE	
-5.00	0.00
-2.50	.33
-2.00	1.68
-1.50	2.32
-1.00	5.53
-.50	9.05
0.00	17.29
.50	33.99
1.00	91.04
1.50	99.59
2.00	99.73
2.50	99.99
3.00	99.99
3.50	100.00
4.00	100.00

oel Shore Bar

	1	2	3	4	5	6	7	
SIEVE SIZE	CUMULATIVE PERCENT							SIEVE SIZE
-2.00	0.00		0.00					-2.00
-2.00	.00	0.00	.32	0.00	0.00	0.00	0.00	-2.00
-1.50	.00	.20	.71	.33	.02	.10	.07	-1.50
-1.00	.75	.20	.00	.20	.03	.30	.00	-1.00
-.50	.00	.27	1.02	.77	.06	.59	1.02	-.50
0.00	1.00	.20	1.31	1.39	.07	1.15	1.01	0.00
.50	1.07	.20	2.33	3.23	.13	2.00	.07	.50
1.00	0.91	1.00	0.02	0.73	1.05	13.12	13.10	1.00
1.50	27.79	00.01	79.00	67.59	76.70	05.70	01.02	1.50
2.00	90.02	01.00	00.00	91.50	93.05	90.00	99.02	2.00
2.50	99.00	00.01	00.03	97.70	97.23	97.03	00.00	2.50
3.00	99.97	00.02	00.70	00.33	00.50	00.02	00.00	3.00
3.50	00.00	100.00	00.05	00.70	00.01	00 00	00.00	3.50
4.00	100.00		00.00	00.03	00.00	00.00	00.03	4.00
4.50			100.00	100.00	100.00	100.00	100.00	4.50

MOMENT STATISTICS

	MEAN SIZE 1.01	MEAN SIZE 1.00	MEAN SIZE 1.31	MEAN SIZE 1.20	MEAN SIZE 1.13	MEAN SIZE 1.20	MEAN SIZE .07
	STANDARD DEVIATION .00	STANDARD DEVIATION .00	STANDARD DEVIATION .00	STANDARD DEVIATION .00	STANDARD DEVIATION .00	STANDARD DEVIATION .00	STANDARD DEVIATION .00
	SKEWNESS -2.02	SKEWNESS -3.23	SKEWNESS -3.06	SKEWNESS -.22	SKEWNESS .00	SKEWNESS 1.60	SKEWNESS .00
	KURTOSIS 21.20	KURTOSIS 12.00	KURTOSIS 17.00	KURTOSIS 0.00	KURTOSIS 3.00	KURTOSIS 10.02	KURTOSIS 3.00
PERCENT GRAVEL	.00	.00	.00	.00	.00	.00	.00
PERCENT SAND	99.00	99.00	99.35	99.00	99.00	99.20	00.00
PERCENT MUD AND CLAY	0.00	0.00	.02	.10	.00	.00	.01

	8	9	10	11	12	13	14	
SIEVE SIZE	CUMULATIVE PERCENT							SIEVE SIZE
-2.00	0.00	0.00	0.00			0.00		-2.00
-1.50	.00	.00	.00		0.00	00		-1.50
-1.00	.00	.00	.00	0.00	.00	.12		-1.00
-.50	.01	.00	.00	.01	.00	.22		-.50
0.00	1.01	.00	.00	.01	.10	.93	0.00	0.00
.50	.00	0.00	0.00	.00	.00	1.07	.03	.00
1.00	0.07	.03	11.00	1.00	0.10	10.50	1.02	1.00
1.50	00.07	00.03	00.00	22.07	00.71	01.00	10.00	1.50
2.00	01.00	00.07	00.01	00.10	00.00	00.00	00.71	2.00
2.50	00.02	00.00	07.77	00.00	00.00	07.00	07.00	2.50
3.00	00.00	00.00	00.01	00.07	00.20	00.00	00 70	3.00
3.50	00.77	00.00	00.00	00.00	00.00	00.00	00 00	3.50
4.00	00.00	00.00	00.00	100.00	00.00	00 07	100 00	4.00
4.50	100.00	100.00	100.00		100.00	100 00		4.50

MOMENT STATISTICS

	MEAN SIZE 1.00	MEAN SIZE 1.02	MEAN SIZE 1.00	MEAN SIZE 1.71	MEAN SIZE 1.20	MEAN SIZE 1.00	MEAN SIZE .00
	STANDARD DEVIATION .00	STANDARD DEVIATION .00	STANDARD DEVIATION .00	STANDARD DEVIATION .00	STANDARD DEVIATION .00	STANDARD DEVIATION .00	STANDARD DEVIATION .00
	SKEWNESS .00	SKEWNESS .01	SKEWNESS .00	SKEWNESS .00	SKEWNESS .00	SKEWNESS .01	SKEWNESS .00
	KURTOSIS .00	KURTOSIS 13.00	KURTOSIS 10.00	KURTOSIS .00	KURTOSIS 17.00	KURTOSIS .00	KURTOSIS .00
PERCENT GRAVEL	.00	.00	.00	0.00	.00	.00	.00
PERCENT SAND	99.00	99.00	99.00	100.00	99.00	99.07	100.00
PERCENT MUD AND CLAY	.00	.00	.00	.00	.00	.01	.00

...el Shore Bar (cont'd)

	15	16	17	18	19	20	21	
SIEVE SIZE	CUMULATIVE PERCENT							SIEVE SIZE
+2.00	0.00	0.00	0.00	0.00			1.21	-2.00
+1.50	.01	.02	.10	.39	0.00		.04	-1.50
+1.00	.04	.04	.21	1.25	.01		.10	-1.00
+.50	.21	.11	.24	2.23	.01	0.00	.29	-.50
0.00	.59	.25	.37	4.84	.02	.01	.44	0.00
+.50	1.04	.44	1.11	7.47	.04	.04	1.73	.50
1.00	12.78	4.97	10.13	17.00	1.74	.17	11.44	1.00
1.50	87.31	69.50	77.87	40.24	23.05	12.79	42.44	1.50
2.00	99.71	92.27	90.[illegible]	48.38	64.00	84.17	84.87	2.00
2.50	99.88	99.19	[illegible]2	99.52	97.54	97.44	98.44	2.50
3.00	99.91	99.58	99.69	99.84	99.78	99.71	99.82	3.00
3.50	99.91	99.89	99.90	99.88	99.89	99.98	99.97	3.50
4.00	99.96	99.93	99.96	99.97	99.99	99.97	99.93	4.00
4.50	100.00	100.00	100.00	100.00	100.00	100.00	100.00	4.50
MOMENT STATISTICS								
	MEAN SIZE 1.27	MEAN SIZE 1.04	MEAN SIZE 1.33	MEAN SIZE 1.06	MEAN SIZE 1.71	MEAN SIZE 1.78	MEAN SIZE 1.01	
	STANDARD DEVIATION .43	STANDARD DEVIATION .43	STANDARD DEVIATION .61	STANDARD DEVIATION .60	STANDARD DEVIATION .34	STANDARD DEVIATION .30	STANDARD DEVIATION .44	
	SKEWNESS 1.17	SKEWNESS .84	SKEWNESS -.27	SKEWNESS -1.30	SKEWNESS .72	SKEWNESS .44	SKEWNESS .17	
	KURTOSIS 12.16	KURTOSIS 8.88	KURTOSIS 11.28	KURTOSIS 7.86	KURTOSIS 4.04	KURTOSIS 4.03	KURTOSIS 4.14	
PERCENT GRANULES	.00	.04	.21	1.21	.01	0.00	.16	
PERCENT SAND	99.08	99.87	99.75	98.73	99.96	99.97	99.81	
PERCENT SILT AND CLAY	.12	.07	.04	.05	.03	.03	.03	

	32	33	34	35	36	37	38	
SIEVE SIZE	CUMULATIVE PERCENT							SIEVE SIZE
+2.00	0.00		0.00		0.00	0.00	1.04	-2.00
+1.50	.01		.01	0.00	.01	.04	.17	-1.50
+1.00	.33	0.00	.01	.04	.03	1.20	.22	-1.00
+.50	.10	.03	.02	.04	.03	2.23	.47	-.50
0.00	.10	.04	.04	.04	.03	3.07	.27	0.00
+.50	.28	.19	.21	.15	.11	7.77	.59	.50
1.00	2.06	3.02	3.08	1.04	1.02	9.03	99.99	1.00
1.50	30.03	20.02	19.05	4.56	22.04	28.81	99.95	1.50
2.00	81.52	96.02	94.98	79.34	87.53	92.97	[illegible]	2.00
2.50	98.21	99.04	98.01	99.06	98.[illegible]	98.77	99.79	2.50
3.00	97.99	99.65	99.23	97.92	99.24	99.93	99.97	3.00
3.50	99.53	99.89	99.84	99.89	99.84	99.94	99.98	3.50
4.00	99.84	99.94	99.84	99.97	99.92	99.92	99.98	4.00
4.50	100.00	100.00	100.00	100.00	100.00	100.00	100.00	4.50
MOMENT STATISTICS								
	MEAN SIZE 1.09	MEAN SIZE 1.08	MEAN SIZE 1.04	MEAN SIZE 1.07	MEAN SIZE 1.71	MEAN SIZE 1.42	MEAN SIZE [illegible]	
	STANDARD DEVIATION .18	STANDARD DEVIATION .39	STANDARD DEVIATION .44	STANDARD DEVIATION .41	STANDARD DEVIATION .44	STANDARD DEVIATION .34	STANDARD DEVIATION .44	
	SKEWNESS .48	SKEWNESS .86	SKEWNESS 1.46	SKEWNESS 1.23	SKEWNESS .34	SKEWNESS -1.71	SKEWNESS -.15	
	KURTOSIS 10.21	KURTOSIS 4.44	KURTOSIS 7.44	KURTOSIS 16.34	KURTOSIS .47	KURTOSIS 11.7	KURTOSIS 7.1	
PERCENT GRANULES	.31	.04	.01	.24	.01	1.24	.12	
PERCENT SAND	99.38	99.93	99.93	99.74	99.97	98.76	99.86	
PERCENT SILT AND CLAY	.32	.03	.06	.03	.02	.00	.02	

Noel Shore Bar (cont'd)

SIEVE SIZE	29	30	31	32	33	34	35	SIEVE SIZE
SIEVE SIZE	CUMULATIVE PERCENT							
-2.00	0.00	0.00		0.00	0.00			-2.00
-1.50	.23	.01	0.06	.03	.3-	0.00		-1.50
-1.00	.61	.73	.01	.14	.00	.11	0.00	-1.00
-.50	.85	.92	.02	.16	.50	.4-	.02	-.50
0.00	.00	1.22	.03	.25	.03	.27	.00	0.00
.50	.79	2.10	.22	.00	2.10	1.02	.22	.50
1.00	3.00	0.51	3.50	2.01	0.02	3.00	1.00	1.00
1.00	20.05	54.24	48.13	23.20	+1.00	34.01	24.37	1.50
2.00	80.10	92.00	69.05	87.00	90.00	88.02	91.39	2.00
2.50	90.79	90.00	90.00	90.17	99.15	90.24	99.03	2.50
3.00	99.74	99.77	99.01	99.29	99.00	99.24	99.00	3.00
3.50	99.93	99.92	99.97	99.76	99.97	99.74	99.96	3.50
+.00	99.97	99.98	99.98	99.98	99.99	99.99	99.9	+.00
+.50	100.00	100.00	100.00	100.00	100.00	100.00	100.00	+.50
MOMENT STATISTICS								
	MEAN SIZE 1.03	MEAN SIZE 1.00	MEAN SIZE 1.09	MEAN SIZE 1.09	MEAN SIZE 1.02	MEAN SIZE 1.04	MEAN SIZE 1.02	
	STANDARD DEVIATION .00	STANDARD DEVIATION .01	STANDARD DEVIATION .01	STANDARD DEVIATION .01	STANDARD DEVIATION . 0	STANDARD DEVIATION .07	STANDARD DEVIATION .37	
	SKEWNESS -1.10	SKEWNESS -1.07	SKEWNESS .25	SKEWNESS -.10	SKEWNESS -1.04	SKEWNESS -.27	SKEWNESS .04	
	KURTOSIS 15.01	KURTOSIS 13.72	KURTOSIS 6.36	KURTOSIS 17.12	KURTOSIS 10.20	KURTOSIS 6.03	KURTOSIS 5.04	
PERCENT GRANULES	.01	.79	.01	.14	.00	.13	0.28	
PERCENT SAND	99.00	99.17	99.97	99.78	99.00	99.70	99.01	
PERCENT SILT AND CLAY	.03	.04	.02	.10	.02	.11	.11	

SIEVE SIZE	36	37	38	39	40	41a	41b	SIEVE SIZE
SIEVE SIZE	CUMULATIVE PERCENT							
-2.00		0.03	0.00				0.00	-2.00
-1.50	0.00	.1-	.07	0.00	0.00	0.00	.00	-1.50
-1.00	.00	.10	1.05	.01	.02	.13	.00	-1.00
-.50	.20	.24	1.05	.10	.20	.17	1.01	-.50
0.00	.60	.00	1.35	.20	.20	.20	1.01	0.00
.50	.02	1.24	1.00	.02	.25	1.05	1.05	.50
1.00	1.00	0.04	1.00	.07	.31	2.00	1.00	1.00
1.50	1.00.0	27.62	0.00	1.00	2.00	1.57	7.52	1.50
2.00	43.03	90.50	59.45	61.01	52.75	10.00	27.00	2.00
2.50	97.00	98.02	92.07	97.10	92.02	69.74	82.90	2.50
3.00	99.00	99.73	99.24	99.30	99.00	93.03	91.01	3.00
3.50	99.03	99.99	99.05	99.03	99.04	96.75	99.07	3.50
+.00	99.02	99.98	99.94	99.92	99.90	97.19	99.07	+.00
+.50	100.00	100.00	100.00	100.00	100.00	99.20	99.29	+.50
						100.00	100.00	5.00
MOMENT STATISTICS								
	MEAN SIZE 1.00	MEAN SIZE 1.00	MEAN SIZE 1.00	MEAN SIZE 1.70	MEAN SIZE 1.01	MEAN SIZE 1.20	MEAN SIZE 1.1	
	STANDARD DEVIATION .01	STANDARD DEVIATION .00	STANDARD DEVIATION .0	STANDARD DEVIATION .39	STANDARD DEVIATION .01	STANDARD DEVIATION .23	STANDARD DEVIATION .00	
	SKEWNESS -.00	SKEWNESS -3.33	SKEWNESS .17	SKEWNESS -.01	SKEWNESS -.01	SKEWNESS -.21	SKEWNESS -2.17	
	KURTOSIS 51.00	KURTOSIS 77.01	KURTOSIS 22.07	KURTOSIS 6.32	KURTOSIS 7.00	KURTOSIS 13.00	KURTOSIS 1< 71	
PERCENT GRANULES	.00	.10	1.3	.01	.00	.20	1. 1	
PERCENT SAND	99.00	99.05	98.03	99.96	99.00	99.00	99..	
PERCENT SILT AND CLAY	.00	.02	0.00	.03	.00	.7-	.71	

Noel Shore Bar (cont'd)

SIEVE SIZE	43a CUMULATIVE PERCENT	43b	43	44	45a	45b	46a	SIEVE SIZE
-3.00			0.00			0.03		-2.50
-2.50			.00			.03		-2.00
-2.00			.00			.11	0.03	-1.50
-1.50			.00	0.00	0.00	.11	.06	-1.00
-1.00			.00	.03	.02	.11	.06	-.50
-.50	0.00		.00	.06	.07	.17	.06	0.00
0.00	.01	0.00	.09	.15	.22	.27	.02	.50
.50	.01	.00	.13	.35	1.17	.02	.05	1.00
1.00	.02	.02	.19	1.98	2.00	2.06	.06	1.50
1.50	.04	.04	.50	2.00	2.00	12.17	10.57	2.00
2.00	13.06	57.11	27.00	25.91	51.91	81.77	99.70	2.50
2.50	69.78	98.00	78.03	83.35	87.00	95.03	99.00	3.00
3.00	96.90	99.19	96.05	99.15	98.38	99.07	99.20	3.50
3.50	99.07	99.96	98.93	99.00	99.20	99.02	99.02	4.00
4.00	99.27	99.10	99.00	99.00	99.35	99.00	99.00	4.50
5.00	100.00	100.00	100.00	100.00	100.00	100.00	100.00	5.00
MOMENT STATISTICS								
MEAN SIZE	2.03	2.03	2.22	1.70	1.61	2.16	2.00	MEAN SIZE
STANDARD DEVIATION	.43	.00	.53	.49	.43	.45	.00	STANDARD DEVIATION
SKEWNESS	1.76	1.99	.07	.00	.17	-.21	.00	SKEWNESS
KURTOSIS	10.16	11.80	11.07	6.75	7.72	7.25	6.76	KURTOSIS
PERCENT GRANULES	0.00	0.00	.00	.03	.02	.11	.03	
PERCENT SAND	99.27	99.16	99.92	99.03	99.33	98.69	99.03	
PERCENT SILT AND CLAY	.73	.02	1.00	.02	.05	1.20	.36	

SIEVE SIZE	46b CUMULATIVE PERCENT	47a	47b	48a	48b	49a	49b	SIEVE SIZE
-3.00							0.03	-3.00
-2.50	0.03				2.46		.03	-2.50
-2.00	.01	0.00		0.00	.02		.09	-2.00
-1.50	.03	.00	0.00	.00	.03		.19	-1.50
-1.00	.09	.03	.00	.02	.05	0.00	.32	-1.00
-.50	.38	.03	.01	.06	.10	.01	.00	-.50
0.00	.93	.17	.05	.26	.23	.02	1.09	0.00
.50	3.38	.07	.08	2.22	2.28	.06	2.24	.50
1.00	26.01	9.57	10.01	59.25	31.71	22.00	39.07	1.00
1.50	72.35	49.68	51.01	95.27	78.93	76.32	97.95	1.50
2.00	99.00	89.35	89.00	98.13	92.38	93.13	99.79	2.00
2.50	99.84	99.27	98.58	99.84	98.07	99.67	99.91	2.50
3.00	99.92	99.81	99.12	99.38	97.06	99.87	99.95	3.00
3.50	99.99	99.29	99.58	99.93	98.76	99.91	99.98	3.50
4.00	100.00	100.00	100.00	100.00	100.00	100.00	100.00	4.00
MOMENT STATISTICS								
MEAN SIZE	1.75	2.36	2.31	2.56	1.77	1.76	1.96	
STANDARD DEVIATION	.58	.00	.09	.05	.08	.01	.03	
SKEWNESS	.00	1.31	.03	1.93	1.07	1.33	.21	
KURTOSIS	7.36	8.36	7.89	12.25	6.00	6.37	8.36	
PERCENT GRANULES	.03	.38	0.00	.08	.33	0.06	.14	
PERCENT SAND	99.36	99.24	99.38	99.90	98.73	99.63	99.00	
PERCENT SILT AND CLAY	.61	.71	.78	.01	1.00	.30	.86	

Noel Shore Bar (cont'd)

SIEVE SIZE	S0 CUMULATIVE PERCENT	S1	S2	S3	S4	SIEVE SIZE
-3.00				0.00		-2.50
-2.50				3.32	0.00	-2.00
-2.00			0.00	0.00	1.57	-1.50
-1.50	0.00	0.00	.50	10.14	1.77	-1.00
-1.00	.02	.05	.98	0.00	1.94	-.50
-.50	.14	.19	1.26	2.70	1.99	0.00
0.00	.39	.16	2.20	0.00	2.01	.50
.50	.95	.26	0.77	1.53	0.00	1.00
1.00	3.66	.78	24.35	89.11	25.83	1.50
1.50	61.57	0.00	88.02	97.04	78.27	2.00
2.00	69.27	63.41	94.73	99.20	98.61	2.50
2.50	98.02	93.37	99.32	99.57	99.08	3.00
3.00	99.05	99.21	99.85	99.71	99.66	3.50
3.50	99.96	99.85	99.96	99.75	99.93	4.00
4.00	99.98	99.93	99.98	99.85	99.95	4.50
4.50	100.00	100.00	100.00	100.00	100.00	5.00

MOMENT STATISTICS

	S0	S1	S2	S3	S4
MEAN SIZE	1.00	1.94	1.38	0.02	1.22
STANDARD DEVIATION	.60	.91	.61	1.19	.66
SKEWNESS	-.76	.08	-1.17	.27	-2.03
KURTOSIS	8.35	7.73	7.25	2.81	14.00
PERCENT GRANULES	.02	.05	.98	00.01	1.94
PERCENT SAND	99.94	99.88	99.36	99.00	98.32
PERCENT SILT AND CLAY	.04	.07	.02	.15	.04

SELMA BAR

SIEVE SIZE	[1] a CUMULATIVE PERCENT	[1] b	[1] c	[1] d	[1] e	SIEVE SIZE
[illegible]	[illegible]	[illegible]	[illegible]	[illegible]		[illegible]
[illegible]	[illegible]	[illegible]	[illegible]	[illegible]	[illegible]	[illegible]
[illegible]	[illegible]	[illegible]	[illegible]	[illegible]	[illegible]	[illegible]
[illegible]	[illegible]	[illegible]	[illegible]	[illegible]	[illegible]	[illegible]
[illegible]	[illegible]	[illegible]	[illegible]	[illegible]	[illegible]	[illegible]
[illegible]	[illegible]	[illegible]	[illegible]	[illegible]	[illegible]	[illegible]
[illegible]	[illegible]	[illegible]	[illegible]	[illegible]	[illegible]	[illegible]
[illegible]	[illegible]	[illegible]	[illegible]	[illegible]	[illegible]	[illegible]
[illegible]	[illegible]	[illegible]	[illegible]	[illegible]	[illegible]	[illegible]
[illegible]	[illegible]	[illegible]	[illegible]	[illegible]	[illegible]	[illegible]
[illegible]	[illegible]	[illegible]	[illegible]	[illegible]	[illegible]	[illegible]
[illegible]	[illegible]	[illegible]	[illegible]	[illegible]	[illegible]	[illegible]
[illegible]	[illegible]	[illegible]	[illegible]	[illegible]	[illegible]	[illegible]
[illegible]	[illegible]	[illegible]	[illegible]	[illegible]	[illegible]	[illegible]
[illegible]	[illegible]	[illegible]	[illegible]	[illegible]	[illegible]	[illegible]

MOMENT STATISTICS

	[1] a	[1] b	[1] c	[1] d	[1] e
MEAN SIZE	[illegible]	[illegible]	[illegible]	[illegible]	[illegible]
STANDARD DEVIATION	[illegible]	[illegible]	[illegible]	[illegible]	[illegible]
SKEWNESS	[illegible]	[illegible]	[illegible]	[illegible]	[illegible]
KURTOSIS	[illegible]	[illegible]	[illegible]	[illegible]	[illegible]
PERCENT GRAVEL	[illegible]	[illegible]	[illegible]	[illegible]	[illegible]
PERCENT SAND	[illegible]	[illegible]	[illegible]	[illegible]	[illegible]
PERCENT SILT AND CLAY	[illegible]	[illegible]	[illegible]	[illegible]	[illegible]

SIEVE SIZE	[2] a CUMULATIVE PERCENT	[2] b	[2] c	[2] d	[2] e	SIEVE SIZE
[illegible]	[illegible]					
[illegible]	[illegible]	[illegible]	[illegible]	[illegible]	[illegible]	[illegible]
[illegible]	[illegible]	[illegible]	[illegible]	[illegible]	[illegible]	[illegible]
[illegible]	[illegible]	[illegible]	[illegible]	[illegible]	[illegible]	[illegible]
[illegible]	[illegible]	[illegible]	[illegible]	[illegible]	[illegible]	[illegible]
[illegible]	[illegible]	[illegible]	[illegible]	[illegible]	[illegible]	[illegible]
[illegible]	[illegible]	[illegible]	[illegible]	[illegible]	[illegible]	[illegible]
[illegible]	[illegible]	[illegible]	[illegible]	[illegible]	[illegible]	[illegible]
[illegible]	[illegible]	[illegible]	[illegible]	[illegible]	[illegible]	[illegible]
[illegible]	[illegible]	[illegible]	[illegible]	[illegible]	[illegible]	[illegible]
[illegible]	[illegible]	[illegible]	[illegible]	[illegible]	[illegible]	[illegible]
[illegible]	[illegible]	[illegible]	[illegible]	[illegible]	[illegible]	[illegible]
[illegible]	[illegible]	[illegible]	[illegible]	[illegible]	[illegible]	[illegible]
[illegible]	[illegible]	[illegible]	[illegible]	[illegible]	[illegible]	[illegible]
[illegible]	[illegible]	[illegible]	[illegible]	[illegible]	[illegible]	[illegible]
[illegible]	[illegible]	[illegible]	[illegible]	[illegible]	[illegible]	[illegible]
[illegible]	[illegible]	[illegible]	[illegible]	[illegible]	[illegible]	[illegible]

MOMENT STATISTICS

	[2] a	[2] b	[2] c	[2] d	[2] e
MEAN SIZE	[illegible]	[illegible]	[illegible]	[illegible]	[illegible]
STANDARD DEVIATION	[illegible]	[illegible]	[illegible]	[illegible]	[illegible]
SKEWNESS	[illegible]	[illegible]	[illegible]	[illegible]	[illegible]
KURTOSIS	[illegible]	[illegible]	[illegible]	[illegible]	[illegible]
PERCENT GRAVEL	[illegible]	[illegible]	[illegible]	[illegible]	[illegible]
PERCENT SAND	[illegible]	[illegible]	[illegible]	[illegible]	[illegible]
PERCENT SILT AND CLAY	[illegible]	[illegible]	[illegible]	[illegible]	[illegible]

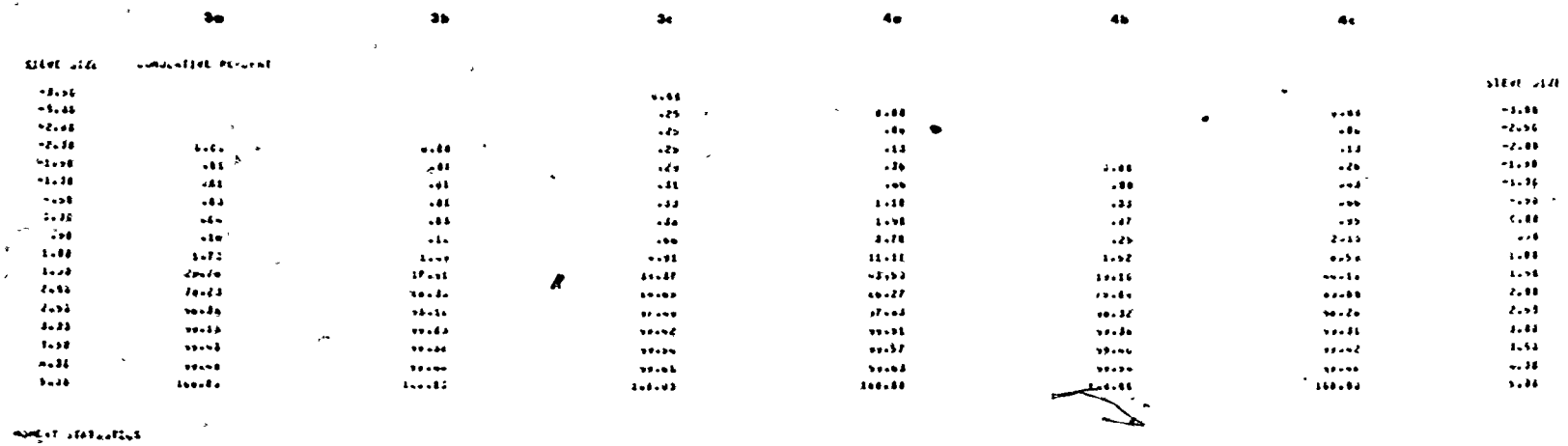

Selma Bar (cont'd)

SIEVE SIZE	3a CUMULATIVE PERCENT	3b	3c	4a	4b	4c	SIEVE SIZE
[illegible]			[illegible]				
[illegible]			.25	0.00		[illegible]	-3.00
[illegible]			.25	.0[illegible]		.06	-2.50
-2.38	0.0[illegible]	0.00	.25	.13		.13	-2.00
[illegible]	.01	.01	.29	.30	[illegible]	.20	-1.50
-1.38	.01	.01	.31	[illegible]	.00	.44	[illegible]
[illegible]	.03	.01	.33	1.10	.33	.66	[illegible]
[illegible]	[illegible]	.05	.36	1.98	.37	.95	0.00
[illegible]	.10	.1[illegible]	.60	3.70	.25	2.13	[illegible]
1.00	1.72	1.[illegible]	[illegible]	11.11	1.52	6.54	1.00
[illegible]	[illegible]	17.[illegible]	[illegible]	[illegible]	1[illegible].16	[illegible]	1.50
[illegible]	70.[illegible]	[illegible]	[illegible]	60.27	[illegible]	[illegible]	2.00
[illegible]	[illegible]	[illegible]	[illegible]	87.0[illegible]	90.32	[illegible]	2.50
[illegible]	[illegible]	[illegible]	[illegible]	[illegible]	[illegible]	[illegible]	3.00
[illegible]	[illegible]	[illegible]	[illegible]	99.57	[illegible]	[illegible]	3.50
[illegible]	[illegible]	[illegible]	[illegible]	[illegible]	[illegible]	[illegible]	[illegible]
[illegible]	100.00	100.0[illegible]	100.03	100.00	100.00	100.00	5.00

MOMENT STATISTICS

	3a	3b	3c	4a	4b	4c
MEAN SIZE	[illegible]	1.90	1.01	1.02	1.03	1.[illegible]
STANDARD DEVIATION	[illegible]	[illegible]	[illegible]	.42	[illegible]	[illegible]
SKEWNESS	1.12	.03	-1.20	[illegible]	[illegible]	[illegible]
KURTOSIS	[illegible]	[illegible]	21.12	10.[illegible]	[illegible]	13.[illegible]
PERCENT GRAVEL	[illegible]	.31	.31	.06	[illegible]	[illegible]
PERCENT SAND	[illegible]	[illegible]	[illegible]	[illegible]	[illegible]	[illegible]
PERCENT SILT AND CLAY	[illegible]	[illegible]	[illegible]	.37	[illegible]	[illegible]

SIEVE SIZE	5a CUMULATIVE PERCENT	5b	5c	5d	SIEVE SIZE
				[illegible]	-3.00
				[illegible]	-2.50
-2.38		0.00	0.03	[illegible]	-2.00
[illegible]	0.0[illegible]	.02	[illegible]	.07	-1.50
-1.38	.01	[illegible]	[illegible]	[illegible]	-1.00
[illegible]	[illegible]	[illegible]	[illegible]	.18	-.50
[illegible]	[illegible]	[illegible]	.39	.12	0.00
[illegible]	.13	[illegible]	[illegible]	.23	.50
1.38	[illegible]	1.51	2.07	1.[illegible]	1.00
[illegible]	7.[illegible]	[illegible]	21.1[illegible]	[illegible]	1.50
[illegible]	[illegible]	[illegible]	60.37	71.25	2.00
[illegible]	[illegible]	[illegible]	92.71	[illegible]	2.50
[illegible]	[illegible]	[illegible]	97.05	[illegible]	3.00
[illegible]	[illegible]	[illegible]	[illegible]	[illegible]	3.50
[illegible]	[illegible]	[illegible]	[illegible]	[illegible]	[illegible]
[illegible]	100.00	100.00	100.00	100.00	5.00

MOMENT STATISTICS

	5a	5b	5c	5d
MEAN SIZE	[illegible]	1.70	1.0[illegible]	1.0[illegible]
STANDARD DEVIATION	[illegible]	[illegible]	[illegible]	.51
SKEWNESS	1.15	.36	1.17	.70
KURTOSIS	[illegible]	[illegible]	[illegible]	12.27

Selma Bar (cont'd)

SIEVE SIZE	6a CUMULATIVE PERCENT	6b	6c	6d	SIEVE SIZE
-∞.00	0.00				-3.50
-3.50	.01		0.00		-3.00
-3.00	.01		.03	0.00	-2.50
-2.50	.01		2.07	.12	-2.00
-2.00	.09		2.07	.36	-1.50
-1.50	.59	0.00	2.07	.78	-1.00
-1.00	.04	.01	3.00	1.17	-.50
-.50	.70	.02	3.12	1.75	0.00
0.00	.91	.04	3.24	2.01	.50
.50	1.1[illegible]	.05	3.95	4.15	1.00
1.00	2.[illegible]	.06	7.02	7.91	1.50
1.50	17.22	9.59	30.26	29.02	2.00
2.00	68.90	68.20	76.21	66.84	2.50
2.50	89.20	88.50	94.72	88.79	3.00
3.00	97.90	98.20	99.06	98.06	3.50
3.50	98.50	99.34	99.63	99.07	4.00
4.00	98.72	99.47	99.69	99.24	4.50
9.00	100.00	100.00	100.00	100.00	5.00

MOMENT STATISTICS

MEAN SIZE	1.09	MEAN SIZE 2.04	MEAN SIZE 1.61	MEAN SIZE 1.73
STANDARD DEVIATION	.72	STANDARD DEVIATION .47	STANDARD DEVIATION .92	STANDARD DEVIATION .76
SKEWNESS	-2.05	SKEWNESS .76	SKEWNESS -2.06	SKEWNESS -1.82
KURTOSIS	28.28	KURTOSIS 7.61	KURTOSIS 15.09	KURTOSIS 8.03
PERCENT GRANULES	.00	.01	3.88	1.17
PERCENT SAND	98.80	99.47	96.09	98.87
PERCENT SILT AND CLAY	1.20	.53	.91	.76

SIEVE SIZE	7a CUMULATIVE PERCENT	7b	7c	7d	7e	SIEVE SIZE
-∞.00		0.00			0.00	-1.00
-2.00		.07	0.00		.01	-1.00
-1.50		.04	.03		.02	-.50
-1.00	.00	.04	.03	0.00	.03	0.00
-.50	.01	.05	.04	.01	.13	.50
0.00	.02	.05	.05	.04	.01	1.00
.50	.05	.03	.06	.21	13.00	1.50
1.00	.37	.11	.08	3.97	64.21	2.00
1.50	10.00	74.00	12.23	90.31	97.01	2.50
2.00	67.02	91.04	78.23	98.84	98.50	3.00
2.50	97.02	98.77	95.[illegible]	99.01	99.07	3.50
3.00	99.35	99.08	98.[illegible]	99.27	99.26	4.00
3.50	99.61	99.29	99.[illegible]	99.36	100.00	5.00
4.00	99.99	99.38	99.48	99.36		
5.00	100.00	100.00	100.00	100.00		

MOMENT STATISTICS

MEAN SIZE	1.79	MEAN SIZE 1.46	MEAN SIZE 1.40	MEAN SIZE 2.05	MEAN SIZE 1.22
STANDARD DEVIATION	.61	STANDARD DEVIATION .63	STANDARD DEVIATION .62	STANDARD DEVIATION .67	STANDARD DEVIATION .8
SKEWNESS	1.62	SKEWNESS 1.23	SKEWNESS 1.63	SKEWNESS 1.82	SKEWNESS 1.26
KURTOSIS	15.69	KURTOSIS 10.76	KURTOSIS 11.36	KURTOSIS 7.00	KURTOSIS 4.22
PERCENT GRANULES	0.00	.04	.33	0.00	.01
PERCENT SAND	99.99	99.36	99.37	99.86	99.11
PERCENT SILT AND CLAY	.01	.62	.06	.04	.88

Selma Bar (cont'd)

SIEVE SIZE	8a CUMULATIVE PERCENT	8b	8c	8d	8e	SIEVE SIZE
-3.00	0.00					
-2.50	.00				0.00	-2.50
-2.00	.00	0.00	0.00	0.00	.02	-2.00
-1.50	.19	.00	.00	.00	.05	-1.50
-1.00	.15	.15	.00	.12	.14	-1.00
-.50	.28	.27	.12	.20	.14	-.50
0.00	.35	.46	.25	.36	.35	0.00
.50	.66	1.59	1.07	1.04	1.20	.50
1.00	2.06	6.78	6.22	5.04	6.52	1.00
1.50	46.50	46.09	47.01	46.58	46.02	1.50
2.00	76.66	96.78	96.25	78.78	76.02	2.00
2.50	99.98	98.05	98.17	93.34	92.16	2.50
3.00	98.95	98.81	99.27	97.76	97.25	3.00
3.50	99.58	99.47	99.37	99.14	97.67	3.50
4.00	99.93	99.92	99.92	98.44	98.16	4.00
5.00	100.00	100.00	100.00	100.00	100.00	5.00

MOMENT STATISTICS

	8a	8b	8c	8d	8e
MEAN SIZE	1.77	1.50	1.58	1.69	1.72
STANDARD DEVIATION	.43	.44	.21	.44	.47
SKEWNESS	.17	.46	.94	1.24	1.28
KURTOSIS	11.02	8.00	18.69	9.06	8.26
PERCENT GRAVELS	.31	.15	.00	.12	.18
PERCENT SAND	99.38	99.66	99.34	98.31	98.80
PERCENT SILT AND CLAY	.31	.00	.00	1.56	1.02

SIEVE SIZE	9a CUMULATIVE PERCENT	9b	9c	SIEVE SIZE
-2.50	0.00		0.00	-2.50
-2.00	.01		.04	-2.00
-1.50	.01		.04	-1.50
-1.00	.01		.00	-1.00
-.50	.01	0.00	.13	-.50
0.00	.04	.02	.16	0.00
.50	.05	.04	.29	.50
1.00	.32	.10	1.49	1.00
1.50	9.10	9.10	30.07	1.50
2.00	50.11	64.37	72.03	2.00
2.50	89.10	98.29	99.14	2.50
3.00	99.20	99.04	99.17	3.00
3.50	99.92	99.36	99.33	3.50
4.00	99.10	99.92	99.91	4.00
5.00	100.00	100.00	100.00	5.00

MOMENT STATISTICS

	9a	9b	9c
MEAN SIZE	2.04	1.97	1.82
STANDARD DEVIATION	.18	.13	.09
SKEWNESS	1.16	1.02	.68
KURTOSIS	8.16	18.89	19.09
PERCENT GRAVELS	.31	.36	.04
PERCENT SAND	99.10	99.62	99.33
PERCENT SILT AND CLAY	.61	.04	.63

CROWE'S FORESHORE

SIEVE SIZE	1	2	3	4	5	6	7	SIEVE SIZE
	CUMULATIVE PERCENT							
-2.50						0.00		-3.50
-2.00						.05		-3.00
-1.50					0.00	.06		-2.50
-1.00				0.00	.01	.06		-2.00
-.50	0.00		0.00	.04	.20	.06		-1.50
0.00	.04	0.00	.04	.16	.67	.06	0.00	-1.00
.50	.07	.00	.05	.25	1.10	.06	.02	-.50
1.00	.14	.01	.06	.41	1.94	.09	.06	0.00
1.50	.26	.04	.12	.65	4.02	.12	.14	.50
2.00	.50	.08	.19	1.22	7.00	.14	.32	1.00
2.50	.85	.28	.32	2.71	14.77	.24	.76	1.50
3.00	2.04	.92	.54	4.87	28.00	.42	2.01	2.00
3.50	10.72	3.04	1.29	9.79	50.14	.74	5.01	2.50
4.00	41.41	12.04	41.15	47.69	78.35	2.07	13.74	3.00
5.00	97.51	42.99	83.00	88.00	94.07	9.21	34.04	3.50
6.00	98.91	67.76	97.65	92.49	98.88	15.00	58.26	4.00
7.00	99.21	89.00	99.15	95.04	99.68	24.00	81.23	5.00
8.00	99.51	94.36	99.69	98.29	99.88	41.00	94.63	6.00
9.00	99.71	97.36	99.85	98.84	99.91	77.15	98.05	7.00
10.00	100.00	100.00	100.00	100.00	100.00	100.00	100.00	10.00

MOMENT STATISTICS

	1	2	3	4	5	6	7
	O	O	MEAN SIZE 3.01	MEAN SIZE 3.12	MEAN SIZE 2.98	O	O
			STANDARD DEVIATION 1.08	STANDARD DEVIATION 1.29	STANDARD DEVIATION 1.08		
			SKEWNESS 2.83	SKEWNESS 3.21	SKEWNESS 2.00		
			KURTOSIS 15.07	KURTOSIS 19.92	KURTOSIS 15.56		
ACENT GRANULES	0.00	3.08	.04	.16	.57	.06	3.05
ACENT SAND	91.31	85.90	83.01	92.20	95.24	13.36	10.26
ACENT SILT AND CLAY	20.69	00.04	16.95	7.61	00.20	00.30	01.00

NOTE: O MOMENT STATISTICS - CAN NOT BE COMPUTED DISTRIBUTION IS OPEN ENDED AT FINE END

APPENDIX III

CURRENT DATA

III.1 CURRENT MEASUREMENTS

The measurement of current velocities (speed and direction) were made at selected locations in Cobequid Bay (Figure 4.1; Table III-1) based on the geographic location and the boundary type so that representative current data could be systematically collected from different parts of the bay and over different bed configurations.

Station positions were marked with 0.4 m diameter fluorescent-coloured spherical buoys. The buoys were moored with sand-filled burlap-bags (filled weight about 50 kg) buried approximately 0.5 m deep on the intertidal sand bars or with two 0.6 m long, three-pronged steel grappling hooks on the subtidal channel beds. Fluorescent flags were attached to several of the buoys to make them easier to locate from a distance. Buoy positions were located by direct sighting during daylight hours. At night, or during foggy weather, buoy positions were found by dead reckoning and with the use of the echo sounder (and a good deal of luck). A small, battery-powered, flashing light was used for night locations when one was available.

Current measurements were made during two scales of time and by two different techniques: (i) vertical velocity profiles measured at a single station at periodic intervals (generally every 15 to 30 minutes) during a complete tidal cycle (i.e., ebb and following flood phase of a cycle); (ii) measurements made periodically at a single height above the bed by automatic recording current meters, to measure the current variations during the lunar cycle (i.e., spring to neap tide differences). The equipment and techniques used for these two types of measurement will be discussed separately.

Velocity Profile Measurements

Vertical velocity profiles were measured during selected tidal cycles at various locations (Figure 4.1; Table III-1) with a Kelvin-

T A B L E III- 1

SUMMARY OF TIDAL CHARACTERISTICS FOR PROFILE MEASUREMENTS

Location[1]	Date	Range[2]			Coefficient[3]		
		Ebb	Flood	Mean	Ebb	Flood	Mean
NOEL BAY BAR							
1A	June 14/71	12.0	11.8	11.9	.745	.732	.739
B	June 18/71	11.6	12.0	11.8	.722	.747	.735
C	July 16/71	11.6	11.9	11.7	.719	.740	.729
D	Aug. 3/72	11.1	11.6	11.3	.690	.719	.704
2A	June 16/71	11.8	11.9	11.9	.734	.742	.738
B	July 14/71	12.4	12.5	12.5	.772	.776	.774
3A	July 3/71	9.5	9.9	9.7	.589	.616	.603
B	July 5/71	9.8	10.4	10.1	.607	.645	.626
C	July 17/71	11.2	11.6	11.4	.694	.720	.707
4	July 12/71	12.7	12.6	12.7	.791	.780	.785
5	July 13/71	12.7	12.6	12.7	.787	.781	.784
6A	July 19/71	10.8	11.4	11.1	.671	.707	.689
B	Aug. 4/72	11.0	11.5	11.3	.681	.715	.698
7	July 23/71	12.0	11.6	11.8	.747	.722	.735
8	July 23/71	12.0	11.6	11.8	.747	.722	.735
EAST NOEL BAR							
1	July 29/71	10.3	10.4	10.4	.639	.648	.643
2	Aug. 1/72	11.8	12.0	11.9	.734	.747	.741
GREAT VILLAGE BAR	Aug. 21/73	11.1	11.5	11.3	.688	.712	.700
CENTRE BAY	July 6/73	11.8	11.7	11.8	.731	.725	.728
MIDDLE CHANNEL	Aug. 1/73	13.1	12.9	13.0	.812	.799	.806

T A B L E III- 1 (Cont'd)

SUMMARY OF TIDAL CHARACTERISTICS FOR PROFILE MEASUREMENTS

Location[1]	Date	Range[2] Ebb	Flood	Mean	Coefficient[3] Ebb	Flood	Mean
NOEL SHORE BAR							
1	Aug. 10/71	13.3	13.3	13.3	.827	.824	.825
2A	Aug. 12/71	12.5	12.6	12.6	.778	.785	.781
B	Aug. 13/71	11.9	12.1	12.0	.736	.751	.743
3	Aug. 14/71	11.1	11.5	11.3	.692	.713	.702
4	Aug. 15/73	11.9	11.8	11.9	.737	.731	.734
5	July 26/73	11.1	11.8	11.5	.688	.731	.709
6	Aug. 17/73	12.0	11.9	12.0	.743	.737	.740
7	Aug. 20/73	11.5	11.8	11.7	.712	.731	.722
8	Aug. 17/71	10.4	10.8	10.6	.643	.673	.658
9	July 23/73	11.1	11.4	11.3	.688	.706	.697
10	July 20/73	11.6	11.6	11.6	.719	.719	.719
11	July 25/73	10.8	11.5	11.2	.669	.712	.691
SELMA BAR							
1A	July 11/72	13.3	12.7	13.0	.823	.789	.806
B	July 18/72	10.3	10.5	10.4	.640	.654	.647
C	June 28/73	11.6	12.5	12.1	.731	.775	.753
D	July 5/73	12.4	12.2	12.3	.768	.756	.762
2A	Aug. 7/71	12.7	12.4	12.6	.787	.770	.779
B	July 13/72	13.0	12.6	12.8	.806	.781	.794
C	July 20/72	9.6	10.0	9.8	.593	.618	.606
D	June 20/73	11.2	11.0	11.1	.694	.681	.688
E	July 3/73	13.4	13.0	13.2	.830	.806	.818
F	July 10/73	9.9	10.4	10.2	.613	.644	.629
3A	July 4/72	11.5	11.7	11.6	.711	.729	.720
B	July 28/72	11.8	12.1	12.0	.734	.751	.743
4A	July 7/72	11.4	12.1	11.8	.709	.752	.730
B	July 22/72	9.7	10.2	10.0	.602	.634	.618
5A	July 6/72	11.3	11.9	11.6	.701	.737	.719

T A B L E III - 1 (Cont'd)

SUMMARY OF TIDAL CHARACTERISTICS FOR PROFILE MEASUREMENTS

Location[1]	Date	Range[2] Ebb	Flood	Mean	Coefficient[3] Ebb	Flood	Mean
SELMA BAR Cont'd.							
5B	July 21/72	9.5	10.0	9.8	.589	.620	.605
C	July 4/73	12.8	12.6	12.7	.793	.781	.787
6A	Aug. 3/71	10.3	9.9	10.1	.639	.612	.625
B	July 12/72	13.2	12.7	13.0	.821	.791	.806
C	July 19/72	9.9	10.2	10.1	.612	.631	.622
D	June 25/73	10.8	11.3	11.1	.669	.700	.684
E	June 27/73	11.3	12.0	11.7	.700	.743	.722
F	July 9/73	10.2	10.5	10.4	.632	.650	.641
7A	July 17/72	10.9	11.0	11.0	.677	.681	.679
B	June 11/73	10.5	10.9	10.7	.650	.675	.663
8A	July 5/72	11.3	11.8	11.6	.703	.730	.716
B	Aug. 13/73	11.3	11.1	11.2	.702	.689	.696
9	Aug. 10/72	12.2	12.4	12.3	.757	.771	.764
10	Aug. 6/71	12.1	11.8	12.0	.751	.732	.741
11	Aug. 2/71	9.3	9.9	9.6	.576	.612	.594
12	Aug. 5/71	11.5	11.1	11.3	.711	.688	.700
13	June 13/73	10.6	11.1	10.9	.659	.688	.672
14	June 19/73	11.3	11.2	11.3	.700	.694	.697
15	June 14/73	10.6	11.1	10.9	.657	.688	.672
16	July 11/73	9.9	10.4	10.2	.613	.644	.629
17	Aug. 14/72	11.3	11.3	11.3	.701	.703	.702
18	Aug. 9/72	12.1	12.5	12.3	.753	.778	.765
19A	July 19/73	11.6	11.5	11.6	.719	.712	.716
B	Aug. 5/73	10.9	11.1	11.0	.675	.688	.681
20A	July 25/72	10.8	11.3	11.1	.668	.704	.686
B	Aug. 15/72	10.7	10.8	10.8	.664	.671	.668

NOTE: 1. Current measurement locations are given in Figure 4.1.
Letters designate repeated measurements at a location.

NOTE: 2. Tidal range is based on information given in the Canadian Tide and Current Tables (C.H.S., 1971, 1972 and 1973).

3. Tidal coefficient is the predicted tidal range^2 divided by the maximum tidal range of 16.1 m (Canadian Tide and Current Tables, C.H.S., 1973). This value is used by some workers as a dimensionless tidal range for the comparison of one area to another (e.g., Allen and Klingebiel, 1969).

Hughes 'direct reading' current meter (Fig. I. 1E; Table III - 2). Profiles could not be measured very close to the bed because of the relatively large size of the current meter and because the boundary was composed of sand that could be scoured by flow moving around the current meter. The meter was lowered to a point 0.5 m from the boundary and readings of current speed and direction were recorded at half-meter intervals from the bottom to the water surface. The measurement of a complete profile required from three to five minutes. Each current speed recorded by the operator represents the approximate average speed from a 10 to 15 second measurement interval at each profile point (i.e., an estimated time-average velocity). Complete profile measurements were repeated every 15 to 30 minutes during the ebb and following flood phase of the tidal cycle.

Measurement of the total water depth for each profile were made with the echosounder. Approximately 25 kg of streamlined weight was attached to a 0.5 m long bridle suspended below the current meter to keep the suspending wire vertical and to aid in the location of the bottom when the meter was lowered (particularly in strong currents). The total depth determined from the wire length was checked against the echosounder reading. The relative positions of the current meter at each point in the profile was noted with respect to calibration marks, spaced at 0.5 m intervals, along the hauling wire. Comparison of wire measurements with depth measured from the echo sounder showed little difference, thus no depth corrections were required to compensate for drag on the meter and wire.

The velocity profiles were measured from the bottom to the surface because the bottom position could always be easily determined by rapidly lowering the meter until the haul-wire just went slack. The bottom was difficult to detect, and in some instances impossible, if the meter were slowly lowered to the bottom as one must do if measuring the velocity profile from the water surface to the bottom. By measuring the profiles from the bottom to the surface, the relative positions of the meter with respect to the bottom were more precisely known and therefore more reliable because the first reading at 0.5 m was readily known. Accurate positioning of the bottom reading is important not only to the location of the other read in the but

that this reading has on the results of regression analysis (see following section on analysis of velocity profiles).

Profile measurements were made at more than 40 locations (Fig. 4.1) during the three summers of field work. This represents more than 1200 individual velocity profiles and over 11,000 individual readings. Many stations were reoccupied more than once (Table III - 1) so that the changes of velocity due to the variation of tidal range during the lunar cycle could be observed.

Automatic Recording Current Measurements

The automatic recording current meter was used to record variations in the tidal currents during the lunar cycle. Three different types of recording current meters (Table III - 2) were used during the three field seasons: a model 021 Plessey (Fig. I-1D), an Anderaa (no model number available) and a model 381 HCM Braincon. The current meters were capable of measuring and automatically recording speed and direction at pre-set time intervals for extended periods ranging up to a maximum of about seven weeks (Table III - 3). Measurements were stored either on magnetic tape as an audible binary code (Plessey and Anderaa) or on photographic film as arc lengths and indicator positions (Braincon). In whatever stored format, the recorded measurements had to be machine or manually translated to velocity units.

The recording current meters were secured to a tubular steel davit that was supported by a 200 kg, circular, steel reinforced concrete base (Fig. I - 1D). In location on the seabed, the horizontal axis of the meter was approximately 0.5 m above the boundary. When moored on intertidal areas, a cork float was attached to the propellor or rotor of the meter to prevent it from free-wheeling in the wind at low tide.

During the three field seasons, these meters were used at nine different locations (Fig. 4.1) both in subtidal channels and on some of the intertidal sand bars. Unfortunately, not all measurements with these meters were without problems.

TABLE III - 2

CURRENT METERS

	Speed (knots)	Direction (degrees)	Miscellaneous
1. Direct Reading			
Kelvin-Hughes	0.1-6.0 ±2% full scale	0-360°±1.5°	propellor-type
2. Automatic Recording			
Plessey	0.1-5.0 ±3% f.s.	0-360°±2°	propellor-type magnetic tape recording
Anderaa	0.1-5.0 ±3% f.s.	0-360°±2°	savonius rotor vane magnetic tape temperature = -1 to 25°C±0.025°
Braincon	0.1-5.0 ±3% f.s.	0-360±2°	savonius rotor vane photographic film

T A B L E III - 3

SUMMARY OF OPERATION PERIODS FOR THE AUTOMATIC RECORDING CURRENT METERS

1. 1971 - Plessey Current Meter

Noel Bay Bar	NB-6	July 7 to July 19
	NB-8	July 19 to August 1
	NB-1	August 1 to August 19

2. 1972 - Anderaa Current Meter

Selma Bar	SB-1	June 28 to July 27
	SB-20	July 22 to August 15
	SB-3	June 28 to July 28
	SB-17	July 28 to August 14

3. 1973 - Braincon Current Meter

Channels west of Selma Bar	SB-18	June 12 to July 19
	NSB-10	June 12 - Lost

III.2 ANALYSIS OF THE CURRENT DATA

Velocity Profiles

The velocity profile data was analyzed by the least squares method of regression analysis (for further discussion of the method, see Davis, 1973, p. 192-221; Guttman and Wilks, 1965, p. 243-247; and Krumbein and Graybill, 1965, p. 286-295) to compute the theoretical velocity distribution for each profile. The velocity (u) at each point in the profile was the dependent variable, and the distance from the boundary (y) was the independent variable. Each profile was regressed as: (i) a first-order, linear model with log y as the independent variable (Eqn. 4.18); and (ii) a second-order, or quadratic model with y and y^2 as the independent variables (Eqns. 4.8 and 4.19).

The least square line approximating the linear form is

$$u = A_o + A_1 \log_{10} y \qquad (4.22)$$

where $A_o = Y_o$, the intercept of the regression line on the depth axis, and A_1, the slope of the line, is equal to

$$A_1 = \frac{u_1 - u_2}{\log_{10} y_1/y_2} \qquad (4.23)$$

The value of u_* is determined from

$$u_* = \frac{A_1 \kappa}{2.3} \qquad (4.24)$$

if the value of κ is assumed to be 0.4.

The least square quadratic has the equation

$$u = A_o + A_1 y + A_2 y^2 \qquad (4.25)$$

which, rewritten in terms of Eqns. 4.8 and 4.19, has the form

$$u = (u_{max} - C_2 u_*) + \frac{(2C_2 u_*)}{D} y - \frac{(C_2 u_*)}{D^2} y^2 \qquad (4.26)$$

A_o, A_1 and A_2 are constants determined by solving simultaneously the normal equations for the least square quadratic. C_2, defined for Eqn. 4.19, is equal to 9.6 (Hama, 1954).

To test the 'goodness-of-fit' and the improvement of fit with the quadratic model versus the linear model, the significance of the correlation coefficients (Arkin and Colton, Table 22, 1963) and the F-test significance (from Table 13), were evaluated. The results of these tests are discussed in Chapter 4.3.

The validity of the assumption made in Eqn. 4.14, that y_o was small compared to y and thus could be neglected, was also tested. For the first approximation, it was assumed that y_o could be neglected in $\log_{10}(y + y_o)$, and the velocity (u) was regressed against the distance from the bed (y) for each point in the profile. The calculated intercept value ($A_o = y_o$) from the first approximation was used in the second approximation in which $\log_{10}(y + y_o)$ was regressed against each velocity value in the profile. Successively higher approximations were made in a similar manner (up to ten iterations) until the y_o values converged.

Point Velocity Data

The point velocity data collected with the automatic recording current meters was compiled and edited into summary form (Appendix III.4) with the help of Messrs. R. R. Lively and E. Verge (Coastal Oceanography, Environment Canada) using several packaged programs in the computing facilities of the Bedford Institute of Oceanography. The data are listed as frequency distributions of current speed and direction.

III.3 LISTING OF VERTICAL VELOCITY PROFILE DATA

The following is a listing of the vertical velocity profile data measured in Cobequid Bay, including: date, time (A.D.T.), station number and the current speed, direction and depth from the bottom for each point in the profile. Depth and speed are listed in CGS units (i.e., cm/s); direction is in degrees relative to 'true' north.

NOEL BAT BAR

DATE - 14/ 6/71 **1a**

TIME	DEPTH	VEL	DIR
929			
946			
603			
619			
631			
708			
720			
824			
848			
911			
930			
950			
1317	50.30	77.16	280
1348			
1350			
1408			
1414			
1430			
1508			
1532			
1603			
1625			
1730			

DATE - 14/ 6/71 **1b**

TIME	DEPTH	VEL	DIR
926			
1030			
1032			
1100			
1130			
1209			
1230			
1302			
1310			
1349	50.30	30.35	326
1352	50.30	77.15	357
1720	53.69	61.21	145
1730			
1745			
1800			
1830			
1940			
2000			
2020			

DATE - 14/ 7/71 **1c**

TIME	DEPTH	VEL	DIR
800			
805			
830			
900			
910			
1000			
1030			
1100			
1130			
1230			

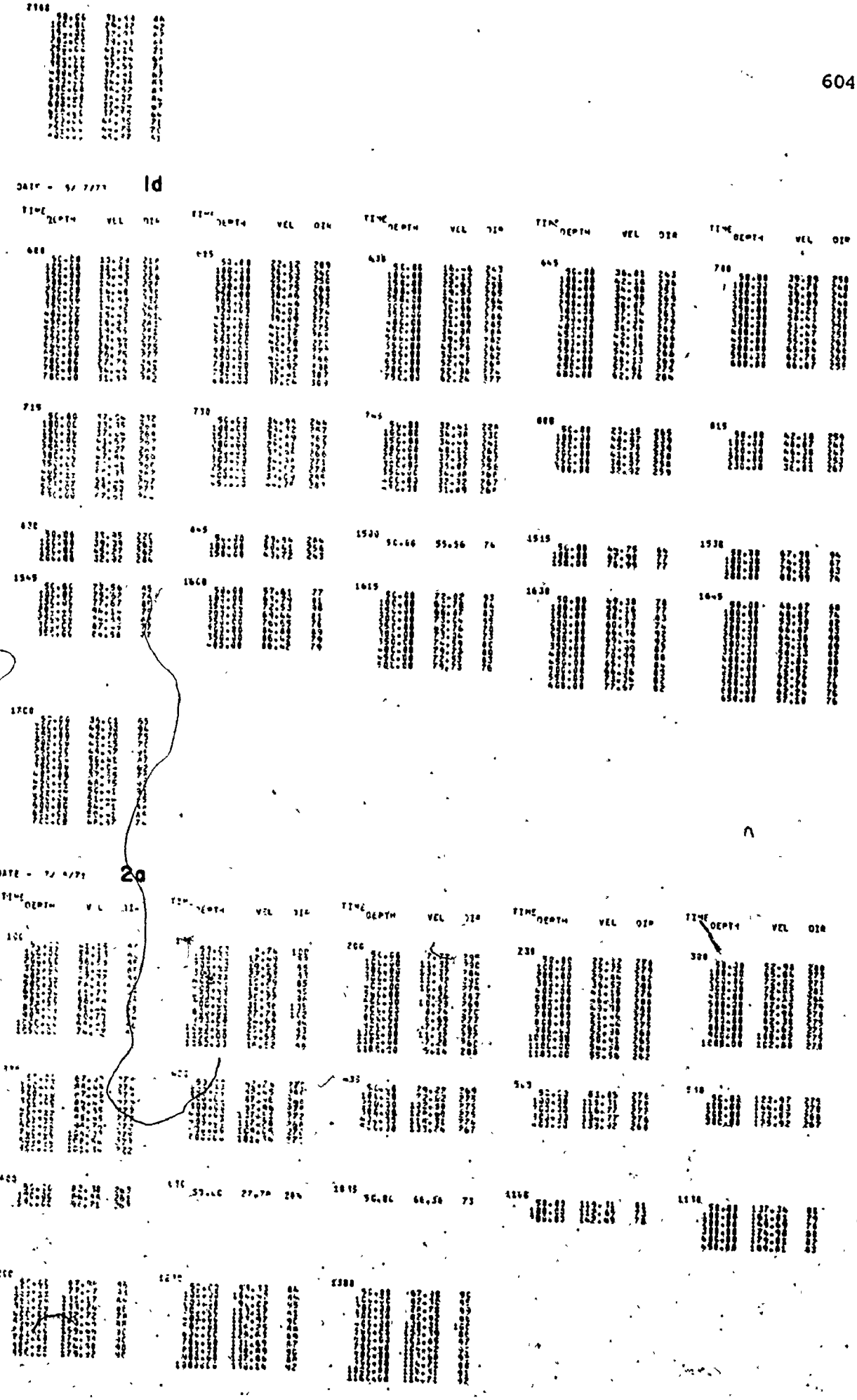
1d
2a

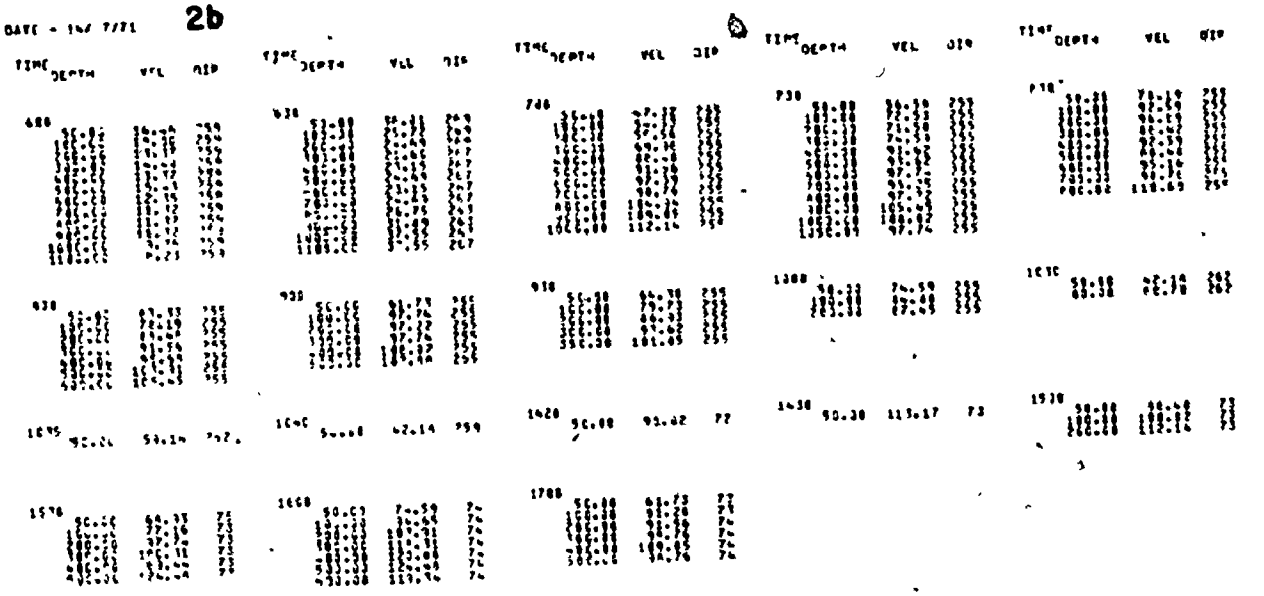
2b
TIME DEPTH VEL DIR

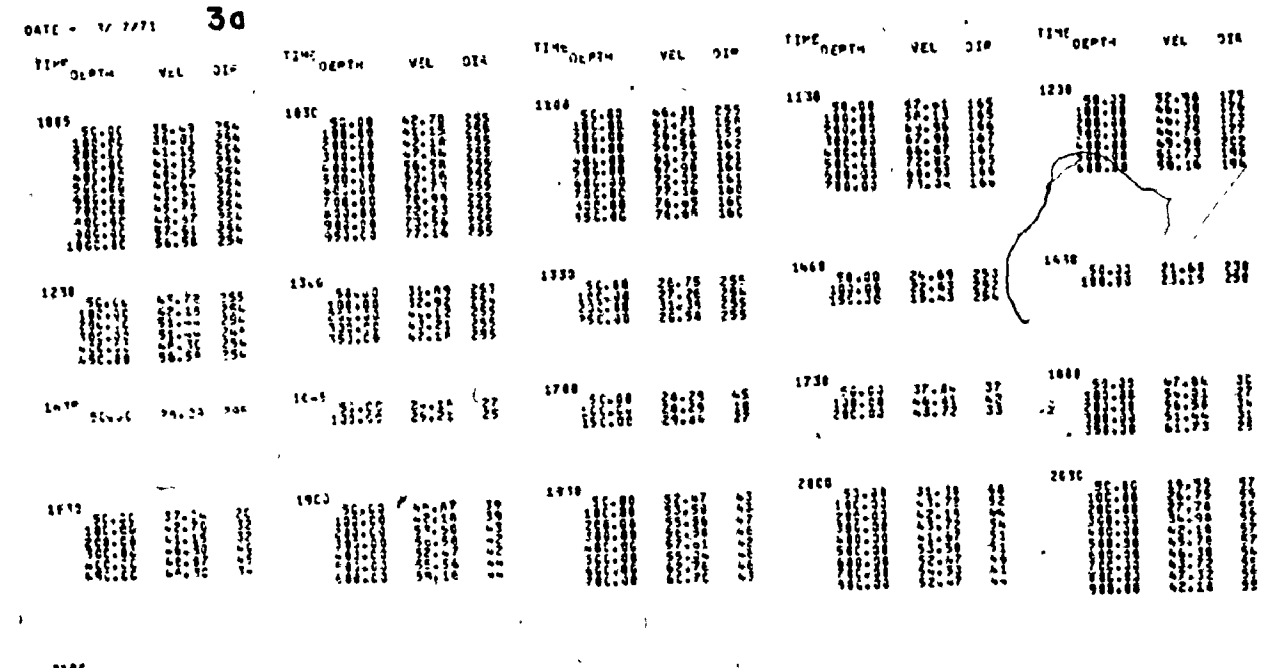
3a
TIME DEPTH VEL DIR

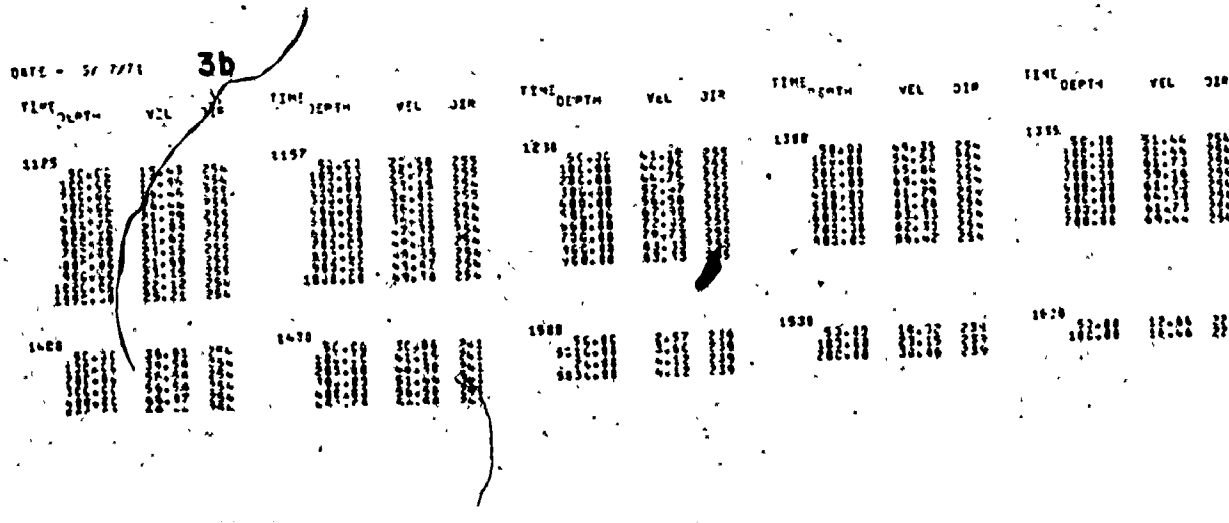
3b
TIME DEPTH VEL DIR

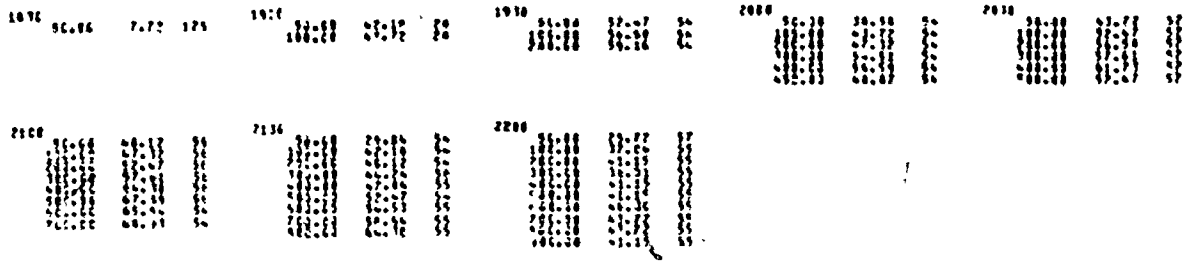

DATE = [illegible]

3c

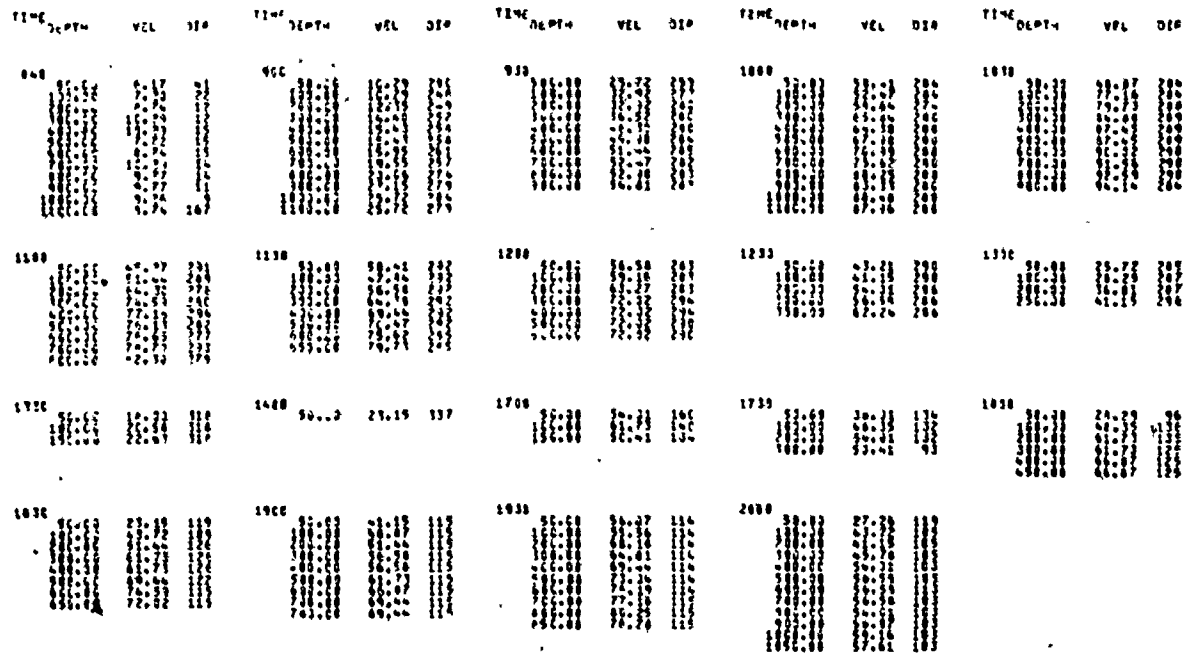

DATE = [illegible]

4

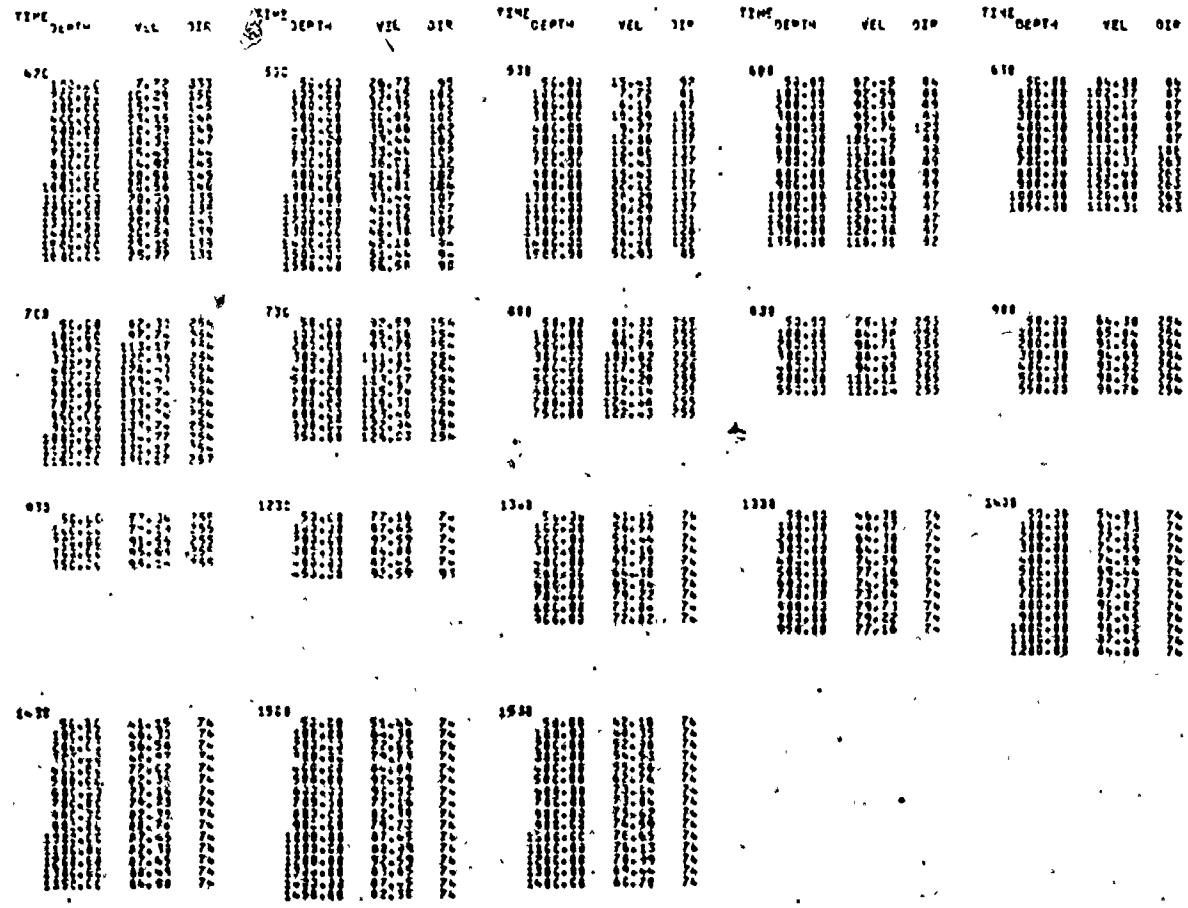

5

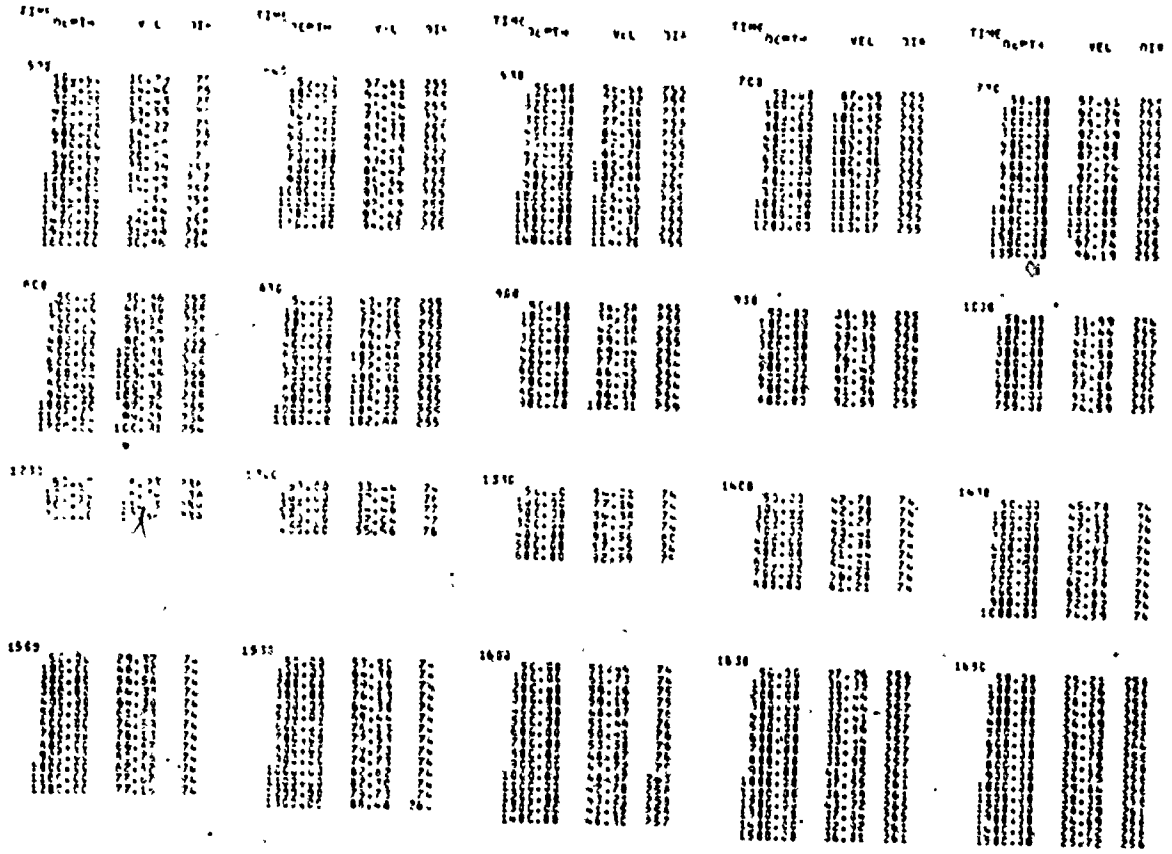

6a

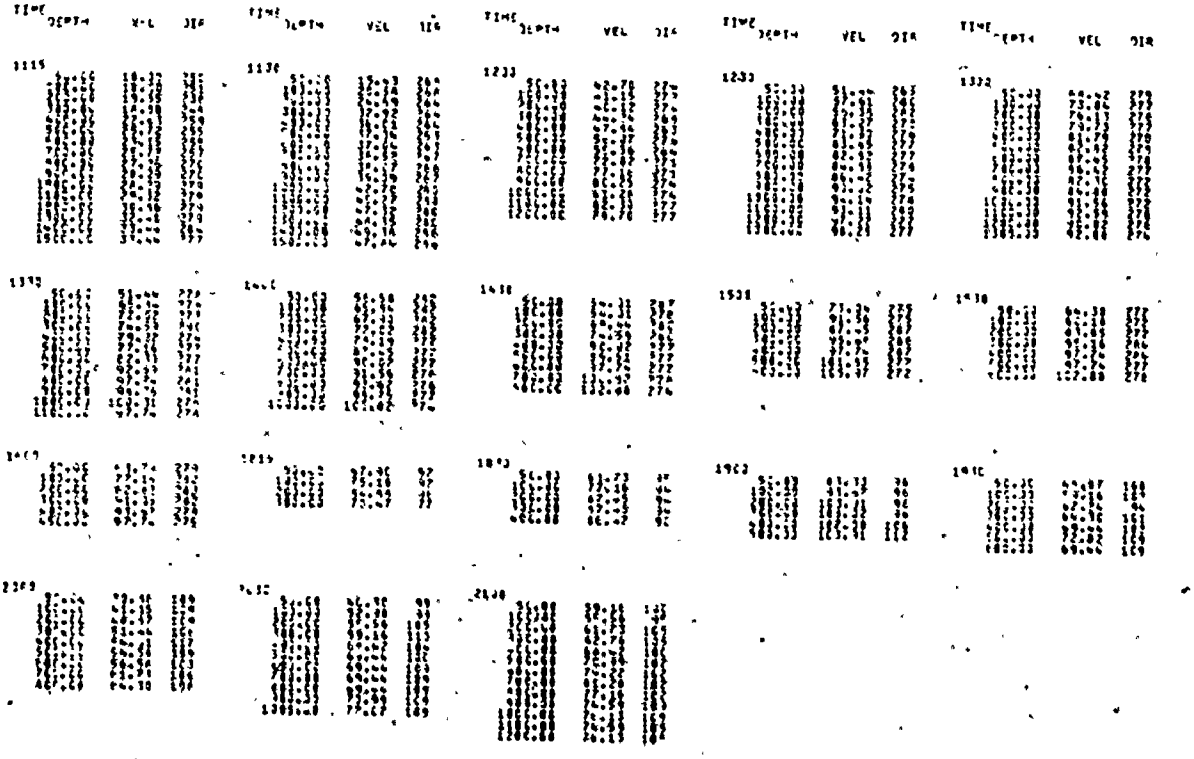

6b

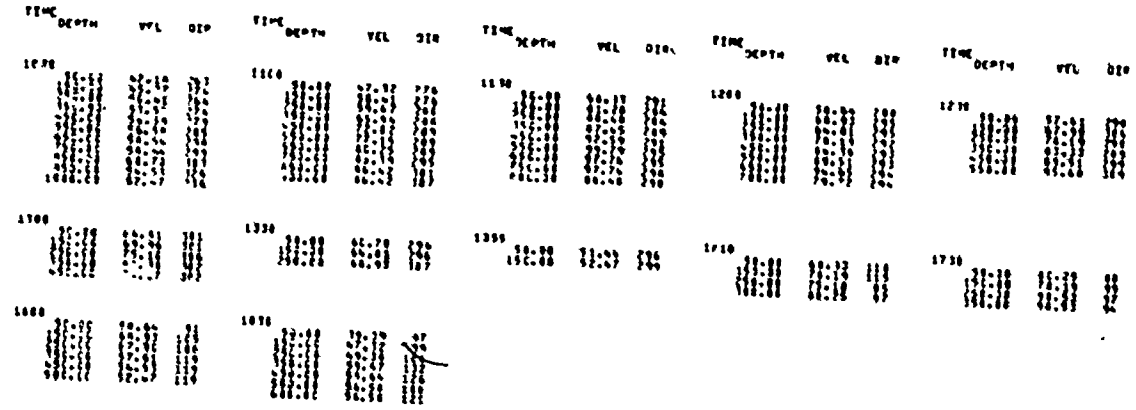

7

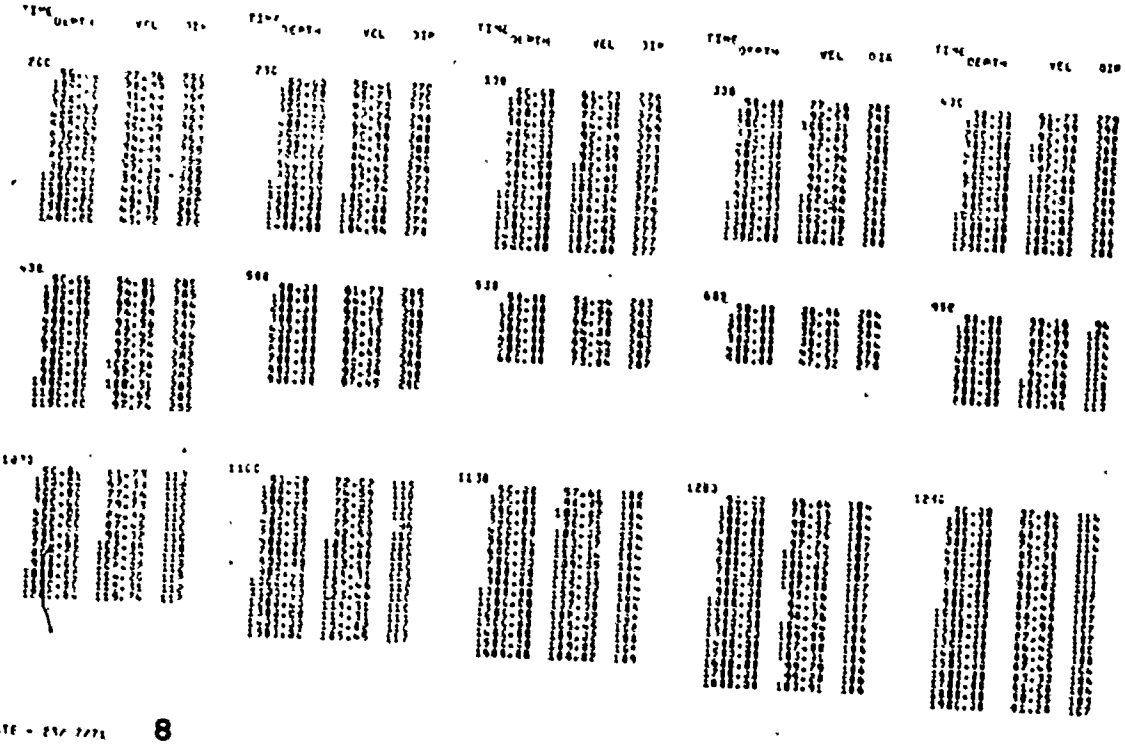

8

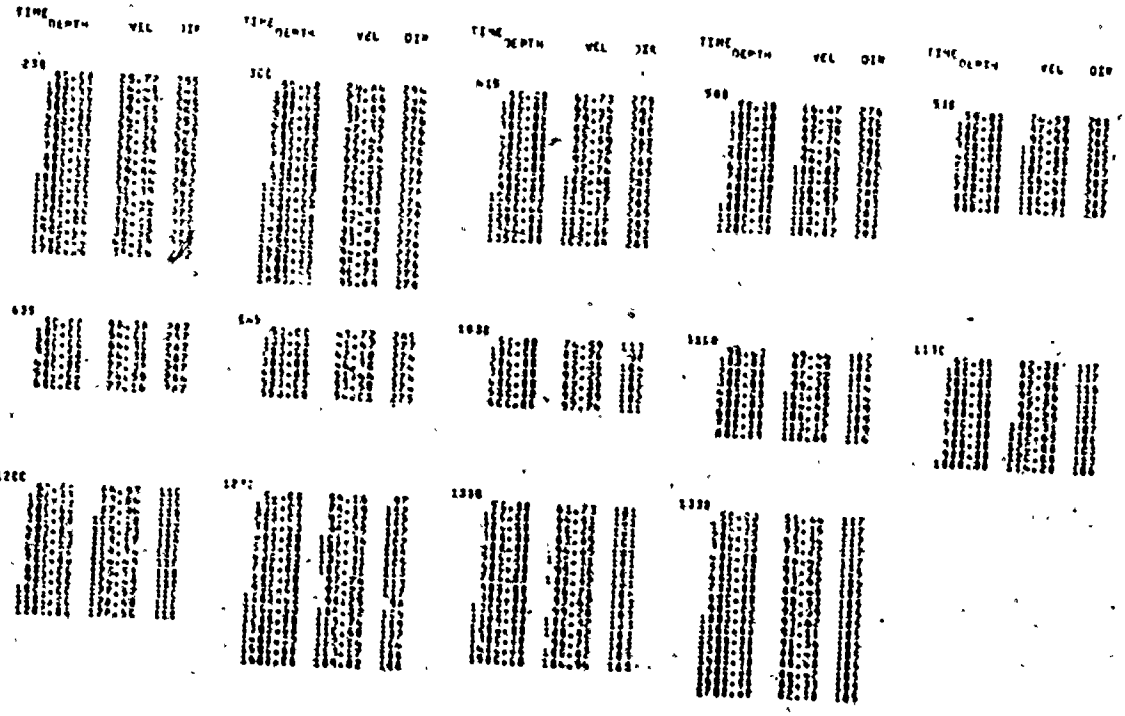

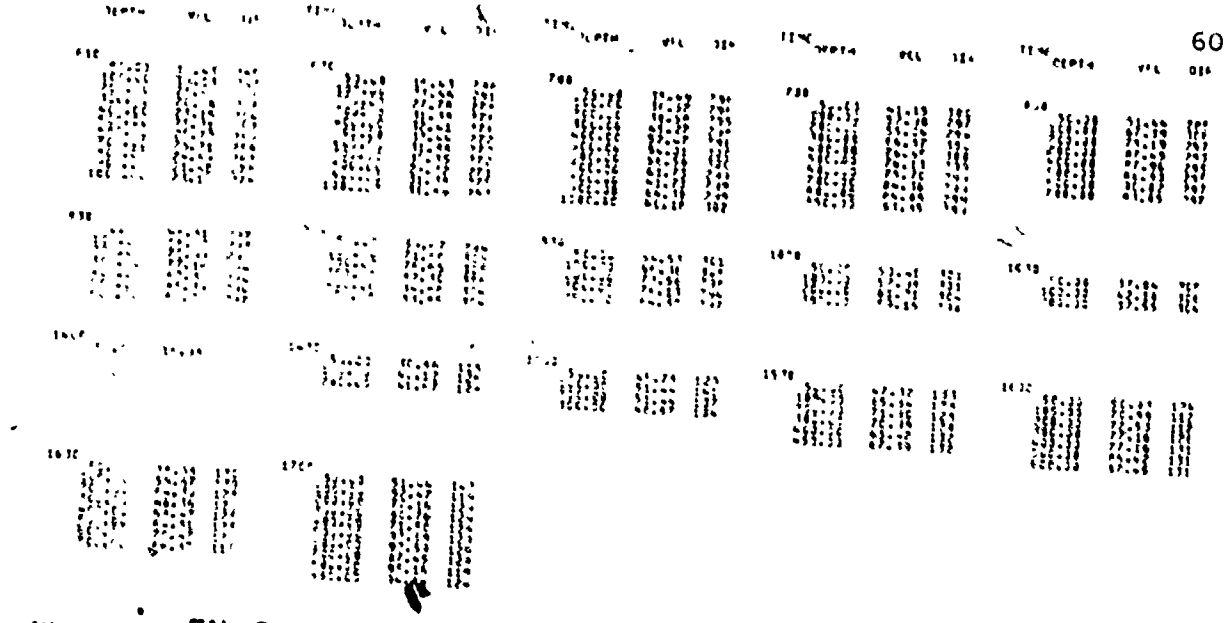

EN-2

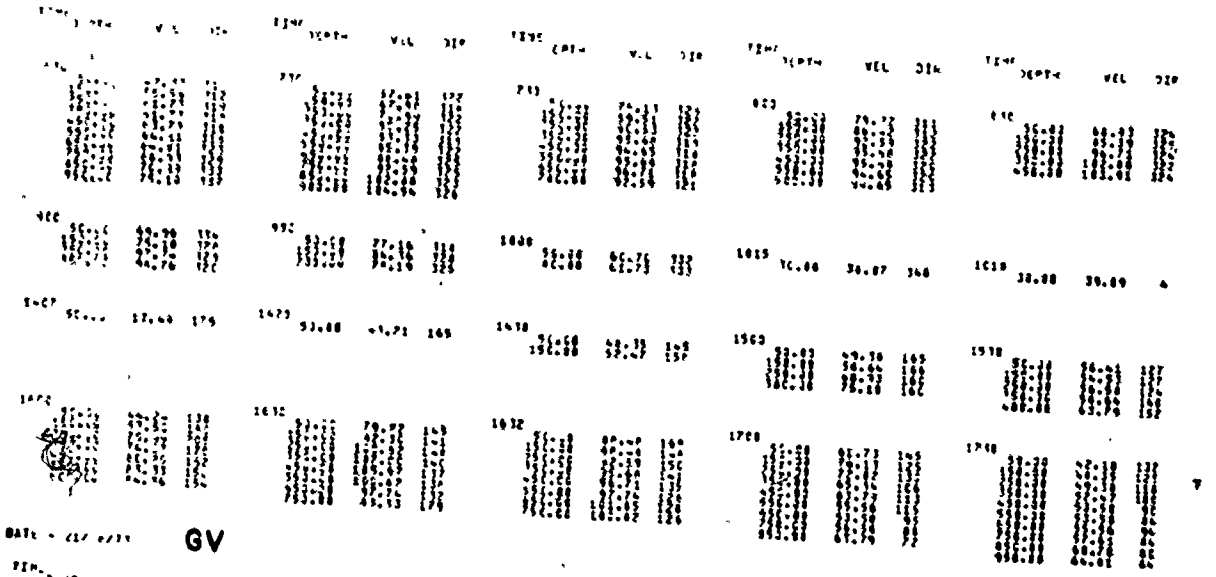

GV

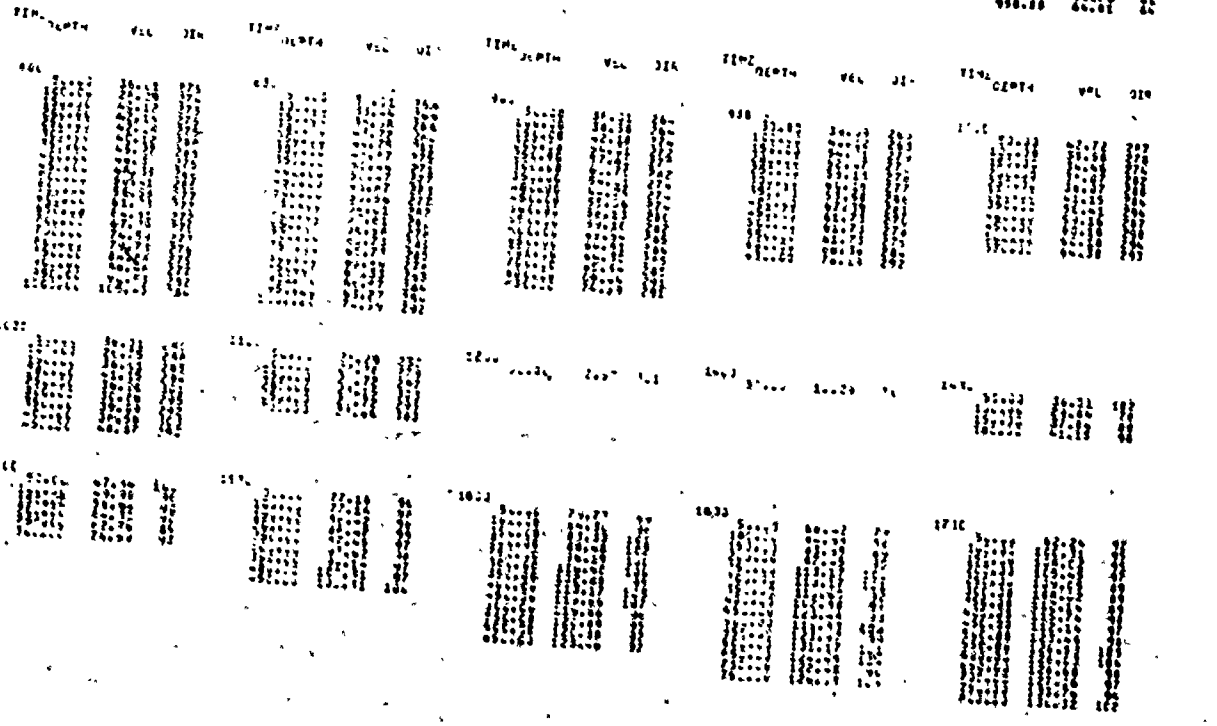

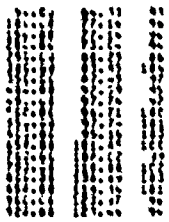

DATE - 17/8/73 **centre bay -- north of NB**

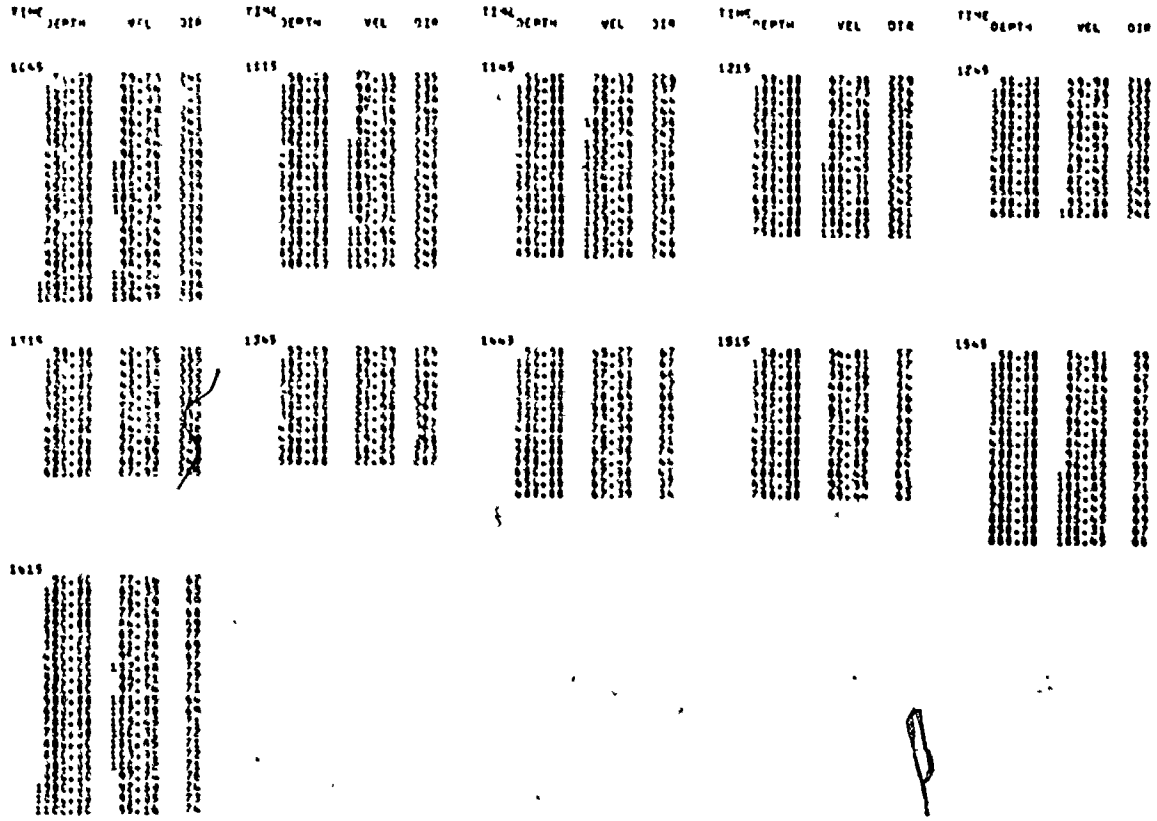

DATE - 17/8/73 **Middle Channel**

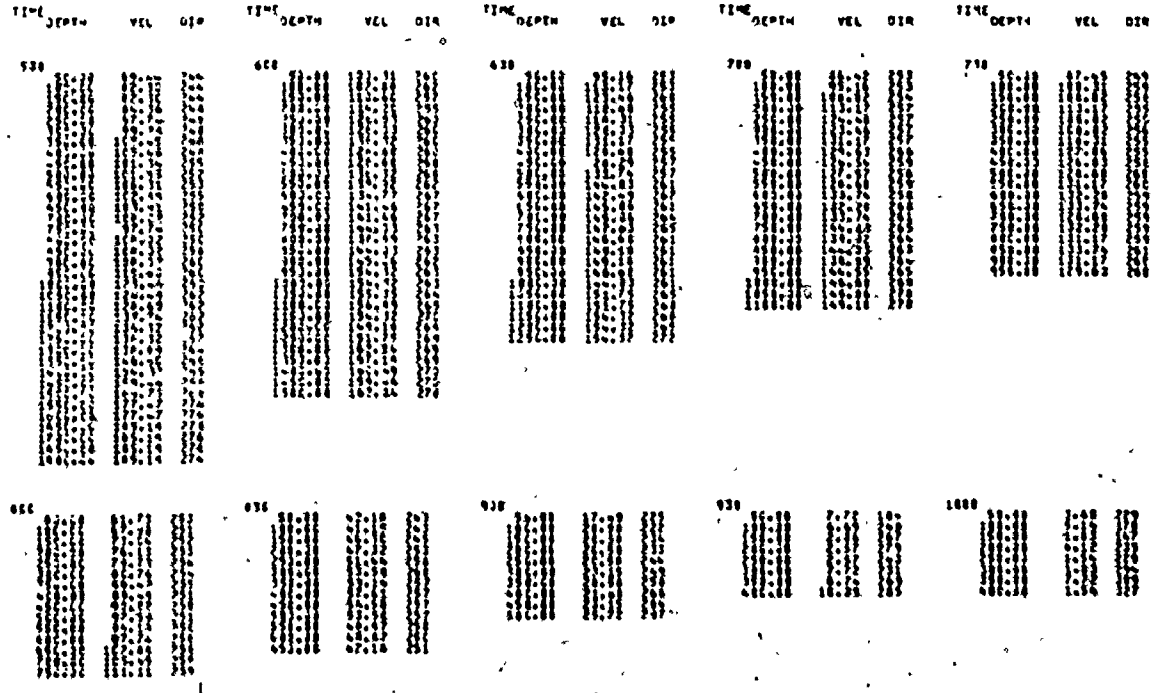

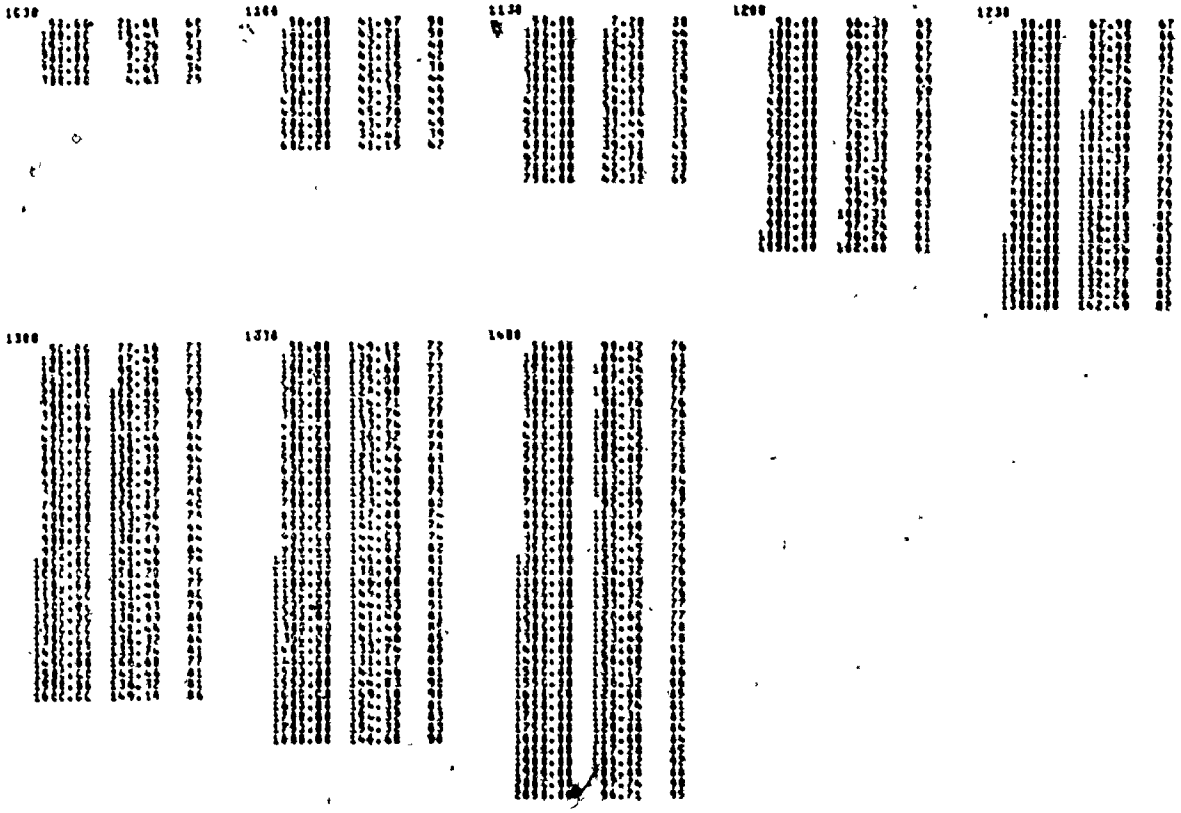

BAR

1

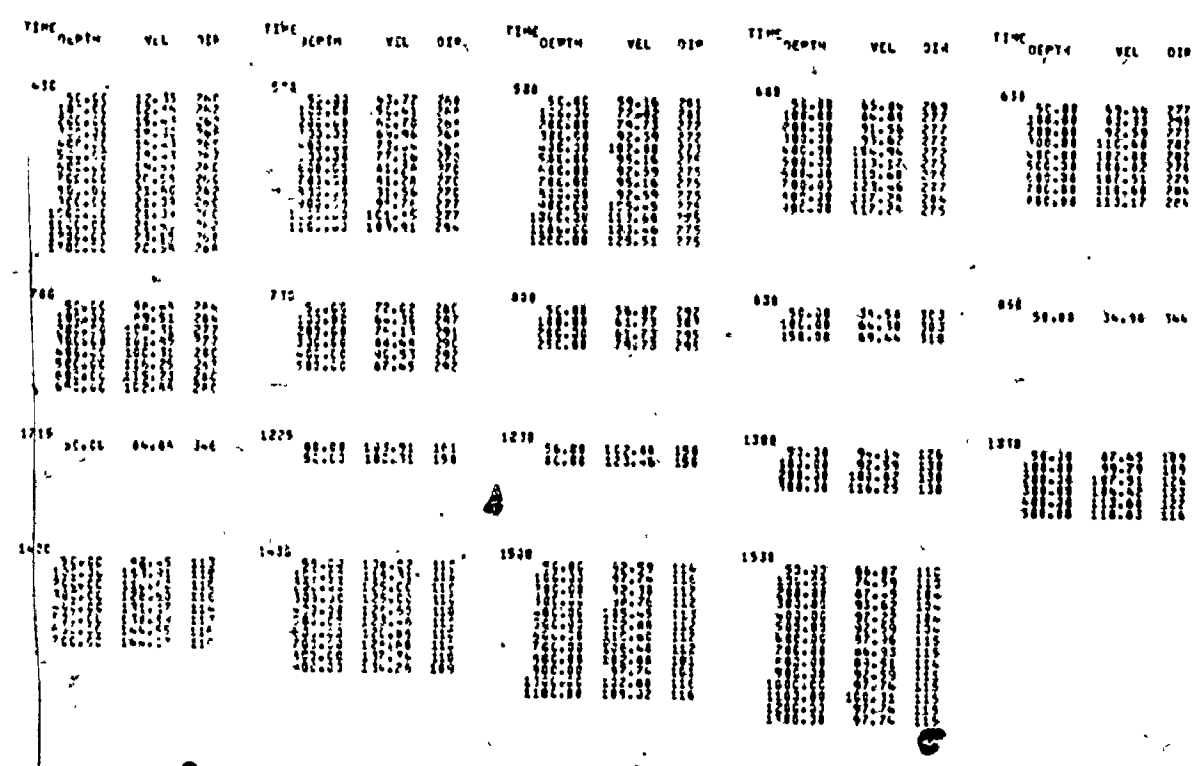

2a

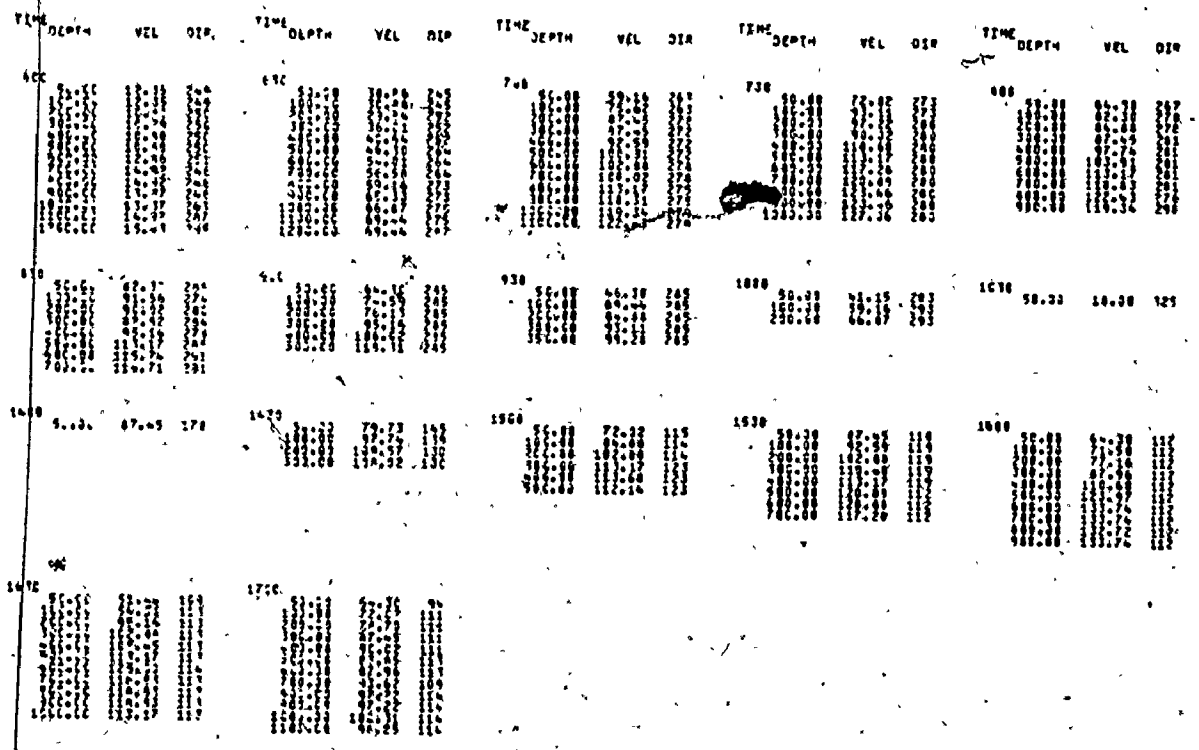

2b

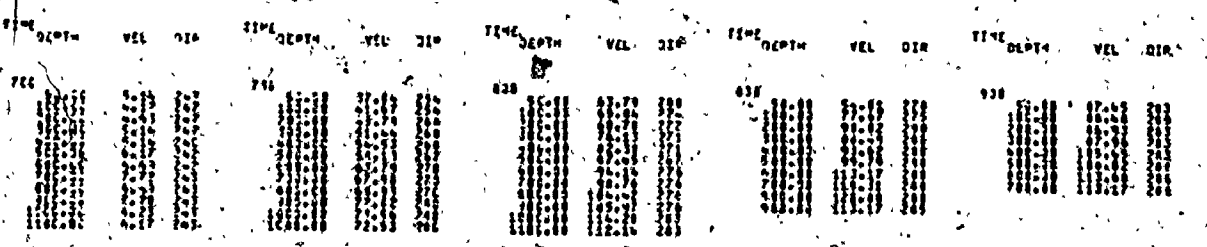

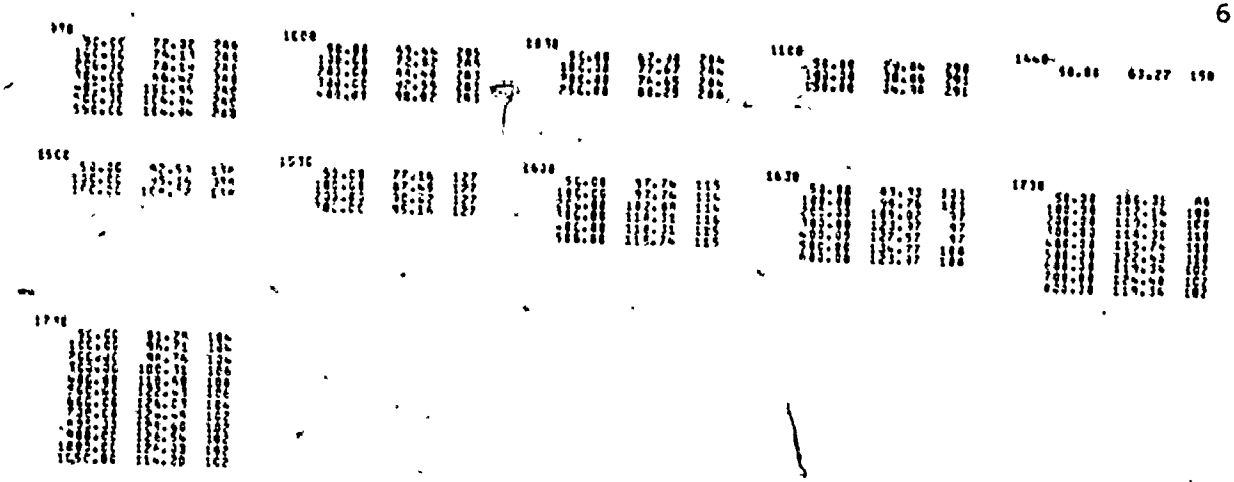

DATE - 14/ 5/71 3

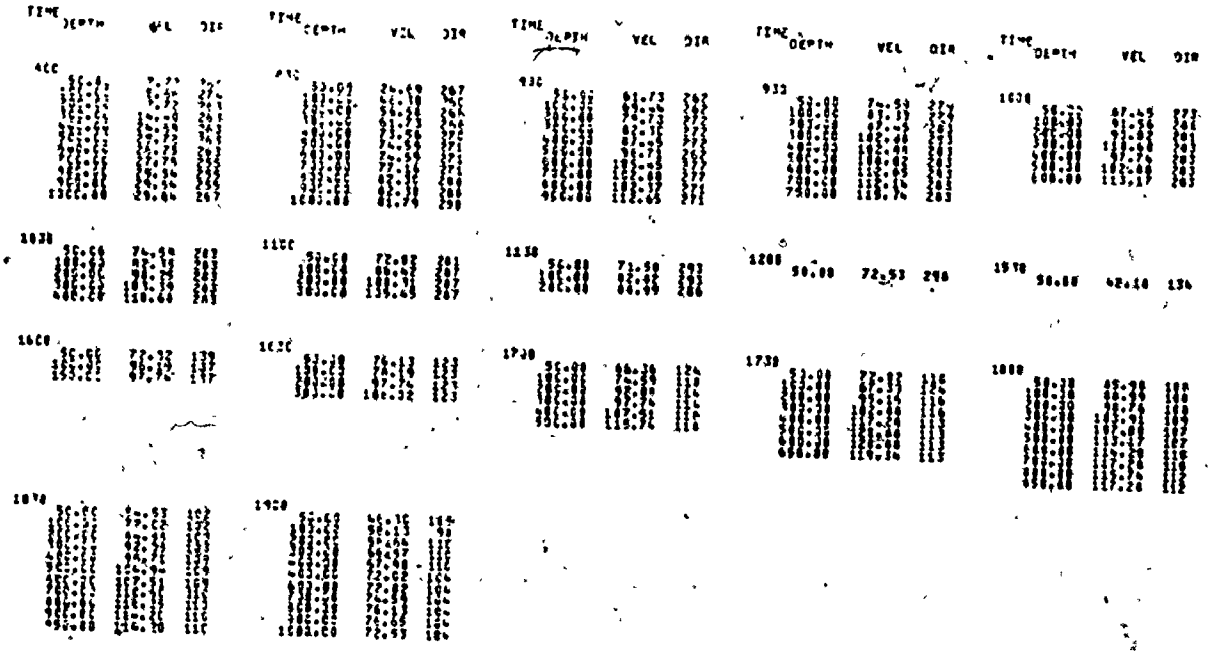

DATE - 15/ 6/73 4

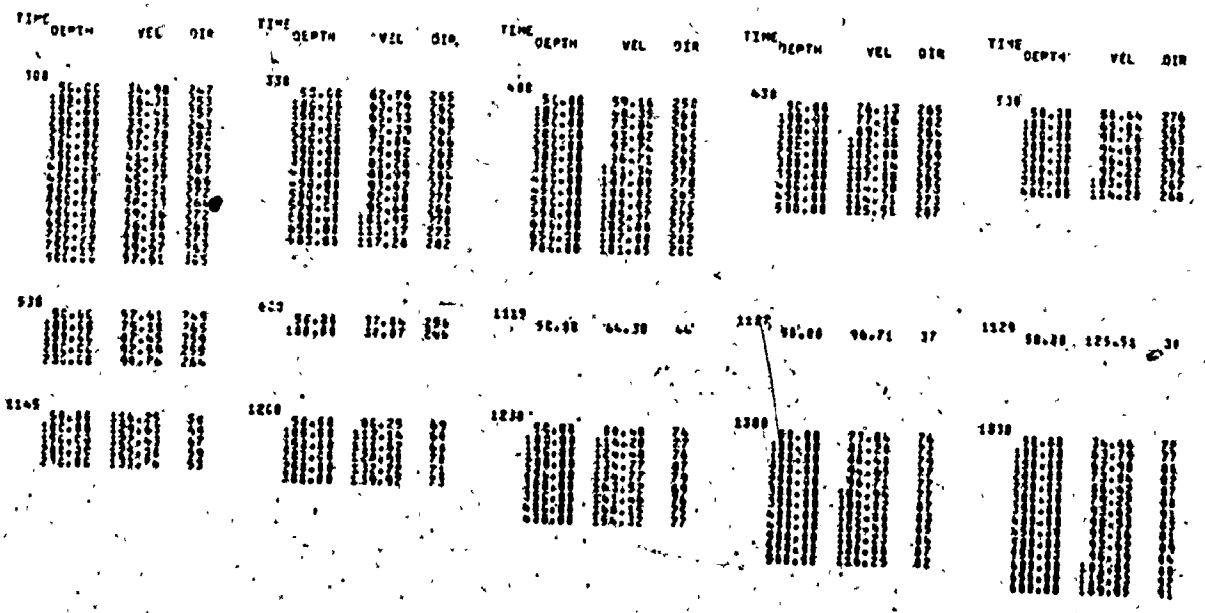

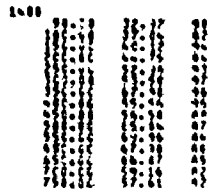

DATE - 7/ 7/77 5

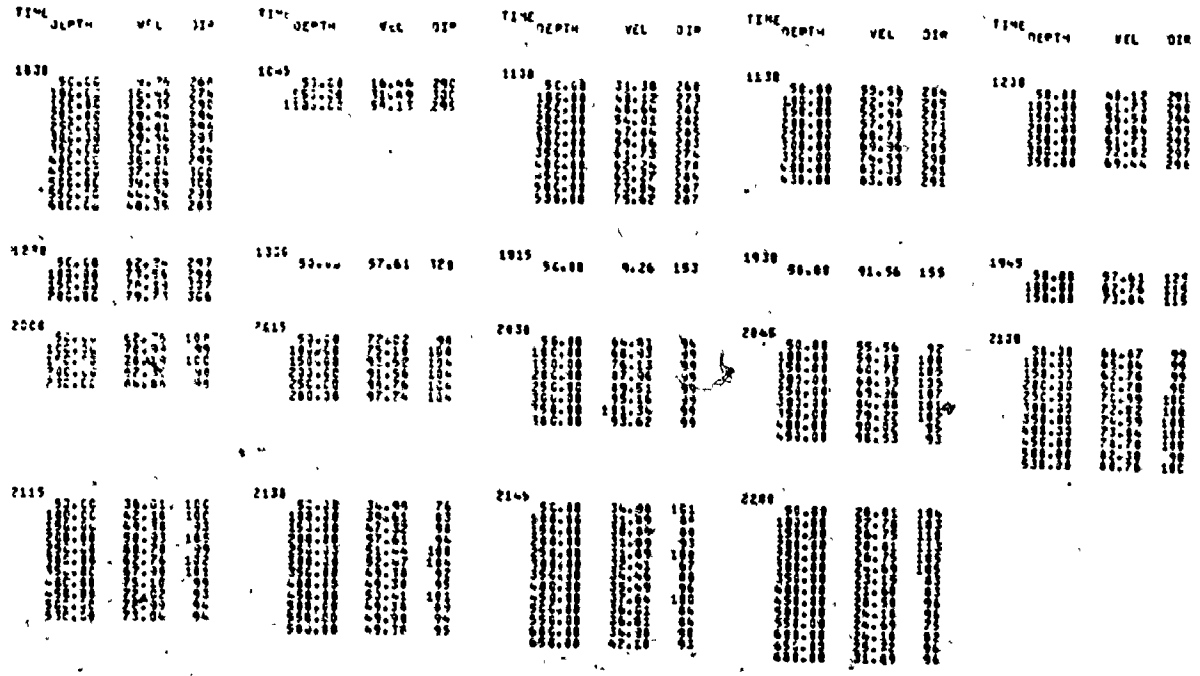

DATE - 8/ 7/77 6

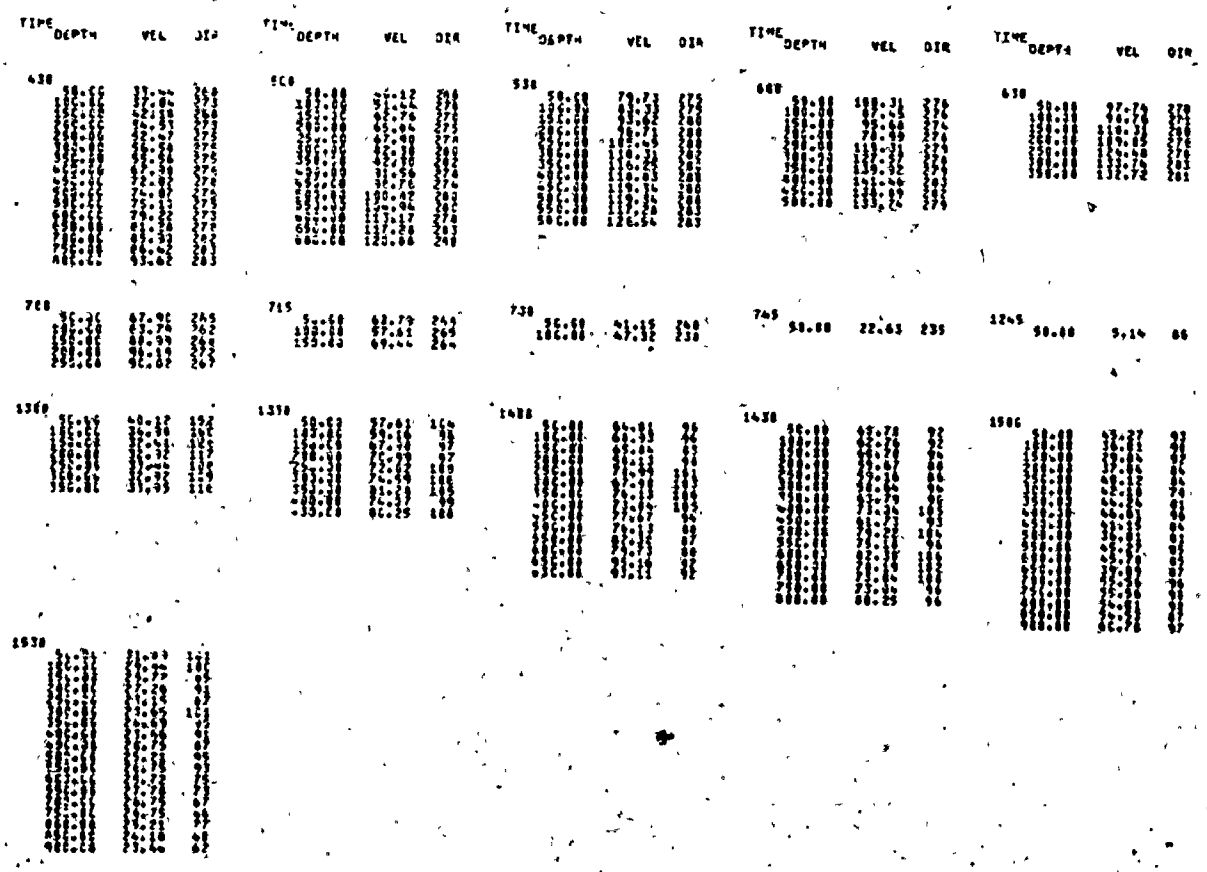

DATE = 28/ 4/71 **7**

TIME	DEPTH	VEL	DIR
630			
700			
730			
800			
830			
900			
930			
1000			
1030			
1100			
1130			
1200			
1230			
1300			
1330			
1400			
1430			
1500			
1530			
1600			
1630			
1700			

DATE = 29/ 4/71 **8**

TIME	DEPTH	VEL	DIR
1100			
1130			
1200			
1230			
1300			
1400			
1430			
1500			
1530			
1600			
1630			
1700			
1730			

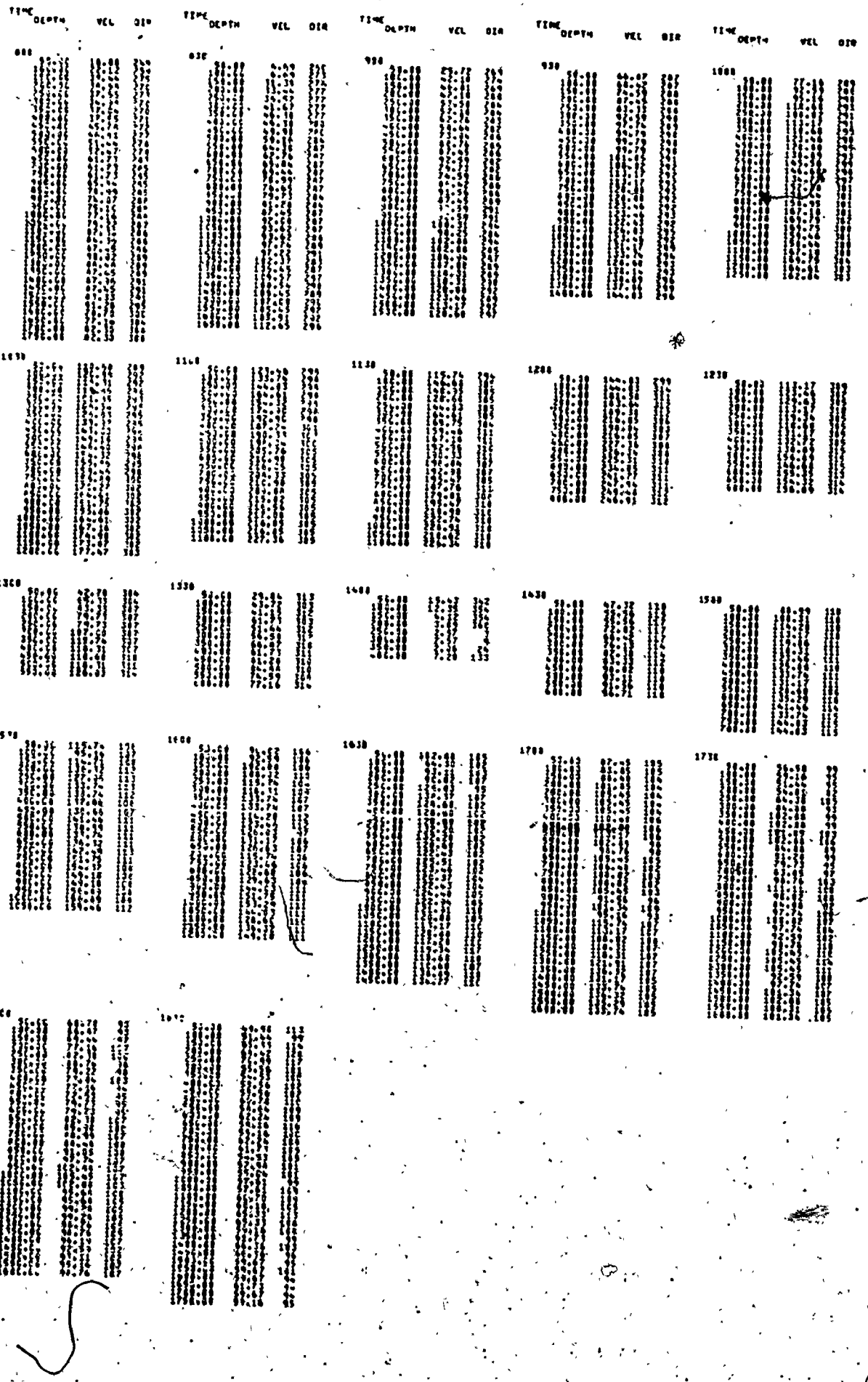
TIME DEPTH VEL DIR
TIME DEPTH VEL DIR
TIME DEPTH VEL DIR
TIME DEPTH VEL DIR
TIME DEPTH VEL DIR

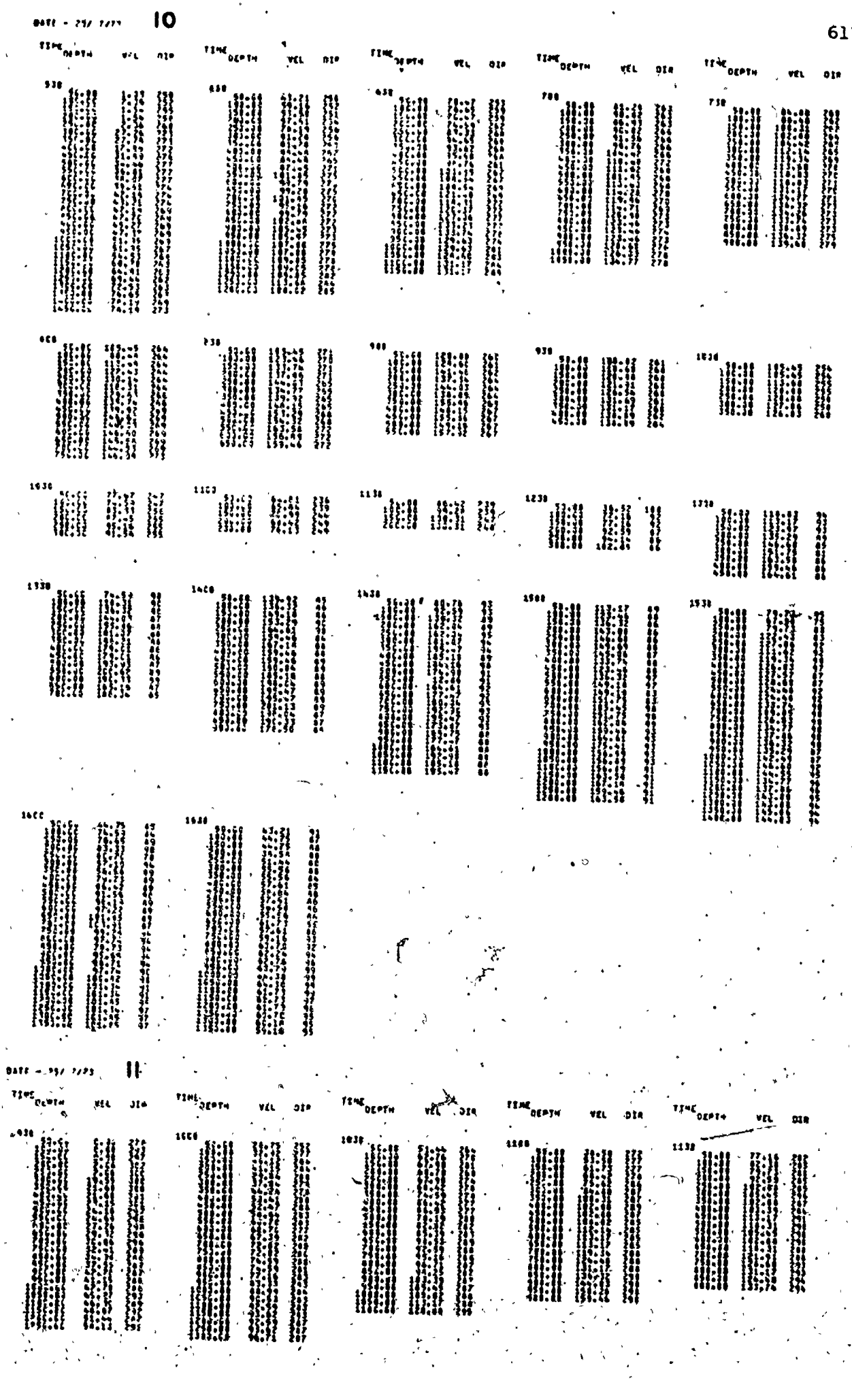

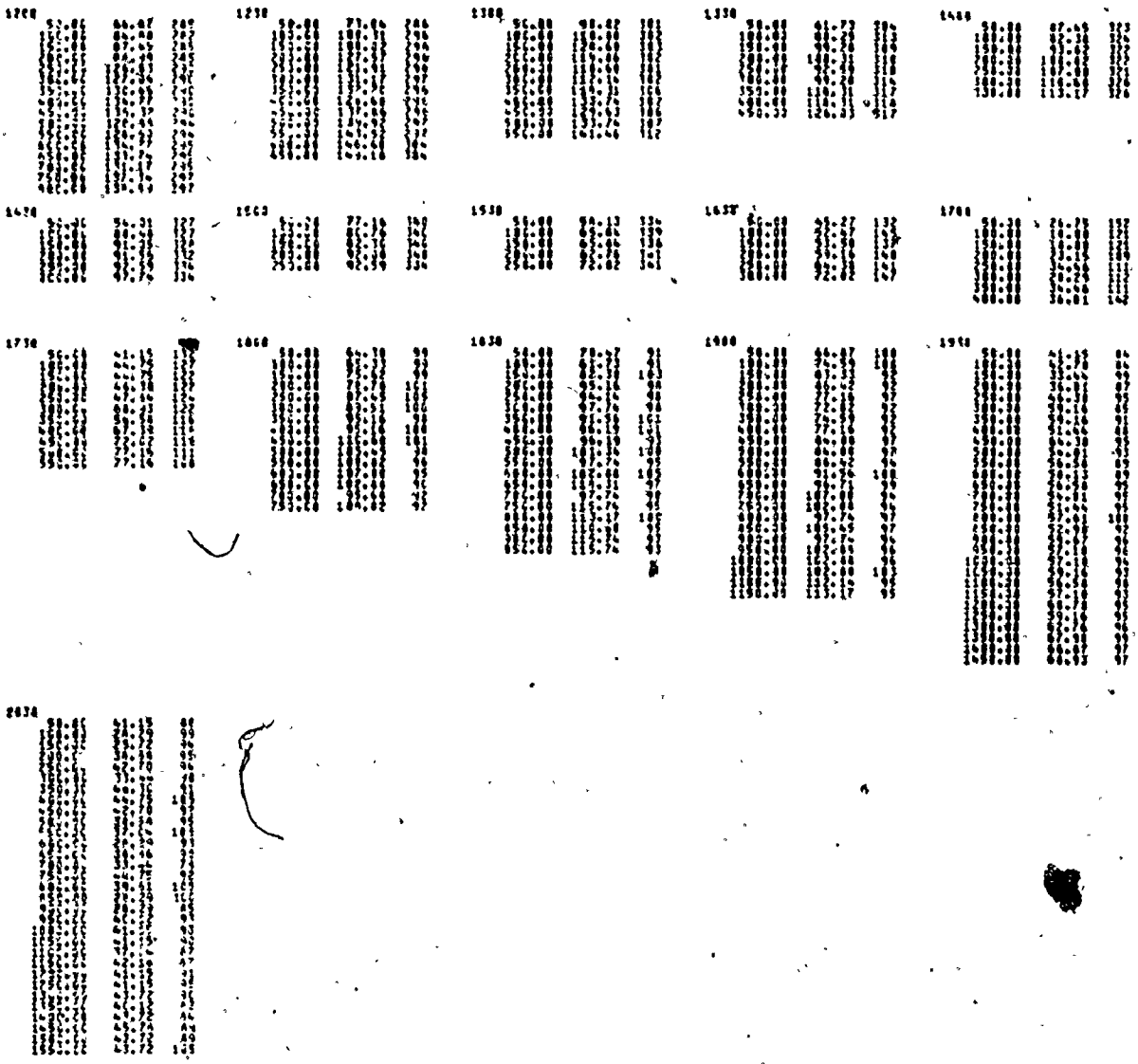

SELMA BAR

1a

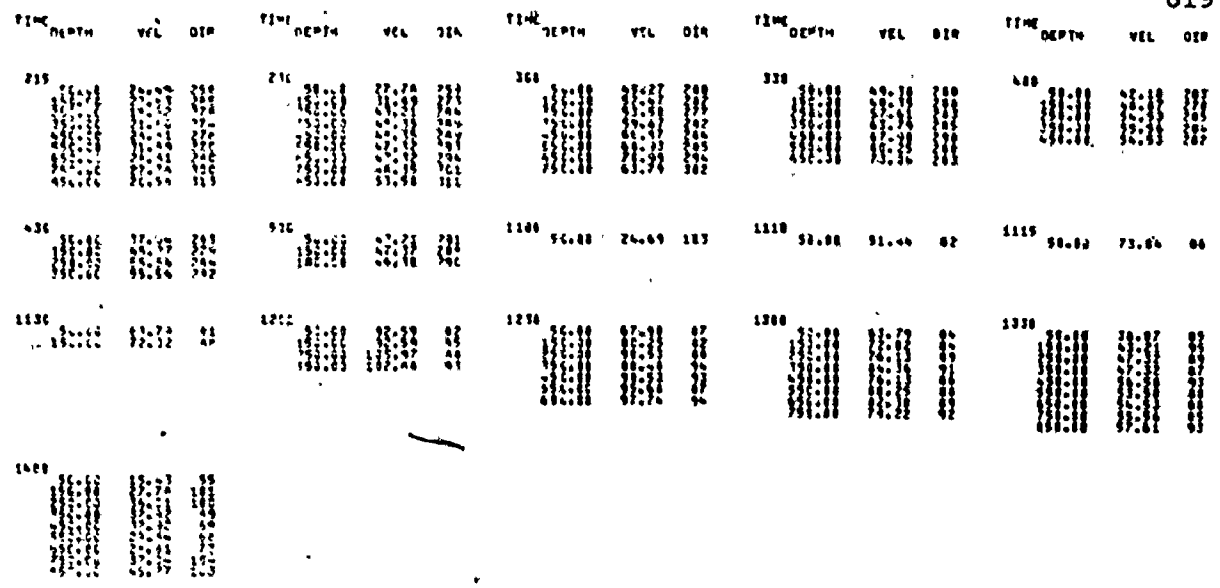

1b

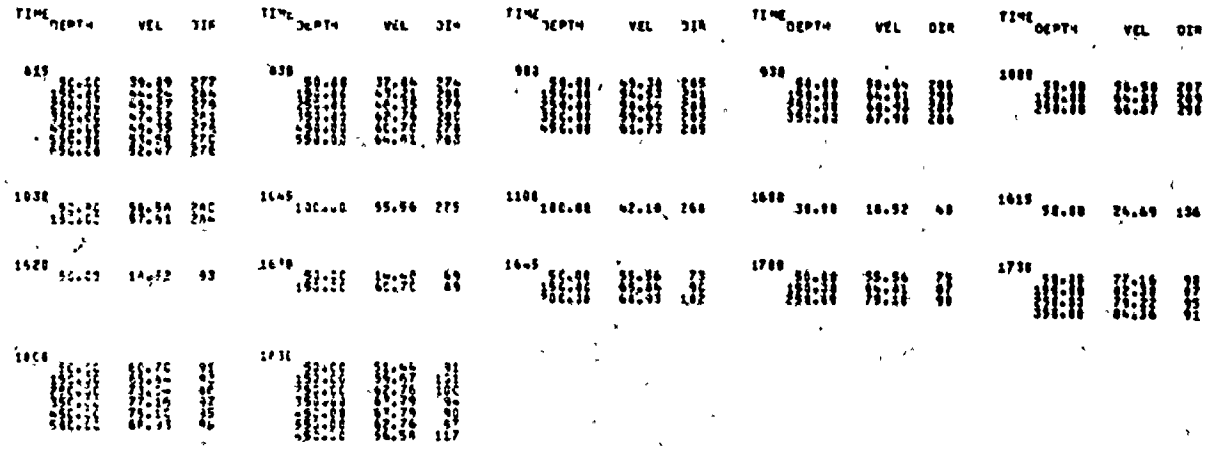

1c

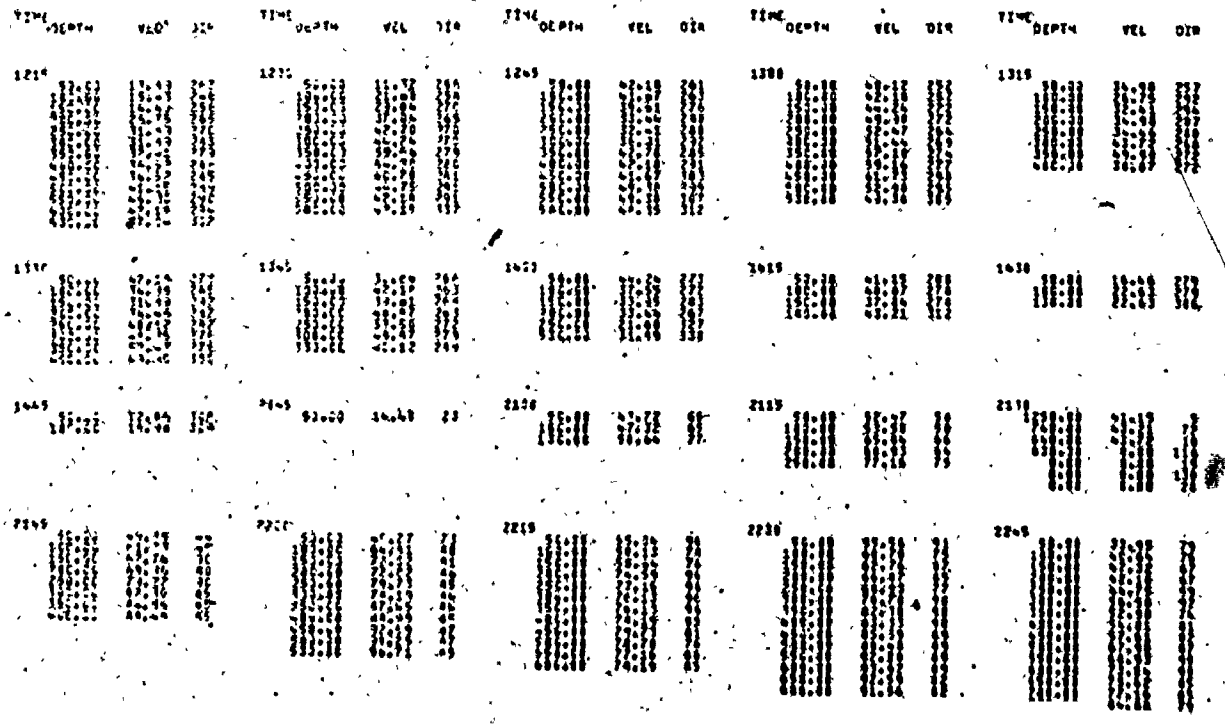

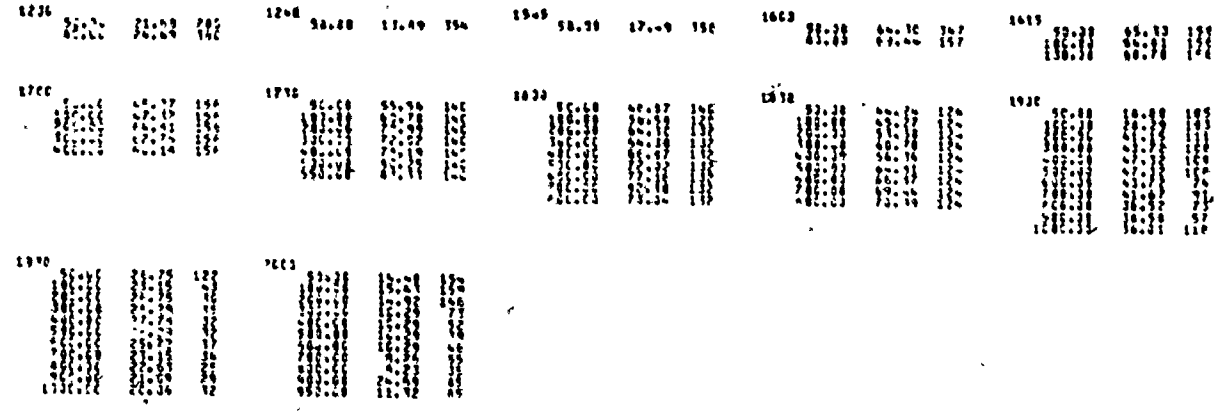

DATE - 1/ 8/72 **1d**

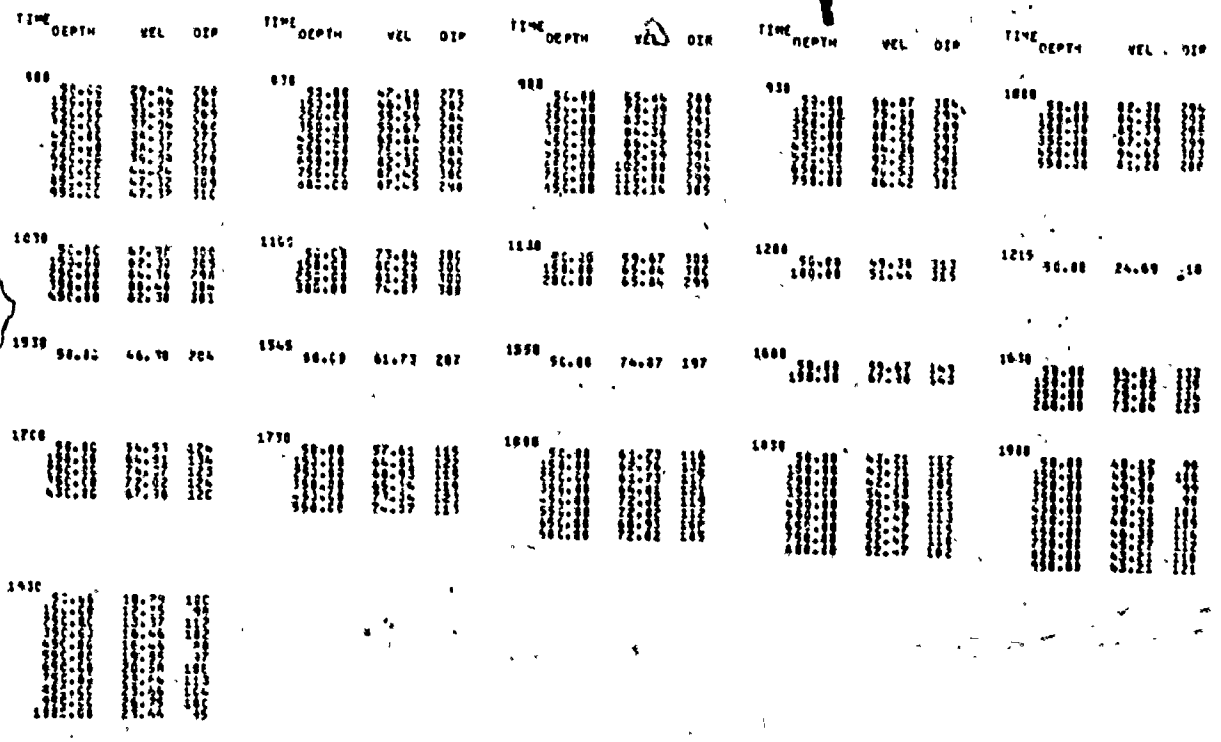

DATE - 1/ 9/72 **2a**

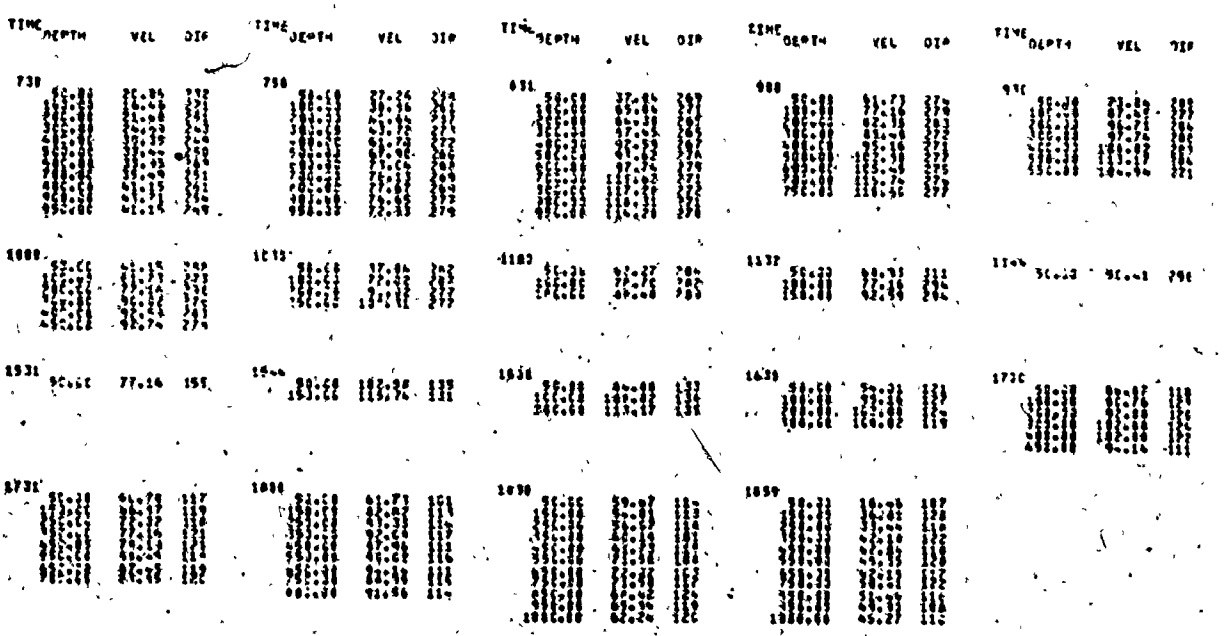

DATE - 23/ 7/72 **2b**

TIME	DEPTH	VEL	DIR
400			
430			
500			
530			
600			
630			
700			
730	50.30	31.35	304
745	50.80	26.75	300
1200	50.00	52.67	163
1230	53.30	46.50	94
1300			
1330			
1400			
1430			
1500			
1530			

DATE - 23/ 7/72 **2c**

TIME	DEPTH	VEL	DIR
930			
1000			
1030			
1100			
1130			
1200			
1230			
1300	50.00	41.15	289
1315	50.00	22.63	275
1330	50.00	22.63	286
1715	50.00	22.01	147
1730	53.00	50.01	105
1745			
1800			
1830			
1900			
1930			
2000			
2030			

DATE - 28/ 6/73 **2d**

TIME	DEPTH	VEL	DIR
500			
515			
530			
545			
630			
615			
630			
645			
700			
715			
730			
745			
800			
815			
830			
845	550.00	27.03	276
900	52.00	24.00	295
1300	50.00	59.07	95
1330			
1345			

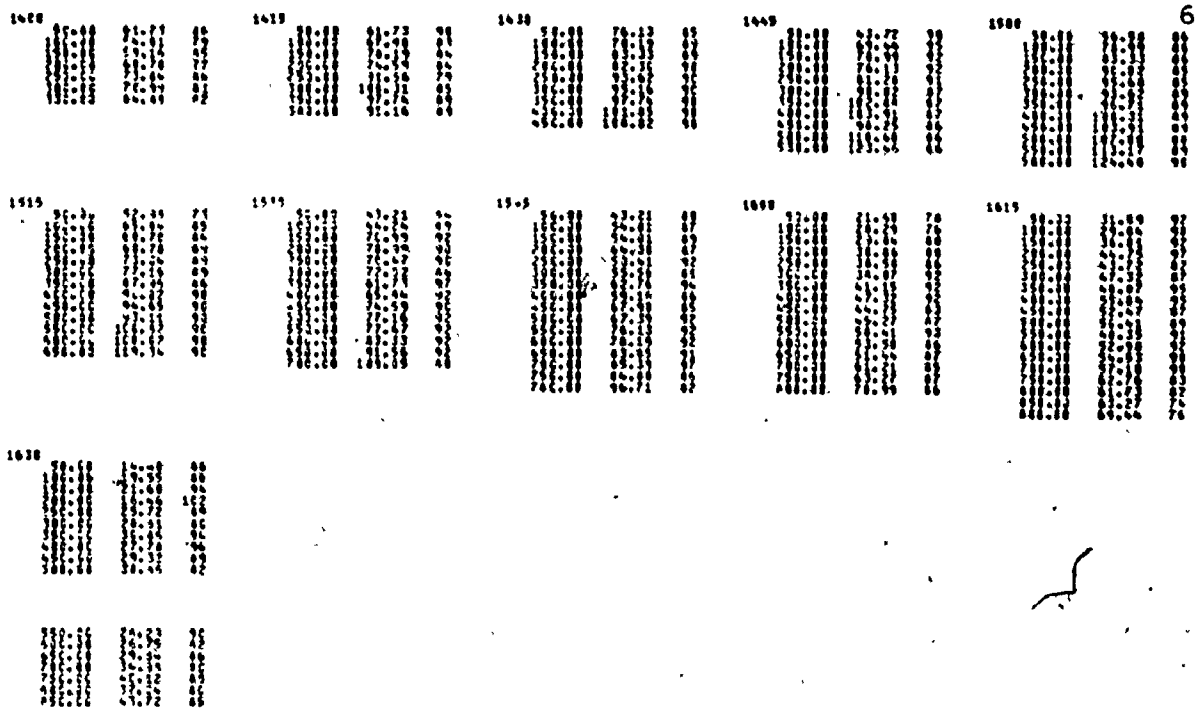

DATE - 9/ 7/73 **2e**

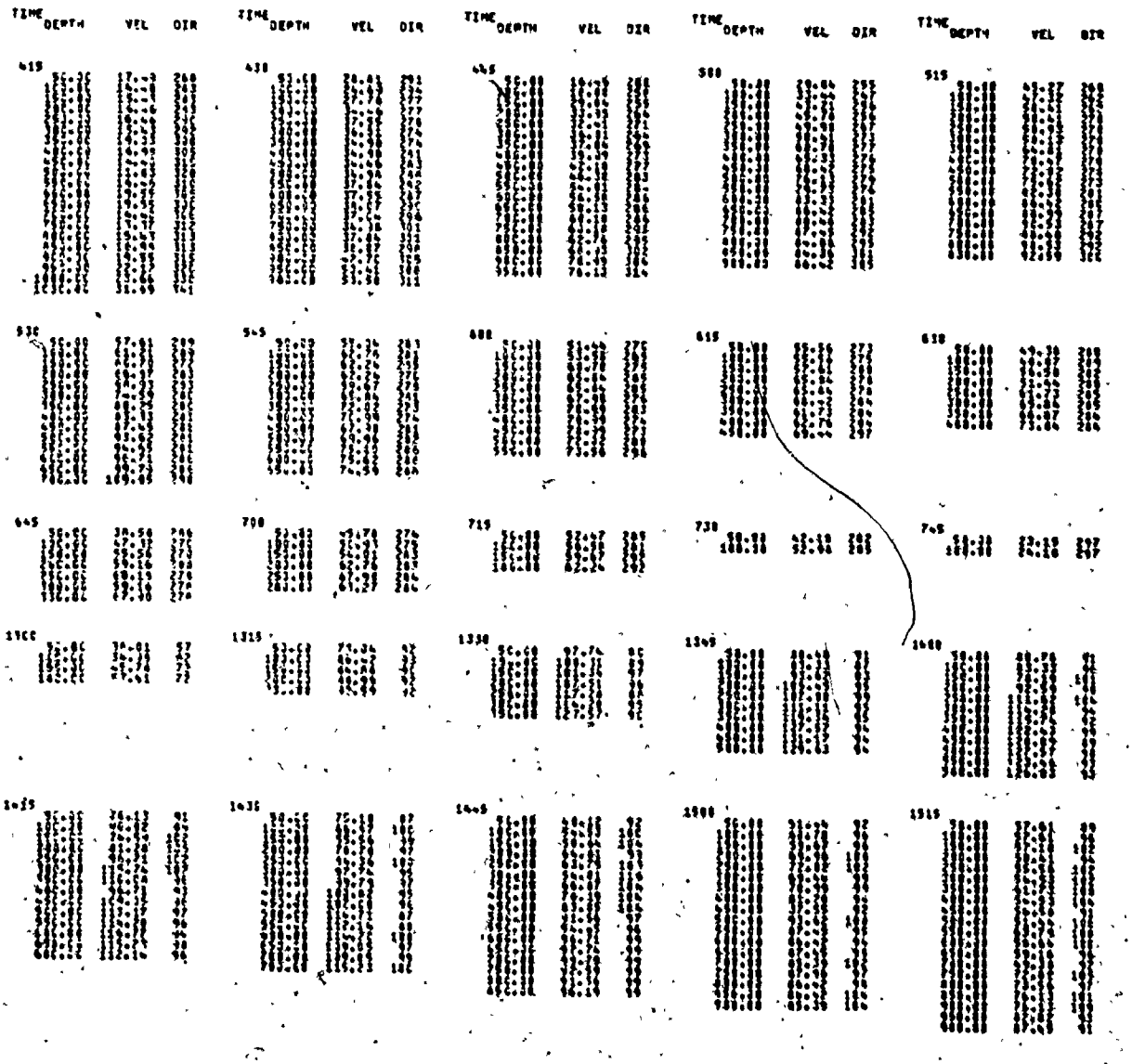
TIME DEPTH VEL DIR
TIME DEPTH VEL DIR
TIME DEPTH VEL DIR
TIME DEPTH VEL DIR
TIME DEPTH VEL DIR

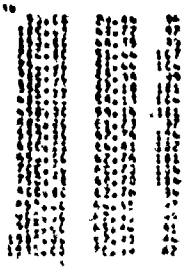

DATE - 12/ 7/72 **2f**

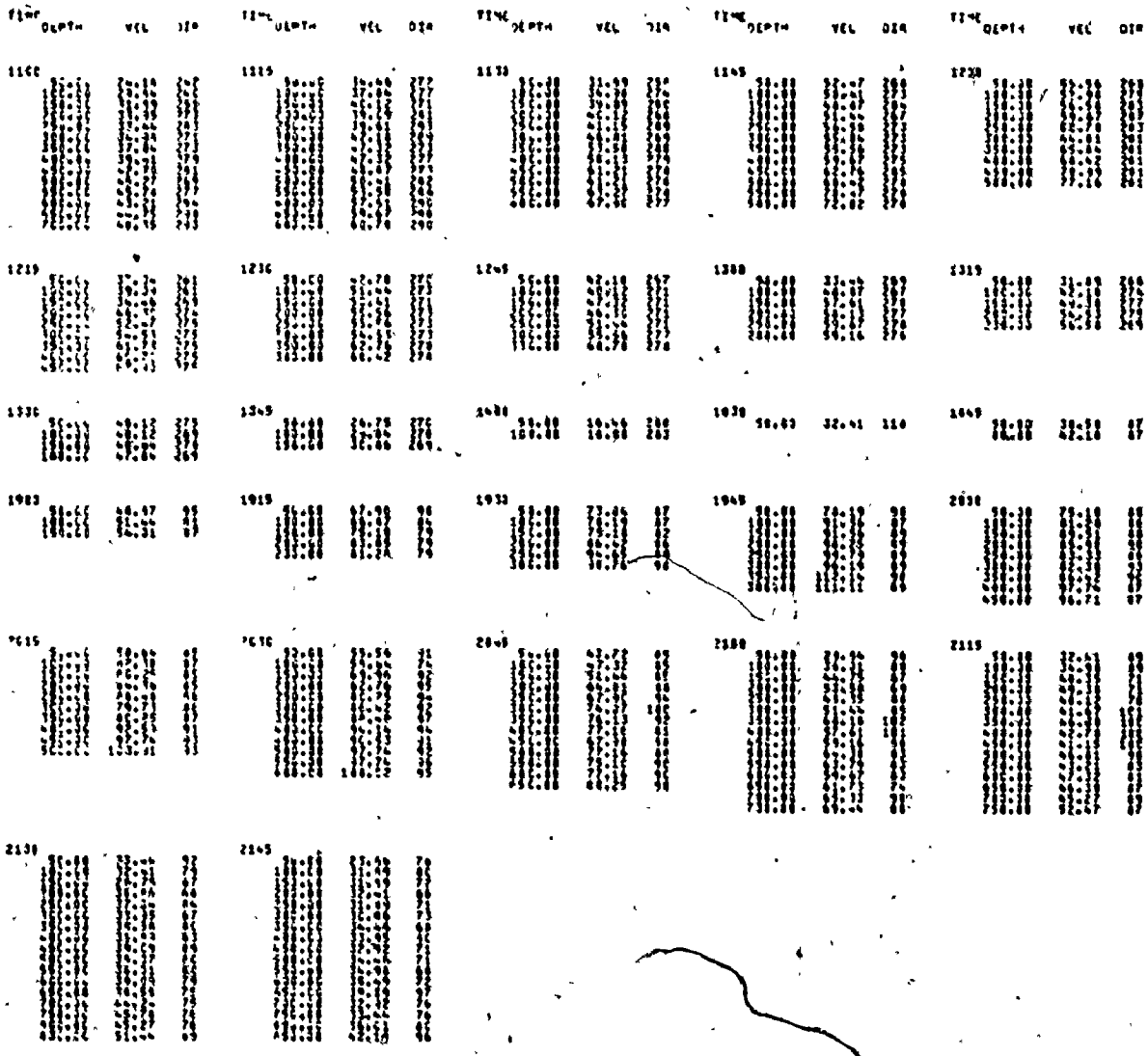

DATE - 12/ 7/72 **3a**

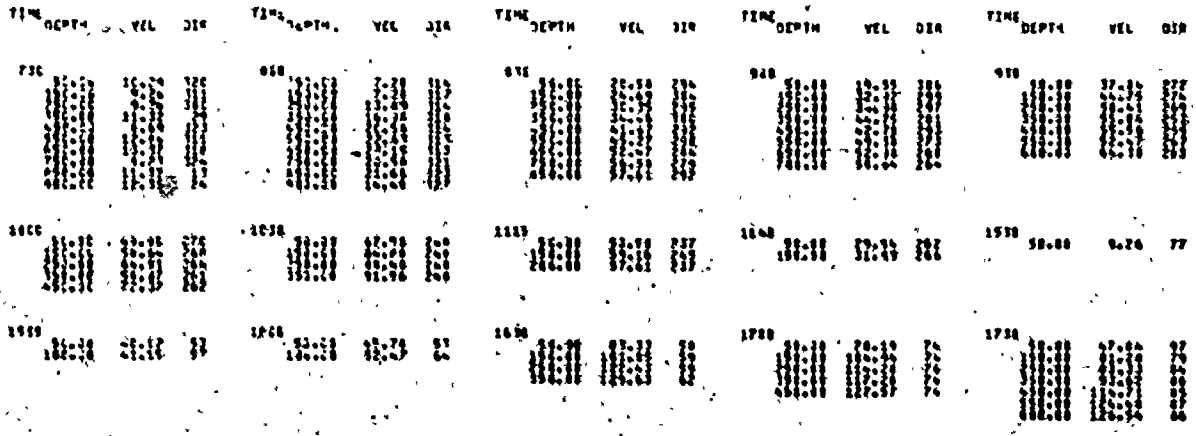

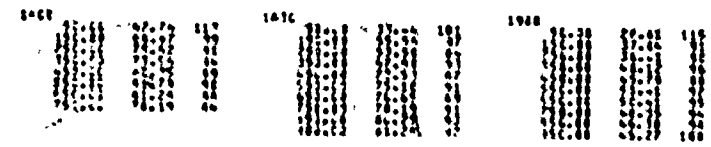

DATE - 2/ 7/72 **3b**

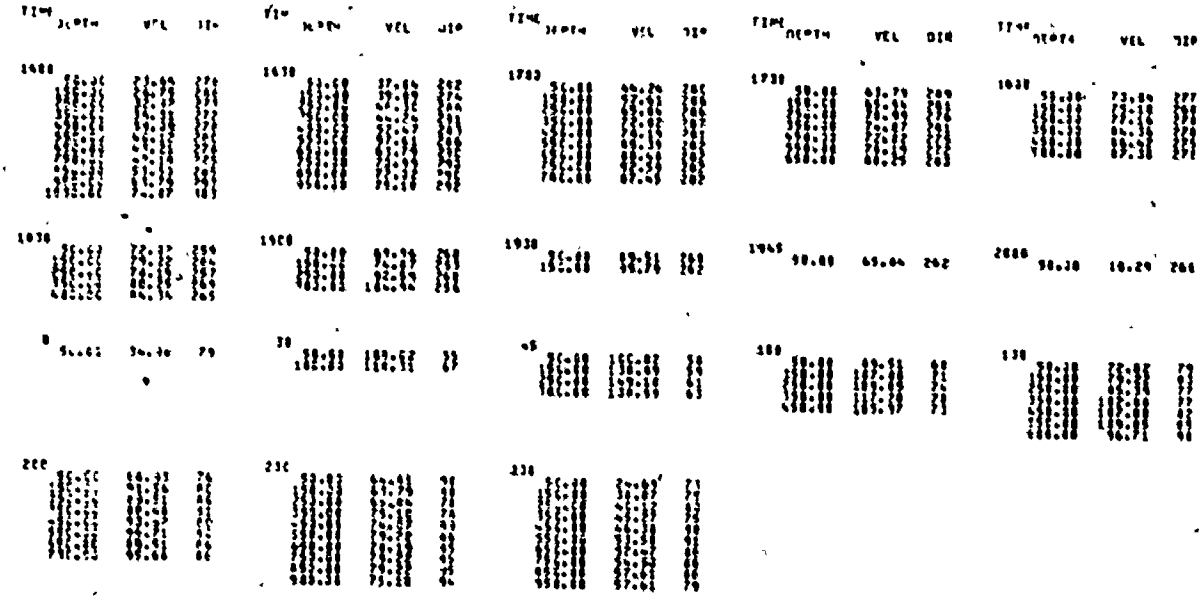

DATE - 2/ 7/72 **4a**

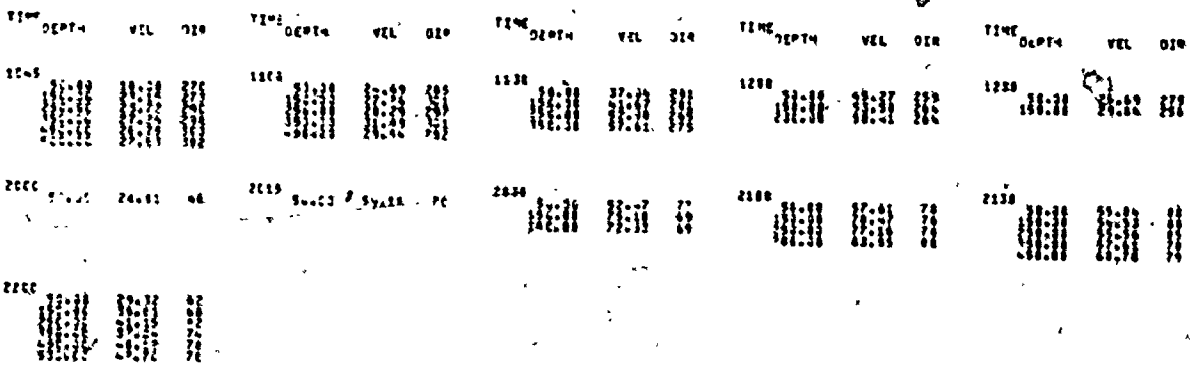

DATE - 22/ 7/72 **4b**

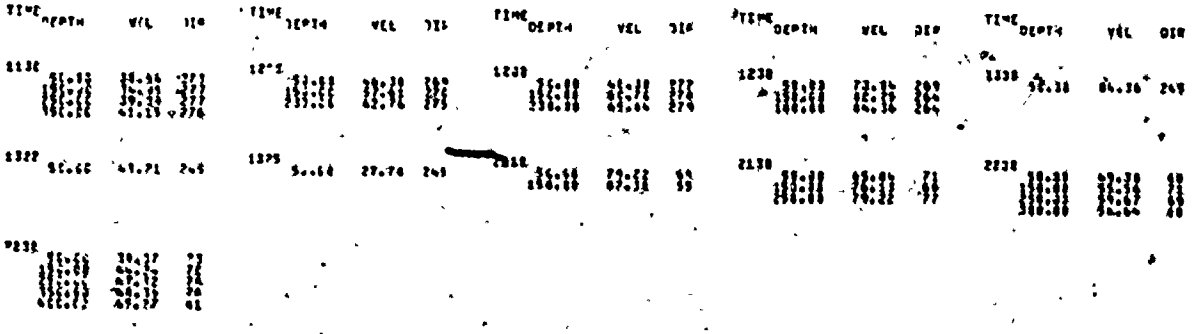

DATE - 2/ 7/72 **5a**

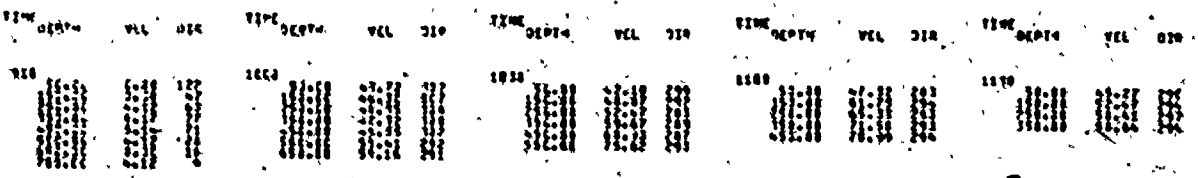

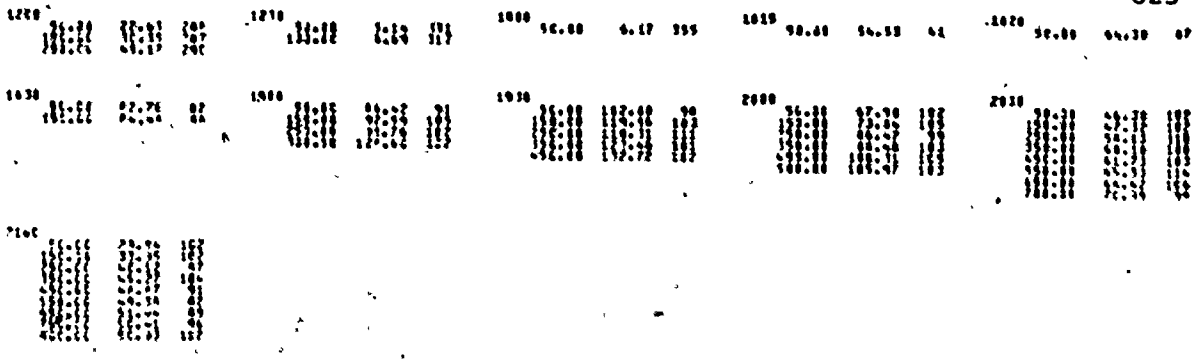

5b

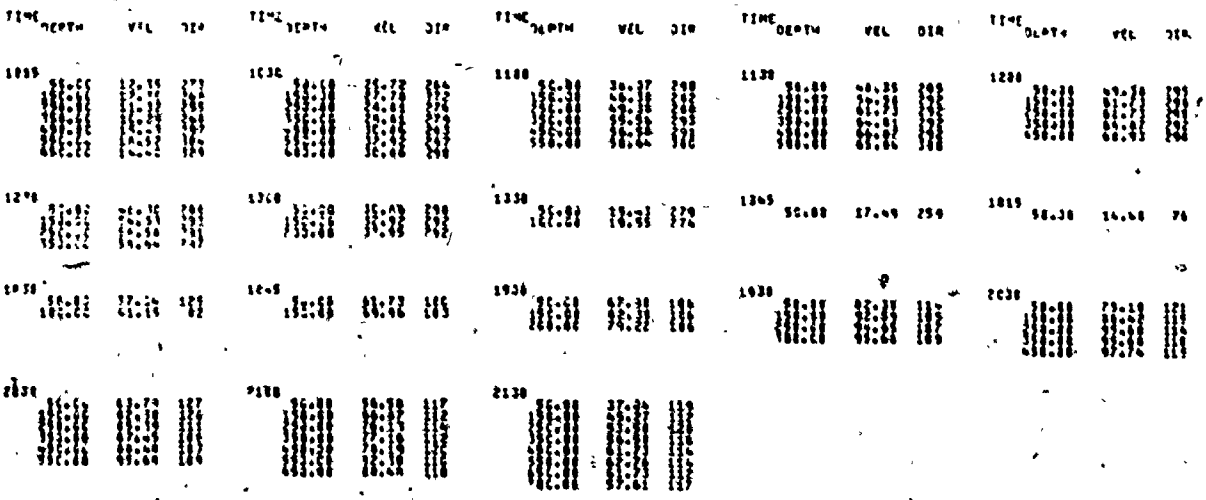

5c

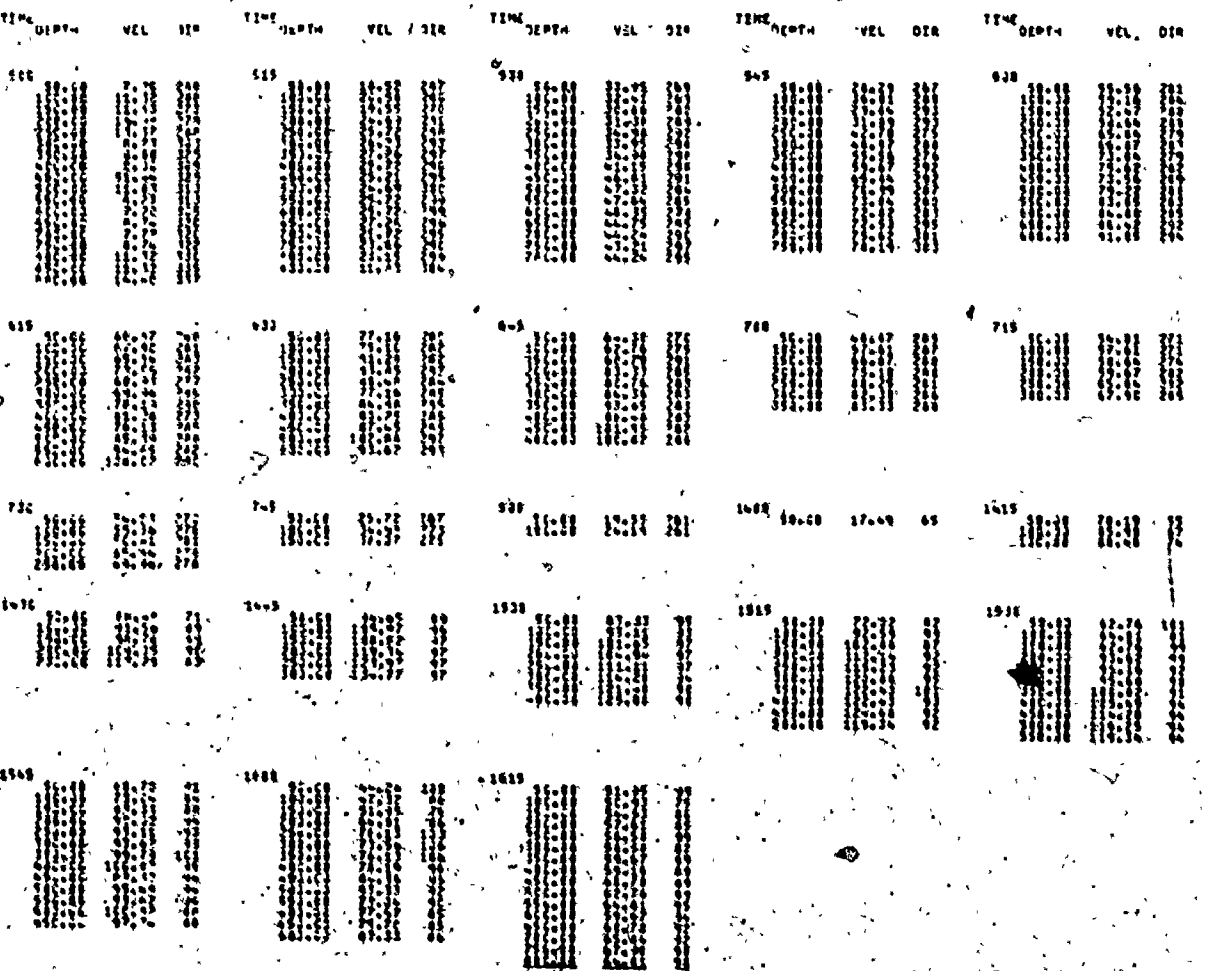

6a

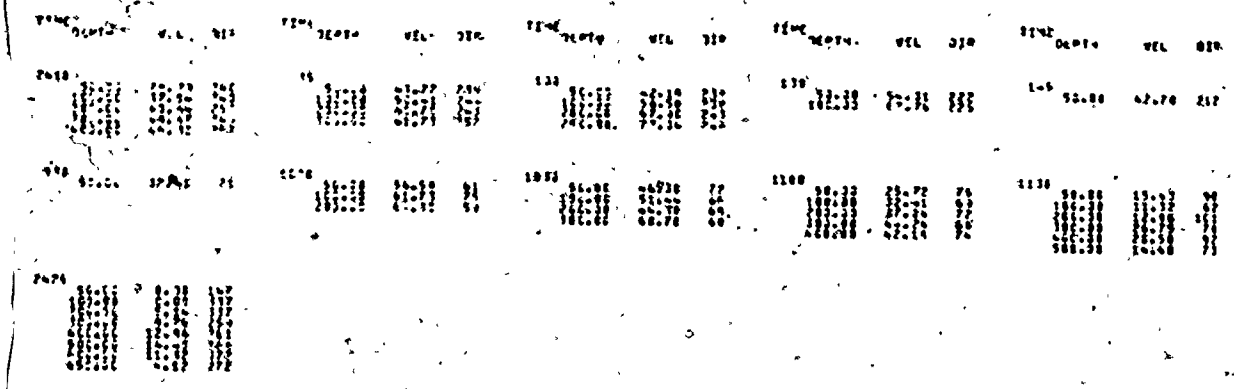

6b

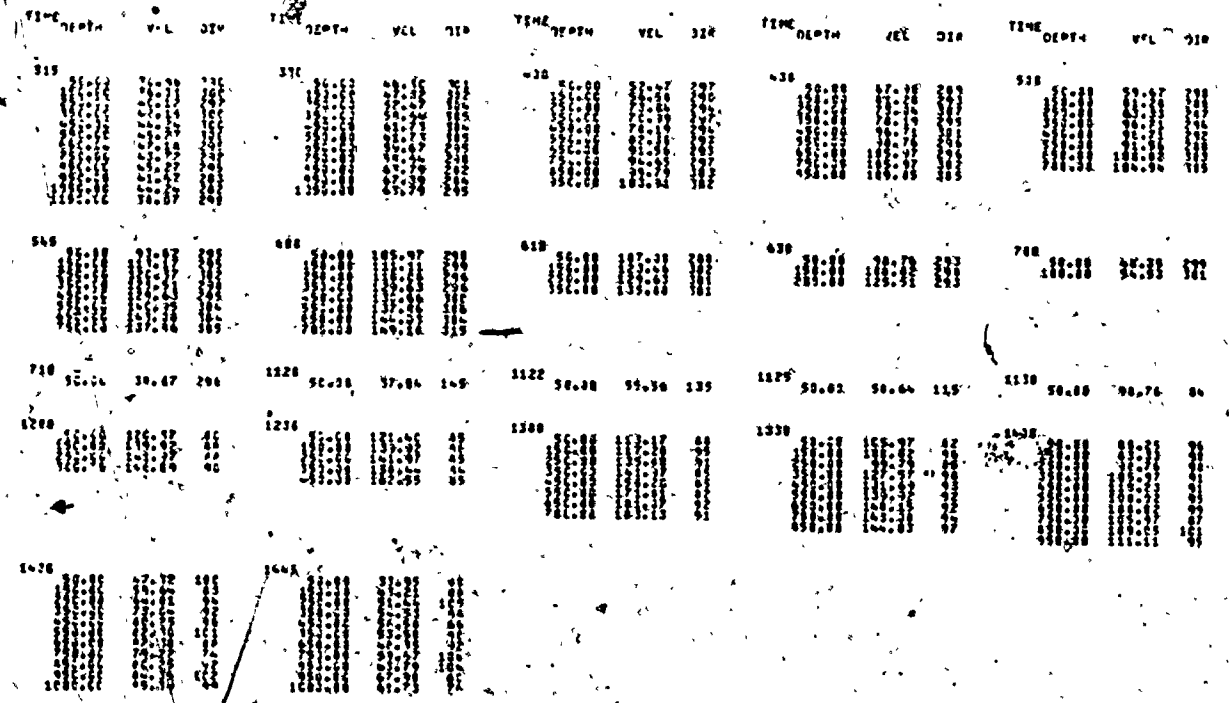

6c

6d

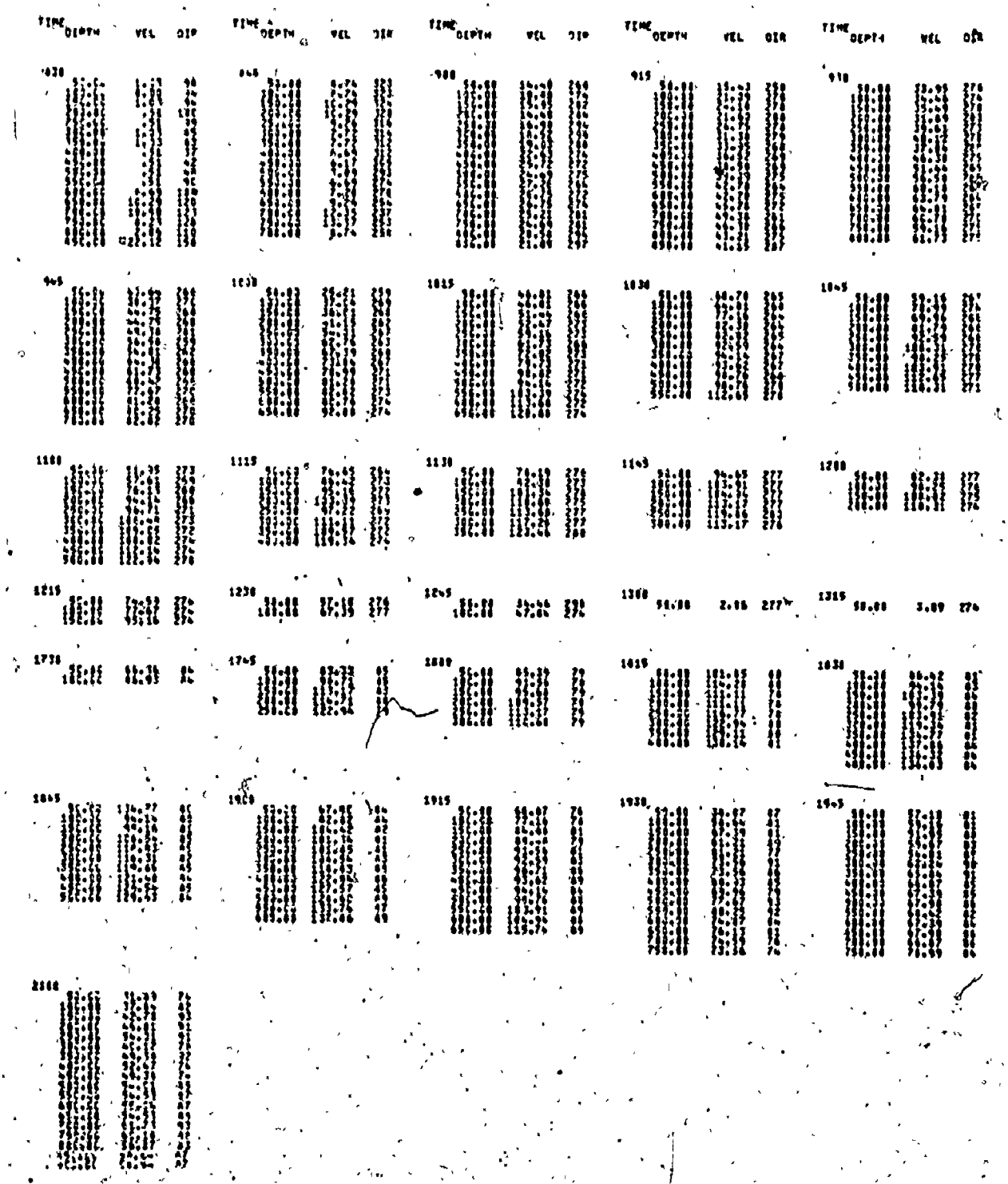

6e

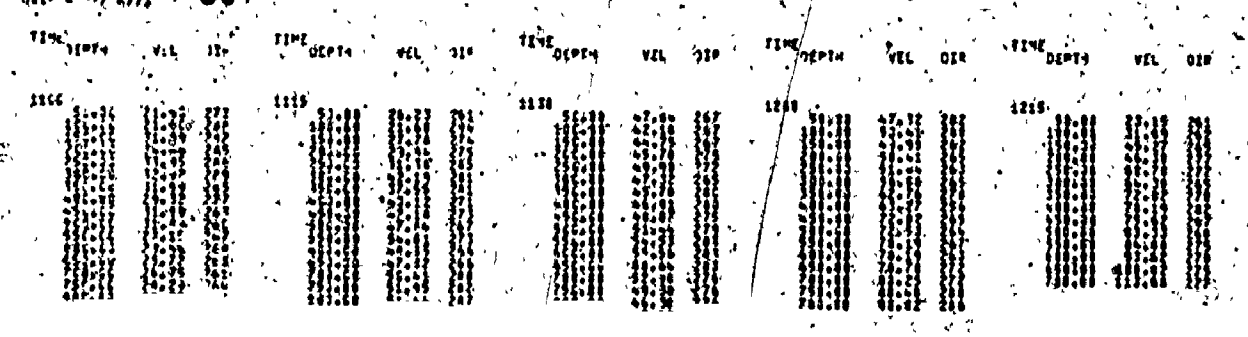

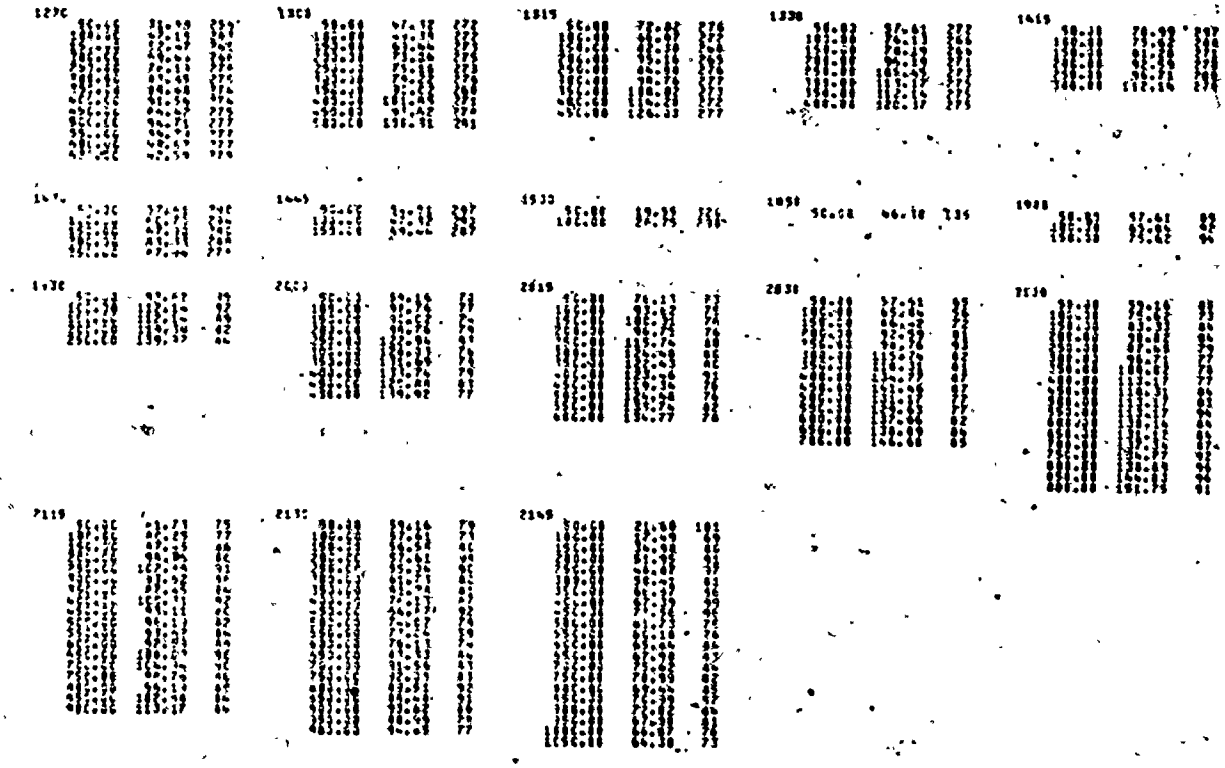

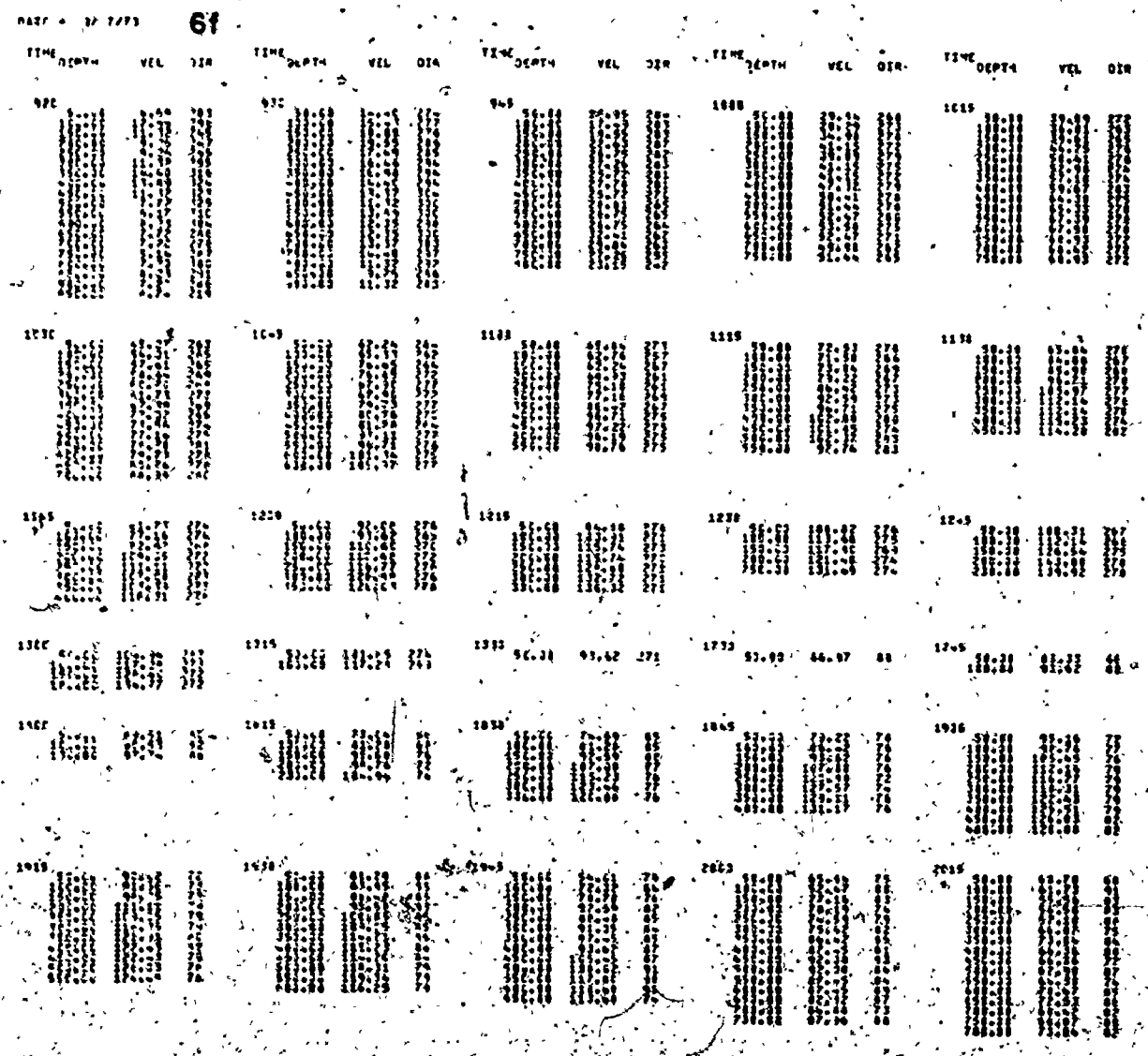
TIME
DEPTH
VEL
DIR

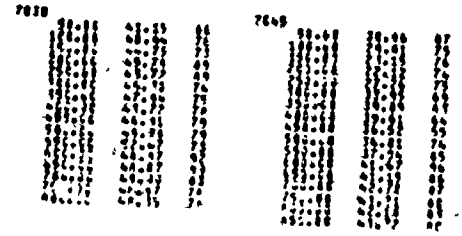

DATE = 17/ 7/72 **7a**

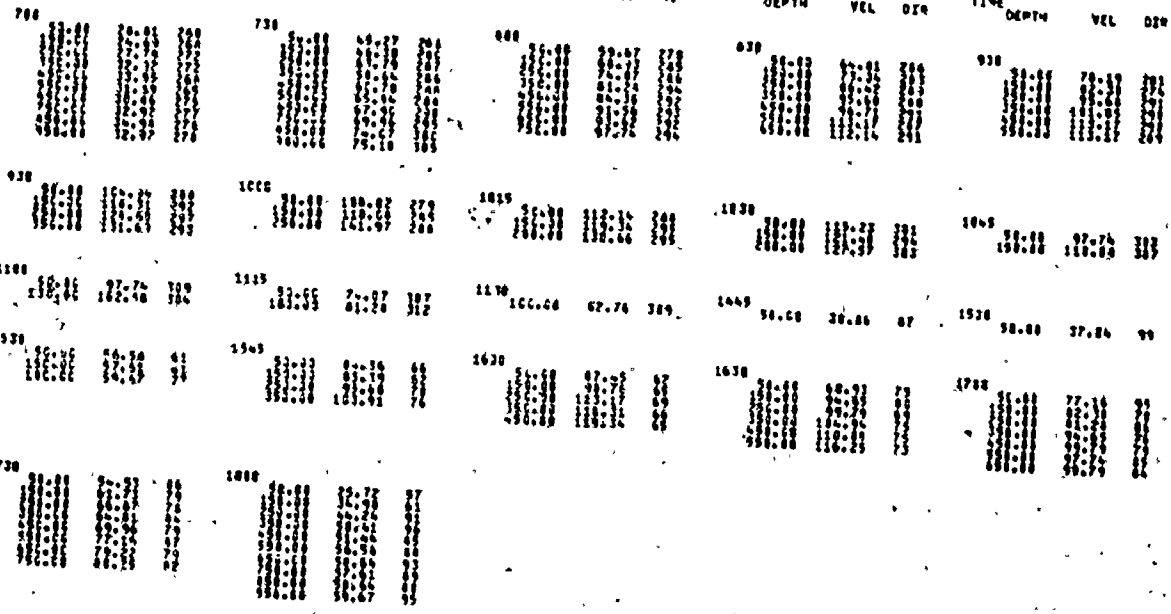

DATE = 11/ 6/73 **7b**

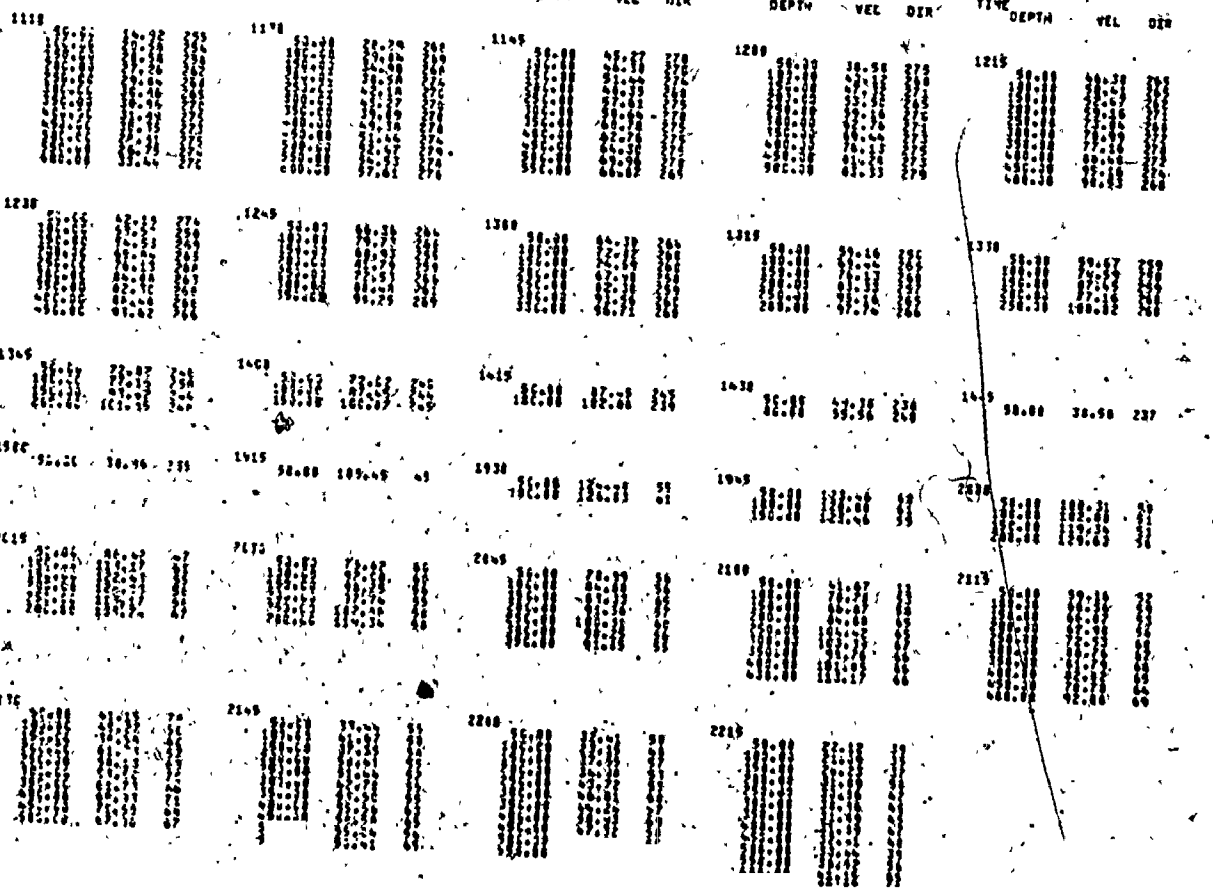

DATE - 5/ 7/77 **8a**

TIME	DEPTH	VEL	DIR
830			
1100			
1630			

TIME	DEPTH	VEL	DIR
900			
1115	56.69	22.07	298
1900			

TIME	DEPTH	VEL	DIR
930			
1740	56.88	14.48	61
1930			

TIME	DEPTH	VEL	DIR
1000			
1745	58.38	13.69	92

TIME	DEPTH	VEL	DIR
1010			
1830			

DATE - 15/ 7/77 **8b**

TIME	DEPTH	VEL	DIR
210			
1300			

TIME	DEPTH	VEL	DIR
300			

TIME	DEPTH	VEL	DIR
1230			

TIME	DEPTH	VEL	DIR
1200			

TIME	DEPTH	VEL	DIR
1230			

DATE - 15/ 8/77 **9**

TIME	DEPTH	VEL	DIR
1500			
1730			
170			

TIME	DEPTH	VEL	DIR
1510			
1800	53.68	27.78	229

TIME	DEPTH	VEL	DIR
1530			
20	56.88	53.58	79

TIME	DEPTH	VEL	DIR
1630			
30			

TIME	DEPTH	VEL	DIR
1700			
100			

DATE - 5/ 9/77 **10**

TIME	DEPTH	VEL	DIR
30			
330			
930			

TIME	DEPTH	VEL	DIR
300			
930	56.69	18.98	255

TIME	DEPTH	VEL	DIR
130			
900	55.69	54.87	97

TIME	DEPTH	VEL	DIR
250			
1020			

TIME	DEPTH	VEL	DIR
210			
1030			

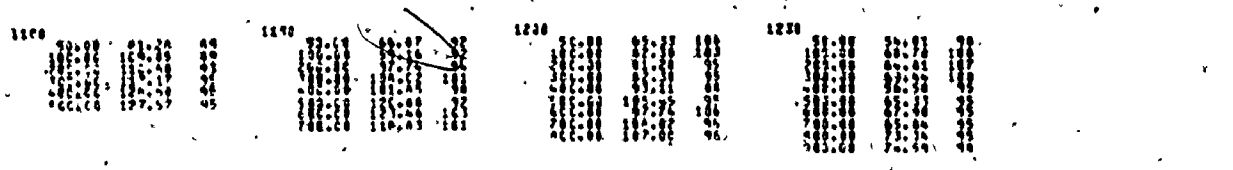

DATE = 2/ 4/71 11

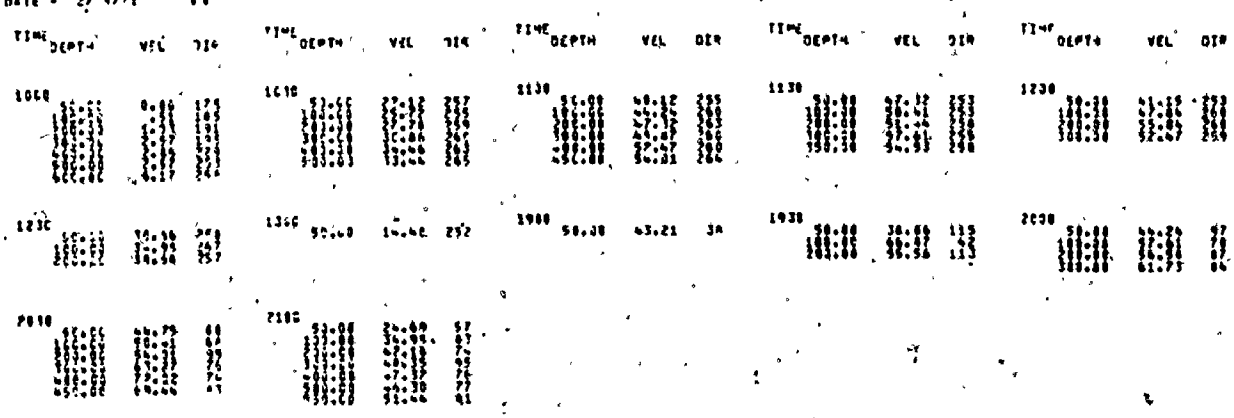

DATE = 3/ 4/71 12

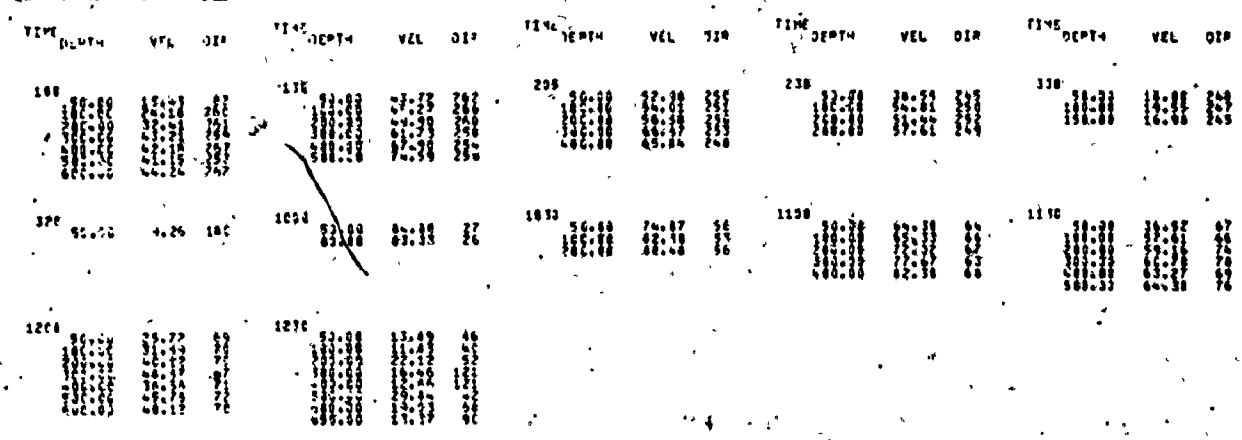

DATE = 13/ 4/71 13

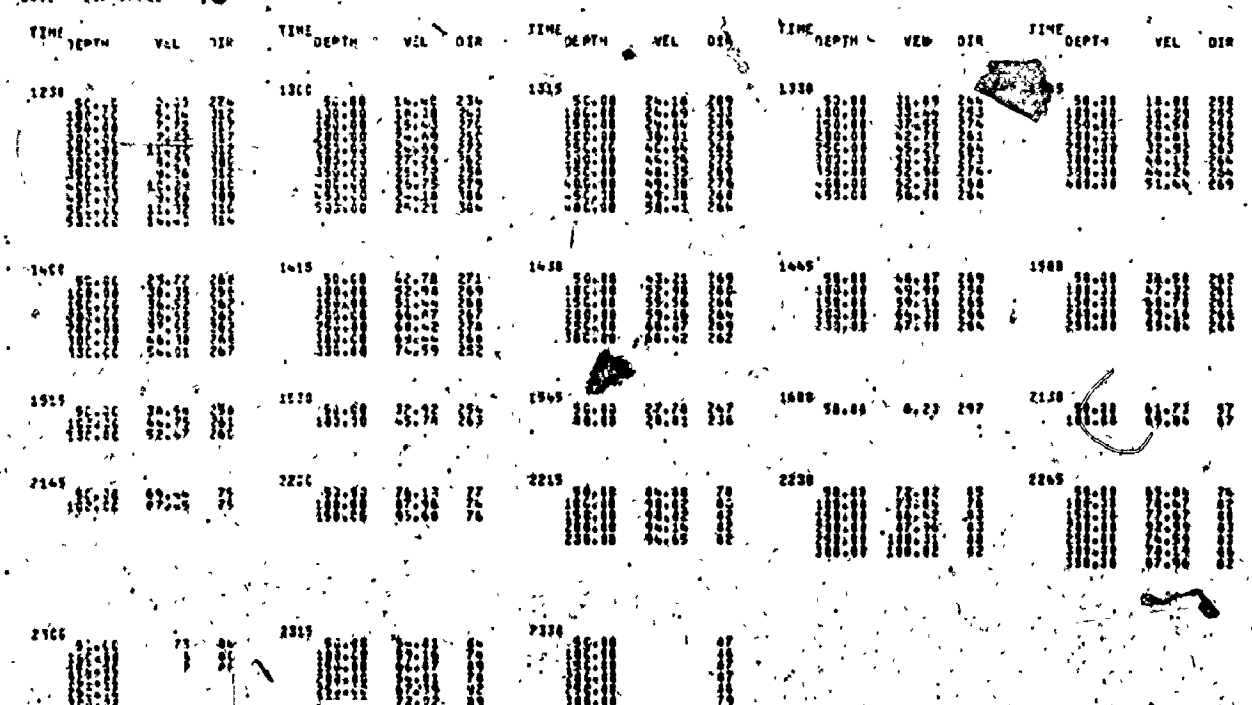

DATE = 14

TIME	DEPTH	VEL	DIR
430			
445			
500			
515			
530			
545			
600			
615			
630			
645			
700			
715			
730			
1315			
1330			
1345			
1400			
1415			
1430			
1445			
1500			
1515			

DATE = 15

TIME	DEPTH	VEL	DIR
1330			
1345			
1400			
1415			
1430			
1445			
1500			
1515			
1530			
1545			
2200			
2215			
2230			
2245			
2300			
2315			
2330			
2345			
0			

DATE = 16

TIME	DEPTH	VEL	DIR
1130			
1145			
1200			
1215			
1230			

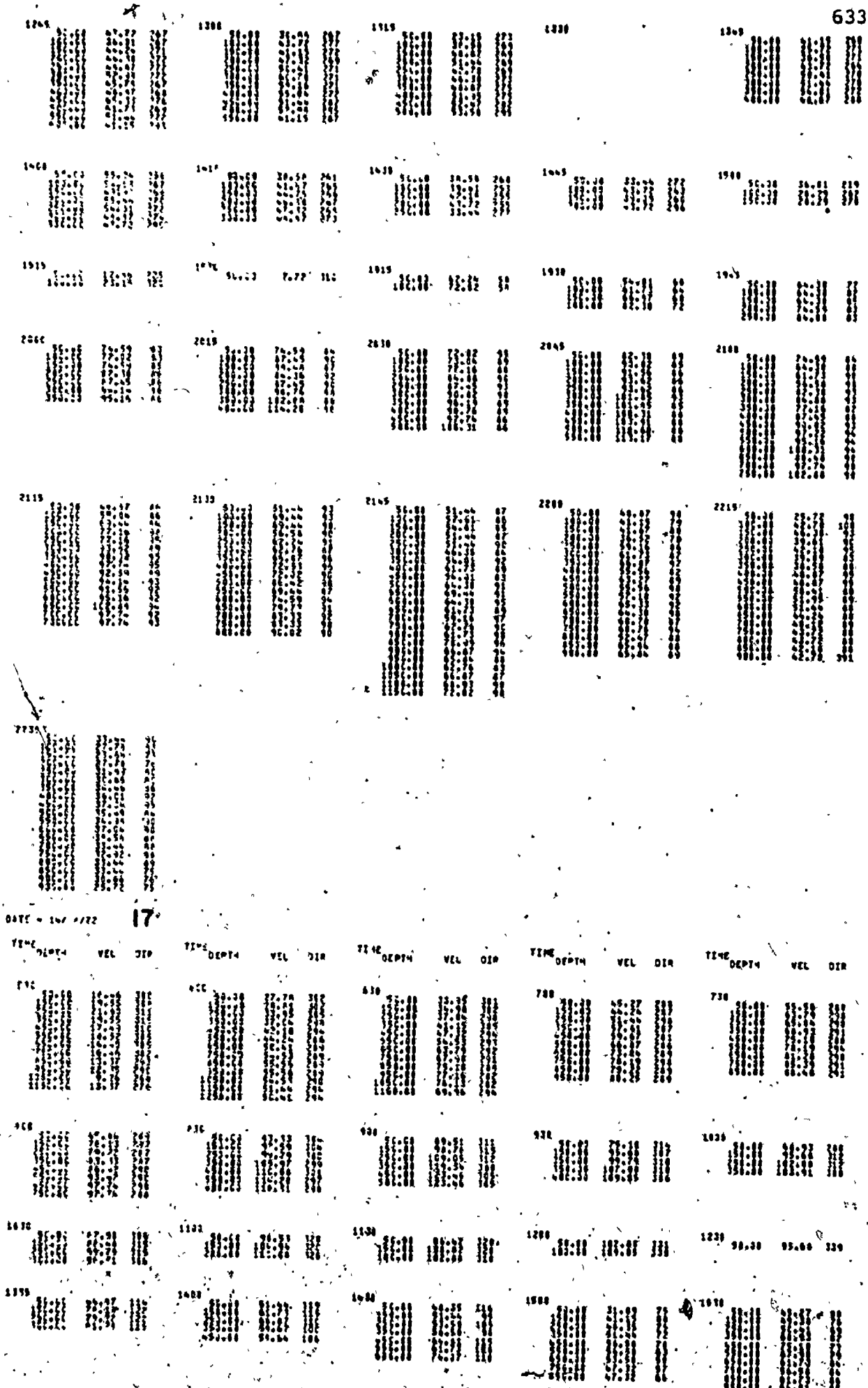

17

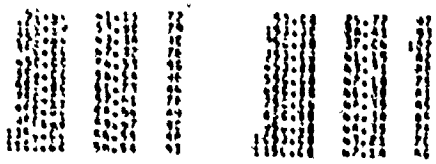

DATE - [illegible] 18

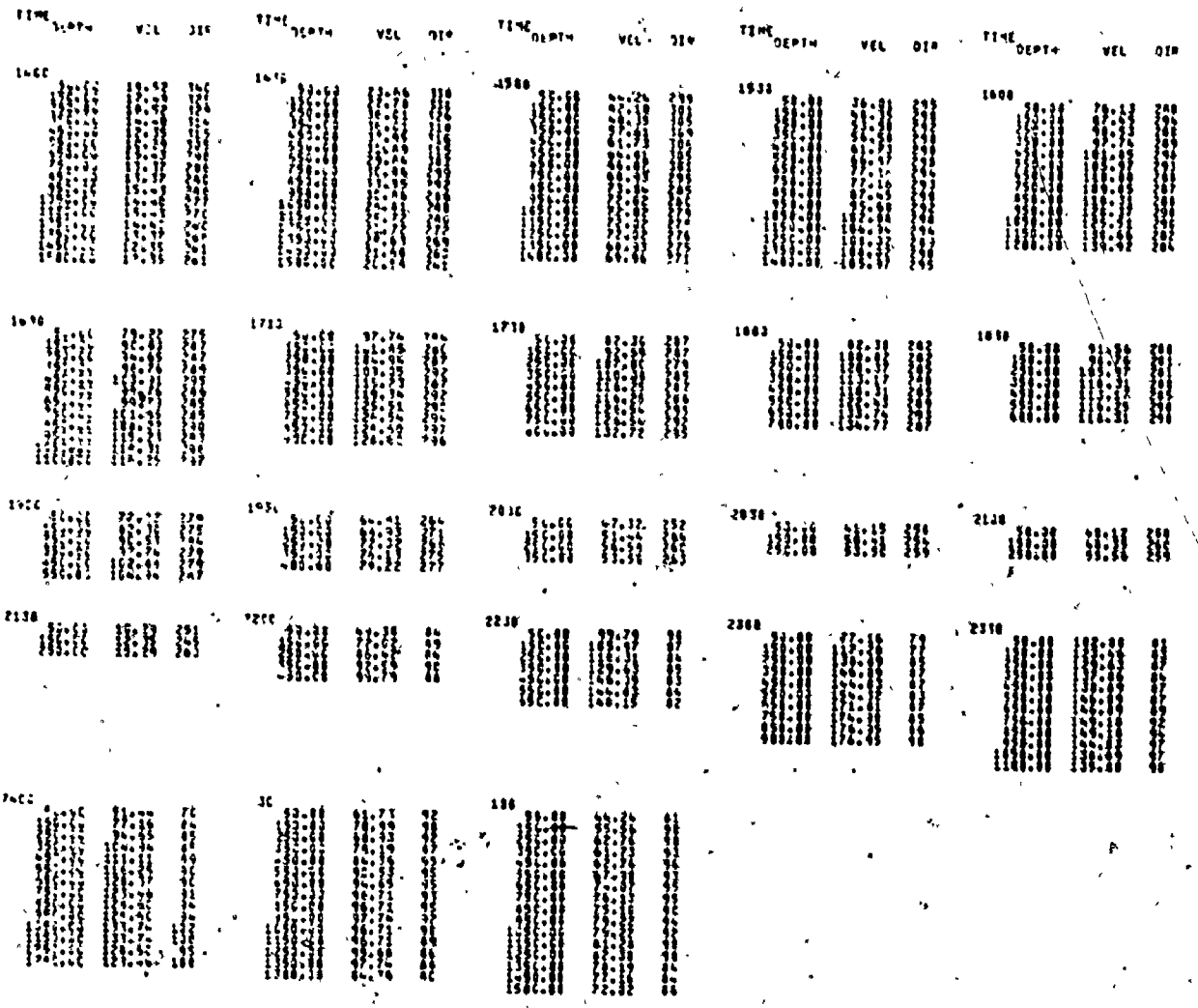

DATE - [illegible] 19a

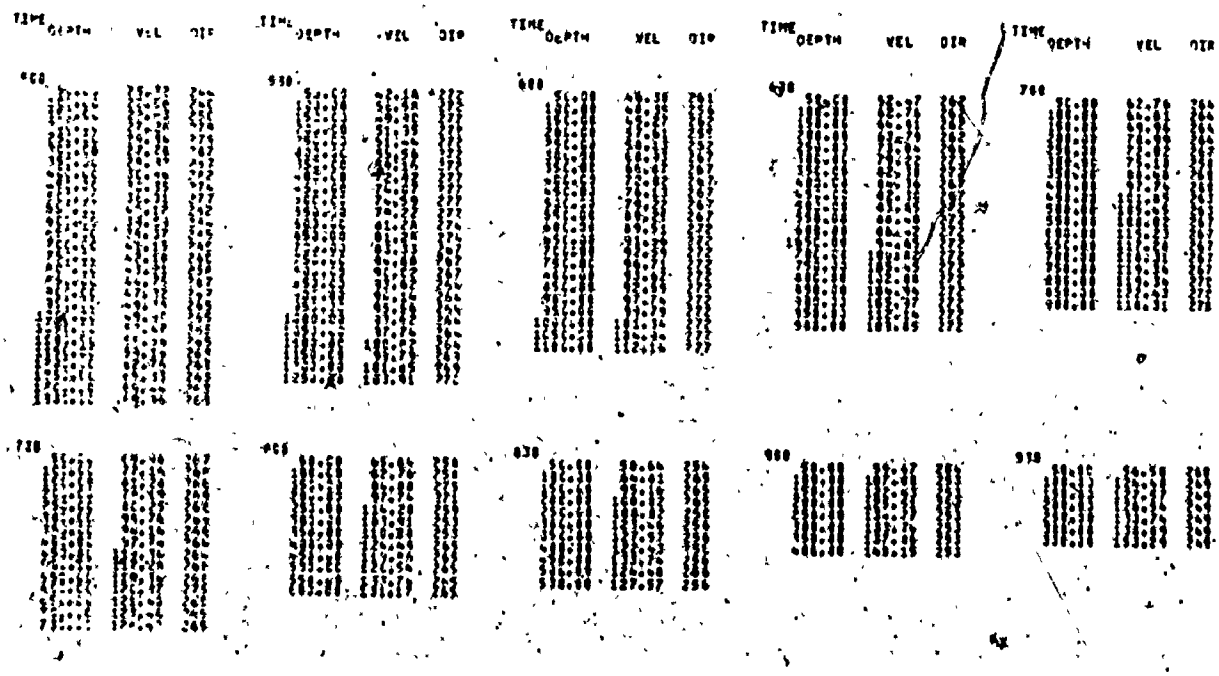

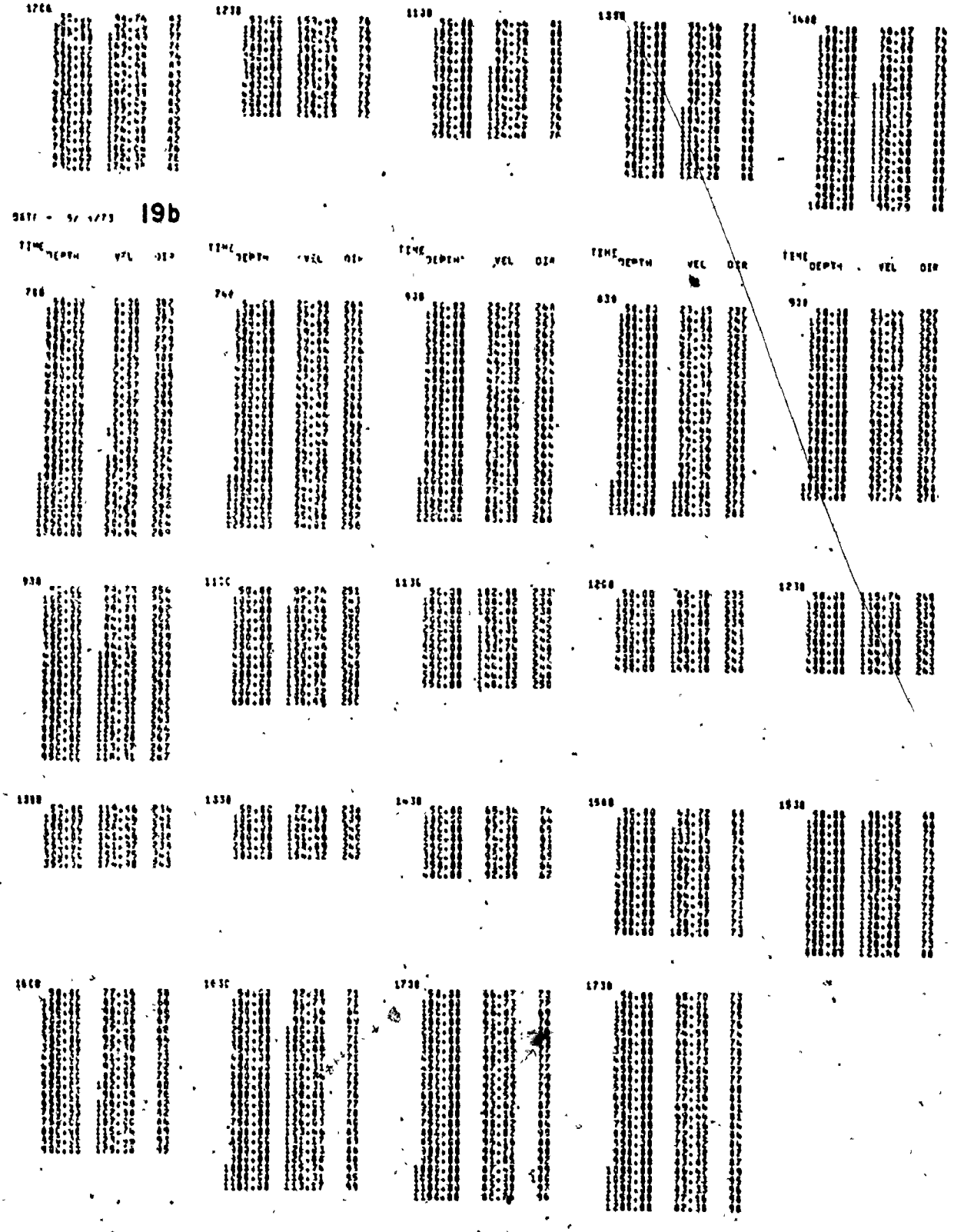
19b
20a

DATE = 15/ 4/77 **20b**

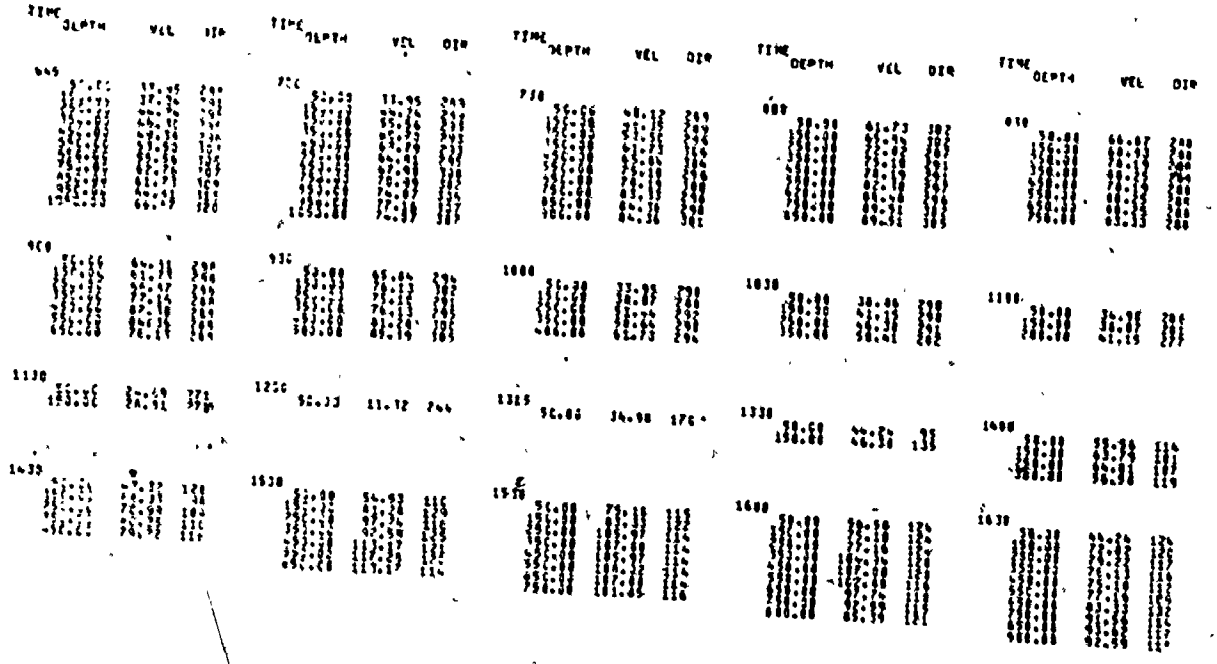

III.4: SUMMARY OF AUTOMATIC CURRENT METER MEASUREMENTS

Frequency distribution summaries of the point velocity data (current speed and direction 0.5 m from the bottom) measured at NB-1, NB-6, NB-8, SB-1, SB-3, SB-17 and SB-20 (see Fig. 4.1 for locations). Speed is listed in knots (1 Knot = 0.5144 m/s) and direction in degrees relative to 'true' north.

NOEL BAY BAR I

FREQUENCY DISTRIBUTION OF DIRECTION AND RATE KNOTS

DIR	000 TO 019	020 TO 039	040 TO 059	060 TO 079	080 TO 099	100 TO 119	120 TO 139	140 TO 159	160 TO 179	180 TO 199	200 TO 219	220 TO 239	240 TO 259
000-009	013	004	001			001	002	002					
010-019	003	002	002	001	002	007	007						
020-029	003	002	001		002	001							
030-039		001	003	001	001			001					
040-049	003	004	002										
050-059	003	002					003						
060-069	004	001	001			002							
070-079	006	005	005										
080-089	005	010	011	004	003	004	001						
090-099	010	008	010	021	008	015	007	001					
100-109	001	022	009	006	032	056	002	015					
110-119	013	001	012	016	042	079	002	014					
120-129	014	007	021	025	034	033	032	001					
130-139	034	013	017	017	033	015	006	008					
140-149	013	017	013	011	025	014	010	001					
150-159	013	011	004	001	013	007	003						
160-169	017	001	003	002	002	001							
170-179	001												
180-189													
190-199													
200-209													
210-219		001											
220-229													
230-239													
240-249													
250-259													
260-269													
270-279													
280-289													
290-299													
300-309													
310-319							001						
320-329													
330-339													
340-349													
350-359	012	[illegible]	[illegible]	[illegible]	[illegible]	013							
	171	164	125	[illegible]	[illegible]	236	116	43	0	0	[illegible]	0	0

DIR	260 TO 279	280 TO 299	300 TO 319	320 TO 339	340 TO 359	360 TO 379	380 TO 399	400 TO 419	420 TO 439	440 TO 459	460 TO 479	480 TO 499	
000-009													25
010-019													24
020-029													9
030-039													9
040-049													9
050-059										001			9
060-069													8
070-079													16
080-089													42
090-099													80
100-109													165
110-119													243
120-129													157
130-139													149
140-149				001									108
150-159													66
160-169													24
170-179													1
180-189													0
190-199													0
200-209													0
210-219													1
220-229													0
230-239													0
240-249													0
250-259													0
260-269													0
270-279													0
280-289													0
290-299													0
300-309													0
310-319													1
320-329													0
330-339													0
340-349													0
350-359													21
	0	0	0	1	0	0	0	0	0	1	0	1	1187

NO. OF [illegible] IS 0

SELMA BAR 3

FREQUENCY DISTRIBUTION OF DIRECTION AND RATE KNOTS

DIR	000 TO 019	020 TO 039	040 TO 059	060 TO 079	080 TO 099	100 TO 119	120 TO 139	140 TO 159	160 TO 179	180 TO 199	200 TO 219	220 TO 239	240 TO 259	260 TO 279	280 TO 299	300 TO 319	320 TO 339	340 TO 359	360 TO 379	380 TO 399	400 TO 419	420 TO 439	440 TO 459	460 TO 479	480 TO 499	
005-009	012																									12
010-014	002																									2
015-019					001																					1
020-024	001	001																								2
025-029				001					001																	2
030-034	002	002			001	001																				6
035-039			006	005	001		001	002										001								15
040-044	010	007	013	015	021	010	010	005	009	005	005	006	003	002				001								122
045-049	015	016	024	025	022	018	017	010	018	013	008	004	004	008		002	001	001								208
050-054	007	003	003	002	004	007	002	002	004					002			002	001								47
055-059	001		003	001	002		002		001		001															11
060-064		001			002	001	003		001																	8
065-069					002																					2
070-074		001					001																			2
075-079			001	001							001					001										4
080-084		001		001							001															3
085-089		001		001																						2
090-094					002																					2
095-099	001			001		001							001													3
100-104				001	001				001	001			001													5
105-109	001			001	002		001		001	001																7
110-114	003	002	002	001	001		002	001						001												13
115-119	006	003	001	001	003	001			001			001		001	001											19
120-124	004	003		003						001																16
125-129	003		002	004	001	003	004	004		003	002	002		001			001									32
130-134	011	003	003	002	003	005	004	007	006	005	004	001	003	002	002		002									67
135-139	010	013	012	020	018	017	021	012	028	020	017	011	006	004	004											236
140-144	009	003	001	003	005	003	001	003	003	003	001		002													46
145-149	002		001	001	001					001				001												7
150-154	001																									1
155-159	001																									1
160-164																										0
165-169																										0
170-174	001																									1
175-179																										0
180-184																										0
	115	71	93	89	79	91	19	1	1	0	0	0	0	0												
	1	1	91	72	66	52	25	22	3	2	0	0	0	0												917

SELMA BAR 20

FREQUENCY DISTRIBUTION OF DIRECTION AND RATE KNOTS

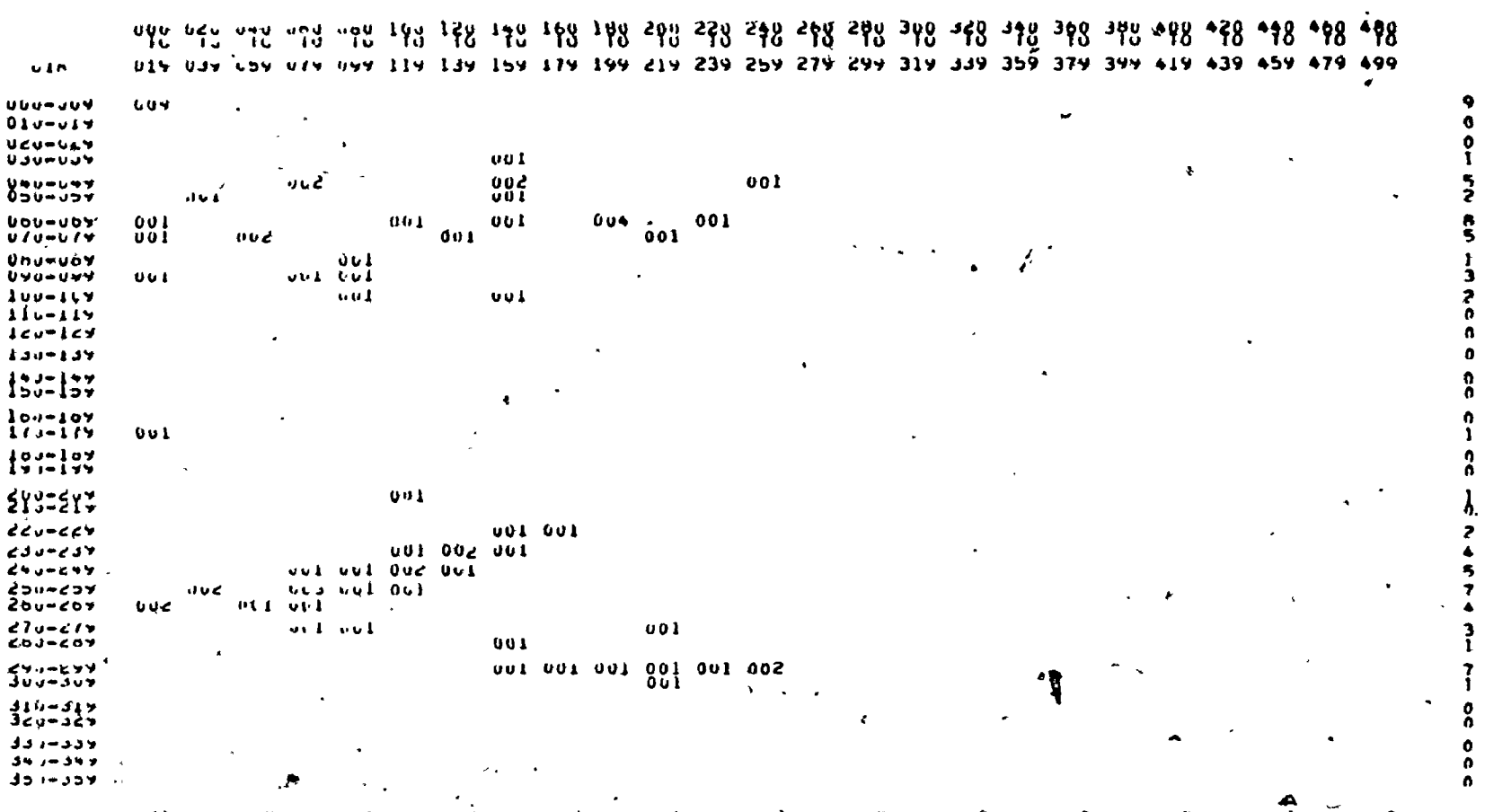

SELMA BAR 17

PERCENT DISTRIBUTION OF DIRECTION AND RATE KNOTS

DIR.	000	020	040	060	080	100	120	140	160	180	200	220	240	260	280	300	320	340	360	380	400	420	440	460	480	
	1-	10	10	10	10	10	10	10	10	10	10	10	10	10	10	10	10	10	10	10	10	10	10	10	10	
	019	039	059	079	099	119	139	159	179	199	219	239	259	279	299	319	339	359	379	399	419	439	459	479	499	
000-009	003		002					001					001													7
010-019			001																							1
020-029												001														1
030-039	001			01																						2
040-049																										0
050-059		001	001	001							001															4
060-069	001	001	001					001		002			001		001											8
070-079	002	003	004			002	002				001	001			001		002	001								21
080-089	003	000	000	000	001	001	002	002	003	002	002	002	001			001		001								42
090-099	010	000	003	003	002	005	008	004	004	005	005	002	003	002	002	001		001								66
100-109	011	003	000	004	000	001	001	002	002	001	001			002	001	001										48
110-119	000	004	000	001	004	003		002	001		001				001											31
120-129	001	003	001	001		001	001			001		001	001				001									12
130-139	002	002	001		003	002																				10
140-149	003	002	004	002			003	001				002	003	002												22
150-159	005	002	001	003	001	001		004	002	001			001					001								22
160-169	002	004	003	003	002	003	001	002	004			003		001												26
170-179	000		001	002			002			001																12
180-189	010	004	002	001			001				001			001												27
190-199	002	003									001															30
200-209	010	003				001			001																	18
210-219	003	002	001	001																						6
220-229	000	002	002		002	001	002	001	003	002		001														22
230-239			002	001							001		001	001		001										7
240-249	003		001									002	001	002	001											10
250-259	001		001			002	001	001	001	001	001	002	001	001												14
260-269	003	001	001	000	000	001	000	000	001	000	000	000	001		001											72
270-279	000	001	001	001	001	001	002	000	001		001															34
280-289	002	003	000	000	000	001	001	002	001			001	001	001	002	001		001								52
290-299	002	002	001		003	001	002			003						001										17
300-309							001		001																	2
310-319																										0
320-329																										0
330-339																										0
340-349																										0
350-359																										0
	153	71	42	30	37	28	29	24	22	18	13	10	8	5	10	6	0	0	0	0	0	0	0	0	0	648

SELMA BAR I

FREQUENCY DISTRIBUTION OF DIRECTION AND RATE KNOTS

DIR	000 TO 019	020 TO 039	040 TO 059	060 TO 079	080 TO 099	100 TO 119	120 TO 139	140 TO 159	160 TO 179	180 TO 199	200 TO 219	220 TO 239	240 TO 259	260 TO 279	280 TO 299	300 TO 319	320 TO 339	340 TO 359	360 TO 379	380 TO 399	400 TO 419	420 TO 439	440 TO 459	460 TO 479	480 TO 499	
000-009	012																									12
010-019	002								001																	3
020-029				001		002	002	001	002																	8
030-039	001	002	002	002	003	004	007	010	006	004	003	005	002	001												52
040-049	011	003	010	001	000	002	008	007	012	006	003	001	004	001												77
050-059	003	001	001			001	002	003	009	011	006	003	003	001	002											46
060-069	010	002	002	005	006	007	008	011	011	011	010	005														99
070-079	009	005	010	010	013	017	016	014	012	007	003	001														121
080-089	003	003	004	005	003	001				001				001					001							23
090-099	002	003	001																							6
100-109	001																									1
110-119	001					001		001																		3
120-129		001	001	001																						3
130-139							001																			1
140-149																										0
150-159	001		001																							2
160-169			002																							2
170-179	001	002																								3
180-189	001			001	001																					3
190-199			001																							1
200-209																										0
210-219	002						001		003					001			001									8
220-229	001			001	002	002	010	020	022	007	002		001													103
230-239	002	003	002	002	007	010	028	023	007	002	001															87
240-249	002	002	001	010	010	020	028	003		001																75
250-259	010	010	012	017	020	017	005																			94
260-269	010	014	017	010	008	003			001				002													65
270-279	014	002	001		001																					18
280-289	011	003	005									001	002		001											22
290-299	001	002	001	001										001												8
300-309																										0
310-319			001	001	001																					3
320-329																										0
330-339	001																									1
340-349	001																									1
350-359		001			001			001		001		001														5
	13	11	14	10	12	16	23	11	09	05	02	01	14	3	0	1	0	1	0	0	0	0	0	0	0	
	11		11		16		11		09		05		17		0		0		0		0		0		0	972

NOEL BAY BAR 8

FREQUENCY DISTRIBUTION OF DIRECTION AND RATE KNOTS

DIR	000 TO 019	020 TO 039	040 TO 059	060 TO 079	080 TO 099	100 TO 119	120 TO 139	140 TO 159	160 TO 179	180 TO 199	200 TO 219	220 TO 239	240 TO 259	260 TO 279	280 TO 299	300 TO 319	320 TO 339	340 TO 359	360 TO 379	380 TO 399	400 TO 419	420 TO 439	440 TO 459	460 TO 479	480 TO 499	
000-009	024	001																								25
010-019	008																									8
020-029	010	002	004	011	002																					29
030-039	004		001	004	003	002																				14
040-049	004	001																								5
050-059	004	004																								8
060-069	013	001																								14
070-079	007	002																								9
080-089	027	010	007	001	002	001	002																			44
090-099	051	022	010	022	023	015	009	004																		163
100-109	035	024	029	006	013	009	001	003		001																377
110-119	053	032	048	007	007	001	004	013	002																	441
120-129	028	033	007	007	004	008	013	006		001																357
130-139	011	003		003	004	005																				28
140-149	011																									11
150-159	011	001																								12
160-169	000																									0
170-179			002																							2
180-189																										0
190-199																										0
200-209																										0
210-219																										0
220-229																										0
230-239																										0
240-249																										0
250-259																										0
260-269																										0
270-279																										0
280-289																										0
290-299																										0
300-309																										0
310-319																										0
320-329																										0
330-339																										0
340-349																										0
350-359	006		001																							7
	365		165		132		115		25		2		0		0		0		0		0		0		0	
		131		293		211		52		2		0		0		0		0		0		0		0		1560

NOEL BAY BAR 6

FREQUENCY DISTRIBUTION OF DIRECTION AND RATE KNOTS

A P P E N D I X IV

HYDRAULIC PARAMETERS

IV.1 METHODS OF CALCULATION

Two fundamental fluid properties used in some of the following calculations are the kinematic viscosity (ν) and the density of seawater (ρ). Values for these properties were determined from tables in Mikaye and Koizumi (1948, Tables I and II) and Cox (1965, assuming an average seawater temperature of 15°C (see section 2.4) and an average salinity of 30 o/oo.

$$\rho = 1022.15 \text{ kg/m}^3$$

$$\nu = 1.189 \times 10^{-6} \text{ m}^2/\text{s}$$

Other constants included:

$$\rho_s = 2650.00 \text{ kg/m}^3$$

$$g = 9.8062 \text{ m/s/s}$$

$$\kappa = 0.40$$

The mean tidal ranges and times of high water in Appendix IV.2 were determined from the Canadian Tide and Current Tables (C.H.S., 1971, 1972 and 1973) for Burntcoat Head. The mean range is the average of the ebb and flood ranges for the given tidal cycle. The mean coefficient is the mean tidal range divided by the maximum tidal range (i.e., 16.1 m) at Burntcoat Head (Allen, 1976 b).

The hydraulic parameters listed in Appendix IV.2 were derived as follows (from left to right; S.I. units):

(a) Time

ADT = absolute Atlantic Daylight Time

From HW = hours from the time of high water at Burntcoat Head

(b) Total Depth = vertical distance from still-water level to bottom; determined by echo sounding and(or) cumulation of measurement increments from vertical velocity profiles; measured in metres.

(c) Bot. Dir. = direction of tidal currents 1 m from the bottom.

(d) Mean Speed = $\bar{u}$ = average of the vertical profile point velocities at 0.2D and 0.8D above the bottom.

(e) Stnd. Speed = mean speed standardized on the mean tidal range at Burntcoat Head (11.7 m)

$$= \frac{(\bar{u})(11.7)}{\text{mean range of particular ebb and flood}}$$

(f) Speed at 1 m = u_1 = current speed 1 m from bottom, determined from the linear regression line fitted to each vertical velocity profile.

(g) Stnd. Dev. = standard deviation of vertical profile current speeds.

(h) Turb. = turbulence coefficient (Section 4.3)

$$= \sum_{i=1}^{n} \left[\frac{\text{estimated speed - observed speed}}{n-2}\right]^{\frac{1}{2}} \Big/ u_*$$

where n = the total number of point measurements per velocity profile and i = the i th point measurement.

(i) Froude No. = $Fr = \dfrac{\bar{u}}{(gD)^{\frac{1}{2}}}$

(j) Reynolds No. = $Re = \dfrac{\bar{u}D}{\nu}$

(k) Discharge = $q = \bar{u}D$ = discharge in m^3/s per unit width of flow.

(l) Shear Vel. = $u_* = (gDS)^{\frac{1}{2}} = (A_1)\ (\kappa)/2.3$

where A_1 = the slope of the regression line fitted to each vertical velocity profile.

(m) Shear Stress = $\tau_o = u_*^2 \rho$

(n) Stream Power = $\omega = \tau_o \bar{u}$

(o) Sediment Discharge = q_{st} = the unit total sediment transport; See discussion on following page.

(p) Energy Slope = $S = \dfrac{u_*^2}{gD}$

(q) $zo = y_o = A_o$ = roughness height = depth intercept of the regression line fitted to each vertical velocity profile.

(r) KS = equivalent grain roughness of the boundary

$$= 10^{\left[\log D + 1.04 - \frac{1}{2.03(f)^{\frac{1}{2}}}\right]}$$

(s) $F = f$ = Darcy-Weisbach friction factor = $\frac{8u_*^2}{\bar{u}}$

(t) $N = n$ = the number of velocity point measurements per vertical profile.

(u) Corr. Coef. = r = correlation coefficient of the linear regression fitted to the measured vertical velocity profiles; see Davis, J.C. (1973, p. 192-221).

Sediment Discharge

The Ackers and White (1973; White, 1972) total sediment load transport function is relatively simple to use because only seven properties of the bed-material and flow, that can be derived from field observations or estimation from tables, are required, i.e., grain size (d_{50} or d_{35}), specific gravity of sediment (s, assumed to equal 2.65), mean flow velocity ($\bar{u}$, from the vertical velocity profiles, shear velocity (u_*, estimated from the slope of the regression line fitted to the measured vertical velocity profiles), depth of flow (D), kinematic viscosity of flow (ν, estimated from tables in Mikaze and Korzumi (1948) and Cox (p. 102-104, in Riley and Skirrow, 1965) and acceleration due to gravity (g, equal to 9.8062 m/s^2).

The transport function is based on three dimensionless relations: grain size (D_{gr}), particle mobility (F_{gr}) and sediment transport (G_{gr}). The dimensionless grain diameter (D_{gr}) resolves to the cube root of the ratio of the immersed sediment weight to viscous forces of the flow (a type of grain Reynolds number),

$$D_{gr} = d\left[\frac{9(s-1)}{\nu^2}\right]^{1/3}$$

and is a general expression that applies to fine, medium and coarse grained sediments.

The sediment mobility (F_{gr}) depends on the sediment grain size and the properties of the flow, i.e., whether the sediment is moved primarily as a 'near' bed process or largely in suspension. Ackers and White (1973) assumed that "the effective shear stress bears a similar relationship to mean stream velocity as with a plane grain-textured surface at rest" if ripples or dunes were present. The general sediment mobility relation is the square root of the ratio of the effective flow shear force to the immersed weight of a layer of sediment

$$F_{gr} = \frac{u_*^n}{\sqrt{gd(s-1)}} \left[\frac{\bar{u}}{\sqrt{32}\ \log_{10}\frac{10D}{d}}\right]^{1-n}$$

where n is a transition exponent depending on grain size. From a computer optimization of the results of sediment transport experiments of their own (Ackers and White, 1973) and other investigators, it was determined that the limits of particle size transition for fine, medium and coarse grained sediments were: (i) D_{gr} values less than one for fine grained bed materials (d_{50} = less than 0.04 mm); (ii) D_{gr} values between one and sixty for medium grained materials (d_{50} = 0.04 to 2.5 mm); and (iii) D_{gr} values greater than sixty (d_{50} = greater than 2.5 mm). The transport function was tested, however, only with grain sizes from 0.04 to 4.0 mm because particle sizes smaller than 0.04 (silt) were considered to have cohesive properties. For transitional grain sizes ($1.0 < D_{gr} \leq 60$ or $0.04 < d_{50} \leq 2.5$mm)

$$n = 1.0 - 0.56\ D_{gr}$$

and for coarse grain sizes ($D_{gr} > 60$ or $d_{50} > 2.5$mm)

$$n = 0.0$$

The dimensionless sediment transport relation (G_{gr}) is based on the work done in moving the sediment per unit time and the flow stream power, expressed as a ratio of the effective flow shear forces to the immersed weight of a layer of sediment times the efficiency of the transport process

$$G_{gr} = \frac{Xd}{sD}\left[\frac{u_*}{\bar{u}}\right]^n$$

where X = mass sediment flux per unit mass flow rate, or the transport of bed material expressed as a concentration weight (p.p.m.).

The dimensionless sediment transport function is related to the dimensionless grain size (D_{gr}) and the particle mobility (F_{gr}), both of which are dependent on the grain size transition exponent (n),

$$G_{gr} = f(D_{gr}, F_{gr})$$

Analysis of data from various sources and computer optimization of the various coefficients and variables, resulted in a general transport function for fine to coarse grained sediments,

$$G_{gr} = C\left(\frac{F_{gr}}{A} - 1\right)^m$$

where C = coefficient in the transport function, A = value of F_{gr} at which sediment transport begins and m = exponent in sediment transport function. For transitional grain sizes ($1.0 < D_{gr} \leq 60$)

$$A = \frac{0.23}{\sqrt{D_{gr}}} + 0.14 \qquad C = 10^{(2.86 \log_{10} D_{gr} - (\log_{10} D_{gr})^2 - 3.53)}$$

$$m = \frac{9.66}{D_{gr}} + 1.34$$

and for coarse sizes ($D_{gr} > 60$)

$$A = 0.17 \qquad C = 0.025$$

$$m = 1.5$$

The sediment flux (X) is calculated in "parts per million by weight of fluid flux" and is easily converted to transport rates in units of volume per unit time per unit width by multiplying through with unit flow discharge and mean water density.

Ackers and White (1973) compared the sediment transport rates using d_{50} and d_{35}, but found the results inconclusive. d_{50} was used for the calculations in this study.

IV.2 DERIVED HYDRAULIC PARAMETERS

The following is a list of the derived hydraulic parameters determined from the vertical current velocity profiles. See Appendix IV.1 for explanation of parameters.

NOEL BAY BAR

LOCATION 1A DATE 16/ 6/71

TIDAL CHARACTERISTICS

TIME ON (EDT) 917

MEAN RANGE 11.09

MEAN COEF. .74

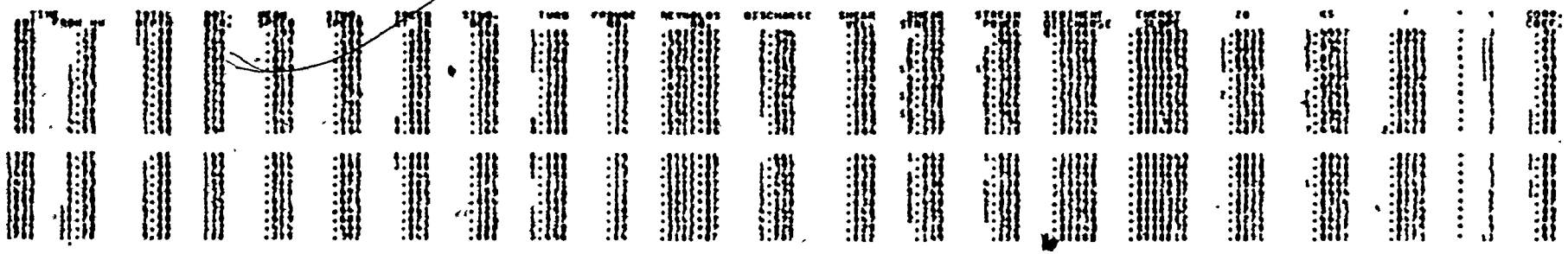

LOCATION 1B DATE 16/ 6/71

TIDAL CHARACTERISTICS

TIME ON (EDT) 917

MEAN RANGE 11.03

MEAN COEF. .73

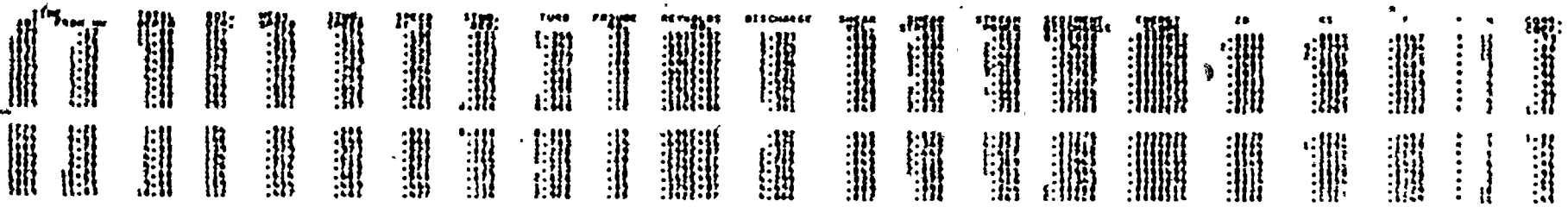

LOCATION 1C DATE 16/ 7/71

TIDAL CHARACTERISTICS

TIME ON (EDT) 752

MEAN RANGE 11.02

MEAN COEF. .72

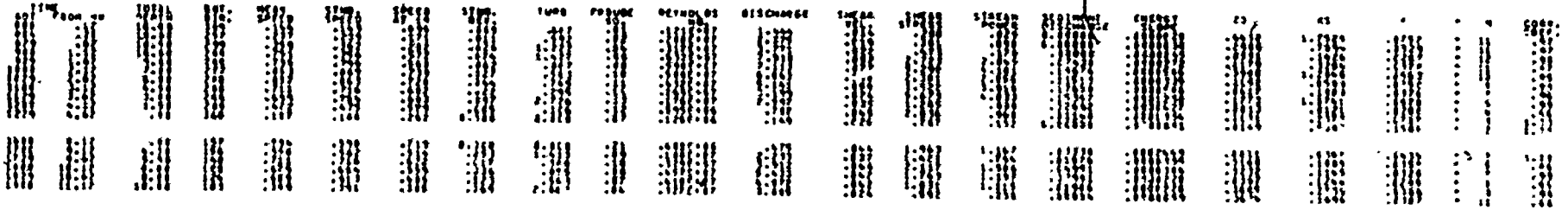

Noel Bay Bar (cont'd)

LOCATION [illegible] DATE [illegible]

TIDAL CHARACTERISTICS

TIME HW (EDT) 912

MEAN RANGE 12.27

MEAN COEF. .79

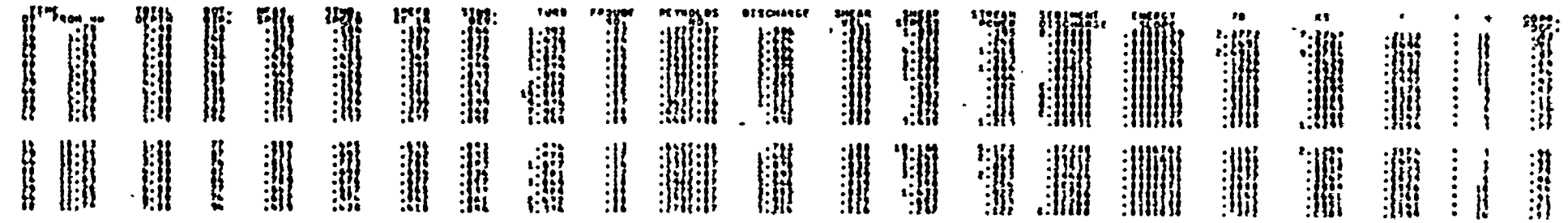

LOCATION 28 DATE 22 8/81

TIDAL CHARACTERISTICS

TIME HW (EDT) 127

MEAN RANGE 12.54

MEAN COEF. .79

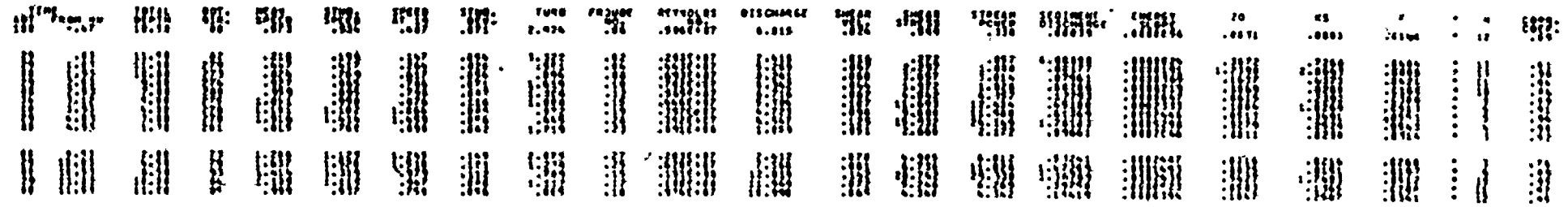

LOCATION 29 DATE 23/ 7/82

TIDAL CHARACTERISTICS

TIME HW (EDT) 347

MEAN RANGE 12.72

MEAN COEF. .79

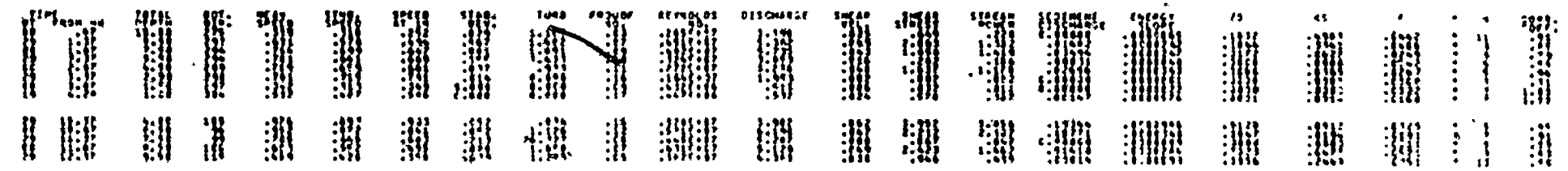

Noel Bay Bar (cont'd)

LOCATION 3A DATE 3/ 7/71

TIDAL CHARACTERISTICS

TIME MN (EDT) 942
MEAN RANGE 9.71
MEAN COEF. .49

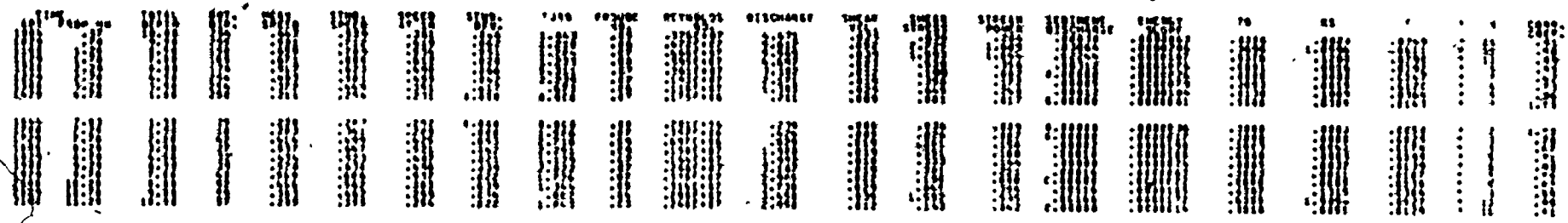

LOCATION 3B DATE 3/ 7/71

TIDAL CHARACTERISTICS

TIME MN (EDT) 1125
MEAN RANGE 10.88
MEAN COEF. .53

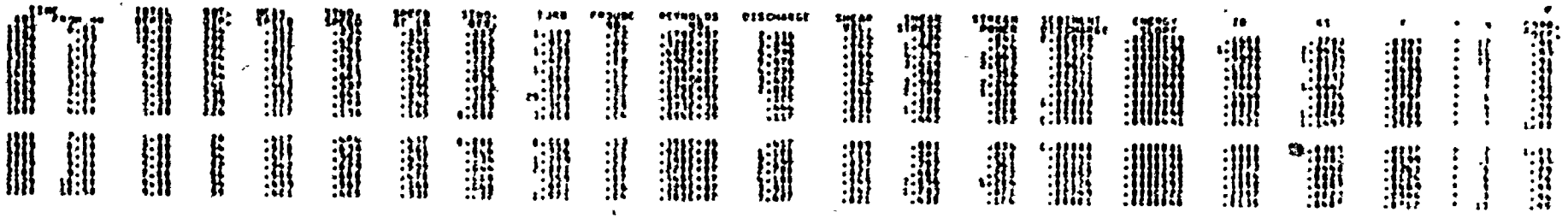

LOCATION 3C DATE 17/ 7/71

TIDAL CHARACTERISTICS

TIME MN (EDT) 957
MEAN RANGE 11.39
MEAN COEF. .71

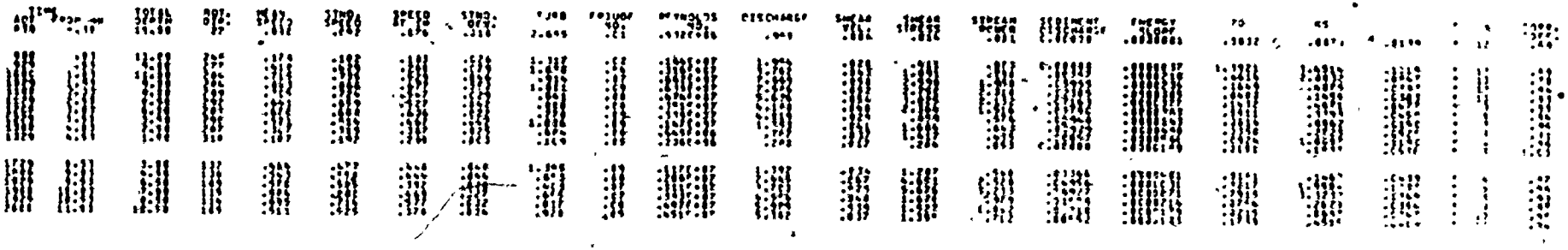

Noel Bay Bar (cont'd)

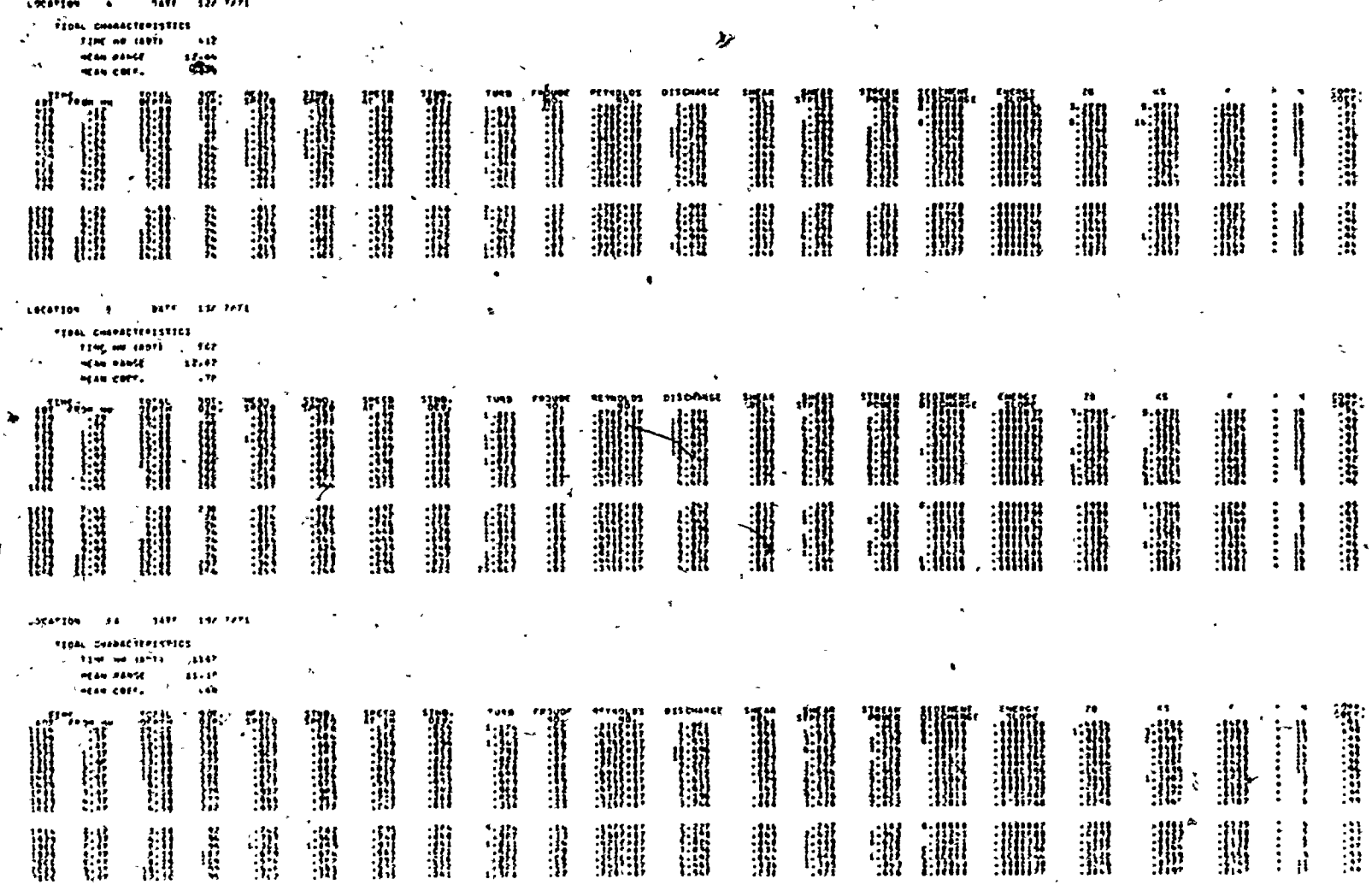

Noel Bay Bar (cont'd)

LOCATION 68 DATE 6/ 6/72

TIDAL CHARACTERISTICS

TIME HW (EDT) 6:7

MEAN RANGE 11.74

MEAN COEF. .72

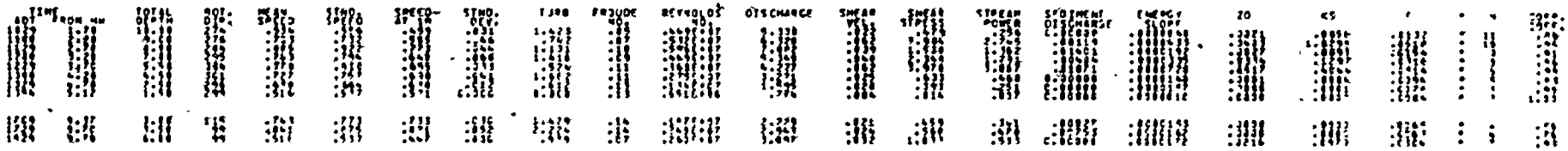

LOCATION 7 DATE 7/7 7/71

TIDAL CHARACTERISTICS

TIME HW (EDT) 6:7

MEAN RANGE 11.79

MEAN COEF. .71

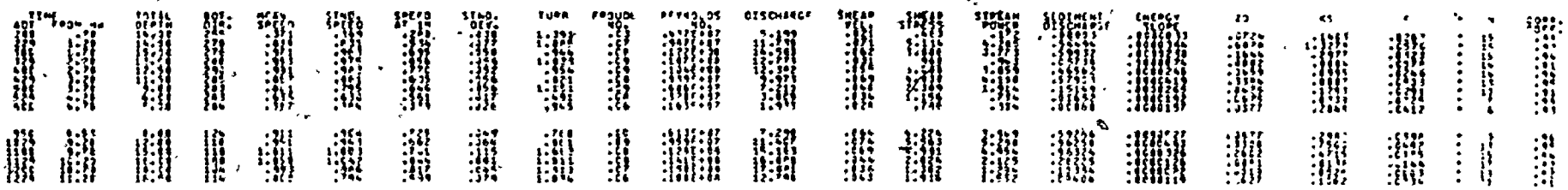

LOCATION 8 DATE 7/ 7/71

TIDAL CHARACTERISTICS

TIME HW (EDT) 7:7

MEAN RANGE 11.81

MEAN COEF. .71

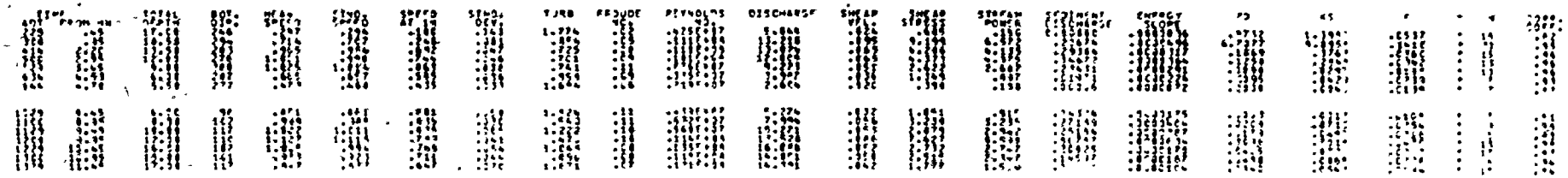

EAST NOEL BAR

LOCATION ENJ DATE 20/ 7/71

TIDAL CHARACTERISTICS

TIME HW (EDT) 859

MEAN RANGE 10.34

MEAN COEF. .64

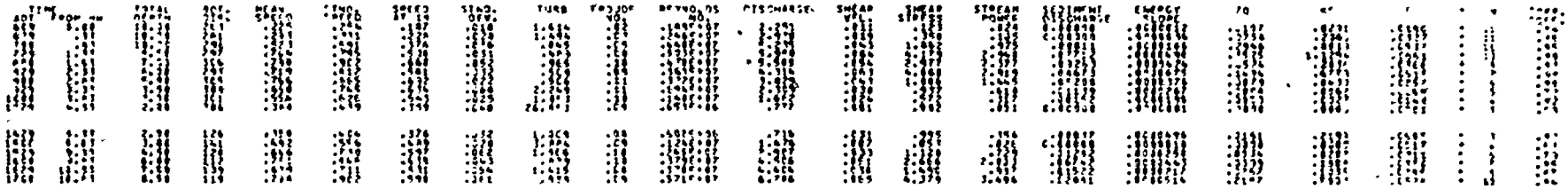

LOCATION ENJ DATE 17/ 8/72

TIDAL CHARACTERISTICS

TIME HW (EDT) 942

MEAN RANGE 11.93

MEAN COEF. .74

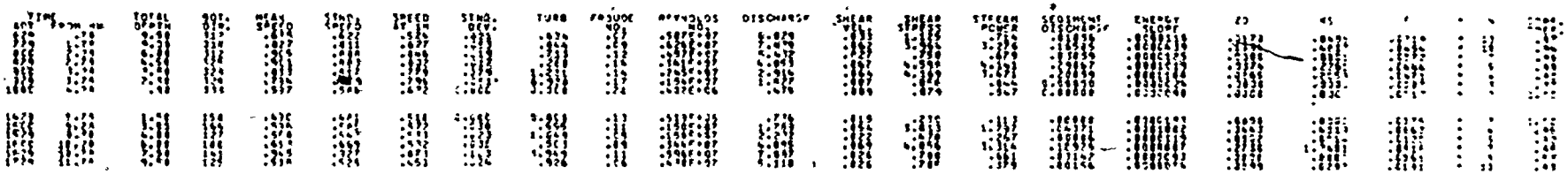

GREAT VILLAGE BAR

LOCATION GV1 DATE 21/ 8/72

TIDAL CHARACTERISTICS

TIME HW (EDT) 632

MEAN RANGE 11.27

MEAN COEF. .70

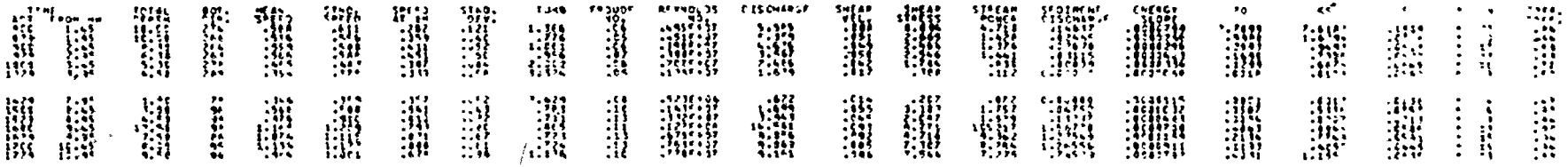

Middle CHANNEL

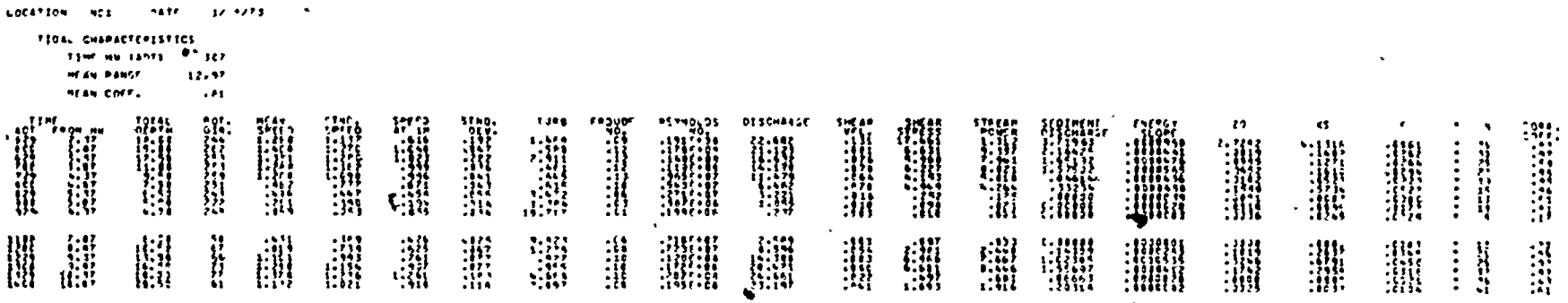

CENTRE BAY

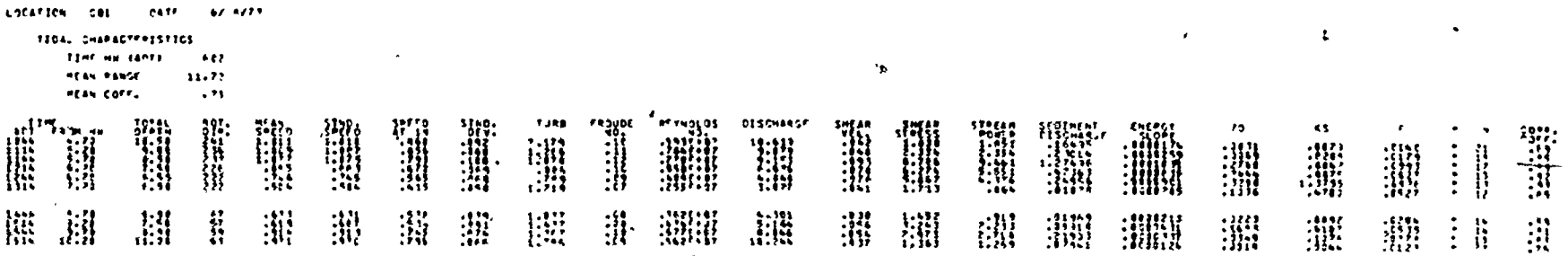

NOEL SHORE BAR

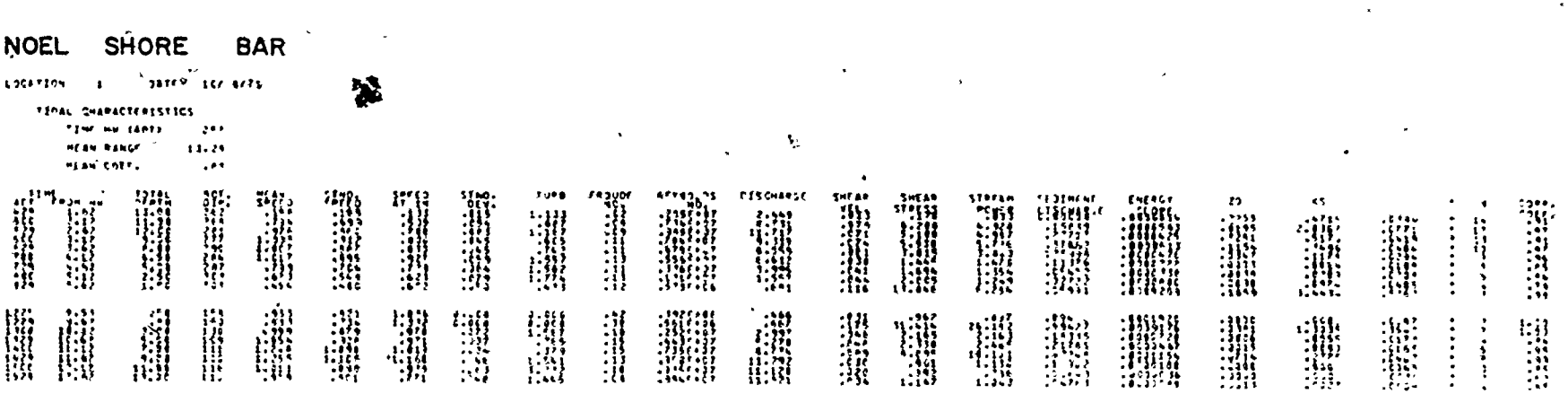

Noel Shore Bar (cont'd)

LOCATION 28 DATE 12/ 6/71

TIDAL CHARACTERISTICS

TIME HW (EDT) 4:37

MEAN RANGE 12.59

MEAN COEF. .78

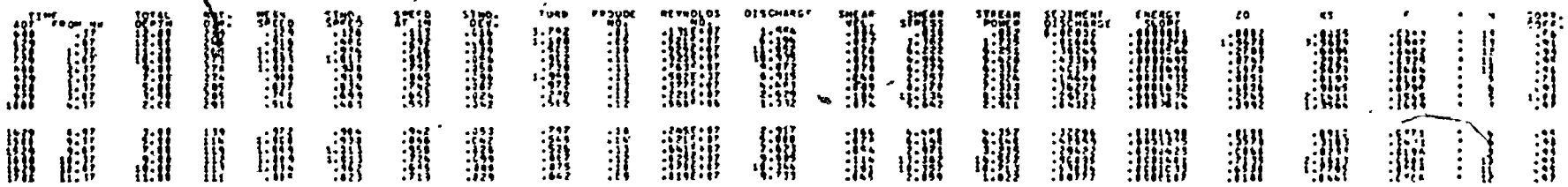

LOCATION 29 DATE 13/ 6/71

TIDAL CHARACTERISTICS

TIME HW (EDT) 6:32

MEAN RANGE 11.97

MEAN COEF. .74

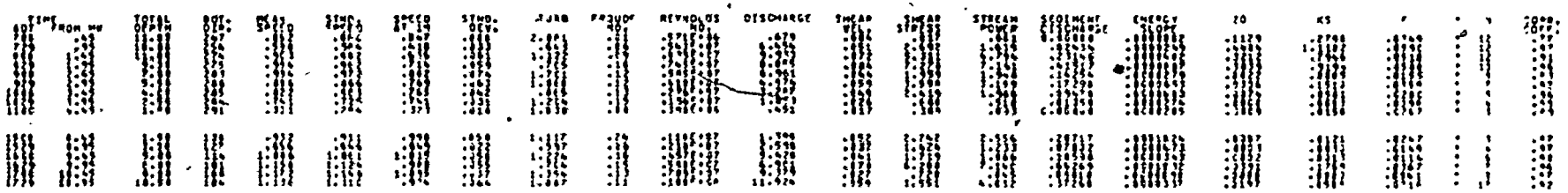

LOCATION 3 DATE 14/ 6/71

TIDAL CHARACTERISTICS

TIME HW (EDT) 7:27

MEAN RANGE 11.31

MEAN COEF. .70

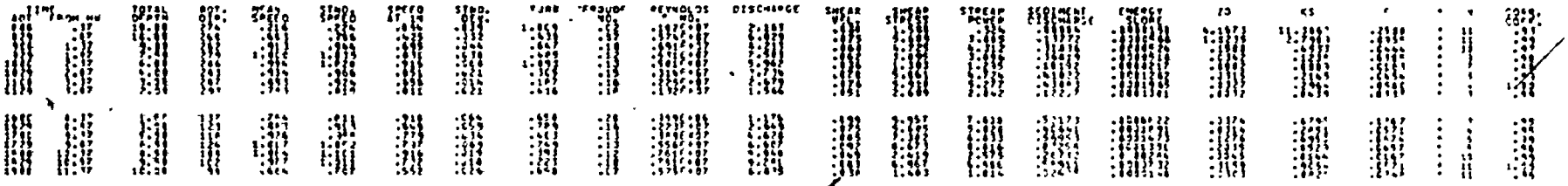

Noel Shore-Bar (cont'd)

LOCATION 4 DATE 17/ 8/73

TIDAL CHARACTERISTICS

TIME HW (EDT) 217

MEAN RANGE 11.8?

MEAN COEF. .73

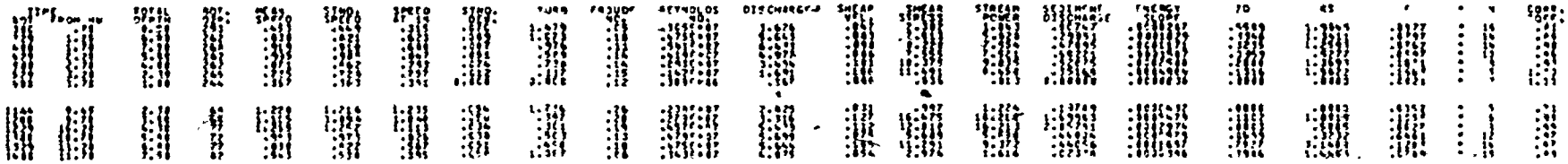

LOCATION 4 DATE 26/ 7/73

TIDAL CHARACTERISTICS

TIME HW (EDT) 1852

MEAN RANGE 11.4?

MEAN COEF. .71

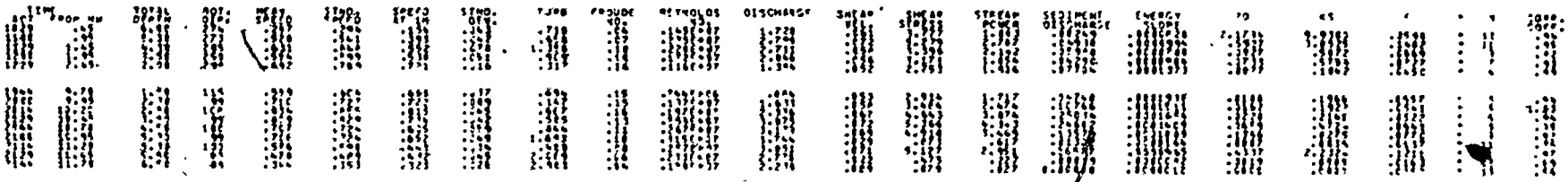

LOCATION 4 DATE 17/ 8/73

TIDAL CHARACTERISTICS

TIME HW (EDT) 257

MEAN RANGE 11.9?

MEAN COEF. .74

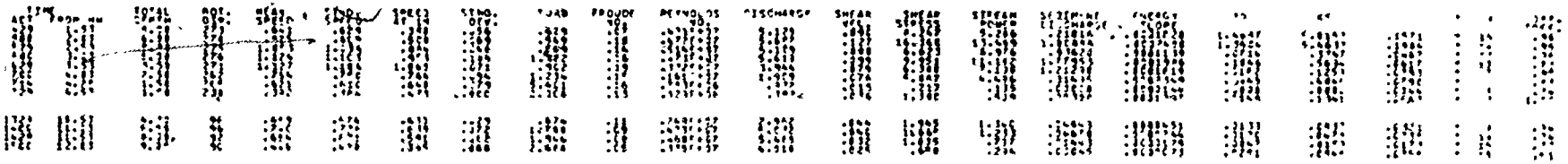

Noel Shore Bar (cont'd)

LOCATION 7 DATE 28/ 9/73

TIDAL CHARACTERISTICS
TIME HW (EDT) 0:37
MEAN RANGE 11.6?
MEAN COEF. .?2

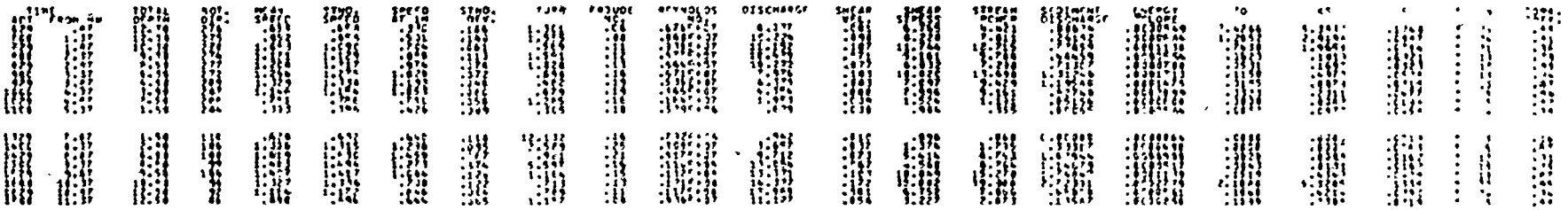

LOCATION 8 DATE 17/ 9/73

TIDAL CHARACTERISTICS
TIME HW (EDT) 10:57
MEAN RANGE 10.0?
MEAN COEF. .??

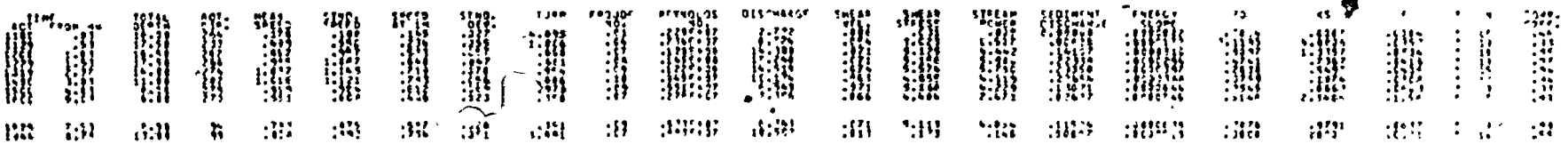

LOCATION 8 DATE 23/ 9/73

TIDAL CHARACTERISTICS
TIME HW (EDT) 6:?
MEAN RANGE 11.??
MEAN COEF. .??

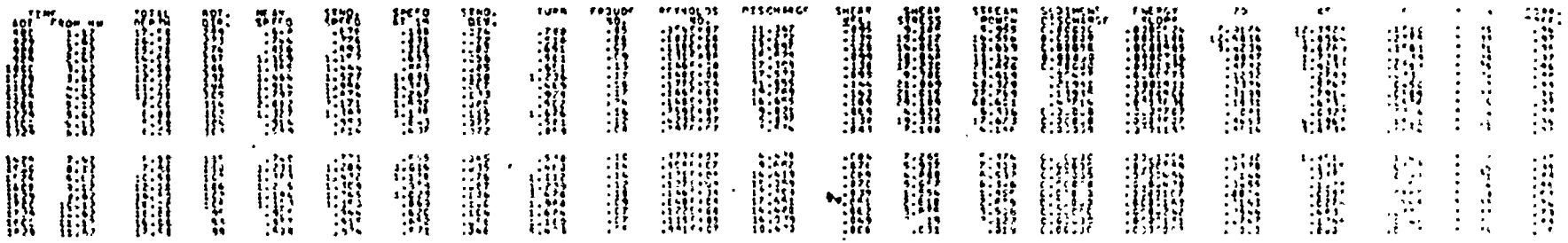

Noel Shore Bar (cont'd)

LOCATION 10 DATE 28/ 7/73

TIDAL CHARACTERISTICS

TIME HW (GDT) 437

MEAN RANGE 11.97

MEAN COEF. .72

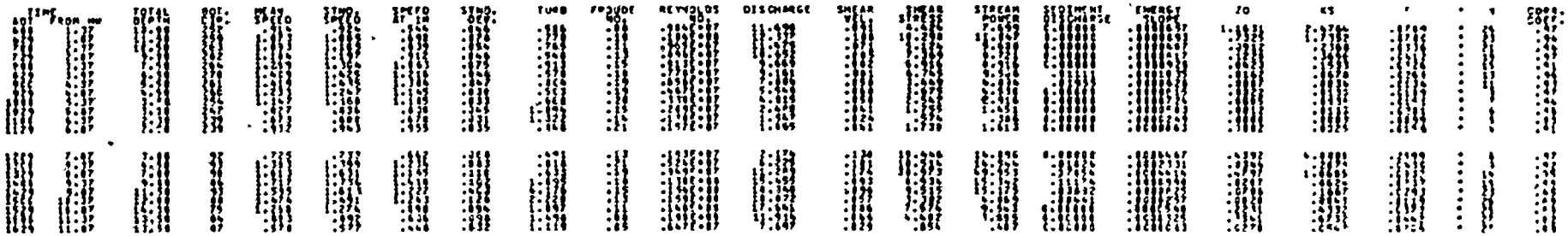

LOCATION 11 DATE 29/ 7/73

TIDAL CHARACTERISTICS

TIME HW (GDT) 852

MEAN RANGE 11.12

MEAN COEF. .69

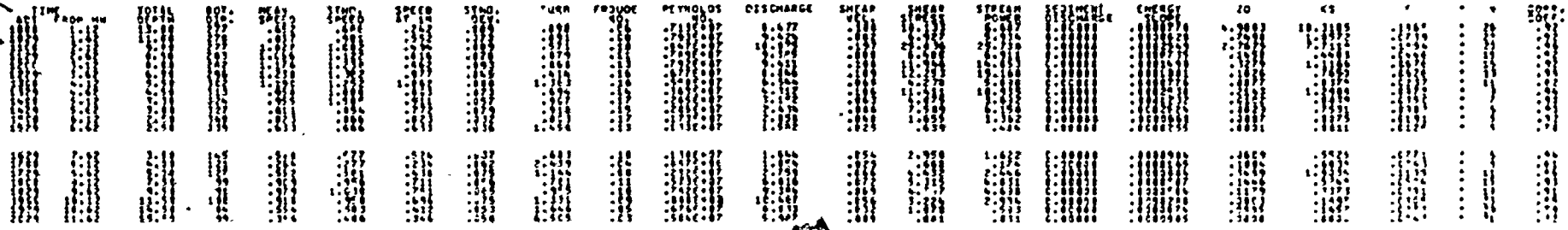

SELMA BAR

LOCATION 1A DATE 11/ 7/72

TIDAL CHARACTERISTICS

TIME HW (EDT) 127

MEAN RANGE 12.96

MEAN COEF. .81

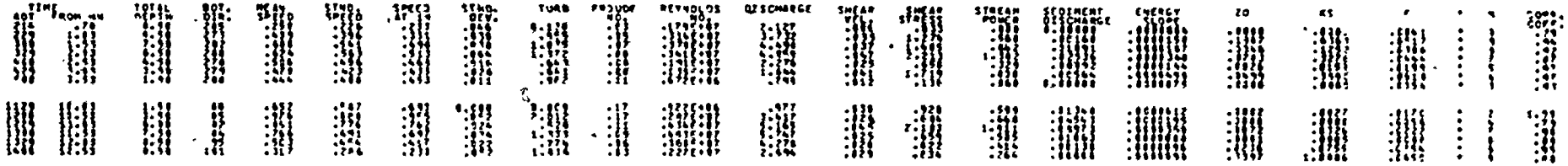

LOCATION 1B DATE 10/ 7/72

TIDAL CHARACTERISTICS

TIME HW (EDT) 707

MEAN RANGE 10.42

MEAN COEF. .69

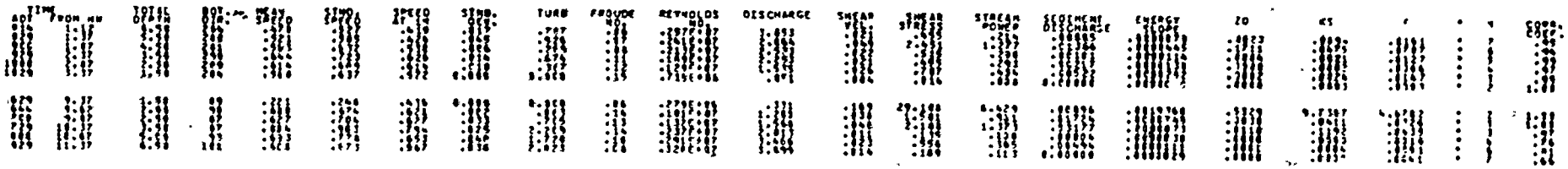

LOCATION 1C DATE 20/ 6/73

TIDAL CHARACTERISTICS

TIME HW (EDT) 1127

MEAN RANGE 12.12

MEAN COEF. .75

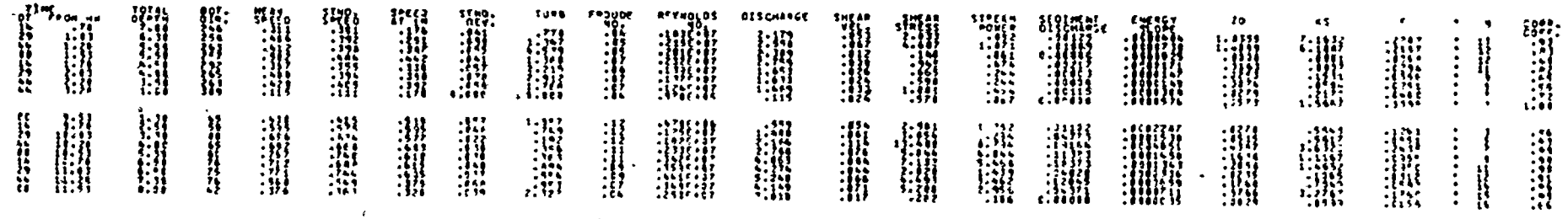

Selma Bar (cont'd)

LOCATION 19 DATE 5/ 6/72

TIDAL CHARACTERISTICS

TIME HW (EDT) 742

MEAN RANGE 11.34

MEAN COEF. .78

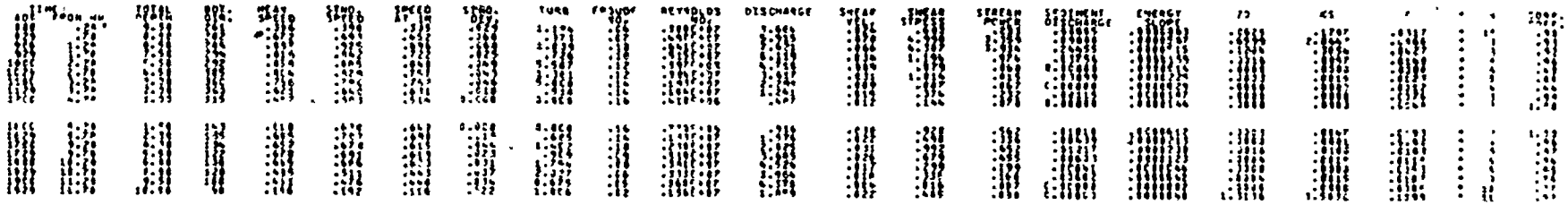

LOCATION 20 DATE 16/ 6/72

TIDAL CHARACTERISTICS

TIME HW (EDT) 737

MEAN RANGE 11.69

MEAN COEF. .74

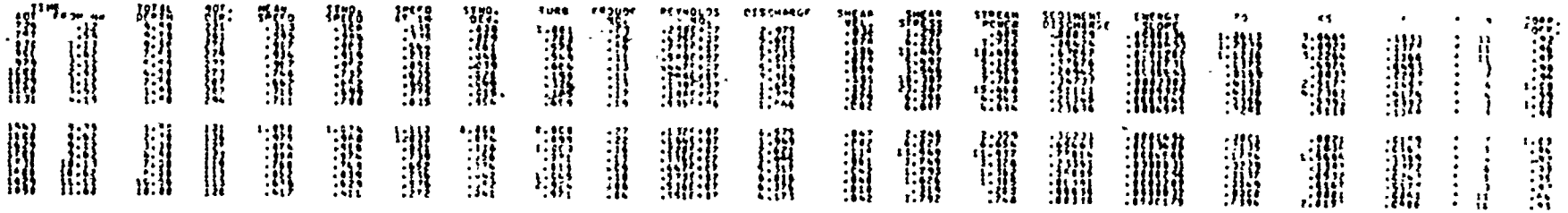

LOCATION 20 DATE 16/ 7/72

TIDAL CHARACTERISTICS

TIME HW (EDT) 657

MEAN RANGE 12.66

MEAN COEF. .77

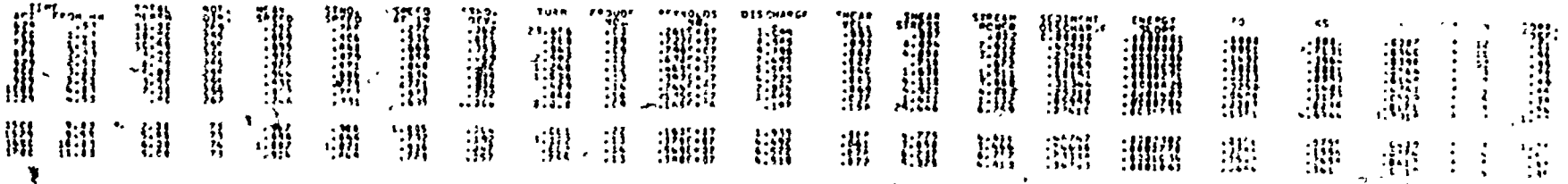

Selma Bar (cont'd)

LOCATION [illegible] DATE [illegible]

TIDAL CHARACTERISTICS

TIME HW (EDT) [illegible]

MEAN RANGE [illegible]

MEAN COEF. [illegible]

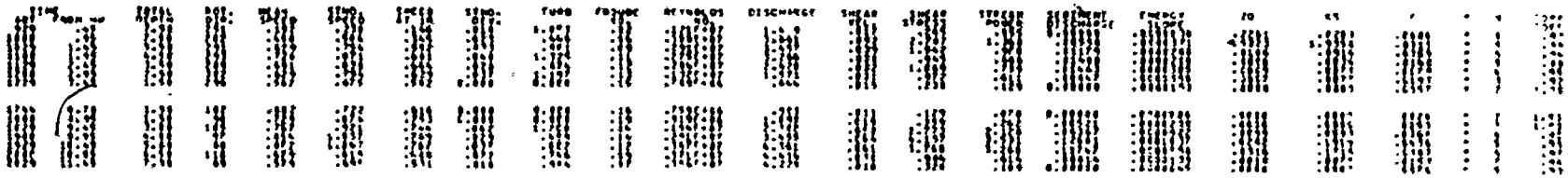

LOCATION [illegible] DATE [illegible]

TIDAL CHARACTERISTICS

TIME HW (EDT) [illegible]

MEAN RANGE [illegible]

MEAN COEF. [illegible]

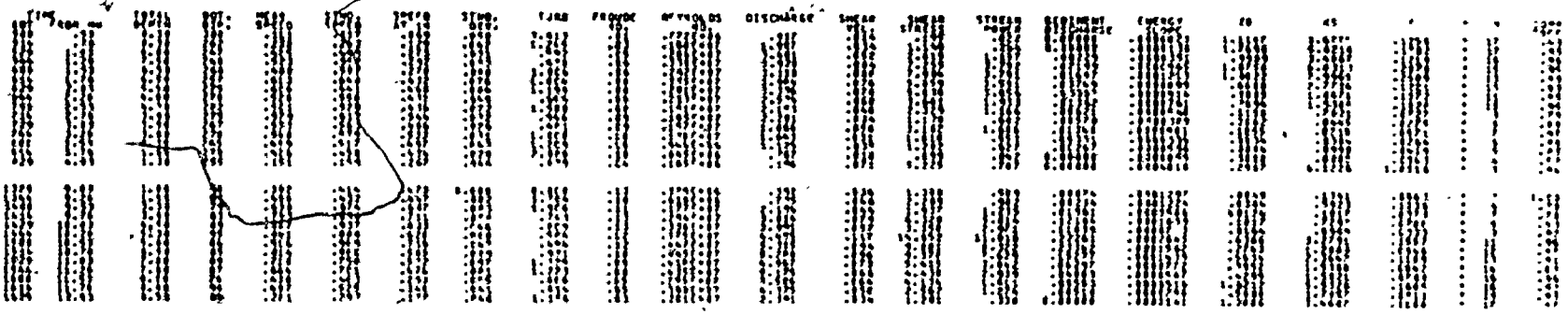

LOCATION [illegible] DATE [illegible]

TIDAL CHARACTERISTICS

TIME HW (EDT) [illegible]

MEAN RANGE [illegible]

MEAN COEF. [illegible]

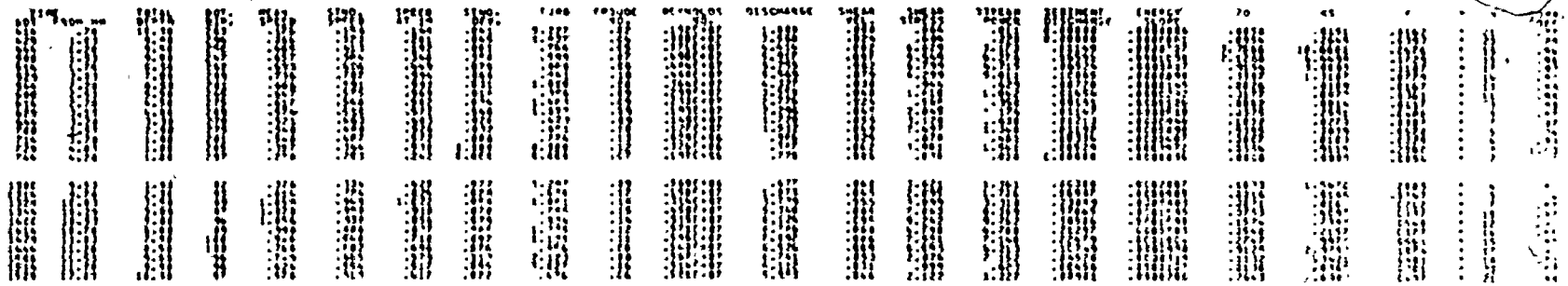

Selma Bar (cont'd)

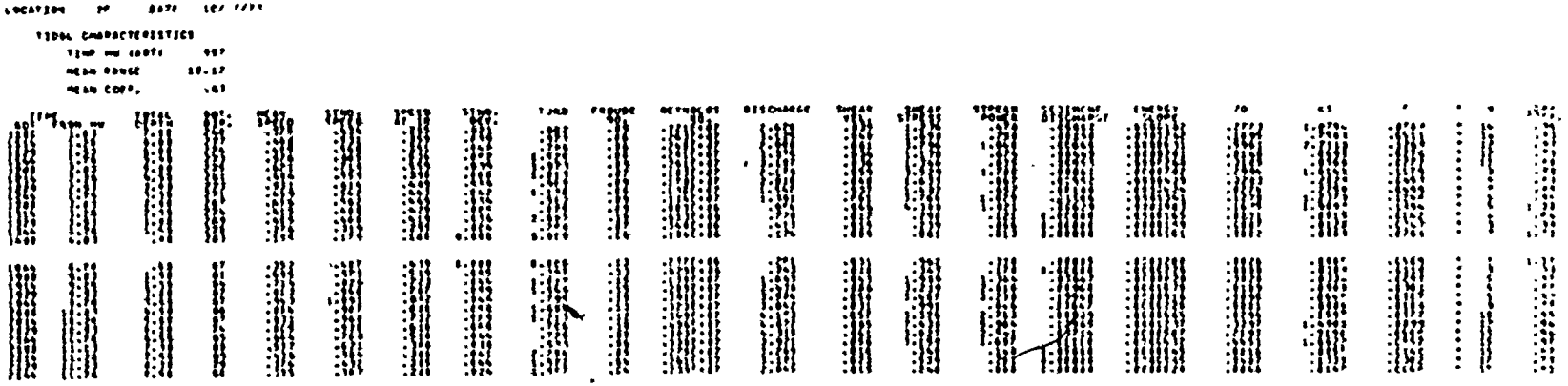

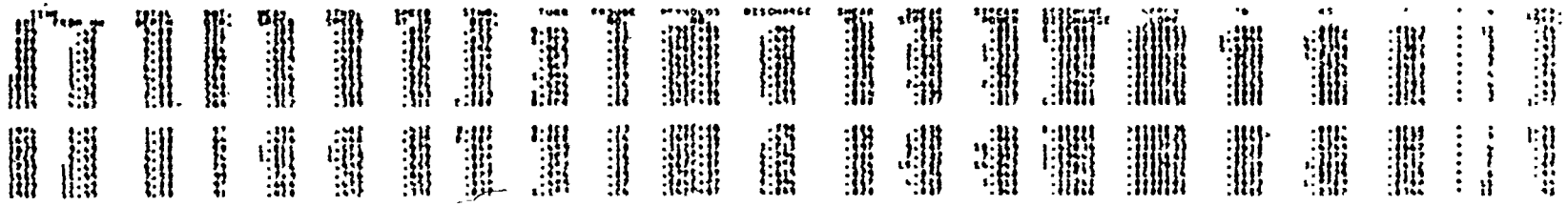

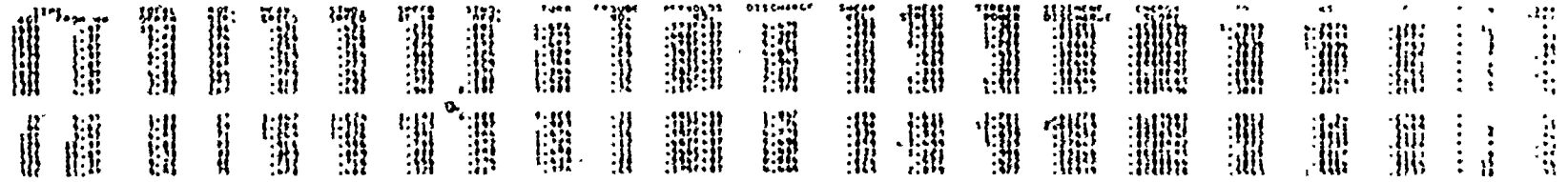

Selma Bar (cont'd)

LOCATION 46 DATE 7/ 7/72

TIDAL CHARACTERISTICS

TIME OF (EDT) EDT

MEAN RANGE 11.7ft

MEAN CURR. .7t

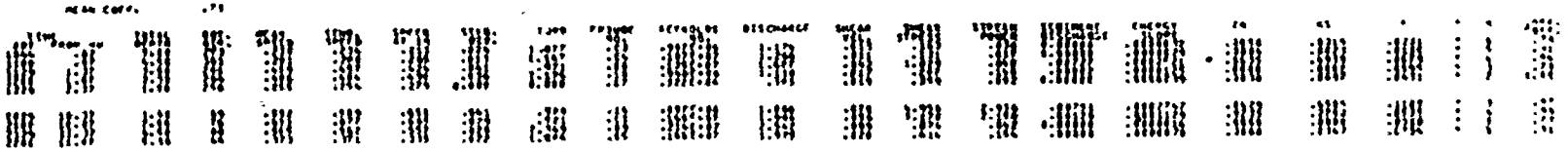

LOCATION 50 DATE 23/ 7/72

TIDAL CHARACTERISTICS

TIME OF (EDT) 1052

MEAN RANGE 6.9ft

MEAN CURR. .6t

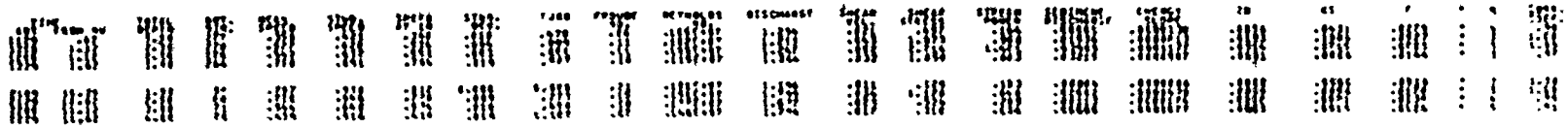

LOCATION 54 DATE 6/ 7/72

TIDAL CHARACTERISTICS

TIME OF (EDT) 907

MEAN RANGE 11.5ft

MEAN CURR. .7t

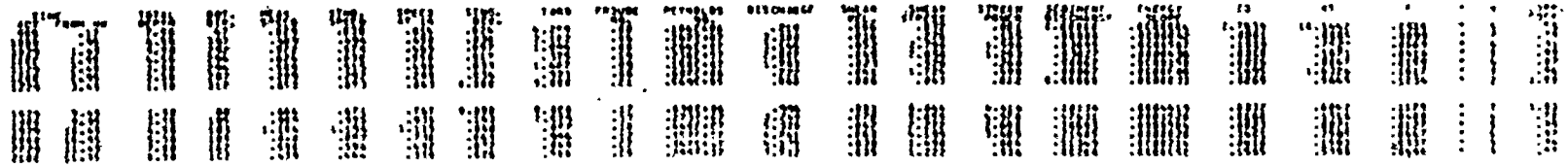

LOCATION 58 DATE 20/ 7/72

TIDAL CHARACTERISTICS

TIME OF (EDT) 957

MEAN RANGE 9.7ft

MEAN CURR. .6t

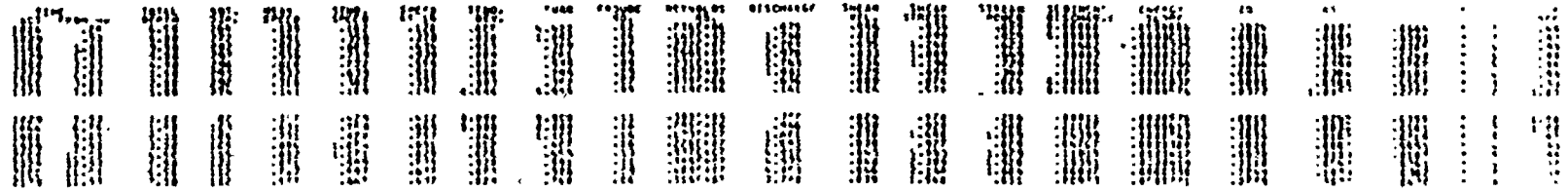

Selma Bar (cont'd)

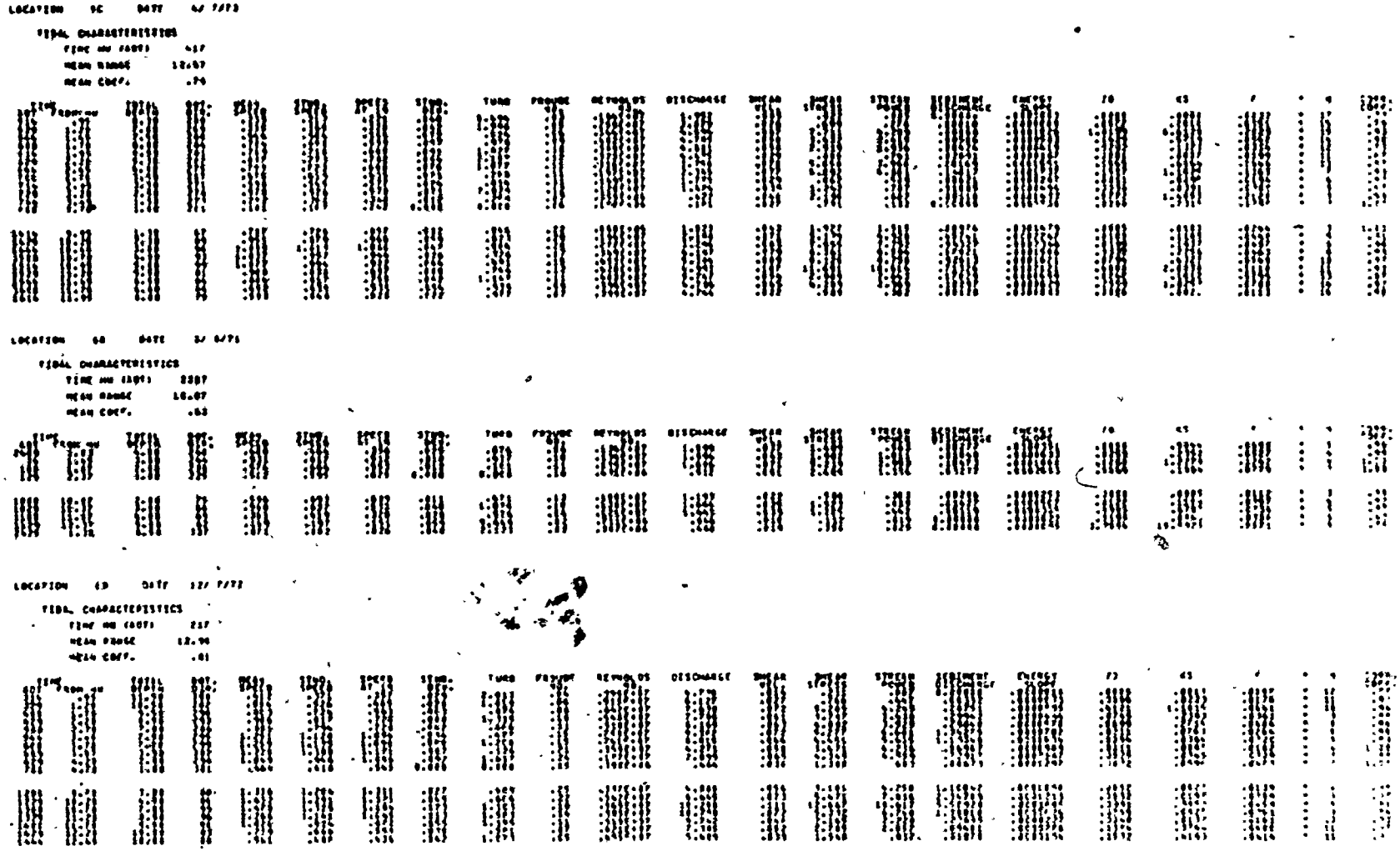

Selma Bar (cont'd)

LOCATION 6C DATE 19/ 7/72

TIDAL CHARACTERISTICS

TIME HW (EDT) 957

MEAN RANGE 10.01

MEAN COEF. .62

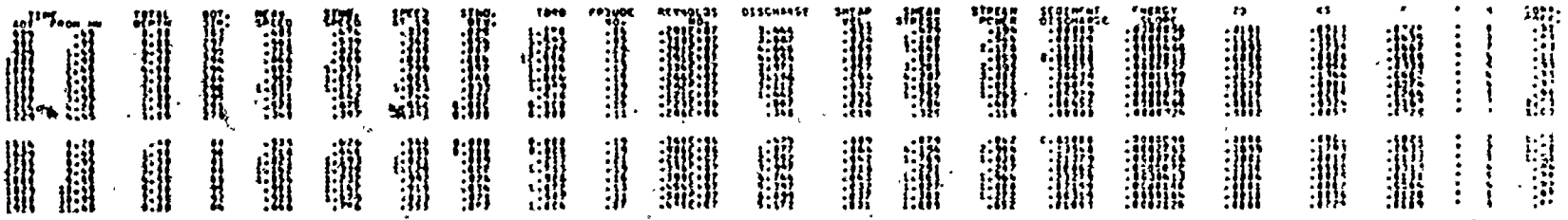

LOCATION 6D DATE 25/ 6/73

TIDAL CHARACTERISTICS

TIME HW (EDT) 827

MEAN RANGE 11.02

MEAN COEF. .68

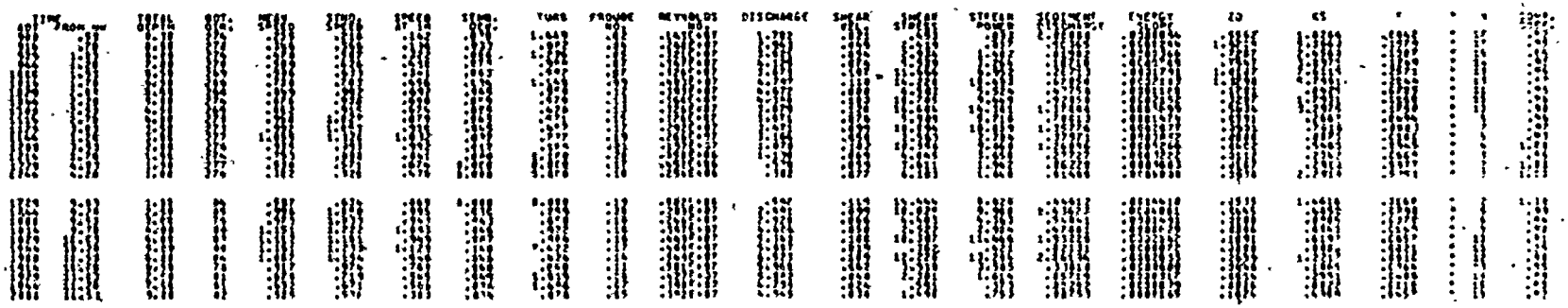

LOCATION 6E DATE 27/ 6/73

TIDAL CHARACTERISTICS

TIME HW (EDT) 1027

MEAN RANGE 11.63

MEAN COEF. .77

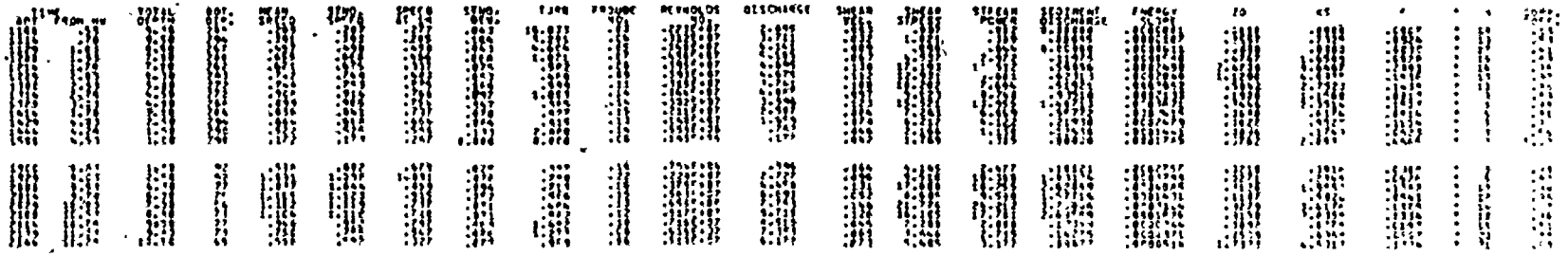

Selma Bar (cont'd)

LOCATION 69 DATE 9/ 7/73

TIDAL CHARACTERISTICS
TIME HW (EDT) 952
MEAN RANGE 10.32
MEAN COEF. .64

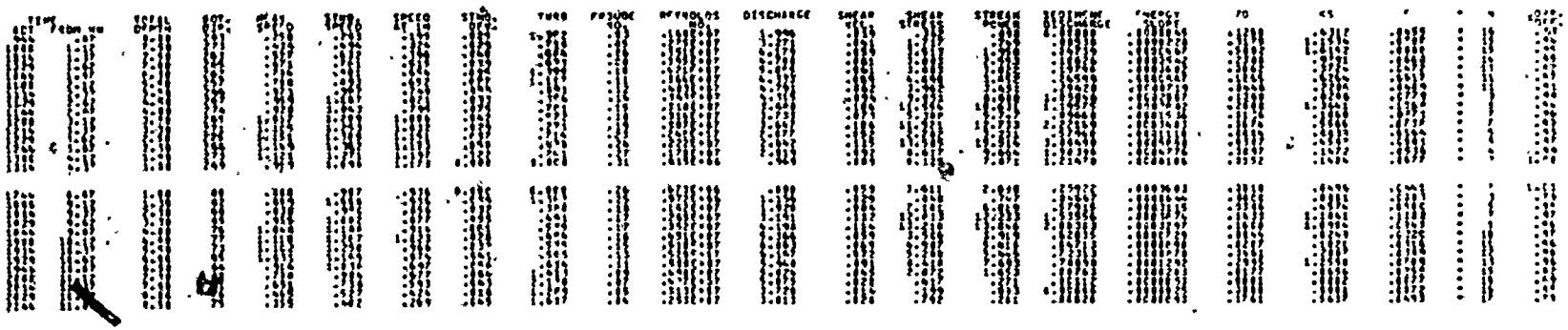

LOCATION 70 DATE 17/ 7/72

TIDAL CHARACTERISTICS
TIME HW (EDT) 617
MEAN RANGE 10.93
MEAN COEF. .68

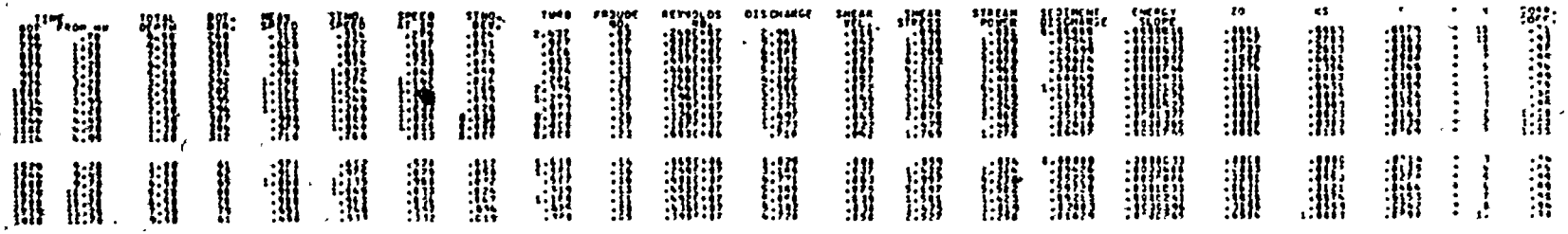

LOCATION 70 DATE 11/ 8/73

TIDAL CHARACTERISTICS
TIME HW (EDT) 1032
MEAN RANGE 10.67
MEAN COEF. .66

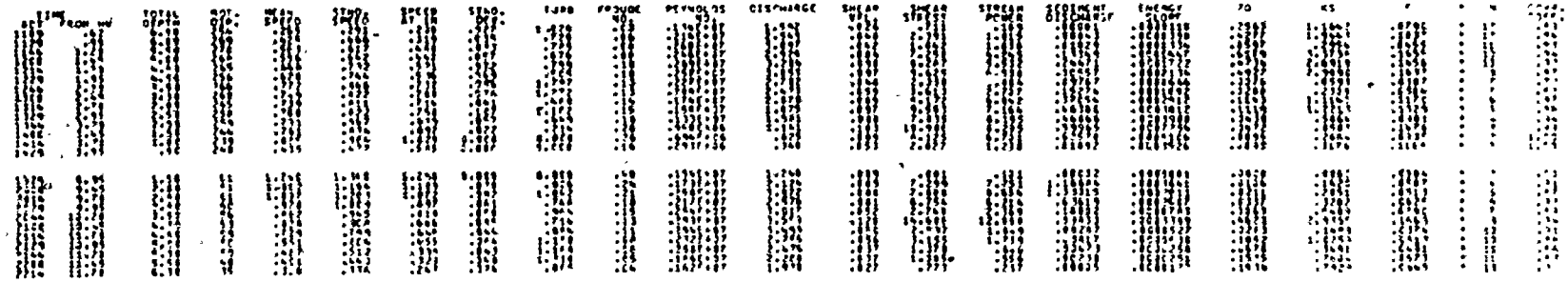

Selma Bar (cont'd)

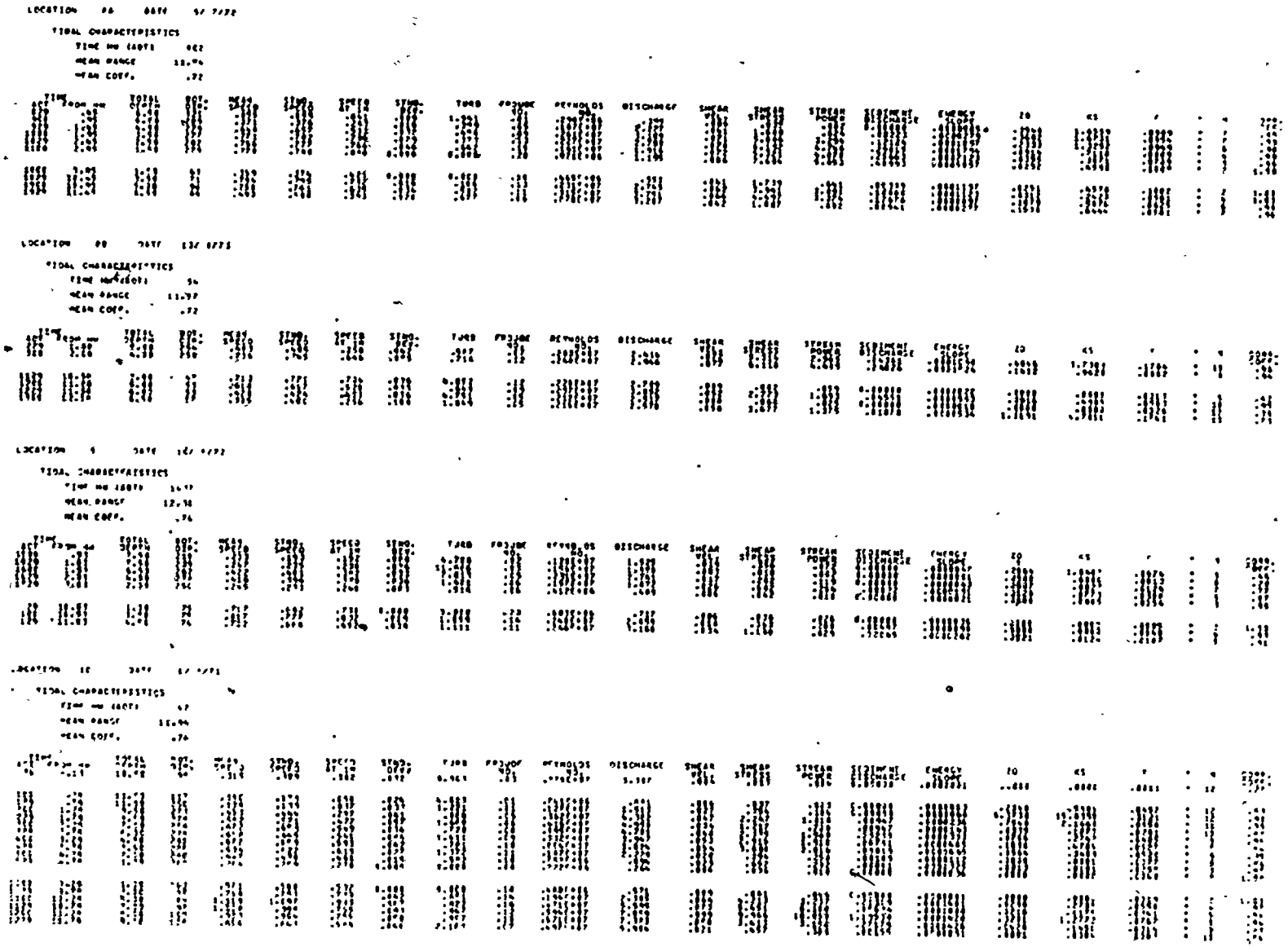

Selma Bar (cont'd)

LOCATION 11 DATE 27 6/71

TIDAL CHARACTERISTICS

TIME MN (EDT) 0?2?

MEAN RANGE 9.?6

MEAN COEF. .?6

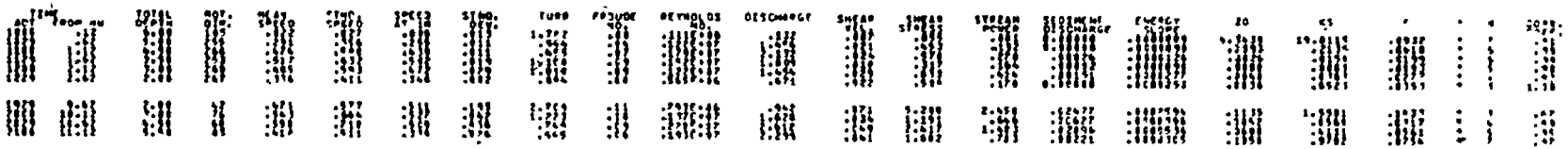

LOCATION 12 DATE ?? 6/71

TIDAL CHARACTERISTICS

TIME MN (EDT) 2357

MEAN RANGE 11.2?

MEAN COEF. .?C

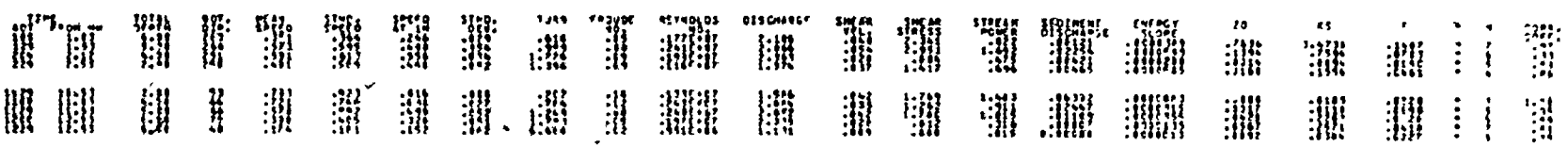

LOCATION 13 DATE 13? 6/?3

TIDAL CHARACTPISTICS

TIME MN (EDT) 1217

MEAN RANGE 10.??

MEAN COEF. .6?

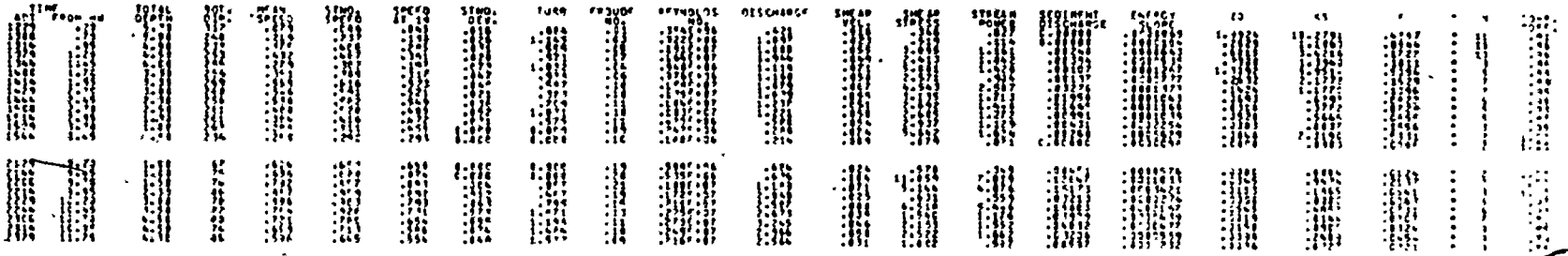

Selma Bar (cont'd)

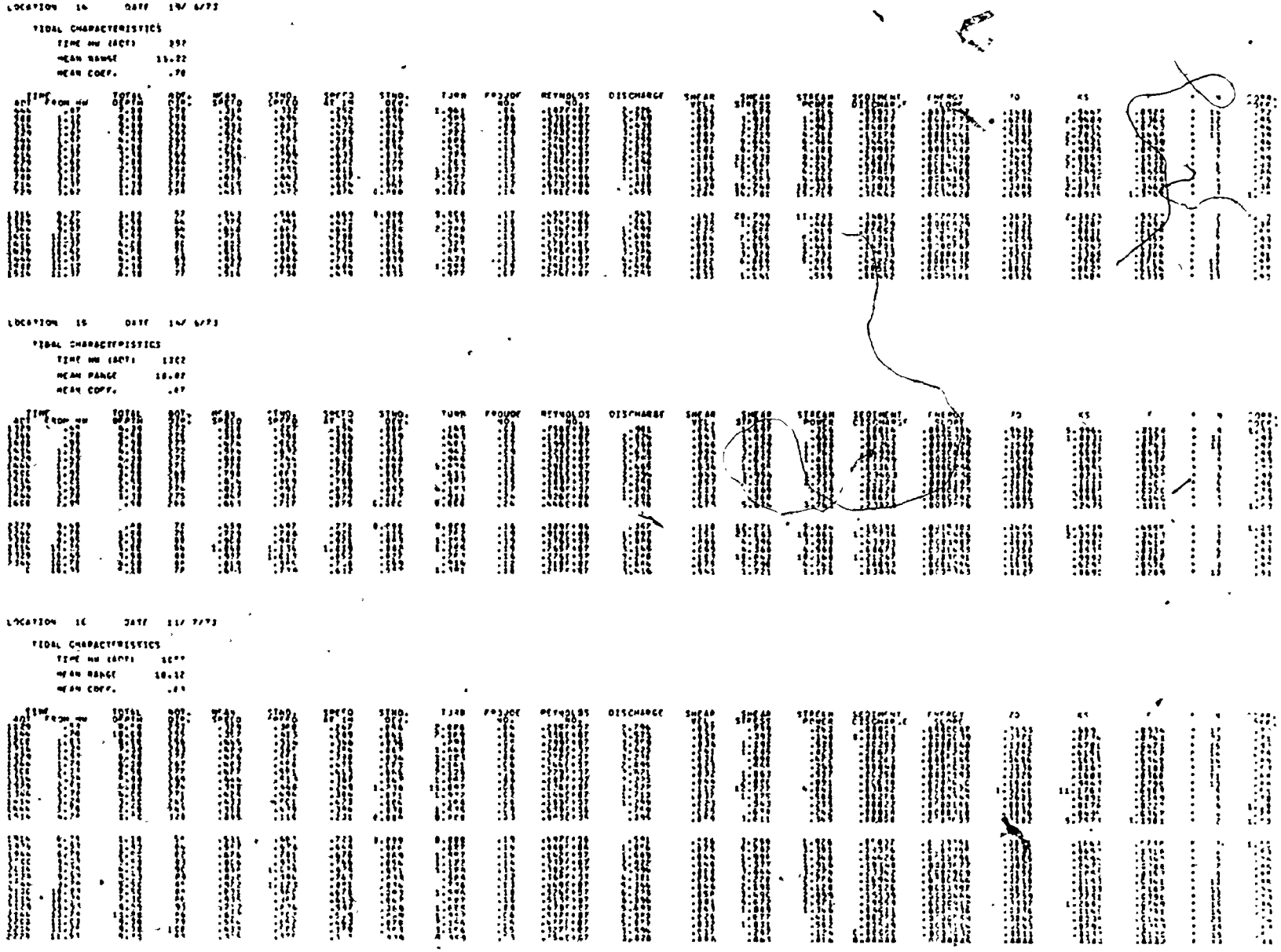

Selma Bar (cont'd)

LOCATION 1P DATE 3/ 8/72

TIDAL CHARACTERISTICS

TIME MN (AST) 0457

MEAN RANGE 11.31

MEAN COEF. .78

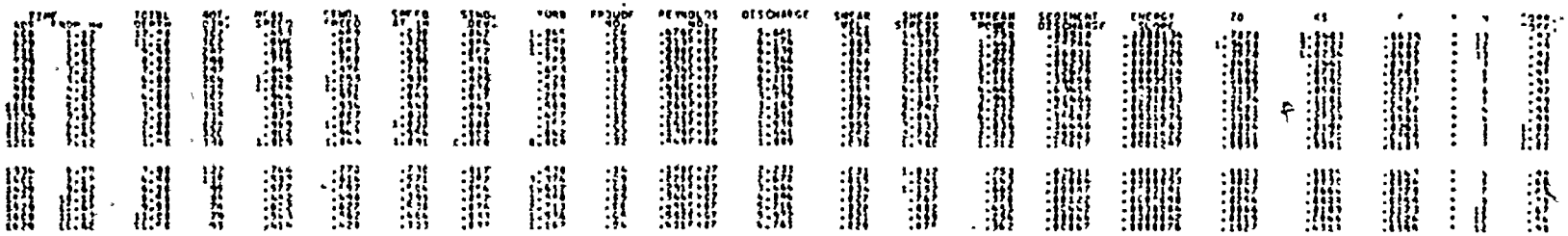

LOCATION 1P DATE 9/ 8/72

TIDAL CHARACTERISTICS

TIME MN (AST) 1142

MEAN RANGE 12.19

MEAN COEF. .77

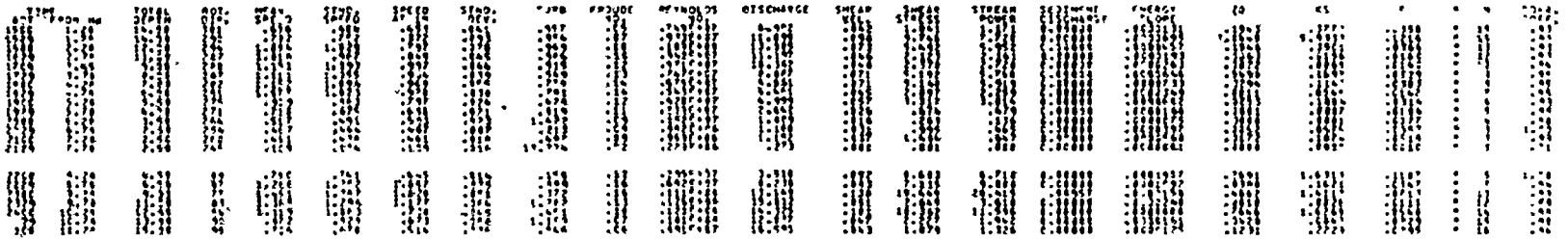

LOCATION 19A DATE 15/ 7/72

TIDAL CHARACTERISTICS

TIME MN (AST) 0857

MEAN RANGE 11.92

MEAN COEF. .72

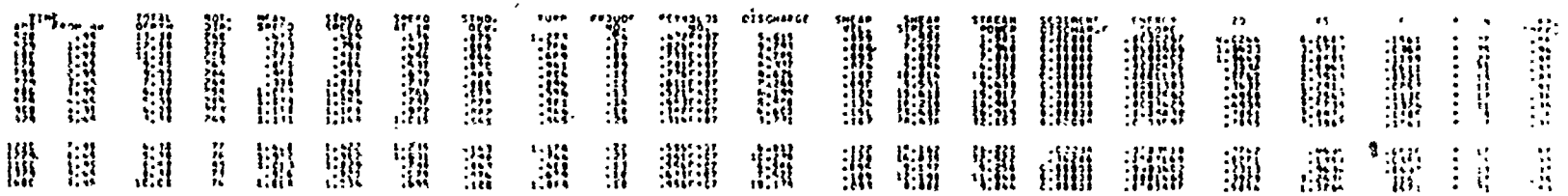

Selma Bar (cont'd)

LOCATION 198 DATE 5/ 6/72

TIDAL CHARACTERISTICS
TIME HW (EDT) 627
MEAN RANGE 10.97
MEAN COEF. .66

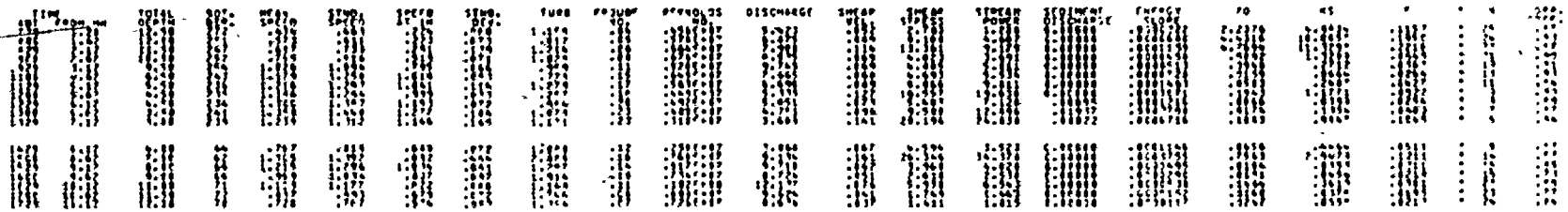

LOCATION 208 DATE 25/ 7/72

TIDAL CHARACTERISTICS
TIME HW (EDT) 1312
MEAN RANGE 11.05
MEAN COEF. .69

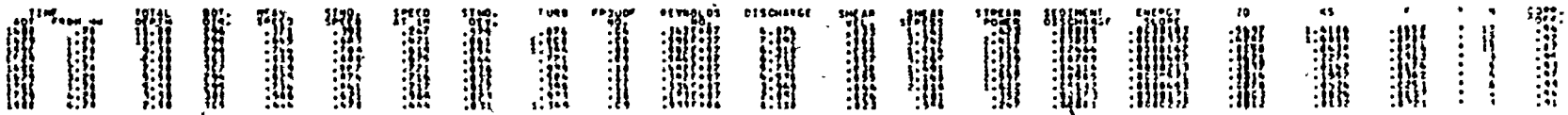

LOCATION 208 DATE 15/ 8/72

TIDAL CHARACTERISTICS
TIME HW (EDT) 527
MEAN RANGE 10.75
MEAN COEF. .67

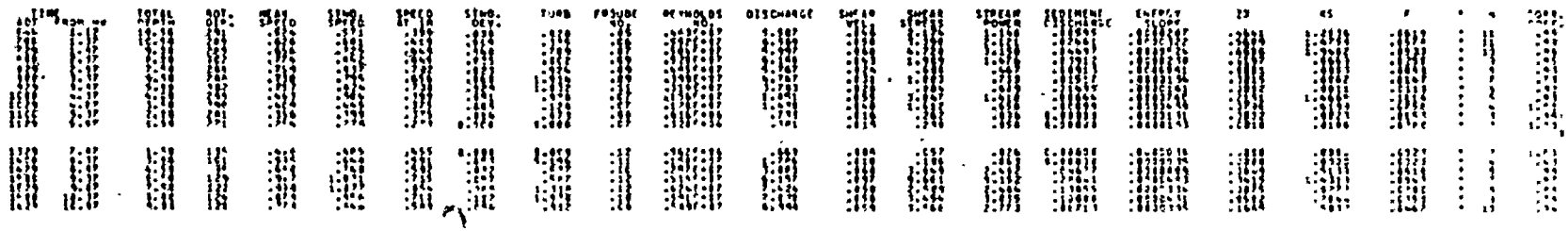

IV.3 UNIT SEDIMENT DISCHARGES RECALCULATED FOR CHANNEL LOCATIONS

The following is a list of the recalculated values of unit sediment discharge for the channel locations (Fig. 4.1) using the average mean grain size from the adjacent sand bars rather than the mean grain size of the grab samples from the channels (e.g., Appendix IV.2).

NOEL BAY BAR

Location 4 12/7/71

Time from HW	Sediment Discharge
.12	0.00000
.78	.00018
1.28	.00001
1.78	.32201
2.28	.20597
2.78	.70416
3.28	.25172
3.78	.44659
4.28	.18202
4.78	.22091
5.28	.13791
8.28	.00620
8.78	.02356
9.28	.04564
9.78	.05975
10.28	.10474
10.78	.04111
11.28	.01981

Location 5 13/7/71

Time from HW	Sediment Discharge
.28	0.00000
.95	.09696
1.45	.31775
1.95	.08623
2.45	.19429
2.95	.46028
3.45	.33204
3.95	.22560
4.45	.24771
4.95	.07842
7.45	0.00000
7.95	.00073
8.45	.13165
8.95	.00086
9.45	.01379
9.95	.06777
10.45	.02762
11.45	0.00000
11.78	0.00000

Location 6A 19/7/71

Time from HW	Sediment Discharge
.12	0.00000
.37	.00147
.87	.05396
1.37	.14688
1.87	.02177
2.37	.15944
2.87	.14775
3.37	.26872
3.87	.13549
4.37	.27958
4.87	.16323
7.12	.00077
7.37	.09757
7.87	.14275
8.37	.01330
8.87	.01155
9.37	.01457
9.87	.01204

Location 6B 4/8/72

Time from HW	Sediment Discharge
1.70	.00038
2.20	.08993
2.70	.07337
3.20	.07113
3.70	.14393
4.20	.00847
4.70	.00146
5.12	0.00000
8.37	.00536
8.70	.01534
9.70	.00362

NOEL BAY BAR (cont'd)

Location 7 22/7/71		Location 8 23/7/71	
Time from HW	Sediment Discharge	Time from HW	Sediment Discharge
.70	.00000	.45	0.00000
1.20	.20962	.95	.20379
1.70	.26561	2.20	.29100
2.20	.05368	2.95	.34337
2.70	.23191	3.45	.23277
3.20	.23044	4.53	.01963
3.70	.08376	4.70	.00006
4.20	.01244	8.45	.04322
4.70	.00029	8.95	.26976
8.53	.25421	9.45	.25003
9.20	.36175	9.95	.85696
9.70	.38411	10.45	.20678
10.20	.17436	10.95	.14498
10.70	.08040	11.45	.06418
11.20	.05704		

NOEL SHORE BAR

Location 9 23/7/73

Time from HW	Sediment Discharge
1.12	.12633
1.62	.38588
2.12	.49681
2.62	.87164
3.12	2.69974
3.62	2.07657
4.12	8.65965
4.62	7.11246
5.12	14.36529
5.62	.97125
6.12	.86786
6.62	.08347
7.62	.19095
8.12	.87840
8.62	1.02032
9.12	.77133
9.62	.20561
10.12	.25813
10.62	.18570
11.12	.10158
11.62	0.00000

Location 10 20/7/73

Time from HW	Sediment Discharge
1.37	.40072
1.87	.81765
2.37	.49659
2.87	.89852
3.37	1.16361
3.87	1.56164
4.37	.95150
4.87	.64134
5.37	.37271
5.87	.07699
6.37	.00580
6.87	.13111
7.87	.44771
8.37	2.16169
8.87	6.94914
9.37	3.49348
9.87	2.79506
10.37	.92118
10.87	1.06323
11.37	.19707
11.87	.00299

Location 11 25/7/73

Time from HW	Sediment Discharge
1.12	.14727
1.62	.27752
2.12	1.41146
2.62	.57260
3.12	1.30132
3.62	1.60856
4.12	.62723
4.62	.69797
5.12	.30526
5.62	.30538
6.12	.07345
6.62	.00505
7.62	.02807
8.12	0.00000
8.62	.04154
9.12	.28544
9.62	.32555
10.12	.16668
10.62	.00408
11.62	0.00000

SELMA BAR

Location 17 14/8/72

Time from HW	Sediment Discharge
1.12	.00358
1.62	.03751
2.12	.04246
2.62	.04892
3.12	.09912
3.62	.26955
4.12	.44689
4.62	.29040
5.12	.34062
5.62	.23847
6.12	.27498
6.62	.19839
7.12	.14989
8.70	.02412
9.12	.00003
9.62	.00751
10.12	.00092
10.62	.00397
11.12	.00035
11.62	.00040

Location 18 9/8/72

Time from HW	Sediment Discharge
1.28	.02007
1.78	.27522
2.28	.50244
2.78	.16521
3.45	.30089
3.78	.55323
4.28	.63242
4.78	.22358
5.28	.19308
5.78	.00895
6.28	.00000
6.78	.00242
7.28	.00451
7.78	0.00000
8.28	.27827
8.78	1.14422
9.28	3.62657
9.78	.59247
10.28	.93070
10.78	.09292
11.28	.03179

Location 19A 19/7/73

Time from HW	Sediment Discharge
.95	.00871
1.45	.21668
1.95	.27059
2.45	.22978
3.45	.64039
3.95	1.07510
4.45	1.25529
4.95	2.16128
5.45	2.40593
7.95	2.93745
8.45	8.41156
6.95	.66729
9.45	.55996
9.95	.62274

Location 19B

Time from HW	Sediment Discharge
1.28	.00694
1.62	.07728
2.12	.22788
2.62	.13418
3.12	.38875
4.62	.64191
5.12	1.13298
5.62	1.83419
6.12	1.07182
6.62	1.95696
7.12	2.50709
8.12	.15175
8.62	3.23545
9.12	.59583
9.62	.17731
10.12	.57734
10.62	.06148
11.12	.02434

SELMA BAR (cont'd)

Location 20A	25/7/72	Location 20B	15/8/72
Time from HW	Sediment Discharge	Time from HW	Sediment Discharge
.78	.00043	1.12	.01167
1.28	.05404	1.37	.04336
1.78	.03276	1.87	.08135
2.28	.13307	2.37	.05354
2.78	.05098	2.87	.00913
3.28	.12865	3.37	.01795
3.78	.06965	3.87	.01581
4.28	.00246	4.37	.01361
4.78	.00029	4.87	.00284
		5.37	0.00000
		5.87	0.00000
		7.87	0.00000
		8.37	0.00000
		8.87	.07582
		9.37	.55793
		9.87	.18924
		10.37	.16686
		10.87	.10777

A P P E N D I X V

BEDFORM MEASUREMENTS

V.1 GENERAL

Comprehensive data about the properties and areal distribution of different types of bedforms on the intertidal bars were collected either simultaneously with sediment sampling on the same grid (Appendix II) or on a completely different grid pattern. Sampling locations are summarized in Figure V.1, V.2 and V.3. The field data are listed in Appendix V.2 for each of the bars.

Bedforms are best described in terms of their size and shape (Allen, 1963, 1968 b, p. 53-66; Harms, 1969; Tanner, 1967). Allen's (1963, Fig. 1 and Table I, 1968 b, p. 60-66) "measures for quantitative description" were used to describe the external morphology of bedforms (Fig. 5.1). Specifically, bedform length (distance between crests, measured perpendicular to the crestline), height (elevation of crest above adjacent trough), ripple index (ratio of length to height), crestline orientation (facing of lee-side dip direction), lee-side slope angle, upper and lower stoss-side slope angles, and crestline continuity (sinuosity; length of bedform crestline relative to the straight-line distance between the ends of the bedform or two reference points on the crestline) were recorded at each grid station. Descriptive notes were made of the bedform morphologies, e.g., scours and spurs, planed-off crests, superposed bedforms, late-stage ebb runoff and emergence features, wave modification features, etc. Measurements and descriptions were supplemented with 35 mm photographs to provide a permanent record for later analysis.

All linear measurements were made with steel (2m) and cloth-woven (30 m) tapes. Bedform heights were determined with a one-meter long, two by five centimeter board, a Brunton compass and the steel tape. One end of the board was placed on the crest of the bedform, and the board was maintained in a horizontal position with the aid of the level on the Brunton (dip-meter set to zero) while the distance was measured from

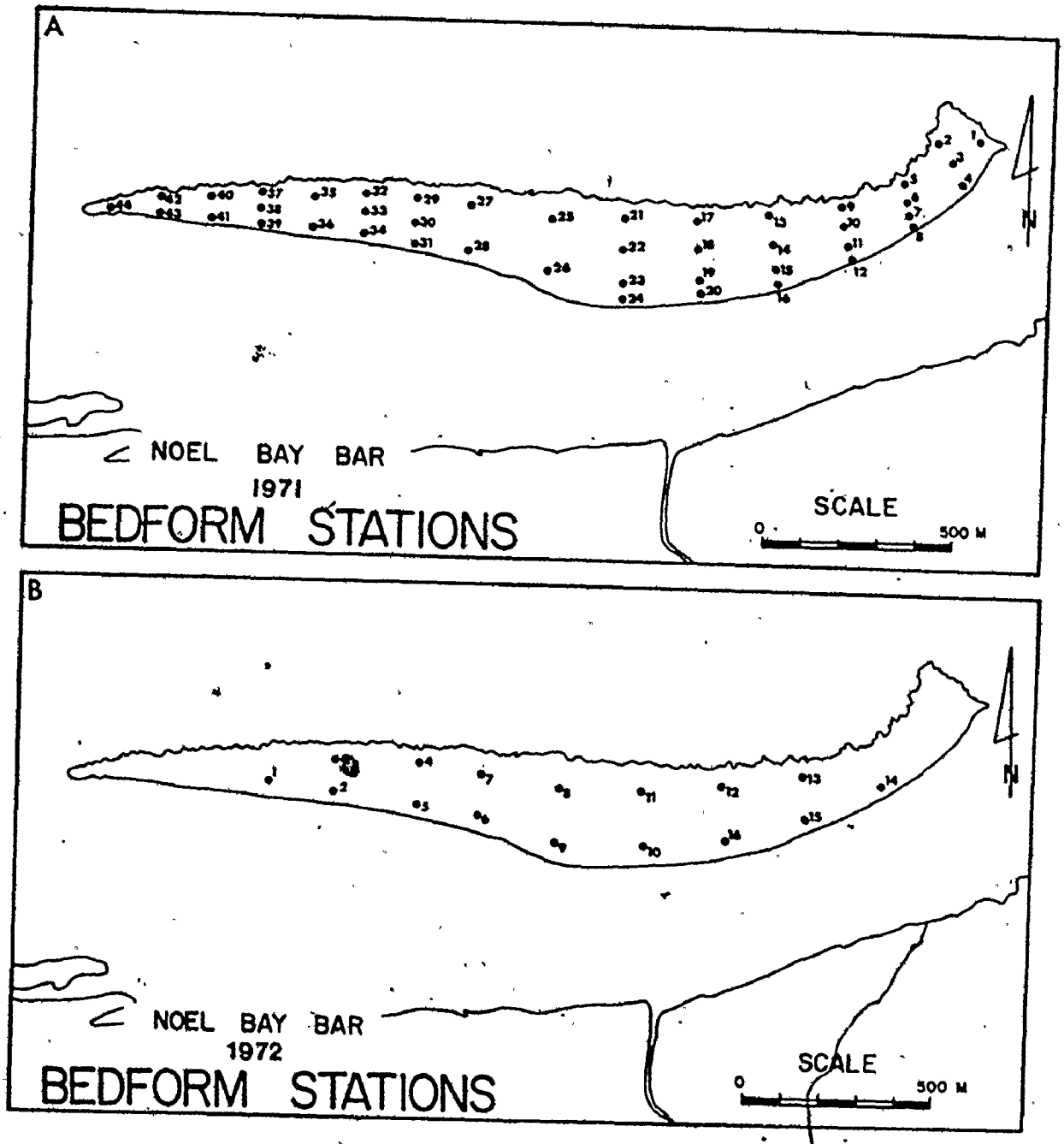

FIGURE V.1: Bedform measurement locations on Noel Bay Bar.

A. 1971

B. 1972

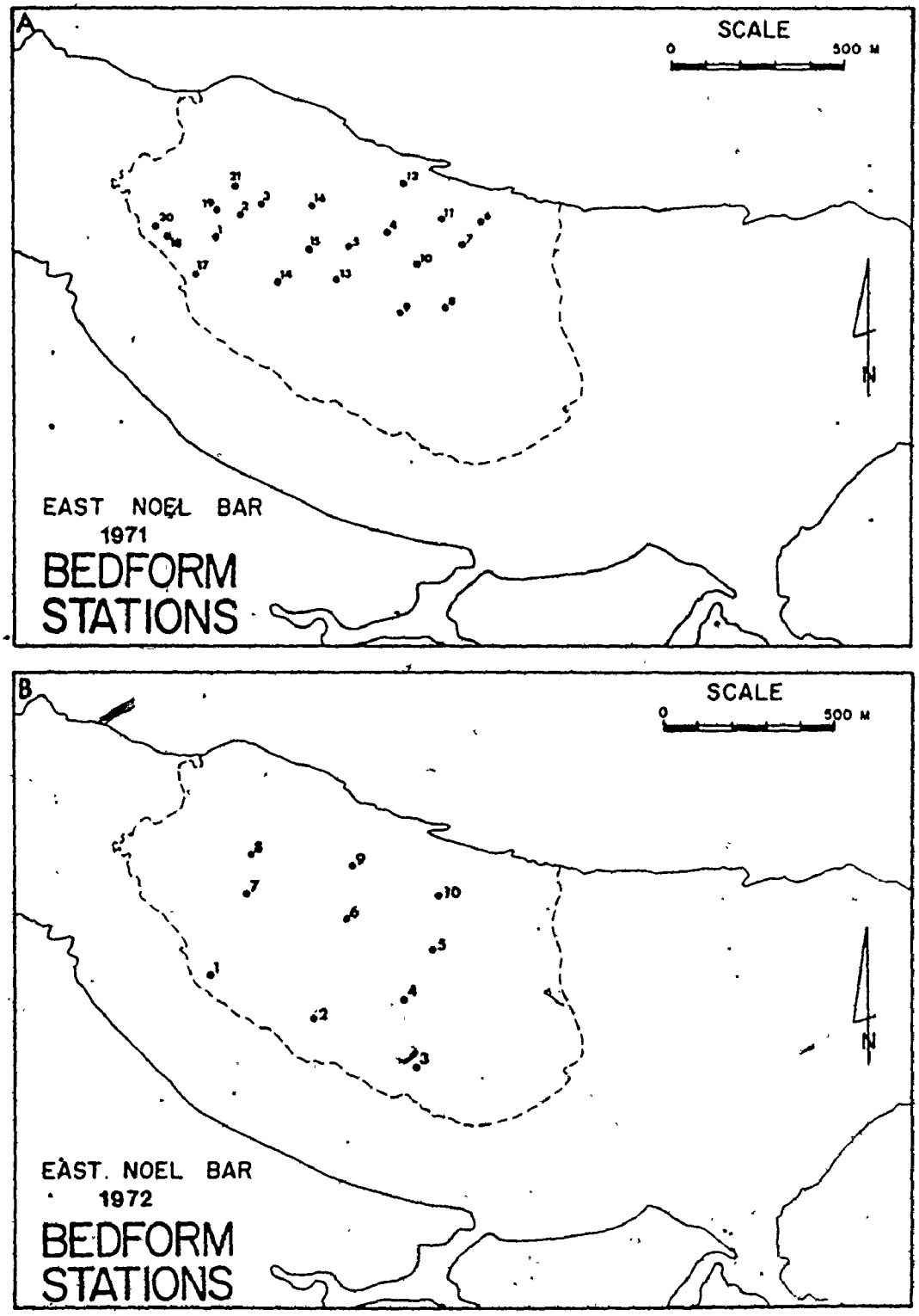

FIGURE V.2: Bedform measurement locations on East Noel Bar.

A. 1971

B. 1972

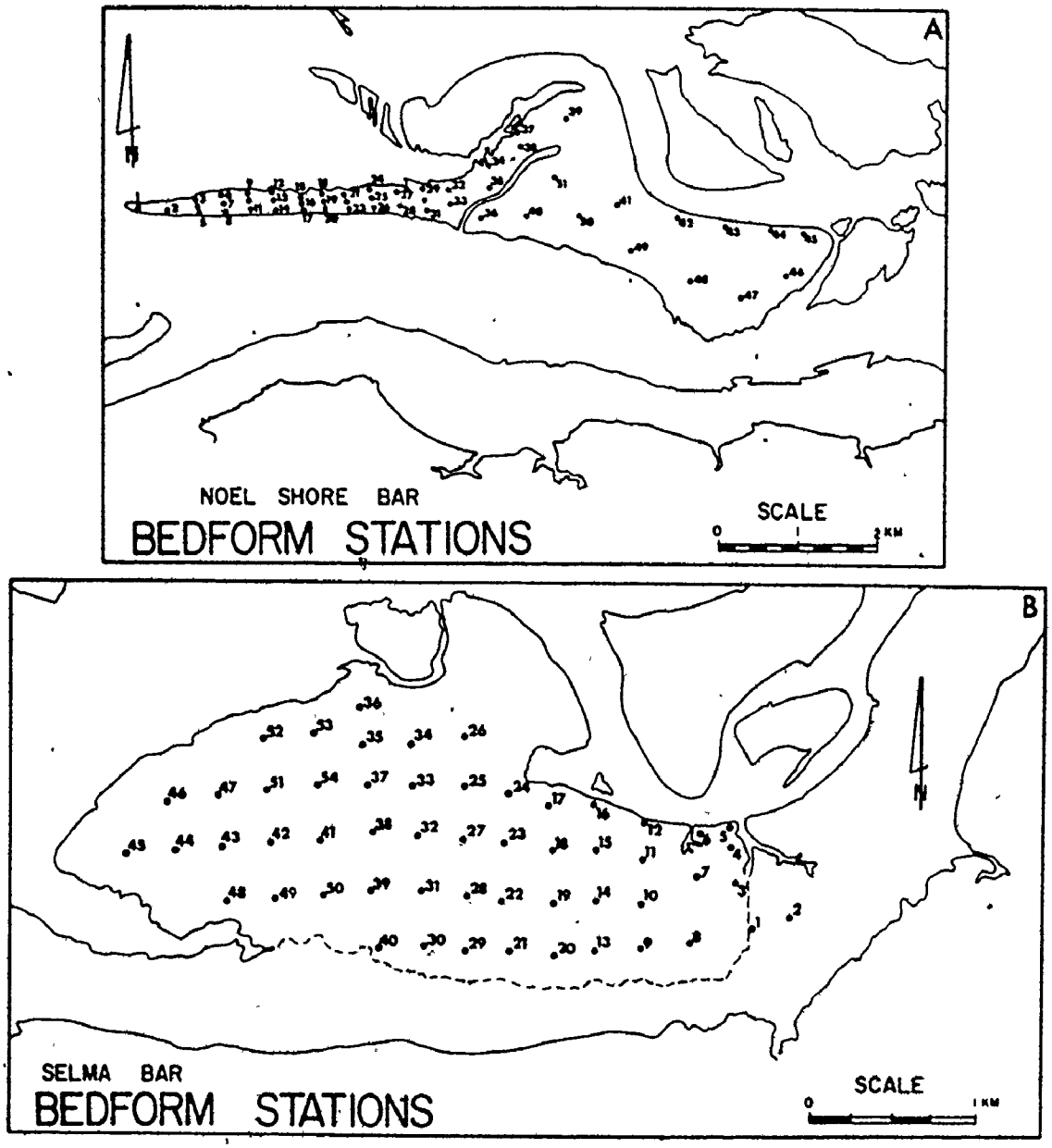

FIGURE V.3: Bedform measurement locations on Noel Shore Bar and Selma Bar.

the lower surface of the board to bedform trough. The Brunton compass was used to determine the bedform orientation and lee-side and stoss-side slope angles. Because the stoss-side of bedforms was commonly irregular due to superposed ripples, the meter board was placed on the upstream surface of bedforms to give a planar base on which the Brunton compass could be set to measure the angle of inclination. Anywhere from three to five measurement repetitions were made at each station.

V.2 TIME-VARIABILITY

The time-variant properties of bedforms on the intertidal bars were examined within two scales of time: (i) during single semidiurnal tidal cycles (ebb and flood); and (ii) during the period of the lunartidal cycle (neap-spring variations).

During single semidiurnal tidal cycles, bedform changes were monitored indirectly with a Raytheon echo-sounder on calm days. Sounding lines were made along pre-marked courses outlined with spherical buoys in a line oriented at right angles to the bedform crestlines. Runs were repeated at one-hour intervals in both up- and down-flow directions during the particular semidiurnal tidal cycle (see discussion by Snishchenko, 1966). This method was successful only with the larger megaripples and sand waves.

A few attempts were made to examine bedforms directly during submerged intervals with SCUBA but water turbidity was too great and flow conditions too hazardous to obtain any information, other than by touch.

The rates of net bedform migration, changes of surface elevation, depths of local scour and variations of bedform length, height, etc., were monitored over periods of several weeks to determine whether the variation of these measures could be correlated to the lunartidal cycle. A simple method of determining rates of net bedform migration, surface elevation change and local scour depths is outlined by Clifton (1969) and Knight (1972). A steel, 'concrete-reinforcing' rod, one to two meters in length by 9.5 mm. was driven into the brinkpoint of a bedform with a hammer to about ninety percent of their length. The sediment surface was marked with a short length of brass wire, and a steel

washer (i.d., 15.9 mm) that was free to slide down the rod was placed on the rod just beneath the wire. Three different networks of stake emplacement were used, either concurrently or separately; (i) the most common method was to position the rods along the brinkline of a single bedform at regular intervals (3 to 5 m); (ii) the rods were placed along the brinklines of two or more different bedforms in the same area; and (iii) anywhere from five to nine stakes were set in a line perpendicular to a bedform crestline and spaced at 1 to 2 m apart. Method (i) was used to determine the net differential brinkline movement of one bedform. The second type of stake emplacement gave differences of net migration for two different bedforms in the same area. The third method was useful for determining local depths of scour and surface elevation changes through a bedform cross-section.

Stake locations were generally the same as the current meter stations. Most stake measurements were made on bars accessible from the shore so that a regular interval of measurement could be maintained regardless of the weather (sometimes a problem for boat operation). Each location was visited at approximately two-day intervals. During each visit, bedform height, length, brinkpoint to stake distance (often in both up- and downflow directions) perpendicular to the crestline and wire and washer distance from the sediment surface were measured. The stakes were reset to the bedform brinkpoint after every measurement.

It was difficult to determine the direction of net migration at some locations because the location was neither ebb- or flood-dominated or else, dominance changed during the lunartidal cycle. This problem was overcome at some stations by dumping fluorescent-painted pebbles (Yasso, 1966; Ingle, 1966, p. 191-195) over the side of the boat at high slack water while at anchor. The painted pebbles marked the outline of the flood current deformed bed before modification of the bed by ebb currents. At low tide, trenches were dug through several bedforms around the ground boat. The outline of the flood generated bedform's stoss-side was marked by pebbles, from which some idea of the net direction of migration could be determined.

V.3 TRENCHES AND PEELS

The internal structures of intertidal bedforms were examined in trench faces and with epoxy-relief peels. Trench faces were an adequate technique of exposing bedform cross-stratification if the sediments had a size distribution with a substantial coarse tail and/or there was some mineralogical separation between the cross-strata, and, if the sediments dried-out sufficiently during low tide emergence of the bedform. This technique did not provide a permanent record of the structures. It was used with success on parts of East Noel and Selma Bars.

Unfortunately, most of the bar sediments were well-sorted, medium sized sands without a prominent coarse-tail and compositional separation. The sediments also remained quite wet throughout low tide periods. To see both large- and small-scale cross-stratification and to provide a permanent record of the sedimentary structures for later detailed examination and presentation, epoxy-relief peels (Barr et al., 1970, Klein, p. 237-241 in Carver, 1971) were taken from the trench faces. Some difficulties recurred with this peel technique because the epoxy did not have sufficient hardening time. After two to three hours in place on the trench peel, the peel was removed before the area was flooded by the incoming tide. If the epoxy was inadequately hardened, it would flow and/or separate from the masonite backing, thus distorting or obliterating any sedimentary structures. In an attempt to solve these problems, the epoxy mixture was modified to equal proportions of the four ingredients, and the peels were left buried in place on the trench face for two semidiurnal tidal cycles. The latter modification allowed the epoxy adequate time to cure, but if the incoming flood tide was particularly strong, the peels were unearthed and eroded (again causing distortion or obliteration of any sedimentary structures). The most consistent results were eventually achieved using the modified epoxy mixture and carefully removing the peels after one emergence period.

It was impossible to make single peels across the full bedform cross-section exposed in the trench face, so small peels, approximately 0.6 by 0.9 m were taken at regular intervals across the trench face (Fig. I.G). Efforts were made to get peels from the deeper parts of

AV	[illegible]	[illegible]	[illegible]	[illegible]	[illegible]	[illegible]	288.	1.66	.73
AV	[illegible]	[illegible]	[illegible]	[illegible]	[illegible]	[illegible]	290.	1.76	.59
AV	[illegible]	[illegible]	[illegible]	[illegible]	[illegible]	[illegible]	296.	1.73	.76
AV	[illegible]	[illegible]	[illegible]	[illegible]	[illegible]	[illegible]	295.	1.73	.73
AV	[illegible]	[illegible]	[illegible]	[illegible]	[illegible]	[illegible]	293.	1.72	.57
AV	[illegible]	[illegible]	[illegible]	[illegible]	[illegible]	[illegible]	296.	1.69	.63
AV	[illegible]	[illegible]	[illegible]	[illegible]	[illegible]	[illegible]	296.	1.77	.52
9	PLOT REP								
AV	[illegible]	[illegible]	[illegible]	[illegible]	[illegible]	[illegible]	278.	1.67	.73
AV	[illegible]	[illegible]	[illegible]	[illegible]	[illegible]	[illegible]	298.	1.63	.67
AV	[illegible]	[illegible]	[illegible]	[illegible]	[illegible]	[illegible]	303.	1.69	.63
17	PLOT REP								
AV	[illegible]	[illegible]	[illegible]	[illegible]	[illegible]	[illegible]	290.	1.78	.59
AV	[illegible]	[illegible]	[illegible]	[illegible]	[illegible]	[illegible]	293.	1.64	.67
AV	[illegible]	[illegible]	[illegible]	[illegible]	[illegible]	[illegible]	285.	1.80	.57
18	PLOT REP								
AV	[illegible]	[illegible]	[illegible]	[illegible]	[illegible]	[illegible]	292.	1.71	.57
AV	[illegible]	[illegible]	[illegible]	[illegible]	[illegible]	[illegible]	296.	1.71	.56
AV	[illegible]	[illegible]	[illegible]	[illegible]	[illegible]	[illegible]	300.	1.92	.61
20	PLOT REP								
AV	[illegible]	[illegible]	[illegible]	[illegible]	[illegible]	[illegible]	316.	1.71	.65
AV	[illegible]	[illegible]	[illegible]	[illegible]	[illegible]	[illegible]	309.	1.69	.59
AV	[illegible]	[illegible]	[illegible]	[illegible]	[illegible]	[illegible]	297.	1.79	.75
AV	[illegible]	[illegible]	[illegible]	[illegible]	[illegible]	[illegible]	310.	1.93	.61
AV	[illegible]	[illegible]	[illegible]	[illegible]	[illegible]	[illegible]	291.	1.76	.76
AV	[illegible]	[illegible]	[illegible]	[illegible]	[illegible]	[illegible]	296.	1.81	.54
AV	[illegible]	[illegible]	[illegible]	[illegible]	[illegible]	[illegible]	292.	1.73	.56
AV	[illegible]	[illegible]	[illegible]	[illegible]	[illegible]	[illegible]	299.	1.93	.51
AV	[illegible]	[illegible]	[illegible]	[illegible]	[illegible]	[illegible]	6.	.78	.57
AV	[illegible]	[illegible]	[illegible]	[illegible]	[illegible]	[illegible]	291.	1.82	.57
AV	[illegible]	[illegible]	[illegible]	[illegible]	[illegible]	[illegible]	291.	1.69	.76
AV	[illegible]	[illegible]	[illegible]	[illegible]	[illegible]	[illegible]	296.	1.69	.77
AV	[illegible]	[illegible]	[illegible]	[illegible]	[illegible]	[illegible]	298.	1.79	.56
AV	[illegible]	[illegible]	[illegible]	[illegible]	[illegible]	[illegible]	287.	1.81	.63
AV	[illegible]	[illegible]	[illegible]	[illegible]	[illegible]	[illegible]	304.		
AV	[illegible]	[illegible]	[illegible]	[illegible]	[illegible]	[illegible]	291.	1.74	.59
AV	[illegible]	[illegible]	[illegible]	[illegible]	[illegible]	[illegible]	296.	1.81	.56
AV	[illegible]	[illegible]	[illegible]	[illegible]	[illegible]	[illegible]	309.	1.77	.78
AV	[illegible]	[illegible]	[illegible]	[illegible]	[illegible]	[illegible]	308.	1.66	.66
AV	[illegible]	[illegible]	[illegible]	[illegible]	[illegible]	[illegible]	293.	1.78	.53
AV	[illegible]	[illegible]	[illegible]	[illegible]	[illegible]	[illegible]	302.	1.84	.63
AV	[illegible]	[illegible]	[illegible]	[illegible]	[illegible]	[illegible]	291.	1.77	.59
AV	[illegible]	[illegible]	[illegible]	[illegible]	[illegible]	[illegible]	310.	1.82	.78
AV	[illegible]	[illegible]	[illegible]	[illegible]	[illegible]	[illegible]	288.	1.78	.75
AV	[illegible]	[illegible]	[illegible]	[illegible]	[illegible]	[illegible]	286.	1.73	.57

NOEL BAY BAR, 1972

BEUFORM LOCN	MEASUREMENT, LENGTH	HEIGHT	L/H	LEE	WALK	AZ
1	3.00	8.00	37.50	20.0	3.0	
1	3.00	11.50	26.10	21.0	3.0	
1	4.00	9.50	42.10	19.0	2.0	
AV	3.50	9.70	34.07	22.0	2.3	298.
2	4.00	12.00	33.30	18.0	2.0	
2	9.50	17.00	34.20	21.0	3.0	
2	7.00	13.00	53.80	19.0	3.0	
AV	5.00	13.70	38.99	18.0	2.6	274.
3	4.20	11.00	37.30	30.0	3.0	
3	4.40	13.00	36.50	30.0	4.0	
3	3.50	8.00	43.80	27.0	3.0	
AV	4.20	11.30	37.20	29.0	4.3	308.
4	7.00	17.00	40.50	27.0	3.0	
4	3.50	12.00	29.20	26.0	4.0	
4	5.00	14.00	35.70	26.0	3.0	
AV	4.20	13.30	31.50	27.7	4.0	288.
5	7.00	20.00	32.10	24.0	4.0	
5	5.00	20.00	32.10	24.0	3.0	
5	8.00	21.00	26.60	24.0	0.0	
AV	7.30	29.70	30.70	24.0	3.0	278.
6	6.00	70.00	8.60	23.0	4.0	
6	10.00	72.00	13.90	23.0	7.0	
6	12.50	55.00	22.70	27.0	3.0	
AV	9.50	69.70	14.40	25.0	4.7	268.
7	8.00	17.00	31.00	30.0	3.3	
7	3.00	15.00	20.00	30.0	4.0	
7	3.50	13.00	26.90	29.0	3.0	
AV	4.20	13.70	26.73	29.4	4.2	305.
8	7.00	10.50	42.40	29.0	7.0	
8	7.70	17.00	45.30	29.0	7.0	
8	8.00	13.00	40.20	29.0	3.0	
AV	8.30	15.50	44.32	29.0	8.5	305.
9	8.30	24.20	37.30	27.0	3.3	
9	4.10	23.00	17.80	28.5	4.5	
9	6.00	21.00	28.60	29.0	3.0	
AV	6.10	22.50	27.11	21.2	3.7	277.
10	3.20	13.50	40.70	29.0	4.0	
10	2.00	13.00	15.40	29.0	4.0	
10	3.50	11.50	30.40	29.0	3.5	
AV	3.70	12.70	29.13	29.0	3.8	302.
11	2.10	7.00	30.00	29.0	3.4	
11	2.40	10.00	24.00	30.0	3.0	
11	2.00	12.00	21.70	27.0	3.0	
AV	2.40	9.70	24.44	21.3	4.7	300.
12	2.40	10.00	12.00	27.0	3.0	
12	3.40	10.00	17.50	29.0	4.0	
12	2.90	10.00	10.10	31.0	3.0	
AV	2.70	17.30	13.41	20.7	4.0	298.
13	3.00	11.00	27.30	29.0	3.0	
13	3.00	20.00	15.00	31.5	3.0	
13	2.50	14.00	17.50	30.0	3.0	
AV	2.66	15.00	18.07	30.2	4.3	298.
14	2.00	27.00	8.30	29.5	1.5	
14	3.20	20.00	11.00	30.5	3.0	
14	3.00	25.00	13.00	31.0	3.0	
AV	2.40	22.30	10.10	30.2	2.5	295.
15	2.00	20.00	10.00	20.0	3.0	
15	2.00	10.00	11.00	31.0	4.0	
15	00.00	5.00	31.50	2.0	-0.0	
AV	1.00	22.70	7.93	30.3	3.7	305.
16	2.10	12.00	17.00	27.0	3.0	
16	2.00	13.00	13.30	27.0	3.0	
AV	2.10	13.00	14.00	27.0	3.0	310.

EAST NOEL BAR 1971

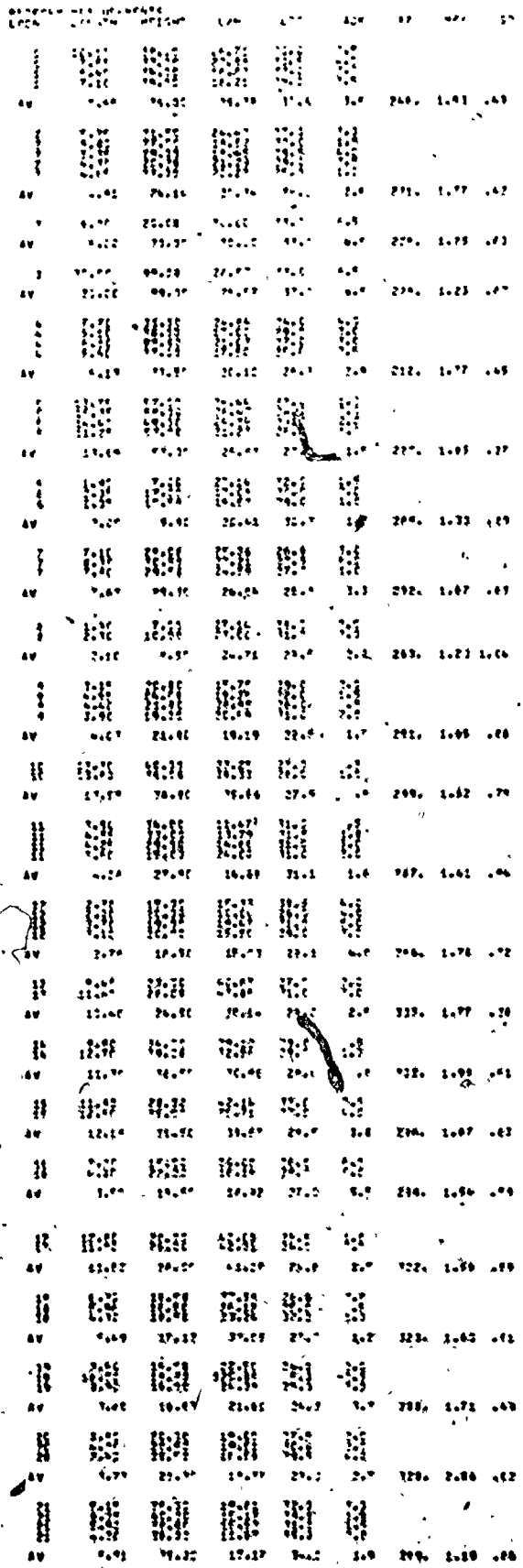

EAST NOEL BAR 1972

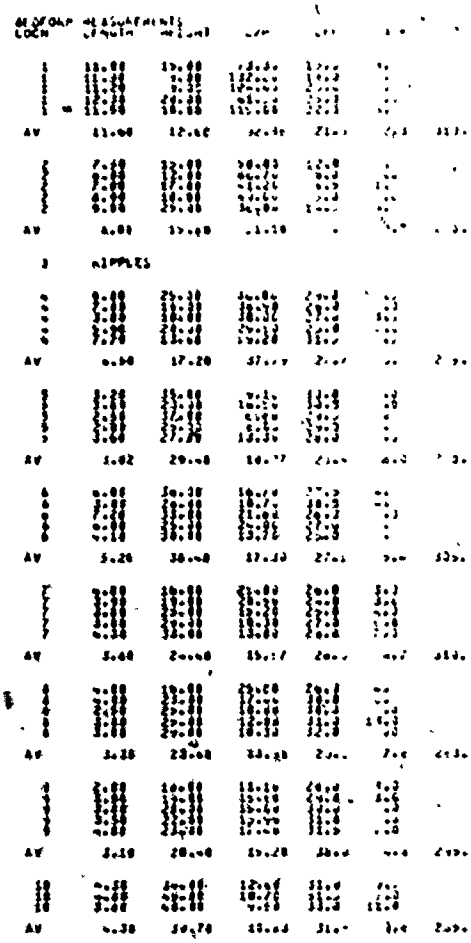

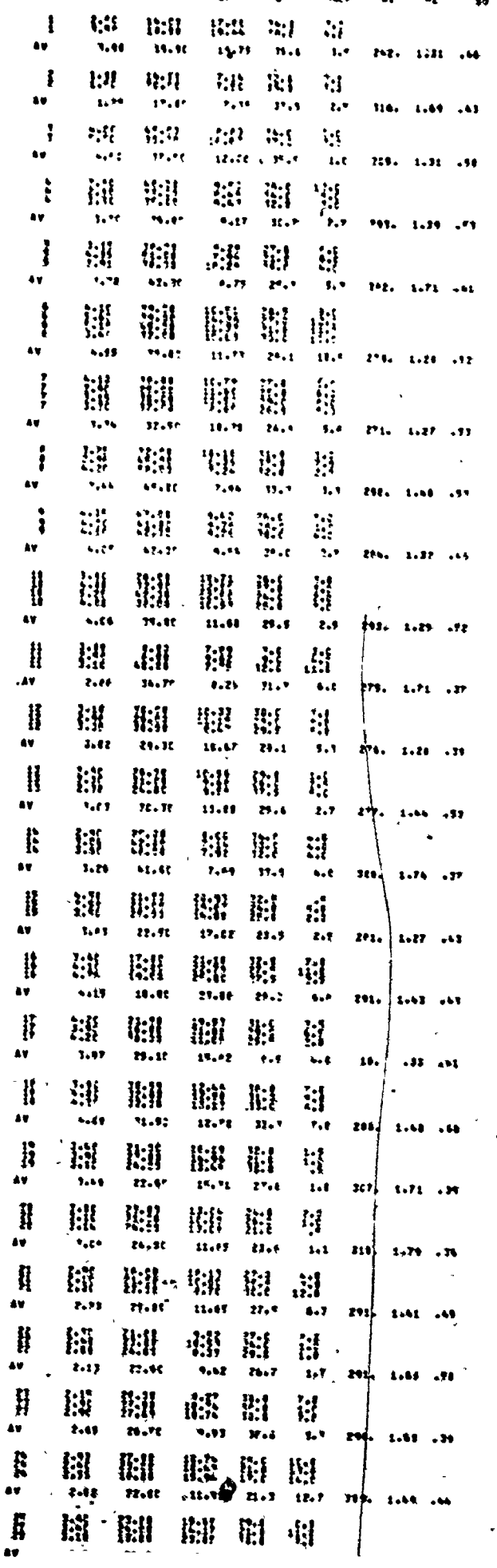

SELMA BAR 1972